



University of Strathclyde
Department of Pure and Applied Chemistry

Synthesis Enabled Drug Discovery

Thesis submitted to the University of Strathclyde in fulfilment of the requirements
for the degree of Doctor of Philosophy

Storm Hassell-Hart

**Academic Supervisor: Professor William Kerr BSC, PhD, CChem,
FRSC, FRSE**

**Industrial Supervisors: Dr Vipulkumar K. Patel, Dr Gemma V.
White**

Declaration of Copyright

This thesis is the result of the author's original research. It has been composed by the author and has not been previously submitted for examination which has led to the award of a degree.

The copyright of this thesis belongs to the author under the terms of the United Kingdom Copyright Acts as qualified by University of Strathclyde Regulation 3.50. Due acknowledgement must always be made of the use of any material contained in, or derived from this thesis.

Signed:

Date:

Abstract

This thesis describes the development and application of key organic synthesis methods to enable two different drug discovery projects: the development of inhibitors of lipoprotein-associated phospholipase A₂ (Lp-PLA₂), and the bromodomain and extra terminal (BET) family.

Studies have implicated the phospholipase Lp-PLA₂ in a range of different disease states, including cardiovascular disorders, diabetic macular oedema, and Alzheimer's disease. With the aim of developing novel inhibitors of Lp-PLA₂, a fragment screening approach was used to identify small, ligand efficient, cyclic borolane inhibitors. The potency and selectivity could be enhanced by careful structure guided growth.

The novel cyclic borolane template posed a number synthetic challenges. The first section of the thesis describes the synthesis and evaluation of a novel subset of pyridone borolane inhibitors of Lp-PLA₂. This research led to the identification of a novel iridium-mediated carbenoid insertion reaction that was applicable to all borolane analogues. Development and optimisation of this reaction led to methodology which was employed in our laboratories to rapidly assemble a range of synthetically challenging borolane analogues in high yields. This led to the identification of a key pyridyl borolane. The established iridium chemistry provided the ability to rapidly enable scale-up and biological evaluation of this compound. Further synthetic research led to the identification of a new concise asymmetric route to provide the desired key compound in excellent yields and enantioselectivities.

The second section of the thesis describes the development of a novel, synthetically challenging series of BET inhibitors. Inhibition of the BET family of bromodomains has been implicated in a range of different disease states, including cancer. The work describes the development of a new series of constrained BET inhibitors, to remove a functional group of concern. This new series was found to retain the potency exhibited by the original series, without the potentially reactive functionality. If required, this series could form the basis of a new research project and be developed into a novel series of BET inhibitors by further elaboration.

Confidential – Property of GSK – Do Not Copy

In addition to this, the synthetic work on the BET series led to the identification of a new rhodium-catalysed, directed C-H activation reaction. It was envisaged that this methodology could be applied to enable the more facile synthesis of a diverse range of medicinal chemistry targets.

Acknowledgements

Firstly, I would like to thank my academic supervisor Professor William Kerr from the University of Strathclyde for his continuous support throughout my PhD and the opportunity to spend time in his laboratories. The breadth of his scientific knowledge is something that inspires me to continue learning and pushing myself. In addition to this I am extremely grateful for the amount of time he has dedicated to teaching and developing both my chemical and presentation skills. I would also like to acknowledge my internal examiner Professor John Murphy for his continued interest in all aspects of my PhD and for his stimulating, although sometimes stressful, conversations.

In addition to Professor Kerr, this PhD would have been impossible without the support of both my industrial supervisors, Dr Vipulkumar Patel and Dr Gemma White. The frank and honest discussion with Vipul, as well his passion for science and continued care for my development, have taught me so much and I continue to respect and admire him. Gemma deserves more credit than I can put down here and I do not believe I could have reached this stage without her. Her diligent supervision in all aspects of my PhD, despite our totally different personalities, has been amazing and I am eternally grateful for this, even if I don't always show it!

I would also like to acknowledge the members, both past and present, of the Kerr group, the industrial PhD scheme, and the FDU. I have learnt so much from our interactions and discussions and feel privileged to have been a part of both groups. Although I cannot name all of your individual contributions, which are extensive to say the least, I want say a special thank you to Tom and Nick, both of whom have helped me enjoy my PhD so much. I also want to thank my industrial placement student Julie, your hard-work and passion for science meant you were a pleasure to supervise and I know you will thrive on your own PhD!

I also want to thank the numerous other people at GSK and the University of Strathclyde who have been so kind, patient, and welcoming over my PhD. So many people have taken time to help me and teach me new skills, not reluctantly but with a smile on your faces. I have been overwhelmed by kind offers of help and support than have contributed to both my development and enjoyment of my PhD. I hope wherever I end up that I always work with people like you.

Confidential – Property of GSK – Do Not Copy

I would like to thank everyone that has been and is involved in the industrial PhD scheme. Thank you to both Professor Harry Kelly and Professor William Kerr for founding this unique collaborative PhD scheme. I cannot imagine another PhD that would provide the amazing breadth of knowledge and experience that I have gained on the scheme and I only wish I could stay on longer! Again thank you both for your continued support on a more personal level and care over the well-being of every student, it's something I really appreciate. I would also like to say thank you to Dave Allen, Head of the Respiratory Therapy Area Unit and Chief Chemist and Dr Patrick Vallenge, President of GSK Pharmaceutical R&D for their continued support for the programme, as well as the time spent to take a personal interest in the research and people involved. A big thank you also goes to Andrea Malley for being instrumental in the organisation of the programme, without you I don't think any of this would be possible.

Finally, and maybe most importantly, I need to say a huge thank you to all my family; Harts, Hassells, and Goldings. You all have been so understanding and taken such good care of me over the past few years, and even before that. I owe you all a huge amount for all the love and support, although I regret to inform you that I may have more time for you all once I finish my PhD!

If there is one person that deserves the most thanks of all it is the love of my life, my wonderful wife Lara. To list the ways you have helped and supported me would take much more than the size of this thesis. I know how much you have had to put up with me, look after me, and be there for me and it's been truly wonderful.

Contents

Declaration of Copyright	i
Abstract.....	ii
Acknowledgements	iv
Contents	vi
Glossary of Terms	xii
Chapter 1: Synthesis of Borolanes as Inhibitors of Lp-PLA ₂	1
1.1 Introduction	2
1.1.1 Lipoprotein-associated Phospholipase A ₂ (Lp-PLA ₂) and the Phospholipases ...	2
1.1.2 The Role of Lp-PLA ₂ in Disease	4
1.1.3 The Catalytic Mechanism of Lp-PLA ₂ and the Consequences for Inhibitor Design	5
1.1.4 Strategies for Inhibition of Lp-PLA ₂	8
1.1.5 Discovery and Development of Boron-based Inhibitors of Lp-PLA ₂	13
1.1.5.1 High-throughput Screening Approach to the Discovery of Lp-PLA ₂ Inhibitors and the Development of Darapladib	13
1.1.5.2 Fragment-based Screening	15
1.1.5.3 Discovery of an Efficient Borolane Fragment	17
1.1.5.4 Elaboration of the Core Borolane Structures (1.1.1)	18
1.1.5.5 Optimisation of the Borolane Core	22
1.1.5.6 Development of a Borolane Pre-candidate Molecule	24
1.1.6 Synthesis of the Borolanes	27

1.1.6.1 Initial Medicinal Chemistry Synthesis of the Borolane Pre-candidate (1.1.12)	27
1.1.6.2 Synthetic Difficulties with Borolane Synthesis	29
1.1.6.3 Influence of the Pyridyl Groups on the Synthetic Strategy	30
1.1.6.4 Influence of the Nitrile Unit on Synthetic Strategy	33
1.1.6.5 Aniline Reactivity	35
1.1.6.6 Chirality of the Borolanes	36
1.1.7 Project Aims	37
1.2 Investigations into an Alternative Pyridone Core	39
1.2.1 Initial Pyridone Borolanes	39
1.2.2 Alternative Pyridone Isomer	39
1.2.3 Retrosynthesis and Common Reaction Steps	41
1.2.4 Synthesis of 6-Bromopyridin-2(<i>1H</i>)-one (1.2.5) and 6-Iodopyridin-2(<i>1H</i>)-one (1.2.8)	43
1.2.5 Development of a Reliable Method to Generate <i>N</i> -Alkylated Pyridone Molecules	45
1.2.5.1 Initial Halo Pyridone Alkylation Reaction Studies	45
1.2.5.2 Interconversion of <i>O</i> -Allyl Pyridones to <i>N</i> -Allyl Pyridones	47
1.2.5.3 Conversion of <i>N</i> -Allyl Pyridone into the Epoxy Derivative (1.2.10)	50
1.2.5.4 Alternative 4-Bromopyridone Isomer Studies	51
1.2.5.5 Previous Studies on Pyridone Alkylation	52
1.2.5.6 Optimisation of the Pyridone Alkylation to Favour <i>N</i> -Alkylation	53
1.2.5.7 Rationalising the Results of the Alkylation Study	59
1.2.6 Synthesis of the Alcohol Intermediate (1.2.27)	60
1.2.7 Borylation of the Racemic Alcohol (1.2.28)	63
1.2.8 Comparison of the Two Pyridone Borolane Isomers	69
1.2.9 Investigations Towards the Synthesis of the B-ring Pyridone (1.1.41)	70
1.3 Improving Synthetic Methodology for the Synthesis of the Pre-candidate Borolane (1.1.12) and Related Analogues	72
1.3.1 Issues with the Original Pre-candidate Borolane (1.1.12) Synthesis	72

1.3.2 The Use of Diazomethane to Access α -Chlorocarbonyls	72
1.3.3 The Use of Sulfur Ylides to Access α -Chlorocarbonyls; an Alternative to Diazomethane	73
1.3.4 The Use of Sulfur Ylides as Carbenoid Sources	76
1.3.5 β -Keto Sulfur Ylide Synthesis	79
1.3.6 Exploring the Source of Water in Ylide Formation	82
1.3.7 Investigations into the Formation of α -Chloro Carbonyl (1.3.1)	86
1.3.8 Iridium Carbenoid-mediated N-H Insertion Reaction.....	87
1.3.9 Studies into the Iridium Carbenoid Insertion Reaction	90
1.3.10 Studies into the Deactivation of the Iridium Catalyst	93
1.3.11 Further Optimisation of the Iridium Insertion Reaction	100
1.3.12 Scale-up of the Pre-candidate (1.1.12) Utilising Iridium-mediated Methods ..	102
1.3.13.1 Applicability of the Sulfur Ylide Chemistry to Other Targets	104
1.3.13.2 Synthesis of the Aniline Fragment	105
1.3.13.3 Iridium-mediated Coupling Reaction and Subsequent Reduction	106
1.3.13.4 Borylation of the Thiadiazole-containing Alcohol (1.3.35).....	107
1.3.14 Further Expansion of the Iridium Methodology	108
1.4 Investigations into the Key Borylation Step.....	110
1.4.1 Issues with the Borylation	110
1.4.2 Mechanistic Considerations and the Source of Dehalogenation	110
1.4.3 Determination of the Source of Dehalogenation	112
1.4.4 Investigations into Borylation at the Ketone Stage	113
1.4.5 Optimisation of the Borylation Reaction	115
1.4.6 Improved Synthesis of Borolane Analogues	116
1.5 Asymmetric Synthesis of the Borolane Pre-candidate (1.1.12). 117	
1.5.1 Asymmetric Reduction of the Ketone (1.3.13)	117
1.5.2 Enzymatic Reduction	119
1.5.3.1 Chemical Enantioselective Reduction of Ketone (1.3.13) – CBS Reduction	121

1.5.3.2 Chemical Enantioselective Reduction of Ketone (1.3.13) – Asymmetric Hydrogenation	122
1.5.4 Alternative Route to the Pre-Candidate Borolane (1.1.12)	124
1.5.5 Synthesis of the α -Keto Acid (1.5.6)	125
1.5.6 Asymmetric Reduction of the Ketone (1.5.6).....	126
1.5.7 Amide Coupling and Completion of the Synthesis	129
1.6 Conclusion	132
Chapter 2: Design and Synthesis of a Novel Bromodomain and Extraterminal Domain (BET) Inhibitors and Discovery of a New C-H Activation Protocol.....	134
2.1 Introduction	135
2.1.1 Bromodomain and Extra Terminal (BET) Proteins	135
2.1.2 BET Protein Family Architecture	137
2.1.3 Bromodomain Structure and Inhibition	138
2.1.4 High-throughput Screening Approach to the Discovery of BET Inhibitors ...	143
2.1.5 Elaboration of the BZP ‘Hit’	144
2.1.5.1 WPF Shelf Region	148
2.1.5.2 ZA Channel	148
2.1.5.3 Substitution at the 8-Position	149
2.1.6 Removal of the Alkene.....	149
2.1.7 Alternative Methods to Mimic the BZP Conformation	152
2.1.8 BET Project Aims/Objectives	153
2.2 Investigations into the Tricyclic Core (2.1.13)	154
2.2.1 Previous Synthesis of the Carbon Skeleton	154
2.2.2 Retrosynthetic Analysis of the Tricyclic Core	157
2.2.3 Synthesis of the Halogenated Amine	159
2.2.4 Initial Palladium-mediated C-H Activation/Halogenation	162

2.2.5 Optimisation of the Palladium-mediated C-H Activation/Halogenation	165
2.2.6 Rhodium-mediated C-H Activation/Halogenation	169
2.2.7 Synthesis of the Tricyclic Core (2.2.10)	179
2.2.7.1 The Use of Enolate Cross-Coupling	179
2.2.7.2 Heck Reaction and Reduction	182
2.2.8 Biological Evaluation of the Tricyclic Core	185
2.2.9 Conclusion and Further Progression of the Series	190
2.3 Development of a Novel Rhodium C-H Activation Methodology	191
2.3.1 Rhodium(III) Catalysed Halogenation Reaction Investigation	191
2.3.2 Use of the Group 9 Metals in C-H Activation and Heterocyclic Synthesis	192
2.3.2.1 Initial Report, the Synthesis of Isocoumarins	192
2.3.2.2 Use of Additives in Group 9-Mediated C-H Activation Reactions	193
2.3.2.3 Mechanism of Rhodium(III)-Mediated C-H Activation	193
2.3.2.4 Use of Internal Oxidants	195
2.3.2.5 Alternative Group 9 Directed C-H Activation Reactions	196
2.3.3 Potential Applications of the New Directing Group C-H Methodology	197
2.3.4 Initial Screening of Rhodium(III)/Iridium(III) C-H Activation Conditions ..	198
2.3.5 Optimisation of the C-H Activation Reaction: Validation and Solvent Screening	205
2.3.6 Optimisation of the C-H Activation Reaction: Exploring the Role of the Additives	210
2.3.7 Investigations into Alternative Directing Groups.....	217
2.3.8 Exploring the Influence of Temperature on the Ratio of Mono-/Di-C-H Activation	221
2.3.9 Evaluating of the Potential Double C-H Activation Process	224
2.3.10 Exploring Alternative Alkynes	225
2.3.11 Alternative C-H Activation Reactions – Heck Reaction	229
2.3.12 Conclusions and Future Work	233

3. Experimental	237
3.1 Lp-PLA ₂ Experimental Section	241
3.2 BET Experimental Section	298
4. Appendix	348
4.1 Lp-PLA ₂ and PLA ₂ -VIIB Biological Assay Information	348
4.2 Determination of <i>N/O</i> -Alkylation	350
4.3 BET Biological Assay Information	351
5. Bibliography	353

Glossary of Terms

°C	Degrees Celsius
Ac	Acetyl
ACN	Acetonitrile
AD	Alzheimer's disease
Ala	Alanine
Ar	Aromatic
BD	Bromodomain
BET	Bromodomain and extraterminal domain
BINAP	2,2'-Bis(diphenylphosphino)-1,1'-binaphthyl
Boc	<i>tert</i> -Butyloxycarbonyl
BP	By-product
br	Broad
Bu	Butyl
BZP	Benzazapinone
CAL	<i>Candida antarctica</i> lipase
CBS	Corey-Bakshi-Shibata
CDI	1,1'-Carbonyldiimidazole
COE	Cyclooctene
Cp*	1,2,3,4,5-Pentamethylcyclopentadienyl
CPM	7-Diethylamino-3-(4'-maleimidylphenyl)-4-methylcoumarin
d	Doublet
DBU	1,8-Diazabicyclo[5.4.0]undec-7-ene
DCE	1,2-Dichloroethane
DCM	Dichloromethane
DG	Directing group

Confidential – Property of GSK – Do Not Copy

DIPEA	<i>N,N</i> -Diisopropylethylamine
DME	Dimethoxyethane
DMF	<i>N,N</i> -Dimethylformamide
DMSO	Dimethyl sulfoxide
DNA	Deoxyribonucleic acid
DPEN	1,2-Diphenyl-1,2-ethylenediamine
Dppb	1,4-Bis(diphenylphosphino)butane
Dppf	1,1'-Bis(diphenylphosphino)ferrocene
E_A	Activation energy
EDG	Electron donating group
ee	Enantiomeric excess
eq	Equivalent
Et	Ethyl
EWG	Electron withdrawing group
FDA	Food and Drug Administration
FRET	Fluorescence resonance energy transfer
GBC	General base catalyst
Gln	Glutamine
h	Hour
HA	Heavy atoms
HPLC	High-performance liquid chromatography
HTS	High-throughput screening
IBX	2-Iodoxybenzoic acid
IPA	<i>iso</i> -Propyl alcohol
ⁱ Pr	<i>iso</i> -Propyl
IR	Infra-red
KHMDS	Potassium hexamethyldisilazide

KJ	Kilojoule
LCMS	Liquid chromatography–mass spectrometry
LDA	Lithium diisopropylamide
LE	Ligand efficiency
LHMDS	Lithium bis(trimethylsilyl)amide
Lp-PLA ₂	Lipoprotein-associated phospholipase A ₂
LUMO	Lowest unoccupied molecular orbital
m	Multiplet
M	Molar
MDAP	Mass directed automatic purification
<i>m</i> -CPBA	<i>meta</i> -Chloroperoxybenzoic acid
Me	Methyl
MeCN	Acetonitrile
2-MeTHF	2-Methyltetrahydrofuran
MIDA	Methyliminodiacetic acid
min	Minute
MOE	Molecular operating environment
mol	Moles
MW	Molecular weight
NBS	<i>N</i> -Bromosuccinimide
NIS	<i>N</i> -Iodosuccinimide
NMR	Nuclear magnetic resonance
<i>n</i> -BuLi	<i>n</i> -Butyllithium
OPLS	Optimized potentials for liquid simulations
P	Product
PAF	Platelet activating factor
PAF-AH	Platelet activating factor-acetylhydrolase

Confidential – Property of GSK – Do Not Copy

Piv	Pivalic
Ph	Phenyl
Phe	Phenylaniline
PK	Pharmacokinetic
pK_a	Logarithmic acidic dissociation constant
PLA ₂ -VIIB	Phospholipase A ₂ -VIIB
PPA	Polyphosphoric acid
Py	Pyridyl
q	Quartet
quin	Quintet
ROESY	Rotating-frame nuclear Overhauser effect spectroscopy
RT	Room temperature
R _t	Retention time
SAR	Structure-activity relationship
Ser	Serine
SM	Starting material
S _N Ar	Nucleophilic aromatic substitution
SPR	Surface plasma resonance
sxt	Sextet
t	Triplet
T	Time
T3P	2,4,6-Tripropyl-1,3,5,2,4,6-trioxatriphosphorinane-2,4,6-trioxide
TBD	1,5,7-Triazabicyclo[4.4.0]dec-5-ene
<i>t</i> -Am	<i>tert</i> -Amyl
^t Bu	<i>tert</i> -Butyl
TBME	<i>tert</i> -Butyl methyl ether
TBSCl	<i>tert</i> -Butyldimethylsilyl chloride

Confidential – Property of GSK – Do Not Copy

TEAB	Tetraethylammonium bromide
Tf	Trifluoromethanesulfonyl
THF	Tetrahydrofuran
2-thio-PAF	1- <i>O</i> -Hexadecyl-2-deoxy-2-thio- <i>S</i> -acetyl- <i>sn</i> -glyceryl-3-phosphorylcholine
TIPS	Triisopropylsilyl
TIPS-EBX	1-[(Triisopropylsilyl)ethynyl]-1,2-benziodoxol-3(<i>1H</i>)-one
TLC	Thin layer chromatography
TMS	Tetramethylsilane
TMSCN	Trimethylsilyl cyanide
Ts	Tosyl
UV	Ultraviolet
WB	Whole-blood

Chapter 1

Synthesis of Borolanes as Inhibitors of Lp-PLA₂

1.1 Introduction

1.1.1 Lipoprotein-associated Phospholipase A₂ (Lp-PLA₂) and the Phospholipases

Lipoprotein-associated phospholipase A₂ (Lp-PLA₂) is a 45 kDa enzyme, consisting of 441 amino acid residues, which hydrolyses oxidised phospholipids in low density lipoprotein.¹ As the enzyme was first identified due to its ability to mediate the hydrolysis of platelet activating factor (PAF) (**Figure 1.1.1**), it is also often referred to as platelet activating factor-acetylhydrolase (PAF-AH).²

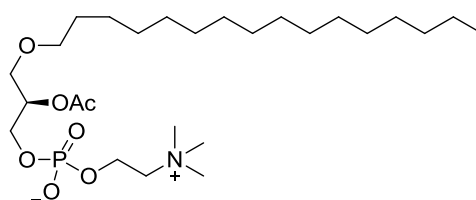


Figure 1.1.1 – Structure of platelet activating factor, PAF.^{3,4}

PAF is a phospholipid within the glycerophospholipid family (**Figure 1.1.2a**). All phospholipids contain a central glycerol core, which is also present in the related glycerolipids.⁵ The two families are differentiated by the presence of the polar phosphate head group in phospholipids.⁴

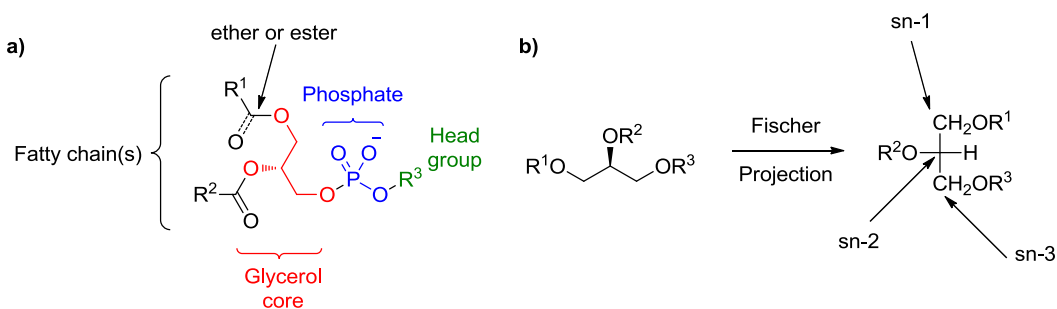


Figure 1.1.2 – a) General structure of phospholipids/glycerophospholipids.⁴ b) Fischer projection of a glycerol core and the labelling of the carbons.⁶

The glycerol carbons of both families share the same nomenclature, and are denoted sn-1, sn-2, and sn-3, where sn stands for stereospecifically numbered.⁶ These names are derived from the Fischer projection of the glycerol core. The central glycerol carbon is referred to as the sn-

2 carbon.⁶ In the Fischer projection the oxygen group on this carbon is represented orientated to the left.⁷ In this conformation the carbon above is labelled the sn-1 carbon, and the carbon below the sn-3 carbon (**Figure 1.1.2b**). The Fischer projection is still commonly used to represent the three dimensional structure of carbohydrates. This is in contrast with the majority of other molecules in which the representation of chirality has been supplanted by other more versatile methods, such as those derived from the Cahn–Ingold–Prelog rules.⁸

Lp-PLA₂ is a member of a family of enzymes, called the phospholipase A₂ superfamily.⁹ Phospholipases are characterised by their ability to hydrolyse at least one of four key bonds that form the core backbone of all phospholipids (**Figure 1.1.3**).^{5,10} The diverse family is further classified into four main categories, according to the position and nature of the bond hydrolysed by the enzymatic activity.¹¹ Phospholipase A (PLA) enzymes hydrolyse one of the two potential ester bonds in the substrate. Phospholipase B (PLB) enzymes hydrolyse both the ester bonds in their substrates. Phospholipase C (PLC) and phospholipase D (PLD) hydrolyse the two different bonds in the phosphate ester.

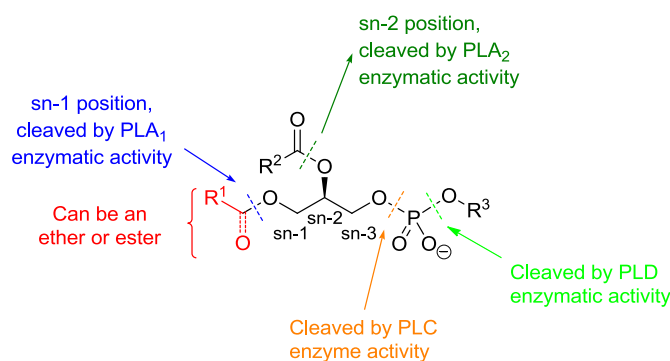


Figure 1.1.3 - Structure of the phospholipid core and the locations of enzymatic hydrolysis.¹¹

The phospholipase A₂ family's name is derived from their ability to hydrolyse the sn-2 acetyl bond of phospholipid substrates. The letter denotes the type of hydrolysis catalysed and the number indicates the position of the bond hydrolysed (**Figure 1.1.3**).⁵ While the PLA₂ classification represents only a small proportion of the total active phospholipase family, it still encompasses a large and diverse number of enzymes.² The identity of individual members is defined according to the nature of the substrate and the relative distributions of both the enzyme and the substrate within the organism.¹²

Lp-PLA₂ is synthesised primarily by white blood cells, which then secrete the enzyme into the blood.² The enzyme subsequently circulates in the blood in a constitutively active form, and associates with both high and low density lipoproteins. The enzyme has evolved to only recognise substrates with short or truncated chains at the sn-2 position.^{2,13} These shorter chains bear a structural resemblance to PAF and are commonly associated with degradation products of larger molecules.¹⁰ This evolution prevents the uncontrolled and unregulated degradation of all accessible phospholipids. This ensures that, under typical pharmacological conditions, key phospholipids, such as those that comprise the cellular membrane, are protected from hydrolysis. Hydrolysis of these phospholipids can result in cell lysis, therefore the process requires stringent regulation within the organism.^{10,14}

1.1.2 The Role of Lp-PLA₂ in Disease

Downstream molecules produced by Lp-PLA₂-mediated lipid hydrolysis have been implicated in the development of various different disease states, most notably atherosclerosis and Alzheimer's disease (AD).^{10,15,16} Small molecule inhibitors of Lp-PLA₂, such as rilapladib and darapladib (**Figure 1.1.4**), have recently been progressed through phase II and phase III clinical trials by GSK, for the treatment of AD and atherosclerosis, respectively.^{17–20} In addition, darapladib has been progressed to phase II clinical trials for the treatment of diabetic macular edema.²¹

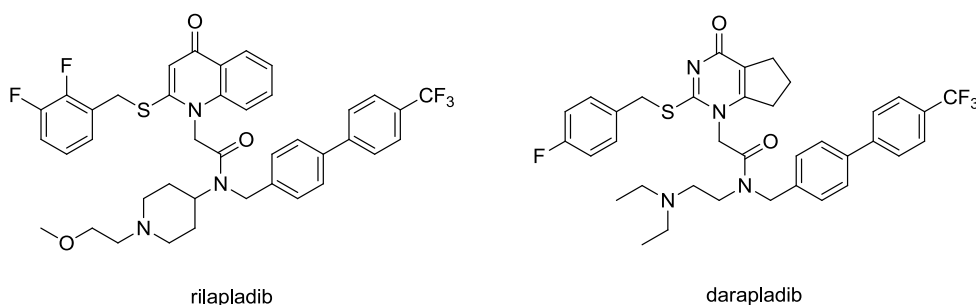


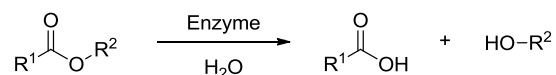
Figure 1.1.4 – Structures of rilapladib and darapladib.

Darapladib (SB-480848) represents the most advanced small molecule inhibitor of Lp-PLA₂. The molecule was discovered by scientists at SmithKline Beecham (**Figure 1.1.4**) and has recently completed two large scale phase III clinical trials.^{22,23} The primary endpoint in these trials was a significant reduction in the incidence of cardiovascular events, in patients on standard of care.²⁴ Unfortunately, the primary endpoint was not met in either of these studies.^{19,20} Despite these results, there is a requirement for further therapeutic agents, that

have the potential to inhibit of Lp-PLA₂ activity, for the treatment of AD and diabetic macular oedema.

1.1.3 The Catalytic Mechanism of Lp-PLA₂ and the Consequences for Inhibitor Design

Lp-PLA₂ mechanistically belongs to a larger classification of enzymes, the serine esterases, which hydrolyse esters to carboxylic acids (**Scheme 1.1.1**).^{4,25} The hydrolysis occurs through nucleophilic attack on the carbonyl moiety of the ester by a catalytic serine. This serine is part of the catalytic triad, which also includes histidine and aspartic acid residues in a linear arrangement, and is a common motif in serine proteases.^{9,26,27} The linear orientation of these residues allows the modulation of the nucleophilicity of the serine hydroxyl group. In addition to this, the orientation of these key residues allows them to perform other critical parts in the catalytic cycle (**Scheme 1.1.2**), including fulfilling the roles of general acid and base catalysts.²⁸



Scheme 1.1.1 – General reaction catalysed by serine esterases.

The catalytic cycle begins with recognition of the substrate and binding within the Lp-PLA₂ active site (**Scheme 1.1.2**). The tertiary structure of the protein has evolved to provide complementary binding with the substrate in the active site. The origin of the selectivity for phospholipids with smaller sn-2 chains is derived from the very specific constraints imposed upon the potential substrate by the shape of this active site.¹⁰

The binding of the substrate into the active site initiates the hydrolysis reaction. The first step in the catalytic cycle is the nucleophilic attack upon the ester by the key catalytic serine residue (**Scheme 1.1.2** - Step 1). The substrate is orientated within the active site to ensure the close proximity of these two reacting species. This causes relative concentrations that are significantly higher than those that can be obtained in solution, a further factor implicated in the dramatic rate acceleration observed. The aspartic acid and histidine residues, constituting the remainder of the catalytic triad, promote this nucleophilic attack by increasing the relative nucleophilicity of the serine residue. This effect originates from formation of a hydrogen bond between the catalytic aspartic acid and histidine residues, increasing the basicity of the histidine by several orders of magnitude; the pK_a of the histidine is estimated to increase from

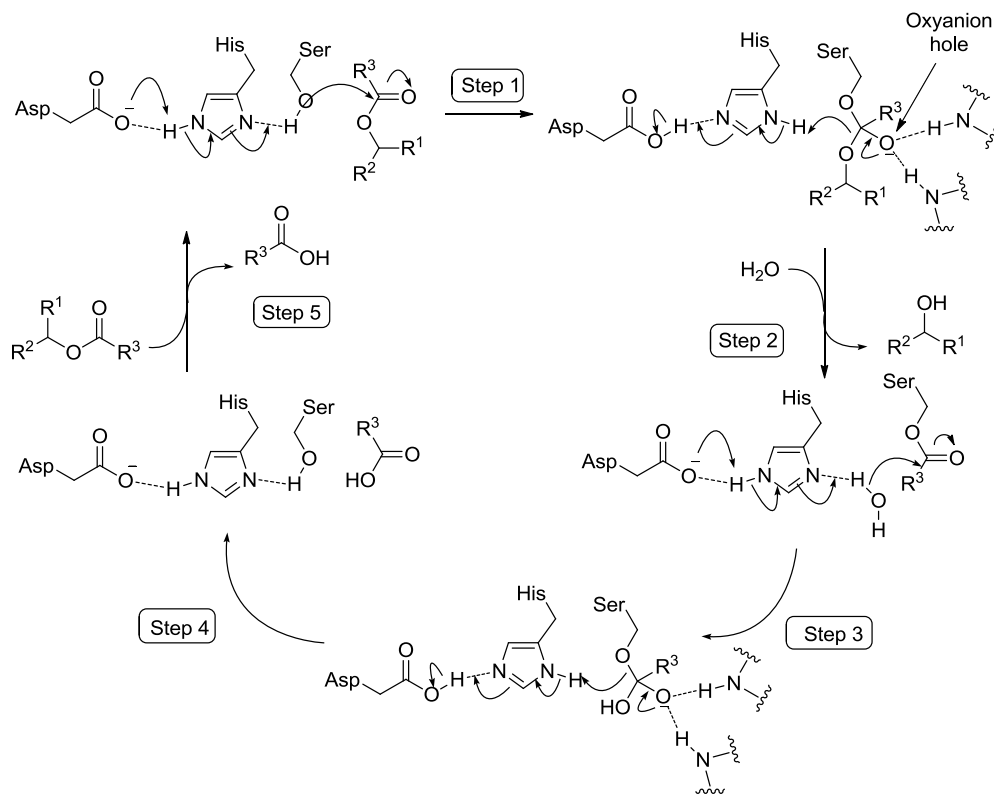
7 to 12 as a result of this hydrogen bond formation.^{4,29} The increased basicity of the histidine allows the residue to function as a general base catalyst (GBC), deprotonating the serine residue during the nucleophilic attack. This prevents the energetically unfavourable accumulation of positive charge upon the serine as this step progresses, lowering the activation energy for this step and increasing the reaction rate.

The nucleophilic action of the hydroxyl of the serine residue on the carbonyl moiety of the ester functionality results in formation of a thermodynamically unfavourable tetrahedral oxyanion intermediate (**Scheme 1.1.2** - Step 1). The resulting accumulation of negative charge in this intermediate species is stabilised through the orientation of this intermediate into the, so-called, oxyanion hole. This dissipates the negative charge through the formation of hydrogen bonds to several N-H bonds of the protein's backbone, stabilising the intermediate. The intermediate then rapidly breaks down to regenerate the more energetically favourable carbonyl species and liberates the free alcohol (**Scheme 1.1.2** - Step 2). The breakdown of this intermediate is assisted by the histidine functioning as a general acid catalyst, providing a proton to the leaving group to prevent the build-up of negative charge.²⁹ Again, this activity is enabled through hydrogen bonding and subsequent proton transfer between the histidine and aspartic acid residue.²⁸

The alcoholic product of the breakdown of the tetrahedral intermediate is displaced from the active site, allowing the coordination of a water residue within the active site and release of the alcohol into the circulatory system. The water can now act as a nucleophile, attacking the enzyme acetyl intermediate to initiate the release of the covalently bound serine residue (**Scheme 1.1.2** - Step 3), in an analogous fashion to that of the initial serine attack (**Scheme 1.1.2** - Step 1). As observed previously, the histidine acts as a general base catalyst with the modulation of this action provided through the key hydrogen bond with the aspartic acid residue.²⁹ This nucleophilic attack produces an alternate tetrahedral intermediate, again exhibiting the stabilisation of the negative charge through the action of the oxyanion hole as discussed previously. The breakdown of the second tetrahedral intermediate (**Scheme 1.1.2** – Step 4) occurs in comparable fashion to that of the initial tetrahedral intermediate formed earlier in the cycle, with both the histidine and aspartic acid residue fulfilling the same functions.

The collapse of the tetrahedral intermediate restores the catalytic serine residue to the initially observed state and produces the free acid within the active site. This is liberated from the active

site by binding of another phospholipid substrate equivalent, expelling the acid moiety into the circulation system (**Scheme 1.1.2** - Step 5). The catalytic cycle can now repeat, hydrolysing further phospholipid substrates.



Scheme 1.1.2 - The catalytic cycle of Lp-PLA₂.²⁸

As mentioned above, in addition to the catalytic triad, the enzyme active site contains another critical region for the catalytic action of the enzyme – the oxyanion hole (**Scheme 1.1.2**). This region stabilises the accumulation of negative charge on the carbonyl oxygen of the ester in the transition state, through the donation of hydrogen bonds from backbone N-H residues.³⁰ This interaction is only significant during the formation of tetrahedral intermediates, so the enzyme provides preferential stabilisation of the higher energy intermediate.³¹ The importance of this interaction upon the reaction rate can be rationalised by consideration of a simplified energy diagram for the first step of catalytic process for the native type enzyme and a theoretical enzyme without the presence of the oxyanion hole (**Figure 1.1.5**).³²

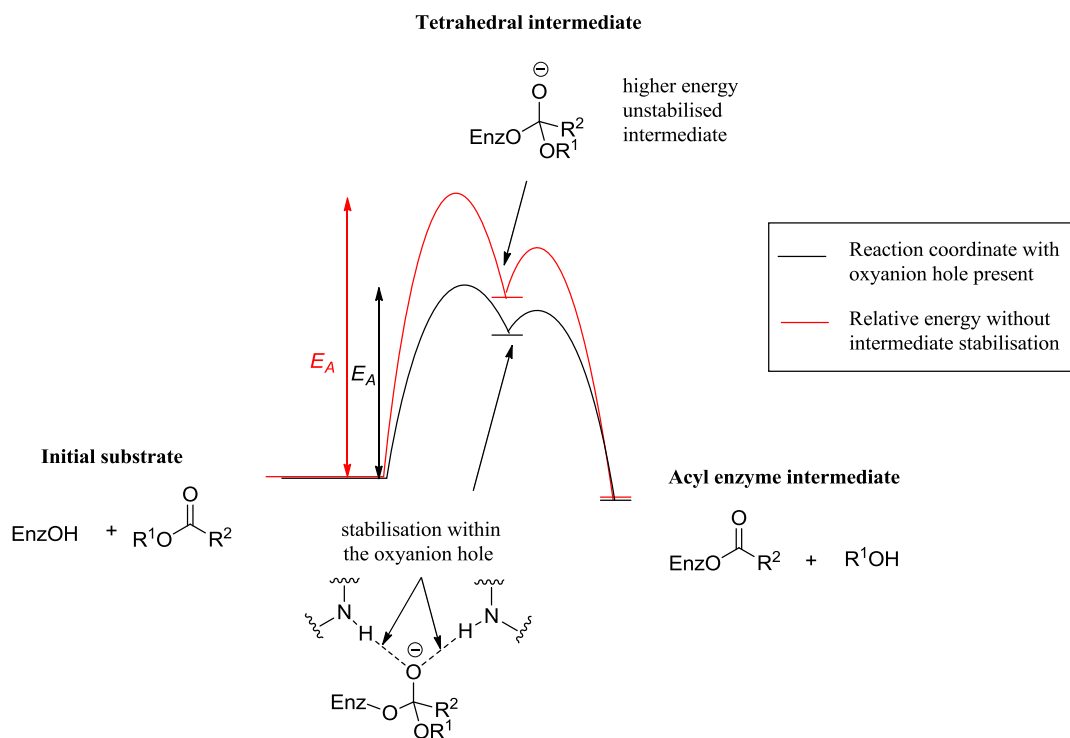


Figure 1.1.5 - Theoretical energy diagram to demonstrate the influence of the oxyanion hole on the rate of enzyme catalysis.²⁸

Consideration of the two reaction coordinates clearly demonstrates the significance of the oxyanion hole on the rate of catalysis. The energy of the higher energy tetrahedral intermediate, and the associated transition state, is lowered by the formation of several favourable hydrogen bonding interactions. This subsequently decreases the energy difference between the ground state and the higher energy states and, consequentially, causes a reduction in the required activation energy (E_A) for the native enzyme.³² This significant energy difference between the E_A of the two cases results in dramatic rate enhancements for hydrolysis. In combination with the activity of the catalytic triad, rate increases observed can be many orders of magnitude greater than that of the uncatalysed reaction in an aqueous medium.

1.1.4 Strategies for Inhibition of Lp-PLA₂

In order to rationally design improved inhibitors of Lp-PLA₂, in addition to a comprehensive understanding of the catalytic mechanism, knowledge of the enzyme active site topology is highly advantageous. Therefore, the publication of the X-ray crystal structure of Lp-PLA₂, by

Bahnon and Samanta in 2008,²⁶ significantly enhanced the available data to enable the systematic design of alternative Lp-PLA₂ inhibitors.

Consideration of the catalytic cycle for the action of Lp-PLA₂ (**Scheme 1.1.2**) allows the identification of two key regions of the active site that can be potentially targeted by small molecule inhibitors, in order to attenuate the enzymatic activity: the serine of the catalytic triad and the oxyanion hole.³¹ The requisite properties for binding to these regions are substantially different and result in inhibitors that display both different modes of action, and physicochemical property profiles.

Darapladib binds in the Lp-PLA₂ active site through coordination to the oxyanion hole. A schematic representation of the mode of binding and subsequent inhibition of Lp-PLA₂ manifested by darapladib is outlined below (**Figure 1.1.6**).

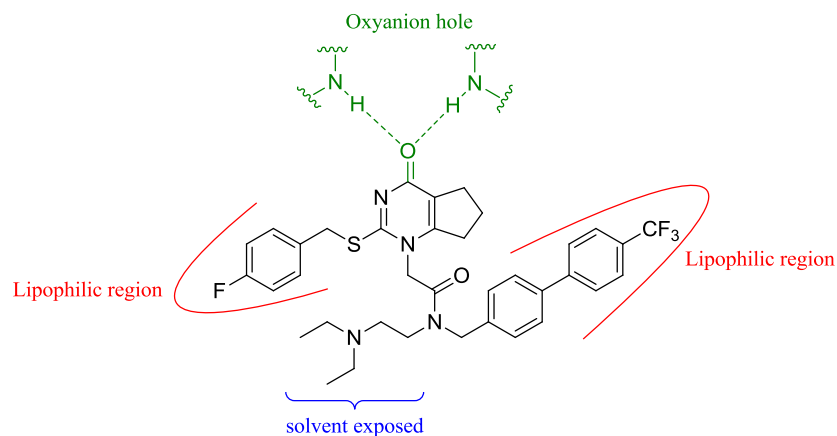


Figure 1.1.6 – Key binding features of darapladib.

The key binding interaction for darapladib with Lp-PLA₂ is the occupation of the oxyanion hole by the pyrimidinone carbonyl group.³³ The remainder of the molecule is the conclusion of significant medicinal chemistry optimisation work, completed by colleagues in the 1990's, which was conducted without knowledge of the mode of binding for this class of inhibitor.^{22,23} Elaboration of the pyrimidinone carbonyl core by the addition of the aromatic groups led to an increase in enzyme binding potency. Improved solubility was obtained through identification of a region where basic amine groups could be tolerated. The specific solvent exposed amine in darapladib was the result of significant optimisation work.^{22,23} Overall, the molecule does not have any covalent interactions with the enzyme and is classified as a non-covalent inhibitor.³⁴

Darapladib readily binds and dissociates from the enzyme active site and, exhibits well defined binding kinetics, most importantly showing a relatively short lifetime for the enzyme-inhibitor complex. As darapladib occupies the same site as the substrate, binding of this inhibitor precludes endogenous substrate binding and *vice versa*. This type of inhibition is defined as competitive. Therefore, the overall classification of darapladib is a non-covalent, reversible, competitive enzyme inhibitor.³⁴

An alternative mode of inhibition of proteases is the formation of at least one covalent bond between the enzyme and inhibitor, in contrast to the inhibition displayed through coordination to the oxyanion hole. General methods to inhibit serine proteases have received significant attention around the investigation of inhibitors which form covalent bonds with the conserved catalytic triad.³⁵ Consequentially, a wide range of structurally distinct covalent inhibitors have been discovered, which include peptidyl halomethyl ketone inhibitors (**Scheme 1.1.3**), such as the γ -chymotrypsin inhibitor (2*S*)-Ac-Ala-Phe-CH(CH₃)Cl (**Figure 1.1.7**).^{35,36}

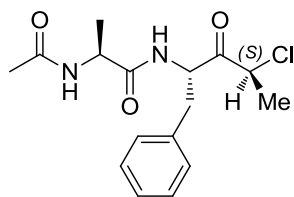
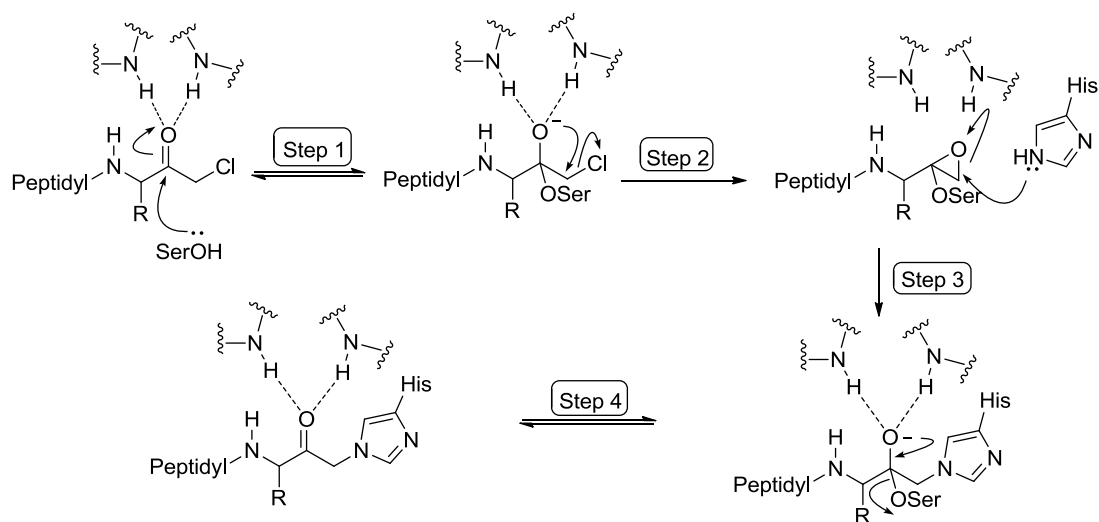


Figure 1.1.7 – Structure of the γ -chymotrypsin inhibitor (2*S*)-Ac-Ala-Phe-CH(CH₃)Cl.^{35,36}



Scheme 1.1.3 – General mode of covalent inhibition of serine esterases by peptidyl halomethyl ketone inhibitors.³⁵

The inhibitor binds the enzyme in an analogous fashion to the native substrates, such as PAF. The electrophilic carbonyl is attacked by the serine residue of the catalytic triad (**Scheme 1.1.3** – Step 1).³⁵ The resulting oxyanion occupies the oxyanion hole, stabilising the intermediate species, as seen in the previous example (**Scheme 1.1.2** – Step 1). The anion now undergoes an irreversible intramolecular displacement of the chlorine to generate an epoxide (**Scheme 1.1.3** – Step 2), instead of breaking down as observed with the phospholipid substrates. Nucleophilic attack by the histidine of the catalytic triad can now occur to form a second covalent bond to the inhibitor. The resulting unstable oxyanion can break down to release the catalytic serine residue (**Scheme 1.1.3** - Step 4), however the covalent bond to the histidine is not broken. Therefore, endogenous substrate binding is prevented by the permanent occupation of the enzyme active site by the inhibitor.⁴

The enzyme is covalently bonded to the inhibitor through the enzymatic action, so peptidyl halomethyl ketone inhibitors are a type of suicide inhibitor.³⁵ The name suicide inhibitor is derived from the enzyme itself causing the irreversible inhibition which permanently deactivates the enzyme.⁴ Typically covalent binding is irreversible, as is observed in the case of peptidyl halomethyl ketone inhibitors (**Scheme 1.1.3**). The irreversible nature and the potential to react with other nucleophiles within the body increases the requirements for high levels of selectivity, which can be challenging to obtain.³⁷ Any off target inhibition can have dramatic and undesirable side effects, since beneficial and required biological processes and functions can be adversely affected. Further, enzymatic activity can only be restored through the synthesis of new enzymes, resulting in the manifestation of effects of irreversible inhibition for prolonged time periods. While there are a wide range of safe medicines which utilise covalent inhibition, this mode of inhibition is often less attractive than the corresponding reversible inhibition strategies.³⁸

Although the majority of covalent inhibitors are commonly associated with irreversible enzymatic inhibition, reversible covalent inhibitors can be utilised for certain applications.³⁷ This strategy is attractive as it further mitigates any concerns about off-target irreversible inhibition, as well as displaying a distinct binding profile compared to other strategies.³⁹ Reversible covalent bonding between the inhibitor and the enzyme may lead to longer residence times, relative to the non-covalent inhibitors. The slow release of the inhibitor can sequester the enzyme, theoretically enabling lower doses to achieve desirable levels of

inhibition.³⁹⁻⁴¹ Additionally, coordination to the enzyme can deliver a protective function, preventing metabolism and subsequent excretion of the inhibitor from the body.

One approach that can be utilised in the development of reversible covalent inhibitors is the incorporation of boron into small molecules. Boron species, such as boronic acid and esters, are commonly associated with sp^2 geometries, with a vacant p orbital that is prone to coordination or stabilised by electron donation from adjacent heteroatom lone pairs (**Figure 1.1.8**).⁴² The oxyphilic nature of boron and the coordinatively unsaturated character of these species allows for coordination to nucleophilic residues, such as the oxygen in the side chain of the catalytic serine of Lp-PLA₂. The coordination of oxygen to the vacant orbital generates a tetrahedral boronate complex, through the formation of a formally dative covalent bond. It is envisaged that off target interactions will be reduced in boron species as a consequence of the propensity of boron to coordinate to oxygen centres. This prevents species without a free hydroxyl from forming strong interactions with the boron centre, minimising the number of species that can form significant interactions with the Lewis acidic base molecule. Unlike the irreversible inhibition, the boronate species can slowly dissociate back into the constituent molecules, avoiding the toxicity and off-target issues which are often associated with covalent inhibitors.⁴³

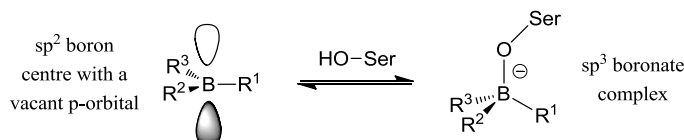


Figure 1.1.8 – The reversible nature of boron-enzyme complexation.

Although boron has rarely been utilised in drug molecules, several boron-containing drugs are on the market or in clinical development. This demonstrates that both the required PK and toxicity profiles are attainable for boron-containing molecules. This is exemplified by the proteasome inhibitor, Velcade[®] (**Figure 1.1.9**), which was granted Food and Drug Administration (FDA) approval for treatment of relapsed multiple myeloma and mantle cell lymphoma in 2006.^{44,45}

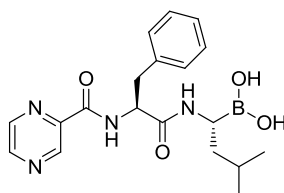


Figure 1.1.9 – Structure of the boron containing drug, Velcade®.⁴⁴

The reversible binding mode and the established safety of boron-containing molecules, has recently resulted in them receiving significant attention as prospective drugs for a variety of different diseases.⁴⁶ In order to develop alternative inhibitors of Lp-PLA₂, boron-containing molecules were identified for investigation.

1.1.5 Discovery and Development of Boron-based Inhibitors of Lp-PLA₂

There are several different recognised approaches to identifying start points or ‘hits’ in drug discovery, including fragment-based screening and high-throughput screening (HTS). These approaches generate ‘hits’, i.e. molecules which are identified based upon a certain set of criterion, dependent on the screening method used. These hit molecules can then be developed into potential drugs through careful optimisation and elaboration.

1.1.5.1 High-throughput Screening Approach to the Discovery of Lp-PLA₂ Inhibitors and the Development of Darapladib

Darapladib was developed from a hit identified through a HTS approach. Two structurally similar molecules (**Figure 1.1.10**), differentiated by the nature of the linker, were identified. Significant optimisation work of these molecules resulted in darapladib (**Figure 1.1.10**).⁴⁷

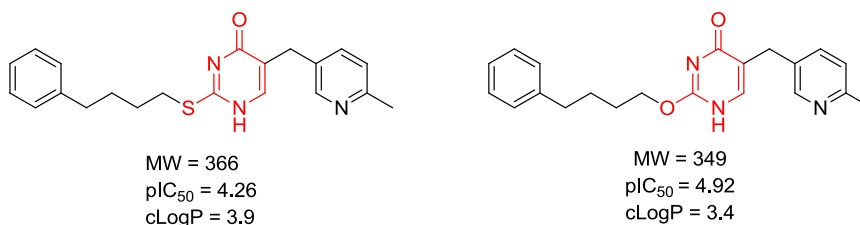
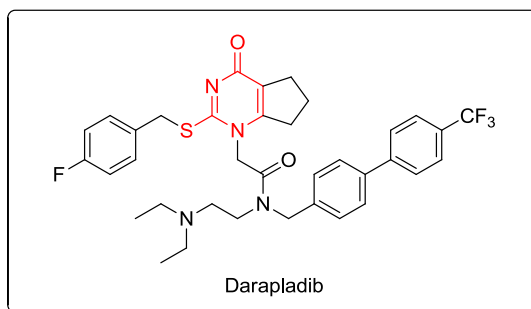


Figure 1.1.10 – HTS hits which represented the start point of darapladib development, highlighting the conserved core structure.⁴⁷

HTS is used to identify molecules which show significant binding affinity or biological activity for the target of interest.^{48,49} HTS libraries of approximately 2 million compounds are typically assessed, allowing a wide range of different molecules to be rapidly screened. The MW of the compounds identified through HTS is typically between 250-600 Daltons.⁵⁰ A potential drawback of HTS screening methods is that the significant binding affinity/biological activity of large hits may be derived from the molecule forming multiple weak, sub-optimal interactions with the enzyme binding pocket (**Figure 1.1.11**) and, therefore, are not necessarily ligand efficient (*vide infra*).

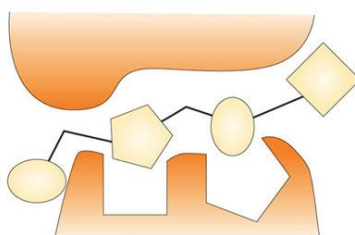


Figure 1.1.11 – Schematic representation of a HTS hit, highlighting the sub-optimal interactions between the molecule (yellow) and the enzyme binding site (orange).⁵¹

As the HTS hit is optimised to improve binding affinity, the molecules typically become larger to enable the formation of additional interactions with the enzyme to increase the binding potency. This often results in increased lipophilicity, which is considered to have a detrimental

effect on the likelihood of a molecule's progression to becoming an active pharmaceutical agent.⁵¹ Lipophilicity is commonly assessed through the calculated parameter cLogP, and has been identified as one of the key parameters in drug discovery.⁵² Analysis of the properties of drugs and potential drugs has shown lipophilicity is a dominant factor in undesirable off-target binding interactions within the body and is, therefore, a major source of developmental attrition.⁵³ As larger molecules are often more lipophilic in nature, different screening methods can be utilised to develop lower molecular weight hits.

1.1.5.2 Fragment-based Screening

One alternative or complementary hit identification method to HTS is fragment screening. Fragment-based screening methods are used to identify small, ligand efficient molecules.^{51,54} The fragments identified typically only show weak binding affinities as a consequence of the small number of interactions formed in the binding pocket. Subsequently, ligand efficiency (LE) is used to assess the efficiency of the binding interactions between the fragment and the enzyme (**Equation 1.1.1**), rather than the binding potency.⁵⁵

$$\text{Ligand Efficiency (LE)} = \frac{\text{Change in Gibbs free energy of binding}}{\text{Number of Heavy atoms (HA)}} \approx \frac{\text{pIC}_{50}}{\text{HA}}$$

Equation 1.1.1 – Ligand efficiency.⁵⁵

Typically, for a fragment-based screening approach, a minimum LE threshold of 0.3 is recommended for the initial hits.⁵⁶ In order to maximise the likelihood of a fragment being developed into clinical molecule, maintaining LE throughout the optimisation process is highly desirable. However, in cases where the initial hit's LE value greatly exceeds 0.3, a decrease in the LE value is often observed.

The primary advantage of fragment-based screening over HTS is the physiochemical properties of the hits identified. Smaller molecules are identified with the MW of fragment hits typically being < 300 Daltons.⁵⁰ This lower MW is a consequence of the selection being based on LE rather than potency. The identified fragments have clearly defined binding interactions, with the majority of atoms in the fragment directly contributing to binding (**Figure 1.1.12a**).⁵¹ The resulting fragments can then be carefully grown to increase the binding potency, while retaining the highly efficient binding nature of the initial fragment (**Figure 1.1.12b**).

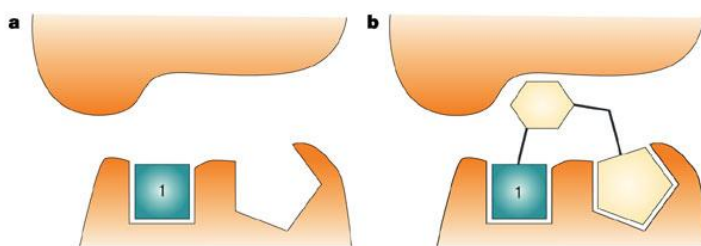


Figure 1.1.12 – a) Typical binding of small fragments, forming highly efficient binding interactions at one binding site; b) Schematic diagram of fragment growth/elaboration into the binding site, forming new interactions while retaining efficiency.⁵¹

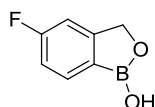
A variety of different methods have been devised to quantify the quality of molecules throughout the drug discovery process. The “rule of five” is the most recognised approach to assessing the quality of molecules during lead optimisation.⁵⁷ In an analogous fashion to the formulation of the “rule of five”, analysis of the hits generated from early fragment screens found they conformed to a “rule of three”.⁵⁸ The rules state that a fragment should fulfil the following criteria:

- Molecular weight < 300 Daltons, ensuring there is scope for elaboration of the fragment while maintaining solubility and low lipophilicity, which is often problematic for larger molecules.
- cLogP < 3. The cLogP is a calculated measure of the lipophilicity.⁵⁹ Maintaining low lipophilicity reduces the chance of off-target toxicological effects.
- Number of hydrogen bond donors and acceptors < 3. Low numbers of hydrogen bonds are required for bioavailability. A large amount of hydrogen bonding is associated with poor membrane penetration and bioavailability.^{60,61} Therefore, despite the additional solubility benefits, high levels of hydrogen bonding interactions are undesirable.
- Number of freely rotatable bonds < 3. Experimental evidence has shown correlation between the number of rotatable bonds and the bioavailability and potency of a molecule.⁶¹ As the number of rotatable bonds increases the bioavailability and the

potency decrease, therefore low numbers of rotatable bonds are desirable in drug development.

Fragment libraries have subsequently been assembled according to these guidelines. This ensures that the hits identified from the fragment screen possess ideal properties for further development into lead compounds.^{54,58}

To identify novel inhibitors of Lp-PLA₂, a fragment binding screen was undertaken in association with Astex Pharmaceuticals, to complement previous HTS investigations. A small cyclic borolane (**Figure 13**) was identified as a hit in the initial screen, displaying weak, ligand efficient binding to Lp-PLA₂.^{62,63} This finding was followed up by a second fragment binding screen, utilising a boron fragment set containing 150 diverse molecules developed within our laboratories.⁶⁴



pIC₅₀ (Lp-PLA₂) = <4.0 (3.7*)
LE = 0.46*

Figure 1.1.13 – The initial cyclic borolane hit identified.⁶² *Donates values obtained from an alternative/historical Lp-PLA₂ assay.

1.1.5.3 Discovery of an Efficient Borolane Fragment

The second fragment screen identified borolane fragment (**1.1.1**) (**Table 1.1.1**).⁶⁵ The borolane fragment showed efficient, although weak, binding to Lp-PLA₂, with a pIC₅₀ of 3.4 and LE of 0.42. In addition to this, the fragment (**1.1.1**) also displayed good lipophilicity with chromLogD_{7.4} < 3.

Molecule	chromLogD _{7.4}	pIC ₅₀ (Lp-PLA ₂)	pIC ₅₀ (PLA ₂ -VIIB)	% Inhibition (1000 nM)	LE
 1.1.1	2.8	3.4	<3.0	51	0.42

Table 1.1.1 – Profile of the initial borolane fragment.^{65,66} Details of the assay protocols are displayed in the **Appendix** section.

The development of this core (**1.1.1**) has been the subject of significant investigation within our laboratories in collaboration with Astex Pharmaceuticals.⁶⁷⁻⁶⁹ Efforts have primarily been focused upon developing two aspects of the initial molecule:

1. Growth of the fragment to improve the enzyme binding potency, while maintaining efficient binding and good physiochemical properties, such as solubility and lipophilicity.
2. Investigation of alternative core structures to further refine the properties of the fragment core. Although other ring structures, such as 5,6 and 7,6 were also identified as potential cores (**Figure 1.1.14**), further medicinal chemistry indicated that the 6,6-borolanes display the optimal vectors and orientation within the active site for elaboration, and were therefore prioritised for further study.⁷⁰ However, other 6,6 ring structures, most notably heterocyclic cores, were not present in the fragment screen. This necessitated further investigations into the core structure to achieve the optimal balance of potency, selectivity, and pharmacokinetic (PK) properties required for progression.

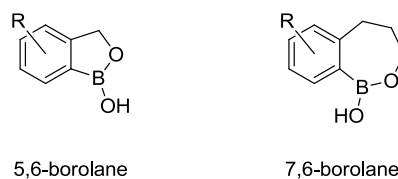


Figure 1.1.14 – The structures of the 5,6- and 7,6-borolane cores.

The work within our laboratories on both aspects of the fragment (**1.1.1**) development is outlined in the following sections.

1.1.5.4 Elaboration of the Core Borolane Structure (1.1.1)

The weak binding ligand efficient borolane fragment (**1.1.1**) required careful growth to obtain the required potency, selectivity, and PK profile. A variety of different vectors were investigated for growth of the initial fragment (**1.1.1**), aided by consideration of previous SAR work and the X-ray crystallographic data.⁷¹ The key focus of development of these core structures was to increase the bind affinity for Lp-PLA₂ and reduce the relative levels of binding to the closely related enzyme, PLA₂-VIIB.

PLA₂-VIIB is a very closely related phospholipase that is expressed in the white blood cells.^{12,72} Its function currently remains undetermined. The risk of inhibiting PLA₂-VIIB has not been established, however compounds in clinical trials exhibit greater than 100-fold selectivity for Lp-PLA₂ over PLA₂-VIIB.^{19,73} As these compounds/assets display no toxicity in biological and clinic trials, maintaining this 100-fold selectivity window reduces the chance of observing toxicological effects related to PLA₂-VIIB inhibition in development. For example, darapladib exhibits a selectivity of over 1800-fold for Lp-PLA₂ over PLA₂-VIIB.⁷⁴

Borolane (**1.1.1**) showed comparable potency for Lp-PLA₂ and PLA₂-VIIB (**Table 1.1.1**). This suggests that the two active sites share very similar topology. Therefore, while the structure of PLA₂-VIIB is undetermined, models based upon the structure of Lp-PLA₂ can be used for predictive purposes to help design inhibitors that display preferential binding to Lp-PLA₂ over PLA₂-VIIB. Careful structure guided growth of the fragment has resulted in highly selective, 100-fold for Lp-PLA₂ over PLA₂-VIIB, potent inhibitors of Lp-PLA₂, pIC₅₀ (Lp-PLA₂) > 7, with cLogP values below 5 as recommended by Lipinski *et al.*⁵⁷

The development of these potent and selective molecules began with the addition of directly linked aromatic groups to the core which provided a significant increase in Lp-PLA₂ binding potency relative to the initial fragment (**1.1.1**) (**Figure 1.1.15**). Addition of the tolyl ring (**1.1.2**) produced a 1000-fold increase in the potency of the molecule for Lp-PLA₂.⁷⁵ However, this resulted in increased measured lipophilicity, with a chromLogD_{7.4}⁷⁶ of 6.0 due to the addition of the aromatic ring, and retention of significant off-target interactions with PLA₂-VIIB. Despite the lack of selectivity over PLA₂-VIIB, the encouraging increase in Lp-PLA₂ potency, resulted in initiation of growth along this vector. Unfortunately, further elaboration of the aromatic group was detrimental to the potency. Therefore, an alternative strategy, whereby a –CH₂- linker was introduced, was explored.

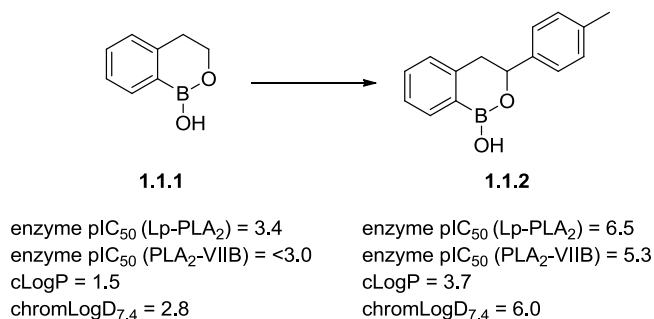
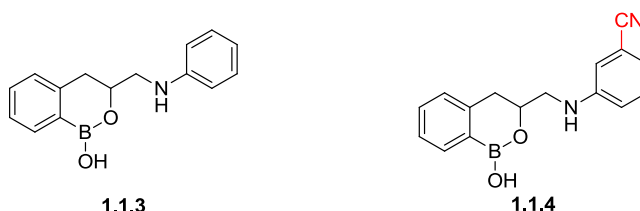


Figure 1.1.15 – Early elaboration of the borolane core.^{65,75–77}

Replacement of the tolyl ring with a $-\text{CH}_2\text{NHPh}$ group led to borolane (**1.1.3**) (**Figure 1.1.16**), which is equipotent against Lp-PLA₂ with directly-linked analogue (**1.1.2**).⁷⁸ Subsequent addition of a nitrile group at the *meta*-position (**1.1.4**) led to a significant increase in Lp-PLA₂ potency, without changing the levels of PLA₂-VIIB inhibition, enhancing the selectivity profile (**Figure 1.1.16**).⁷⁹



enzyme pIC₅₀ (LP-PLA₂) = 6.9
enzyme pIC₅₀ (PLA₂-VIIB) = 5.9

selectivity (LP-PLA₂ over PLA₂-VIIB) = 16

enzyme pIC₅₀ (LP-PLA₂) = 8.2
enzyme pIC₅₀ (PLA₂-VIIB) = 5.7

selectivity (LP-PLA₂ over PLA₂-VIIB) = 222

Figure 1.1.16 – Development of the borolane linkers, illustrating the importance of the nitrile (**1.1.4**) group for Lp-PLA₂ potency and selectivity over PLA₂-VIIB.^{78,79} Details of the assay protocol and the derivation of the selectivity for Lp-PLA₂ are displayed in the **Appendix** section.

Based on X-ray crystallographic analysis, the addition of the nitrile functionality allows the formation of an additional hydrogen bond with the Lp-PLA₂ active site.⁸⁰ As illustrated in **Figure 1.1.17**, the borolane (**1.1.4**) clearly shows the hydrogen-bond between the nitrile and the backbone N-H of Phe357.⁸¹

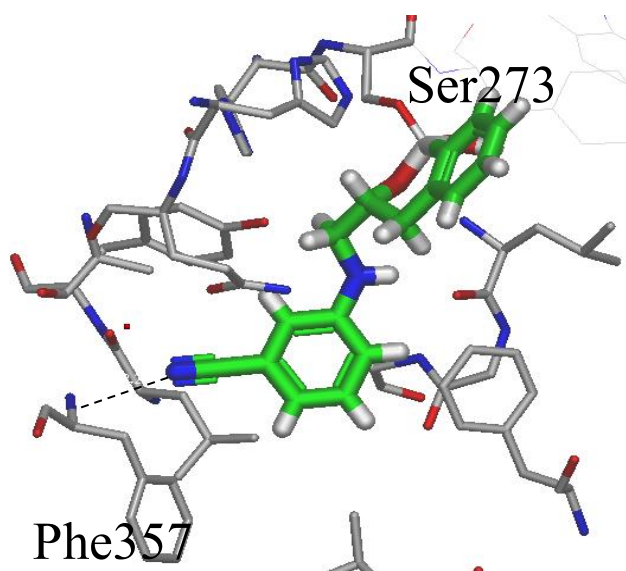


Figure 1.1.17 – X-ray crystallographic structure of borolane (green) (**1.1.4**) bound in the active site of Lp-PLA₂ (PSILO: 6HYZO). The key hydrogen-bond (3.22 Å) between the nitrile and Phe357 is highlighted. The covalent bond to Ser273 is also indicated.⁸¹

It is postulated that in PLA₂-VIIB, subtle differences in the shape of the active site preclude this hydrogen-bonding interaction. Therefore, the formation of the additional binding interaction in Lp-PLA₂ leads to an increased relative binding potency over PLA₂-VIIB and enhanced selectivity. However, in the absence of X-ray crystallographic data for PLA₂-VIIB this cannot be confirmed.

The addition of fluorine to the *para*-position (**1.1.5**) was able to further increase the Lp-PLA₂ potency, with 100-fold selectivity over PLA₂-VIIB being achieved (**Figure 1.1.18**). Unfortunately, the aniline components of both borolanes (**1.1.4** and **1.1.5**) are Ames positive, indicating that these compounds are potentially genotoxic.⁸² Further addition of an extra aromatic ring, the A-ring, led to the discovery of compounds structurally similar to borolane (**1.1.6**). The additional ring further enhanced Lp-PLA₂ potency and selectivity while removing the genotoxicity risks.^{83–85} The chloropyridyl analogue was found to be one of the least lipophilic of these A-rings, while retaining the selectivity over PLA₂-VIIB.

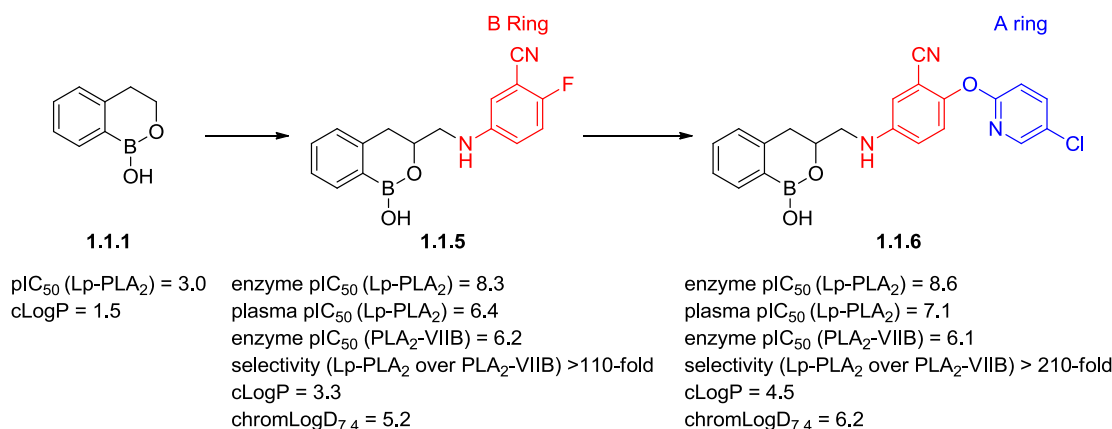


Figure 1.1.18 – Evolution of the borolanes through addition of a B-ring (**1.1.5**) or A-/B-ring (**1.1.6**) combination.^{83–85}

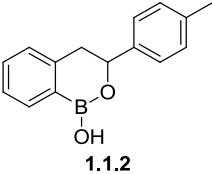
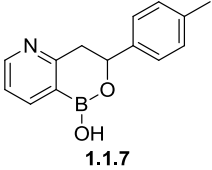
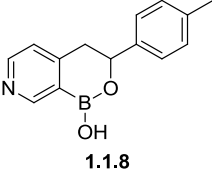
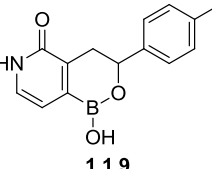
Despite significant increases in potency for Lp-PLA₂ and selectivity over PLA₂-VIIB, the increased lipophilicity relative to the original hit (**1.1.1**) remained a concern. It was hypothesised that a reduction in lipophilicity of borolane (**1.1.6**) may reduce the cell drop-off observed in the plasma assay (**Figure 1.1.18**). One potential solution to the issue of increased lipophilicity is the replacement of the aryl borolane core with more polar structures.

1.1.5.5 Optimisation of the Borolane Core

Development and modifications of the core structure have received considerable investigation within our laboratories.⁶⁸ The key objective of these optimisation studies was a reduction in lipophilicity of the borolane template, without a significant detrimental effect upon the potency and selectivity. Reduced lipophilicity is highly desirable, as high lipophilicity is commonly associated with off-target toxicity due to promiscuity and can also reduce the bioavailability of the molecule. For example, increases in lipophilicity have been demonstrated to show strong correlation with p450 binding and subsequent metabolism.⁸⁶ The increased polarity due to metabolic activity increases the rate of clearance and subsequently reduces the bioavailability of the compound.⁶¹

As previously discussed, elaboration of the initial fragment (**1.1.1**) led to the development of the directly linked molecule (**1.1.2**). This small fragment displays a relatively high lipophilicity, as assessed by the cLogP or chromLogD_{7,4} parameters. The cLogP value of 3.7 (**Figure 1.1.15**) exceeds the value of three recommended by the “rule of three” and, therefore, is a concern for further development without leading to high lipophilicity and the problems

associated with this.⁵⁸ No heterocyclic analogues of 6,6 borolane (**1.1.1**) were present in the initial fragment set. As directly linked tolyl analogue (**1.1.2**) was of interest, the corresponding heterocyclic analogues were synthesised to explore the effect on physiochemical properties, potency, and selectivity over PLA₂-VIIB (**Table 1.1.2**).

Molecule	chrom LogD _{7.4}	cLogP	pIC ₅₀ (Lp- PLA ₂ enzyme)	pIC ₅₀ (PLA ₂ - VIIB enzyme)	pIC ₅₀ (Lp- PLA ₂ plasma)	Selectivity ^b	LE
 1.1.2	6.0	3.7	6.5 ^a	5.3 ^a	-	-	-
 1.1.7	3.4	2.2	6.6	4.9 (n=2) <5.0 (n=2)	5.4	48	0.50
 1.1.8	3.5	2.2	5.5	5.7 (n=1) < 5.0 (n=1)	< 5.0	-	0.42
 1.1.9	1.2	1.0	6.2	6.0	5.3	6	0.45

^aData was collected using an alternative assay and therefore the values obtained are not directly comparable. ^bSelectivity was assessed by measuring the ratio of the level of inhibition in enzymatic assays after 180 minutes for Lp-PLA₂ and after 60 minutes for PLA₂-VIIB.

Table 1.1.2 – The effect of modification of the borolane core structure upon the lipophilicity, Lp-PLA₂ binding potency, and selectivity over PLA₂-VIIB.^{77,87–89}

A reduction in lipophilicity was observed in all three instances of the aryl replacement with heterocyclic rings (**1.1.7-1.1.9**) (**Table 1.1.2**), with high LE observed in each case. The pyridine isomer (**1.1.8**) showed the lowest potency of the heterocyclic cores. Therefore, this core was less attractive for further development compared to the alternative pyridine isomer (**1.1.7**), which has the same calculated lipophilicity while retaining potency. The greatest reduction in the lipophilicity was observed for the pyridone core (**1.1.9**). However, this core has comparable binding activity for Lp-PLA₂ and PLA₂-VIIB. These heterocyclic variations

of (1.1.2) demonstrate the potential to reduce the lipophilicity, whilst maintaining Lp-PLA₂ binding potency and, in some instances, low levels of selectivity over PLA₂-VIIB. Significant work still remains in order to investigate other core structures.

X-ray crystallographic data of the enzyme inhibitor complex was obtained for multiple examples of each core, including directly-linked, B-ring, and A-/B-ring analogues, to deduce the binding modes and ensure that they were comparable.⁹⁰ In all instances the 6,6-borolane cores occupied the same region of the active site, forming covalent bonds to the catalytic serine and projecting the elaborated groups along similar vectors within the active site (**Figure 1.1.19**). The conserved binding mode of the 6,6-borolanes gave confidence that the SAR could be transferred between other elaborated analogues.

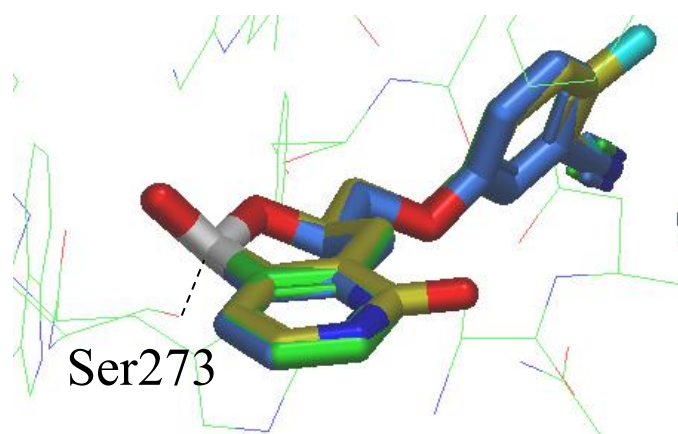


Figure 1.1.19 – X-ray crystallographic data demonstrating the conserved binding mode of the borolanes for aryl (green, PSiLO:7FQVL), pyridone (yellow, PSiLO:5MDOK) and pyridyl (blue, PSiLO: 6ZOKM) borolanes within the Lp-PLA₂ active site.^{77,88,90}

1.1.5.6 Development of a Borolane Pre-candidate Molecule

Knowledge from introduction of polarity into the borolane core (**Table 1.1.2**) was applied to the elaborated A-/B-ring analogue (1.1.6) (**Figure 1.1.20**). This led to the discovery of the pre-candidate molecule (1.1.10), which had the required potency, selectivity, and PK profile for further development.

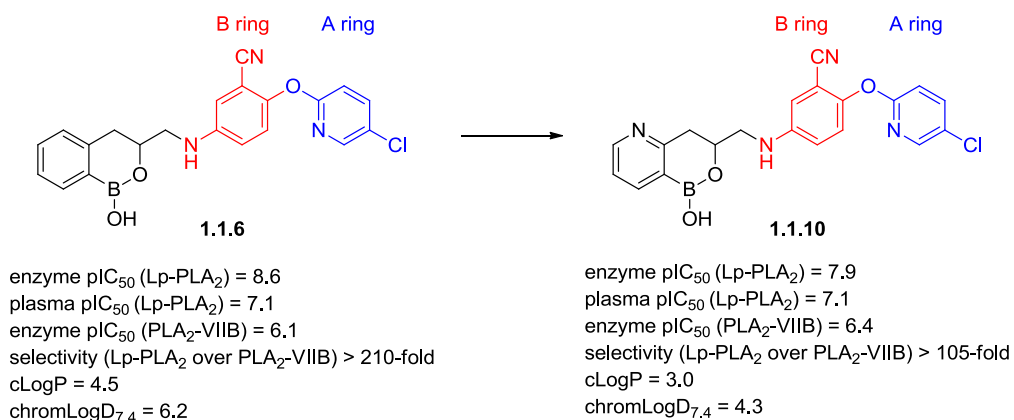
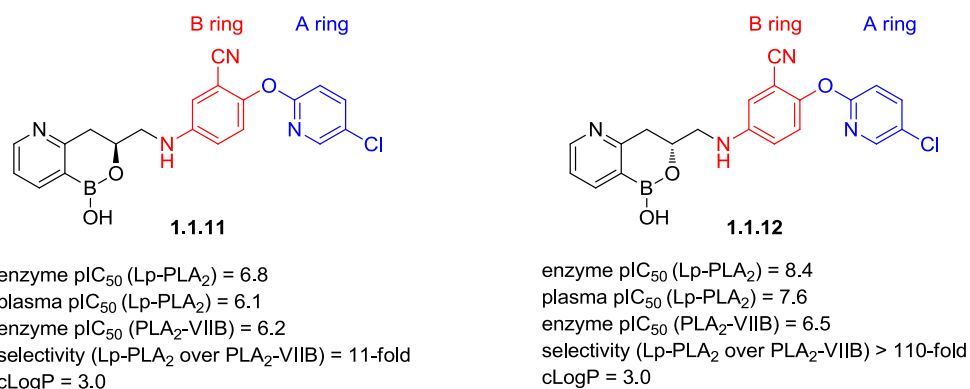


Figure 1.1.20 – Development of the pre-candidate (**1.1.10**).^{85,91}

Replacement of the aryl borolane core in (**1.1.6**) gave pyridyl borolane (**1.1.10**), giving significant changes in the biological properties of the molecules.⁹¹ Gratifyingly, a highly advantageous decrease in the lipophilicity is observed for (**1.1.10**) relative to (**1.1.6**), in analogous fashion to the direct linked compounds (**Table 1.1.2**). Although the potency for Lp-PLA₂ in enzymatic assays is reduced for the pre-candidate (**1.1.10**), the potency in plasma assays is retained. This suggests the lower lipophilicity of pyridyl borolane (**1.1.10**) reduces off-target lipophilic interactions, meaning more compound is available to inhibit Lp-PLA₂. The additional levels of available compound can therefore compensate for the reduction in binding potency, leading to comparable plasma inhibition potencies for both the aryl (**1.1.6**) and pyridyl (**1.1.10**) analogues. A decrease in the selectivity for Lp-PLA₂ over PLA₂-VIIB is observed. However, the critical value of 100-fold selectivity is retained by the molecule, which, it is envisaged, would reduce the chance of any findings related to inhibition of PLA₂-VIIB in the clinic.

Enzyme active sites possess chiral recognition, as a consequence of the inherent chirality of the natural amino acids which constituent the protein.²⁹ Therefore, one enantiomer of chiral small molecule inhibitors may characteristically show a greater binding affinity for the active site. This effect is observed in the pre-candidate molecule (**1.1.10**). The racemic pre-candidate molecule was separated into individual enantiomers. Subsequent biological assessment of the separate enantiomers identified one enantiomer (**1.1.12**) as being more potent and selective than the alternative enantiomer (**1.1.11**) (**Figure 1.1.21**).⁹²



*Stereochemistry of the more potent enantiomer was tentatively assigned using the X-ray crystallographic data of the Lp-PLA₂ protein ligand complex.*⁹³

Figure 1.1.21 – Biological data for the enantiomers of the pre-candidate molecule (**1.1.10**).⁹²

X-ray crystallographic studies suggested that the more potent and selective enantiomer was found to be the *R*-enantiomer (**1.1.12**) (**Figure 1.1.22**).⁹³ The chirality of the molecule could be clearly resolved, in addition to other key interactions between the inhibitor and the active site. These include the covalent bond of the catalytic Ser273 to the boron centre, and several hydrogen bonding interactions to the backbone of Phe357 and the NH₂ of Gln352.

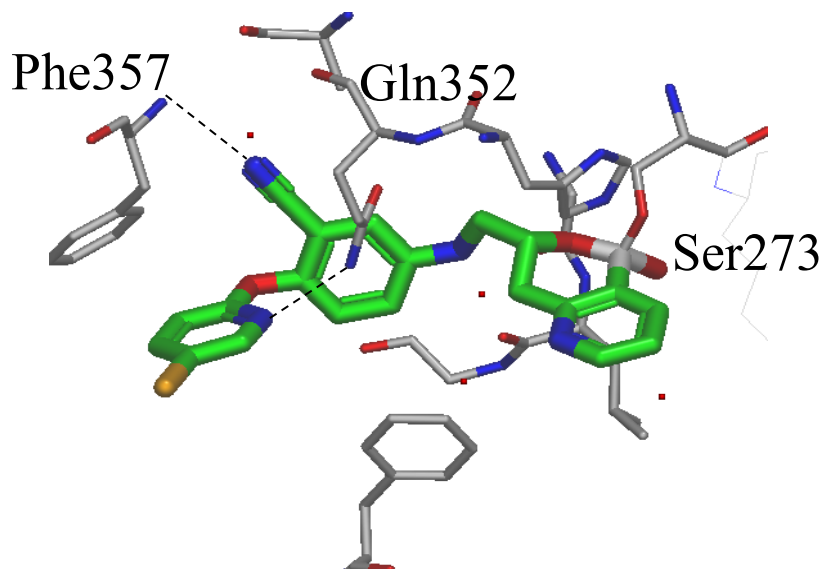


Figure 1.1.22 – X-ray crystallographic structure of pyridyl borolane (**1.1.12**) (green) bound in the Lp-PLA₂ active site (PSILO:4VAAO). Key hydrogen bonding interactions to Phe357 and Gln352 can be observed, in addition to the covalent bond with Ser273.⁹³

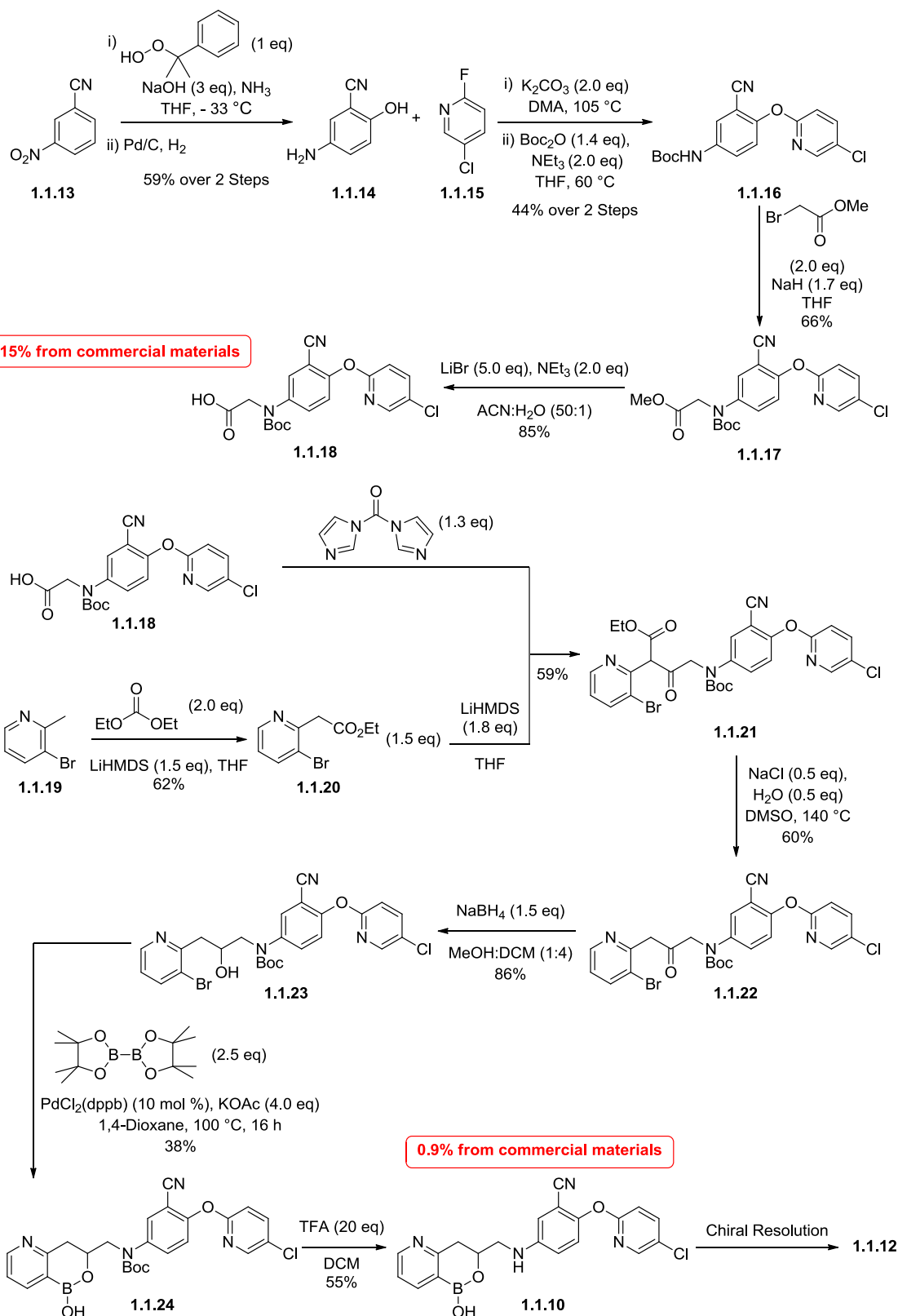
Chiral separation and X-ray crystallography of other borolanes has demonstrated that this is a reoccurring pattern, with the *R*-enantiomer displaying greater potency and selectivity in the

majority of molecules assessed.⁸⁰ The improved profile of the *R*-enantiomer (**1.1.12**) led to this molecule being selected as a pre-candidate. To reach candidate status, significant quantities (> 45 g) of pyridyl borolane (**1.1.12**) was required for toxicological studies.

1.1.6 Synthesis of the Borolanes

1.1.6.1 Initial Medicinal Chemistry Synthesis of the Borolane Pre-candidate (1.1.12)

Extensive synthetic investigations around the borolane series within our laboratories led to the development of the first synthesis of the racemic borolane pre-candidate (**1.1.10**) (**Scheme 1.1.4**). This synthesis was able to provide sufficient quantities, approximately 100 mg, of the racemic borolane (**1.1.10**) to enable both biological evaluation and chiral resolution of the molecule for further testing.



Scheme 1.1.4 – Medicinal chemistry synthesis of the pre-candidate molecule (1.1.12).⁹¹

The synthesis begins with peroxide-mediated oxidation of the commercially available 3-nitrobenzonitrile (**1.1.13**), followed by palladium-catalysed hydrogenation of the nitro group to give the aminophenol (**1.1.14**). S_NAr reaction of the aminophenol (**1.1.14**) with the fluoro-pyridine (**1.1.15**) gives the A-/B-ring containing aniline required for synthesis of (**1.1.12**). This aniline was subsequently protected using Boc anhydride to produce (**1.1.16**). Deprotonation of the amide N-H proton generates the anionic nucleophilic nitrogen centre, which readily reacts with the commercially available methyl bromoacetate to form the protected aniline (**1.1.17**). Ester hydrolysis of the methyl ester (**1.1.17**) gave (**1.1.18**) in an overall yield of 15% from commercial starting materials.

The synthesis of the left-hand side of the molecule is initiated by deprotonation of commercially available 3-bromo-2-methylpyridine (**1.1.19**), followed by quenching the anion with diethyl carbonate to give (**1.1.20**). The left-hand side and right-hand side components are coupled by the reaction of the electrophilic activated carboxylic acid (**1.1.18**) with the enolate derived from (**1.1.20**), formed by LHMDS. Decarboxylation of (**1.1.21**) under Krapcho's decarboxylation conditions,⁹⁴ followed by reduction of the ketone gave the alcohol intermediate (**1.1.23**). Palladium-catalysed Miyaura borylation of the bromine in alcohol (**1.1.23**) gave the cyclic borolane product (**1.1.24**), which was converted into the pre-candidate molecule (**1.1.10**) through TFA-mediated deprotection.

Overall, the synthesis of the racemic pre-candidate (**1.1.10**) was accomplished in a total of 11 linear steps with a total yield of 0.9%. Chiral chromatography of the racemic borolane (**1.1.10**) was required to produce the desired *R*-enantiomer (**1.1.12**), further diminishing the product yield. With the requirement for activating and protecting groups, the synthesis was deemed inappropriate to provide the greater amounts of borolane (**1.1.12**) required for toxicological studies. A minimum of 45 g of the borolane (**1.1.12**) are required for complete safety and biological assessment.

1.1.6.2 Synthetic Difficulties with Borolane Synthesis

The synthesis to the pre-candidate (**1.1.12**) described above (**Scheme 1.1.4**) was obtained after significant synthetic effort within our laboratories.⁹¹ The long linear sequence highlighted a number of synthetic difficulties that require additional exploration. It has also been noted that the challenges are inherent to the structural template and are observed in the majority of the borolanes studied, and not just the pre-candidate (**1.1.12**).⁹⁵ Features of the pre-candidate

(1.1.12) that complicate the synthetic strategy are shown in (Figure 1.1.23). Each of these features is discussed, in turn, in the following sections.

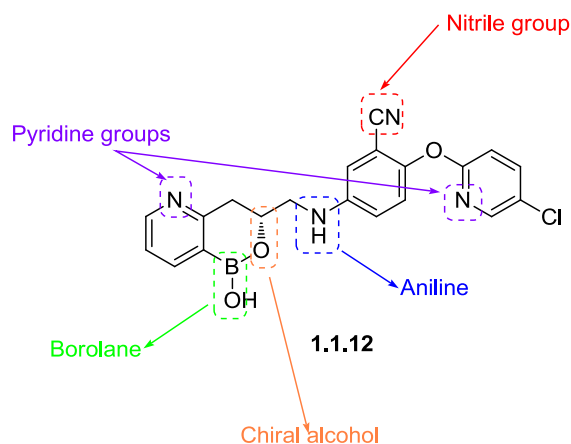


Figure 1.1.23 – Structure of the borolane pre-candidate (1.1.12) with the problematic regions highlighted.

1.1.6.3 Influence of the Pyridyl Groups on the Synthetic Strategy

Despite the benefits that incorporation of the pyridyl units, instead of the homoaryl groups, confers on the molecules within this series, this substitution is also associated with increased synthetic difficulties. The first problem associated with pyridine is related to the nitrogen lone pair (Figure 1.1.24). Unlike the corresponding aryl groups, the nitrogen of pyridine possesses an available sp^2 lone pair. The ability of the lone pair to chelate to a variety of different species, such as metals or Lewis acids, and partake in nucleophilic substitution reactions has been well established.^{96–99} Difficulties in the borylation reaction may be attributed to the pyridine coordinating to and interacting with the metal catalyst, having a detrimental effect upon the reaction. This chelating ability also has implications upon other synthetic procedures, such as the use of other transition metal catalysts, acids, or Lewis acids, with the number of possible reactions being limited by the tolerance of the reagents towards pyridine.

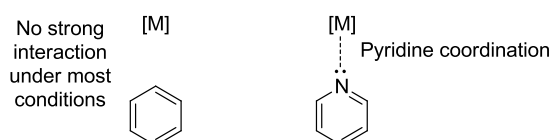


Figure 1.1.24 – An example of the potential issues with replacement of aryl groups with pyridyl groups.

The electron-deficient nature of pyridine is also well established.^{100,101} In the case of the borolanes, the electron-deficiency manifests itself in several ways. The first potential problem is increase in the acidity of the substituents adjacent to the ring relative to aryl analogues, which can be readily observed by consideration of the pK_a values (**Figure 1.1.25**).

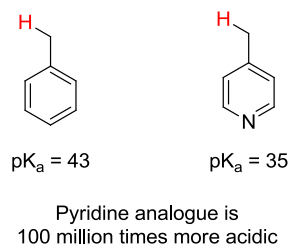
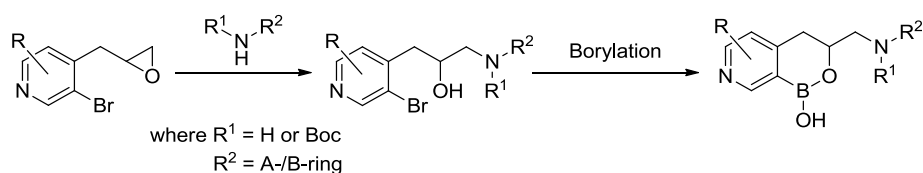


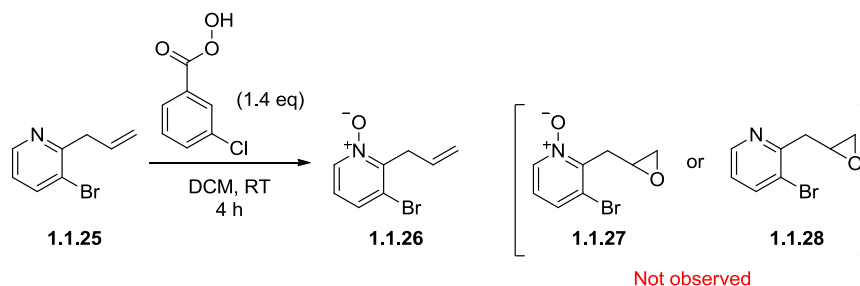
Figure 1.1.25 – Comparison of acidity for aryl and pyridyl groups in DMSO.^{100,102}

One early synthetic strategy explored to access the borolanes was through the use of epoxide electrophiles. The use of epoxides with homoaryl analogues was able to successfully produce a variety of different borolane analogues for the elaboration studies. It was envisaged that this methodology could be applied to the synthesis of pyridyl borolanes (**Scheme 1.1.5**).



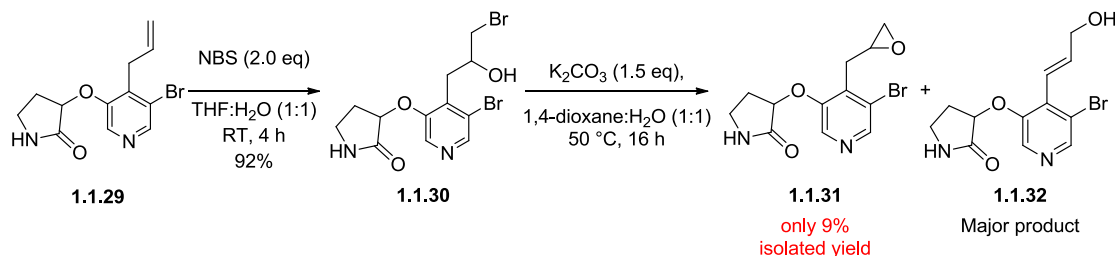
Scheme 1.1.5 – Proposed method to access pyridyl borolanes through epoxide chemistry.

Unfortunately, for pyridyl analogues the direct interconversion of allyl groups into the corresponding epoxides was unsuccessful. A variety of different reagents and conditions were assessed for this transformation, including the use of the peracid *m*-CPBA (**Scheme 1.1.6**).¹⁰³ No epoxide formation was observed under the reaction conditions with only the *N*-oxide (**1.1.26**) being generated under the reaction conditions. Attempts to form the epoxide through sequential *N*-oxide formation followed by epoxidation through the use of an excess of peracid were similarly unsuccessful.



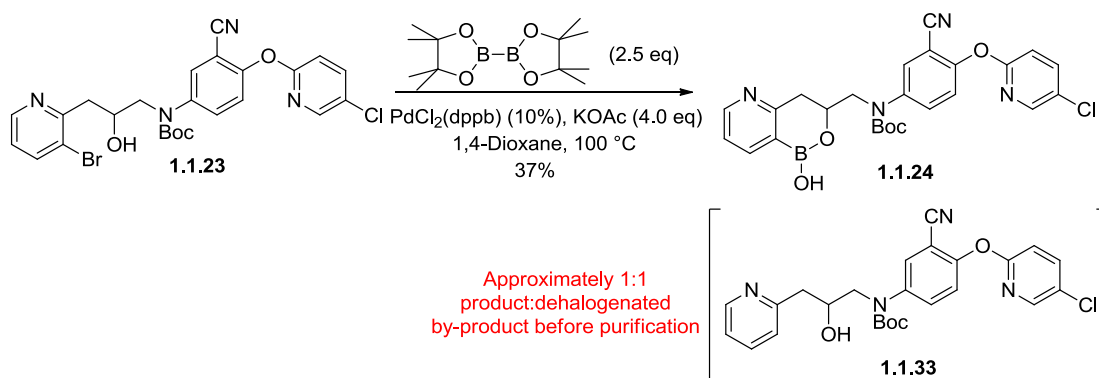
Scheme 1.1.6 – Attempted *m*-CPBA-mediated oxidation of allyl pyridyl (1.1.25) to the corresponding epoxide (1.1.28) or *N*-oxide epoxide (1.1.27).¹⁰³

Epoxide formation *via* the bromohydrin intermediate was investigated as an alternative method to access the key epoxide intermediates (**Scheme 1.1.7**).¹⁰⁴ Facile formation of the bromohydrin intermediate (1.1.30) was observed through treatment of the allyl compound (1.1.29) with aqueous NBS. Unfortunately, base-mediated ring closing of the bromohydrin intermediate (1.1.30) to give the epoxide (1.1.31) suffered from significant elimination to open the epoxide, generating undesirable allylic alcohol (1.1.32) as the major reaction product. The reaction was found to proceed in very low yields of less than 10% and was, therefore, considered inappropriate as a synthetic strategy. Other epoxidation methods have been investigated but were also found to be unsuccessful.



Scheme 1.1.7 – Attempted method to access pyridyl epoxide intermediates (1.1.31) *via* bromohydrin intermediates (1.1.30).¹⁰⁴

The second issue with the electron-deficient nature of the pyridine relates to the borylation stage (**Scheme 1.1.4**). Issues with the borylation of electron-deficient heteroaromatic substrates have been extensively documented.¹⁰⁵ The predominant issue with the reaction is the propensity for the substrate to undergo dehalogenation, either through dehalogenation directly or de-borylation of the resulting product (**Scheme 1.1.8**).¹⁰⁶



Scheme 1.1.8 – The issues with pyridyl (**1.1.23**) dehalogenation in the Miyaura borylation to give borolane (**1.1.24**) and des-bromo compound (**1.1.33**).¹⁰⁶

The electron-deficient pyridyl aromatic (**1.1.23**) promotes the undesirable dehalogenation or deborylation, with a significant increase in dehalogenation/deborylation relative to the analogous homoaryl borylation reaction. As the product and by-product share similar polarities and lipophilicity, purification of borolane (**1.1.24**) often requires multiple chromatographic separations, causing substantial reductions in the yield of the reaction.¹⁰⁶

1.1.6.4 Influence of the Nitrile Unit on Synthetic Strategy

In an analogous fashion to the pyridine discussed previously, the introduction of a nitrile functionality provides an additional nitrogen lone pair. The lone pair occupies an sp orbital and is known to chelate to a range of different metallic species, again potentially limiting the available synthetic transformations (**Figure 1.1.26**).¹⁰⁷

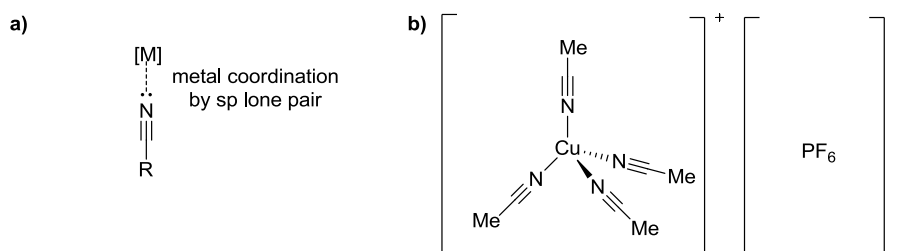
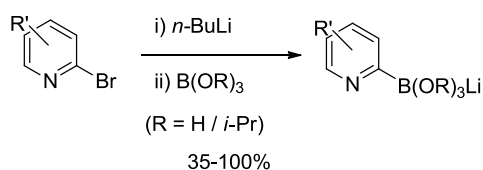


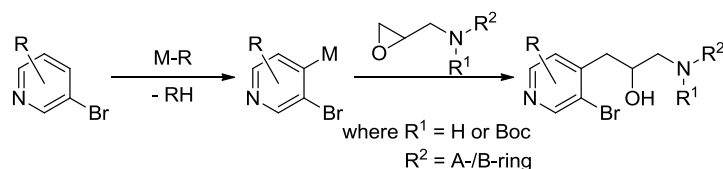
Figure 1.1.26 – a) The typical mode of nitrile coordination to metal species. b) Tetrakis(acetonitrile)copper(I) hexafluorophosphate, an example of nitrile coordination.¹⁰⁷

Nitrile groups are also renowned for their poor functional tolerance to a range of different reaction conditions, most notably based on the attack on nitriles by organometallic reagents. The use of organometallic reagents is a common method for the production of boron compounds, typically through metal-halogen exchange and subsequent quenching with a boron-based electrophile (**Scheme 1.1.9**).^{105,108} This methodology has been applied to a nitrile pyridine substrate (**Scheme 1.1.9**).¹⁰⁸ However, poor yields, the use of a simple substrate, and the requirements for cryogenic conditions to inhibit side reactions, all detract from this method.



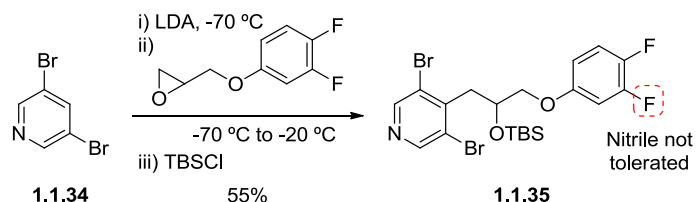
Scheme 1.1.9 – An example of organometallic-mediated borylation of bromopyridine.¹⁰⁸

In the absence of the key nitrile group, it is envisaged that organometallic chemistry could be utilised at several stages of the borolane synthesis. Organometallic-mediated borylation (**Scheme 1.1.9**) was proposed as a potential solution to the dehalogenation observed under Miyaura reaction conditions (**Scheme 1.1.8**). However, the susceptibility of the nitrile functionality to organometallic attack precludes this type of borylation to introduce the boron centre. Organometallics could also be used for the coupling of the pyridyl and aniline portions of the borolanes (**Scheme 1.1.10**).



Scheme 1.1.10 – Proposed method to access the borolanes utilising organometallic (M-R) attack on epoxide electrophiles to furnish the key alcohol intermediates, prior to borylation.

This method had been successfully utilised within our laboratories for the synthesis of a range of borolanes which did not possess the nitrile functionality (**Scheme 1.1.11**).¹⁰⁹ Unfortunately, this methodology was not compatible with the cyano unit, with undesirable attack upon the nitrile occurring in preference to epoxide opening.

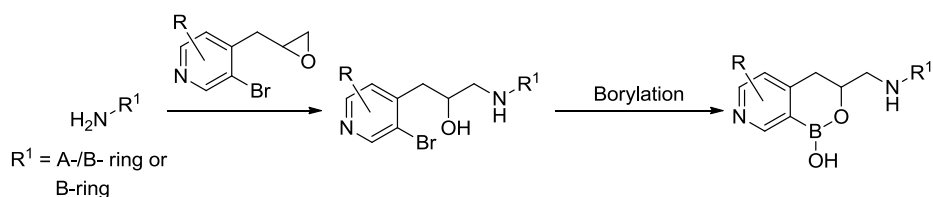


Scheme 1.1.11 – Organometallic-mediated methods to access the borolanes.¹⁰⁹

A range of different metallic species were investigated for the desired epoxide-opening reaction, including lithium, zinc, copper, and magnesium species.^{109,110} Typically the reactivity of organometallic species increases as the ionic character of the metal-carbon bond increases.¹¹¹ As the lithium-bond possesses the greatest ionic character, and therefore the greatest reactivity, poor functional group tolerance is often observed with these reagents. The other metal species were investigated due to the decreased reactivity, resulting in increased functional group tolerance of these species.^{112,113} Unfortunately, in all cases investigated the reaction conditions did not tolerate the nitrile functionality, with either direct attack of the organometallic reagent upon the nitrile or no significant reaction being observed.

1.1.6.5 Aniline Reactivity

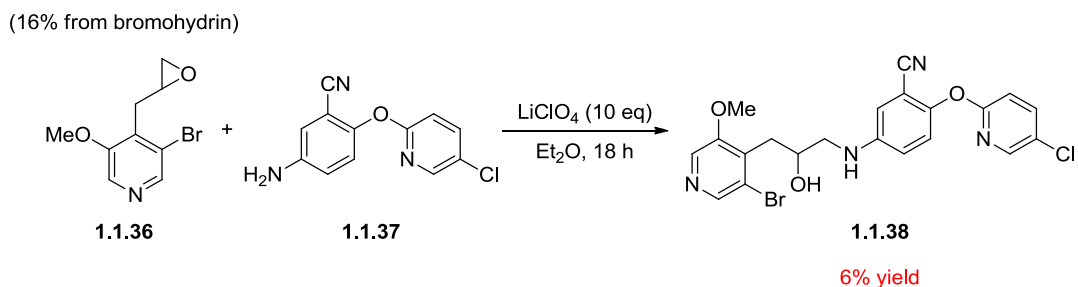
The nucleophilic ability of anilines has been extensively studied.^{114,115} Anilines typically only display weak nucleophilic ability, as a consequence of the conjugation of the nitrogen lone pair with the π -system of the aromatic ring. This limits the conditions under which anilines will react, often requiring either highly activated electrophiles or formal deprotonation of the aniline. It was envisaged that the aniline could undergo nucleophilic attack upon an appropriate electrophile, such as an epoxide, to synthesise borolane analogues (**Scheme 1.1.12**).



Scheme 1.1.12 – Proposed method to access the borolanes through nucleophilic attack by the aniline component of the borolane.

The aniline component of the borolane (**1.1.12**) displays uncharacteristically low reactivity towards electrophiles. The unprotected aniline displays minimal nucleophilic reactivity under

a wide range of different conditions, including reductive amination and epoxide opening, as exemplified below (**Scheme 1.1.13**).¹¹⁶

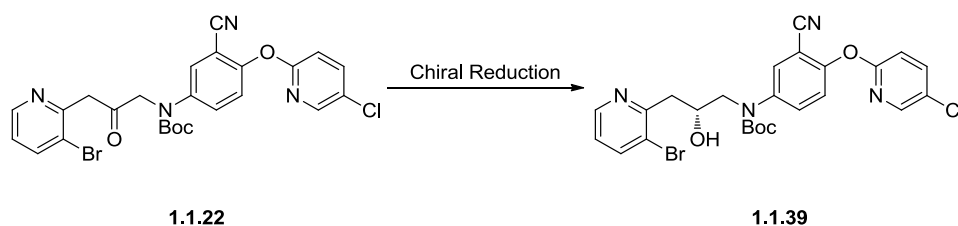


Scheme 1.1.13 – An illustration of the poor aniline reactivity.¹¹⁶

The failure of the aniline to react with a variety of different electrophiles led to the requirement for the Boc protection (**Scheme 1.1.4**). The reduction in pK_a when going from the aniline to the corresponding amide, due to increased conjugate base stabilisation, enables the deprotonation of amide derivatives by strong bases, such as sodium hydride. However, this requirement for strong bases to affect the deprotonation, limits the number of possible electrophiles. The difficulties encountered with this key bond formation, and the requirement for the Boc protecting group, led to the protracted linear synthesis as previously delineated.

1.1.6.6 Chirality of the Borolanes

The significant differences in the properties of the two enantiomers necessitates that enantiopure borolane (**1.1.12**) is accessed. It was envisaged that the reduction of the ketone (**1.1.22**) could be conducted asymmetrically to allow control of this stereocenter (**Scheme 1.1.14**).



Scheme 1.1.4 – Proposed asymmetric reduction.

Within our laboratories a range of different asymmetric reductions have been investigated. The poorly defined steric environment meant that no enantioselectivity was observed under

Corey-Bakshi-Shibata (CBS) conditions¹¹⁷ or with enzymatic reductants.¹¹⁸ In this latter regard, several different keto-reductase enzymatic panels have been screened, with no successful asymmetric induction being observed thus far. The inability to conduct the reaction asymmetrically or utilise enantiopure starting materials means that chiral separation is required to provide the required enantiomer. Investigations into the chiral reduction are ongoing.

1.1.7 Project Aims

Although significant work has been conducted within our laboratories around the preparation of the key borolanes, identifying improved synthetic routes is considered a high priority. Two main issues remain to be investigated, and will be addressed within this project:

- 1) Exploration of the synthesis and biological properties of alternative borolane core fragments and elaborated analogues. As outlined in section 1.5.5, the variation of the core structure can have dramatic influences upon the properties of the molecule. A range of different core structures still remains to be investigated and different cores will be studied as part of this project (**Figure 1.1.27**).

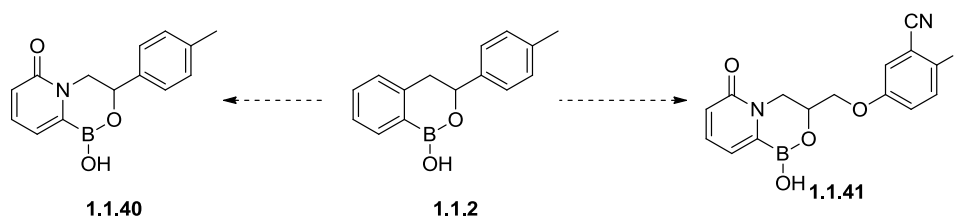


Figure 1.1.27 – The development of alternative borolanes (**1.1.40** and **1.1.41**) designed to test an alternative pyridone core structure.

- 2) To devise a suitable synthesis of the pre-candidate molecule (**1.1.12**), which will allow facile access to this pre-candidate and other borolane analogues. The synthesis has the following requirements:
 - A reduction in the number of linear synthetic steps from 11.
 - An improvement in the overall yield of the pre-candidate to facilitate scale-up of the pre-candidate (**1.1.12**) in sufficient quantities to allow further biological and toxicological assessment.
 - Improved green chemistry metrics, and increased atom economy, through a removal of the requirement for protecting and activating groups, as well as reducing the need for column chromatography.

- Synthetic introduction of chirality.

1.2 Investigations into an Alternative Pyridone Core

1.2.1 Initial Pyridone Borolanes

Borolane (**1.1.9**) (**Table 1.1.2**) demonstrated that a reduction in lipophilicity can be obtained by introducing heteroatoms into the core. A diverse range of analogues of pyridone heterocycle (**1.1.9**) have been synthesised within our laboratories, differentiated by various substituents at R² and functionalisation of the pyridone nitrogen (**Figure 1.2.1**). Variation of these substituents was able to achieve high potencies of Lp-PLA₂ binding, with pIC₅₀ values exceeding 7, as well as demonstrating the lowest lipophilicity values of the cores assessed.¹¹⁹

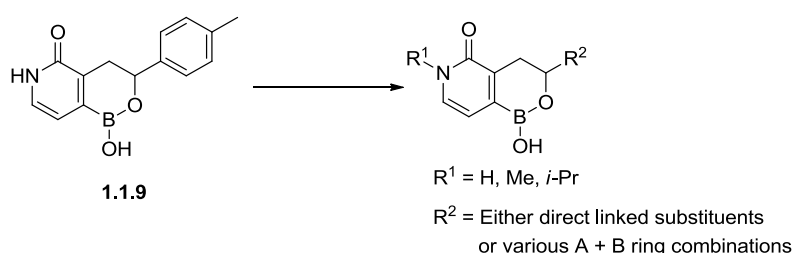


Figure 1.2.1 – Generalised structure of the pyridone borolanes based on pyridone borolane (**1.9**).¹¹⁹

Disappointingly, the pyridone core suffered from less than 100-fold selectivity for Lp-PLA₂, with significant PLA₂-VIIB inhibition, regardless of the R¹ or R² substituent on the borolane (**Figure 1.2.1**). The work on this core was therefore suspended as a consequence of the poor selectivities relative to comparable molecules in other series, with selectivities typically being an order of magnitude lower for the pyridones (**Table 1.1.2**).

1.2.2 Alternative Pyridone Isomer

Despite the poor selectivity over PLA₂-VIIB for pyridone-borolane analogues (**Figure 1.2.1**), alternative pyridone cores were of interest due to the reduction in lipophilicity. *In-silico* modelling using a model of PLA₂-VIIB built from the crystal structure of Lp-PLA₂ suggested that the pyridone borolane regioisomer (**Figure 1.2.2**) had the potential to provide enhanced selectivity over PLA₂-VIIB, compared to the pyridone isomer (**1.1.9**).³³ The improved selectivity could be a result of changes to the core structure, which would cause subtle alterations to the binding mode of the borolane core in the enzyme. However, any postulated

changes in selectivity require experimental determination, as a consequence of the associated uncertainty of the PLA₂-VIIB model.

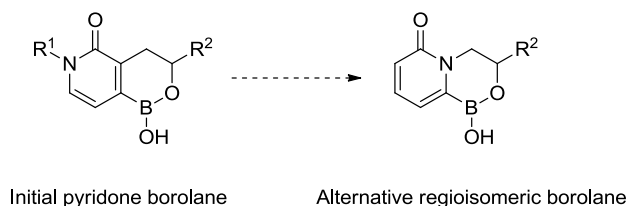


Figure 1.2.2 – Structures of the two different pyridone borolane isomers.

To determine the potential of the alternative pyridone borolane core to be developed into an effective inhibitor of Lp-PLA₂, the relative potency and selectivity of this core needed to be determined in comparison to other borolane cores. To assess this, two unprecedented pyridoborolane compounds (**1.1.40** and **1.1.41**) were designed for synthesis (**Figure 1.2.3**). As previously discussed, the SAR from these compounds could be utilised to predict the properties of more elaborated analogues, as all the different borolane cores made to date adopted the same binding mode as one another (**Figure 1.1.19**), regardless of the linker. Therefore, by comparison of the properties of pyridones (**1.1.40** and **1.1.41**) to those of other core analogues, the potential of the new core could be analysed, without necessitating the synthesis of a wide range of analogues. If the core showed potential, then further more elaborated analogues could be synthesised.

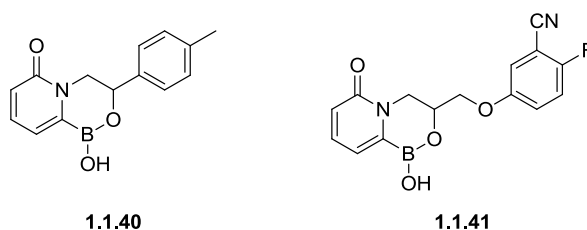


Figure 1.2.3 – The two key pyridones designed for investigation into the alternative pyridone regioisomer.

The B-ring containing pyridone (**1.1.41**) was selected to ascertain the relative potency of the core compared to other B-ring analogues (**Figure 1.2.4**). The corresponding B-ring analogues have been found to exhibit high potencies and moderate selectivities, allowing the relative potency of the alternative pyridone core (**Figure 1.2.2**) to be deduced. The *O*-alkyl linker was attractive from a synthetic perspective, as it circumvents the issues with the aniline linker

(Section 1.1.6.5). If ether (1.1.41) was found to be of interest, synthesis of the corresponding aniline linked analogues could then be explored.

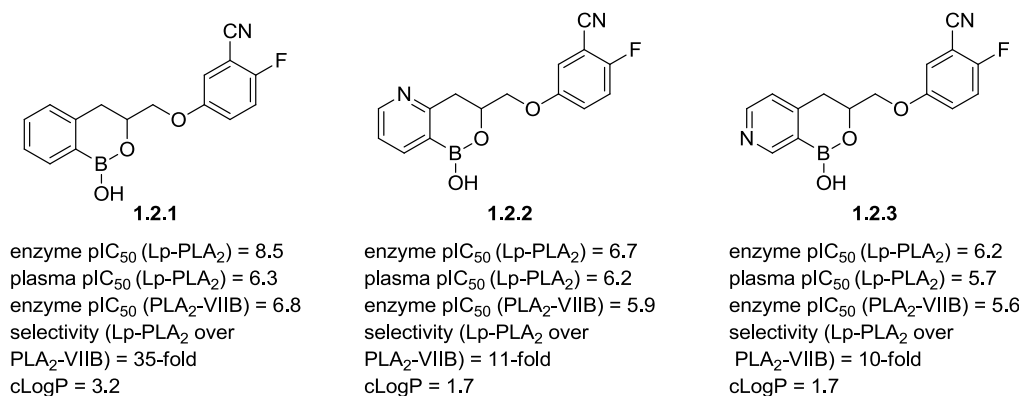
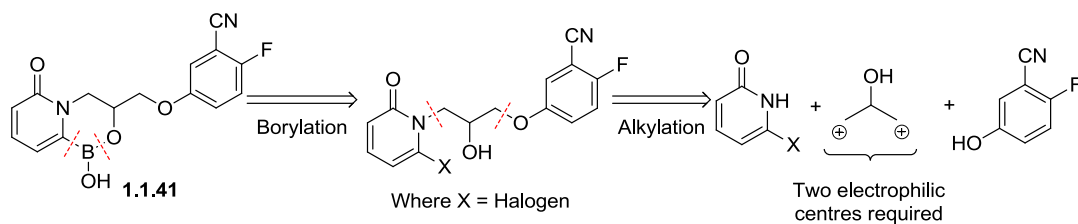


Figure 1.2.4 – Other borolane cores comparable to analogue (1.1.41), sharing the same B-ring. ^{120–122}

The directly linked aryl pyridone (1.1.40) was designed to test the potency and selectivity of the alternative core. Directly linked analogues to this molecule exist in all four major series of the core structures (Table 1.1.2) and, therefore, the selectivity relative to the other heterocyclic borolane cores can be deduced. This core was also selected due to the relative simplicity of the molecule, avoiding the synthetic issues encountered with more elaborated structures, such as nitrile/pyridine chelation and aniline functionalisation (Sections 1.1.6.3 – 1.1.6.5).

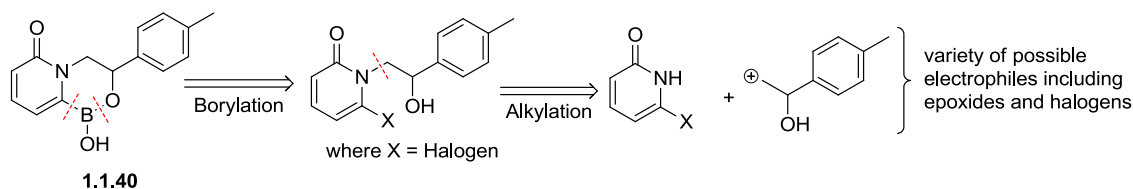
1.2.3 Retrosynthesis and Common Reaction Steps

The retrosynthesis of the B-ring containing pyridone (1.1.41) is illustrated in Scheme 1.2.1. It was planned to install the boron functionality in the final step of the synthesis, using the bromo alcohol intermediate. Work within our laboratories on other borolane analogues has typically utilised borylation and spontaneous cyclisation of analogous alcohols as the final synthetic step.⁶⁸ The ‘boronic acid’ group is introduced as the final synthetic step to avoid issues with aryl-B bond stability, challenges in purification, and poor tolerance to a range of reaction conditions.^{42,123} The requisite alcohol can be accessed through alkylation reactions. In contrast to the direct linked compound (*vide infra*), two alkylations are required to build the skeleton of the intermediate: halo pyridone and phenol alkylations. These alkylations could be conducted in either order and both orders were explored to establish the optimal method to access the final compound (1.1.41).



Scheme 1.2.1 – Retrosynthetic analysis of the B-ring containing pyridone (**1.1.41**).

The retrosynthetic analysis of the directly linked pyridone (**1.1.40**) is displayed below (**Scheme 1.2.2**) and is similar to the B-ring analogue (**1.1.41**). The required alcohol intermediate can be accessed through alkylation of the corresponding 3-halopyridone with an appropriate electrophilic species. Depending on the identity of the halogen, different methods have been established to access the 3-halopyridone species from a variety of different commercially available starting materials.^{124–126}



Scheme 1.2.2 – Retrosynthetic analysis of the directly linked pyridone borolane (**1.1.40**).

Comparison of the two retrosynthetic analyses (**Scheme 1.2.1** and **Scheme 1.2.2**) allows easy identification of the similarities in the potential routes. Both synthetic pathways require synthesis of the halo pyridone molecule, followed by *N*-alkylation with an appropriate electrophile. The syntheses also utilise the same final borylation step to give the borolane analogues (**1.1.40** and **1.1.41**).

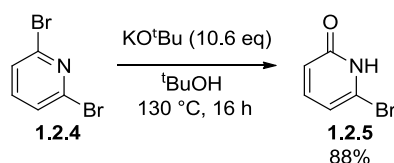
These synthetic similarities are shared between all the potential borolanes derived from this pyridone core. The development of reliable synthetic methodologies to access these two analogues (**1.1.40** and **1.1.41**) will allow the rapid exploration of subsequent analogues, if these species prove to have high potencies for Lp-PLA₂ and selectivities over PLA₂-VIIB.

1.2.4 Synthesis of 6-Bromopyridin-2(1H)-one (1.2.5) and 6-Iodopyridin-2(1H)-one (1.2.8)

The first stage of the investigation was the development of high yielding methods to access the common bromopyridone (**1.2.5**) (**Scheme 1.2.3**) and iodopyridone (**1.2.8**) (**Scheme 1.2.4**) starting materials. For the investigation, the bromopyridone (**1.2.5**) and iodopyridones (**1.2.8**) were selected as potentially useful borylation partners. The different steric and electronic properties were anticipated to result in slightly different reactivity profiles of the pyridones.

The halogen identity influences several aspects of the synthesis. Differences in the Hammett substituent constants, σ (*para*) = 0.232 for bromine and σ (*para*) = 0.276 for iodine, reflect the different electronic influences of the halogens.¹²⁷ The larger value for iodine reflects the increased electron-withdrawing character of the iodine, therefore, slowing the reaction rate in processes which cause an accumulation of positive charge and vice-versa. It is postulated that this may influence the pyridone alkylation process. The steric differences of the halogens can be accounted for using a similar approach: the Taft equation.¹²⁸ The difference in reactivity is likely to be most pronounced in the borylation reaction, where the rate of oxidative addition is dependent upon the carbon-halogen bond strength. The weaker carbon-iodine bond leads to increased rates of oxidative addition and may lead to a beneficial reaction profile.¹²⁹

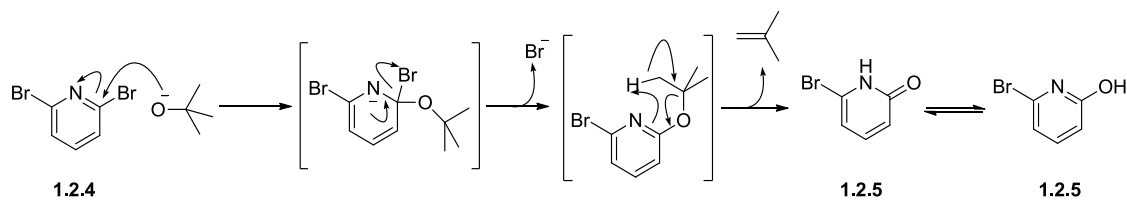
The synthesis of the bromopyridone (**1.2.5**) was reported in 1974 by Sauer *et al.* in one step from the commercially available 2,6-dibromopyridine (**1.2.4**), which repeated in good yield (**Scheme 1.2.3**).¹²⁵ Utilising this procedure over 30 g of the desired pyridone (**1.2.5**) has subsequently been synthesised by the contract research organisation, GVKBio, providing sufficient material for further investigations.¹³⁰



Scheme 1.2.3 – Synthesis of 3-bromopyridone (**1.2.5**).

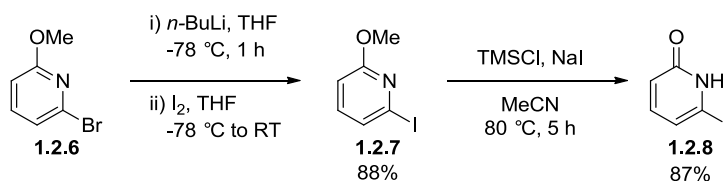
The proposed mechanism of the transformation is outlined below (**Scheme 1.2.4**).¹²⁵ The reaction begins with nucleophilic attack on the pyridine system (**1.2.4**) by the *t*-butoxide nucleophile, localising the negative charge onto the electronegative nitrogen centre. The resulting intermediate rapidly breaks down to restore the thermodynamically favourable

aromatic system, expelling a bromide anion. The resulting intermediate undergoes β -elimination to generate the 3-bromopyridone and eliminate gaseous isobutene, which is entropically favourable.



Scheme 1.2.4 – Proposed mechanism of formation of the 3-bromopyridone (**1.2.5**).

The synthesis of the iodopyridone (**1.2.8**) has also previously been reported in the literature, by Curran *et al.* in 1996.¹²⁴ In this case the molecule is synthesised through a two-step synthetic sequence, and involved isolation and purification through chromatographic methods at both stages. This methodology was applied to the synthesis of the iodopyridone (**1.2.8**) as detailed below (**Scheme 1.2.5**).



Scheme 1.2.5 – The two-step synthesis of the iodopyridone (**1.2.8**).

Lithium-halogen exchange of the bromo pyridine (**1.2.6**) at -78 °C yielded the lithium anion, which, using iodine as the electrophile, gave the iodide (**1.2.7**). Subsequent demethylation to give the iodopyridone (**1.2.8**) was achieved through treatment of methoxy pyridine (**1.2.7**) with TMSI, generated *in-situ* from the reaction between TMSCl and NaI. This two step synthesis provided the desired pyridone (**1.2.8**) in 77% overall yield from commercial materials.

With methods established to access the bromo and iodopyridone species, the focus of the synthesis shifted to the first key disconnection, the *N*-alkylation reaction.

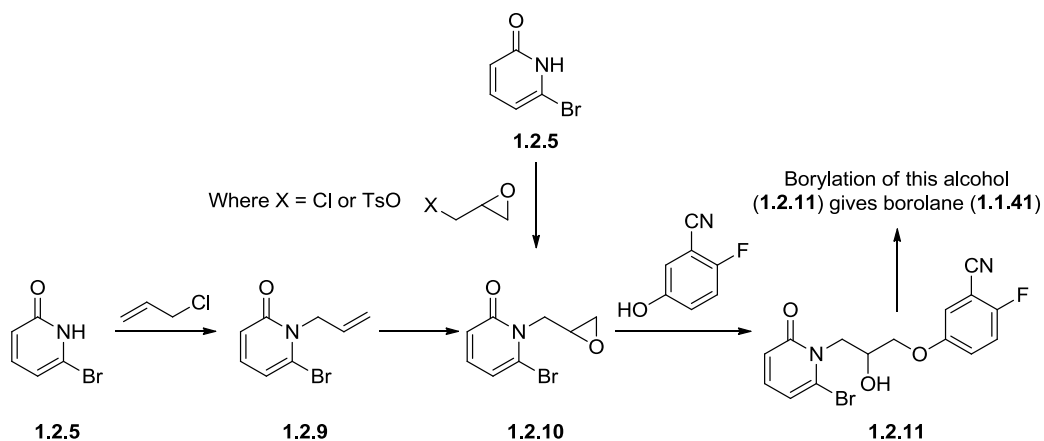
1.2.5 Development of a Reliable Method to Generate *N*-Alkylated Pyridone Molecules

1.2.5.1 Initial Halo Pyridone Alkylation Reaction Studies

Pyridones are ambidentate nucleophiles, possessing nucleophilic oxygen and nitrogen centres. Despite the prevalence of pyridones in both natural products and drugs, there are no general conditions in the literature for *N*-alkylation of pyridones.^{131,132} The literature suggests variable success in achieving *N*-alkylation over *O*-alkylation, so the identification of robust methodology to efficiently affect the *N*-alkylation of 3-halopyridones was required.

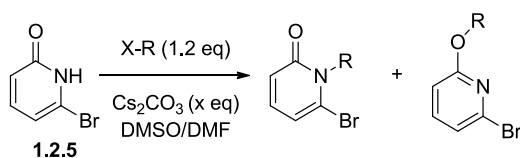
A significant proportion of the reactions in the literature utilise polar aprotic solvents, typically DMSO or DMF, and carbonate bases, such as Cs₂CO₃ or K₂CO₃, to achieve selective *N*-alkylation^{133–136} and, therefore, these conditions were utilised in the initial studies. In particular, the success of the DMSO/Cs₂CO₃ methodology used by Stenkamp *et al.* to promote *N*-alkylation of a range of different pyridones with tosylate electrophiles,¹³⁴ meant that this system was utilised in the first reactions attempted (**Table 1.2.1**).

The initial experiments utilised the bromopyridone (**1.2.5**) as the nucleophile. This intermediate was chosen due to the availability compared to the iodo derivative (**1.2.8**). The electrophiles were selected to provide facile access to the B-ring pyridone borolane (**Scheme 1.2.6**). Epoxides (**1.2.12** and **1.2.13**) are particularly attractive electrophiles because they possess two electrophilic centres. This removes the requirement for additional manipulation after the initial nucleophilic attack, unlike the allyl electrophile (**1.2.14**). Additionally, as the chiral epoxides (**1.2.12** and **1.2.13**) are commercially available, it is envisaged that this would allow for facile control of the stereocenter in the final borolane (**1.1.41**), without the need for any stereoselective transformations or chiral resolution steps.



Scheme 1.2.6 – Methods to access borolane (1.1.41), utilising epoxy or allyl electrophiles and subsequent epoxidation.

The results of the initial studies to determine the *N*-:*O*-alkylation ratio are outlined below (Scheme 1.2.7 and Table 1.2.1).



Scheme 1.2.7 - General procedure for the *N*-:*O*-alkylation ratio studies.

Entry	Electrophile	Base	T (°C)	Ratio (N:O) ^a	% Yield (N:O)
1	1.2.12	Cs ₂ CO ₃ (2.5 eq)	60	19:81	0:5 ^{b,c}
2	1.2.13	Cs ₂ CO ₃ (1.2 eq)	85 ^d	24:76	0:31 ^{b,c}
3	1.2.14	Cs ₂ CO ₃ (1.2 eq)	85 ^d	30:70	28 (1.2.19):68 (1.2.18)

^aRatio of products was determined by LCMS analysis of the crude reaction mixture prior to purification

^bBoth epoxide reactions showed significant by-product formation in the LCMS analysis; masses and isotopic patterns provided putative evidence of epoxide opening through the action of a second equivalent of pyridone. ^cProduct isolation was inhibited by volatility issues and/or product instability.

^dReactions conducted at elevated temperatures according to the observation that elevated temperatures favour N-alkylation.¹³⁷

Table 1.2.1 – Results of the initial bromopyridone (**1.2.5**) alkylation study to explore N:O selectivity. A discussion relating to the assignment of the N:O-alkylation products is contained in the relevant **Appendix** section.

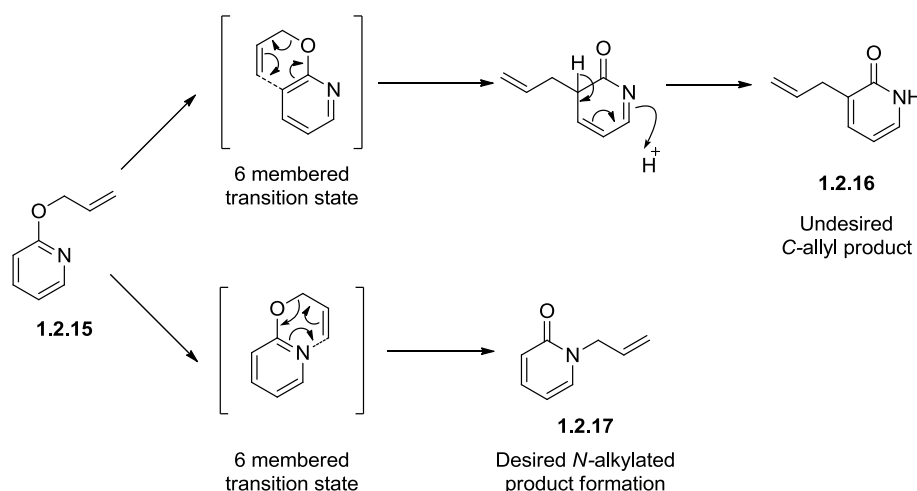
Unexpectedly, despite the reports in the literature, all alkylations with the 6-bromopyridine (**1.2.5**) under these conditions led predominately to formation of the undesirable O-alkylated product. While the transition to the softer epichlorohydrin (**1.2.13**) and allyl chloride (**1.2.14**) electrophiles and elevated temperatures were able to increase N-alkylation, the proportion of O-alkylation still significantly outweighed that of N-alkylation.

The significant by-product formation, low levels of N-alkyl product formation, and difficult isolation (due to product volatility or instability and difficulty in removing the by-products through chromatographic methods) meant that the use of the epoxides as electrophiles was not pursued further. Use of the allyl chloride (**1.2.14**) resulted in predominately O-alkylated product formation. Despite this, it was noted in the literature that this ether could be converted into the desired product through a palladium-catalysed rearrangement.¹³⁸

1.2.5.2 Interconversion of O-Allyl Pyridones to N-Allyl Pyridones

The Claisen type reaction in the absence of a metal catalyst has been reported on several different O-allyl pyridones and pyridone derived structures, from work conducted during the

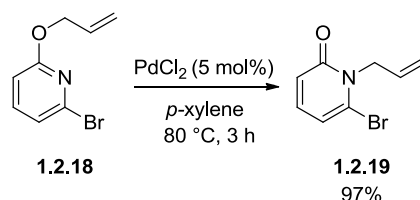
1960s by Moffett, Dinan, and Tieckelmann (**Scheme 1.2.8**).^{139,140} This reaction allows the conversion of the *O*-allylated substrate (**1.2.15**) into the desired *N*-allylated product (**1.2.17**), maximising the net yield of the *N*-allyl species from the corresponding pyridone. However, reactions have been reported to only proceed in poor yields, with significant quantities of the carbon allyl pyridone (**1.2.16**) and unreacted starting material (**1.2.15**) being observed under the reaction conditions (**Scheme 1.2.8**).



Scheme 1.2.8 - Sigmatropic rearrangement of allyl pyridones (**1.2.15**) into *N*-allylated product (**1.2.17**) and the *C*-allyl by-product (**1.2.16**).¹⁴⁰

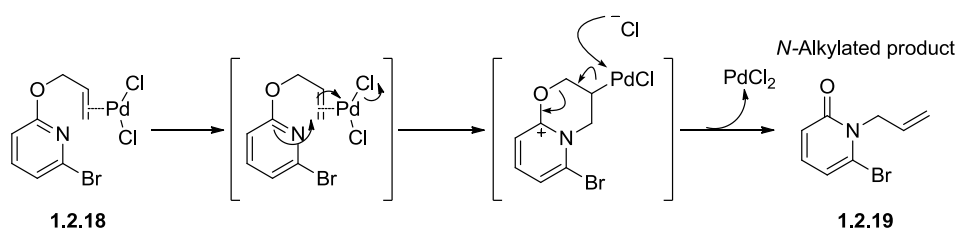
The reaction required high temperatures, in excess of 250 °C, and gave approximately equal amounts of the two products, in addition to the unreacted starting material. Therefore, although the reaction could plausibly lead to an overall increase in the quantities of the desired *N*-allylated product, the poor yields (15-25%) and difficult separations detract from using this method.^{139,140} This method demonstrated that the interconversion is possible but would require further refinement.

More recent developments by Yoshida *et al.* in 2003 show that significant improvements to the yields and selectivity of the reaction were possible using a palladium-catalysed Overman rearrangement.^{138,141} Gratifyingly, application of this method to the conversion of *O*-allyl bromopyridone (**1.2.18**) into *N*-allyl pyridone (**1.2.19**) was successful (**Scheme 1.2.9**).



Scheme 1.2.9 – Palladium-catalysed Overman rearrangement to synthesise the 1-allyl-6-bromopyridin-2(*1H*)-one (**1.2.19**).

This rearrangement was demonstrated with palladium (II) chloride, although the transformation has been reported with both palladium (0) and palladium (II) catalysts.¹³⁸ The addition of the palladium catalyst enables the use of significantly lower temperatures, and limits the amount of carbon allyl by-product formation. In the case of the *O*-allyl bromopyridone (**1.2.18**), palladium (II) catalyst was selected to avoid oxidative addition into the C-Br bond. The exact reaction pathway depends on the oxidation state of the catalyst employed. The postulated mechanism for the Pd(II)-catalysed process is displayed in **Scheme 1.2.10**.



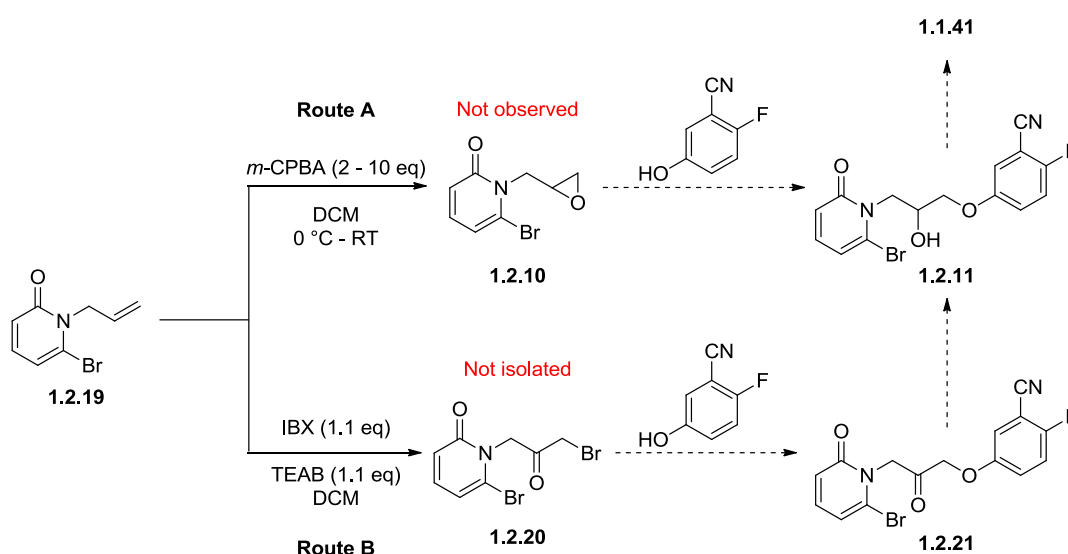
Scheme 1.2.10 - Proposed mechanism of the Overman rearrangement.

The reaction is initiated by coordination of the Pd(II) catalyst to the alkene π -system. This activates the alkene to nucleophilic attack in an analogous fashion to activation observed in the Wacker oxidation.¹⁴² Nucleophilic attack on the activated alkene by the nitrogen forms the cyclic intermediate, displacing one of the two chloride ligands. Nucleophilic attack by the resulting chloride anion causes the breakdown of the cyclic species, generating the *N*-alkylated product (**1.2.19**) and restoring the Pd(II) catalyst. Mechanistically, nucleophilic attack through the nitrogen is required, which circumvents the formation of the carbon allyl by-products.

1.2.5.3 Conversion of *N*-Allyl Pyridone into the Epoxy Derivative (1.2.10)

The method to readily access the *N*-allyl pyridone (**1.2.19**) was now established, so investigations into the functionalisation of the resulting alkene were initiated.

Attempts to functionalise the alkene focused upon accessing either the corresponding epoxide (**1.2.10**) (Scheme 1.2.11 – Route A) or α -bromo carbonyl electrophiles (**2.20**) (Scheme 1.2.11 – Route B). It was envisaged that both of these electrophiles would allow facile access to a range of different A- and B-ring analogues by reaction with an appropriate nucleophile. However, in the first instance, borolane (**1.1.41**) was targeted.



Scheme 1.2.11 – Route A - Attempted *m*-CPBA-mediated epoxidation of (**1.2.19**) to form (**1.2.10**). **Route B** - Attempted IBX-mediated α -bromo ketone (**1.2.20**) synthesis from (**1.2.19**).

The epoxidation of the alkene (**1.2.19**) through treatment with the peracid, *m*-CPBA, was analysed with variable equivalents of the peracid (Scheme 1.2.11, Route A). The reaction was conducted with up to ten equivalents of the peracid. However, in all reactions no desired epoxide was observed, with only significant decomposition being observed through LCMS analysis.

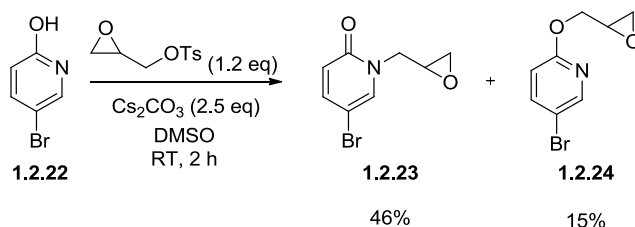
The use of IBX and TEAB to synthesise α -bromo carbonyls from terminal alkenes was reported in 2011 by Akamanchi *et al.*¹⁴³ Application of these conditions to the pyridone alkene (**1.2.19**) led to putative evidence of the desired product according to LCMS analysis. However, confirmation of the product identity was not obtained because the proposed α -bromo carbonyl

(**1.2.20**), if formed, was unstable, with decomposition occurring at either work-up or subsequent purification stages. Attempts to replicate the reaction using substrates reported in the literature were similarly unsuccessful. Therefore, the IBX work was concluded at this stage.

The difficulties encountered accessing both the epoxide (**1.2.10**) and the α -bromo ketone (**1.2.20**), *via* the *N*-allyl intermediate (**1.2.19**), meant that an alternative strategy was required. Alternative epoxidation methods were considered for the transformation, for example titanium-catalysed epoxidation methods commonly employed in the Sharpless asymmetric epoxidation.¹⁴⁴ However, the difficulties in the epoxidation of comparable pyridyl analogues (Section **1.1.6.3**) meant that establishing an alternative synthetic route was prioritised. Direct alkylation of the halo pyridone nitrogen was, therefore, revisited starting with studies into the influence of the halogen upon the reactivity of the pyridones.

1.2.5.4 Alternative 4-Bromopyridone Isomer Studies

The low yields of the *N*-alkylation of pyridone (**1.2.5**) (**Table 1.2.1**) were disappointing, as the conditions were anticipated to predominately produce *N*-alkylation based on previous literature precedent.^{133–136} Further investigation was required to enhance the proportion of *N*-alkylation. There were several postulated reasons for the poor yields of the protocol: either the methodology was incompatible with the pyridone nucleophile or electrophiles studied, or the protocol favoured *O*-alkylation. To ascertain which factor was responsible for the observed product ratios, the reaction with the tosylate epoxide (**Table 1.2.1** – Entry 1) was replicated with the 4-bromopyridone isomer (**Scheme 1.2.12**). It was postulated that if the undesired preference for *O*-alkylation was a consequence of the pyridone nucleophile, variation of the substitution pattern should result in a deviation of the *N*:*O* product distribution observed.



Scheme 1.2.12 - Alkylation of the regioisomeric pyridone (**1.2.22**).

The reaction showed a favourable reversal in the ratio of *N*:*O* alkylation relative to that seen with the 3-bromopyridone (**1.2.5**), with the dominant product being the *N*-alkylated molecule (**1.2.23**). The reduced isolated yields were thought to be a consequence of side-product formation; LCMS analysis suggested that epoxide opening by a second pyridone equivalent was occurring as a significant side-reaction. Regardless of this, the encouraging product ratios suggest that the position of the halogen is crucial in determination of the *N*:*O* selectivity. It is postulated that the halogen adjacent to nitrogen inhibits nucleophilic attack through either steric or electronic influences. Two explanations for this inhibition are plausible: either the size of the halogen sterically inhibits the attack through this centre or inductive withdrawal of electron density by the electronegative halogen decreases the nucleophilicity. The relative influences of these two factors remained to be determined, however, the observed ratios from experiments with the corresponding iodo derivatives may be able to elucidate the dominant factor (*vide infra*).

1.2.5.5 Previous Studies on Pyridone Alkylation

As previously discussed, pyridones are ambidentate nucleophiles. Typically the molecules exist in a tautomeric equilibrium (**Figure 1.2.5**), where the exact ratio of pyridone form to hydroxypyridine form is strongly dependent upon both the solvent and the substitution of the pyridone.¹⁴⁵ In polar media the pyridone form is found to be the dominant tautomer, while decreasing the solvent polarity is found to shift the equilibrium towards the hydroxypyridine form.¹⁴⁶

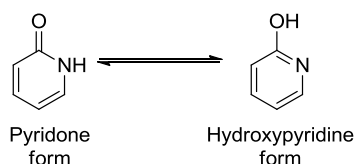
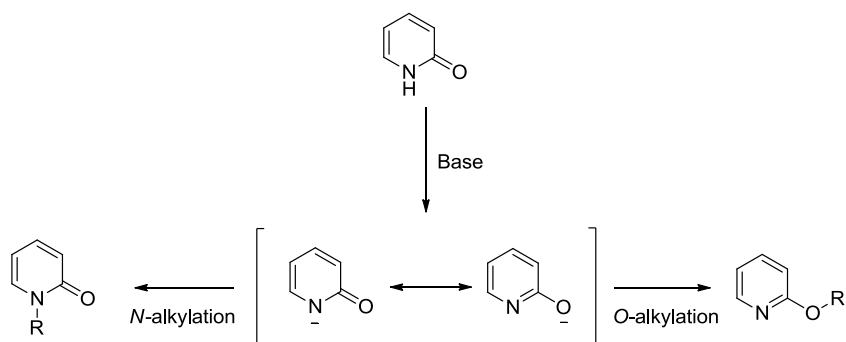


Figure 1.2.5 – Tautomeric equilibrium of the pyridones.¹⁴⁵

Alkylation reactions of pyridones are typically conducted by the treatment of the pyridone with an appropriate base and electrophile, although Lewis-acid mediated reactions have also been employed for pyridone alkylation reactions.¹⁴⁷ As has already been observed, both these methods generally lead to a mixture of *N*- and *O*-alkylated products (**Scheme 1.2.13**).



Scheme 1.2.13 – General reactivity of pyridone nucleophiles to provide *N*- and *O*-alkylated products.

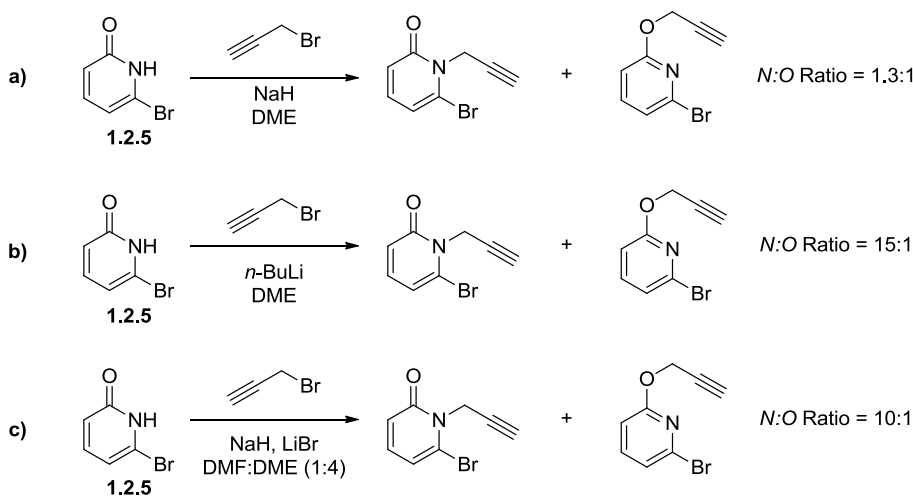
The product distribution of *N*- vs *O*-alkylation is influenced by a wide range of factors. Studies have implicated that solvent, base, electrophile, and temperature selection all play significant roles in the product distribution.^{133,136,137,148–150} In addition to this, the exact nature of the pyridone has also been demonstrated to influence the ratio of *N*:*O*-alkylation observed.

The first systematic investigation into the roles of the solvent, cation, and electrophile was conducted in 1967 by Tieckelmann *et al.*¹⁵⁰ The experiments demonstrated the subtle factors that control the regioselectivity, with the solvent selection, cation identity, steric bulk of the electrophile, and the leaving group all mediating significant effects upon the product distribution. Often the results of the alkylation reactions are highly substrate specific, giving rise to the wide range of conditions utilised within the literature. This substrate specificity can be clearly observed upon comparison of the experiments with the pyridone regioisomers (**1.2.5** and **1.2.22**).

1.2.5.6 Optimisation of the Pyridone Alkylation to Favour *N*-Alkylation

With the knowledge that the *N*- vs. *O*-alkylation could be switched to favour *N*-alkylation of pyridone (**1.2.22**), further studies were deemed important to overcome the intrinsic bias of the 2-halopyridones towards *O*-alkylation. Analysis of the literature allowed identification of two different strategies to promote *N*-alkylation of pyridones. As previously discussed, *N*-alkylation can be favoured through careful optimisation of the conditions with the base, solvent, and electrophile all playing significant roles. The alternative method to conduct the reaction is through the use of Lewis acids, activating the electrophile to nucleophilic attack.¹⁴⁷

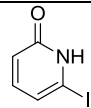
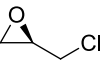
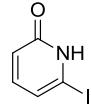
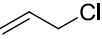
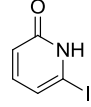
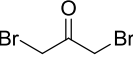
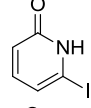
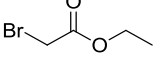
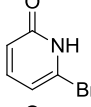
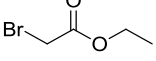
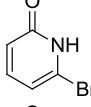
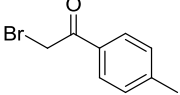
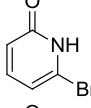
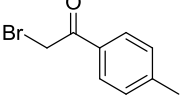
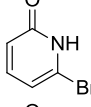
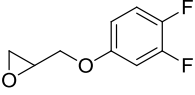
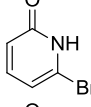
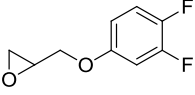
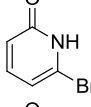
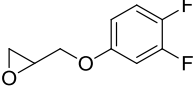
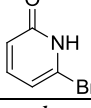
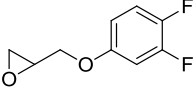
In 1995, Curran *et al.* investigated the same pyridone core structures, bromopyridone (**1.2.5**) and iodopyridone (**1.2.8**), and the resulting alkylation product distributions under a variety of different conditions. Comparison of the reactions of 2-halopyridones in DME and DMF led the authors to conclude that a less polar solvent had a modest, yet beneficial influence upon the proportion of *N*-alkylation observed.¹⁵¹ However, it was found that the factor that had the greatest influence upon the product distributions was the cation identity. In particular, the presence of lithium species was found to cause a dramatic increase in the amount of *N*-alkylated product formed, although no mechanistic rationale for this result was presented. The authors found that the highest levels of *N*-alkylation were observed with the organometallic lithium base, *n*-BuLi.¹⁵¹ However, the use of *n*-BuLi had issues associated with it, including: the need for cryogenic conditions, the potential for undesirable lithium-halogen exchange, and incomplete reaction progression. To overcome these issues, it was demonstrated that selectivities of comparable magnitudes could be attained through the use of alternative base species with the inclusion of lithium bromide additives. Under these conditions complete reaction progression was observed and the issues with temperature and potential side reactions were avoided. A summary of these results is displayed below (**Scheme 1.2.14**).



Scheme 1.2.14 – Summary of the study conducted by Curran *et al.* a) Results of alkylation in the less-polar solvent, DME. b) Alkylation results with organometallic lithium, after 3 days 20% starting material still remained. c) Alkylation results with lithium additives.¹⁵¹

The use of Lewis acids to give exclusively *N*-alkylation has been reported by Malkondu *et al.* who utilised combinations of CdI₂ and BF₃.OEt as the Lewis acids in the reactions.¹⁴⁶ This methodology was particularly attractive due to the use of electrophilic epoxides in the study, the advantages of which have been previously discussed.

Building upon the work detailed by Curran *et al.* and Malkondu *et al.* a second study into the alkylation was undertaken. To develop the greatest understanding and optimal conditions a wide range of different electrophiles were investigated (**Table 1.2.2**), which could then be used to access either the direct-linked borolane (**1.1.40**) or the B-ring analogue (**1.1.41**) through subsequent manipulation.

Entry	Pyridone	Electrophile	Conditions	T (°C)	Ratio (N:O) ^a	% Yield (N:O)
1			NaH, LiBr (2.0 eq) DME/DMF (4:1)	65	0 ^b	0
2			NaH, LiBr (2.0 eq) DME/DMF (6:1)	65	77:23	76:N/A
3			NaH, LiBr (2.0 eq) DME/DMF (4:1)	65	0 ^b	0
4			NaH, LiBr (2.0 eq) DME/DMF (4:1)	65	84:16	83:0
5			NaH, LiBr (2.0 eq) DME/DMF (4:1)	65	93:7	82:0
6			NaH, LiBr (2.0 eq) DME/DMF (4:1)	65	62:38	51:37
7 ^c			LHMDS (1.0 eq) THF	65	87:13	0 ^e
8 ^d			Cs ₂ CO ₃ (2.5 eq) DMSO	RT to 60	0:100	0:35
9 ^d			BF ₃ .OEt ₂ , DCM	0 to 40	0 ^b	0
10 ^d			NaH, LiBr (2.0 eq) DME/DMF (4:1)	65	100:0	0 ^e :0
11 ^d			Cs ₂ CO ₃ (1.2 eq) LiBr (2.0 eq) DME/DMF (4:1)	65	32:68	N/A ^f

^aRatio of products was determined by LCMS of the crude reaction mixture before isolation and purification. ^bNo product formation was observed in these reactions either during the reaction or in the LCMS of the crude reaction mixture. ^cReaction was conducted with LHMDS as a base instead of NaH. ^dElectrophile was material provided from within our laboratories; if encouraging results were attained then the experiments could be repeated with equivalent nitrile derivatives. ^eIn both instances only very low reaction conversions were observed and therefore no product could be isolated. ^fA complex reaction mixture prevented isolation of the products.

Table 1.2.2 – Results of the alkylation study employing the modified alkylation conditions.

The first two entries (**Table 1.2.2** – Entries 1 and 2) used the same electrophiles as the earlier reaction study (**Table 1.2.1**) to allow a comparison with the initial conditions. The reactions were conducted with the iodopyridone (**1.2.8**) to circumvent the potential volatility issues that had been previously encountered with the bromopyridone derivatives (**Table 1.2.1**). The reaction with the allyl chloride electrophile (**Table 1.2.2** – Entry 2) showed significantly greater *N*-alkylation than the previous experiments, potentially due to the ‘soft’ character of the electrophile. However, this new methodology was incompatible with the epoxide electrophile. It was thought that the basic conditions were leading to elimination reactions *via* epoxide ring opening. The incompatibility of the epoxide electrophile to the reaction conditions was also observed in the reaction with the phenol epoxide (**Table 1.2.2** – Entry 10). In this reaction only trace amounts of product were detected by LCMS. Attempts to isolate and confirm the identity of the product were unsuccessful as the product only constituted a small fraction of the total reaction mixture.

Entries 8-11 (**Table 1.2.2**) detail further investigations into the use of epoxide electrophiles. These experiments were conducted with the B-ring derived epoxide. It was envisaged that the resulting alcohol could be subjected to the borylation conditions to yield the final borolane compound. Attempts to conduct the reaction under standard literature conditions, polar solvent, and soft base, gave exclusively *O*-alkylation (**Table 1.2.2** – Entry 8) in poor yield. Slow reaction kinetics were observed at ambient temperature, therefore, the reaction was heated to facilitate the reaction. While this successfully led to complete conversion of the starting material, LCMS analysis was unable to detect any *N*-alkylation at either temperature. Lewis acid-mediated alkylation employing the conditions developed by Malkondu *et al.* were also investigated.¹⁴⁷ No reaction was observed, even after subjecting the reaction to prolonged reaction times and increased temperatures relative to the literature conditions.

Entry 10 (**Table 1.2.2**) investigated the alkylation of the B-ring derived epoxide under the reaction conditions of Curran *et al.*¹⁵¹ Under these reaction conditions LCMS analysis was only able to detect trace amounts of the desired *N*-alkylated product. Significant undetermined by-product formation meant that the absence of any *O*-alkylated product could not be confirmed. Due to the inherent instability of the epoxide to strongly basic conditions (**Table 1.2.2** – Entry 10), the alkylation with Cs₂CO₃ and LiBr additives was investigated (**Table 1.2.2** – Entry 11). The addition of LiBr gave an improved product distribution relative to the experiment without this additive (**Table 1.2.2** – Entry 8). However, the reaction progression

was poor and significant by-product formation inhibited efforts to isolate the resulting products.

The remaining experiments used α -bromocarbonyls as the electrophilic species (**Table 1.2.2** – Entries 3-7). These are attractive electrophiles for two reasons. They are highly reactive soft electrophiles, as a consequence of the low energy LUMO formed from the overlap between the C-Br σ^* and the C=O π^* antibonding orbitals. It was envisaged that this would favour reaction through the softer nitrogen centre, increasing the proportion of *N*-alkylation observed. The resulting carbonyl functionality could then be utilised in a wide range of further synthetic manipulations to allow facile access to elaborated structures.

Entry 3 (**Table 1.2.2**) details the use of the dibromo acetone electrophile, which theoretically could be used to generate an α -bromocarbonyl electrophile upon reaction with the pyridone nucleophile. It was envisaged that this could then be displaced by an appropriate B-ring nucleophile to couple the pyridone and the B-ring structures together. However, the reaction using this molecule resulted in a very complex reaction mixture, with no discernible product formation.

Entries 4 and 5 (**Table 1.2.2**) utilised an α -bromo ester electrophile, under the conditions devised by Curran *et al.*¹⁵¹ It was envisaged that the resulting ester species could then be used to access the B-ring analogue (**1.1.41**) through several transformations (see **Section 1.2.9**). The halogen identity was found to alter the selectivity profile. In both cases high ratios of *N*-alkylated product were observed, with the bromopyridone (**Table 1.2.2** – Entry 5) showing a greater proportion of the desired *N*-alkylated product. As the iodo derivative led to greater levels of the *O*-alkylated product, this suggests that sterics (as opposed to inductive withdrawal) are responsible for favouring the formation of the *O*-alkylated products in the initial experiments. The preferential product ratio with the bromo derivative (**2.5**) meant that it was selected for further investigations around this core.

Entries 6 and 7 (**Table 1.2.2**) detail the use of the aryl α -bromo ketone as an electrophile, which could subsequently be elaborated to generate the target pyridone borolane (**1.1.40**). Entry 6 details the reaction under the conditions developed by Curran *et al.*¹⁵¹ While the reaction showed a reduction in selectivity and overall yields relative to the ester examples (Entries 4 and 5), satisfactory product formation was still observed. In an effort to improve on this, the reaction was repeated using LHMDS as the lithium base. It was postulated that the

increased steric demands of the base (relative to *n*-BuLi) would prevent the undesirable lithium halogen exchange occurring and, therefore, lead to increased selectivities and yields. However, while there was a significant increase in the proportion of the *N*-alkylated product, the reaction only showed minimal levels of progression and also significant unidentified by-product formation.

Overall, the modifications proposed by Curran *et al.*¹⁵¹ showed significant improvements upon the initial reaction conditions, with the *N*-alkylated product being the major product in a majority of cases. While the reaction methodology was not compatible with epoxide electrophiles, the success with different α -bromocarbonyls means that the use of these species and subsequent elaboration could facilitate the formation of a wide range of different pyridone structures.

1.2.5.7 Rationalising the Results of the Alkylation Study

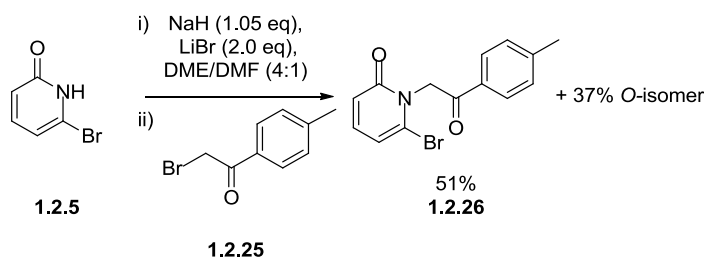
Despite the diverse range of studies into pyridone reactivity and syntheses using pyridone or pyridone derivatives, a rationale for the ratio of *N*-:*O*-alkylation has only recently been presented. In 2010, Mayr *et al.* conducted a study into pyridone reactivity utilising a combination of computational and experimental experiments.¹⁵² The authors concluded that the influence of the cation could be explained through its oxophilic or nitrophilic character. Therefore, oxophilic lithium cations form strong ion-pairs with the oxygen centre, preventing reaction through this centre. Likewise, the use of nitrophilic silver salts results in predominately *O*-alkylation due to the nitrogen-silver ion-pair. Modelling of the energetics of the reaction was also able to show that *N*-alkylation is the thermodynamic product and, in the absence of steric factors, the lower activation energy of this pathway leads to greater levels of *N*-alkylation. In reactions with bulkier electrophiles, the increased steric demands of the nitrogen disfavour this reaction pathway, leading to increased *O*-alkyl product.

The influence of sterics proposed by Mayr *et al.*¹⁵² is in agreement with the data obtained for halogen substitution. A comparison of entries 4 and 5 (**Table 1.2.2**), which only differ in the identity of the halogen in the halopyridone nucleophile, demonstrated a greater proportion of *N*-alkylation was observed with the bromopyridone (**1.2.5**). Increased levels of *O*-alkylation were detected with the iodopyridone (**1.2.8**), as a consequence of the steric bulk of this halogen disfavours the reaction through the adjacent nitrogen centre.

The ion-pair model proposed by Mayr *et al.*¹⁵² is able to rationalise the increased levels of *N*-alkylation upon addition of lithium additives (**Table 1.2.2** – Entries 1 – 6 and 10 – 11) or lithium-based bases (**Table 1.2.2** – Entry 7). The lithium ions preferentially coordinate to the oxygen centre, debilitating nucleophilic attack through this centre. This increases the relative amount of nucleophilic attack through the nitrogen centre, leading to increased levels of *N*-alkylation.

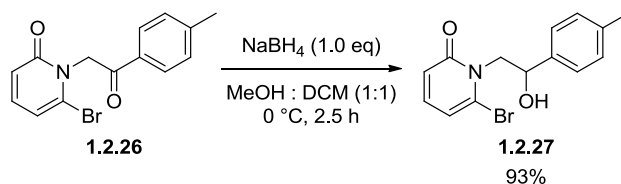
1.2.6 Synthesis of the Alcohol Intermediate (1.2.27)

With conditions to facilitate the *N*-alkylation of the halo pyridones having been established, the synthesis of the directly linked borolane (**1.1.40**) could now be explored. The first step was alkylation of bromopyridone (**1.2.5**) with the commercially available α -bromoketone (**1.2.25**) (**Scheme 1.2.15**), as previously discussed (**Table 1.2.2** – Entry 6).



Scheme 1.2.15 – Pyridone alkylation with the α -bromoketone (**1.2.25**).

Reduction of the ketone (**1.2.26**) could now be utilised to produce the alcohol intermediate (**1.2.27**), prior to the final borylation and cyclisation step. The racemic reduction was conducted using NaBH₄ as the reductant and provided access to the racemic alcohol (**1.2.27**) in high yield (**Scheme 1.2.16**).

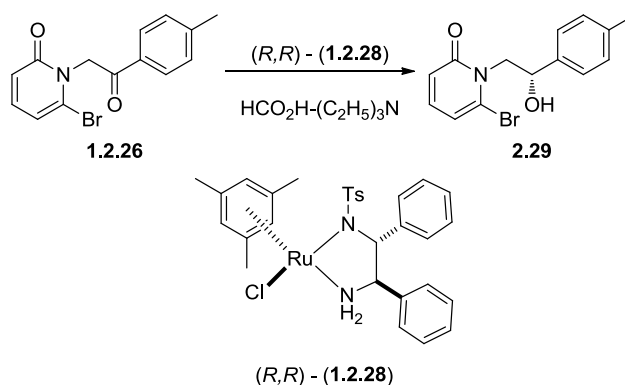


Scheme 1.2.16 – Reduction of ketone (**1.2.26**) to give racemic alcohol (**1.2.27**).

In addition to providing access to the racemic alcohol (**1.2.27**), the ketone intermediate (**1.2.26**) theoretically allows access to enantioenriched intermediates through application of a chiral

reduction protocol. The potential for asymmetric induction is synthetically attractive as it negates the requirement for chiral separation, which is undesirable due to the loss of material and the associated time and cost factors, especially on large-scale. There is a wide number of different asymmetric reduction methods described within the literature.^{117,153} The electronic and steric characteristics of the groups around the ketone mean that two asymmetric reduction protocols were considered for this system.

The aromatic group adjacent to the ketone led to the consideration of a Noyori transfer hydrogenation reaction.¹⁵⁴ The proposed reaction utilises a chiral ruthenium catalyst (**1.2.28**) with an organic hydrogen source to effect the asymmetric reduction of ketone (**1.2.26**) to chiral alcohol (**1.2.29**) (Scheme 1.2.17).



Scheme 1.2.17 – Proposed Noyori transfer hydrogenation reaction.

The Noyori transfer hydrogenation has been utilised on a range of different structures, typically displaying excellent yields and enantioselectivities.¹⁵⁴ Induction of high enantioselectivity is dependent upon aromatic or allyl carbonyls, limiting the substrate scope. The stereoinduction relies upon the formation of a key t-shaped π -interaction between the catalyst and substrate (**Figure 1.2.6**).¹⁵⁵ The absence of a suitable π -system neighbouring the carbonyl means that this interaction cannot exist. Consequentially, there is little preference for one *pseudo*-diastereomeric transition state over the other and enantioselectivity is reduced. This limitation means that this system would not be applicable towards the asymmetric reduction of elaborated A-/B-ring analogues and, therefore, due to this limited utility was not investigated.

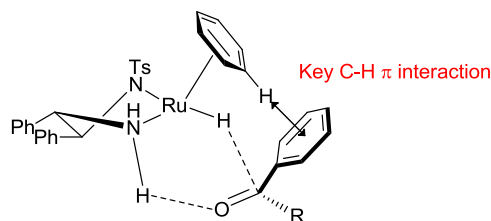
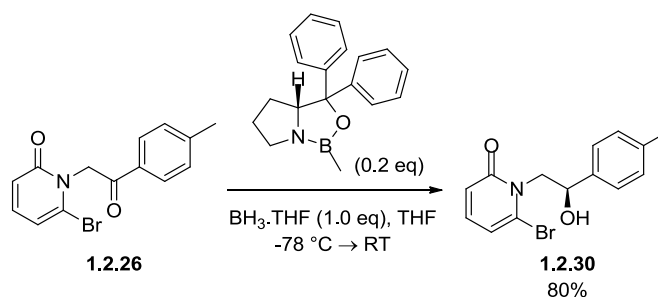


Figure 1.2.6 – The transition state in the Noyori transfer hydrogenation, illustrating the key interaction required for stereocontrol.¹⁵⁵

The second asymmetric reduction protocol considered was the Corey-Bakshi-Shibata (CBS) reduction. This reaction utilises a chiral oxazaborolidine as the catalyst, with a borane derived reductant. The reaction was evaluated utilising the reaction conditions reported by Corey *et al.* to determine if significant levels of stereoselection could be attained (**Scheme 1.2.18**).¹¹⁷



Scheme 1.2.18 - CBS reduction of ketone (**1.2.26**).

The stereoselectivity in the CBS reduction is typically attributed to steric interactions within the cyclic transition state, with an electronic contribution also being observed in some instances (**Figure 1.2.7**). The difference in the steric bulk of the two substituents can be estimated through consideration of the A-values for each substituent, calculated from the energy differences in the conformation of substituted cyclohexane structures. This gives a typical A-value of 3 kcal mol⁻¹ for the tolyl group, with < 2 kcal mol⁻¹ for the alkyl substituent.¹⁵⁶ In terms of ketone (**1.2.26**), the tolyl group exhibits considerably greater steric bulk closer to the reacting centre than the methylene-linked pyridone. As such, the tolyl group is held away from the B-R group of the catalysts within the transition state to minimise steric clashes. This preference differentiates the enantiofaces of the ketone and leads to the observed stereochemistry.

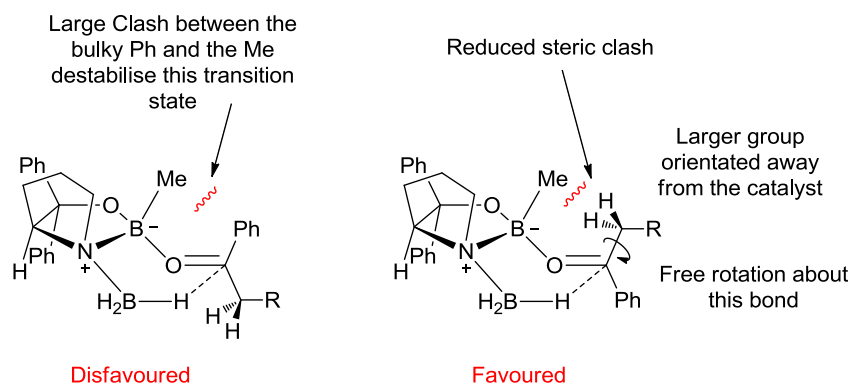


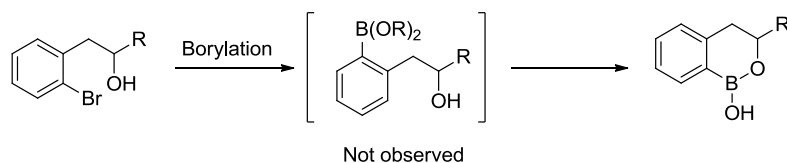
Figure 1.2.7 – Stereocontrol in the CBS reduction.

Gratifyingly the reduction was found to proceed in good yields. The enantioselectivity was determined by formation of the diastereoisomeric esters *via* the reaction of the alcohol (**1.2.30**) with Mosher's acid. The resulting diastereoisomeric mixture was then analysed by NMR and the ratio of the isomers determined. Using this methodology the ee of the reduction was calculated to be approximately 60%. While only modest enantioselectivity was initially observed, it is envisaged that optimisation of the temperature, catalyst, and hydride source should provide further increases in the enantioselectivity, if the biological data for pyridone (**1.1.40**) warrants further investigation.

1.2.7 Borylation of the Racemic Alcohol (1.2.28)

The final step in the synthesis of the directly linked pyridone borolane (**1.1.40**) is the borylation reaction.

It has been shown that under the borylation conditions for the synthesis of other analogues within our laboratories, the presence of the free hydroxyl in close proximity to the boronate ester leads to spontaneous cyclisation and borolane formation, through hydrolysis of the boronate, without the need for an additional cyclisation step (**Scheme 1.2.19**).⁶⁸

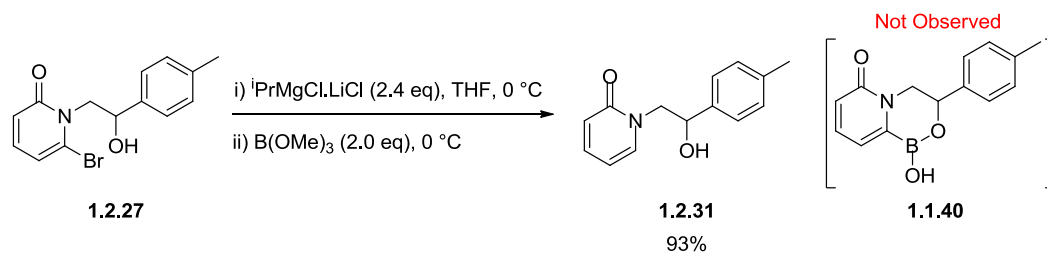


Scheme 1.2.19 – The borylation reaction and spontaneous cyclisation to yield the borolane.

Aryl boronic acids/esters are key synthetic intermediates in organic synthesis, being prevalent in a range of reactions, including the Suzuki cross coupling reaction.^{157,158} Two different synthetic methods are predominately utilised to access these key boronic acid and ester intermediates from the corresponding aryl halide species.

The first method involves treatment with an appropriate organometallic reagent, undergoing transmetallation with a halogen.¹⁰⁸ The resulting metalated species can then undergo transmetallation with a suitable boron species to yield the boronic acid or ester product after work-up. There are several drawbacks to this methodology. The reactive nature of the organometallic reagents, most commonly lithium or magnesium species, means that the reaction is incompatible with a wide range of functionalities. This was of particular concern for the targeted borolanes, which would incorporate a potentially reactive nitrile group,¹⁵⁹ which conveys a large amount of selectivity for Lp-PLA₂ over PLA₂-VIII. (**Figure 1.1.16**). These organometallic reagents are also often highly basic species and could deprotonate the acidic alcohol residue, which may interfere with the reaction. A final drawback of this methodology is that cryogenic conditions are often required, with lithium species typically requiring -100 °C to prevent side reactions leading to borinic and borane products.

The associated difficulties with the reaction utilising lithium reagents has resulted in alternative metal species being investigated. The reaction has been conducted effectively by Colobert *et al.* and others utilising Grignard or turbo Grignard reagents.^{105,160} These reactions have been demonstrated to occur cleanly at significantly higher temperatures and with improved functional group tolerance. The borylation of the pyridone alcohol (**2.27**) was investigated utilising the conditions of Colobert *et al.* (**Scheme 1.2.20**).¹⁶⁰ ⁱPrMgCl•LiCl (TurboGrignard) reagent was explored due to the increased tolerance of this reagent due to the increased kinetic basicity of these species, relative to conventional Grignard reagents.¹⁶¹ This increased basicity favours the magnesium-halogen exchange over nucleophilic attack, reducing the likelihood of side reactions.

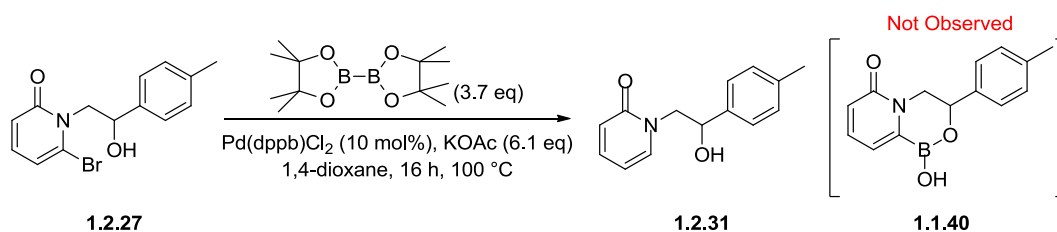


Scheme 1.2.20 - Attempted ¹PrMgCl•LiCl (TurboGrignard)-mediated borylation reaction of bromopyridone (1.2.27).

As alcohol deprotonation occurs prior to magnesium-bromine exchange, at least two equivalents of Turbo Grignard are required for this reaction. Assessment of the reaction mixture by LCMS after treatment with the magnesium species indicated that the reagent underwent facile magnesium halogen exchange, with only the mass of the dehalogenated pyridone species being observed by LCMS analysis. Despite this, the attempt to react this intermediate with the trimethoxy borate was unsuccessful, either due to instability of the magnesium adduct or decomposition of the boronic species during the required acidic workup. The failure of the organometallic borylation meant that the exploration around identifying suitable conditions focused on the second commonly used method, Miyaura borylation.

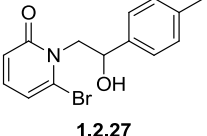
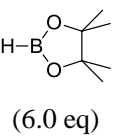
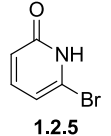
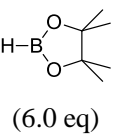
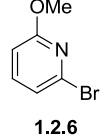
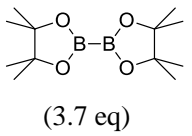
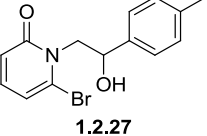
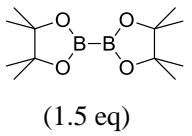
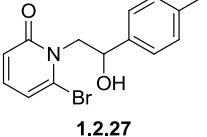
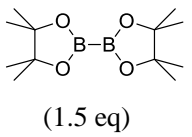
Miyaura borylation was first reported in 1995 and still represents one of the most important methods to access aryl boron compounds.¹⁵⁷ Due to the issues frequently encountered with organometallic reagents, the Miyaura borylation was the typical method used to conduct the key borylation reaction for the synthesis of other analogues within our laboratories.¹⁶² Therefore, this reaction had received considerable attention and optimisation.

Investigations into optimisation of the Miyaura borylation reaction for the borolanes have been found to be highly dependent upon the exact structure of the borolane, with most substrates requiring individual optimisation.¹⁶² Taking this into account the Miyaura borylation was investigated employing a catalytic system which had been successfully utilised in a range of other borolane syntheses (**Scheme 1.2.21**).¹⁶³



Scheme 1.2.21 – Attempted Miyaura borylation reaction.

Under the reaction conditions shown above (**Scheme 1.2.21**) LCMS analysis of the crude reaction mixture showed complete dehalogenation to give pyridone (**1.2.31**), with no desired product formation being detected. It was postulated that the electron-deficient nature of the pyridone was causing destabilisation of either the boron product or a palladium intermediate. Therefore, alternative reaction conditions which promoted the borylation were sought. A series of experiments were conducted in an effort to develop conditions for the borylation of the aryl bromide (**1.2.27**) or other aryl bromide substrates which could be then converted into the desired pyridone (**1.1.40**) (**Table 1.2.3**).

Ar-Br	Borane	Catalyst	Base	T (°C)	Time	Ratio of Desired Product:Dehalogenation
 1.2.27	 (6.0 eq)	Pd(PPh ₃) ₄ (10 mol%)	NEt ₃ (6.0 eq)	100	16 h	No reaction
 1.2.5	 (6.0 eq)	Pd(PPh ₃) ₄ (10 mol%)	NEt ₃ (6.0 eq)	100	2 h	No product detected
 1.2.6	 (3.7 eq)	Pd(dppb)Cl ₂ (10 mol%)	KOAc (6.1 eq)	100 ^a	15 min	No reaction
 1.2.27	 (1.5 eq)	Pd(dppf)Cl ₂ (5 mol%)	KOAc (6.1 eq)	130 ^a	15 min	1:6
 1.2.27	 (1.5 eq)	Pd(dppf)Cl ₂ (5 mol%)	KOAc (6.1 eq)	130 ^a	5 min	1:4

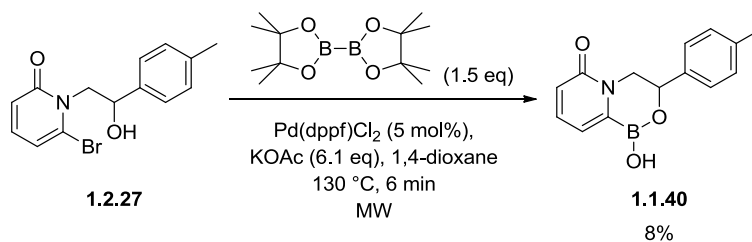
^aReactions conducted under microwave irradiation.

Table 1.2.3 – Investigations towards pyridone borylation through variation of the Miyaura reaction conditions.

The first two experiments (**Table 1.2.3** – Entries 1-2), utilised conditions which had successfully overcome a similar issue of dehalogenation with 3-bromopyridone derivatives.¹⁶⁴ These reaction conditions were assessed with both the alcohol (**1.2.27**) (**Table 1.2.3** – Entry 1) and the 2-bromopyridone (**1.2.5**) (**Table 1.2.3** – Entry 2). In both instances the reaction was unsuccessful. With the 2-bromopyridone alcohol (**1.2.27**) no reaction was observed with only starting material detected after a period of 16 h. In case of the bromopyridone (**1.2.5**), complete conversion of the starting material was observed, but no product formation could be detected. It was postulated that dehalogenation had occurred as no bromine isotopic pattern could be detected through LCMS analysis. Isolation of the product was difficult, potentially due to volatility, and the identity of the product could not be conclusively confirmed.

The final three experiments utilised microwave irradiation, which had been successfully utilised in the synthesis of a variety of different borolanes within our laboratories.¹⁶⁵ The methoxy pyridine (**1.2.6**) (**Table 1.2.3** – Entry 3) was investigated due to the different electronics. It was postulated that the electron-donating oxygen may lead to stabilisation of both reaction intermediates and the boron product and, therefore, enable successful borylation. However, under microwave irradiation no reaction was observed and only starting material remained.

The final experiments (**Table 1.2.3** – Entries 4-5) utilised microwave irradiation in combination with the alcohol pyridone (**1.2.27**). In both instances minimal product (**1.1.40**) formation was observed. The change in the desired product:dehalogenation ratio implied that the borolane was being formed but undergoing deborylation under the reaction conditions. Shorter reaction times were therefore selected to maximise the proportion of borolane product present (**Scheme 1.2.22**).



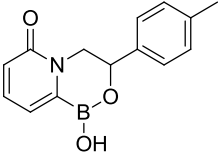
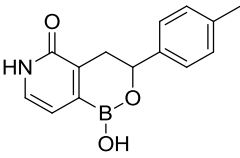
Scheme 1.2.22 – The Miyaura borylation reaction to access the direct-linked borolane (**1.1.40**).

The scheme above outlines the conditions employed to access the direct-linked borolane (**1.1.40**). The poor conversion to desired product (**1.1.40**) necessitated HPLC purification to isolate sufficiently pure material for biological assessment. The low yield of this reaction demonstrates significant optimisation will be required for resynthesis, if necessitated by the biological data.

1.2.8 Comparison of the Two Pyridone Borolane Isomers

With access to the direct-linked pyridone borolane (**1.1.40**) having been established, biological evaluation could now be carried out. The poor yield and difficult purification of the compound meant there was only sufficient material for the enzyme assay. The data is presented in **Table 1.2.4**.

1.2.4.

Pyridone	cLogP	pIC ₅₀ (Lp-PLA ₂)	pIC ₅₀ (PLA ₂ -VIIB)	Selectivity (Lp-PLA ₂ / PLA ₂ -VIIB) ^a
 1.1.40	1.4	5.1 (n=2) <5 (n=1)	4.7 (n=2) <5 (n=1)	4.4
 1.1.9	1.0	6.2	5.3	6.0

^aSelectivity is measured at the time limits of both assays and therefore the values do not directly relate to the values of pIC₅₀ reported.

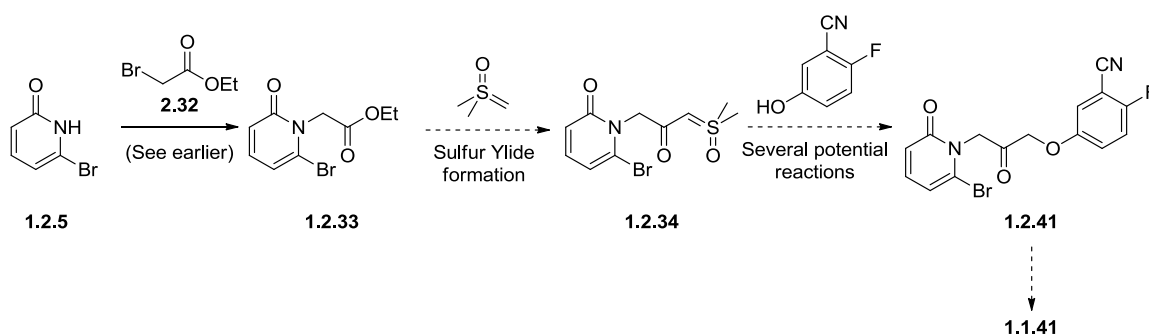
Table 1.2.4 – Comparison of the biological data for two pyridone core regioisomers.^{122,166}

A comparison of analogous structures for the two pyridone series allows the potential of the new core (**1.1.40**) to be evaluated. Disappointingly, the pyridoborolane (**1.1.40**) is less potent than its isomer (**1.1.9**) and has comparable selectivity over PLA₂-VIIB (**Table 1.2.4**). As investigations into the original core (**1.1.9**) were suspended due to the poor selectivity, the further decrease in selectivity for the new core (**1.1.40**) was clearly unacceptable and, therefore, further work on this series was terminated.

This work demonstrated that this new pyridone core was not a valid replacement, suffering from reduced selectivities and potencies relative to analogous borolanes. However, synthetic methodology has been established to access related core replacement analogues, which were previously challenging.

1.2.9 Investigations Towards the Synthesis of the B-ring Pyridone (1.1.41)

Despite the reduced interest in pyridone analogues, research into an appropriate synthetic strategy for synthesis of (1.1.41) has led to the identification of an alternative method to introduce the aniline or phenol linked motifs, which are common in the borolane series. This methodology utilises the potential reactivity of sulfur ylides (Scheme 1.2.23).



Scheme 1.2.23 – Potential method to access pyridone B-ring borolanes (1.1.41) through sulfur ylide chemistry.

The sulfur ylide (1.2.34) can plausibly be accessed from the ester (1.2.33), which itself is generated from the pyridone alkylation reaction with the α -bromocarbonyl electrophile (1.2.23) as previously discussed (Table 1.2.2 - Entry 5). Subsequent, conversion of the resulting ylide to an appropriate electrophile enables the formation of the key N/O bond through nucleophilic substitution by the appropriate aniline or phenol. It was envisaged that a highly electrophilic α -halocarbonyl species (1.2.42) could be accessed from the sulfur ylide intermediate (Figure 1.2.8), with complete control over the site of halogenation.

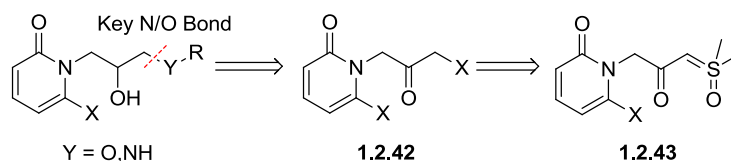


Figure 1.2.8 – The proposed method to form the key bond in the elaborated pyridone borolane, through the use of sulfur ylide and α -halocarbonyl intermediates.

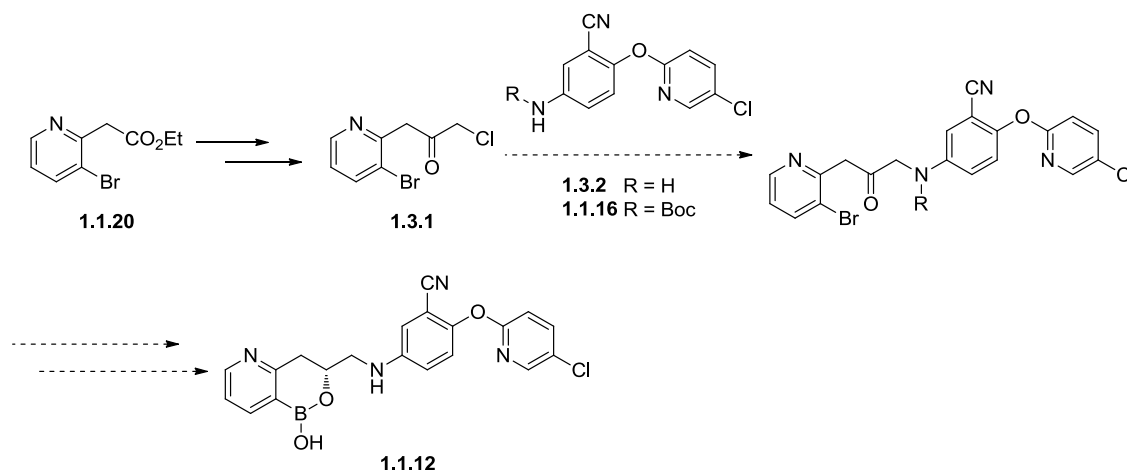
As the pyridone molecules were down-prioritised, as a consequence of the inherent low selectivities for Lp-PLA₂ over PLA₂-VIIB, the proposed synthetic route was not investigated (Scheme 1.2.23). Instead the methodology, discussed above, was applied to develop an

alternative method to access the pre-candidate (**1.1.12**), for which the previous routes have historically suffered from low yields and protracted syntheses (**Scheme 1.1.4, Section 1.6**).⁹¹

1.3 Improving Synthetic Methodology for the Synthesis of the Pre-candidate Borolane (1.1.12) and Related Analogues

1.3.1 Issues with the Original Pre-candidate Borolane (1.1.12) Synthesis

The current synthetic route to the borolane (1.1.12) possesses 11 steps, with a poor overall yield (0.9% from commercial starting materials), and the requirement for both protecting and activating groups (Section 1.1.7). α -Halocarbonyl electrophiles have been previously employed in the synthesis of the alternative pyridone borolane (1.1.40) and the pre-candidate molecule (Scheme 1.1.4 – 1.1.16 \rightarrow 1.1.17.). Based on the effectiveness of this functionality, it was envisaged that the α -halocarbonyl electrophile could be utilised to directly functionalise the pre-candidate aniline. This would reduce the number of steps in the pre-candidate synthesis (Scheme 1.3.1), improving both the yields and corresponding environmental sustainability metric measures. Several potential synthetic strategies were identified to access the desired α -chlorocarbonyl (1.3.1) and these are discussed in the following sections.

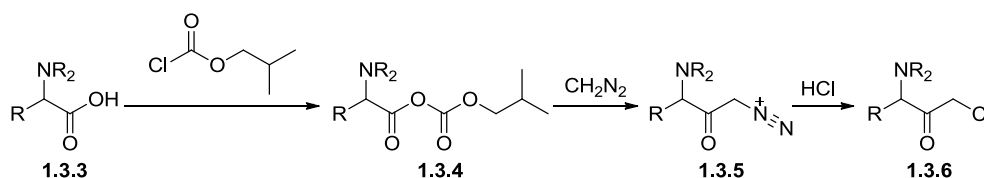


Scheme 1.3.1 – Potential use of α -halocarbonyls to access the keto intermediate on route to pre-candidate molecule (1.1.12).

1.3.2 The Use of Diazomethane to Access α -Chlorocarbonyls

Although the reaction between IBX and terminal alkene substrates has been reported to provide facile access to α -halocarbonyl derivatives,¹⁴³ the previous failures to replicate these

results on both novel and literature substrates (**Section 1.2.5.3**) resulted in alternative methods to synthesise α -halocarbonyls being considered. One such method was developed by Albeck and Persky in 1994, through the use of diazomethane species.¹⁶⁷ The authors exemplified the potential utility of this methodology through the homologation of different amino acids (**Scheme 1.3.2**) to the corresponding α -chloroketones.



Scheme 1.3.2 - Use of diazomethane to access α -chloro carbonyls.²

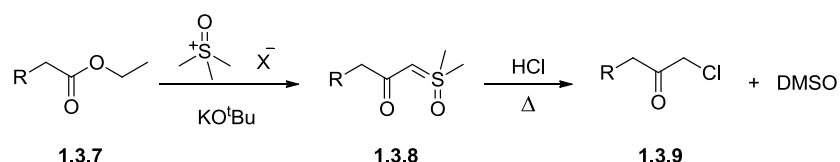
In the examples reported by Albeck and Persky, reaction of the amino acid species (**1.3.3**) with isobutyl chloroformate generated the corresponding mixed anhydride (**1.3.4**).¹⁶⁷ Treatment of this intermediate with diazomethane formed the diazomethyl species (**1.3.5**). The alkyl carbonate by-product rapidly decomposed, to give the corresponding alkoxide species and carbon dioxide, which provided a strong thermodynamic driving force for the reaction. The addition of HCl to the diazomethyl intermediate (**1.3.5**) yielded the α -chlorocarbonyl species (**1.3.6**), with the evolution of nitrogen acting as the driving force for the reaction. The methodology allowed access to less substituted (kinetic) α -chlorocarbonyl molecules, while avoiding potential issues with selectivity for halogen addition at the normally more acidic position.

Despite the sequence being reported to proceed in high yields, and providing facile access to the desired electrophilic species, the explosive and mutagenic nature of diazomethane detracts from the overall viability of this method. Some of the issues with diazomethane can potentially be mitigated through the use of TMS-diazomethane.¹⁶⁸ However, concerns relating to safety and long term scale-up requirements meant that this method was deemed inappropriate for further investigation within our laboratory.

1.3.3 The Use of Sulfur Ylides to Access α -Chlorocarbonyls; an Alternative to Diazomethane

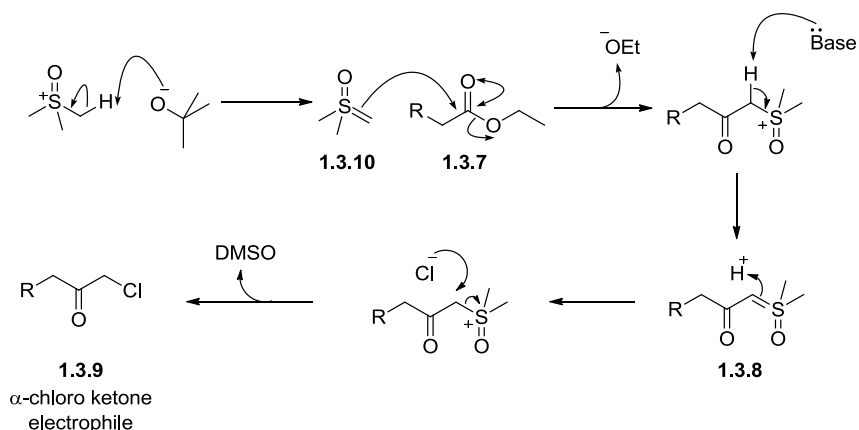
To circumvent the hazards associated with the use of diazomethane, the discovery of alternative methods to enable the transformation of carbonyls into α -halocarbonyls (**Scheme**

1.3.2) has received considerable attention. One potential solution to the use of diazomethane, is the use of sulfur ylide species as a substitute for diazonium functionality, which was published in 2004 by Nugent *et al.*¹⁶⁹ In contrast to the synthesis of the diazonium species, this chemistry methodology employs ester starting materials. Nucleophilic attack on the ester (**1.3.7**) by dimethylsulfoxonium methylide yields the stable β -keto sulfur ylide intermediate (**1.3.8**). On treatment with anhydrous HCl, these ylides are converted to the corresponding α -chloro carbonyls (**1.3.9**), liberating DMSO as the sole by-product (**Scheme 1.3.3**).



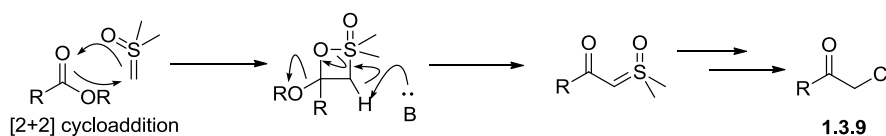
Scheme 1.3.3 - Use of sulfur ylides to access α -chloro ketone species.¹⁶⁹

The postulated mechanism for this transformation begins with the generation of the dimethylsulfoxonium methylide, typically through heating trimethyl sulfoxonium salts with KO^tBu (**Scheme 1.3.4**). Dimethylsulfoxonium methylide (**1.3.10**) then acts as a nucleophile through the more nucleophilic carbon centre, displacing the ethoxide group of the ester (**1.3.7**). Deprotonation of the resulting cation species, by a base such as the ethoxide, generates the stable β -keto sulfur ylide (**1.3.8**), which is typically isolated through recrystallisation or chromatographic methods. Under acidic conditions the ylide is protonated, activating the species to nucleophilic attack. Displacement of the DMSO leaving group by the halide is facilitated by the adjacent ketone π -system, forming the desired α -chloro ketone (**1.3.9**).



Scheme 1.3.4 - Proposed mechanism of α -chloro ketones (**1.3.9**) formation from the corresponding esters (**1.3.7**).

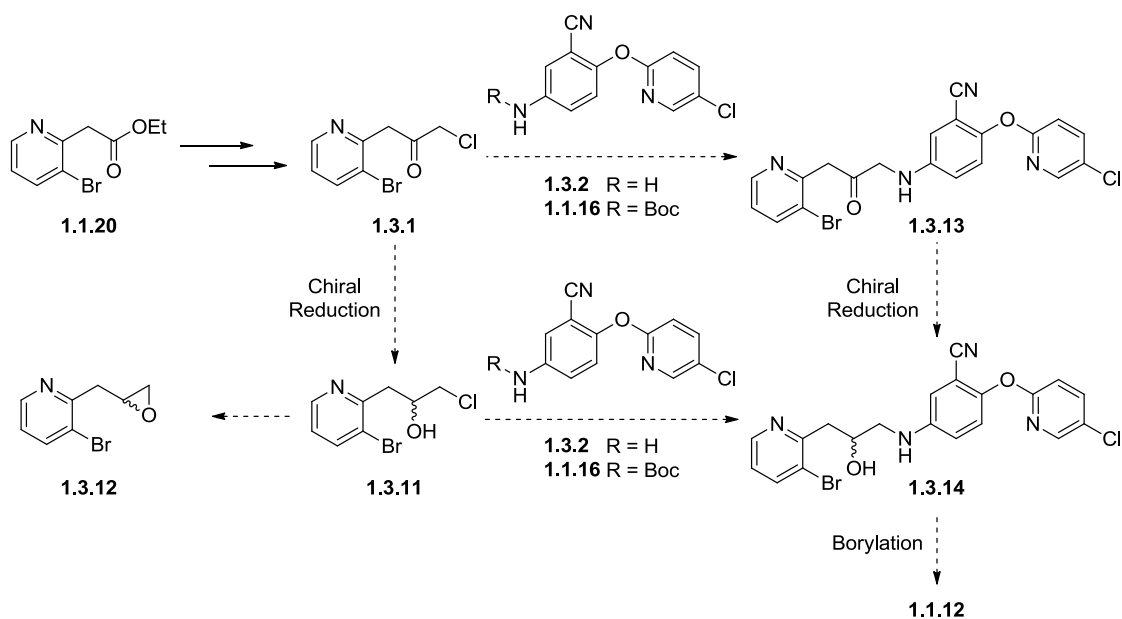
Nugent *et al.* have proposed an alternative mechanism to account for the formation of the β -keto sulfur ylide (**Scheme 1.3.5**).¹⁶⁹ They postulate that the initial interaction between the dimethylsulfoxonium methylide and the ester is a reversible [2+2] cycloaddition, based upon the isolation and characterisation of a stabilised 1,2- λ^6 -oxathietane in 1996 by Kawashima *et al.* (**Scheme 1.3.5**).¹⁷⁰ The resulting cyclo-adduct is deprotonated causing its breakdown to generate the β -keto sulfur ylide and an additional equivalent of base. Treatment of this intermediate with an appropriate acid then generates the α -chloro ketone in an analogous fashion to the previously discussed mechanism (**Scheme 1.3.5**).



Scheme 1.3.5 – Alternative mechanism for the formation of β -keto sulfur ylides.

Attempts to provide conclusive evidence for the reaction mechanism, by Nugent *et al.*, have thus far been unsuccessful.¹⁶⁹ Further mechanistic studies are required in order to deduce which of the two mechanisms is, indeed, occurring.

The sulfur ylide chemistry can potentially provide access to α -halo carbonyl (**1.3.1**) (**Scheme 1.3.6**) from the ester intermediate (**1.1.20**) used in the initial pre-candidate synthesis. It is envisaged that the resultant α -halo carbonyl species (**1.3.1**) can be utilised to access the candidate molecule (**1.1.12**) *via* two alternative routes (**Scheme 1.3.6**). The first route involves nucleophilic displacement with the aniline (**1.3.2**) or the Boc protected aniline (**1.1.16**) equivalent, to give the ketone (**1.3.13**), followed by reduction to give the alcohol (**1.3.14**). Depending on the success of this method the sequence of events could be reversed performing a reduction to give (**1.3.11**). From this intermediate (**1.3.11**) two potential routes to the desired alcohol (**1.3.14**) can be envisaged; either intramolecular displacement of the chloride to form the epoxide (**1.3.12**), followed by nucleophilic ring opening, or direct displacement of the chloride to access the same alcohol intermediate (**1.3.14**).



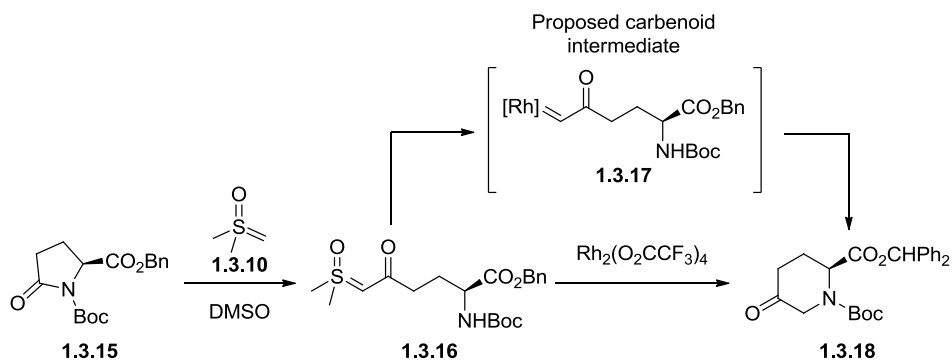
Scheme 1.3.6 – Potential methods to access the pre-candidate molecule from α -chlorocarbonyls.

The improved safety profile and the potential to scale-up the methodology, if necessitated, led to the sulfur ylide route being investigated, in preference to the diazomethane chemistry.

1.3.4 The Use of Sulfur Ylides as Carbenoid Sources

The use of the sulfur ylide group as a diazonium surrogate meant that in addition to being utilised as an effective leaving group (**Scheme 1.3.3**), the sulfur ylides can also plausibly undergo alternative characteristic reactions of diazonium species. One potential transformation identified was the use of sulfur ylides as carbene sources, with the resulting carbenoids potentially undergoing insertion reactions into nucleophilic bonds.¹⁷¹

In 1993, Baldwin *et al.* demonstrated that upon treatment with an appropriate rhodium catalyst, sulfur ylides could be used to access carbenoid species.¹⁷¹ The resulting carbenoid could insert into N-H bonds, evolving DMSO as a by-product. The authors presented the ring expansion below as an example of this methodology (**Scheme 1.3.7**).

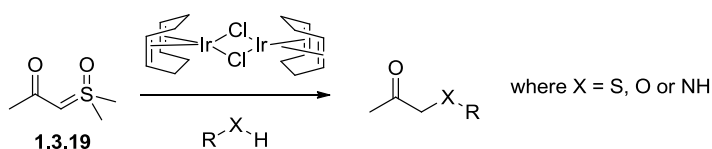


Scheme 1.3.7 - Use of rhodium-catalysed carbene formation and N-H insertion.¹⁷¹

To optimise the reaction yields, the authors assessed a variety of transition metal catalysts.¹⁷¹ Encouragingly, several rhodium catalysts were identified which displayed reasonable activity, with yields for the N-H insertion reaction being between 60-77%. Alternative prospective catalysts were unable to affect the transformation, including several copper catalysts which had previously been implicated in carbene insertion reactions.

Despite the success of the rhodium-catalysed methodology to effectively catalyse the transformation displayed above (**Scheme 1.3.7**), the reaction suffered from several significant drawbacks. These drawbacks included; limited reaction substrate scope and potential issues with DMSO-mediated catalyst deactivation. This meant that this methodology did not receive any further attention for a number of years.

In 2009 the use of sulfur ylides as carbene precursors, and the subsequent insertion reactions, were revisited by Mangion *et al.*¹⁷² The authors initiated an alternative catalyst screen in an attempt to overcome the limitations imposed by the catalyst deactivation, most notably the requirements for high catalyst loadings. Various iridium and rhodium catalysts were screened with a range of alcohols, thiols, and anilines. The [Ir.COD.Cl]₂ dimer displayed the best activity, showing high yields in a variety of solvents and with a range of substrates (**Scheme 1.3.8**). The authors hypothesised that this increased activity is a consequence of the lower affinity of DMSO for the iridium catalyst, reducing catalyst deactivation.



Scheme 1.3.8 - The use of iridium carbene for X-H insertions.¹⁷²

The iridium-catalysed reaction (**Scheme 1.3.8**) was successfully conducted with a wide range of different anilines, thiols, and alcohols.¹⁷² The robustness of the iridium-mediated reaction was subsequently illustrated through the synthesis of MK-7246, showing the reliability of the methodology on a 100 kg scale (**Figure 1.3.1**).¹⁷³ Subsequent work by Mangion *et al.* demonstrated that the reaction can be conducted utilising gold catalysis as an alternative to the iridium catalysis.¹⁷⁴

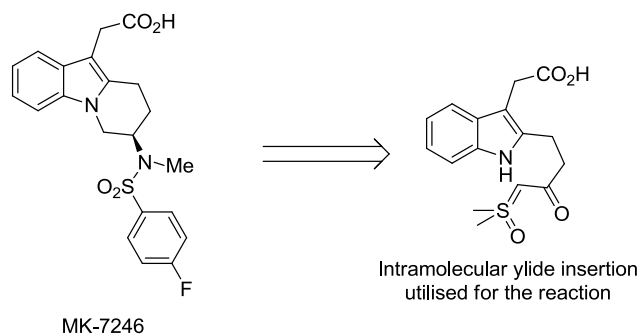
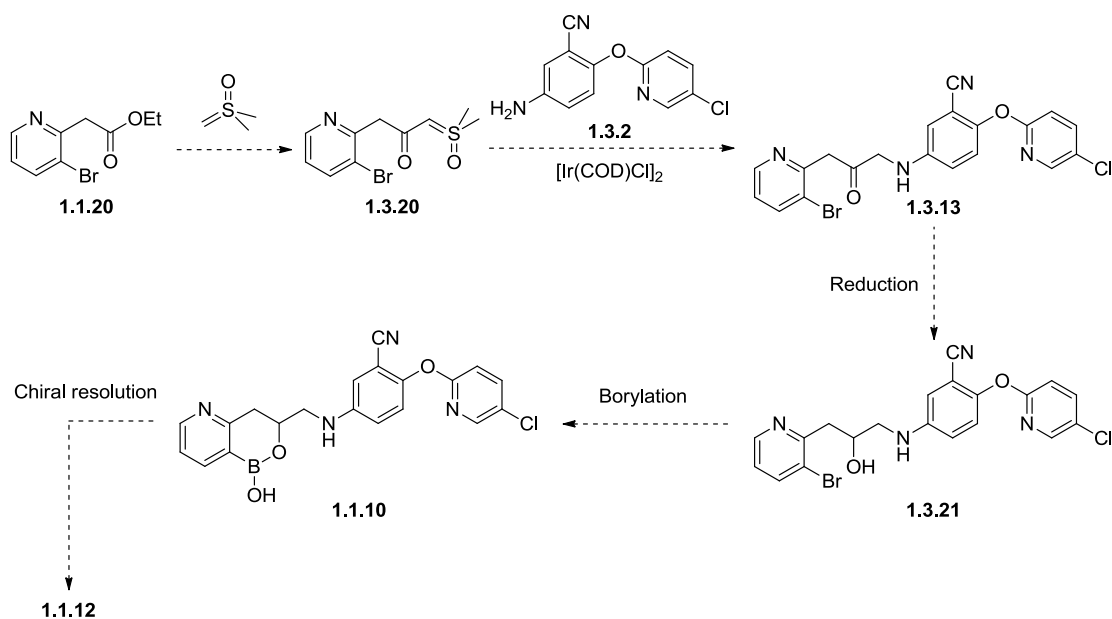


Figure 1.3.1 – The structure of MK-7246 and the ylide utilised in the scale-up synthesis of this molecule.¹⁷³

It was envisaged that the iridium-catalysed process could be applied to synthesis of borolane analogues, removing the need for a protracted linear synthesis. The carbenoid methodology can be utilised to circumvent the formation of the potentially unstable α -chlorocarbonyl (**1.3.11**) and to further reduce the number of synthetic steps (**Scheme 1.3.9**).



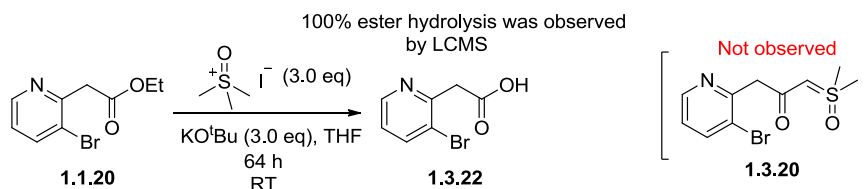
Scheme 1.3.9 – New proposed synthesis of the pre-candidate (**1.1.12**).

As both the iridium-mediated insertion and the α -chlorocarbonyl syntheses pass through the same key β -keto sulfur ylide (**1.3.20**), to enable investigations into both these strategies, a reliable, high yielding protocol for the formation of the ylide was required.

1.3.5 β -Keto Sulfur Ylide Synthesis

While the formation of β -keto ylides from esters is well precedented, examples of the formation of these species in the presence of heterocycles is substantially less established. In the majority of cases for the formation of the sulfur ylides, the same reaction conditions are employed: an excess of base and trimethylsulfoxonium salts in THF. Either trimethylsulfoxonium iodide or chloride is commonly utilised in the reaction.^{169,173,175,176}

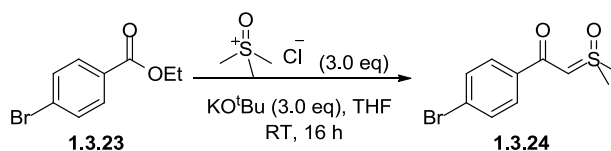
In the synthesis of MK-7246 (**Figure 1.3.1**), trimethylsulfoxonium iodide salts were effectively utilised in the formation of > 60 g of β -keto ylide, in a reasonable 71% yield from the ester.¹⁷³ The efficiency and scalability of this procedure led to this being identified as the starting point in the investigation into the β -keto sulfur ylide (**1.3.20**) formation (**Scheme 1.3.10**).



Scheme 1.3.10 – Attempted β -keto ylide formation using trimethylsulfoxonium iodide.

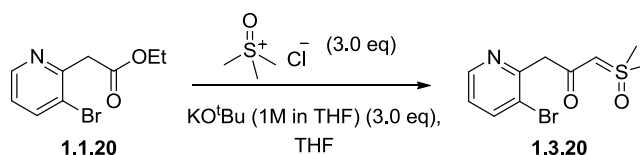
The reaction progression was monitored periodically during the reaction by LCMS analysis. Surprisingly no ylide formation was observed and complete ester hydrolysis to the carboxylic acid (**1.3.22**) occurred under the reaction conditions.

To determine if the inability to form the ylide (**1.3.20**) was a consequence of the heterocyclic substrate (**1.1.20**), the reaction was conducted using a known literature procedure and substrate (**Scheme 1.3.11**).¹⁷² Trimethylsulfoxonium chloride was utilised in the reaction due to improved solubility and light stability relative to the iodide salts.¹⁷⁵



Scheme 1.3.11 - Model reaction to probe sulfur ylide formation.¹⁷²

Monitoring of the reaction progress, under the alternative reactions conditions (**Scheme 1.3.11**), revealed significant product (**1.3.24**) formation (24% of the total reaction composition by LCMS analysis) in addition to starting material (**1.3.23**) and carboxylic acid by-product. The successful ylide formation in this reaction led to these conditions being utilised in a systematic study into the formation of the desired pyridyl β -keto ylide (**1.3.20**). The ylide formation from ester (**1.1.20**) was repeated using trimethylsulfoxonium chloride as the sulfur source (**Scheme 1.3.12**) (**Table 1.3.1**), utilising the conditions of Mangion *et al.*¹⁷²



Scheme 1.3.12 - Conditions for the sulfur ylide formation investigation.

Entry	Temperature (°C)	Amount of hydrolysis observed ^a	Reaction time	Product formation ^a	Remaining Starting material ^a
1	25	8% (10%) ^b	24 h (48 h) ^b	52% (54%) ^b	32% (29%) ^b
2	40	8% (9%) ^b	24 h (72 h)	75% (56%) ^b	14% (0%) ^b
3	50	14%	24 h	71%	7%
4	55	14% (19%) ^b	24 h (48 h)	67% (63%) ^b	10% (0%) ^b
5 ^c	70	9%	18 h	45%	18%

^a Determined by LCMS analysis. ^b Values in brackets correspond to experiments with extended time periods, denoted by the brackets in the time column. ^c Reaction at 70 °C was discontinued after 18 h due to significant by-product formation (representing approximately 30% of the total reaction composition).

Table 1.3.1 - Results of the formation of the sulfur ylide study.

At ambient temperature (**Table 1.3.1** – Entry 1) the reaction progression was found to be significantly slower than comparable literature examples, using this procedure.^{169,172} Complete reaction conversion was not attained at ambient temperature, with no significant reaction progression being observed beyond 24 hours. As the model reaction (**Scheme 1.3.11**) displayed slower reaction kinetics than anticipated, the influence of temperature upon the reaction was investigated.

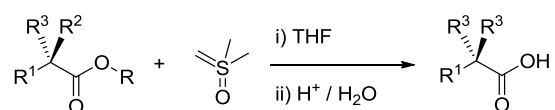
Increased temperatures led to significant increases in the reaction rate and progression in all the experiments, but still did not lead to complete reaction conversion after 24 h. Increasing the duration (**Table 1.3.1** – Entries 2 and 4) to 48 h, gave complete conversion of the starting material but there were increased levels of unidentified by-product formation. This by-product formation was particularly pronounced at 70 °C (**Table 1.3.1** – Entry 5), where only minimal product levels were observed.

The results suggested that the optimal reaction temperature was around 50 °C (**Table 1.3.1** – Entry 3). Conducting the reaction at this temperature provided both high reaction conversions and reaction rates with minimal by-product formation. Therefore, further studies into the formation of the sulfur ylides (and subsequent synthetic manipulation) were conducted at this temperature.

Another significant result from the study was the relatively consistent levels of hydrolysis irrespective of the reaction temperature, representing a considerable loss of product and overall reaction yield. Nugent *et al.* have observed that β -keto sulfur ylides contain unusually strong UV chromophores,¹⁶⁹ therefore LCMS analysis cannot be used to accurately quantify the levels of hydrolysis by-product formed during the reaction, and, therefore, the levels of hydrolytic product are potentially underestimated in the study (**Table 1.3.1**). In order to maximise the reaction yields, a reduction in the levels of hydrolysis was desired. It was thought that one way to achieve this may be through identifying the primary source of water in the reaction in order to reduce the relative water levels present within the current protocol.

1.3.6 Exploring the Source of Water in Ylide Formation

The potential presence of significant levels of water in these reactions is not unprecedented. In 2012 Leggio *et al.* presented the use of trimethylsulfoxium halide salts in combination with a base to hydrolyse a wide range of esters to the corresponding carboxylic acids in high yields, 70-99% (**Scheme 1.3.13**).¹⁷⁷



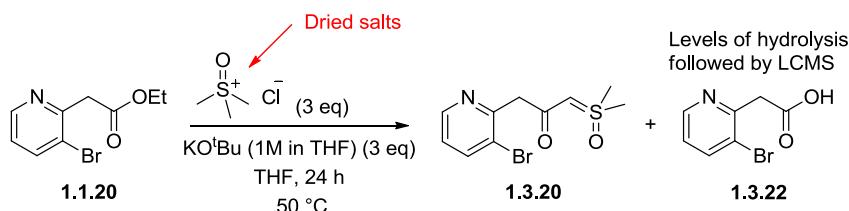
Scheme 1.3.13 - Method to hydrolyse esters to acids utilising dimethylsulfoxonium methylide.¹⁷⁷

The source of oxygen within the carboxylic acid was proposed to be derived from the initial sulfonium salt.¹⁷⁷ In order to identify the source of the oxygen in the carboxylic acid product, isotopic labelling experiments were conducted with Li¹⁸OH and Na¹⁸OH. The lack of ¹⁸O incorporation into the acid was interpreted as evidence for the dimethylsulfoxonium methylide acting as the oxygen source, attacking the ester through oxygen.

In 2013, Nugent *et al.* followed up this work with publication of a detailed study on the formation of sulfur ylides and source of hydrolytic products observed.¹⁷⁵ Computational modelling of the nucleophilic species showed that the largest orbital co-efficient in the HOMO resided upon the carbon of the ylide and, therefore, attack through oxygen, as proposed by Leggio *et al.*,¹⁷⁷ was less plausible.

Nugent *et al.* systemically analysed the water content of each of the reaction components in turn.¹⁷⁵ Trimethylsulfoxonium chloride salts were found to be very hygroscopic, providing the major source of water in the reaction, while only negligible levels of water were found to derive from the solvent and base. The authors utilised two strategies to minimise the water concentrations in the reaction: the addition of drying agents to the reaction, or drying the trimethylsulfoxonium chloride salts prior to the reaction. In both cases the levels of hydrolysis decreased dramatically, with no hydrolysis observed in the reaction with the dried sulfur salts.

To determine if the results reported by Nugent *et al.* were applicable to the levels of hydrolysis observed in the pyridyl ylide (**1.3.20**) formation (**Scheme 1.3.12**, **Table 1.3.1**) a drying experiment was undertaken. In each case the sulfur salts were dried by heating the trimethylsulfoxonium chloride salts under vacuum for the indicated time period (**Table 1.3.2**). The differences in the masses were used to approximate the levels of water content, which were confirmed by Karl-Fischer titration data obtained by colleagues within our laboratories.^{178,179} The dried salts were then utilised in ylide formation (**Scheme 1.3.14**) and the levels of hydrolysis determined through LCMS analysis (**Table 1.3.2**).



Scheme 1.3.14 – Ylide formation and hydrolysis with dried sulfur salts.

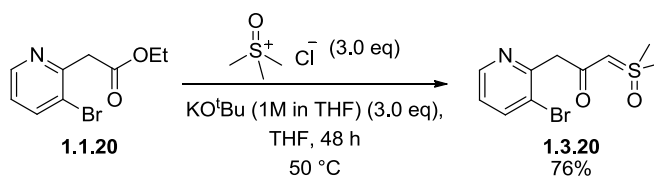
Entry	Temperature (°C)	Time (days)	Mass Before (g)	Mass After (g)	% Change	% of hydrolysis ^a
1	55	5	20.4	19.4	4.7	0.95
2	55	3	10.7	10.6	1.4	N/A ^b
3	60	4	28.1	27.0	3.7	N/A ^b
4	60	2	10.4	10.1	3.4	N/A ^{b,c}

^aEach dried salt was subsequently used in the sulfur ylide formation and the amount of hydrolysis was determined by LCMS analysis. In each case the levels of hydrolysis were too low to allow isolation of the acid. ^bNo hydrolysis was detected in the subsequent experiments when followed by LCMS. ^cAlternative ester used in the ylide formation.

Table 1.3.2 - Results of drying experiments on the mass of trimethylsulfoxonium chloride salts and the levels of hydrolysis by-product observed after this drying. The change in mass was used to estimate the levels of water within the salts.

In all cases the trimethylsulfoxonium salts displayed significant water content (**Table 1.3.2**), estimated from the changes in the mass of the sample, with an average water content of 3.3% by mass. Water levels above 2% are sufficient for complete ester hydrolysis, which accounted for the results seen by Leggio *et al.*¹⁷⁷ All the trimethylsulfoxonium chloride samples (**Table 1.3.2** – Entries 1-4) were different batches provided by Sigma Aldrich. Karl-Fischer titration of an additional sample from Sigma Aldrich (not shown in **Table 1.3.2**) suggested the sample assessed had 7% water by weight.¹⁷⁹ These results suggest that there is significant variation in the water content between samples, which may be due to different storage conditions.

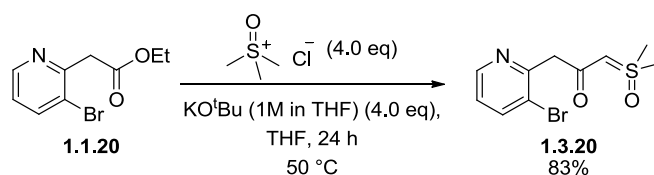
Combination of the results of the temperature dependence and drying experiments led to an improved protocol for formation of sulfur ylide (**1.3.20**), from pyridyl ester (**1.1.20**), being devised. The details of this procedure are displayed below (**Scheme 1.3.15**).



Scheme 1.3.15 - The optimised sulfur ylide formation reaction.

Gratifyingly, no hydrolysis of the ester (**1.1.20**) to the corresponding acid was detected under these reaction conditions. However, complete conversion of the starting material was not observed, with approximately 5% unreacted starting material observed by LCMS analysis after 48 h. The product was isolated by column chromatography to provide the solid crystalline material which was found to be a bench stable reagent, since no decomposition was observed by LCMS analysis after 52 weeks.

Nugent *et al.* demonstrated the importance of the equivalents of the sulfonium salt and the base in the reaction rates and conversion.¹⁷⁵ They postulate that dimethylsulfoxonium methyllide is prone to aggregation within the reaction mixture and, as the reaction progresses, this aggregation removes the active dimethylsulfoxonium methyllide species from the reaction mixture, decreasing the reaction rate. The addition of increased dimethylsulfoxonium methyllide is potentially able to mitigate this factor and increase the reaction rates and overall conversion. This theory currently remains unconfirmed; however, changes in the solvent concentration and to the rate of agitation/stirring may provide more evidence to support this hypothesis. To probe this effect, the reaction was repeated using the dried reagent, with an additional equivalent of both the base and the sulfonium salt, while maintaining a similar reaction concentration (**Scheme 1.3.16**).¹⁷⁵



Scheme 1.3.16 - The ylide (**1.3.20**) formation with an addition equivalent of base and dried trimethylsulfoxonium chloride.

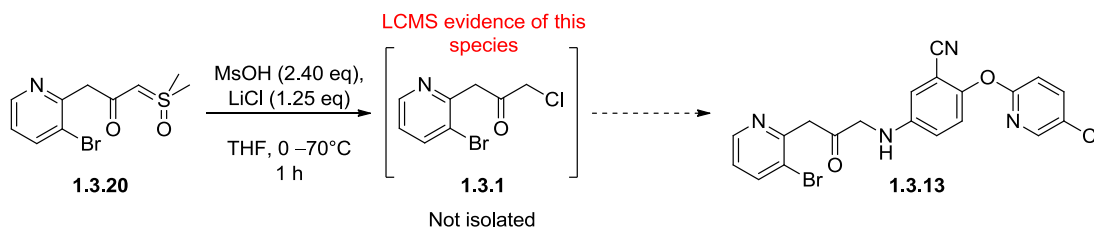
Despite the additional base and sulfur salts being unable to produce a significant change in the reaction yield, the additional equivalents were found to give an increased rate of reaction and conversion with no remaining starting material being observed in the LCMS after 24 h. It is

thought that the major source of product loss in this reaction is during purification, not the reaction itself. The highly polar nature of the ylide product necessitates prolonged chromatographic times, in polar eluents, to liberate the product. It is postulated that product loss and decomposition may occur under these conditions. However, the yields were considered sufficient to proceed with the overall synthetic strategy.

Now that a sufficiently successful method had been established to form the β -keto sulfur ylide (**1.3.20**), focus was shifted to the next stages: formation of the α -chlorocarbonyl electrophile (**1.3.1**) or the iridium-mediated insertion reaction to form the ketone (**1.3.13**).

1.3.7 Investigations into the Formation of α -Chloro Carbonyl (**1.3.1**)

As previously discussed, the treatment of sulfur ylide species with an anhydrous acid and a chloride source, has been reported to generate the corresponding α -chloroketone species.¹⁶⁹ This methodology was, therefore, explored with the sulfur ylide (**1.3.20**), as outlined below (**Scheme 1.3.17**). An additional equivalent of acid was added relative to the standard literature conditions, as the starting material has a basic pyridine moiety, which would sequester the acid under these reaction conditions.

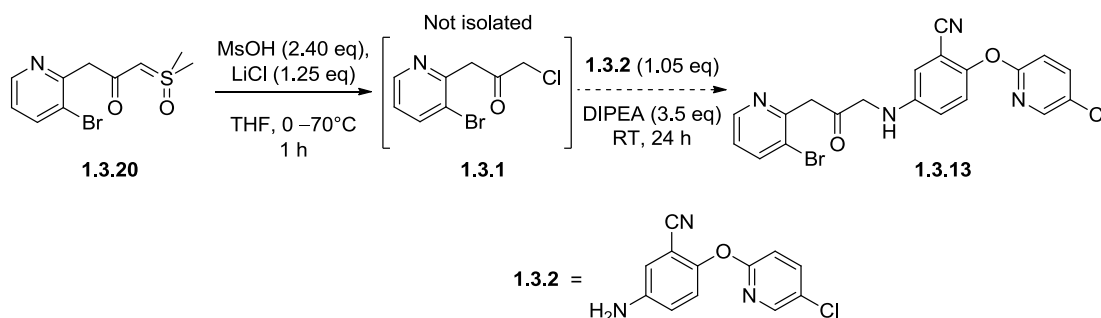


Scheme 1.3.17 – Attempted synthesis of α -chloroketone (**1.3.1**).

Complete conversion of starting material was observed after 1 h, with no remaining starting material detected by LCMS analysis. The major constituent of the crude reaction mixture was thought to be α -chlorocarbonyl (**1.3.1**), with the LCMS analysis of this species being consistent with the isotopic mass pattern of the desired product. However, we were unable to corroborate this by NMR spectroscopy, as the product appeared to be unstable upon work-up and purification.

In an effort to circumvent the issues with isolation of (**1.3.1**) a one-pot reaction was explored; forming the putative α -chloroketone intermediate (**1.3.1**) *in-situ*, before addition of the aniline

(**1.3.2**) under basic conditions (**Scheme 1.3.18**). It was envisaged that this would allow the formation of the desired ketone (**1.3.13**) without the decomposition of α -chloroketone (**1.3.1**). The introduction of the aniline (**1.3.2**) was accompanied by addition of 3.5 equivalents of base, serving the dual purpose of quenching the residual acid from the first step and preventing the accumulation of HCl from the displacement reaction.



Scheme 1.3.18 – Attempted one-pot α -chlorocarbonyl formation and subsequent $\text{S}_{\text{N}}2$ displacement by the aniline (**1.3.2**) to give ketone (**1.3.13**).

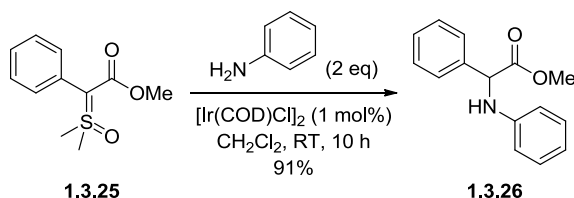
LCMS analysis, of the one-pot reaction, indicated complete conversion of the ylide (**1.3.20**) into the α -chloroketone (**1.3.1**), in an analogous fashion to that previously observed (**Scheme 1.3.17**). However, addition of the aniline (**1.3.2**) and DIPEA (3.5 eq) did not lead to formation of the desired product (**1.3.13**). LCMS analysis after 24 h revealed predominately unreacted aniline and decomposition of the chloroacetyl intermediate.

A postulated reason for the failure of this reaction was the poor nucleophilicity of the aniline (**1.3.2**). This limitation was previously overcome by Boc protection of the aniline, followed by deprotonation using the strong base, NaH, to generate a more nucleophilic species (**Scheme 1.1.4**). Although variation of the reaction conditions, such as increasing the temperature or use of a stronger base, may be beneficial for this reaction, the success of the iridium insertion reaction (*vide infra*) led to the conclusion of this work.

1.3.8 Iridium Carbenoid-mediated N-H Insertion Reaction

As discussed previously, in addition to providing a potential source of α -chlorocarbonyl electrophiles, sulfur ylides can also be utilised as carbenoid sources. The reduction in the number of synthetic steps and the incompatibility of α -chlorocarbonyl functionality with the aniline meant that further investigation was focused on exploring this methodology.

A typical example of the iridium-mediated N-H insertion reaction procedure is outlined in the scheme below (**Scheme 1.3.19**).¹⁷² The reaction was found by Mangion *et al.* in 2009 to readily proceed in high yields at ambient temperatures, with low catalyst loading for the majority of instances, after considerable optimisation.



Scheme 1.3.19 - The first reported iridium mediated N-H insertion reaction.¹⁷²

Despite the impressive yields reported, only a very limited substrate scope was established for this reaction. Mangion *et al.* only utilised relatively simple functionalities and, therefore, the tolerance of the reaction required to be established.¹⁷²

In the case of the aniline (**1.3.2**) and ylide (**1.3.20**), for the synthesis of the pre-candidate (**1.1.12**), there was concern that the significant amount of functionality may not be tolerated under the optimised conditions of Mangion *et al.*¹⁷² For example, the nitrile moiety could deactivate the catalyst through coordination to the metal centre. In the case of pyridine, potential coordination to iridium is well established. Crabtree's catalyst (**1.3.27**) exemplifies the co-ordination of pyridine to iridium, with pyridine acting as one of the ligands in this complex (**Figure 1.3.2**). This binding interaction may cause catalyst debilitation and deactivation.¹⁸⁰

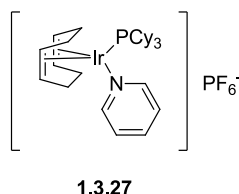
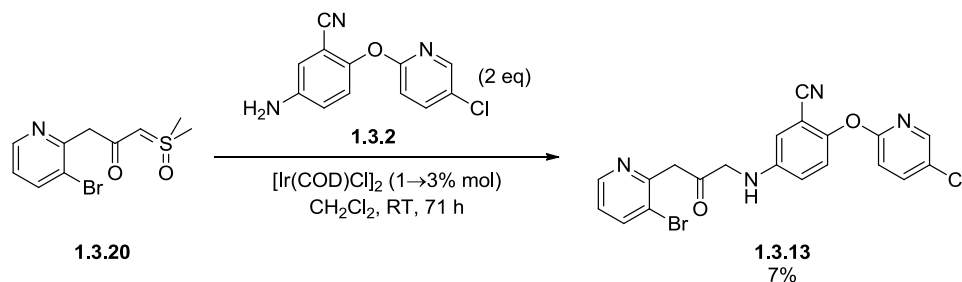


Figure 1.3.2 – Crabtree's catalyst.¹⁸⁰

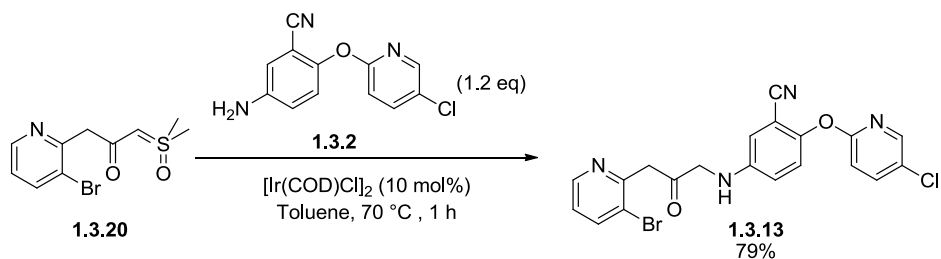
In order to determine the influence of these functionalities, the reaction was conducted on ylide (**1.3.20**) with aniline (**1.3.2**) utilising the conditions developed by Mangion *et al.*¹⁷² The results of this initial experimentation are displayed in **Scheme 1.3.20**.



Scheme 1.3.20 – Initial studies into the N-H insertion of aniline (**1.3.2**) and the sulfur ylide (**1.3.20**).

The reaction was initially conducted using 1 mol% catalyst loading. Monitoring over 24 h by LCMS showed minimal reaction conversion, with only trace amounts of the desired ketone (**1.3.13**) detected. An additional 1 mol% of the catalyst was added to the reaction in an effort to increase the reaction conversion. This addition initially resulted in increased product formation. However, the reaction rapidly stopped, with no further progression after another 24 h. Additional catalyst was added to the mixture, to give a total catalyst loading of 3 mol%, and the reaction stirred for a further 23 h. Again an initial increase in the reaction rate was observed, after which no changes in the reaction composition were observed for the remainder of the reaction duration.

It was hypothesised that the low reaction rate and conversion was a result of undesirable catalyst deactivation by either the nitrile or pyridine groups. As addition of more catalyst was able to increase the conversion of starting material to the required product, this gave confidence that the reaction could be optimised with further work. Literature precedent with more challenging substrates showed that elevating the temperature was beneficial. The impact of raising the temperature and increasing the catalytic loading was therefore evaluated (**Scheme 1.3.21**). The number of aniline equivalents was also decreased to lower the concentration of coordinating functionalities in the reaction mixture.



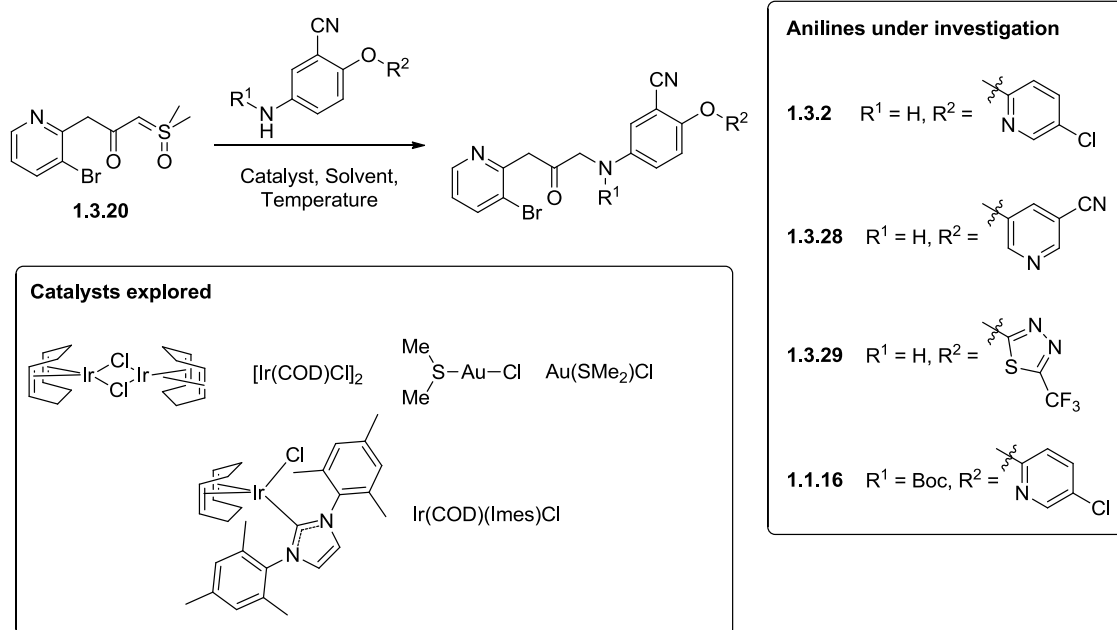
Scheme 1.3.21 – Optimisation of the iridium insertion reaction.

Gratifyingly, the isolated yield on the small scale was 79%. Unfortunately, initial scale-up (>10 g) efforts within our laboratories utilising these reaction conditions led to a reduction in the yield, with 40% isolated product¹⁸¹. However, no other route was able to provide these quantities of ketone (**1.3.13**), without a lower overall yield and increase in the number of synthetic steps. Despite this improvement on the previous synthesis, further optimisation of the reaction was required.

1.3.9 Studies into the Iridium Carbenoid Insertion Reaction

In order to deduce the factors causing lower yields on scale-up, a study into catalyst loadings, temperature, and reagent equivalents were explored to understand the governing processes of the iridium-mediated insertion reaction.

Four different anilines were selected for the insertion investigation (**Scheme 1.3.22**). Aniline (**1.3.2**) is the parent aniline in the A/B ring fragment of the pre-candidate (**1.1.10**) and is consequently of particular significance in the study. Aniline (**1.3.28**) represents an A-/B-ring combination which was synthesised as part of the medicinal chemistry SAR exploration.¹⁸² If the nitrile was responsible for the decreased reactivity through catalyst deactivation, this effect would be more pronounced with increased nitrile functionalities present in aniline (**1.3.28**). In addition to this, the pyridine nitrogen is more exposed, potentially allowing more efficient metal coordination. Aniline (**1.3.29**) is based around an unusual thiadiazole core structure. Synthetic attempts to access the corresponding borolane to this structure had been unsuccessful due to the instability of this fragment. The aniline monomer was selected to test the tolerance of sensitive functionalities to the reaction conditions. The final aniline (**1.1.16**) is the Boc protected version of (**1.3.2**). Increased steric bulk of this species may aid asymmetric ketone reduction further on in the synthetic route, by sterically defining the two enantiofaces of the ketone.



Scheme 1.3.22 – General scheme for the insertion reaction, highlighting the identities of the anilines and catalysts under investigation.

Entry	Aniline	Solvent	Temperature (°C)	Eq. of aniline	Catalyst	Catalyst loading	Yield (%) ^d
1		DCM	25	2.0		1-3%	7 ^a
2		DCM	25	1.5		10%	N/A ^b
3	1.3.2	Toluene	70	1.5	$[\text{Ir}(\text{COD})\text{Cl}]_2$	1%	N/A ^b
4		Toluene	45	1.5		10%	43 ^c
5		Toluene	70	1.2		10%	34
6		Toluene	70	2.0		10%	60
7		Toluene	70	1.1		10%	20
8	1.3.28	Toluene	70	1.5	$[\text{Ir}(\text{COD})\text{Cl}]_2$	10%	21
9		Toluene	70	2.0		10%	49
10	1.3.29	Toluene	70	1.5	$[\text{Ir}(\text{COD})\text{Cl}]_2$	10%	37
11		Toluene	70	2.0		10%	58
12	1.1.16	Toluene	70	2.0	$[\text{Ir}(\text{COD})\text{Cl}]_2$	10%	0
13		DCM	25	1.5	$\text{Ir}(\text{COD})(\text{Imes})\text{Cl}^{183}$	10%	0
14	1.3.2	Toluene	70	2.0	$\text{Ir}(\text{COD})(\text{Imes})\text{Cl}^{183}$	10%	0
15		Toluene	70	2.0	$\text{Au}(\text{SMe}_2)\text{Cl}$	10%	0

^aAdditional catalyst was added a regular intervals – see above for more details. ^bThe reactions were observed to proceed to completion by LCMS with no remaining ylide. However there was significant by-product formation and therefore attempts to isolate the product were unsuccessful. ^cIncreased amounts of by-products were observed at 45 °C with reduced crude product by LCMS. ^dThe yields may have been reduced due to unanticipated solubility issues upon column chromatography.

Table 1.3.3 - Results of N-H insertion studies using ylide (**1.3.20**) and varying the catalyst, temperature, and reaction stoichiometry.

The Au(SMe₂)Cl catalyst (**Table 1.3.3** – Entry 15) which had been designed by Mangion *et al.* was found to be incompatible with this system, with no product formation being observed.¹⁷⁴ When the authors reported this catalyst, they commented on the catalyst inability to effectively catalyse the N-H insertion of carbamates, a weaker nucleophile. The authors attribute this failure to the reduced electrophilicity of the gold carbene, relative to the iridium carbene. The surprisingly poor nucleophilicity of the aniline (**1.3.2**) and the increased steric bulk, relative to the simple examples of Mangion *et al.*, may therefore prevent the reaction with the less electrophilic carbene species. The failure of the Boc protected aniline (**1.1.16**) to undergo N-H insertion reactions (**Table 1.3.3** – Entry 12) may be similarly attributed to the reduced nucleophilicity and even greater steric bulk, relative to aniline (**1.3.2**).

The Ir(COD)(Imes)Cl catalyst developed by Kerr *et al.* was explored as a potential catalyst due to its well-established reversible binding to pyridine.¹⁸³ If pyridine coordination was contributing to catalyst deactivation, then it was envisaged that this catalyst should display increased activities and subsequently increased yields. Disappointingly, this catalyst was found to be inactive in this reaction, both at ambient and elevated temperatures.

Increasing the reaction temperatures to either 45 °C or 70 °C was found to have a beneficial effect upon the reaction. In the case of aniline (**1.3.2**), raising the temperature increased the yields from less than 10% at ambient temperature (**Table 1.3.3** – Entries 1-2), to over 40% at 45 °C and above (**Table 1.3.3** – Entries 4 and 6). Increasing the temperature from ambient temperature (**Table 1.3.3** – Entry 2) to 45 °C (**Table 1.3.3** – Entry 4), as well as changing the solvent from DCM to toluene to allow access to higher reaction temperatures, with 1.5 equivalents of the aniline (**1.3.2**), increased both the levels of product formation and reduced the levels of the by-product formation.

Increasing the temperature to 70 °C (**Table 1.3.3** – Entry 5) led to further reductions in the by-product levels and improved product formation in the crude reaction mixture, as well as increased reaction rates, as assessed by LCMS.

The overall decrease in the isolated yield (**Table 1.3.3** – Entry 5), relative to the 45 °C experiment (**Table 1.3.3** – Entry 4), was thought to be a consequence of variations in the purification method employed, rather than the increase in ylide equivalents. All experiments apart from Entry 4, **Table 1.3.3** were purified through solid loading onto Florisil and

subsequent flash column chromatography. This method led to unanticipated compound loss due to crystallisation of product on the surface of the silica column. Eluting the column with a polar solvent after purification was found to liberate more material. In the case of the experiment carried out at 45 °C (**Table 1.3.3** – Entry 4), the reaction mixture was liquid loaded due to the increased levels of by-products. In this instance, washing the column with high polarity solvent did not liberate any further product. Therefore, this modification to the purification may have circumvented the solubility issues and, therefore, caused a disproportionately high yield, relative to (**Table 1.3.3** – Entry 5). However, the greatest yield was observed at 70 °C (**Table 1.3.3** – Entry 6), with two equivalents of the aniline (**1.3.2**).

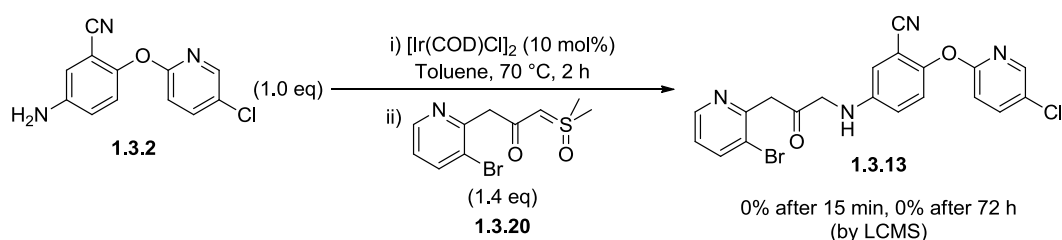
At 70 °C the [Ir(COD)Cl]₂ catalyst was found to be competent for the three non-protected anilines (**1.3.2**, **1.3.28**, and **1.3.29**). Increased aniline equivalents (**Table 1.3.3** – Entries 7-9), from 1.1 to 2.0, were also found to increase the overall yield of the reaction from 19% to 49% in the case of aniline **1.3.28**. In all cases, the unreacted aniline was stable under the reaction conditions and could be recycled after isolation by column chromatography. The yields for the reactions with the two anilines (**1.3.2** and **1.3.29**) were found to be comparable (**Table 1.3.3** – Entries 6 and 11), with slight reductions in the yield for the aniline (**1.3.28**) (**Table 1.3.3** – Entry 9), which contains two nitrile functionalities. It was proposed that this could be a consequence of increased interference by the coordinating nitriles, but further data would be required to more fully support this proposal.

1.3.10 Studies into the Deactivation of the Iridium Catalyst

As discussed previously (**Section 1.1.6**) the presence of both pyridyl and nitrile groups have been shown to coordinate to metal centres and inhibit catalysis.^{96–99,107} The requirements for higher temperatures and catalyst loading, relative to the conditions reported by Mangion *et al.*, imply that the pyridyl or the nitrile groups in both the ylide and the anilines interact with the iridium catalyst. This hypothesis is supported by the initial experiment (**Scheme 1.3.20**) where additional catalyst was found to give a small increase in product levels before no further progression was observed. In order to deduce which functionality is responsible for this potential deactivation, several experiments were conducted.

The first two experiments were designed to ascertain if the aniline reactant (**1.3.2**) is responsible for the catalyst deactivation, and to demonstrate whether the catalyst is inhibited under the reaction conditions. To probe this hypothesis, the aniline (**1.3.2**) was added to a

mixture of the catalyst and solvent at 70 °C, 2 h prior to the addition of the ylide (**1.3.20**) (**Scheme 1.3.23**). Previous observations confirmed the decomposition of the ylide (**1.3.20**) under the reaction conditions, therefore, the reaction stoichiometry was inverted. Inversion of the stoichiometry ensured the ylide (**1.3.20**) was present to perform the reaction, and the decomposition of excess ylide enhanced the ability to monitor the reaction by LCMS and facilitated the purification of the product, if necessary.

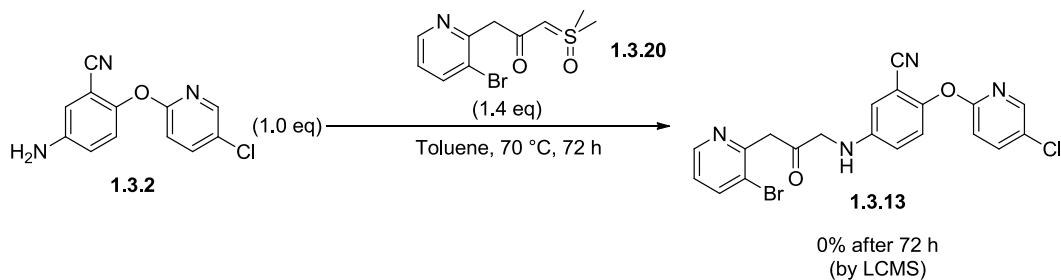


Scheme 1.3.23 – Probing the potential deactivation of the catalyst by aniline (**1.3.2**).

The pre-addition of the aniline prior to the ylide dramatically influenced the N-H insertion reaction (**Scheme 1.3.23**), causing complete catalyst deactivation. To demonstrate that these changes were mediated by the aniline (**1.3.2**), rather than the action of a potential degradation by-product, the mixture was assessed by LCMS immediately after aniline addition, and again after 2 h, prior to the ylide addition. In both instances the same LCMS spectra were obtained suggesting that aniline (**1.3.2**) is stable under the reaction conditions, and that any changes in the reaction profile can therefore be attributed to the aniline (**1.3.2**) interacting with the catalyst. LCMS analysis of the reaction composition, 15 minutes after the ylide (**1.3.20**) addition, showed very slight changes, with the only significant change being the observation of 3% of a new unidentified by-product. After 72 h, no ketone (**1.3.13**) was observed by LCMS, with the major components of the reaction mixture being: 51% aniline (**1.3.2**), 10% unknown by-product, and 5% ylide (**1.3.20**), with lower levels of other by-products which may correspond to the loss of DMSO from the ylide (**1.3.20**).

In previous examples (**Section 1.3.9**), under comparable reaction conditions, without the pre-addition of the aniline (**1.3.2**), complete conversion of the ylide had been observed within 1 h for a range of different aniline substrates. With no product formation being observed after 72 h with the pre-addition of the aniline (**1.3.2**), this suggests that an irreversible interaction between the aniline (**1.3.2**) and the catalyst is occurring, resulting in a complete loss of activity. Although some consumption of the ylide (**1.3.20**) was observed under the reaction conditions, it was hypothesised that this is a consequence of thermal instability of the ylide, rather than

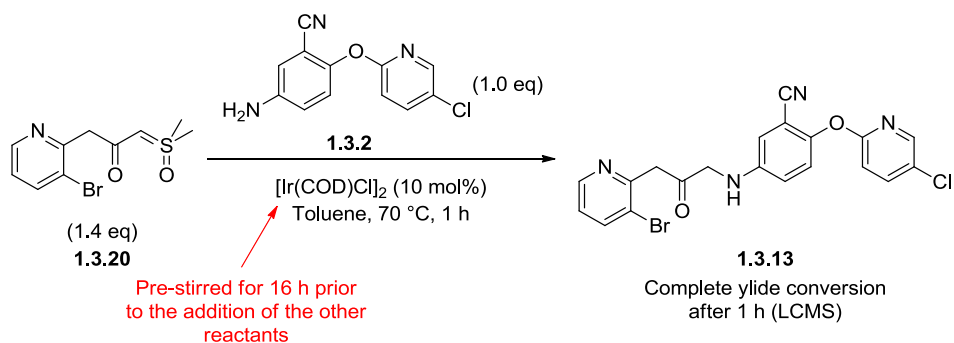
any iridium-mediated processes. To confirm this, the reaction conditions were replicated without the iridium catalyst (**Scheme 1.3.24**).



Scheme 1.3.24 – Exploring the thermal stability of the ylide (**1.3.20**).

As anticipated, under these reaction conditions no desired product was formed. Again, the same unidentified by-product was formed, with significant levels of the aniline and reduced levels of the ylide. The comparable reaction profile to the deactivation study (**Scheme 1.3.23**) demonstrates that the catalyst is indeed having no impact on the reaction progression in either reaction.

As previously discussed (**Section 1.1.6**) interaction and deactivation of metal complexes by both nitrile and pyridyl functionalities is well-established. This supports the hypothesised deactivation of the catalyst by the aniline (**1.3.2**). However, an alternative is also plausible. The loss of catalytic activity could also potentially be attributed to the decomposition of the catalyst under the elevated reaction temperatures. To confirm that this was not the case, the insertion N-H was replicated, however, the catalyst was stirred in toluene at 70 °C prior to the addition of the aniline (**1.3.2**) and the ylide (**1.3.20**) (**Scheme 1.3.25**).

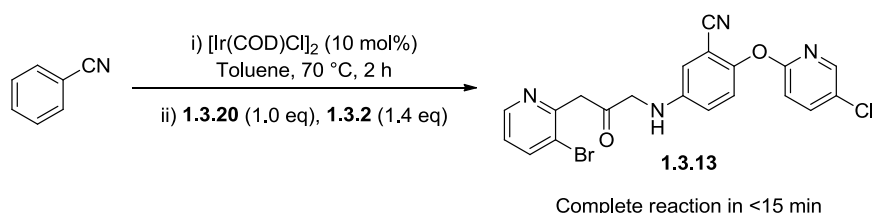


Scheme 1.3.25 – Assessing the catalyst stability under typical N-H insertion reaction conditions.

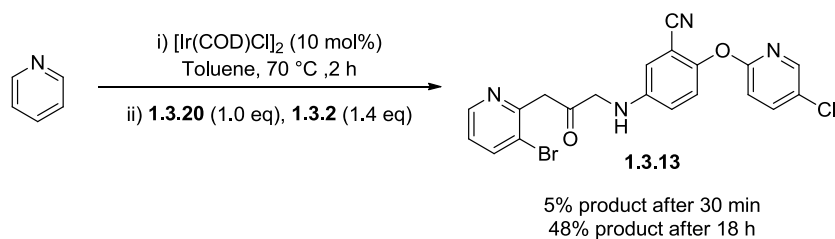
Gratifyingly, under these reaction conditions, a comparable reaction profile was observed relative to previous examples (e.g. **Scheme 1.3.21**), with only the unreacted aniline (**1.3.2**) and the product (**1.3.13**) being detected in significant levels by LCMS analysis. This confirms that it is the influence of the aniline (**1.3.2**) which is responsible for the loss in catalytic activity observed in the earlier experiments (e.g. **Scheme 1.3.23**), rather than catalyst degradation under the reaction conditions.

With the aniline (**1.3.2**) being determined as the major source of deactivation, investigations into how this deactivation is manifested were initiated. As previously discussed, it was thought that this loss of activity was a consequence of either the pyridyl or nitrile groups. Although the aniline functionality could also theoretically coordinate to the metal, the wide range of different anilines utilised previously under milder reaction conditions with lower catalyst loadings by Mangion *et al.*,¹⁷² suggests that the aniline is not responsible for the significant catalyst deactivation observed.

In order to explore which one of the pyridyl or nitrile groups were responsible for the catalyst deactivation, two experiments were designed (**Scheme 1.3.26** and **Scheme 1.3.27**). The first experiment (**Scheme 1.3.26**) involved the pre-incubation of the catalyst with benzonitrile and the second (**Scheme 1.3.27**) with pyridine, prior to the addition of the aniline (**1.3.2**) and ylide (**1.3.20**). The relative rates of the reaction could then be utilised to determine which functionality has a great influence on the catalyst.



Scheme 1.3.26 - Assessing the influence of the aromatic nitrile functionality on the insertion reaction.



Scheme 1.3.27 – Assessing the influence of the pyridyl functionality on the insertion reaction (product formation was determined by LCMS analysis).

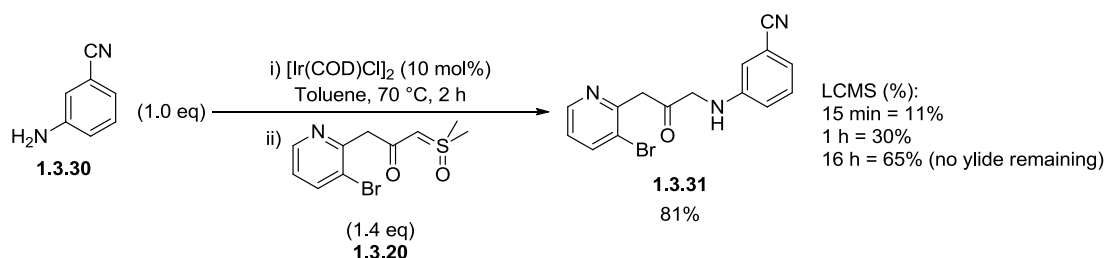
In the case of the benzonitrile example (**Scheme 1.3.26**), no decrease in the reaction rate was observed, with a comparable reaction profile to the previous examples (e.g. **Scheme 1.3.20**) excluding the benzonitrile. This result strongly suggests that the nitrile group is not the major cause of the catalytic loss and that the nitrile group is tolerated under the reaction conditions.

In contrast to this, the addition of pyridine to the reaction caused a dramatic decrease in the reaction rate, with only 5% product being detected after 30 minutes (**Scheme 1.3.27**). Although complete conversion of the ylide was observed after protracted reaction times, 18 h, LCMS analysis suggested lower levels of product were formed, in addition to increased levels of the ketone by-product formed by the loss of DMSO. However, in comparison to the initial deactivation experiment (**Scheme 1.3.23**), significant reactivity is still retained.

This implies that although pyridine complexes the iridium catalyst, this interaction is reversible under the reaction conditions. Initially the pyridine sequesters the catalyst, before slowly dissociating from the iridium and enabling the formation of the active catalyst. The slight decrease in the yield, in addition to the increased levels of by-product formation, may therefore be attributed to the thermal decomposition of the ylide as previously observed (**Scheme 1.3.24** and **Scheme 1.3.25**). However, despite this loss of activity, this is unable to explain the total loss of catalytic activity observed with the elaborated aniline (**1.3.2**) (**Scheme 1.3.23**).

With both the studies with simplified pyridyl and nitrile substrates been unable to explain the total loss of catalytic activity, further studies were necessitated. It was postulated that the differences in the both electronic and steric environment of the pyridyl group in aniline (**1.3.2**) may serve to strengthen the interaction with the iridium centre, causing irreversible catalyst inhibition. To confirm that the aniline (**1.3.2**) pyridyl group is indeed responsible for the deactivation, rather than the aniline or the nitrile, the insertion reaction was conducted with

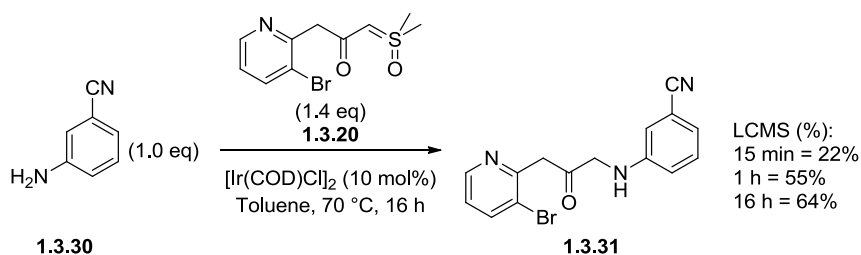
the alternative truncated aniline (**1.3.30**). It was envisaged that the absence of the pyridyl unit would lead to rapid insertion, even in the case of pre-stirring the catalyst with the aniline (**1.3.2**) (**Scheme 1.3.28**) due to the absence of the deactivating functionality.



Scheme 1.3.28 – Iridium mediated N-H insertion of the truncated aniline (**1.3.30**).

Gratifyingly, the reaction proceeded to completion, with an isolated yield of 81%. However, unexpectedly, the reaction was found to proceed significantly slower than the comparable elaborated anilines (e.g. **Scheme 1.3.21**). Although this could be indicative of some coordination of the catalyst by the aniline (**1.3.30**), an alternative explanation is that the insertion occurs slower with the more electron poor aniline (**1.3.30**), leading to a slower attack on the iridium carbenoid, and subsequently a increased reaction time.

To determine which of these effects is operative, the reaction was repeated without the pre-stirring of the catalyst and the aniline (**Scheme 1.3.29**). If a significant difference in the reaction rate was observed this would suggest that either the nitrile or the aniline groups in the substrate (**1.3.30**) contribute to iridium deactivation.

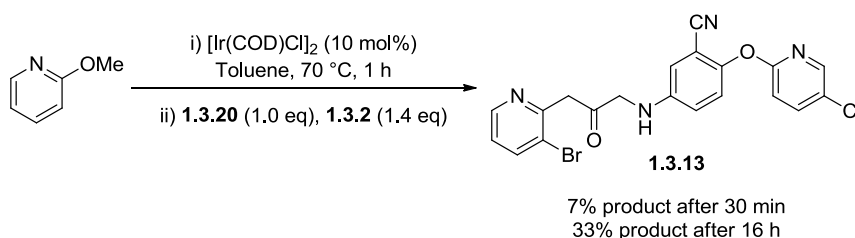


Scheme 1.3.29 – Iridium mediated N-H insertion of aniline (**1.3.2**) without the pre-stirring of the aniline and the catalyst.

In comparison to the pre-stirring experiment (**Scheme 1.3.28**), LCMS analysis showed a small increase in the reaction rate (**Scheme 1.3.29**) without the pre-addition step. However, in both

cases the reaction profile obtained was almost identical, with around 65% product at the end of the reaction, in addition to the excess aniline, catalyst, and toluene. Therefore, although the addition of the aniline species may mediate a small influence on the reaction rate which could be due to a weak coordination, the overall slower rate relative to the extended aniline (**3.2**) may be a consequence of the reduced nucleophilicity of the aniline. In the case of the extended aniline, the additional electron-donation from the oxygen may enhance the nucleophilicity of the aniline helping facilitate the reaction. Analysis of other anilines with a variety of electron-donating and withdrawing groups may be able further support this hypothesis. However, this is beyond the current scope of this report.

With several inhibition experiments having now been conducted, the greatest levels of catalyst deactivation were observed with pyridine (**Scheme 1.3.27**) and the extended aniline (**1.3.2**) (**Scheme 1.3.23**). However, there was still significant disparity between these two results, with the pyridine example still showing significant reaction conversion. It was postulated that in the case of the extended aniline (**1.3.2**), the additional electron-donating oxygen enhances the coordinating ability of the pyridine, resulting in stronger coordination and greater catalyst deactivation. To assess this, a final experiment was conducted in analogous fashion to the previous pyridine experiment (**Scheme 1.3.27**), but using electron rich 2-methoxy pyridine (**Scheme 1.3.30**).



Scheme 1.3.30 – Investigating the influence of the electron rich 2-methoxy pyridine on the N-H insertion reaction.

Surprisingly, no significant change in the reaction profile was observed with 2-methoxy pyridine, relative to the pyridine example (**Scheme 1.3.27**). Complete reaction conversion was observed by LCMS analysis after 16 h, with the lower percentage area being influenced by the stronger chromophore of the 2-methoxy pyridyl, relative to the pyridine. Therefore, despite protracted reaction rates in both pyridyl cases (**Scheme 1.3.27** and **Scheme 1.3.30**), these additives are unable to explain the complete loss of activity with the elaborated aniline (**3.2**). Interestingly, the inhibition studies with both the nitrile (**Scheme 1.3.26** and **Scheme 1.3.28**)

and pyridyl substrates (**Scheme 1.3.27** and **Scheme 1.3.30**) suggest that both these functionalities are tolerated under the reaction conditions.

In conclusion, these studies demonstrate that aniline (**1.3.2**) is able to interact with the iridium catalyst in a fashion which cannot be accounted for by consideration of any of the functionalities which comprise the molecule in isolation. The strength of this interaction, observed by the irreversible inhibition, could mean that a bidentate interaction is formed, for example through the pyridyl and the nitrile, or the pyridyl and the π cloud of the adjacent aniline. Alternatively, it could be due the steric environment of the coordinating functionality, preventing any dissociation from the iridium catalyst.

To further understand this observation, the next proposed stage in the inhibition studies would be using various elaborated anilines, such as those in the previous study (**Table 1.3.3**). The change in the A-ring and the corresponding influence on the inhibition may enable the source of this interaction to be determined. Other experiments utilising anilines without the pyridyl, ether linker, or nitrile may also increase the understanding of the process occurring.

However, due to the scarcity of the aniline derivatives and the considerable effort required to synthesise them, further studies were not conducted. It has been demonstrated that the aniline (**1.3.2**) irreversibly deactivates the catalyst, which necessitates the modified temperature and reaction protocol relative to that of Mangion *et al.*¹⁷²

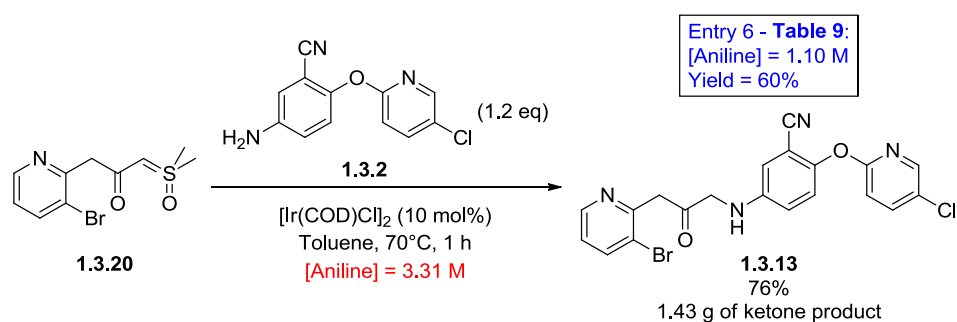
1.3.11 Further Optimisation of the Iridium Insertion Reaction

With the understanding generated from the N-H insertion studies (**Table 1.3.3**) and the inhibition work (**Section 1.3.10**), further modifications to the insertion reaction were explored to enable a high yielding and scalable reaction to be developed.

Evidence that the ketone products suffer from poor solubility (**Table 1.3.3** – Entry 4) meant that liquid phase loading was adopted going forward as the standard method of purification in order to maximise yields. It was envisaged that this would prevent any product loss due to the product not being correctly dissolved onto the column, which appeared to occur with solid loading protocols.

In the previous successful N-H insertion reactions (for example **Table 1.3.3**), analysis of the crude reaction mixtures predominately showed the desired ketone, unreacted aniline, and smaller percentages of a wide range of unidentified by-products. Although in all experiments complete conversion of the ylide (**1.3.20**) was observed, this did not always lead to high yields of the desired ketone (e.g. **Table 1.3.3** – Entry 7). This suggested that although all the ylide was converted to the iridium carbenoid, this species was highly unstable, and rapidly decomposed or underwent undesirable side reactions in the reaction mixture.

It was therefore postulated that the correlation between the yields and the equivalents of the aniline (**Table 1.3.3**) were a consequence of the increased concentrations of the aniline in the reaction mixture, increasing the rate of the desired reaction and reducing the proportion of undesired carbenoid decomposition. To test this hypothesis the reaction was repeated with an increased concentration of the aniline (**1.3.2**) (**Scheme 1.3.31**), relative to the previous experiments (e.g. **Table 1.3.3** – Entry 6).

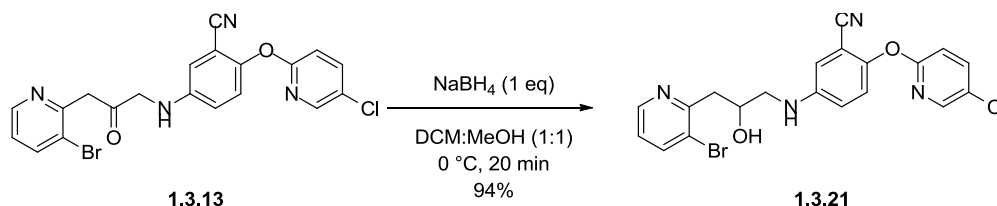


Scheme 1.3.31 – The modified iridium insertion reaction with increased reaction concentration.

Gratifyingly, increasing the concentration of aniline gave significant increases in the reaction yield of (**1.3.13**) from (**1.3.2**) and (**1.3.20**), observed in both the crude LCMS and the isolated yields, as well improving the sustainable chemistry metrics through reduction of the solvent volume. In addition to this, the number of aniline equivalents could be reduced to 1.2 equivalents, while still maintaining the good yield. This improvement to the reaction allowed the gram scale reaction to be performed with good yields (76%).

As a protocol for a high yielding, large scale iridium-mediated insertion had now been demonstrated (**Scheme 1.3.31**) the resulting reduction was investigated. The resulting ketone

(**1.3.13**) could be readily reduced with NaBH₄ to yield the alcohol (**1.3.21**) in excellent yields (**Scheme 1.3.32**).



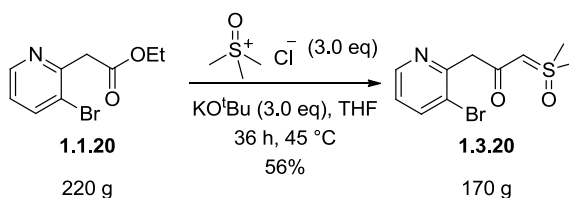
Scheme 1.3.32 –Racemic reduction of the ketone (**1.3.13**).

1.3.12 Scale-up of the Pre-candidate (1.1.12) Utilising Iridium-mediated Methods

The sulfur ylide methodology developed provides significantly improved access to the late stage intermediate (**1.3.21**) to form pre-candidate (**1.1.12**) (**Scheme 1.3.35**). The synthesis reduces the number of steps in addition to removal of the requirements for protecting groups and activating groups.

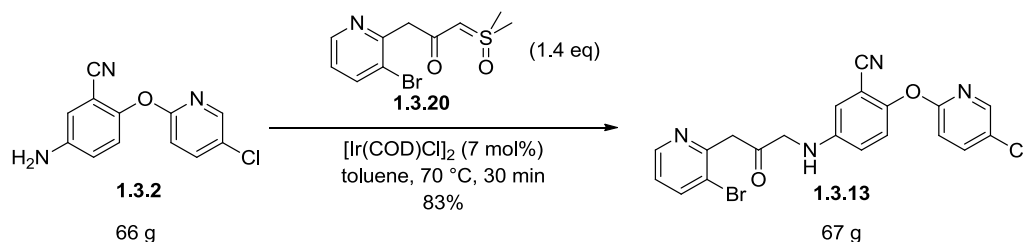
The success of this chemistry has led to it being utilised in scale-up operations of the pre-candidate molecule (**1.1.12**) by the contract research organisation, GVKBio. Several minor modifications to the ylide formation (**Scheme 1.3.33**) and subsequent insertion reactions (**Scheme 1.3.34**) have been made to optimise the process for scale-up.

The procedure below (**Scheme 1.3.33**) represents the modified ylide (**1.3.20**) formation reaction. The need for chromatography has been removed by alterations to the work-up procedure. An aqueous wash, followed by trituration with diethyl ether was able to avoid the need for chromatography. These modifications also led to a slight reduction in the isolated yield, from 80% to 64% but this is offset by the absence of chromatographic methods. Using this method, reactions on >100 g scale can readily be conducted.¹⁸⁴



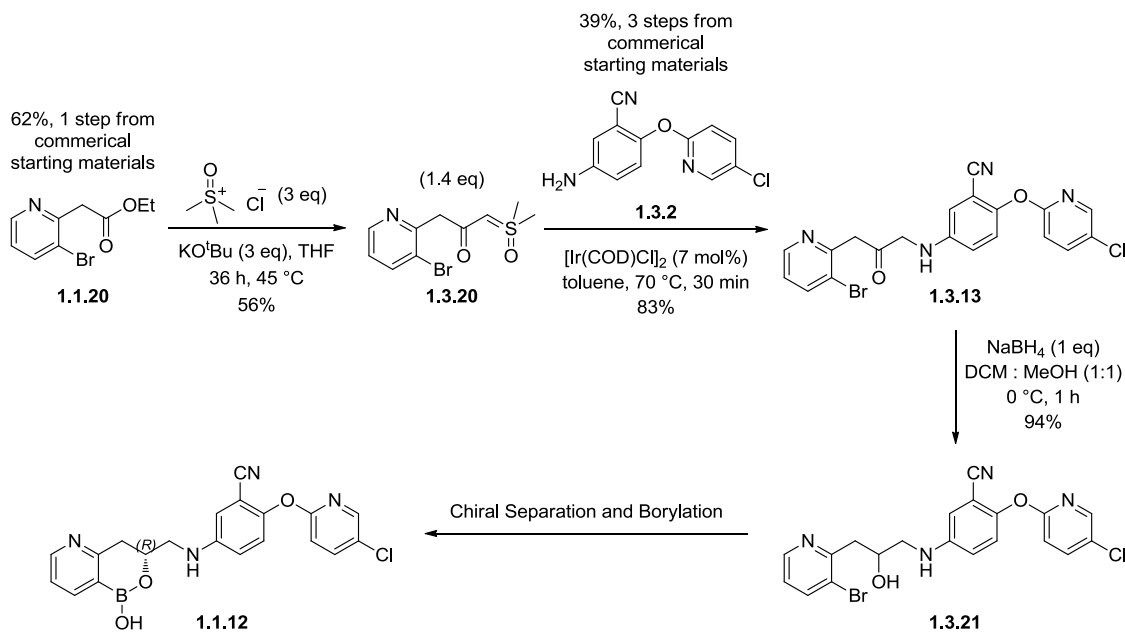
Scheme 1.3.33 – Reaction conditions for the scale-up of the sulfur ylide (**1.3.20**).¹⁸⁴

It has been found that the crude ylide can be utilised in the iridium-mediated N-H insertion without any detrimental effect upon the reaction yields (**Scheme 1.3.34**). In order to aid the separation and to maximise the total yields of the synthesis, the stoichiometry of the reaction was reversed (**Scheme 1.3.34**).¹⁸⁵ The use of the ylide in excess, leads to almost complete consumption of the aniline. The excess ylide (**1.3.20**) breaks down under the reaction conditions. This leaves the ketone as the major constituent of the reaction mixture, enabling facile purification.



Scheme 1.3.34 – Scale-up of the iridium insertion reaction to afford ketone (**1.3.13**).¹⁸⁵

Utilising this chemistry, multiple grams of the pre-candidate molecule have been synthesised (**Scheme 1.3.34**). This new route has a reduction in the total number of linear synthetic steps, from 11 (**Scheme 1.1.4**) to 6 (**Scheme 1.3.35**). The overall yield has increased from 0.9% to 8.0%. The route is also more sustainable and displays greater atom efficiency due to the absence of protecting and activating groups. This chemistry is now the main synthetic method to access borolane pre-candidate (**1.1.12**), enabling access to large quantities of material, which were previously inaccessible.



Scheme 1.3.35 – The scale-up route to the borolane pre-candidate (**1.1.12**).¹⁸⁵

1.3.13.1 Applicability of the Sulfur Ylide Chemistry to Other Targets

Establishment of a concise, high yielding method to access the pre-candidate (**1.1.12**) not only has ramifications for progression of the pre-candidate molecule (**1.1.12**), but the route can also be applied to other potential borolane targets. This methodology has the potential to allow rapid synthesis of borolane analogous and provide access to previously inaccessible synthetic targets.

The applicability of the chemistry towards previously inaccessible synthetic targets is outlined in the following example. The thiadiazole target (**1.3.32**) (**Figure 1.3.3**) contains a diverse range of functionalities which had inhibited previous synthetic attempts to access the molecule, for example when utilising an analogous strategy to that detailed in **Scheme 1.1.4**.

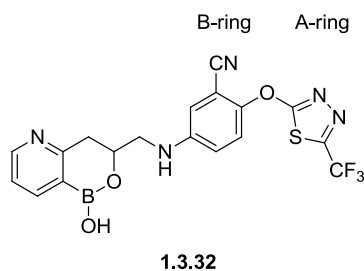
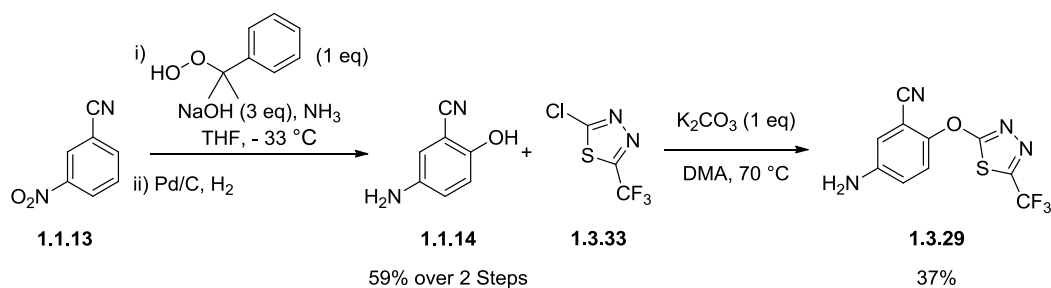


Figure 1.3.3 - Structure of the borolane (**1.3.32**) selected to demonstrate the scope of the iridium chemistry.

The A/B ring combination exemplified in thiadiazole (**1.3.32**) was initially proposed as part of the lead optimisation. Unsuccessful efforts were made to combine this aniline motif with several different borolane cores. The failure to synthesise the molecule was due to two key factors. The first factor was the poor stability of the A-ring, which decomposed under a variety of reaction conditions.¹⁸⁶ The most significant A-ring decomposition was observed in the final borylation step reaction. The second issue was the protracted nature of the synthetic route.¹⁸⁷ This meant that significant loss of material reduced the quantities available for the final reaction step, preventing a systematic approach into the improvement of the borylation process. It was envisaged that synthesis of the aniline (**1.3.29**) and subsequent reaction with ylide (**1.3.20**) would overcome these previous issues.

1.3.13.2 Synthesis of the Aniline Fragment

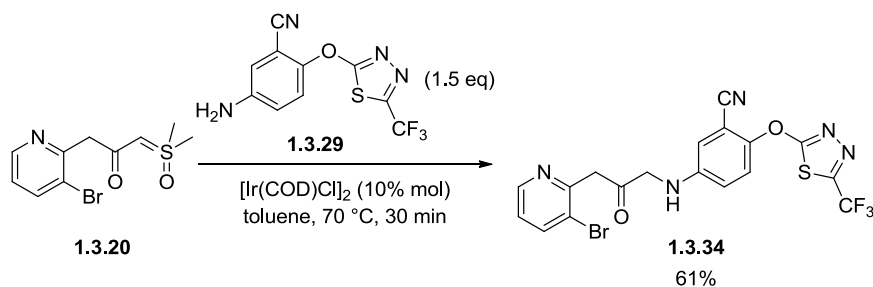
Previous synthetic investigations established a reliable method to access the aniline (**1.3.29**) (**Scheme 1.3.36**).¹⁸⁸ The synthesis utilises an analogous strategy to that of the synthesis of the pre-candidate aniline (**1.3.2**), coupling the two rings together with an S_NAr reaction (**Scheme 1.3.36**). Base-mediated S_NAr of the common aniline (**1.1.14**) with the commercially available thiadiazole species (**1.3.33**) gave the required starting material on a multi-gram scale (**1.3.29**).²¹



Scheme 1.3.36 – Synthesis of the aniline component of the thiadiazole borolane (1.3.29).²¹

1.3.13.3 Iridium-mediated Coupling Reaction and Subsequent Reduction

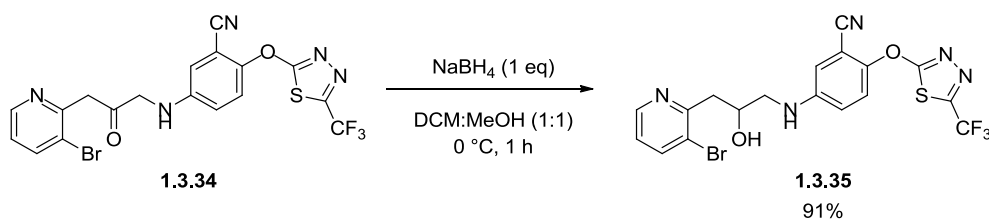
The optimised ylide insertion chemistry was applied to the synthesis of thiadiazole borolane (1.3.32) (Figure 1.3.3). The results of the application of this methodology are displayed below (Scheme 1.3.37).



Scheme 1.3.37 – The iridium-mediated N-H insertion reaction with the thiadiazole aniline (1.3.29) to afford ketone (1.3.34)

The reaction provided a gram of the ketone (1.3.34) for further synthetic manipulation and in good yield, illustrating the success of the chemistry on a moderate scale. Despite reduction of the number of equivalents of the aniline (1.3.29) used, the previous yield was maintained (Table 1.3.3 – Entry 11). This provides more evidence for the significance of the reaction concentration as the more dilute example was only able to provide a yield of 37% on small scale (Table 1.3.3 – Entry 10).

The ketone reduction was conducted in analogous fashion to the pre-candidate molecule synthesis (Scheme 1.3.32). Gratifyingly the NaBH₄-mediated reduction was found to proceed in good yields with no reduction of the thiadiazole ring structure being observed (Scheme 1.3.38).

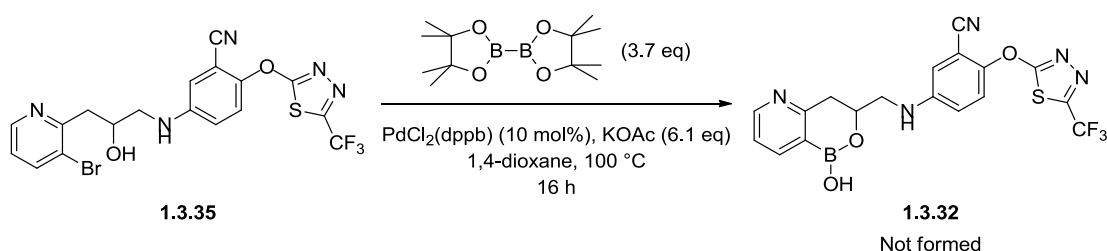


Scheme 1.3.38 – Reduction of the thiadiazole containing ketone (**1.3.34**).

This series of synthetic steps was able to provide facile access to the alcohol intermediate (**1.3.35**) prior to borylation. The short, reliable synthesis was able to provide sufficient material to investigate the borylation, while previous syntheses typically only provided sufficient material to assess one set of borylation conditions.

1.3.13.4 Borylation of the Thiadiazole-containing Alcohol (**1.3.35**)

Based upon the relative success with the borylation in the pre-candidate synthesis, these conditions were chosen as a starting point of the borylation investigation. It was envisaged that due to the homology between the two alcohol substrates, the borylation reaction would proceed successfully with the thiadiazole compound. The reaction is displayed below (**Scheme 1.3.39**).

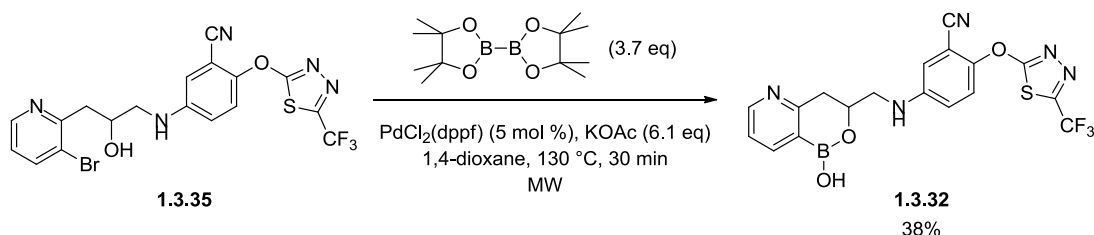


Scheme 1.3.39 – Attempted borylation using thermal reaction conditions.

The reaction was monitored periodically by LCMS. No product formation was detected throughout the reaction. After 16 h a multi-component reaction profile was detected, including starting material and fragmentation products. This result was consistent with the results of previous borylation studies carried out in our laboratories with the thiadiazole ring structure present.^{186,187}

Attention was switched to conducting borylation reactions under microwave conditions, utilising a $\text{Pd}(\text{dppf})\text{Cl}_2$ catalyst, as these conditions had been successful in the pyridone borolane synthesis (**Scheme 1.2.22**). It was hypothesised that the success with the unstable

pyridone implies that this represents a more tolerant borylation method. The results of the microwave reaction are displayed below (**Scheme 1.3.40**).



Scheme 1.3.40 – Borylation of the thiadiazole (**1.3.35**) to afford borolane (**1.3.32**) under microwave irradiation conditions.

Gratifyingly, conducting the reaction under microwave conditions was able to produce significant product (**1.3.32**) with only minimal dehalogenation/deborylation or thiadiazole decomposition. This allowed the assessment of the potency of the previously unobtainable A-/B-ring combination.

Although the borolane (**1.3.32**) suffered from poor selectivity for Lp-PLA₂ over PLA₂-VIIB (**Table 1.3.4**) this rapid synthesis allowed facile assessment of a previously unobtainable target, demonstrating the wider applicability of this methodology.

Structure	cLogP	pIC ₅₀ (Lp-PLA ₂ enzyme)	pIC ₅₀ (Lp-PLA ₂ plasma)	pIC ₅₀ (PLA ₂ -VIIB enzyme)	Selectivity
	2.0	7.9	7.2	6.4	62

Table 1.3.4 – Biological data for thiadiazole borolane (**1.3.32**).¹⁸⁹

1.3.14 Further Expansion of the Iridium Methodology

The success of the iridium methodology has led to this method becoming the standard synthesis for elaborated borolane structures, supplanting other longer synthetic routes for lead optimisation synthetic targets. The methodology is attractive due to the short, high yielding processes and the capability of late stage diversification of the A-/B-ring motifs.

A wide range of A-/B-ring variations of the pyridyl borolane core have been rapidly assembled utilising ylide (**1.3.20**) and variation of the aniline. **Figure 1.3.4** shows some examples of analogues accessed *via* the ylide chemistry from elsewhere in our laboratories, demonstrating the substrate scope.^{190–192}

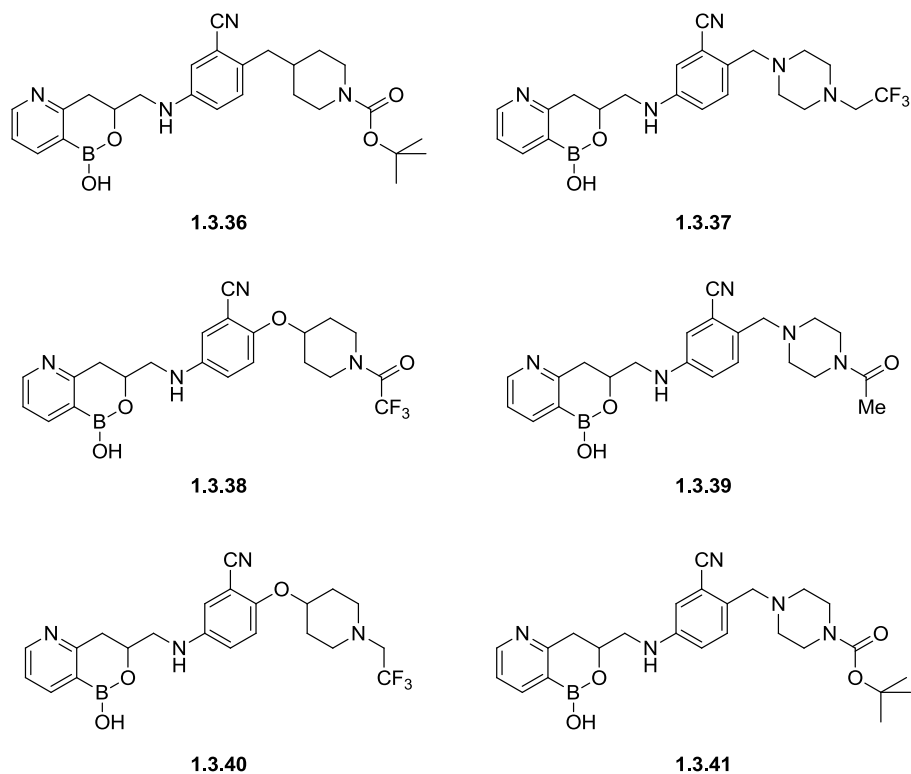


Figure 1.3.4 – Examples of borolanes synthesised utilising the ylide chemistry from ylide (**1.3.20**).^{190–192}

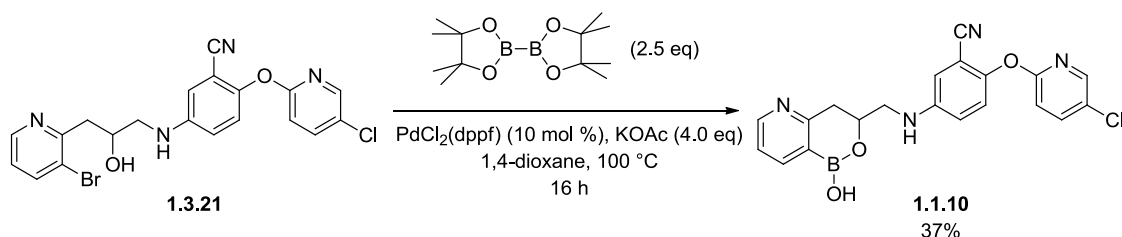
The examples in **Figure 1.3.4** illustrate the impact that the borolane chemistry has conveyed upon the SAR work. The analogues could be rapidly synthesised using the iridium methodology, allowing a vast array of different functionalities to be rapidly assessed. Without this synthetic methodology giving rapid access into the to A-/B-ring systems, a complete assessment of the wide range of A- and B-rings would not have been feasible, due to the synthetic intractability and time constraints. The examples above (**Figure 1.3.4**) represent a small subset of borolanes which have been synthesised utilising this chemistry.

1.4 Investigations into the Key Borylation Step

1.4.1 Issues with the Borylation

As previously discussed, borylation is typically the last synthetic step in the synthesis of the borolane analogues. Although the ylide chemistry shortened the synthesis and increased the yields, the borylation reaction remained inefficient, with yields typically below 40%. Typically the borylation reaction is associated with undesirable dehalogenation, causing significant reduction in yields. Additionally, the polarities of the product and by-product are very similar, complicating the purification stages. Therefore, to ensure sufficient purity for biological assessment, the molecules often require several purification stages, further diminishing the reaction yields.

Although multiple methods for the introduction of the boron centre exist, due to issues of functional group tolerance (**Section 1.1.6**), this is accomplished through a Miyaura borylation reaction. Typical reaction conditions are displayed below (**Scheme 1.4.1**).



Scheme 1.4.1 – Example of the Miyaura borylation to give the racemic pre-candidate molecule (**1.1.10**).⁹¹

1.14.2 Mechanistic Considerations and the Source of Dehalogenation

For the synthesis of simple borolane analogues, the Miyaura borylation reaction was found to proceed in reasonable yields, typically above 60%, within our laboratories.^{68,193} However, the elaborated structures often displayed diminished yields, with typical yields of less than 40% being observed (**Scheme 1.4.1**).^{91,106} In order to develop an improved procedure, the mechanism of the reaction was analysed to establish whether this offered any insights on how to improve the yield by modifying the reaction conditions. The accepted mechanism of the Miyaura borylation is displayed below (**Figure 1.4.1**).

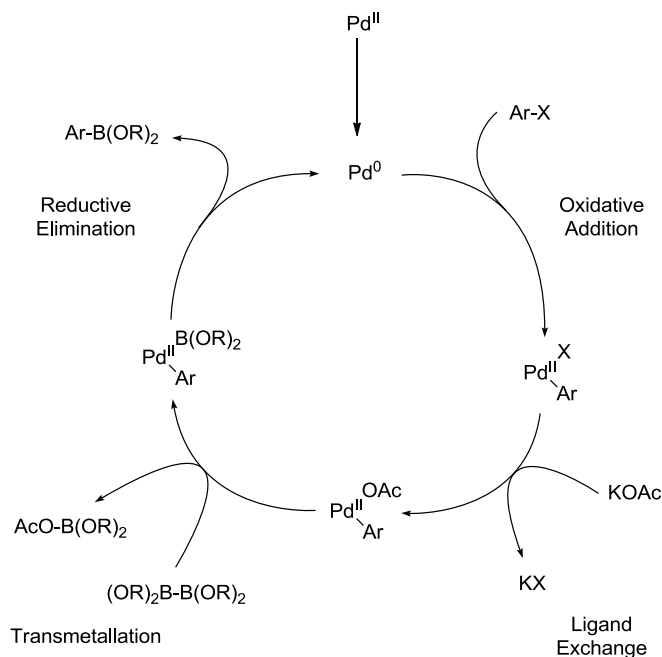


Figure 1.4.1 – The proposed mechanism of the Miyaura borylation for a Pd(II) catalyst.¹⁵⁷

The catalytic cycle begins with Pd(0), which in the case of Pd(dppf)Cl₂ is generated *in-situ* under the reaction conditions. In the first step of the catalytic cycle, the Pd(0) complex undergoes oxidative addition into the aryl-halide bond, forming a Pd(II) intermediate.¹⁵⁷ Displacement of the halide ligand by the acetate group generates a second Pd(II) species. This species undergoes transmetalation with the boron species to form a Pd(II) boron complex, liberating the second boron atom as a boron acetate complex. This can now undergo reductive elimination to liberate the boron product and regenerate the catalyst, which can then repeat the catalytic cycle.

Analysis of the reaction composition in the borolane formation (**Scheme 1.4.1**) shows complete consumption of the bromide starting material (**1.3.21**) under the reaction conditions. The major by-product is the *des*-bromo species, demonstrating that the oxidative addition process is readily occurring under these reaction conditions. The success of the oxidative addition means that the dehalogenation can plausibly occur at two different stages in the catalytic cycle (**Figure 1.4.2**). Either the intermediate Pd(II) species may breakdown prior to the reductive elimination step, or the boron containing product may undergo deborylation under the reaction conditions. In order to develop a more effective borylation procedure, the dominant dehalogenation pathway needs to be determined.

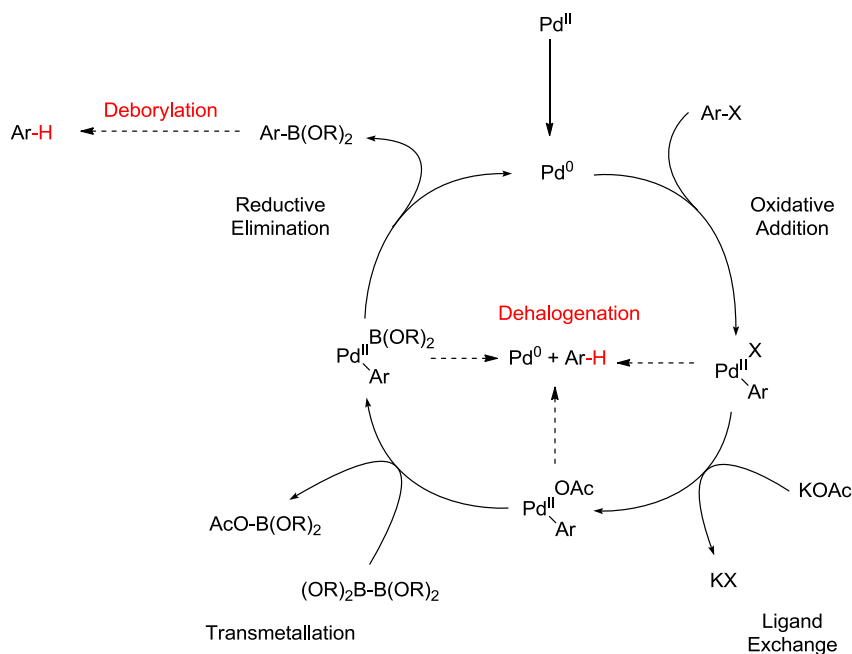
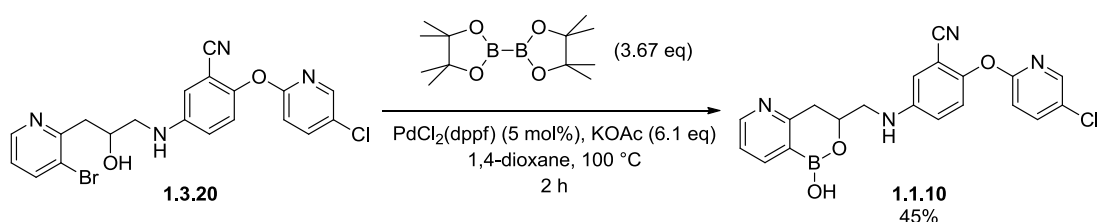


Figure 1.4.2 – The Miyaura borylation catalytic cycle with the potential points of dehalogenation or deborylation indicated.

1.4.3 Determination of the Source of Dehalogenation

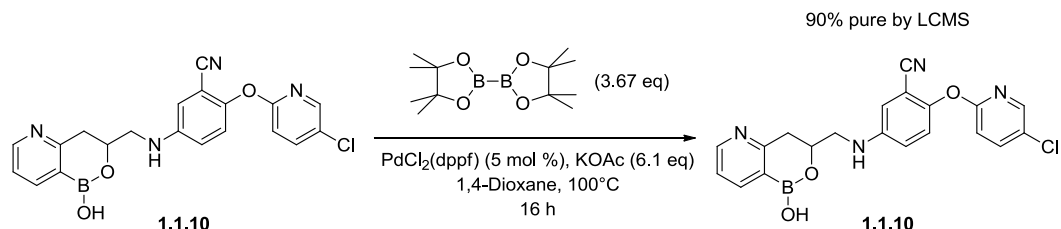
In order to deduce the dominant mode of dehalogenation, two experiments were conducted. The first experiment (**Scheme 1.4.2**) involved conducting the borylation reaction under the standard conditions but with a prolonged reaction time. The levels of dehalogenation were monitored throughout the reaction to determine any variation in the desired product:dehalogenation product ratio.



Scheme 1.4.2 – Experiment to probe the source of the dehalogenation.

After 2 h LCMS analysis revealed consumption of the starting material (**1.3.20**), with 55% product (**1.1.10**) and 26% of the corresponding *des*-bromo by-product. The reaction was retained under these reaction conditions for an additional 14 h, after which it was reassessed by LCMS. LCMS analysis revealed no significant changes in the reaction composition at this

point. The reaction was concluded at this point and the mixture subjected to HPLC purification. Due to the similar polarity of the two products only 45% yield of **1.1.10**, with 89% product purity by LCMS was attained at this step. This crude mixture was then resubjected to the reaction conditions (**Scheme 1.4.3**).



Scheme 1.4.3 – Assessment of the borolane stability under Miyaura reaction conditions.

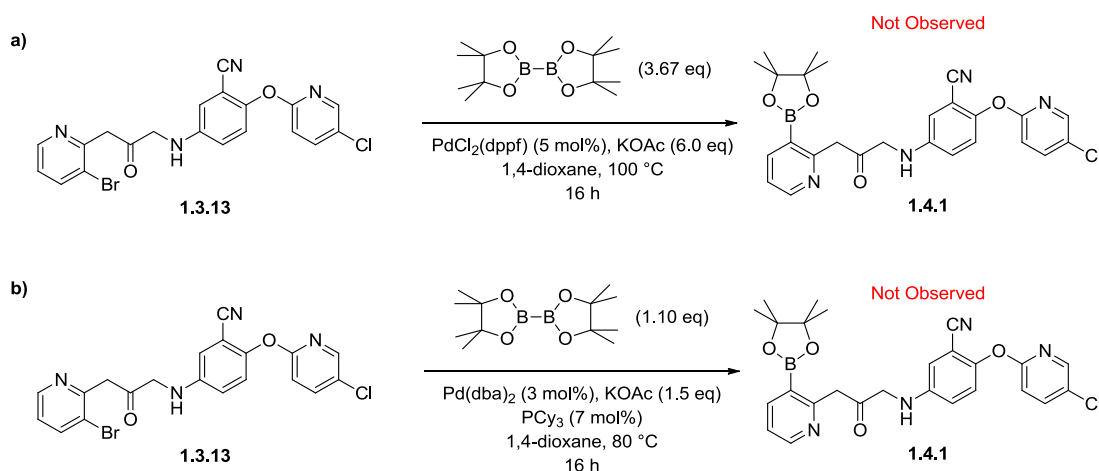
The reaction containing (**1.1.10**) (**Scheme 1.4.3**) was heated at 100 °C for 4 h, after which LCMS analysis revealed no deborylation had occurred. The reaction was continued for an additional 12 h, after which LCMS analysis still revealed no significant change in the reaction composition.

The two experiments (**Scheme 1.4.2** and **Scheme 1.4.3**) demonstrate that the borolane product is stable under the reaction conditions. This suggests that the dehalogenation is occurring due to side reactions of the Pd(II) species, rather than deborylation of the resulting borolane. With the point of dehalogenation having been established, focus could now be directed to overcoming this limitation.

1.4.4 Investigations into Borylation at the Ketone Stage

A number of different parameters for investigation were identified. One of these was the role of the alcohol moiety in the bromide starting materials. It was proposed that the alcohol may exert an influence upon the reaction; potentially coordinating to the catalyst and slowing the rate of transmetallation or alternatively providing the hydrogen source for the dehalogenation reaction. To investigate this potential role, borylation at the ketone stage (**1.3.13**) was chosen for investigation (**Scheme 1.4.4**). It was envisaged that if the yield of borylation at the ketone stage (**1.3.13**) was improved compared to the corresponding reaction of the alcohol (**1.3.20**) the final compound could be accessed through ketone reduction of the borylated product (**1.4.1**).

Two different sets of borylation conditions were assessed. The first set (**Scheme 1.4.4a**) utilised the same conditions as the previous experiments to allow a direct comparison of the reactions. The second set of conditions (**Scheme 1.4.4b**) explored were reported by Ishiyama *et al.*, who identified a highly active catalyst system through screening a variety of palladium sources and phosphine ligands.¹⁹⁴ This catalyst system demonstrated high yields for the borylation reaction, even on typically unreactive substrates, such as aryl chlorides.



Scheme 1.4.4 – a) Attempted borylation utilising standard borylation conditions. b) Attempted borylation utilising the literature conditions.¹⁹⁴

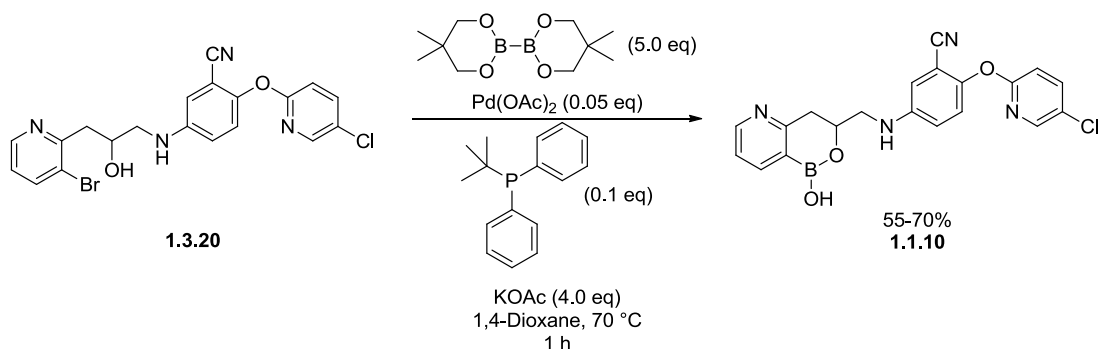
The progression of both reactions was monitored periodically by LCMS. Unfortunately, no product formation was detected at any stage in either instance. After prolonged periods a complicated mixture of unidentifiable by-products was observed with the only identified product being the aniline (**1.3.2**). The presence of the aniline (**1.3.2**) suggests that degradation of the starting material occurs under the reaction conditions, however, the exact mechanism of this is unknown. It was postulated that the failure of the ketone (**1.3.13**) to undergo borylation under the reaction conditions, could be attributed to the increased relative acidity of the protons between the pyridine and ketone. It was envisaged that ketone (**1.3.13**) could undergo tautomerisation under the reaction conditions to form the corresponding enol. This species could then either chelate the palladium metal, or by the formation of a planar system inhibit the oxidative addition into the Ar-Br bond.

As attempts to conduct the borylation prior to reduction failed, no further investigations into the ketone borylation were conducted. Further synthetic effort was focused instead on further optimisation of the borylation of the alcohol (**1.3.20**).

1.4.5 Optimisation of the Borylation Reaction

Although the initial Miyaura borylation conditions (**Scheme 1.4.1**) were identified from significant optimisation work on a small model substrate, subsequent work has revealed that the success of these borylation conditions appears to be highly substrate dependent. Despite these conditions being appropriate for the model substrate, the increased complexity of the pre-candidate alcohol (**1.3.20**) meant that further optimisation was required for the borylation of this extended analogue.

Therefore, a rigorous optimisation study was undertaken elsewhere within our laboratories. The parameters explored in this investigation were; temperature, solvent, catalyst, boron source, and the equivalents of each species. After several iterations of design, significantly improved reaction conditions were identified for the borylation (**Scheme 1.4.5**).¹⁹⁵ The application of these conditions enabled the completion of the scale-up operations by the contract research organisation, GVKBio,¹⁹⁶ enabling large scale biological testing to occur.



Scheme 1.4.5 – Optimised borylation reaction which was appropriate for multiple-gram scale synthesis of borolane (**1.1.10**).¹⁹⁵

The fundamental issue with the initial reaction conditions was the competing dehalogenation reaction (**Scheme 1.4.1**). Although the mechanism of this is still undetermined, the stages at which the undesirable dehalogenation could occur were previously considered (**Figure 1.4.2**).

The change in boron source and the increased number of equivalents of this reagent are postulated to increase the rate of transmetalation and, subsequently, minimise the rate of undesired breakdown after oxidative insertion. Although an in-depth comparison of the rates of transmetalation of different boron species during the Miyaura borylation is not available,

kinetic data for the comparable Suzuki-Miyaura reaction is available. In Carrow and Hartwig's 2011 publication exploring the mechanism of transmetalation in the Suzuki-Miyaura reaction, it was demonstrated that pinacol boronic esters underwent significantly slower transmetalation than the comparable neopentyl boronic esters.¹⁹⁷ This can be attributed to the steric bulk around the boron centres. In the pinacol derivatives the boron centre is significantly more hindered and, therefore, undergoes transmetalation slower than the less hindered neopentyl species.

Although the role of the temperature in dehalogenation has not been proven, it is postulated that the temperature influences the stability of the palladated intermediates. At higher temperatures it is proposed that the complexes are unstable, and therefore decompose prior to transmetalation and borylation, yielding the dehalogenated by-product. Therefore, lower temperatures, such as the 70 °C described above (**Scheme 1.4.5**), compared to the 100 °C of the previously optimised reactions (**Scheme 1.4.1**), are beneficial for the reaction. The improved catalyst system is also thought to more readily undergo oxidative addition than the Pd(dppf)Cl₂ system, therefore, enabling the reaction to be conducted at the desired lower temperatures.¹⁹⁵

Under the modified conditions, almost quantitative conversion from pyridyl bromide (**1.3.20**) to borolane (**1.1.10**) was observed by LCMS, with only minimal levels of dehalogenation. Unfortunately, the purification methods employed still utilised prolonged column chromatography and it is thought that the major loss of product occurs during this step, not during the reaction. If the molecule is candidate selected, further work into the purification method utilised will be conducted within our laboratories.

1.4.6 Improved Synthesis of Borolane Analogues

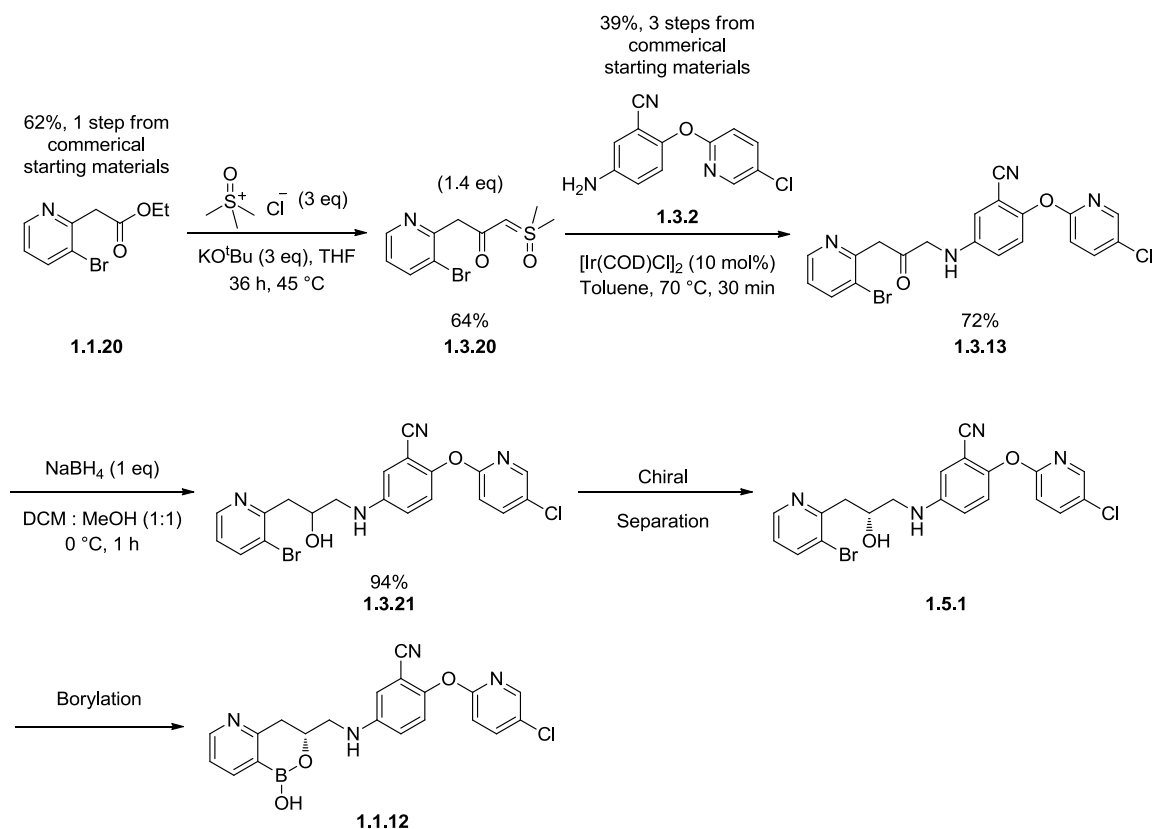
The combined improvement of the borylation reaction, and the introduction of the iridium methodology (**Section 1.3**) enabled facile access to a range of elaborated borolane analogues in significantly increased yields compared to the initial synthetic strategies discussed previously. In addition to this, the improvements to the borylation reaction have greatly simplified the synthesis of almost all borolane derivatives; increasing the yields of the reaction and reducing the by-product formation, greatly aiding subsequent purification and isolation. With these improved conditions, the methodology has been established to rapidly allow the synthesis of significant quantities of borolane molecules for biological assessment.

1.5 Asymmetric Synthesis of the Borolane Pre-candidate (1.1.12)

1.5.1 Asymmetric Reduction of the Ketone (1.3.13)

As previously mentioned, significant improvements to the synthetic route to access pre-candidate borolane (1.1.12) has been made through the use of a key iridium-mediated insertion reaction (Section 1.3), as well as optimisation of the borylation reaction (Scheme 1.4.5). In addition to this, the concise route and late stage diversification has enabled the rapid synthesis of a range of synthetically challenging analogues for biological evaluation (Figure 1.3.4).

The racemic reduction of ketone (1.3.13) to the alcohol (1.3.21), meant that the pre-candidate synthesis still necessitated a chiral resolution to provide the desired borolane *R*-enantiomer (1.12) (Scheme 1.5.1). While this route provided sufficient quantity of material to enable extensive biological evaluation, in terms of cost, practicality, and environmental aspects, this route is inappropriate for further scale-up operations. Therefore, development of an enantioselective reduction protocol was explored.



Scheme 1.5.1 – Synthesis of the pre-candidate (**1.1.12**) utilising chiral separation to provide the desired *R*-enantiomer.

Asymmetric reduction of ketones is dependent on differentiation of the *Re* and *Si* faces of the substrate (**Figure 1.5.1**).¹⁹⁸ In the case of the racemic reduction of ketone (**1.3.13**), the achiral nature of the borohydride reducing agent and the substrate mean that the transition states for hydride addition to the *Re* and *Si* faces are of equal energy. There is no energetic preference for the formation of one enantiomer and a racemic mixture is formed.

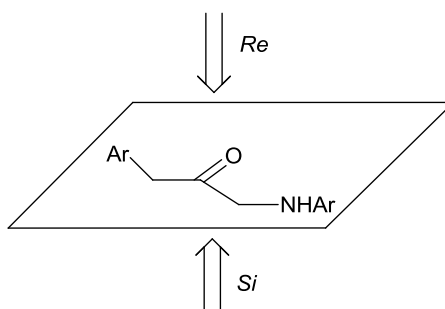


Figure 1.5.1 – Labelling the *Re* and *Si* faces of ketone (**1.3.13**).¹⁹⁸

For achiral substrates, enantioselectivity can theoretically be obtained by the use of a chiral reducing agent/catalyst.¹¹⁷ In order to establish enantioselectivity, the interaction between the substrate and the chiral reagent needs to preferentially lower the energy of either the *Re* or *Si* face addition transition state (**Figure 1.5.2**).¹⁹⁹ The enantiomeric excess (ee) of a reaction is dependent on two main factors. The first is the energy difference between the diastereomeric transition states formed between the chiral catalyst and prochiral substrate.²⁰⁰ The larger the energy difference between the transition states, the greater the ee obtained. The second is the rate of the potential reverse reaction, oxidation to the ketone. In cases when significant reoxidation occurs, enantioselectivity is eroded by equilibration of the two alcohol enantiomers.²⁰¹

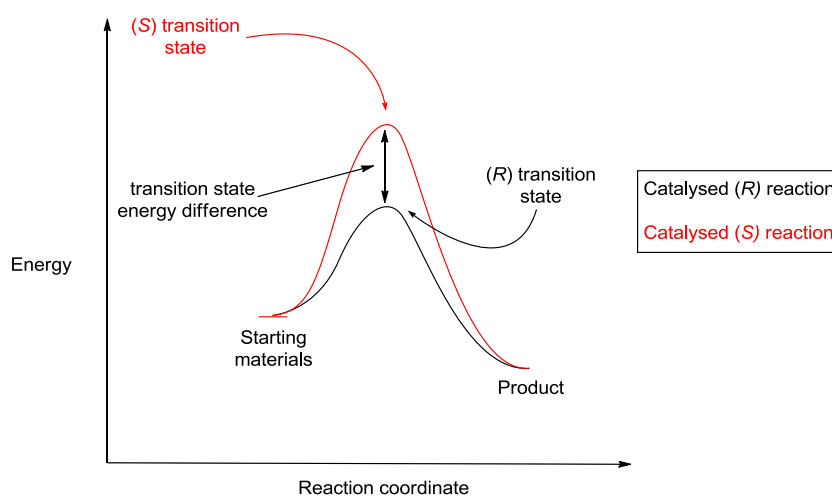


Figure 1.5.2 – Example reaction coordinates for an enantioselective reaction.¹⁹⁹

There are a variety of different methods that can be utilised to differentiate between the *Re* and *Si* faces of a ketone substrate. Typically, sterics, electronics, and coordinating groups are employed to achieve asymmetric reduction reactions.^{117,153} Subsequently, the catalyst/reagent systems that achieve high enantioselectivities are often highly substrate dependent. Commonly used methods to perform asymmetric reductions include both chemical and enzymatic systems. Both of these were investigated for the asymmetric reduction of the ketone (**1.3.13**) to enable the development of an enantioselective synthesis.

1.5.2 Enzymatic Reduction

Enzymatic reactions are of interest to the chemistry community as the reactions are typically more environmentally friendly than comparable chemical processes, due to the aqueous

conditions used.²⁰² Enzymes display exceptionally high chemoselectivity and enantioselectivity in asymmetric processes, but can only catalyse a limited number of reactions, with highly specific substrates.^{203–206} Subsequently, obtaining a compatible enzyme for a non-natural substrate can be difficult.

Both the Boc protected substrate (**1.1.22**), from the initial medicinal chemistry synthesis (**Section 1.1**), and the unprotected ketone (**1.3.13**) were screened against a variety of ketoreductase panels, both from our laboratories and external sources (**Figure 1.5.3**).^{207,208} It was envisaged that screening two electronically/sterically differentiated ketones (**1.1.22** and **1.3.13**) would increase the likelihood of a compatible enzyme being identified.

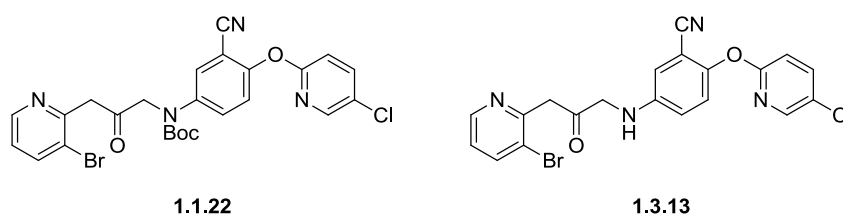


Figure 1.5.3 – Ketone substrates screened against the enzyme ketoreductase panels .

Unfortunately, despite the wide range of enzymes screened, no ketoreductases able to effect an acceptable enantioselective transformation were identified for the Boc substrate (**1.1.22**).¹¹⁸ For the unprotected substrate (**1.3.13**), screening of enzyme panels developed within our laboratories successfully identified several enzymes which were able to reduce the ketone in high enantioselectivities.²⁰⁹ One enzyme, *Saccharomyces cerevisiae* methylglyoxal reductase (GRE2),²¹⁰ was able to generate the desired enantiomer in 94% ee, albeit in modest conversions.

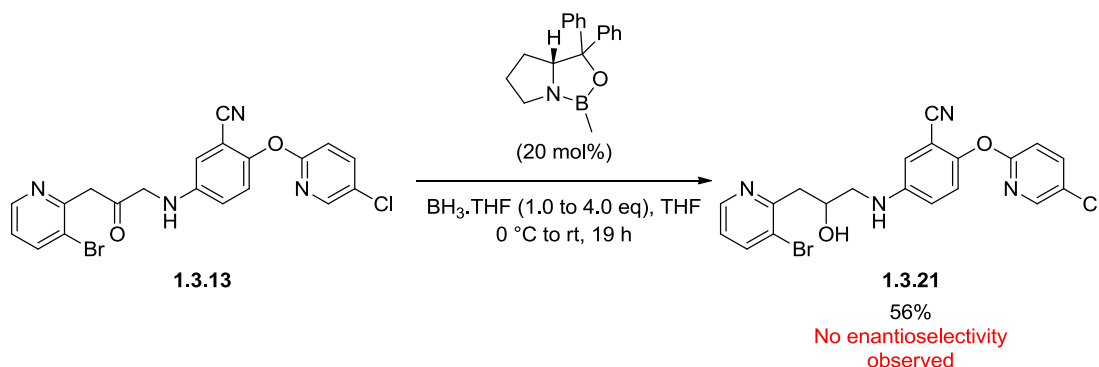
Follow-up investigations into this transformation were subsequently initiated.²¹¹ Despite the encouraging enantioselectivity, the enzymatic reaction does not proceed to completion. Efforts to improve the conversion through variation of the temperature, between 35-50 °C, and the pH of the reaction, between 6.5-8, were explored within our laboratories.²¹¹ However, even under the optimal reaction conditions, 40% of the unreacted ketone still remained after prolonged reaction times (>48 h). It was postulated that this was a consequence of the reverse oxidation reaction occurring under the reaction conditions, establishing an equilibrium between the product (**1.5.1**) and the ketone (**1.3.13**). Typically this limitation is overcome by manipulation of the reaction conditions to favour precipitation of the desired product (**1.5.1**) out of the

reaction medium, preventing the reverse reaction. In this case, the increased solubility of the alcohol (**1.5.1**), relative to that of the ketone (**1.3.13**), prevented the use of this strategy.

Due to the sensitive nature of enzymes, the scope for further optimisation of the solvent system and the reaction temperature are significantly limited. Further development of a high yielding and selective enzymatic reduction procedure would require embarking on an evolutionary program, using *Saccharomyces cerevisiae* methylglyoxal reductase (GRE2)²¹⁰ as a starting point. Despite recent advances, from random mutagenesis to more rational design processes, this is still a long and intensive process.^{212–214} Therefore, other asymmetric options were selected for investigation in preference to the enzymatic reduction.

1.5.3.1 Chemical Enantioselective Reduction of Ketone (**1.3.13**) – CBS Reduction

With the issues encountered with the enzymatic reduction, several alternative chemical enantioselective reduction methods were identified. The CBS reduction (**Section 1.2.6**) of the ketone (**1.3.13**) was initially explored.¹¹⁷ Unfortunately, no enantioselectivity was attained (**Scheme 1.5.2**).



Scheme 1.5.2 – Attempted CBS reduction of ketone (**1.3.13**).

This absence of enantioselectivity is postulated to be a consequence of the poorly defined and differentiated steric environment of the ketone (**1.3.13**). It is thought that the secondary carbon centres adjacent to the ketone result in the majority of the steric bulk of the molecule being localised away from the catalyst during the reaction. The potential for free rotation around the carbon bonds means that the bulky substituents can be orientated away from the catalyst,

alleviating the steric clashes responsible for the facial selectivity (**Figure 1.5.4**). Subsequently, no detectable levels of stereinduction were observed.

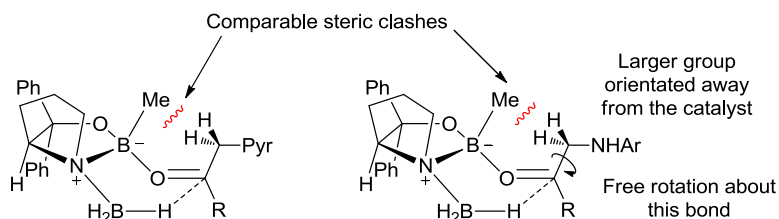
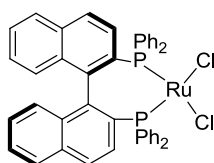


Figure 1.5.4 – Proposed transition states for *Re* and *Si* face reductions of ketone (**1.3.13**) highlighting the minimal differences in steric clashes between the two.

1.5.3.2 Chemical Enantioselective Reduction of Ketone (**1.3.13**) – Asymmetric Hydrogenation

Another method commonly utilised to generate chiral alcohols is the enantioselective hydrogenation of ketones. These reactions most commonly exploit chiral ruthenium catalysts to differentiate between the *Re* and *Si* faces of ketones.²¹⁵ The importance of these catalysts was acknowledged in 2001, when Ryoji Noyori was awarded the Nobel Prize in Chemistry for his development of the first of these complexes.²¹⁶ The initial catalysts utilised a Ru-BINAP complex (**Figure 1.5.5**) and were dependent on coordinating functionalities, such as esters, for enantioselectivity.²¹⁶ However, the evolution of these catalysts, for example the inclusion of chiral amine groups, has expanded the substrate scope and removed the necessity for coordinating groups.²¹⁷



1.5.2

Figure 1.5.5 – Structure of the chlororuthenium-BINAP complex (**1.5.2**), an example of one of the original complexes presented by Noyori for asymmetric ketone hydrogenations.²¹⁶

In order to develop an enantioselective hydrogenation of the pre-candidate ketone (**1.3.13**), a variety of ruthenium catalysts were screened for catalytic activity. This led to the identification of (*R*)-RUCY-XylBINAP (**1.5.3**)²¹⁸, a diamine catalyst derived from the initial BINAP catalyst

(1.5.2) (Figure 1.5.6). This catalyst displayed the greatest activity, with over 90% conversion for the hydrogenation of the ketone (1.3.13).

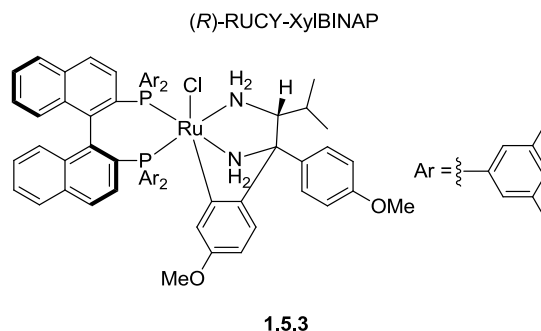
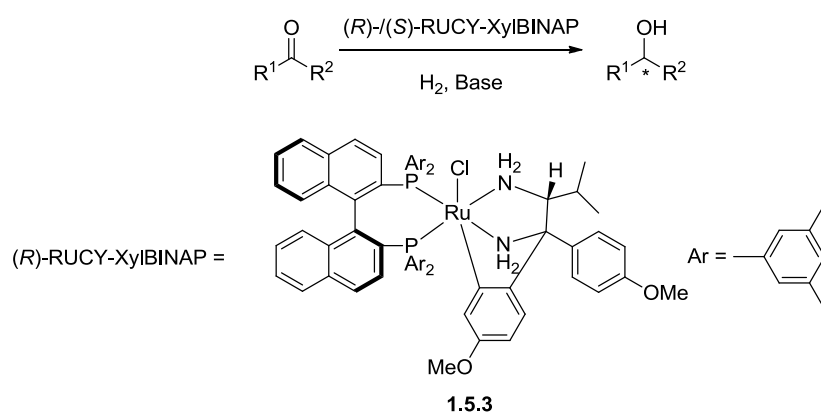


Figure 1.5.6 - (R)-RUCY-XylBINAP (1.5.3).

In 2011 Ohkuma *et al.*, in collaboration with Takasago International Corporation, presented the use of the commercially available (R)-RUCY-XylBINAP catalyst (1.5.3) for the enantioselective hydrogenation of a range of ketones (Scheme 1.5.3).²¹⁸ Substrates which are cited as being difficult for asymmetric hydrogenation, including several base-labile and bicyclic ketones, were effectively and selectively reduced. The novel bicyclic catalyst system displayed greater activities and selectivities than the commercially available Noyori-type catalysts in both literature and our own studies.



Scheme 1.5.3 - (R)-RUCY-XylBINAP (1.5.3) asymmetric hydrogenation of ketones.²¹⁸

In order to develop a scalable, high yielding, enantioselective asymmetric hydrogenation protocol, a rigorous design of experiment (DoE) was initiated.^{219,220} The DoE is a powerful synthetic tool for optimisation of chemical reactions utilising computer designed experiments.²¹⁹⁻²²¹ The experiments are designed to probe a range of variables, and identify the significance of each. The analysis of these experiments can direct further experimentation

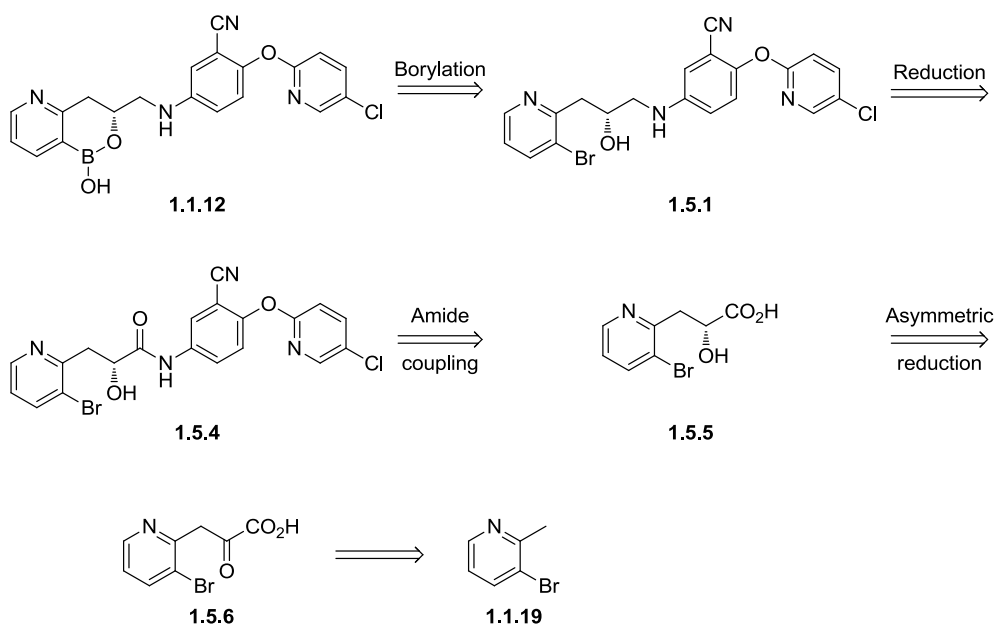
and iterations of optimisation. The power of this technique is the efficiency of the process, limiting the number of experiments required to determine the maximum amount of information.

Several iterations of the experimentation to optimise the reaction were conducted, investigating parameters temperature, concentration, base identity, stoichiometry, and hydrogen pressure. The combination of protic solvents and strong inorganic bases, most notably KO^tBu, was able to yield chiral alcohols in excess of 90% ee.

Unfortunately, as the investigations were transferred to larger scales, with aim of further enhancing the yields and enantioselectivities, the reactions were hampered by the poor solubility of the ketone (**1.3.13**). The low solubility of the ketone in a range of solvents resulted in precipitation of the starting material, incomplete reactions, and issues with reproducibility. This unforeseen difficulty cast doubts on the initial design of experiment work, as the optimisation of the conditions may have been driven by solubility rather than the catalyst activity and enantioselectivity. This additional complication prevented any correlation between the yield/enantioselectivities and the other parameters being determined. Further studies and substantial synthetic investigation are necessitated to development an asymmetric route to the pre-candidate (**1.1.12**) *via* ketone (**1.3.13**). The significant limitations of this strategy meant that the development of alternative synthetic route was prioritised.

1.5.4 Alternative Route to the Pre-Candidate Borolane (1.1.12)

The poorly defined and differentiated steric and electronic environment of the ketone (**1.3.13**) inhibits the development of an asymmetric synthesis. In order to enhance the facial selectivity of the reduction a new route was devised, utilising the asymmetric reduction of an well differentiated α -keto acid (**1.5.6**) (**Scheme 1.5.4**).



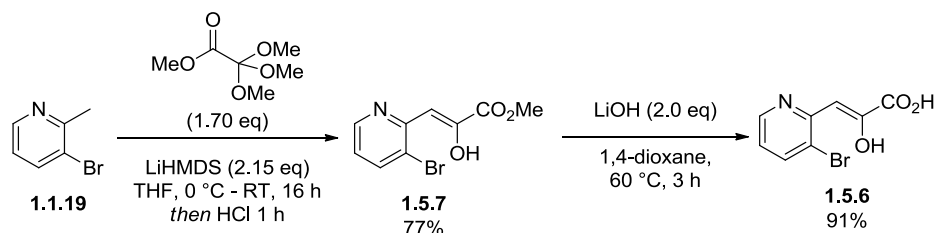
Scheme 1.5.4 – Proposed asymmetric route to the pre-candidate borolane (**1.1.12**) utilising an asymmetric reduction of the α -keto acid (**1.5.6**) to construct the stereocenter in the product.

The route was designed to converge on the chiral alcohol (**1.5.1**), enabling the borylation reaction as the final step in the synthesis, *vide supra*. It was envisaged that the formation of the synthetically challenging C-N bond (**Section 1**) could be achieved by amide coupling, with a selective reduction of the resulting amide (**1.5.4**) synthesising the chiral alcohol (**1.5.1**). The carboxylic acid coupling partner (**1.5.5**) can be accessed in-turn from the corresponding ketone (**1.5.6**). In contrast to the ketone (**1.3.13**), this substrate is electronically and sterically well defined and possesses a potential coordinating carboxylic acid motif. It was postulated that high enantioselectivities could therefore be attained from the reduction of this substrate. This keto-acid (**1.5.5**) can then be accessed from the commercially available bromopyridine (**1.1.19**) previously utilised (**Section 1.1.6**).

1.5.5 Synthesis of the α -Keto Acid (**1.5.6**)

It was envisaged that the asymmetric hydrogenation substrate (**1.5.6**) could be accessed through deprotonation of the acidic methyl group of the bromopyridine (**1.1.19**), followed by quenching with an appropriate electrophile. Due to the acidic proton of the carboxylic acid, this acid functionality could not be directly installed, as it would quench the nucleophile, preventing the attack. It was envisaged that the use of corresponding ester could circumvent this problem, which could be hydrolysed to the desired acid (**1.5.6**). Unfortunately, the diester

electrophiles required for this reaction are susceptible to undergoing multiple nucleophilic attacks, potentially preventing the formation of the desired product and instead forming a mixture of addition products. An elegant solution to this problem was provided by Medina *et al.* who utilised *ortho*-esters as a protected ester group for the preparation of a comparable pyridine analogue.²²² A subsequent acidic work-up stage is able to then give the desired ester (1.5.7) (Scheme 1.5.5). This could then, in turn, be converted to the corresponding acid (1.5.6), by treatment with lithium hydroxide (Scheme 1.5.5).



Scheme 1.5.5 – Preparation of the keto-acid (1.5.7).

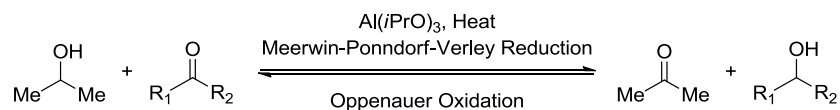
Gratifyingly, deprotonation with LHMDS, quenching with the *ortho* ester, and acidic work-up yielded the keto-ester (1.5.7) in a 77% yield (Scheme 1.5.5). NMR analysis demonstrated that in DMSO, this species was found to exist exclusively as the enol tautomer, presumably due to the enhanced conjugation with the aromatic ring in this tautomer. The hydrolysis of this intermediate (1.5.6) provided access to the desired acid (1.5.6) in a 70% yield over 2 steps. NMR analysis showed that the acid also exists as exclusively the enol tautomer in the polar DMSO solvent, although the ratio is predicted to change depending on the solvent polarity.

1.5.6 Asymmetric Reduction of the Ketone (1.5.6)

With a robust, high yielding method to access the keto-acid (1.5.6) established, attention was transferred to the asymmetric reduction. Due to the well defined ketone, it was envisaged that milder reaction conditions for the reduction could be developed than those utilised for the ketone (1.3.13), without the requirement for high catalyst loadings and hydrogen pressures (Section 1.5.3.2), which often necessitates the use of specialist reaction vessels and has associated safety risks.

It was thought that the use of transfer hydrogenation would provide an alternative reduction protocol, without the requirement for a hydrogen atmosphere. Instead the reaction utilises a sacrificial hydrogen source, which is in turn oxidised under the reaction conditions. The first

transfer hydrogenation reaction was the seminal aluminium *iso*-propoxide mediated Meerwein-Ponndorf-Verley reduction (**Scheme 1.5.6**).²²³



Scheme 1.5.6 – Example of the Meerwein-Ponndorf-Verley reduction.²²³

Since the initial report of the Meerwein-Ponndorf-Verley reduction, significant advances have been made in the field of transfer hydrogenation. The use of transition metal catalysts has significantly enhanced the reaction scope, reactivity, and enabled the development of enantioselective variants of the reactions. The first example of ruthenium catalysts being employed in asymmetric transfer hydrogenation was reported by Noyori *et al.* in 1995.²²⁴ Since this publication, improvements to the reaction conditions, most notably the use of formic acid as an irreversible hydrogen source by generating gaseous carbon dioxide,^{225,226} and further development of the catalysts, to enhance the catalyst stability, activity, and enantioselectivity observed, have been reported.^{227,228}

One of the most significant developments in transfer hydrogenation catalysts was the introduction of tethered ligands, pioneered by Wills *et al.*^{229–231} It was envisaged that these catalysts would be superior to the non-tethered counterparts in two main ways. The tridentate coordination was envisaged to increase both the catalyst stability and activity, preventing catalyst decomposition and degradation. The tridentate coordination is also used to restrict the rotation around the aromatic ring (**Figure 1.5.7**), increasing the rigidity of the complex and enhancing the levels of enantioselectivity.

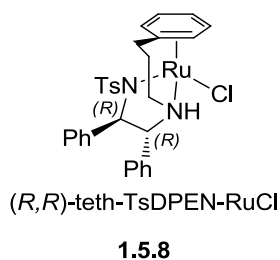
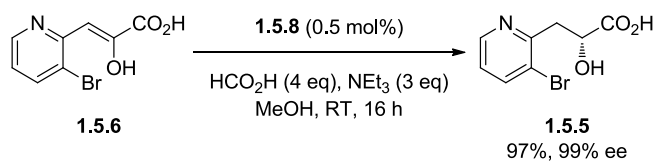


Figure 1.5.7 – Structure of one of the ruthenium tethered catalysts designed by Wills *et al.*²³¹

To evaluate the potential asymmetric transfer hydrogenation, the tethered catalyst (**1.5.8**) was explored for the reduction of the keto-acid (**1.5.6**) (**Scheme 1.5.7**). Formic acid was employed

as the irreversible hydrogen source, preventing the reverse reaction and an erosion of both the yield and enantioselectivity.



Scheme 1.5.7 – Asymmetric transfer hydrogenation of the keto-acid (**1.5.6**). The stereochemistry was assigned through synthesis of the alcohol (**1.5.1**) and comparison to HPLC trace of the desired enantiomer obtained by chiral resolution.²³²

Gratifyingly, under the reaction conditions the ketone/enol was found to be reduced in both high yields and enantioselectivities. The stereochemistry was confirmed by comparison to the chiral HPLC traces of both enantiomers of the alcohol (**1.3.20**) later on in the synthesis.²³² For the ruthenium catalysed asymmetric transfer hydrogenation, the stereoselectivity is generally attributed to the formation of a key CH/ π interaction between the aryl of the substrate and the catalyst (**Figure 1.5.8a**).²³³ For some specific classes, most notably imines, the selectivity is also attributed to the formation of a hydrogen bond between the protonated nitrogen and the catalyst (**Figure 1.5.8b**).²³⁴

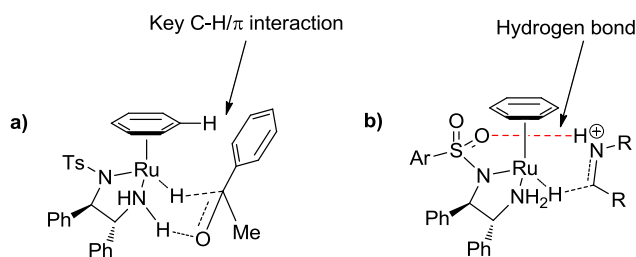


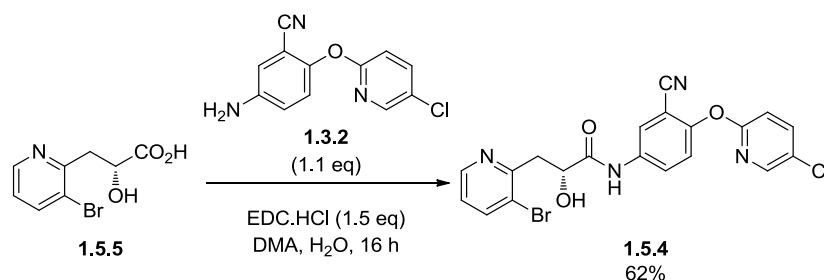
Figure 1.5.8 – **a)** Illustration of the CH/ π interaction for enantioselectivity in α -substituted ketones;²³³ **b)** Role of hydrogen bonding for enantioselectivity in imine asymmetric transfer hydrogenation.²³⁴

For the keto-acid (**1.5.6**), the observed enantioselectivity, forming the (*R*)-enantiomer (**1.5.5**), suggests that the lower energy transition state has the acid occupying the same position as the aromatic ring in the example (**Figure 1.5.8a**). Although the acid can potentially act as a hydrogen bond donor, the planar nature of the conjugated keto acid (**1.5.6**) and large ring size required to form this bond potentially inhibits this mode of induction. Instead it is proposed that the acid forms a π -interaction with the aromatic ring, leading to the observed selectivity

in an analogous fashion to that of aromatic ketone example (**Figure 1.5.8a**). Further work would be required to confirm this hypothesis.

1.5.7 Amide Coupling and Completion of the Synthesis

With a high yielding, enantioselective route to the chiral acid (**1.5.5**) being established, attention was turned to the amide coupling reaction with the aniline fragment (**1.3.2**). The amide coupling with the EDC coupling agent was identified as a potential method to couple the two halves of the molecule (**Scheme 1.5.8**).

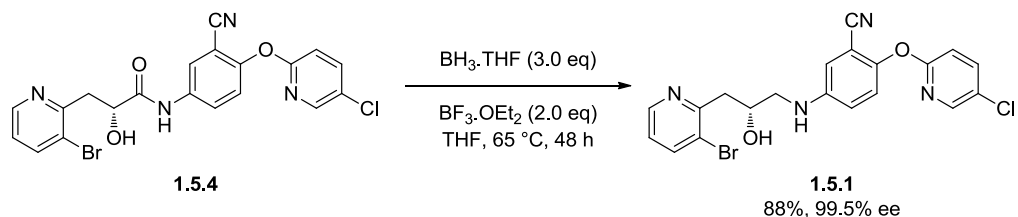


Scheme 1.5.8 – Amide coupling reaction to synthesise the amide (**1.5.4**).

Gratifying, the desired amide (**1.5.4**) was formed under the reaction conditions in moderate yields, despite the unprotected nucleophilic alcohol. It was envisaged that the alcohol could attack the coupling agent or one of the intermediates formed during the coupling reaction, preventing the reaction occurring and leading to the formation of by-products. Under the EDC conditions, no significant by-product formation was observed, with high conversion to the desired product, despite the diverse range of functionality.

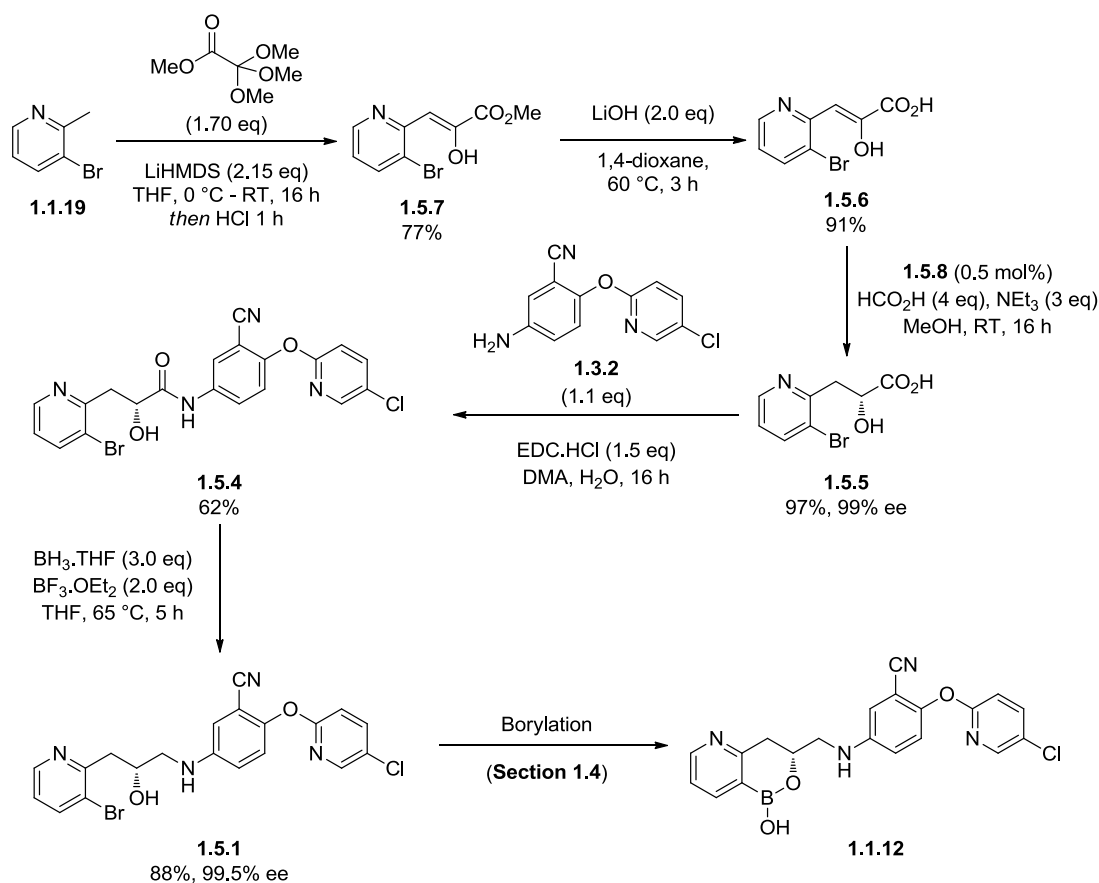
Chiral HPLC analysis was unable to determine the enantiomeric excess after this reaction, as the minor isomer could not be discerned. To determine the enantiomeric excess and to confirm that no racemisation of the chiral center occurred in the synthesis, the amide (**1.5.4**) was carried forward to the reduction reaction. As the racemic alcohol (**1.3.20**) was previously synthesised, this could then be used as a reference for the chiral HPLC.

Due to the susceptibility of the nitrile group to reduction and the potential racemisation of the acidic α -chiral centre, borane was selected as a reducing agent. It was envisaged that the Lewis basic nature of the amide would enable selective amide reduction, in the presence of the nitrile *via* preferential coordination to the amide carbonyl (**Scheme 1.5.9**).



Scheme 1.5.9 – Selective reduction of the amide (**1.5.4**) to give the enantioenriched alcohol (**1.5.1**).

Gratifyingly, under the reaction conditions the chemoselective reduction of the amide (**1.5.4**) was observed in high yields with no racemisation, with LCMS analysis unable to discern any undesirable nitrile reduction. Chiral HPLC analysis, in reference to the racemic alcohol (**1.3.21**), was able to confirm that no racemisation occurred under the reaction conditions. It is envisaged that further optimisation of this final reduction, either through the continued use of borane or alternative selective reduction protocols,^{235,236} could be used to develop a large scale enantioselective synthesis (**Scheme 1.5.10**), with the synthesis converging on the alcohol intermediate (**1.5.1**) prior to borylation/cyclisation (**Section 1.4**).



Scheme 1.5.10 – Asymmetric synthesis of the key alcohol intermediate for the synthesis of the active borolane isomer (**1.1.12**).

Overall the synthesis of the alcohol (**1.5.1**) was accomplished in a concise 5 step synthesis, in an overall yield of 37%. This route offered significant improvements to the iridium-mediated synthesis (**Section 1.3**); including increased yields, a reduction in discreet purification steps and increased sustainability metrics, including the removal of the chiral resolution stage. The requirement for chiral separation lowers the overall yield by at least 50%, increases the use of solvents and purification equipment, and is impractical for larger scale synthetic operations. The major loss of material (**Scheme 1.5.10**) occurred predominately during the unoptimised amide coupling stage. If further scale-up was required, then optimisation of this stage could further increase the already excellent overall yield.

1.6. Conclusion

In summary, significant progress has been made towards the aims outlined at the start of the research project (**Section 1.1**), with all of the aims of the project accomplished, having a profound impact on the design of Lp-PLA₂ inhibitors. These achievements are outlined below:

- 1) The synthesis of the challenging novel pyridone borolane (**1.1.40**) has been achieved, representing the first example of this borolane core structure. A small number of compounds were designed to evaluate the core, without the requirement for a large number of analogues. The borolane (**1.1.40**) enabled assessment of the novel pyridone core's potential to develop a potent and selective Lp-PLA₂ inhibitor. The matched-pair analysis demonstrated that the pyridone series would be unable to provide the minimal selectivity required for further development. This expedited the development of the pyridyl borolane (**1.1.12**), allowing further SAR to be focused on this core substructure.
- 2) Dramatic improvements to the synthesis of the synthetically challenging borolanes have been made. The application of the iridium carbenoid chemistry (**Section 1.3**) significantly reduced the initial length of the synthetic route to the pre-candidate borolane (**1.1.12**). The methodology was able to rapidly synthesise the complex borolane, facilitating scale-up efforts to enable comprehensive biological evaluation, as well as improving the green metrics and yields of the synthesis. In addition to this, the chemistry developed was applied to the synthesis of other complex analogues of interest which had previously been synthetically challenging with protracted routes. Overall, the research was instrumental in delivering efficient access to the pre-candidate borolane (**1.1.12**), underpinning both scale-up and SAR work within our laboratories.
- 3) Several asymmetric reduction protocols have been evaluated to enable the enantioselective synthesis of borolane (**1.1.12**). Unfortunately, due to solubility and conversion issues, none of these were appropriate for scale-up. A new concise route was devised which was able to converge on the key alcohol (**1.5.1**). The overall synthesis was 5 steps in 37% yield, increased from the 4% yield of the racemic protected substrate (**1.1.23**) in the initial medicinal chemistry route. The desired

Confidential – Property of GSK – Do Not Copy

enantiomer of the alcohol (**1.5.1**) was produced with high enantiomeric excess (99.5% ee) preventing the requirement for chiral resolution. In addition to this, there remains the potential for extended optimisation to further increase these yields, enabling enantioselective scale-up synthesis if the molecule is progressed further towards a externally utilised drug.

Chapter 2

Design and Synthesis of a Novel Bromodomain and Extraterminal Domain (BET) Inhibitors and Discovery of a New C-H Activation Protocol

2.1. Introduction

2.1.1. Bromodomain and Extra Terminal (BET) Proteins

The diploid human genome consists of approximately 6 billion base pairs,²³⁷ contained within 23 pairs of chromosomes. The average length of a DNA base pair is 0.34 nm long, therefore, each human diploid cell contains over 2 meters of DNA.²³⁸ To enable efficient gene transcription, packaging of the genetic information, and to inhibit DNA damage, the DNA is compacted into chromatin in the nucleus (**Figure 2.1.1**).²³⁹

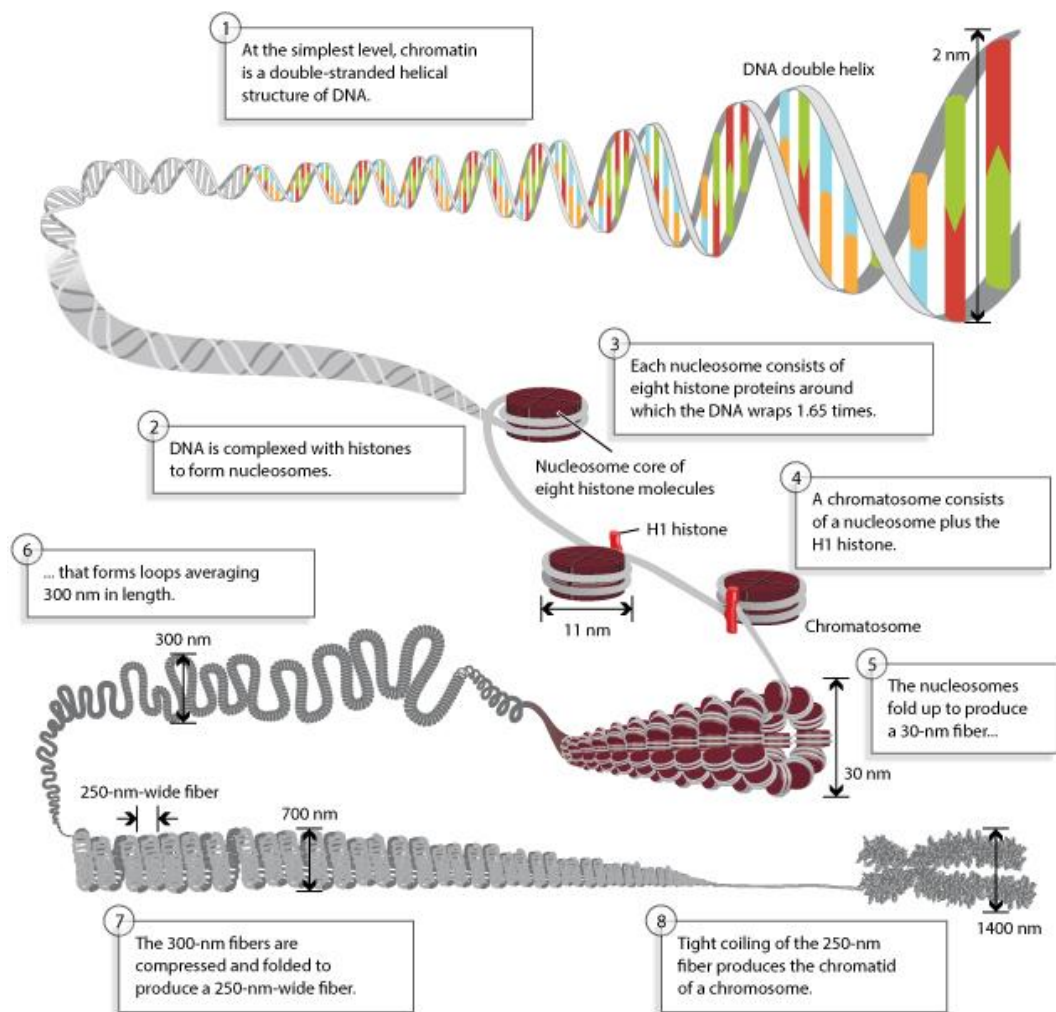


Figure 2.1.1 – Levels of DNA organisation from double stranded DNA (1), to the chromosome (8).²³⁸

Within the eukaryotic cell, chromatin formation begins with the interaction between the double stranded DNA helix and the histones (**Figure 2.1.1** – Number 2).²³⁸ The histones are a family of positively charged, low MW proteins consisting of 5 discrete members; H1, H2A, H2B, H3, H4.²⁴⁰ The positively charged histones form strong electrostatic interactions with the negatively charged phosphate backbone of the DNA, enabling the tight coiling of the DNA helix around the histones. The histones are organised into 8 protein clusters, which are referred to as nucleosomes (**Figure 2.1.1** – Number 3). The nucleosomes are in-turn organised into sequentially higher order structures (**Figure 2.1.1** – Numbers 4-8), eventually leading to the formation of the chromosomes (**Figure 2.1.1** – Number 8).

Acetylation of histone lysine residues is a fundamental post-transcriptional protein modification.²⁴¹ This causes a neutralisation of the positively charged amino acid chain, weakening the interaction between the histone and the negatively charged DNA backbone. This results in a loosening of the DNA winding around the histone, forming an open chromatin state, allowing increased levels of gene transcription. The open state allows a variety of proteins to access the DNA, and the histone acetylation patterns direct the recruitment of proteins to the region of the DNA, both processes enabling gene transcription.²⁴²

Bromodomains are a class of protein domain characterised by the ability to recognise acetylated histone lysine residues.²⁴² Upon histone recognition and binding, the bromodomain containing proteins can elucidate a range of pathways, including regulation of gene transcription. Within the human genome there are 61 distinct bromodomains, encoded in 46 bromodomain containing proteins. Proteins containing bromodomains are subdivided into 8 groups. The members of each group possess similar sequence lengths with over 30% sequence homology (**Figure 2.1.2**). One of these 8 groups is the bromodomain and extra terminal (BET) family (**Figure 2.1.2**, Group 3).

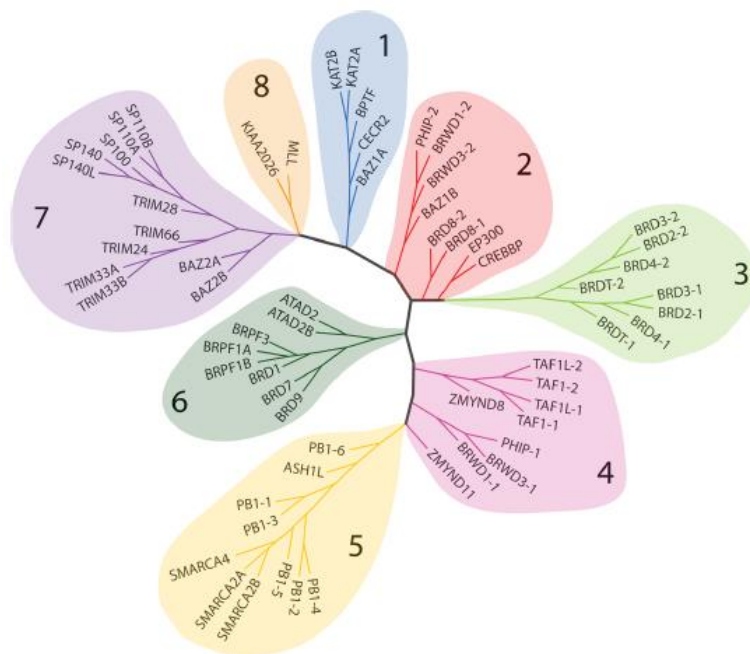


Figure 2.1.2 – Phylogenetic tree of human bromodomain proteins with the BET family highlighted in light green, group 3.²⁴²

The members of the BET bromodomain family are associated with transcription activation and propagation.²⁴³ Abnormal increases in acetylation of histone lysines has been implicated in irregular levels of gene expression, which can give rise to a variety of different disease states including; cancer, diabetes, inflammation, and cardiovascular disorders.²⁴⁴ Due to the central role of the BET family in both recognition of the acetylated lysines and subsequent transcription, inhibition of these domains can rebalance the levels of gene expression, having a profound therapeutic impact on patients.

2.1.2 BET Protein Family Architecture

Bromodomain containing proteins are multi-domain proteins and the presence of a bromodomain confers the ability to recognise acetylated histone lysine residues, *vide supra*.²⁴⁵ The accompanying domains then determine the function of the protein and the influence on gene expression.

The BET family are a family of tandem bromodomain containing proteins, with two structurally related bromodomains referred to as BD1 and BD2 (**Figure 2.1.3**).²⁴⁶ These two bromodomains can recognise different acetylation patterns on the histones. Consequentially,

selective inhibition of one of the bromodomains, BD1 or BD2, may give rise to distinct therapeutic effects relative to non-selective inhibition, known as pan-BET inhibition.

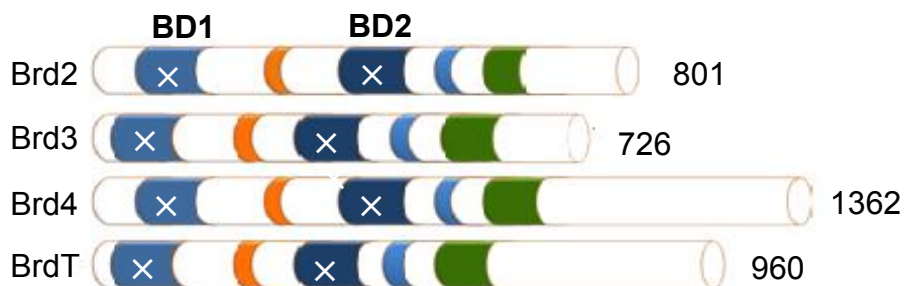


Figure 2.1.3 – Domain structure of four BET proteins highlighting the two distinct bromodomains, BD1 and BD2, in addition to the variable overall protein length.²⁴⁷

2.1.3 Bromodomain Structure and Inhibition

Since the solving of the first bromodomain structure in 1999, more than half of the bromodomain three-dimensional structures have been elucidated.^{245,248} In all instances, the bromodomain is formed from a conserved bundle of four anti-parallel α -helices (**Figure 2.1.4**). The substrate specificity is then determined by the variations in the loops linking these helices.

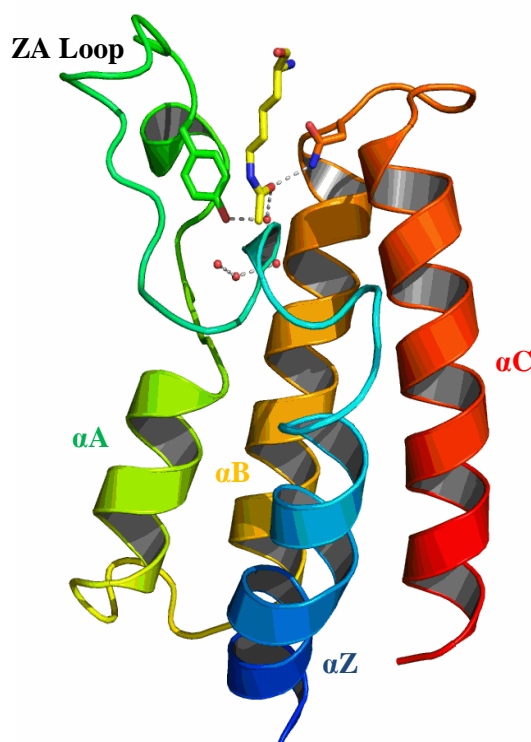


Figure 2.1.4 – Structure of a typical bromodomain with four distinct α -helices, α A, α B, α C, and α Z.²⁴⁹ The acetylated lysine binding in the recognition site is highlighted in yellow. Water molecules are depicted by red circles.²⁵⁰

The BET family bromodomains, recognise and bind the acetylated lysine through interactions with conserved asparagine and tyrosine residues. The acetyl carbonyl forms two hydrogen bonds: a direct hydrogen bond with the asparagine and a through water hydrogen bond to the tyrosine, formed with one of four highly conserved waters in the active site (**Figure 2.1.5**).

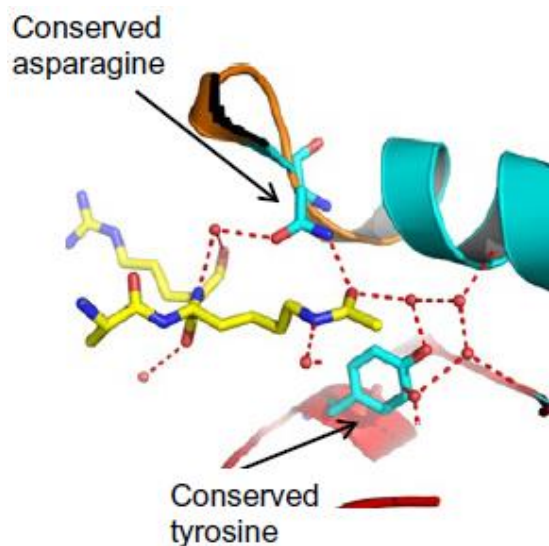


Figure 2.1.5 – Bromodomain binding of acetylated lysine (yellow) in the binding site.²⁴⁵ Conserved water molecules are depicted by red circles.

In the BET family, the binding of the acetylated lysine occurs in a deep, well-defined binding pocket. This has enabled the development of small molecules that bind and occupy this pocket, disrupting and preventing recognition of the acetylated histones.²⁴² Since the disclosure of the first bromodomain inhibitor in 2005, a variety of different BET inhibitors have been reported (**Figure 2.1.6**).

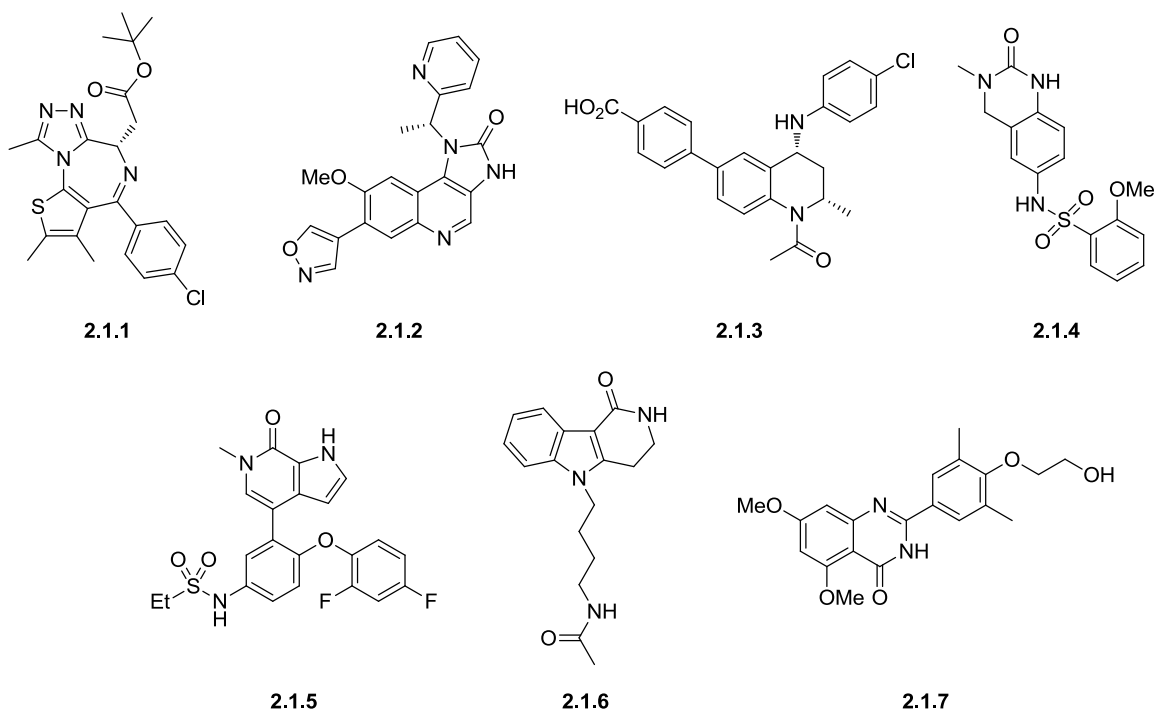


Figure 2.1.6 – Examples of different BET family bromodomain inhibitors.²⁴²

Although there is structural distinction between these templates, the key binding interactions are typically conserved between the series. The majority of the molecules depicted in **Figure 2.1.6** bind deep within the acetyl-lysine binding pocket, interacting with the highly conserved asparagine and tyrosine residues.²⁵¹ A range of different hydrogen bond accepting functionalities are utilised to mimic the binding of the acetyl lysine, forming the key hydrogen bonding interactions. Overlaying the X-ray crystal structures of the acetylated lysine and the inhibitors shows the occupation of the binding site and the homology between the hydrogen bond acceptor groups (**Figure 2.1.7**).

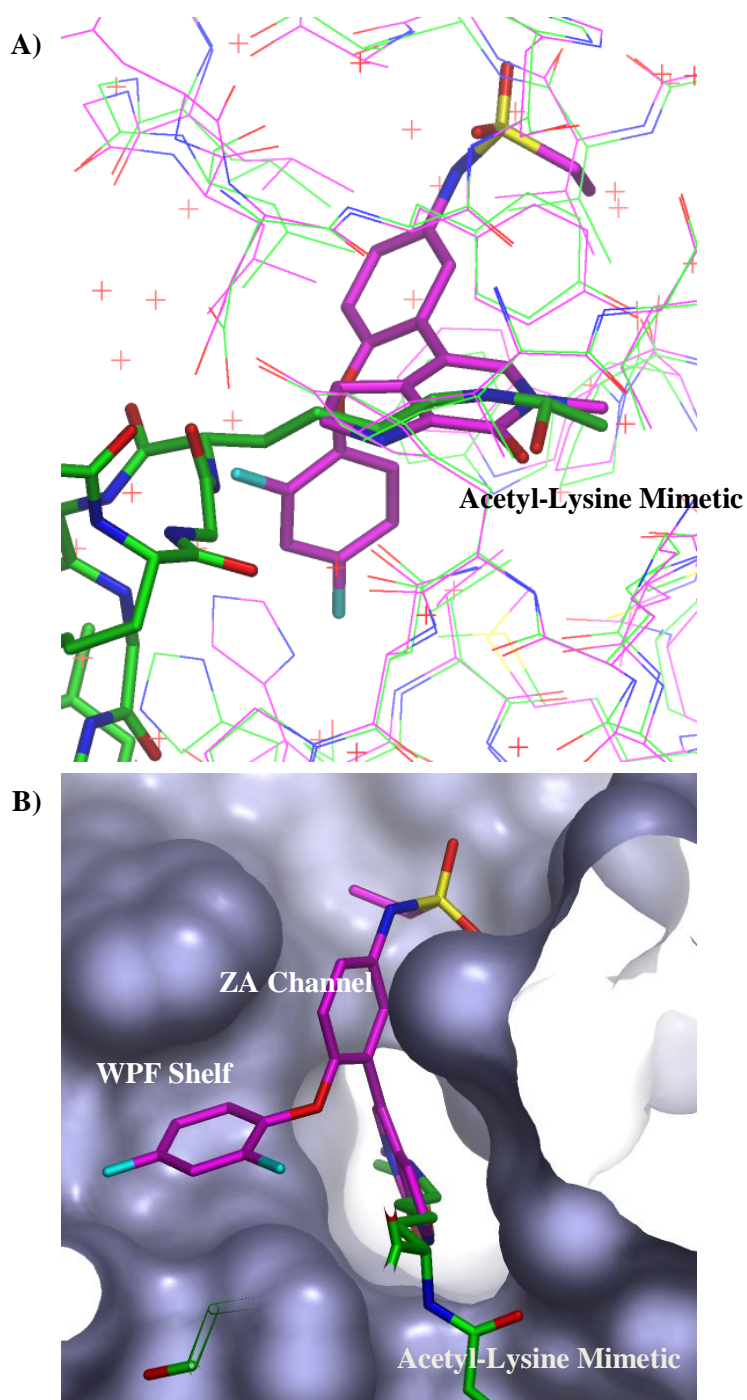


Figure 2.1.7 – A) Example of the overlap in BD2 between the acetylated lysine mimetic of the BET-inhibitor carbonyl (**2.1.5**, Purple, PSILO-7BJGT) and the acetylated lysine (Green, PSILO-2E3K), B) highlighting the key binding features of the molecule.

In addition to the key hydrogen bonding interactions, there are two other well-documented regions of the BET-family binding site, which can be exploited to tune the selectivity and the potency of the inhibitors. Two of the major regions, the WPF shelf and the ZA channel, are

highlighted for the potent BET inhibitor (2.1.5) (Figure 2.1.7). The WPF shelf derives its name from the conserved WPF, tryptophan (W), proline (P), and phenylalanine (F), motif that is present in all BET-bromodomains. This is a hydrophobic region of the binding site and, therefore, inhibitors typically contain lipophilic substituents in this region, such as the difluoro aromatic in (2.1.5) (Figure 2.1.7). The second major vector is growth into ZA channel. This is a narrow hydrophilic channel formed by the ZA loop between the Z and A α -helices (Figure 2.1.4), which is occupied by water molecules in the unbound protein. Inhibitors growing into this vector typically utilise polar or planar functional groups, to maximise the interactions with the binding site.

Despite the wide range of BET inhibitors reported, the biological implications and extended potential therapeutic benefits of BET inhibition mean that there is still global interest in the development of novel BET inhibitors. Novel chemotypes can be utilised for different therapeutic indications, with alternative cores having distinct dosing regimes and exhibiting alternative distribution patterns within the body. Accordingly, it is envisaged that differing physicochemical properties will enable the efficient treatment of various diseases, and therefore a diverse portfolio of BET-inhibitors is highly desirable.

2.1.4 High-throughput Screening Approach to the Discovery of BET Inhibitors

There are a variety of different techniques in drug discovery that are utilised to discover ‘hit’ molecules, i.e. those molecules displaying significant binding affinity or biological activity against a target of interest. For a discussion on the benefits and drawbacks of various techniques see (Section 1.1.5).

In order to discover novel chemotypes as BET inhibitors, historical HTS data was reanalysed from a previous screen in our laboratories.²⁵² A library of 50,000 compounds, designed around potential acetylated lysine mimetics, was screened in a biochemical assay for significant BET-BD1 activity. Approximately 8000 compounds were identified with BD1 activity. Further filtering, based on compounds possessing promising physicochemical properties for further development, reduced this to 1586 compounds of interest. Clustering these based on structural homology and selection of representative examples of each group identified 270 compounds for re-screening, using both biochemical FRET (fluorescence resonance energy transfer) and biophysical SPR (surface plasma resonance) assays, was able to refine the set to a few key molecules for further investigation.

One of these was the small, potent, ligand efficient benzazapinone (BZP) analogue inhibitor (**2.1.8**) of the BET family (**Figure 2.1.7**). This molecule demonstrated comparable inhibition of both BRD4 BD1 and BD2, and represents a previously unexplored chemotype of BET inhibitor. The structural similarities between the BET family bromodomains (**Figure 2.1.3**) means that typically binding potencies are conserved across the family. The assays are typically run in BRD4 due to its robust and reliable nature, with compounds being routinely screened in the other BET proteins to ensure the values obtained are representative of the whole family.

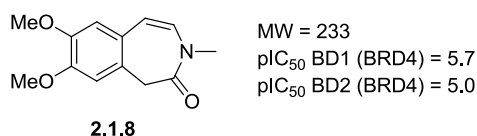


Figure 2.1.7 – Initial benzazapinone (BZP) ‘hit’ (**2.1.8**). BRD4 data is used as representative of the BET family. All potency values expressed herein refer to BRD4 unless otherwise stated.

2.1.5 Elaboration of the BZP ‘Hit’

Since the identification and validation of this initial hit (**2.1.8**), optimisation of this series has been conducted within our laboratories. The aim of this overarching programme was the development of ‘*a candidate quality pan-BET inhibitor*’, i.e. equipotent BD1 and BD2 potencies, as well as displaying desirable physiochemical and pharmacokinetic properties.

The X-ray structure of the BZP hit (**2.1.8**) bound in the BRD2 acetyl lysine binding site (**Figure 2.1.8**) was able to determine the molecule’s binding mode. The amide group acts as an acetylated lysine mimetic, forming hydrogen bonds to both the key asparagine and tyrosine residues (**Figure 2.1.8**). The remainder of the molecule adopts an unusual bent conformation within the active site, potentially disrupting the conjugation between the alkene and the aromatic unit.

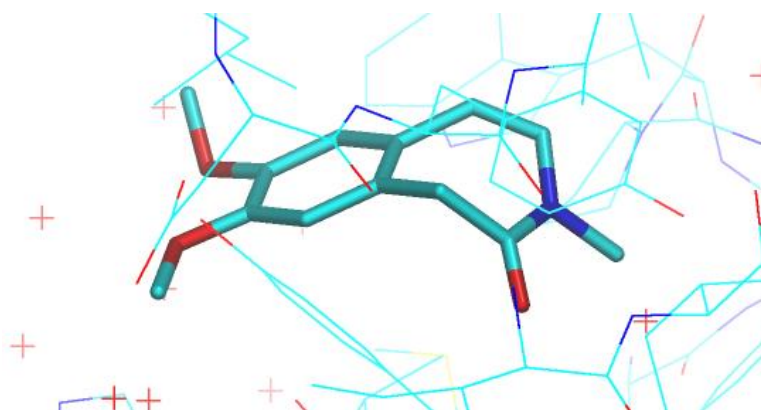


Figure 2.1.8 – X-ray crystal structure of the initial hit (**2.1.8**) bound in the BRD2 BD2 bromodomain (PSILO-8DXIY).

As observed previously, the carbonyl group of the amide acts as the acetylated lysine mimetic. Comparisons between the initial hit (**2.1.8**) (**Figure 2.1.9** - Orange) and an acetylated lysine (**Figure 2.1.9** - Green), used to replicate the histone binding mode, demonstrated that the carbonyl groups occupy almost identical regions of the binding site, both forming hydrogen bonds to key residues (**Figure 2.1.9**).

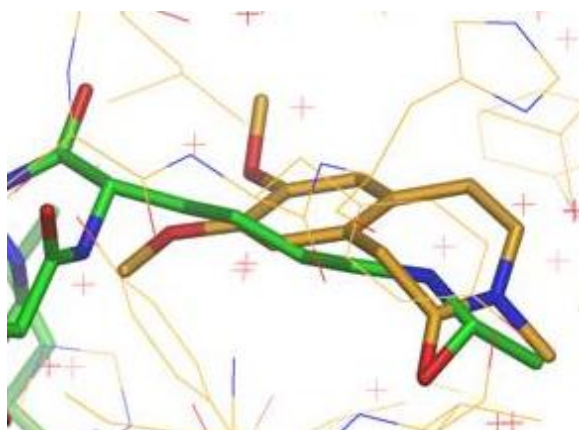


Figure 2.1.9 – Overlaid structures of the BZP hit (**2.1.8**, Orange, PSILO-8DXIY) and the acetylated lysine residue (Green, PSILO-2E3K) highlighting the comparable positions of the two carbonyl groups.

The crystal structure of the initial hit (**Figures 2.1.8** and **2.1.9**) and the already extensive knowledge of the BET proteins within our laboratories was able to guide the development of this core. One of the earliest modifications was the exploration of substitution α to the carbonyl group. Analysis of the crystal structure, and overlaying this with the historical BET-inhibitor

(2.1.5) was able to identify a small binding site in this position, building into the region occupied by the pyrrole group in the historical inhibitor (2.1.5) (**Figure 2.1.10**).

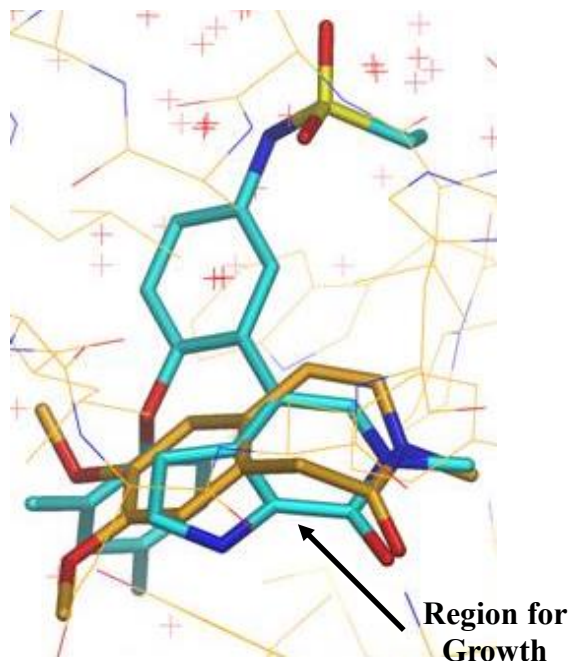


Figure 2.1.10 – Overlay of the initial hit compound (2.1.8, PSILO-8DXIY) and the historical inhibitor (2.1.5, PSILO-7BJGT), highlighting the small pocket for growth/elaboration.

Addition of a methyl group adjacent to the carbonyl in (2.1.8) was found to increase both the BD1 and BD2 potencies. The methyl compound was synthesised as the racemate, which was then subjected to chiral purification methods to afford the single enantiomers.²⁵³

(*R*)-Methyl analogue (2.1.9) increased the BD1 and BD2 potencies by over 10-fold (**Figure 2.1.11**) relative to the initial hit (2.1.8). The (*S*)-methyl enantiomer (2.1.10) was found to have a significant reduction in binding potency. X-ray crystallographic analysis of the active enantiomer (2.1.9) was able to putatively assign the stereochemistry of this enantiomer as the (*R*)-isomer. The chirality of this molecule has subsequently been shown to be crucial for binding activity, with the (*R*)-enantiomer typically being 1.5-2.0 log units more potent than the (*S*)-enantiomer.

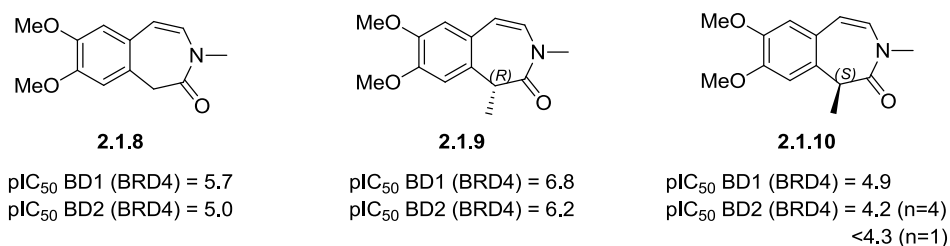


Figure 2.1.11 – Data for the methyl enantiomers. X-ray crystallography was used to assign the stereochemistry of the more potent enantiomer (**2.1.9**).

The stereocentre is postulated to control the major binding conformation of the molecules, dictating whether the major conformation of the compound is bent into the correct binding orientation (see **Figures 2.1.8 - 2.1.10**). Although the inactive/poorly active enantiomer can bend to adopt the correct binding orientation, the enthalpic penalty for the *pseudo*-axial methyl group and the clash between the methyl group and the protein result in a significant loss of binding affinity being observed.

Although significant optimisation of this core has been able to further increase the potencies, as well as modulate the pharmacokinetic (PK) properties of the BZP series, an in depth discussion of this work is beyond the scope of this thesis. However, there are several key learnings from this work that are important for subsequent discussion and will be elaborated on.

The extensive structure activity relationship (SAR) work was able to identify three key vectors for control of the potency, selectivity, and PK properties of the BZPs (**Figure 2.1.12**).²⁵⁴ These explore well-defined regions of the bromodomain binding site that have been extensively documented previously, *vide supra*.

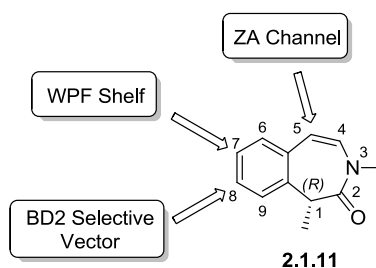


Figure 2.1.12 – Unsubstituted BZP core (**2.1.11**) and the three major vectors for elaboration.

2.1.5.1 WPF Shelf Region

Elaboration of the 7-position builds into the hydrophobic WPF shelf region (Section 2.1.2) and was found to give significant increases in potency for the BZP series, with a variety of groups tolerated in this position. Representative examples are shown below (Figure 2.1.13), with the unsubstituted core (2.1.11) provided for reference.²⁵⁵ Although aromatic groups are tolerated on the WPF shelf, providing increases in both BD1 and BD2 activity, it was desirable to avoid the addition of further aromatic groups to maintain good physicochemical properties, in particular, solubility.

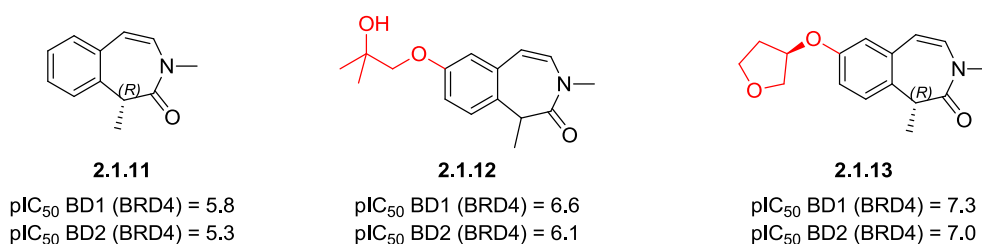


Figure 2.1.13 - Examples of the increased potency of BZP compounds with 7-position substituents relative to that of the unsubstituted core (2.1.11).²⁵⁵

2.1.5.2 ZA Channel

In contrast to the WPF shelf, the SAR work found that the narrow ZA channel (Section 2.1.2) requires planar aromatic substituents, to efficiently occupy this region and further enhance the BZP potencies. The potency increases when combined with a WPF shelf group are typically found to be additive, generating potent pan-BET inhibitors (Figure 2.1.14).²⁵⁶

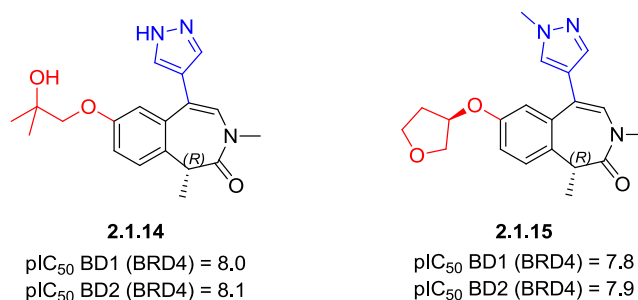


Figure 2.1.14 – Combined ZA channel and WPF shelf substituted BZP compounds.²⁵⁶

2.1.5.3 Substitution at the 8-Position

The final major vector for elaboration of the BZP core is the 8-position. As observed in the initial hit (**2.1.8**), substitution at this position is tolerated. Growth of the core into this region can increase the potency of the molecules (**Figure 2.1.15**).²⁵⁴ In contrast to the 5- and 7-positions, this vector grows towards a region of the domain which is non-conserved between the BD1 and BD2 domains. Therefore, in order to retain the desired *pan*-BET selectivity profile this position only tolerates smaller substituents (**Figure 2.1.15**), with larger substituents often resulting in an undesirable increase in BD2 selectivity.²⁵⁴

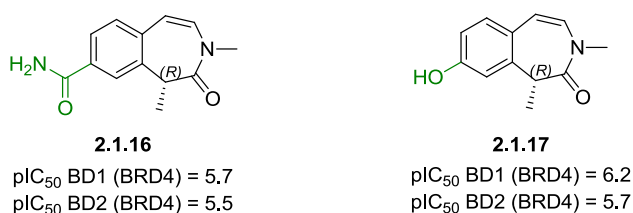


Figure 2.1.15 – Small substituents at the 8-position with *pan*-BET selectivity.

2.1.6 Removal of the Alkene

Despite the diverse range of molecules synthesised and evaluated, several key features are conserved across the BZP series. One of the concerns about the further progression of the BZP series was the presence of the alkene group. Although, to date, there have been no toxicological issues identified with this motif, concerns about potential metabolism or other undesired *in vivo* processes remain, and therefore alternatives were sought.

One potential method to mitigate the risk of the alkene was to remove this group from the core. To determine the influence of the alkene on the potency of the BZP series, saturated analogues of the BZP series were prepared. Unfortunately, in all instances, these analogues displayed a significant reduction in potency relative to the corresponding BZP compounds (**Figure 2.1.16**).²⁵⁴

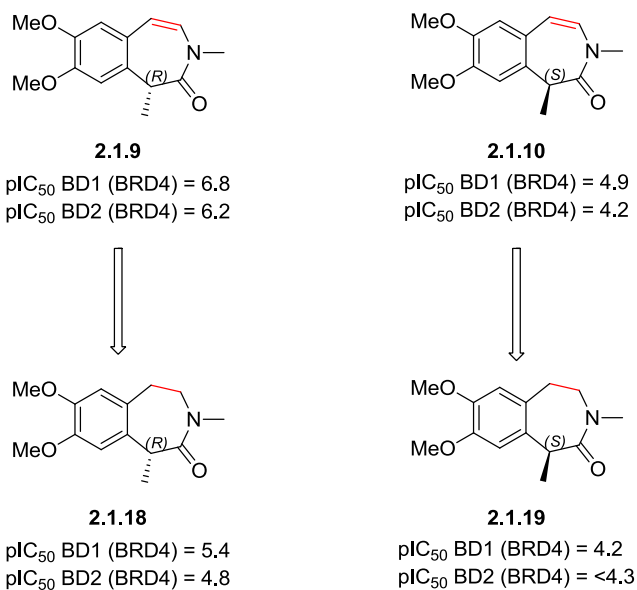


Figure 2.1.16 – Comparison between BZP analogues (**2.1.9** and **2.1.10**) and the saturated analogues (**2.1.18** and **2.1.19**). X-ray crystallography was used to confirm the stereochemistry of the more potent enantiomer.

As observed in the BZP series, the (*R*)-enantiomer (**2.1.18**) displayed greater potency than that of the (*S*)-enantiomer (**2.1.19**). However the dramatic loss of potency for the saturated analogues meant that this core was not suitable for further progression.

In order to understand the role and importance of the alkene for potency, an explanation for the dramatic potency differences was sought. The first potential hypothesis was that the two series exhibited significantly different binding modes. To probe this, the X-ray crystal structures of the saturated analogue (**2.1.18**) and the corresponding BZP (**2.1.9**) were compared (**Figure 2.1.17**).

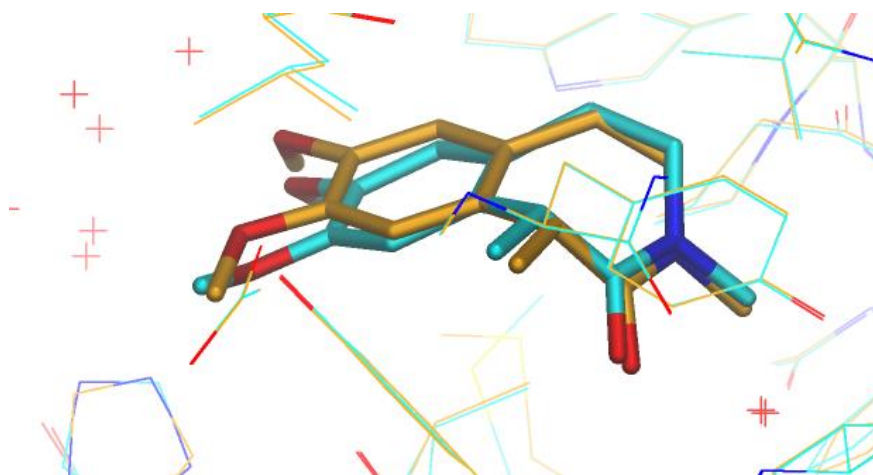


Figure 2.1.17 – BRD2 BD2 X-ray crystal structure overlay of BZP analogue in orange (**2.1.9**, PSILO-9WNNE) and the corresponding saturated analogue in blue (**2.1.18**, PSILO-4NORT).

In both cases the molecules adopt similar binding conformations, with only subtle differences in the binding site. The slight displacement of saturated analogue (**2.1.18**) relative to the BZP (**2.1.9**) is insufficient to explain the dramatically disparate binding potencies. Therefore, an alternative explanation was sought.

As the two analogues both bind the bromodomain in the same fashion, it was postulated that the differences in binding energetics may be attributed to differences in the solution conformations. Molecular mechanics calculations (Maestro, OPLS forcefield in GBSA solvent) for the BZP (**2.1.9**) conformation showed that in solution this molecule exists predominately in one conformation.²⁵⁷ This conformation complements the binding mode and no enthalpic penalty is incurred on binding.

For the saturated analogue (**2.1.18**) the same computational approach suggested that in solution the molecule possesses multiple energetically accessible conformations. Unlike the BZP analogue, the lowest energy conformation did not complement the binding site. The calculated energy difference between the lowest energy solution conformation and the binding conformation was 7 kJ mol^{-1} .²⁵⁷ This enthalpic difference or strain energy can explain the large decrease in the binding energies and potency, between the saturated and unsaturated analogues.

This work demonstrated that in the BZP series, the alkene is important for maintaining the optimal binding conformation. Therefore, the direct removal of this group is unlikely to provide potent pan-BET inhibitors.

2.1.7 Alternative Methods to Mimic the BZP Conformation

As the alkene in the BZP core (2.1.8) restricts the molecule into the required binding conformation, alternative methods to constrain the seven-membered ring in this conformation were sought. A potential alternative tricyclic framework was identified that would mimic the BZP conformation. The 5-membered ring in this tricyclic structure (2.1.20) is proposed to lock the seven-membered ring into the desired binding conformation (Figure 2.1.18) as evidenced by computational modelling. The 5-membered ring of the tricyclic core could be accommodated in the ZA channel region of the protein.

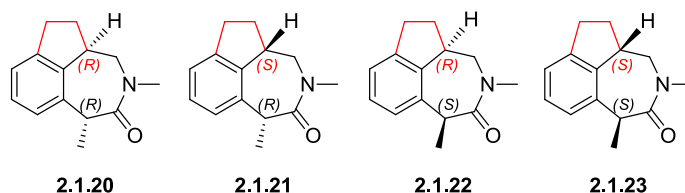


Figure 2.1.18 – Four stereoisomers of the potential tricyclic BZP mimetic.

The presence of two stereogenic centres in the molecule are expected to have a profound influence on the conformation of the tricyclic analogue. With the saturated analogue highlighting the importance of the BET inhibitors conformation, the potential active isomer required identification. Molecular modelling utilising MOE (molecular operating environment) of the individual stereoisomers predicted that the lowest energy conformation of (*R,R*)-isomer (2.1.20) matched that of the active BZP core (Figure 2.1.19).

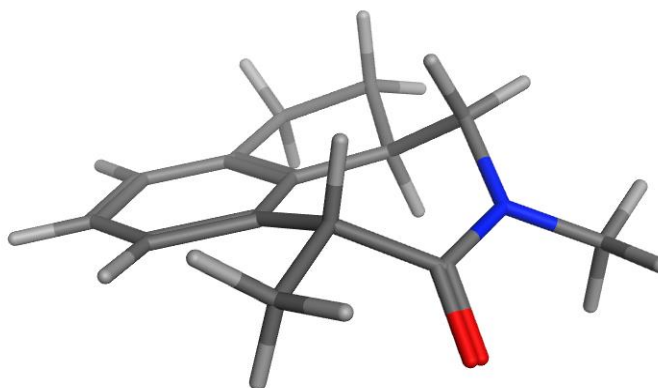


Figure 2.1.19 – MOE (Molecular Operating Environment) energy minimised forcefield structure of the proposed (*R,R*)-tricyclic analogue (**2.1.20**).

Despite the molecular modelling suggesting that the tricyclic analogue (**2.1.20**) possesses a comparable conformation to the BZP series, this required experimental validation. Slight discrepancies in the conformation or the extra carbons atoms may influence the binding and subsequently the potency. In addition to this, elaborated analogues exploring the previously discussed vectors, in attempts enhance potency, require synthesis. This will enable the developability of the tricyclic to be evaluated, as well as demonstrating if the BZP SAR can be transferred to this new series.

2.1.8 BET Project Aims/Objectives

In order to assess the potential of the tricyclic series as BET bromodomain inhibitors and to determine if they necessitate further investigation, this project aims to address several key issues:

- 1) Development of a synthetic route to enable access to the tricyclic analogue (**2.1.20**). To enable a comprehensive comparison to the BZP core (**2.1.11**), the synthesis needs to provide sufficient material, greater than 100 mg, for comprehensive assessment and chiral purification.
- 2) The synthesis and biological testing of a small series of elaborated tricyclic molecules. This will enable the developability of the core to be assessed, and will enable the decision to carry on with the core or terminate the investigations into this analogue.

2.2. Investigations into the Tricyclic Core (2.1.13)

2.2.1 Previous Synthesis of the Carbon Skeleton

At the time of writing, there is no known reported synthesis of the unsubstituted tricyclic core (2.2.20). Only one synthesis of a related molecule (2.2.1), sharing the same tricyclic architecture, has been reported by Weinstock *et al.* In 1987, Weinstock *et al.* published the synthesis of a tricyclic molecule (2.2.1) as an intermediate in their investigations into potential dopamine agonists (Figure 2.2.1).²⁵⁸

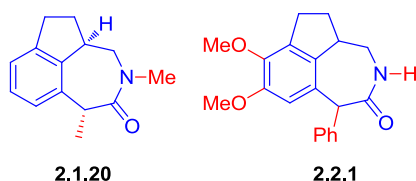
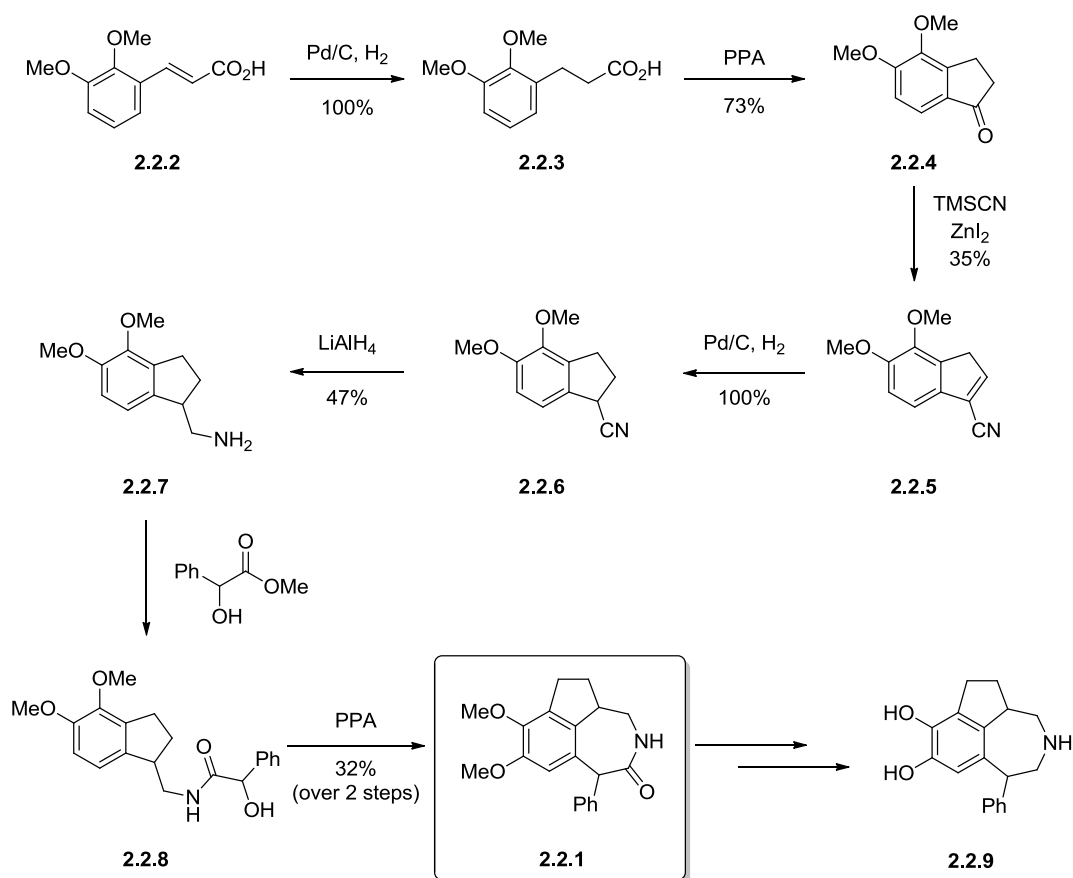


Figure 2.2.1 – Comparison between the desired tricyclic core (2.1.13) and tricyclic intermediate (2.2.1), with the similarities in blue and the differences highlighted in red.²⁵⁸

Comparisons between the two molecules show the significant homology between them. Both molecules possess the same carbon skeleton, amide position, and α -substitution pattern. Despite this, there are also several key differences; the dimethoxy substituents on the aromatic ring, the secondary amide group, and the additional aromatic group in the α position. These variations, in particular the distinct electronic properties from the two aromatic groups (2.2.1), underpin the synthesis of Weinstock *et al.* (Scheme 2.2.1).²⁵⁸



Scheme 2.2.1 – Synthesis of the tricyclic intermediate (**2.2.1**) on route to the dopamine agonist (**2.2.9**).²⁵⁸

The synthesis of Weinstock *et al.* begins with the hydrogenation of the α,β -unsaturated acid (**2.2.2**), followed by subsequent polyphosphoric acid (PPA) mediated Friedel-Crafts acylation to yield the dimethoxy indanone intermediate (**2.2.4**).²⁵⁸ Lewis-acid mediated cyanation and elimination of the alcohol forms the unsaturated nitrile (**2.2.5**), which is subsequently hydrogenated to the saturated nitrile (**2.2.6**). Reduction to the primary amine (**2.2.7**), amide coupling, and a second Friedel-Crafts cyclisation yields the tricyclic intermediate of interest (**2.2.1**).

Overall, the synthesis of the tricyclic intermediate consists of 7 linear steps, with an overall yield of 3.8% as a undefined mixture of *cis*- and *trans*-isomers. Further synthetic manipulations were then utilised to convert this into potential dopamine agonist (**2.2.9**).

Unfortunately, this strategy suffers from several drawbacks which may limit the applicability of this route to access both the unsubstituted core (**2.1.20**) and elaborated analogues. Despite

a relatively low number of steps, the overall yield is poor, with the product being obtained as a mixture of isomers. In particular, the synthesis suffers from several low-yielding steps: three reactions under 50% yield, including a 32% yield for the key-cyclisation to construct the seven-membered ring (**2.2.1**). Although the dimethoxy indanone (**2.2.4**) has subsequently been commercialised, the cost of this reagent is prohibitive, inhibiting its use in scale-up operations.

In addition to the low-yield of the cyclisation, the generality of the final Friedel-Crafts cyclisation to generate the 7-membered ring (**2.2.1**) was also a cause for concern. Two factors may limit the application of this ring closing strategy to the synthesis of desired tricyclic core (**2.1.13**) or other analogues. The electron-rich nucleophilic aromatic ring is anticipated to promote the cyclisation reaction. In the case of the cyclisation reported by Weinstock *et al.* the electron-donating dimethoxy substituents increase the nucleophilicity of the ring, facilitating the Friedel-Crafts reaction.²⁵⁸ Without these groups, or with electron-withdrawing groups, the reduced nucleophilicity of the aromatic unit may inhibit the cyclisation, reducing the already low cyclisation efficiencies. The second factor is the stability of the intermediate electrophilic cation, formed under the strongly acidic reaction conditions. In the example reported by Weinstock *et al.*, the resulting positive charge is stabilised by conjugation with the π -system of adjacent aromatic group (**Figure 2.2.2**). In the absence of this group, the destabilisation of the potential cation may inhibit the reaction or, indeed, promote undesirable side reactions, such as elimination to the unsaturated system (**Figure 2.2.2**). It is significant, that despite the favourable factors promoting cyclisation, Wienstock *et al.* only obtained the desired product in a modest 32% yield. A more efficient synthetic strategy to construct the ring system is, therefore, required.

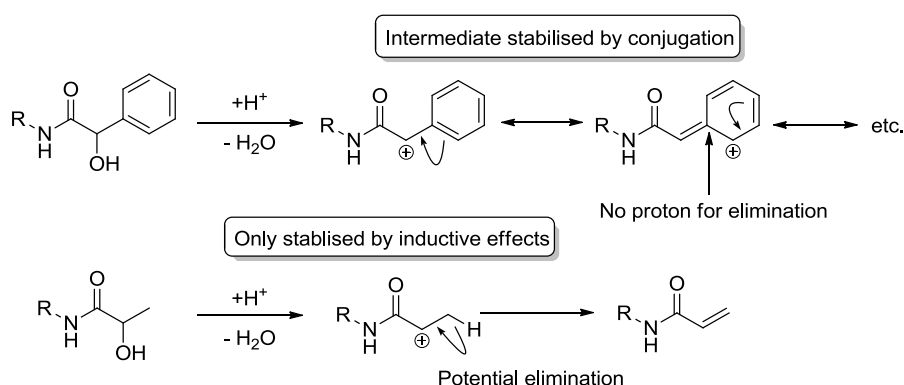


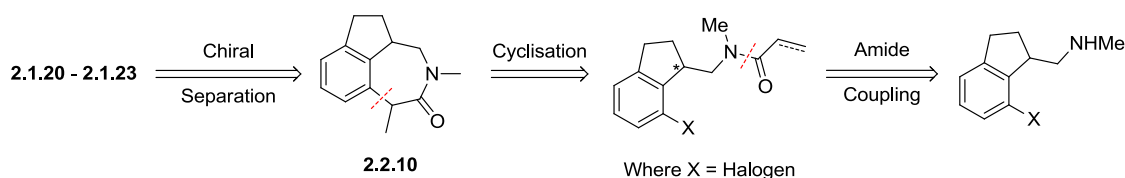
Figure 2.2.2 – Influence of the phenyl group on the intermediate stability and preventing elimination.

In addition to the concerns relating to the viability of the synthetic strategy, the use of toxic reagents detracts further from the synthesis. Most notably TMSCN, represents a safety liability, particularly if scale-up is necessitated. The use of strongly acidic conditions to affect both Friedel-Crafts cyclisation steps also limits the function group tolerance, limiting the synthesis of potential analogues.

Overall, despite the synthesis of Weinstock *et al.* providing access to a comparable core molecule, this route was not appropriate to enable the synthesis of the desired core (**2.1.20**) or elaborated analogues. It was envisaged that a modified strategy, similarly utilising late-stage construction of the seven-membered ring *via* an appropriately functionalised amide, could provide access to the desired core (**2.1.20**).

2.2.2 Retrosynthetic Analysis of the Tricyclic Core

The late-stage retrosynthesis of the desired enantiomer of the tricyclic core (**2.1.20**), constructing the seven-membered ring through an achiral synthetic strategy, is illustrated in (**Scheme 2.2.2**). To enable facile synthesis of the tricyclic core, the initial route was designed without any elements of stereocontrol. The route was planned to enable modification of the strategy to provide an enantioselective synthesis, if the biological evaluation necessitated further investigation, rather than complete redesign of the synthetic strategy being required.

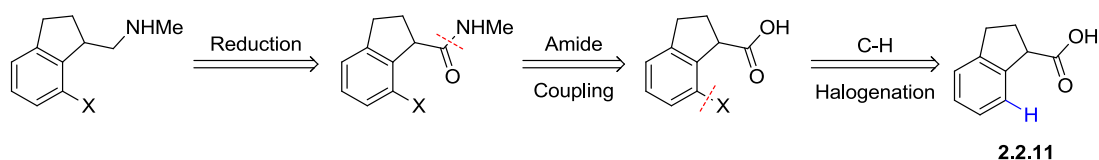


Scheme 2.2.2 – Late-stage retrosynthetic analysis of the tricyclic core (**2.2.10**).

The key step in the synthesis of the achiral tricyclic core (**2.2.10**) was the formation of the 7-membered ring. Due to the limitations of the Friedel-Crafts type cyclisation, *vide supra*, transition metal-mediated cyclisation strategies were considered. Two palladium-catalysed reactions were envisaged: either intramolecular enolate coupling methodologies, or a Heck-type cyclisation followed by reduction.^{259,260} Despite the absence of chiral catalysis/reagents to impart stereocontrol, the close proximity of the second stereocenter (denoted *, **Scheme 2.2.2**), and the predicted well-defined geometry of the cyclised product (**Figure 2.1.19**) are envisaged to convey some diastereoselectivity for the cyclisation. It was hypothesised that if

an asymmetric route was required, control of the marked stereocenter geometry would enable the enantioselective synthesis without requiring further asymmetric methodologies.

Both the non-cyclised amides, alkyl or alkene depending on the cyclisation strategy, can be accessed from a shared amine precursor. Both the corresponding acyl chloride partners are commercially available, enabling facile amide coupling.



Scheme 2.2.3 – Retrosynthetic analysis of the key halogenated amide.

The retrosynthesis of the halogenated amine precursor is outlined in (**Scheme 2.2.3**). The halogenated amine can be accessed *via* reduction of the corresponding amide, with a myriad of different reduction protocols available for this transformation. It was envisaged that this amide could, in turn, be synthesised from the carboxylic acid, *via* a second amide coupling reaction.

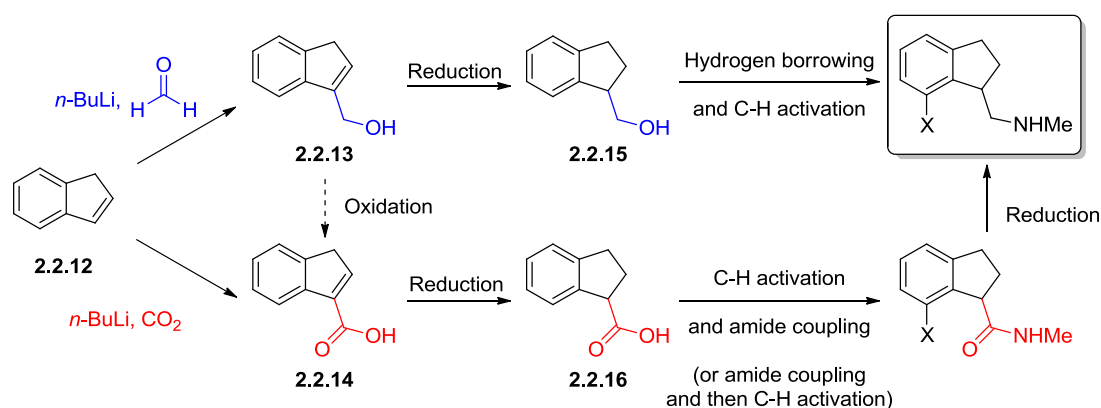
To install the halogen (ideally iodine or bromine due to the weaker bond strengths and subsequent increases in reactivity) a directed C-H activation/halogenation reaction was envisaged. The presence of a coordinating functionality, either the carboxylic acid, amide or amine groups, potentially enables the desired C-H activation/halogenation to be conducted at any of several stages in the synthesis.

The use of carboxylic acids as directing groups in C-H activation is particularly well precedented, including elegant examples from the both the Larrosa^{261–264} and Yu^{265–268} groups. The work from the Yu laboratories is of particular relevance, demonstrating the use of carboxylic acids as directing groups in palladium-mediated C-H activations for a variety of reactions, including halogenations.²⁶⁵ For the desired tricyclic C-H activation, the constrained conformation of the acid on the 5-membered ring (**2.2.11**) is envisaged to facilitate the formation of the 6-membered metallocyclic intermediate, enabling exclusive functionalisation of the desired position. The C-H activation starting materials, either the acid (**2.2.11**) or other species, can be accessed from indene (**2.2.12**), with several different functionalisation

strategies available. The results of the C-H activation, as well as the ease of the synthesis of the precursors and further manipulations will then dictate the overall route employed.

2.2.3 Synthesis of the Halogenated Amine

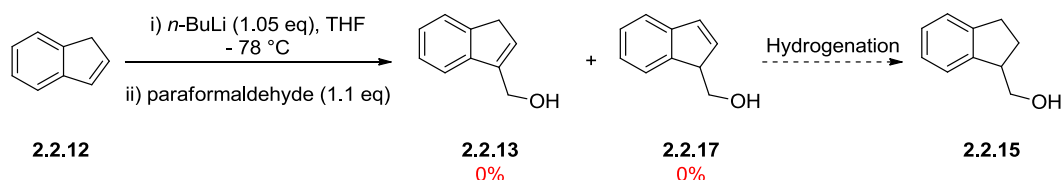
Two concurrent strategies were explored for the functionalisation of indene (**2.2.12**), initially installing either an alcohol (**2.2.13**) or a carboxylic acid group (**2.2.14**). It was envisaged that both species could be accessed through metalation, followed by quenching with an appropriate electrophile (**Scheme 2.2.4**). Both synthetic routes then converge on the desired halogenated amine species. To assess the plausibility of each route and to compare the overall yields, both routes were investigated, as each route possesses potential advantages and drawbacks.



Scheme 2.2.4 – Two convergent strategies to access the key halogenated amide intermediate *via* the alcohol (**2.2.13**) or the acid (**2.2.14**).

In both instances, deprotonation of indene generates the formally aromatic indene anion. Trapping of the indene anion with formaldehyde/paraformaldehyde was envisaged to enable access to the alcohol (**2.2.13**).²⁶⁹ The resulting alcohol could then be hydrogenated to the saturated alcohol (**2.2.15**). Although this would provide access to the racemic alcohol (**2.2.15**), the well-defined internal alkene geometry and the potentially co-ordinating alcohol could facilitate the development of asymmetric variant of this hydrogenation, if required. A hydrogen borrowing approach from this molecule would then enable the synthesis of the corresponding methyl amine, circumventing the requirement for oxidation to enable a more conventional reductive amination procedure.^{270,271} From this intermediate, in addition to the alcohol (**2.2.15**), C-H activation protocols could then be explored.

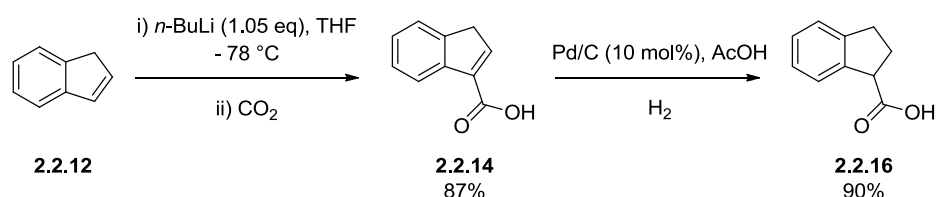
The synthesis of the alcohol (**2.2.15**) has previously been reported in several publications, including that of Ishizone *et al.* in 2015.²⁶⁹ The authors reported that the deprotonation of indene (**2.2.12**), followed by nucleophilic attack on paraformaldehyde, afforded the desired product (**2.2.13**) and the isomer (**2.2.17**) in a combined yield of approximately 60%. It was envisaged that the hydrogenation of the two isomers would then converge on the desired alcohol (**2.2.15**).



Scheme 2.2.5 – Attempted synthesis of indene derived alcohol (**2.2.13**) and convergence on the hydrogenated product (**2.2.15**).

Unfortunately, the initial alkylation could not be replicated, with no significant reaction observed under the conditions of Ishizone *et al.* (**Scheme 2.2.5**). With the inability to access the desired alcohol (**2.2.15**), and concerns about the less-well preceded proposed C-H activation reaction, the alternative pathway (**Scheme 2.2.4**), through the acid intermediate (**2.2.14**), was explored. This route, despite the increased number of steps, possessed greater literature precedent for the key carboxylic acid directed C-H activation. This was therefore prioritised over further investigations into the alcohol route (**2.2.15**).

The synthesis of 2,3-dihydro-1*H*-indene-1-carboxylic acid (**2.2.16**), from indene (**2.2.12**), was previously reported by Braun *et al.* in 2009.²⁷² Gratifyingly, replication of the reported procedures yielded the desired acid (**2.2.16**) in a 78% yield over 2 steps (**Scheme 2.2.6**) after minor optimisation.



Scheme 2.2.6 – Synthesis of 2,3-dihydro-1*H*-indene-1-carboxylic acid (**2.2.16**) using the conditions of Braun *et al.*²⁷²

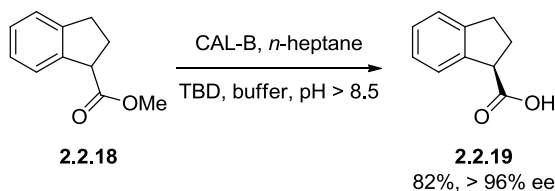
In contrast to the alcohol route (**Scheme 2.2.5**), the first step of the synthesis provided exclusively one product from the first step. It is anticipated that the initial reaction with the

carbon dioxide would produce a non-conjugated product, analogous to the proposed alcohol by-product (**2.2.17**). However, under the basic reaction conditions the resulting alkene migrates to produce the thermodynamically favourable conjugated acid product (**2.2.14**). In the case of the alcohol (**Scheme 2.2.5**), the absence of potential conjugation results in no significant energetic preference for one or the other product (**2.2.13** or **2.2.17**) and therefore a mixture is observed.

In addition to the acid route providing facile access to the desired acid (**2.2.16**) in gram-scale quantities, it also facilitates the potential asymmetric synthesis of the acid if necessary. The single product from the first metalation step (**Scheme 2.2.6**), unlike that for the proposed alcohol (**Scheme 2.2.5**), means that an asymmetric catalytic reduction could be utilised to control the facial selectivity of the reduction, giving rise to a enantioenriched acid.

There are some limitations to this proposed hydrogenation reaction. The asymmetric hydrogenation of comparable literature trisubstituted alkenes are typically conducted under high pressures of hydrogen, using elaborate transition metal catalysts.²⁷³ This suggests that the congested steric environment around this alkene may prove problematic, and both the associated costs of the reagents and experimental limitations may prohibit scale-up operations, if necessitated by biological assessment.

An elegant alternative solution to this problem was provided in 2015 by Braun *et al.*²⁷² The authors investigated the dynamic enzymatic kinetic resolution of the methyl ester (**2.2.18**), to provide access to the optically-enriched acid (**2.2.19**). The authors screened a variety of different esterases, testing for hydrolysis activity and enantioselectivity. After careful optimisation of the reaction conditions, the authors were able to utilise the commercially available enzyme, CAL-B, in combination with the base, 1,5,7-triazabicyclo[4.4.0]dec-5-ene (TBD), to yield the desired acid in excellent yields and enantiomeric excess (**Scheme 2.2.7**).



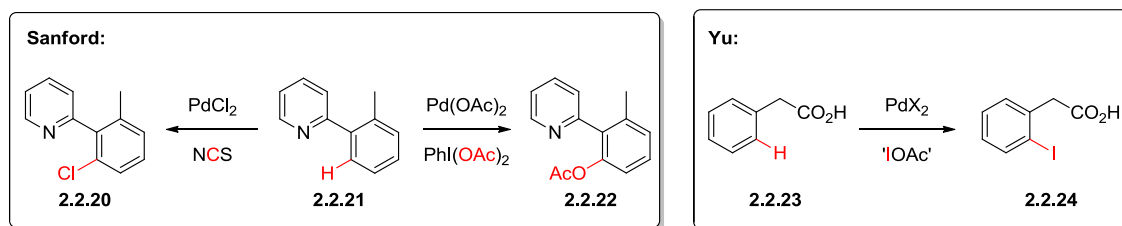
Scheme 2.2.7 – Dynamic enzymatic kinetic resolution to synthesise (*R*)-2,3-dihydro-1*H*-indene-1-carboxylic acid (**2.2.19**).²⁷²

In all but one case, the commercially available esterases assessed showed an enantioselectivity for the (*R*)-enantiomer. It was envisaged that this procedure could be utilised to provide access to the desired (*R*)-enantiomer (**2.2.19**) using environmentally friendly, scalable chemistry, if an asymmetric synthesis was required.

2.2.4 Initial Palladium-mediated C-H Activation/Halogenation

With a robust method to access the acid (**2.2.16**) having been established, the proposed C-H activation process could now be investigated. C-H activation is a broad term, encompassing a wide range of both transition metal-mediated and metal-free processes. Recently C-H activation has received considerable attention from a variety of academic and industrial sources. To enable the synthesis of the halogenated amine derivative (**Scheme 2.2.4**), we required a method to install a halogen or *pseudo*-halogen *ortho* to the carboxylic acid directing group.

Even within the subset of available processes with a carboxylic acid or halogen/*pseudo*-halogen electrophiles, there are still extensive examples of this methodology published. Of particular interest was the work of Sanford *et al.*²⁷⁴ and Yu *et al.* (**Scheme 2.2.7**), *vide supra*.²⁶⁵ In 2009, Sanford *et al.* published the palladium-catalysed, pyridyl-directed, *ortho*-chlorination/acetoxylation. The authors proposed a Pd^{II}/Pd^{IV} catalytic cycle. This was attractive from a synthetic perspective, as it meant that the methodology tolerates halogens within the molecule that would be susceptible to oxidative addition under a Pd⁰ catalytic system. Unfortunately, the major limitation of the methodology was the pyridyl directing group. It was anticipated that the conjugation between the pyridyl group and the aromatic ring locks the conformation, and the strong Lewis basic nature of the pyridyl nitrogen facilitates the *ortho*-metalation process. There were concerns that the addition of the conformational freedom from the addition sp³ linker in the acid (**2.2.16**) may debilitate the reaction. In addition to this, the low reactivity of the chloride may inhibit the final cyclisation process, requiring increased temperatures and more active catalysts to enable oxidative addition within this latter proposed process.



Scheme 2.2.7 – Examples of directed C-H activation work by Sanford and Yu.^{265,274}

More recently, Yu *et al.* published examples of *ortho*-directed C-H activation/iodination of phenylacetic acid derivatives (2.2.23 to 2.2.24).²⁶⁵ The reaction was again proposed to involve a Pd^{II}/Pd^{IV} catalytic cycle, with oxidative addition of the Suárez-type reagent IOAc forming the high oxidation state Pd^{IV} species.²⁷⁵ Due to the instability of IOAc, the methodology employed a combination of iodine and the hypervalent iodine species, PhI(OAc)₂ to form this species *in-situ*.²⁷⁶ The authors also reported that both the starting material (2.2.23) and the product (2.2.24) were susceptible to undesirable decarboxylation reactions. It was suggested decarboxylation could be overcome by running the reactions in the absence of any light sources.

Due to the similarities between the starting substrates and the acid (2.2.16), and the potential to install the reactive iodine group, the conditions reported by Yu *et al.* were selected for initial C-H activation investigations. Despite the resemblance in substrates, the restricted conformation of the acid (2.2.16) and the increased steric demands of this substrate may exert either a positive or negative influence on the reaction. To assess this, the acid was subjected to the conditions reported by Yu *et al.* (**Figure 2.2.2**).²⁶⁵

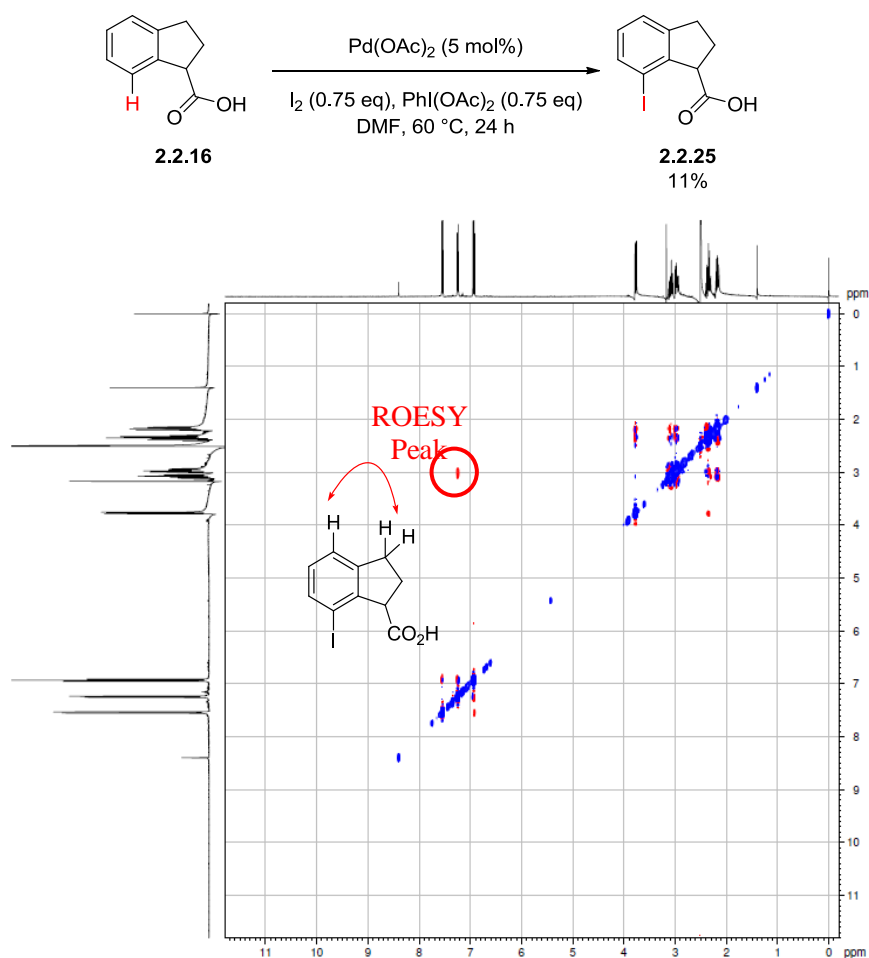


Figure 2.2.2 – Initial investigation into the C-H activation/iodination of the acid (**2.2.16**) and corresponding ROESY spectrum.

Gratifying, under the reaction conditions the desired iodinated product (**2.2.25**) was formed, albeit in low yield. ROESY spectroscopy (**Figure 2.2.2**) was able to confirm that under these conditions iodination was exclusively limited to the desired 7-position, with no non-directed iodination observed.

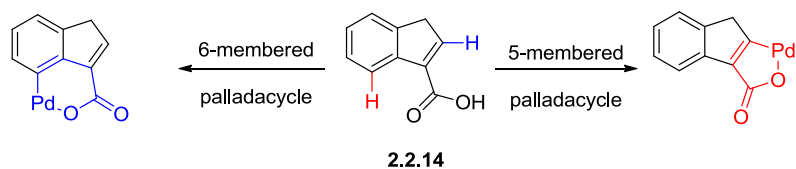
With the viability of the reaction having been demonstrated, attention was turned to the optimisation of the reaction, to enable access to the desired product (**2.2.25**) in synthetically useful yields. The initial reaction had several issues which may have contributed to the low reaction yield. The first was the incomplete reaction conversion, with starting material still observed by LCMS after 24 h. However, at this stage no further reaction progression was observed by LCMS. It is proposed that this was due to the instability of the IOAc species. The breakdown of the oxidant formed *in-situ* would mean that full conversion was not attained. With the relative chromophore strengths of the product (**2.2.25**) and the starting material

(2.2.16) being unknown at this time, determination of an accurate measure of the overall reaction conversion was problematic. If there is a large disparity between the two, then it may be that the LCMS overestimates the levels of the reaction conversion, and that the low conversion was the source of the poor yield attained. Analysis of the reaction mixture was further complicated by fact that the solvent, $\text{PhI}(\text{OAc})_2$ oxidant, and the PhI by-product formed in the reaction mixture are all UV active species.

Another fundamental issue was that of purification. The low yield, 11%, for the initial reaction can also be attributed to the difficulties in the isolation of the product. The acidic nature of both the product (2.2.25) and the starting material (2.2.16), in addition to the by-products from the reaction, meant that the product purification required both normal phase column chromatography and mass directed automatic purification (MDAP) to attain pure sample. This limited the yields and the practicality of the process. Chromatography was further inhibited by the poor chromophore of the product (2.2.25) and the hydrogen bonding nature of the acid groups, adding a further degree of complexity to the purification stage.

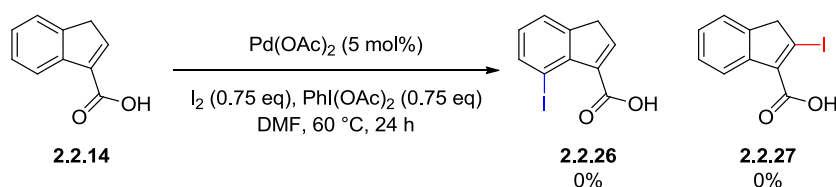
2.2.5 Optimisation of the Palladium-mediated C-H Activation/Halogenation

Before significant optimisation of the reaction of the unsaturated acid (2.2.16) was conducted, the C-H activation protocol was also assessed with the unsaturated acid (2.2.14). The conjugated nature of the acid increases the strength of the UV chromophore of the acid (2.2.14), potentially facilitating the reaction monitoring and subsequent purification. The alkene also removes the potential susceptibility to undergo decarboxylation, by removing the stabilised benzylic site. In addition to this, the increased rigidity may assist with the metalation step, improving the reaction rate and the overall conversion. There were concerns that the additional alkene would provide an alternative site for directed C-H activation (Scheme 2.2.8). However, even if this did occur it could provide a further functional handle for diversification, or could subsequently be removed at a later stage in the synthesis.



Scheme 2.2.8 – Potential sites for directed C-H activation.

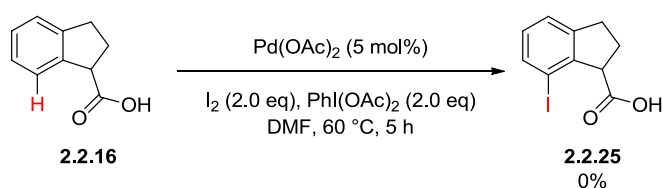
To determine the ratio of product formation, and if there was any benefits to conducting the C-H activation at this earlier stage, the acid (**2.2.14**) was subjected to the conditions of Yu *et al.* (**Scheme 2.2.9**).²⁶⁵ Under the literature conditions, no reaction was observed. After 24 h, the reaction mixture still showed predominately starting material, with low levels of unidentifiable by-products. This demonstrated that the indene species (**2.2.14**) was not a viable substrate for the C-H activation work.



Scheme 2.2.9 – Attempted C-H activation of the acid intermediate (**2.2.14**).

The attention of the subsequent optimisation returned to the saturated system (**2.2.16**), as the feasibility of this reaction had already been established (**Figure 2.2.2**). The first issue that was investigated was the incomplete reaction conversion.

It was thought that the instability of the intermediate IOAc was the major source of the incomplete reaction conversion, *vide supra*. The reaction was, therefore, repeated with significantly larger quantities of iodine and PhI(OAc)₂, increasing from 0.75 equivalents to 2.00 equivalents of each reagent (**Scheme 2.2.10**). With each equivalent of iodine and PhI(OAc)₂ forming two equivalents of IOAc, it was envisaged that the large excess IOAc would be sufficient to attain quantitative reaction conversion.

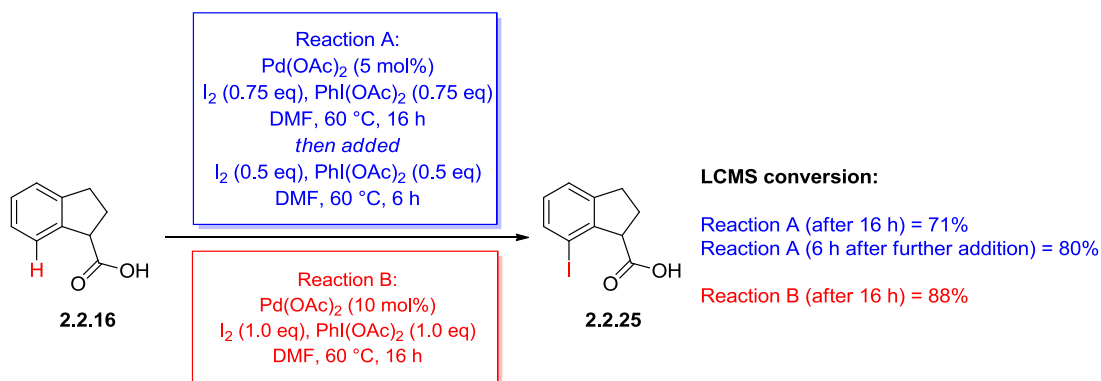


Scheme 2.2.10 – Attempted C-H activation with increased iodine and PhI(OAc)₂ loadings.

Surprisingly, under the reaction conditions with increased loadings, no starting material (**2.2.16**) or product (**2.2.25**) could be discerned by LCMS. In addition to this, a significant increase in the pressure of the reaction vessel was observed. These observations suggest that the increased levels of IOAc cause significant decarboxylation of the acid to occur, with the gaseous evolution of the resulting carbon dioxide causing the pressure increase. A cause for

concern was that neither of the proposed decarboxylated materials, starting material or product, could be discerned by LCMS. The LCMS spectrum after five hours only showed peaks corresponding to the solvent and PhI by-product, both assigned by comparing to reference samples of both species. This suggests that the decarboxylated product/s peaks are obstructed by these peaks and prevents assessment of the levels of decarboxylation. This decarboxylation could be another factor in the low yields observed for the initial reaction (**Scheme 2.2.8**).

There were two potential solutions to attain complete reaction conversion, while avoiding the undesired decarboxylation: either increasing the catalyst loading or portionwise addition of the iodine and PhI(OAc)₂ (**Scheme 2.2.11**). It was envisaged that the increased catalyst loading would increase the overall rate of reaction, assuming the metalation step is rate determining, thereby reducing the proportion of IOAc degradation and increasing the reaction conversion. The portionwise addition was proposed to increase the levels of overall product by maintaining levels of IOAc, without the high quantities which appeared to have caused decarboxylation (**Scheme 2.2.10**). In both instances, the LCMS ratio of product (**2.2.25**) to starting material (**2.2.16**) was used to assess the reaction conversion.

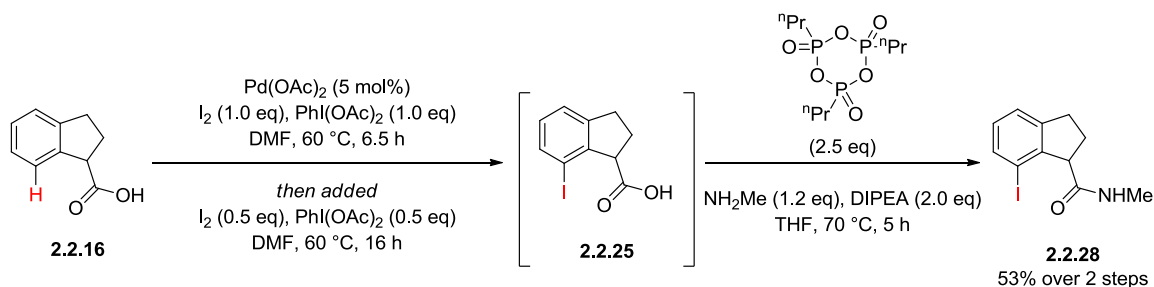


Scheme 2.2.11 – Assessing the influence of the portionwise addition (reaction A) or increased catalyst loading (reaction B) on the overall reaction conversion.

In both instances, LCMS suggested that the modified conditions improved the reaction conversion, relative to the initially explored reaction (**Figure 2.2.2**). The portionwise addition (reaction A, **Scheme 2.2.11**) demonstrated that the addition of further equivalents of IOAc were able to exhibit a small but significant increase in the reaction conversion. The increased catalyst, with a slight increase in substrate loading, was also able to show significant improvements to the overall reaction progression.

With no method to monitor the levels of decarboxylation, attempts were made to purify both reactions to obtain accurate yields for the reactions. Unfortunately, in both instances, the reported work-up protocol and column chromatography were unable to provide the iodinated product (**2.2.25**) in sufficient purity to enable determination of an accurate yield.

Having demonstrated that the problem of low/incomplete reaction conversion could be overcome, the work-up/purification stages were explored in more detail. It was hypothesised that the predominant issue with the isolation was the acid functionalities, inhibiting the purification of the product (**2.2.25**) from other acidic by-products and starting material (**2.2.16**). In order to overcome these issues, the conversion of the crude acid (**2.2.25**) to the corresponding amide (**2.2.28**) was investigated (**Scheme 2.2.12**). It was rationalised that this amide (**2.2.28**) would have reduced interactions with the silica purification media, facilitating purification of the substrate. In addition to this, it would improve the overall green metrics of the synthesis, by reducing the number of purification steps.²⁷⁷



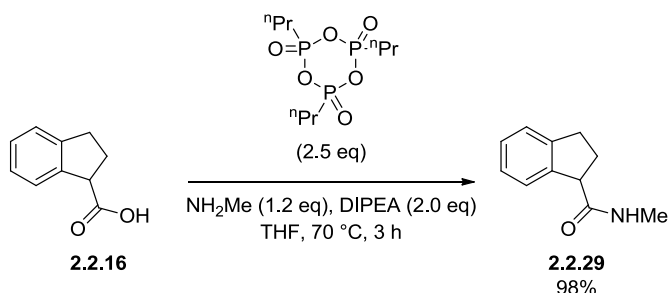
Scheme 2.2.12 – Attempted C-H activation and amide coupling without purification of the intermediate acid (**2.2.25**).

Utilising a combination of the modified conditions; increased initial loading of IOAc precursors and further portionwise addition, was able to give almost complete conversion to the desired acid (**2.2.25**). An extensive work-up procedure, see experimental section for details, utilising the acidic properties of this intermediate, was able to provide material of sufficient purity to be used in the next step without purification. The 2,4,6-tripropyl-1,3,5,2,4,6-trioxatriphosphorinane-2,4,6-trioxide (T3P) mediated coupling of this intermediate (**2.2.25**) yielded the desired amide (**2.2.28**), which could be purified at this stage to give an overall yield of 53% from the acid (**2.2.16**). With the yields for the corresponding C-H activation reported by Yu *et al.* ranging between 62-90%, this yield was within the range

of the literature values. As such no further work into the optimisation of this reaction was conducted.

2.2.6 Rhodium-mediated C-H Activation/Halogenation

With the difficulties in the acid directed C-H activation (**Scheme 2.2.8** – **Scheme 2.2.10**), in addition to the optimisation of this reaction, alternative C-H activation methods were sought. It was envisaged that employing an amide directing group may have several benefits, including facilitating purification, *vide supra*, and preventing the decarboxylation that the carboxylic acid (**2.2.16**) is susceptible to. To prevent the elongation of the synthesis, by requiring changing the amide directing group, C-H activation/halogenation conditions with the methyl amide group were sought. The desired substrate could again be synthesised through the use of T3P-mediated amide coupling reaction in a 98% yield (**Scheme 2.2.13**).



Scheme 2.2.13 – Amide coupling of the acid (**2.2.16**).

The use of amide directing groups in palladium catalysed C-H activation reactions is well precedented (**Figure 2.2.3**). These reactions often utilise specially designed and optimised directing amide functionalities, which then require subsequent removal.²⁷⁸ Despite the excellent yields and reactivities afforded by these groups, the addition and subsequent removal of these groups as well as a further amide coupling reaction, meant that alternative C-H activation methods were sought.

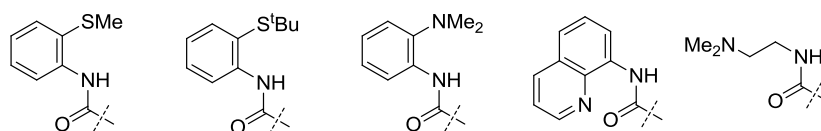
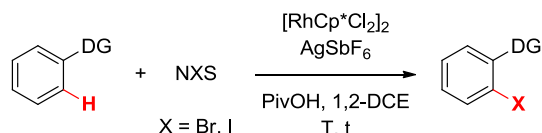


Figure 2.2.3 – Representative examples of amide directing groups for C-H activation reactions.²⁷⁸

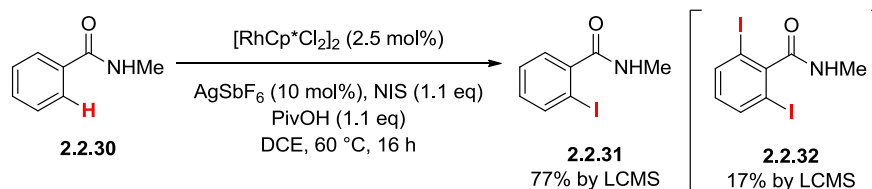
The recent revolution in C-H activation has not just been limited to palladium, with a diverse range of transition metal catalysed C-H activations having been reported, including cobalt,^{279–281} manganese,²⁸² iron,²⁸³ and rhodium.^{284–286} In 2012, Glorius *et al.* reported a rhodium-catalysed *ortho*-bromination/iodination reaction, directed by a range of both carbonyl and heterocyclic directing groups (**Scheme 2.2.14**) in excellent yields.²⁸⁷ In contrast to the palladium process reported by Yu *et al.*, the reaction utilised comparatively mild reaction conditions without the need for the highly reactive IOAc oxidant.²⁶⁵



Scheme 2.2.14 – General scheme for the rhodium-catalysed C-H activation/halogenation.²⁸⁷
DG = directing group.

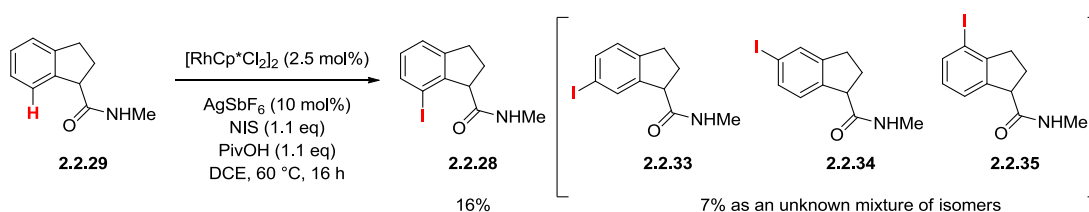
The major limitation of this method, was the position of the directing group. In almost all instances, the directing group was directly attached to the aromatic ring, enabling C-H activation *via* a five-membered metallocycle, not the desired six-membered metallocycle for the tricyclic species targeted within this research. Investigation into the compatibility of this methodology with the desired amide (**2.2.29**) was required.

Included in the diverse range of directing groups reported by Glorius *et al.* were a range of both secondary and tertiary alkyl amides. Despite this wide scope, the use of the NHMe directing group, such as that contained in the amide (**2.2.29**), was not reported. To demonstrate that this group is indeed a viable directing group and that the C-H activation reported by Glorius *et al.* could be replicated, this directing group was assessed in a simplified analogue (**2.2.30**) (**Scheme 2.2.15**).



Scheme 2.2.15 – Rhodium-mediated C-H activation assessing the NHMe amide directing group.

Conducting the reaction under the standard reported conditions demonstrated that the amide was an efficient directing group, with both mono- and di-iodination occurring under the reaction conditions. With the viability of the directing group having been demonstrated, the focus of the research was turned to the reaction of the desired amide (**2.2.29**). In the first instance, the amide substrate (**2.2.29**) was subjected to the same reaction conditions (**Scheme 2.2.16**).



Scheme 2.2.16 – Rhodium-catalysed C-H activation/iodination of the NHMe amide (**2.2.29**).

Gratifyingly, under the standard reaction conditions, the reaction was partially successful. The desired product (**2.2.28**) was isolated in a modest yield as the major product after MDAP purification. In contrast to the model substrate (**2.2.30**), the reaction gave a complex mixture of the other regioisomers (**2.2.34** – **2.2.36**) which could not be separated. The reduction in regioselectivity is attributed to two factors: the increased nucleophilicity of the aromatic ring, enhancing the rate of electrophilic iodination, and the presence of the additional sp^3 carbon linker, reducing the efficiency of the C-H activation step.

The addition of the additional sp^3 linker, removes the amide directing group from direct conjugation with the ring. This has two major influences. In the model substrate (**2.2.30**), the electron-withdrawing amide reduces the relative nucleophilicity of the ring, and therefore inhibits the undesirable electrophilic substitution reaction. With the substrate (**2.2.29**) the C-H activation step is more challenging, with the formation of a six-membered metallocycle instead of the five-membered intermediate in the model substrate. The work of Glorius *et al.* did present some limited examples of six-membered metallocycle formation (**Figure 2.2.4**). However, these substrates all possess heteroatom linkers, increasing the electron density on the directing group to facilitate C-H activation by enhancing the coordination strength to the rhodium(III) metal, and reducing the conformation freedom. In our substrate (**2.2.29**) neither of these factors are present.

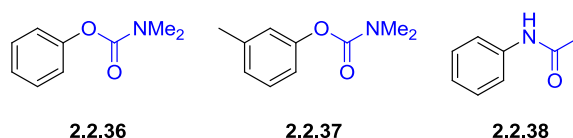


Figure 2.2.4 – Directing groups utilised by Glorius *et al.* that form six-membered metallocyclic intermediates.

With the demonstration of the viability of the novel rhodium-mediated C-H activation (**Scheme 2.2.16**), the research was focused onto understanding the factors which control the regioselectivity and the overall yield of the process. The first factor examined was the influence of the rhodium catalyst. It was envisaged that the desired product (**2.2.28**) could be formed *via* either a rhodium-mediated C-H activation reaction (**Figure 2.2.5** – Pathway A), or the uncatalysed direct electrophilic substitution reaction at this position through nucleophilic attack on the NIS (**Figure 2.2.5** – Pathway B).

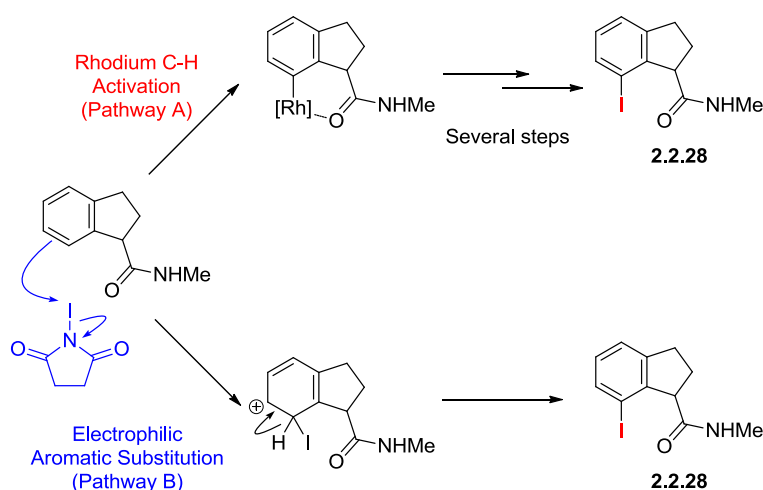
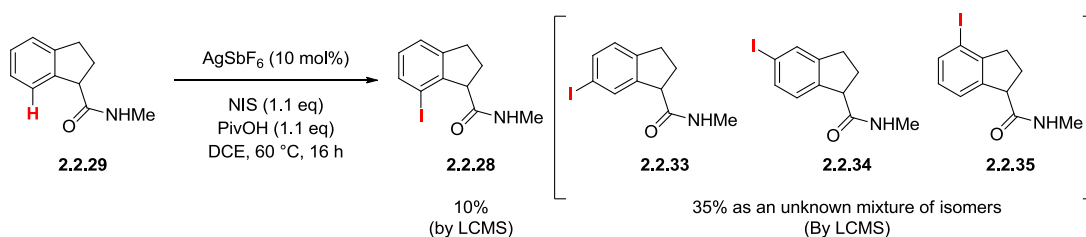


Figure 2.2.5 – Two potential mechanistic pathways to form the iodinated product (**2.2.28**).

To attempt to quantify the relative rates of the two competing pathways, the reaction was replicated in the absence of the rhodium (**Scheme 2.2.17**). Under these conditions, product (**2.2.28**) formation is due to the uncatalysed pathway (**Figure 2.2.5** – Pathway B). By comparing the relative amounts of the other regioisomer formation, the influence of the rhodium on the reaction can then be more accurately assessed.



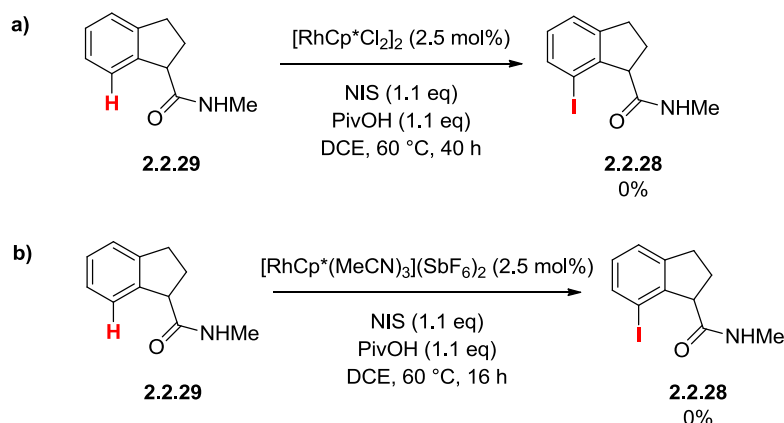
Scheme 2.2.17 – Investigations into the non-rhodium catalysed electrophilic aromatic substitution reaction.

In contrast to the rhodium reaction (**Scheme 2.2.16**), there is an inversion of the regioselectivity, from a product:by-product/s ratio of 2.2:1, to a ratio of 0.28:1, an almost ten-fold decrease in the desired reaction pathway. This demonstrates that the rhodium-mediated C-H activation pathway (**Figure 2.2.5** – Pathway A) is the dominant reaction pathway process with the rhodium present, and that, despite the anticipated difficulties with the C-H activation, the desired reaction is occurring.

With the importance of the rhodium having been established, the next reaction variable that was considered was the role of the silver salts in the reaction. Silver additives are commonly utilised as halophiles in combination with group nine metals.²⁸⁸ These salts serve to remove and sequester the halogen ligands, resulting in the formation of a more activated cationic metal species, enhancing coordination to the directing group. It was postulated that in addition to this role, the silver salts exert an influence on the reactivity of NIS halogen source. In the earlier palladium research, the desired product was formed as exclusively one halogenated regioisomer, with no undesired non-selective electrophilic pathways in evidence, despite the electrophilic iodine in the reaction mixture (**Section 2.2.5**). This suggested that the silver salts may be performing multiple roles under the reaction conditions.

To probe this hypothesis, two experiments were conducted. The first experiment replicated the previously successful reaction (**Scheme 2.2.16**), without the silver additive (**Scheme 2.2.18a**). Despite the influence of the silver salts on the activation of the group nine metals, they are not always necessitated, particularly when strong directing groups are utilised. In addition to assessing if the C-H activation could be conducted in the absence of the silver salts, it also enables the influence of the silver salts on the electrophilic pathway to be assessed. The second experiment (**Scheme 2.2.18b**), utilised an alternative rhodium(III) catalyst, tris(acetonitrile)pentamethylcyclopentadienylrhodium(III) hexafluoroantimonate. This preformed ‘cationic’ rhodium catalyst does not require any prior activation by silver salts,

while retaining or even enhancing the reactivity.²⁸⁷ If no reaction was observed with this catalyst system, it implies that the silver performs multiple roles under the reaction conditions.



Scheme 2.2.18 – a) Attempted C-H activation reaction without silver additives; b) Attempted C-H activation reaction with the alternative rhodium catalyst.

In the absence of the silver no reaction (**Scheme 2.2.18a**), either C-H activation or electrophilic substitution, was observed. This provides evidence that the silver salts are responsible for the electrophilic pathway, increasing the electrophilicity of the iodine species within the reaction mixture. The influence on the C-H activation is less conclusive; either the absence of the reaction is due to the silver serving to activate the NIS towards this pathway, or without the silver the rhodium catalyst is not activated, and no reaction is observed.

The second reaction (**Scheme 2.2.18b**) however, points towards the first explanation. Only trace levels of any product formation, either product or by-product, were observed by LCMS. This provides further evidence for the importance of the silver salts for the reaction. It was proposed that the silver salts act as a Lewis acid, coordinating to the NIS carbonyl group. It is thought that this would cause an elongation and weakening of the nitrogen-iodine bond, facilitating both nucleophilic attack or oxidative addition pathways (**Figure 2.2.6**).

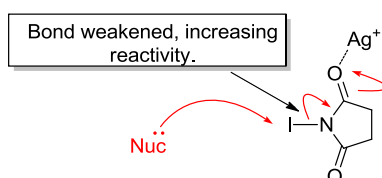
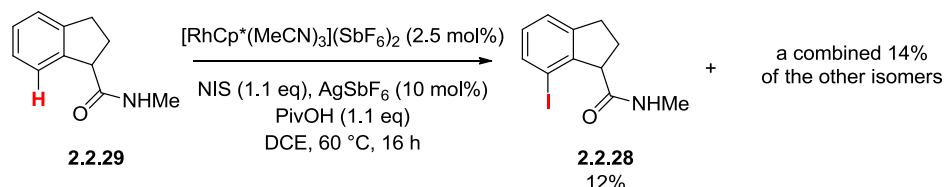


Figure 2.2.6 – Proposed activation of NIS by Lewis acidic silver(I) salts.

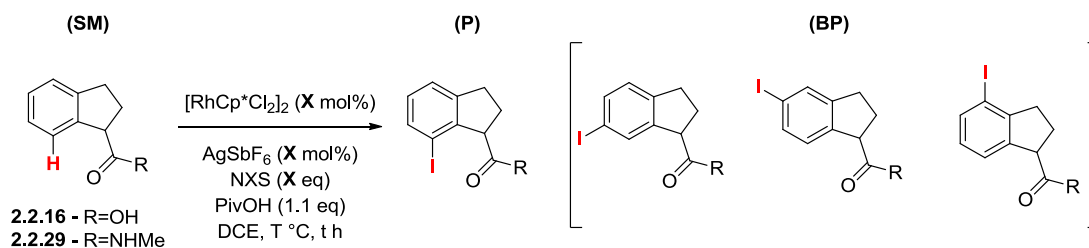
To confirm the hypothesis, the reaction with tris(acetonitrile)pentamethylcyclopentadienylrhodium(III) hexafluoroantimonate was replicated, with the addition of the silver source, AgSbF₆. It was postulated that this would restore the reactivity of the NIS, enabling catalysis with the alternative ‘cationic’ catalyst.



Scheme 2.2.19 – Exploring the influence of the silver salts on the C-H activation reaction.

The addition of the silver salts was able to restore reactivity to the system, enabling both the C-H activation and electrophilic pathways to occur. Since this work was conducted, the use of silver salts to activate NIS for electrophilic substitution reactions has been reported by Sutherland *et al.*²⁸⁹ As part of their work on electrophilic aromatic iodination reactions, the authors screened a small set of potential Lewis acids as prospective catalysts. From this several different silver salts, including AgSbF₆, were identified as catalysts for the reaction. This suggests that the silver behaves in a comparable manner in the C-H activation reactions.

Having established the importance of the silver and rhodium to the C-H activation process, the optimisation was now focused on the temperature and the loading of the catalyst and silver. It was envisaged that the C-H activation pathway (**Figure 2.2.4** – Pathway A) and the electrophilic pathway (**Figure 2.2.4** – Pathway B) would have different dependences on these variables, and therefore the reaction conditions could be varied to prefer the C-H activation pathway. A range of different temperatures, catalyst loadings, and halogen sources were investigated (**Scheme 2.2.20**; **Table 2.2.1**).



Scheme 2.2.20 – General procedure for the investigations into the rhodium mediated C-H activation process.

Entry	Substrate	NXS (X = I, Br)	Catalyst Loading (mol%)	Silver Loading (mol%)	T (°C)	Time (h)	Yield (LCMS%), P:BP:SM ^a	Ratio (P/BP)
1	2.2.29	NBS (1.1 eq)	2.5	10.0	60	16	- ^b	-
2	2.2.16	NIS (1.1 eq)	2.5	10.0	60	16	- ^c	-
3	2.2.29	NIS (1.1 eq)	1.0	4.0	60	16	08:10:23	0.80
4	2.2.29	NIS (1.1 eq)	20.0	80.0	60	24	18:42:22	0.43
5	2.2.29	NIS (1.1 eq)	2.5	2.5	60	16	Trace	-
6	2.2.29	NIS (3.0 eq)	2.5	10.0	25	16 ^d	16:04:67	4.00
7	2.2.29	NIS (1.1 eq)	2.5	10.0	30	16	06:02:22	3.00
8	2.2.29	NIS (1.1 eq)	2.5	10.0	40	16	13:05:24	2.60
9	2.2.29	NIS (1.1 eq)	2.5	10.0	50	16	16:05:17	3.20
10	2.2.29	NIS (1.1 eq)	2.5	10.0	60	16	09:09:18	1.00
11	2.2.29	NIS (1.1 eq)	2.5	10.0	70	16	07:08:23	0.88

^aP = product, BP = unidentified other regioisomer/s, SM = unreacted starting material. ^bComplex mixture was observed by LMCS. ^cComplete conversion of the starting acid was observed, however, no product formation was detected and gaseous evolution was observed. ^dNo further changes were observed after 40 h.

Table 2.2.1 – Investigations into the optimisation of the rhodium-mediated C-H activation reaction.

In addition to the iodination methodology, Glorius *et al.* demonstrated that the rhodium(III) methodology was compatible with NBS (*N*-bromosuccinimide).²⁸⁷ In one example, with the acetyl aniline (**2.2.38**, **Figure 2.2.4**), the authors reported that the attempted C-H activation with NIS instead exclusively formed the undesired *meta*-isomer, presumably through a electrophilic substitution pathway. On changing the halogen source to NBS, the desired

reaction was observed, with the *ortho*-bromo product being obtained in a 89% yield. Although the authors do not comment on this result, it is postulated that even with the influence of the Lewis acidic silver salts, the NBS is significantly less electrophilic, and therefore does not undergo the electrophilic substitution pathway. It was envisaged that the differences in the reactivity could be utilised for the amide (**2.2.29**), favouring the directed C-H activation pathway in preference to that of the electrophilic reaction. Unfortunately, the use of NBS was found to be incompatible with this system (**Table 2.2.1** – Entry 1), instead forming a complex reaction mixture with no discernible product formed. With this poor result, further experimentation was restricted to the iodination reaction.

With the inability to debilitate the electrophilic aromatic substitution reaction, methods to enhance the rate of the C-H activation reaction were sought. Glorius *et al.* utilised a variety of different carbonyl directing groups, with the more electron-rich, bulky, tertiary amides typically being the most efficient directing groups. Despite this, the use of these groups for the desired reaction was undesirable, as this would require the addition of several synthetic steps to the synthesis. The carboxylic acid in (**2.2.16**) was identified as an alternative directing group, which may exhibit an enhanced affinity for the rhodium catalyst and thereby promote the C-H activation reaction. This hypothesis could not be confirmed, as the use of the acid under the standard reaction conditions (**Table 2.2.1** – Entry 2) led to decomposition of either the products or the starting material (**2.2.16**). An increase in pressure in the reaction vessel suggests that this occurs *via* a decarboxylative pathway, however, no by-products were isolated to confirm this.

The influence of the catalyst and silver additive loadings were next investigated (**Table 2.2.1** – Entries 3-5). It was envisaged that changing the relative amounts of these species could influence the relative rates of the two competing pathways, enabling a bias towards of the C-H activation pathway. Unfortunately, both decreasing the silver/rhodium loadings (**Table 2.2.1** – Entry 3) and increasing them (**Table 2.2.1** – Entry 4) had a detrimental effect on the reactions. Lower loading appeared to significantly reduce both reaction pathways, with the majority of the starting material unreacted under these conditions, and a poor product to by-product ratio. Increased loadings gave correspondingly higher levels of conversion of the starting material, approximately 75% conversion. Unfortunately, the increased silver loading appears to be the dominant factor, with the electrophilic products being the major reaction components under these reaction conditions. With the increase in the silver having been demonstrated to lead to increased undesired electrophilic substitution, the relative

stoichiometry of the silver was decreased (**Table 2.2.1** – Entry 5). It was envisaged that despite the four halogens in the rhodium dimer, and therefore the four to one ratio between the catalyst and the silver halophile, that lowering the silver levels could still lead to the formation of active rhodium catalytic species, while decreasing the electrophilic pathway. Disappointingly, this was not observed, with only trace levels of both product and by-products forming under these reaction conditions.

In all instances the reactions did not give complete conversion, with unreacted starting material present. With the Lewis acidic nature of the silver salts enhancing the reactivity of the NIS, it was postulated the NIS was unstable under the reaction conditions, undergoing decomposition. However, increasing the levels of NIS (**Table 2.2.1** – Entry 6) and decreasing the reaction temperature to minimise the potential decomposition, led to a lower reaction conversion. As the reaction was conducted at lower temperatures, this lower conversion could be attributed to the slower reaction. To probe this, the reaction was continued for a further 24 hours, total reaction time of 40 hours. No changes in the reaction composition were observed after this time, suggesting an alternative explanation for the decreased conversion. It could be that any degradation products result in the formation of iodine anions. These, in turn, could coordinate the rhodium and sequester the silver in the reaction mixture, debilitating both reaction pathways.

With changes to the catalyst loading, silver additives, and electrophile all failing to improve the reaction, the influence of temperature was now investigated (**Table 2.2.1** – Entries 7-11). With the low conversion at ambient temperature (**Table 2.2.1** – Entry 6) the minimal temperature threshold was selected to be 30 °C, increasing this incrementally to 70 °C. Two general patterns were observed. An increase in temperature led to increases in the conversion of the starting materials, but a loss in the selectivity. At lower temperatures, a good selectivity between 3:1 and 4:1 for the desired product was observed, but low conversions inhibited the reaction. Conversely, the selectivity had decreased to approximately 1:1 at and above 60 °C. The optimal conditions for the reaction appeared to be at 50 °C (**Table 2.2.1** – Entry 9), balancing the relative selectivity and reactivity. Unfortunately, the reaction still showed significant levels of by-product formation and the starting materials, preventing this methodology from being utilised for the desired halogenation.

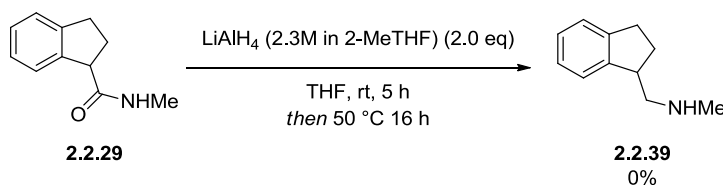
Therefore, work into the rhodium catalysis was concluded at this stage. Although further optimisation, such as the influence of alternative ligands, additives, or solvents remained

unexplored, the increased selectivity and yields of the palladium process (**Section 2.2.5**) meant that this route was utilised for further investigations.

2.2.7 Synthesis of the Tricyclic Core (2.2.10)

2.2.7.1 The Use of Enolate Cross-Coupling

With a robust synthesis of the amide (**2.2.28**) established, the reduction and subsequent amide coupling, to enable investigations into the cyclisation, was explored. A plethora of amide reduction protocols exist, with different reductants, catalysts, and functional group tolerances. The initial investigation utilised lithium aluminium hydride (LiAlH_4) for the reduction of the model amide (**2.2.29**), due to the facile access to this intermediate (**Scheme 2.2.21**).



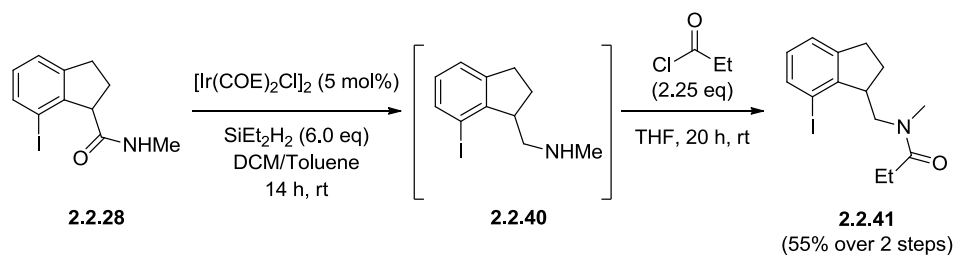
Scheme 2.2.21 – Attempted LiAlH_4 reduction of the model amide (**2.2.29**)

Surprisingly, no reaction was observed at ambient temperature, with the reaction requiring elevated temperatures in order to proceed. Despite the complete reaction under these conditions, after work-up, concentration of the sample led to degradation of the amine (**2.2.39**). The rationale for this degradation remains unclear.

In addition to the potential instabilities of the amine (**2.2.39**), it was envisaged that the basic centre and the weak chromophore of the molecule would inhibit direct isolation of this species. As the investigation was to be applied to the key iodinated amide (**2.2.28**), a mild alternative reduction protocol, followed by direct amide coupling was sought to avoid any issues with instability and isolation.

In 2012, Cheng and Brookhart reported an iridium-catalysed reduction of secondary amides to amines or imines, using diethylsilane as the reductant.²⁹⁰ The mild reaction conditions, clean reaction profiles, and facile work-up conditions reported meant that this was identified as a prospective reduction protocol. It was envisaged that the intermediate amine (**2.2.40**) could be

directly utilised in the next reaction, to give access to the ethyl amide (**2.2.41**) without further purification steps (**Scheme 2.2.22**).

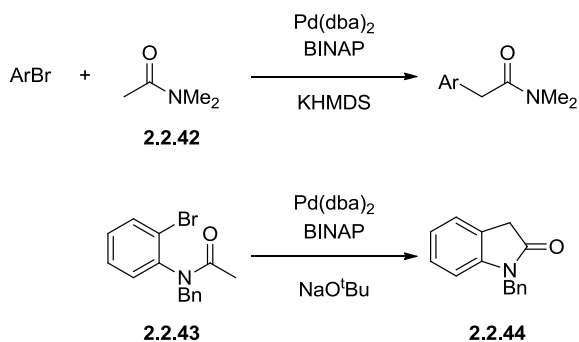


Scheme 2.2.22 – Iridium-catalysed reduction and subsequent amide coupling.²⁹⁰

Gratifyingly, the reduction and subsequent amide formation were found to proceed in good yields, enabling access to the amine and allowing the subsequent cyclisation to be explored. Due to the poor solubility of the starting amide (**2.2.28**) it was necessary to add the additional solvents toluene and DCM to enable the reaction. In addition to this, to increase the overall conversion, the equivalents of the diethylsilane reductant were increased to six from the literature value of four. Using these modifications and the reported work-up protocol afforded crude amine (**2.2.40**), which could then be coupled with the commercial acid chloride to give the ethyl amide (**2.2.41**).

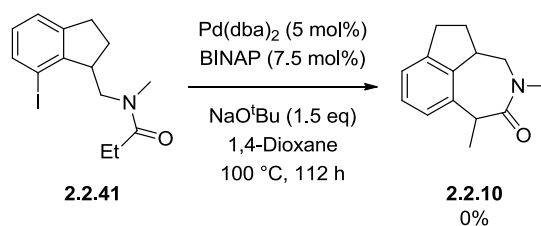
It was envisaged that the resulting amide (**2.2.41**) could be cross-coupled through an enolate cross-coupling protocol. Depending on the identity of the halogen and carbonyl, a variety of different palladium-catalysed protocols exist to affect either *inter*- or *intra*-molecular cross coupling between a nucleophilic enolate and aryl halide/pseudohalide partner.

In 1997 Hartwig *et al.* reported a palladium-catalysed α -arylation of amides to access either α -arylamides or oxindole products,²⁵⁹ as an extension of earlier reported methodologies from the α -arylation of ketones. The authors comment on the relative difficulty of coupling amides, when compared to ketones, due to the increased pK_a of amide derivatives. The authors explored a range of different bidentate phosphine ligands, concluding that BINAP was the most efficient ligand for this desired transformation. Depending on the desired transformation, either sodium *tert*-butoxide or the stronger base potassium hexamethyldisilazide were employed (**Scheme 2.2.23**).



Scheme 2.2.23 – Representative examples of palladium-catalysed α -arylation of amides.²⁵⁹

The authors found for intramolecular cyclisations, the use of sodium *tert*-butoxide was critical for obtaining high yields. Stronger bases, such as potassium hexamethyldisilazide or lithium diisopropylamide, were found to either cause cleavage of the acetyl functionality in the starting material (**2.2.43**) or deactivation of the catalyst, in both cases resulting in low yields. Conversely, the use of weaker bases was found to be insufficient for the reaction, with low or no reaction observed. These conditions were, therefore, applied to the substrate (**2.2.41**) (**Scheme 2.2.24**). Despite the increased ring size, it was envisaged that the conformational restriction imposed on the substrate would promote the potential cyclisation.

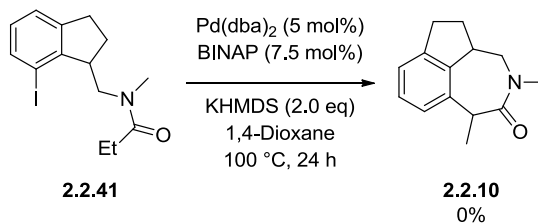


Scheme 2.2.24 – Attempted palladium-mediated cyclisation using sodium *tert*-butoxide as the base.

Unfortunately, under the standard conditions no reaction, cyclisation or otherwise, was observed. The absence of any discernible levels of dehalogenated starting material suggested that the oxidative addition was not occurring under the reaction conditions. This implies that catalyst deactivation was occurring under the reaction conditions, potentially *via* complexation with the amide, as the catalyst system had been demonstrated to undergo oxidative addition into the stronger aryl-bromide bond by Hartwig *et al.*

It was thought that the absence in reactivity could be attributed to the differences in pK_a between the aromatic amide substrate (**2.2.43**) reported by Hartwig *et al.* and the alkyl amide

(2.2.41). The additional delocalisation onto the aromatic ring, stabilises the formal negative charge of the enolate, significantly lowering pK_a of the aromatic amides relative to alkyl amides. The reaction was therefore repeated, utilising the stronger KHMDS base to compensate for the increased pK_a of the substrate (2.2.41) (Scheme 2.2.25).

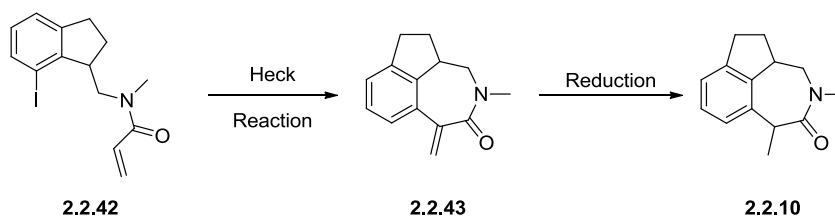


Scheme 2.2.25 - Attempted palladium-mediated cyclisation using the stronger KHMDS base.

Under the reaction conditions (Scheme 2.2.25) no product (2.2.10) or dimerisation, *via* intermolecular enolate coupling, was observed. In contrast to the use of sodium *tert*-butoxide, some dehalogenated starting material was detected. This indicated that the oxidative addition was occurring, suggesting that the failure of the reaction could again be attributed to the enolate coupling sequence. Potentially, the high pK_a of the substrate, still prevents significant levels of the desired enolate in the solution and therefore no cross-coupling reaction occurs. Typically, this issue can be overcome by the use of an even stronger base, such as lithium diisopropylamide. However, the reported catalyst deactivation with stronger bases, *vide supra*, meant that alternative methods to perform the cyclisation were sought in preference to the enolate-coupling methodology.

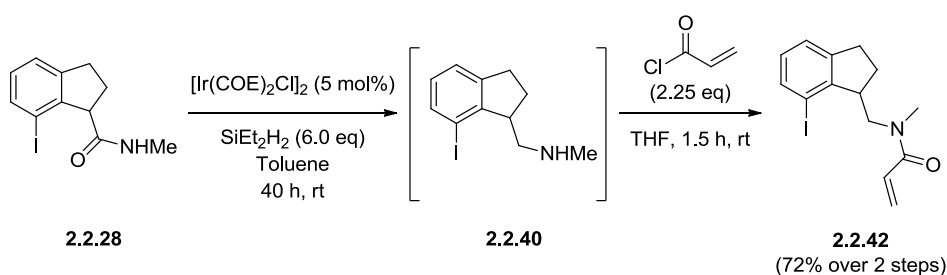
2.2.7.2 Heck Reaction and Reduction

Heck-type chemistry was envisaged to provide an alternative method to effect the formation of the 7-membered ring (Scheme 2.2.26), albeit requiring a further synthetic step to synthesise the desired tricyclic molecule (2.2.10). The intermediate alkene from the initial cyclisation (2.2.26) requires reducing to the desired tricyclic intermediate (2.2.10), adding an additional transformation relative to the proposed enolate coupling route. However, with the failure of the enolate conditions to provide any cross-coupled products, this methodology was investigated.



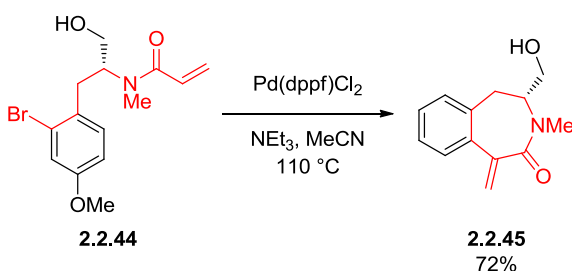
Scheme 2.2.26 – Proposed Heck-mediated cyclisation to access the tricyclic core (**2.2.10**).

To enable investigations into the Heck-reaction and subsequent reduction, a synthesis of the requisite amide was required. Gratifyingly, the amide (**2.2.42**) could be prepared in analogous fashion to the ethyl amide (**2.2.41**), utilising the same iridium-catalysed reduction and amide formation with an alternative commercially available acid chloride (**Scheme 2.2.27**).



Scheme 2.2.27 – Synthesis of the Heck precursor amide (**2.2.42**).

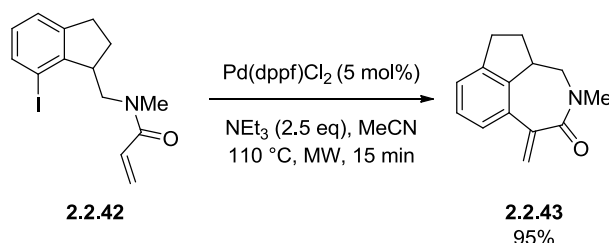
There are a myriad of different Heck reaction protocols, using different substrates, catalysts, solvents, and other additives.^{291,292} In 2009, Donets *et al.* utilised an intramolecular Heck-type reaction between an unsaturated amide and an aryl bromide to synthesise a comparable seven-membered ring (**Scheme 2.2.28**).²⁶⁰



Scheme 2.2.278 – Heck reaction employed by Donets *et al.*²⁶⁰

The high yields for the construction of a less-constrained seven-membered ring, which would disfavour the formation of the ring relative to the amide (**2.2.42**), meant these reaction conditions were identified for exploration. In addition to the less constrained system, Donets

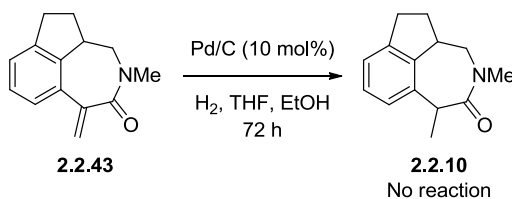
*et al.*²⁶⁰ also utilised a less reactive aryl bromide. It was envisaged that the aryl iodide would undergo more facile oxidative addition, promoting the desired cyclisation (**Scheme 2.2.29**). The authors also reported a reductive Heck reaction, however, the Heck reaction and subsequent reduction was investigated first. If scale-up and further synthesis was required then a reductive protocol could be developed.



Scheme 2.2.29 – Heck cyclisation to access the tricyclic skeleton (**2.2.43**).

Gratifyingly, the desired Heck-reaction was found to give exclusively the desired tricyclic molecule (**2.2.43**). The increased yield relative to that of Donets *et al.* is thought to be due to the constrained system enforced by the five-membered ring and the increased reactivity of the C-I bond.

With the carbon skeleton in place, reduction of the unsaturated system was required to complete the synthesis. It was envisaged that the stereogenic centre would be able to control the facial selectivity of the reduction, giving rise to the desired diastereoisomer *vide supra*, without the requirement for an asymmetric reduction protocol. A palladium-mediated reduction similar to that employed for the reduction of **2.2.14** (**Section 2.2.3**) was investigated (**Scheme 2.2.30**).

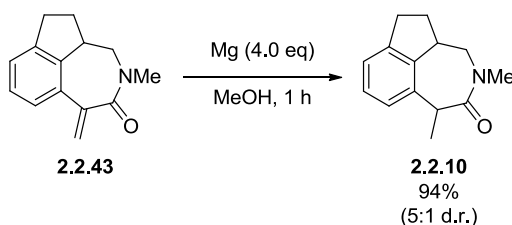


Scheme 2.2.30 – Failed hydrogenation reaction.

In contrast to the previous hydrogenation reaction (**Scheme 2.2.6**), under the Pd-mediated reaction conditions, no hydrogenation was observed. It was postulated that absence of reaction could be attributed to the sterically congested environment, preventing approach by the

heterogeneous palladium catalyst. An alternative method to conduct the reduction was therefore sought.

In 1999, Venkataiah *et al.* reported the use of magnesium and methanol to reduce several dienamides to the corresponding β,γ -unsaturated amides.²⁹³ The authors propose that under these reaction conditions, single electron transfer from the metal sequentially reduces the alkene, with the protic solvent acting as the proton source. The mild reaction conditions, comparatively low equivalents of magnesium, and the selectivity for the conjugated amide, due to the stability of the intermediate radical, were attractive for both this molecule and potentially more elaborated cores, if necessitated. The tricyclic core was therefore assessed under these reaction conditions (**Scheme 2.2.31**).



Scheme 2.2.31 – Magnesium-mediated radical reduction.

Gratifyingly, under the conditions of Venkataiah *et al.* the reduction was found to proceed in excellent yields with a 5:1 diastereoisomeric ratio. The diastereoselectivity is dictated by the presence of the nearby stereocenter, favouring one diastereoisomer. Although the initial reduction was found to give a mixture of diastereoisomers, the major diastereoisomeric pair could be isolated using mass-directed autopurification (MDAP) techniques. Unfortunately, due to the small scale and 5:1 diastereoisomeric ratio, the minor diastereoisomeric pair could not be isolated.

2.2.8 Biological Evaluation of the Tricyclic Core

Isolation of the major diastereoisomeric pair (**2.2.10a**) allowed enzymatic evaluation to determine the potency of this new core (**Figure 2.2.7**). In addition to providing a comparison with the unsubstituted BZP core (**2.1.11**), any enzymatic potency would support the hypothesis of the major diastereoisomeric pair being the (*R,R*)- and (*S,S*)-isomers, as it is hypothesised that only the (*R,R*)-isomer would display any binding affinity (**Section 2.1**).

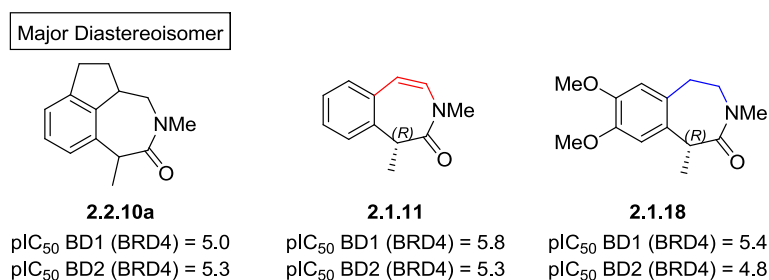


Figure 2.2.7 – Enzymatic data for the major diastereoisomer of the tricyclic core (**2.2.10a**), obtained from the reduction reaction (**Scheme 2.2.31**) relative to that of the unsubstituted core (**2.1.11**), and the saturated analogue (**2.1.18**).

Gratifyingly, the major diastereoisomer of tricyclic core (**2.2.10a**) displayed significant BRD4 binding affinities within the desired pan-BET profile. In addition to this, the pIC₅₀ values displayed by this core are comparable to those exhibited by the enantiopure (*R*)-BZP (**2.1.11**). It was anticipated that the (*R,R*)-enantiomer would display an almost identical potency to that of the chiral BZP (**2.1.11**). This demonstrates that this template provides an alternative to the BZP core, removing the potentially reactive and synthetically challenging alkene group. The racemic tricyclic core (**2.2.10**) also displays comparable binding affinities to the enantiopure saturated analogue (**2.1.18**), despite the absence of substitution.

To enable further biological assessment, and crystallography of the active enantiomer to confirm the stereochemistry, the single enantiomers were required. Chiral purification/separation of the initial mixture of diastereoisomers from the reduction reaction (**Scheme 2.2.30**) was untaken. Unfortunately, under the chiral purification methods only one of the major isomers was isolated as a pure sample (denoted isomer 1), with the other isomer showing approximately 20% of one of the minor diastereoisomers (denoted isomer 2). To determine which was the active enantiomer and to enable X-ray crystallography, these compounds were subjected to both enzymatic and whole-blood (WB) biological evaluation (**Figure 2.2.8**).

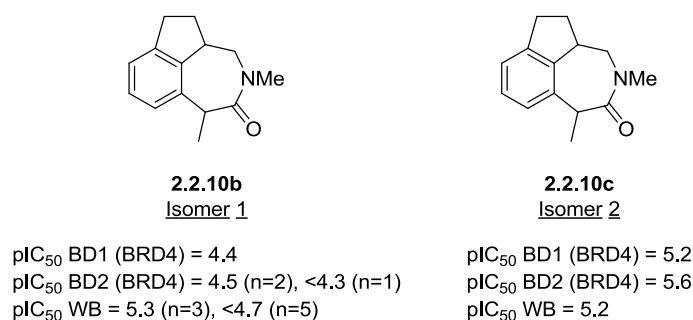
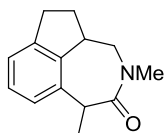


Figure 2.2.8 – Enzyme and whole-blood data for the chirally separated isomers of the tricyclic core (**2.2.10b** and **2.2.10c**). Isomer 1 (**2.2.10b**) is enantiomerically pure and isomer 2 (**2.2.10c**) contained 20% of an undefined minor diastereoisomer, with the major constituent being the opposite enantiomer to that of isomer 1.

Both the enzymatic and WB values showed that isomer 1 (**Figure 2.2.8**) was the less active enantiomer. Surprisingly, the initial WB values obtained for the two isomers were equal, suggesting that the two compounds were equipotent BET-inhibitors in a stimulated blood environment. Subsequent re-testing has revealed that this was a consequence of anomalous results for isomer 1, with additional data points showing no discernible activity in the whole-blood assay.

Unfortunately, due to the impurities in the active isomer (**Figure 2.2.8 – 2.2.10c**), the potency of the active isomer or the stereochemistry of the molecule could not be confirmed. It is plausible that the minor diastereoisomer displays some biological activity. In addition to this, X-ray crystallography cannot be utilised to irrevocably assign the stereochemistry of this compound, as the minor component may crystallise in the active site, leading to an incorrect assignment of the stereochemistry.

Gratifyingly, despite the two diastereoisomers co-eluting under chiral HPLC purification,²⁹⁴ MDAP purification was able to separate the two stereoisomers, *vide supra*. Unfortunately, a pure sample of the minor diastereoisomer could not be isolated, however, an enantiopure sample of the major component of isomer 2 was obtained (Isomer 3, **2.2.10d**). This was re-subjected to the biological evaluation (**Figure 2.2.9**).



2.2.10d

Isomer 3 - major component of isomer 2

pIC₅₀ BD1 (BRD4) = 5.0

pIC₅₀ BD2 (BRD4) = 5.4

Figure 2.2.9 – Enzymatic data for the analytically pure single stereoisomer, major component of isomer 2 after chiral resolution.

Analysis of the single isomer (**2.2.10d**) (**Figure 2.2.9**) showed a comparable potency to the mixture (**Figure 2.2.8**, Isomer 2). This indicates that this is the active isomer, responsible for the observed biological activity. To confirm that this isomer is the hypothesised (*R,R*)-enantiomer (**2.1.20**), X-ray crystallography was used to assign the stereochemistry of this isomer (**Figure 2.2.10**).

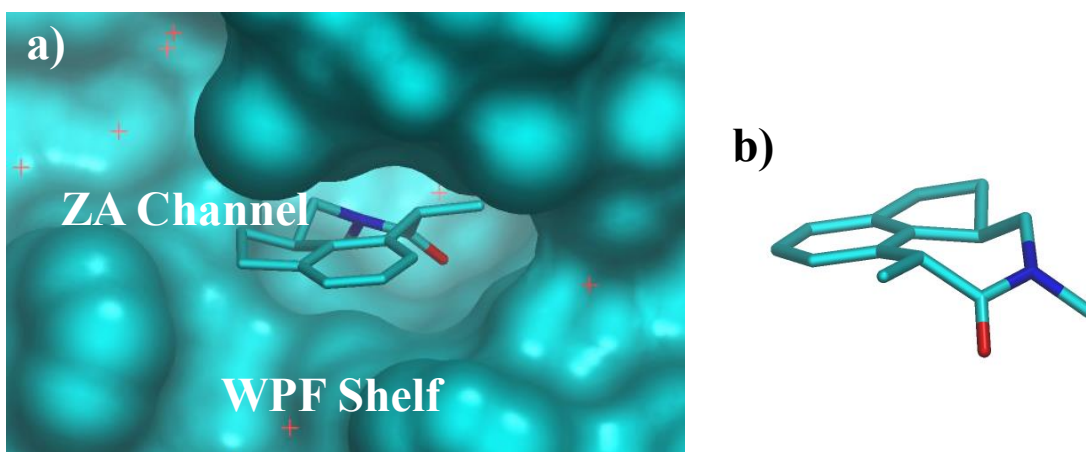


Figure 2.2.10 – a) X-ray structure of the biologically active tricyclic core (**2.1.20**) bound in the BRD2 BD2 C-terminal domain (PSILO-8QNMR) highlighting the vectors for elaboration. b) Structure of the tricyclic molecule with the binding site omitted, clearly showing the stereochemistry of the active enantiomer.

Gratifyingly, the binding mode of the active isomer (**2.1.20**) was clearly resolved, enabling assignment of both the stereocenters. This confirmed that the active enantiomer was the (*R,R*)-isomer, supporting the hypothesis that this would have the desired conformation to mimic the BZP core. The formation of the desired diastereoisomeric pair as the major products from the reduction (**Scheme 2.2.30**), is also envisaged to facilitate an enantioselective synthesis. The conformation control exhibited by the already defined stereocenter in the reduction means that

control of this stereocenter should direct the reduction to the desired face of the unsaturated carbonyl, or enable a subsequent epimerisation to the desired enantiomer (**2.1.20**). Methods to control the stereochemistry of the first chiral center were discussed previously (**Section 2.2.3**).

The close homology between the tricyclic and BZP binding modes can be demonstrated by overlaying the two structures bound in the active site of the protein (**Figure 2.2.11**).

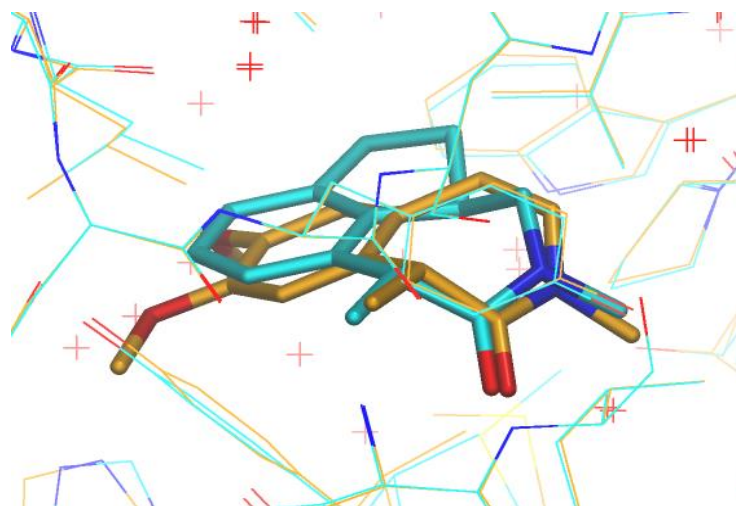


Figure 2.2.11 – X-ray crystal structure of the tricyclic core (**2.1.20**) in blue (PSILO-8QNMR) and the dimethoxy methyl BZP (**2.1.9**) in orange (PSILO-9WNNE), demonstrating the conservation of binding modes.

Analysis of the two compounds (**Figure 2.2.11**) demonstrates that the key amide occupies a comparable position in both analogues, with small displacements in the remainder of the molecule. The key interactions with the BET protein are conserved and similar vectors for growth are available. This allows the significant SAR work from the BZP series to be utilised to further enhance the potency of the tricyclic template.

In contrast to the saturated analogue (**2.1.18**),²⁵⁷ the binding conformation of the tricyclic molecule (**2.1.20**) displays a close homology to the computationally calculated conformation in solution (**Figure 2.1.19**). This reduces the unfavourable entropic and enthalpic penalties to binding observed for the saturated analogue (**2.1.18**), increasing the affinity of the tricyclic core to comparable levels to the BZP series.

2.2.9 Conclusion and Further Progression of the Series

In conclusion, all of the aims outlined at the start of this research project (**Section 2.1**) have been achieved. These achievements are highlighted in the following section:

- 1) A computational approach was able to design a novel BET series as an alternative to a known series within our laboratories (**Figure 2.2.12**). This core was hypothesised to maintain the desired binding conformation of the original series, while removing the potentially reactive alkene functionality.

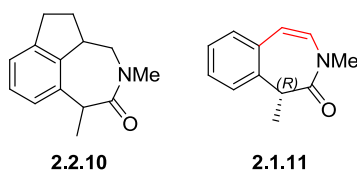


Figure 2.2.12 – Structure of the novel BET series (**2.2.10**) and the known BZP series (**2.1.11**).

- 2) A concise synthesis of the tricyclic molecule (**2.2.10**) was designed and conducted, utilising a directed C-H activation step as the key disconnection. In addition to this, the synthesis was designed to enable a facile asymmetric synthesis of the core, using either chemical or enzymatic methods to control one stereocenter, which then imparts the desired stereochemistry for the second stereocenter. The facile synthesis of elaborated analogues could be conducted using this route, using more functionalised indene acid precursors (**2.2.16** or more elaborated structures).
- 3) The new core was demonstrated to retain the excellent potencies to the original BZP series and increased binding potencies relative to the alternative saturated series (**Section 2.1**). This demonstrates that this represents an alternative to the BZP series, without the potentially reactive alkene liability. If issues with the BZP core are encountered during development, this alternative series will immediately provide a replacement template, without requiring costly hit identification and verification. The comparable vectors between the BZP and tricyclic core enable the significant transfer of SAR between the series, further facilitating development of novel BET inhibitors in shorter timescales, and reduced analogue synthesis.

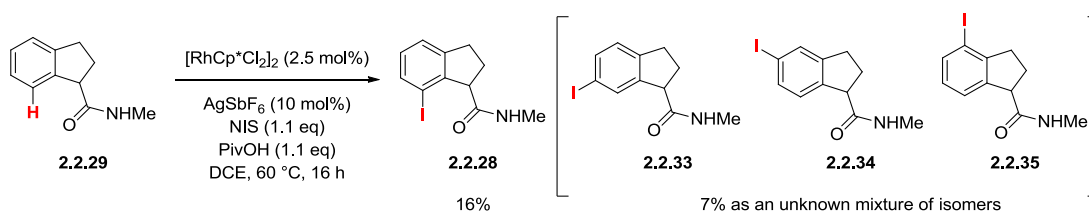
2.3. Development of a Novel Rhodium C-H Activation Methodology

As part of the investigations into the synthesis of the novel tricyclic series, *vide supra*, extensive investigations into the use of amide directed C-H activation/halogenation were conducted. During these investigations a novel rhodium(III) catalysed reaction was demonstrated, albeit in low yields due to competitive non-catalytic reaction pathways (**Section 2.2.6**). The use of simple alkyl amides as directing groups was particularly attractive, eliminating the requirement for more elaborated functionalities.

It was proposed that the major limitation of this methodology was the electrophilicity of the halogen coupling partner and that the use of alternative coupling partners could circumvent this issue. Studies into other coupling partners and directing groups were therefore conducted with the aim of developing further understanding about this reaction and to evaluate the potential of this strategy to provide a new practical synthetic method to access otherwise challenging structures. For example, it was envisaged that this reaction could directly facilitate the synthesis of the challenging BZP core, which suffers from protracted syntheses and low yields for the majority of the analogues in our laboratories.

2.3.1 Rhodium(III)-catalysed Halogenation Reaction Investigation

Although, the rhodium(III)-catalysed halogenation investigations were unable to develop a reliable protocol for the desired C-H activation (**Scheme 2.3.1**), evidence of elevated levels of product (**2.2.28**) indicated that the desired C-H activation process was occurring (**Section 2.2.6**). Initial investigations showed that the problems with this could be traced to the electrophilic partner, NIS, and it was proposed that other less electrophilic species could be utilised with this methodology that are not susceptible to the undesirable non-catalysed processes.



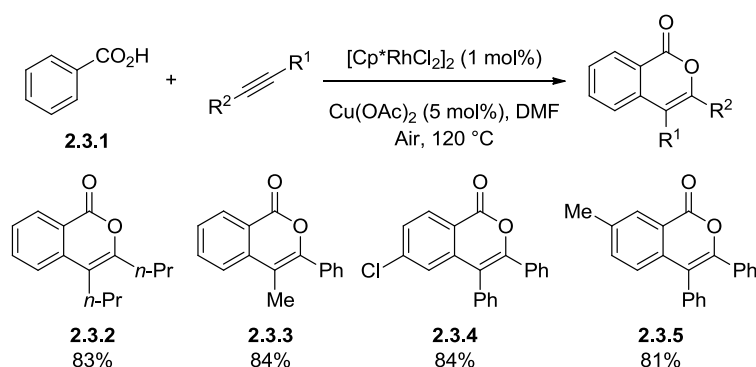
Scheme 2.3.1 – Failed C-H activation/halogenation reaction.

2.3.2 Use of the Group 9 Metals in C-H Activation and Heterocyclic Synthesis

2.3.2.1 Initial Report, the Synthesis of Isocoumarins

The use of the group 9 transition metals in C-H activation methodology is not just limited to rhodium, with the use of iridium²⁸⁵ and, more recently, cobalt catalysis also having been extensively documented.^{279,280,295} One of the most important transformations, particularly from a medicinal chemistry perspective, is the use of the group 9 metals to construct heterocycles. The use of C-H activation can simplify syntheses, removing the requirements for pre-functionalisation, with atoms such as halogens.

The use of rhodium(III) catalysis for the construction of heterocycles was first reported in the 2007 seminal publication by Miura *et al.*²⁹⁶ The authors reported the use of the rhodium(III) catalyst, $[\text{RhCp}^*\text{Cl}_2]_2$, in combination with $\text{Cu}(\text{OAc})_2$ as a co-catalyst, to form isocoumarins *via* cyclisation of a carboxylic acid directing group with an alkyne (**Scheme 2.3.2**). The copper catalyst is proposed to facilitate the reoxidation of rhodium(I) to rhodium(III) under the reaction conditions, in combination with the air atmosphere.

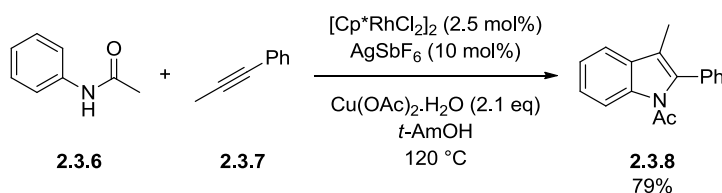


Scheme 2.3.2 – Examples of the rhodium(III) catalysed synthesis of isocoumarins.²⁹⁶

The authors explored a small subset of different rhodium(III) catalysts for the formation of isocoumarins, with the $[\text{RhCp}^*\text{Cl}_2]_2$ catalyst being the only catalyst to show an appreciable activity.²⁹⁶ In addition to the reaction of alkynes, the authors also demonstrated that the same system could be utilised to conduct Heck-type reactions with alkenes.²⁹⁶

2.3.2.2 Use of Additives in Group 9-mediated C-H Activation Reactions

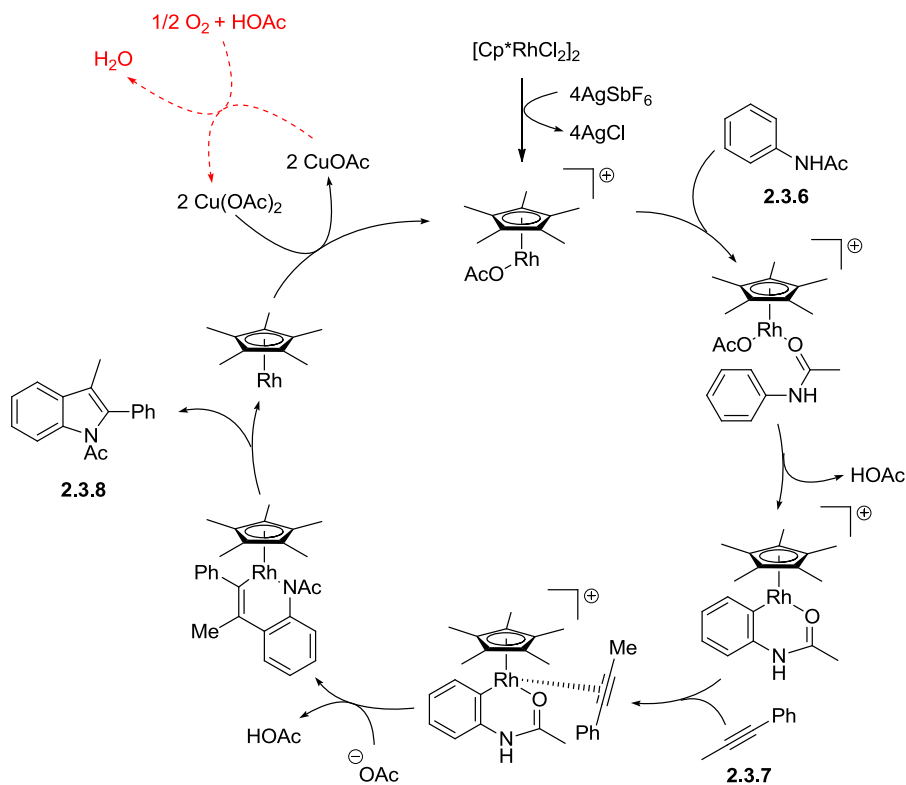
Following the pioneering work of Miura *et al.*,²⁹⁶ a range of alternative directing groups have been employed in the formation of alternative heterocyclic systems. In 2008, Fagnou *et al.* published the use of C-H activation to synthesise a range of indole derivatives (**Scheme 2.3.3**).²⁹⁷ The use of silver salts, in particular AgSbF_6 , was found to promote the reaction leading to increased reaction yields. The amide directing group was used to promote *ortho* C-H activation, with the resulting metallocycle being coupled with an alkyne group, *vide supra*. In contrast to the synthesis of isocoumarins,²⁹⁶ stoichiometric quantities of a copper(I) oxidant were utilised to re-oxidise the rhodium(I) to rhodium(III).



Scheme 2.3.3 – Fagnou indole synthesis using rhodium(III) catalysed C-H activation.²⁹⁷

2.3.2.3 Mechanism of Rhodium(III)-Mediated C-H Activation

The scope of the heterocycles that can be accessed *via* rhodium(III) catalysed C-H activation is by no means restricted to indoles and isocoumarins, with examples of pyrroles,²⁹⁸ isoquinolines,²⁸⁴ isoquinolones,²⁹⁹ and pyridones,³⁰⁰ in addition to a range of other substrates. In all instances, the reaction mechanism is thought to be similar, with the substrates differentiated by the directing group and coupling partner identity, determining the product formed. The proposed mechanism for the indole (**2.3.8**) formation example (**Scheme 2.3.3**) is outlined below (**Scheme 2.3.4**).²⁸⁸

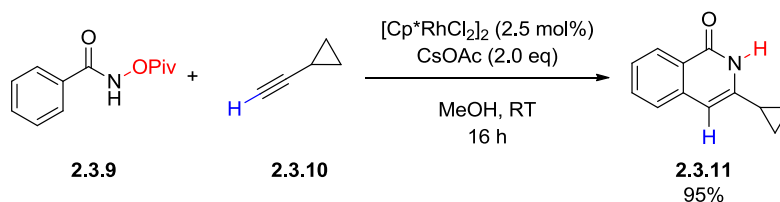


Scheme 2.3.4 – Mechanism of rhodium(III) catalyzed C-H activation for the synthesis of indoles.²⁸⁸

The reaction begins with the formation of the cationic rhodium species, with the silver salts acting as halogen scavengers to increase the reactivity of the rhodium and promote coordination of the directing group, in this instance the acetylated aniline (**2.3.6**). In the absence of the silver salts, the halogen displacement typically requires elevated temperatures and strong coordinating groups, such as the carboxylic acid groups utilised by Miura *et al.*²⁹⁶ The directing group coordination enables the metallocycle formation, through an electrophilic C-H activation process, liberating acetic acid as the by-product. Coordination is presumed to occur through the oxygen due to the conjugated nature of the nitrogen and formation of the thermodynamically preferred six-membered metallocycle. Coordination of the alkyne π -system to the vacant rhodium metal coordination site enables the key C-C bond forming migratory insertion reaction, with the regioselectivity of the reaction controlled predominately by electronic influences.²⁸⁸ At this stage, deprotonation of the directing group NH enables coordination of the nitrogen to the metal, potentially *via* η^3 -coordination of the directing group. Reductive elimination then liberates the product (**2.3.8**), and a low oxidation state rhodium(I) species. Reoxidation to rhodium(III), either through the use of air and catalytic copper oxidant or a stoichiometric copper oxidant, regenerates the active catalyst.

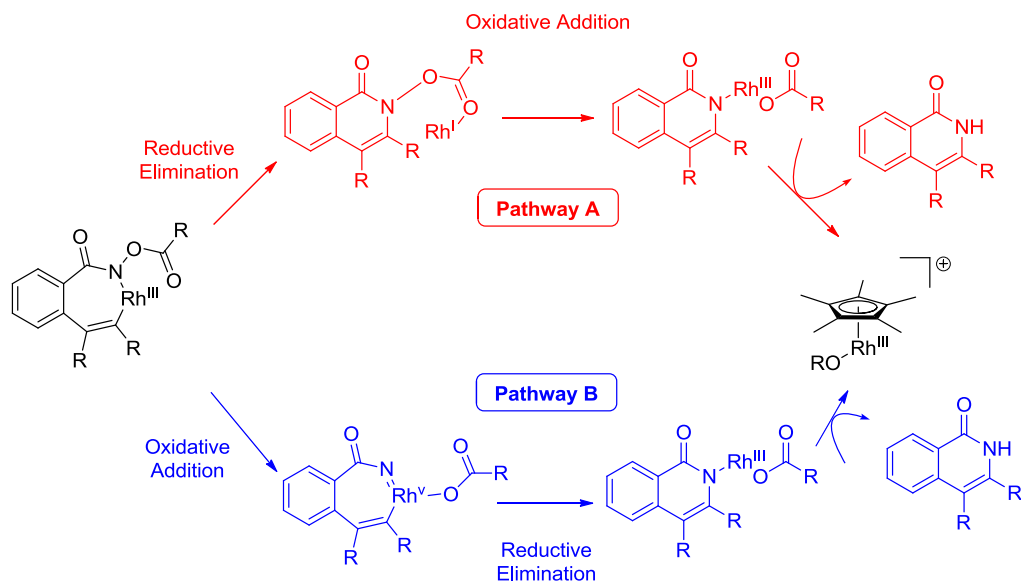
2.3.2.4 Use of Internal Oxidants

One of the primary concerns relating to this class of methodology was the requirement for the additional oxidant to facilitate catalytic turnover, limiting the scope and practicality of the reaction, in addition to raising associated costs.³⁰¹ An elegant solution to this problem is the use of internal oxidants (**2.3.9**), contained within the directing group (**Scheme 2.3.5**).³⁰¹ Under the reaction conditions, the cleavage of the weak N-O bond serves to re-oxidise the catalyst, removing the requirement for the internal oxidant. This methodology significantly increased the scope of the reactions, for example enabling the use of terminal alkynes which were not tolerated by the copper oxidants.



Scheme 2.3.5 - Use of internal oxidants in rhodium(III)-catalysed C-H activation for the synthesis of isoquinolines.³⁰¹

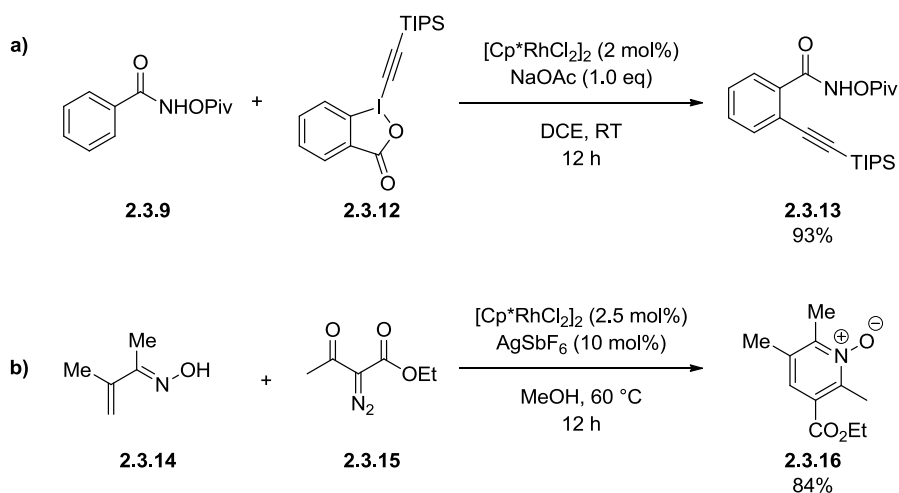
Until 2016, the exact mechanism of the reoxidation by internal oxidants was unconfirmed. Under the typical reaction conditions, N-O bonds were tolerated apart from in the directing group. This demonstrated that the N-O bond is not acting as an oxidant of an isolated rhodium(I) species, but instead oxidises the metal as part of the catalytic cycle before product formation. It was initially proposed that after the reductive addition step of the reaction, the rhodium(I) species formed remains associated with the directing group, enabling oxidation addition into the N-O bond to regenerate the rhodium(III) species (**Scheme 2.3.6 – Pathway A**).³⁰¹ Recent computational investigations have disproved this hypothesis, instead invoking a rhodium(III)/rhodium(V) catalytic cycle (**Scheme 2.3.6 – Pathway B**).³⁰²



Scheme 2.3.6 – Pathway A) Initially proposed mechanism for the use of internal oxidants to regenerate Rh(III),³⁰¹ Pathway B) Computationally supported mechanism proposed by Houk *et al.*³⁰²

2.3.2.5 Alternative Group 9 Directed C-H Activation Reactions

In addition to the formation of heterocyclic systems through coupling with π -systems, group 9-metals have been employed in combination with a range of different partners to give rise to a variety of synthetically versatile intermediates. Elegant examples include the use of the hypervalent iodine reagent TIPS-EBX (**2.3.12**) (1-[(triisopropylsilyl)ethynyl]-1,2-benziodoxol-3(1*H*)-one) to perform electronically reversed Sonogashira reactions (**Scheme 2.3.7a**),²⁸⁶ or the use of diazomalونات to synthesise pyridyl or *N*-oxide derivatives (**Scheme 2.3.7b**),^{303,304} Overall, a huge variety of directing groups, conditions, and products can be utilised or accessed in this type of methodology.



Scheme 2.3.7 – a) Use of TIPS-EBX (**2.3.12**) for Sonogashira type C-H activation reactions,²⁸⁶
 b) Synthesis of pyridyl *N*-oxide derivatives using C-H activation.^{303,304}

2.3.3 Potential Applications of the New Directing Group C-H Methodology

Despite the diverse range of directing groups utilised for group 9 C-H activation, the alkyl amide (**2.2.29**) represented the demonstration of a new type of directing group. The development of this class of directing group could potentially enable the use of the C-H activation reactions to access new classes of substrates that were previously inaccessible (**Figure 2.3.1**), providing significant synthetic value.

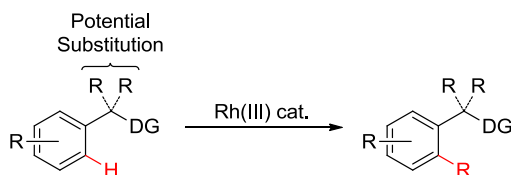
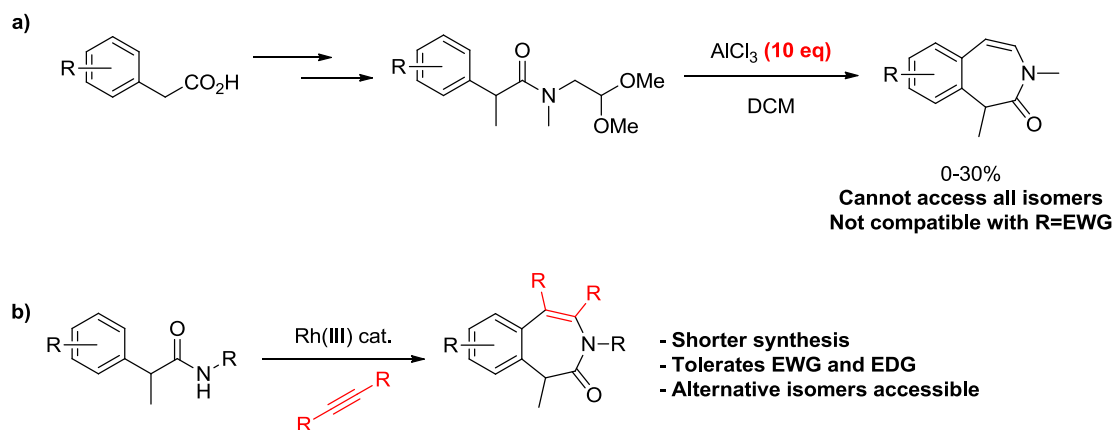


Figure 2.3.1 – New potential mode of Rh(III) C-H activation.

In addition to the wider applications of the methodology, it was also envisaged that this could be applied to the synthesis of the BZP core. At the outset of this research, the only successful synthetic strategy to access the BZP core was the use of a Friedel-Crafts cyclisation. Unfortunately, this reaction proceeded in maximum yields of 30%, required a large excess of the Lewis-acid reagent, and the remainder of starting material was found to decompose under the reaction conditions (**Scheme 2.3.8a**).³⁰⁵ It was envisaged that the use of C-H activation, in an analogous fashion to the synthesis of isoquinolines,³⁰¹ could provide a solution to this preparative challenge (**Scheme 2.3.8b**).



Scheme 2.3.8 – a) Use of the Friedel-Crafts reaction for the synthesis of BZP derivatives, b) Potential use of C-H activation to synthesise the BZP core.

2.3.4 Initial Screening of Rhodium(III)/Iridium(III) C-H Activation Conditions

In order to assess the new class of directing groups and to develop a robust high-yielding C-H activation protocol, a range of conditions which had previously been utilised for C-H activation reactions were assessed. Attempts were made to select a variety of representative conditions, exploring different additives, solvent classes, and temperatures. Several electronically distinct secondary amide directing groups were evaluated (**Figure 2.3.2**), using both alkyl groups and the N-O functionalities commonly associated with internal oxidation of the catalysts (**Section 2.3.2.4**). The initial substrates explored also possessed an α -methyl group to replicate the BZP core as closely as possible.

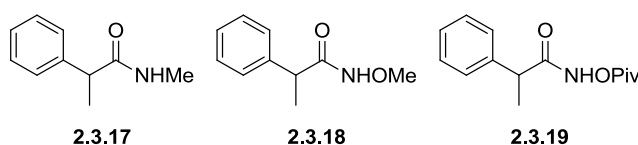
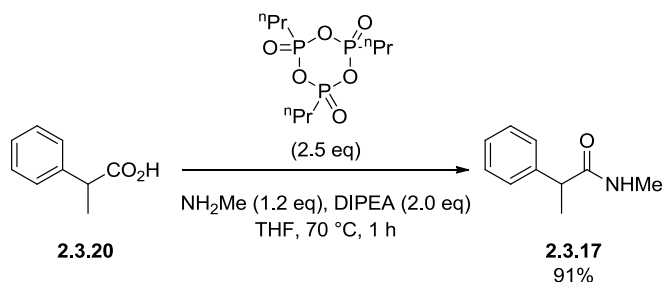


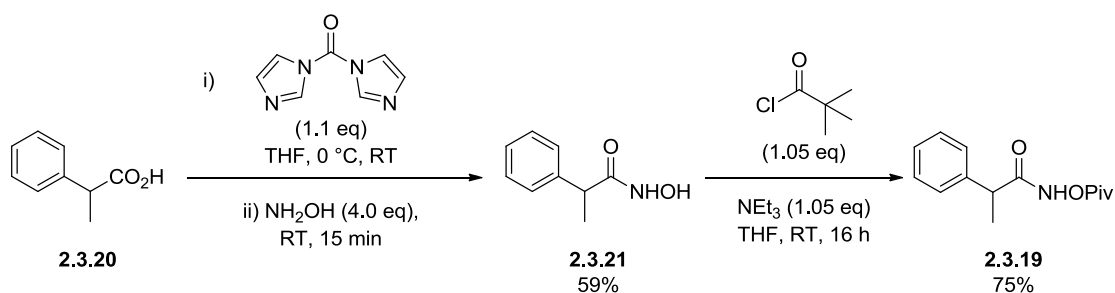
Figure 2.3.2 – Amide directing groups under investigation.

Before the investigations into the C-H activation could be initiated, synthesis of the amide directing groups (**2.3.17**, **2.3.18**, and **2.3.19**) was required. The methyl amide (**2.3.17**) was prepared from the amide coupling of methylamine and the corresponding commercially available carboxylic acid (**2.3.20**) (**Scheme 2.3.9**). An analogous strategy was employed within our laboratories for the synthesis of the NH-OMe substrate (**2.3.18**).³⁰⁶



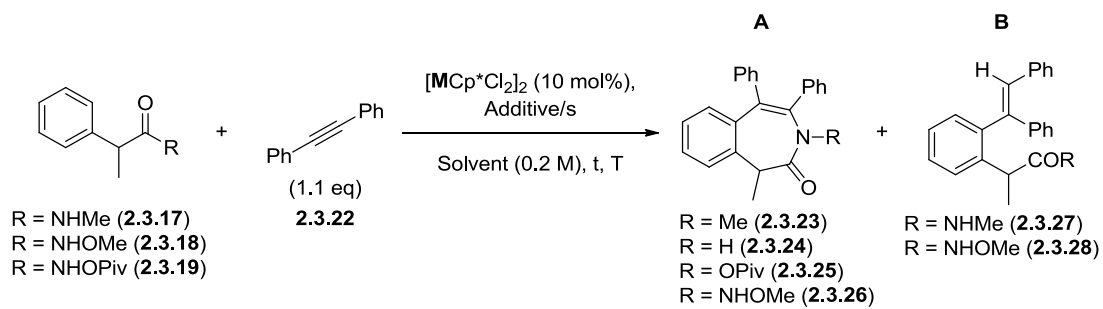
Scheme 2.3.9 - Amide coupling to synthesis the methyl amide starting material.

The OPiv derivative was synthesised in a two step procedure (**Scheme 2.3.10**), starting with the amide coupling of the carboxylic acid (**2.3.20**) with hydroxylamine to synthesise the hydroxyamide (**2.3.21**). Alkylation with the commercially available acid chloride afforded the desired OPiv substrate (**2.3.19**), enabling the investigation into the C-H activation reaction.



Scheme 2.3.10 – Synthesis of the OPiv amide (**2.3.19**).

The diphenyl alkyne (**2.3.22**) was selected for the initial C-H investigations due to its well established literature precedent in this class of reaction, strong UV chromophore, symmetrical nature to avoid regioselectivity issues, and the absence of any terminal alkyne groups which may interfere with the reaction. To enable a direct comparison between the conditions, the catalyst loading was set to 10 mol%, with 1.1 equivalents of the alkyne, and reactions run at a molarity of 0.2 M. It was anticipated that these levels could then be adjusted during subsequent optimisation reactions. The results from the initial screening investigation are presented below (**Scheme 2.3.11** and **Table 2.3.1**).



Scheme 2.3.11 – General scheme for the initial C-H activation studies. **A** denotes cyclised products and **B** denotes uncyclised products.

Entry	R	M	Additive/s (mol%)	Solvent	T (°C)	t (h)	A (%) ^d	B (%) ^d
1 ^a	NHMe	Rh	CsOAc (30)	MeOH	60	90	0	0
2 ^a	NHMe	Ir	CsOAc (30)	MeOH	60	90	0	0
3	NHOMe	Rh	CsOAc (30)	MeOH	60	40	1 (R = H)	2 (R = NHOMe)
4 ^{a,c}	NHOPiv	Rh	CsOAc (30)	MeOH	60	16	0	0
5 ^c	NHOPiv	Ir	CsOAc (30)	MeOH	60	16	0	0
6	NHMe	Rh	CsOAc (200)	MeOH	RT	90	0	0
7 ^c	NHOPiv	Rh	CsOAc (200)	MeOH	RT	72	0	0
8	NHMe	Rh	Cu(OAc) ₂ (210)	^t AmOH	110	16	0	0
9 ^a	NHMe	Rh	CsOAc (200)	^t AmOH	110	72	0	0
10	NHMe	Rh	CsOAc (30)	MeCN	60	90	0	0
11	NHOPiv	Rh	CsOAc (30)	MeCN	60	72	0	0
12 ^a	NHMe	Rh	AgSbF ₆ (40), Cu(OAc) ₂ (220)	DCE	60	144	0	39 (7) ^b
13 ^c	NHOPiv	Rh	AgSbF ₆ (40), Cu(OAc) ₂ (220)	DCE	60	72	0	0
14	NHOMe	Rh	AgSbF ₆ (40), Cu(OAc) ₂ (220)	DCE	60	40	0	0
15	NHMe	Rh	AgSbF ₆ (40), PivOH (110)	DCE	60	16	0	34 (19) ^b
16 ^c	NHOPiv	Rh	AgSbF ₆ (40), PivOH (110)	DCE	60	16	0	0
17	NHOMe	Rh	AgSbF ₆ (40), PivOH (110)	DCE	60	144	0	10 (R = NHOMe)
18	NHMe	Rh	CsOPiv (200), Cu(OAc) ₂ (40)	MeCN	60	60	0	0
19	NHMe	Ir	AgNTf ₂ (40)	DCE	60	72	0	0
20	NHMe	Ir	Ag ₂ CO ₃ (200)	<i>o</i> -xylene	160	24	0	0

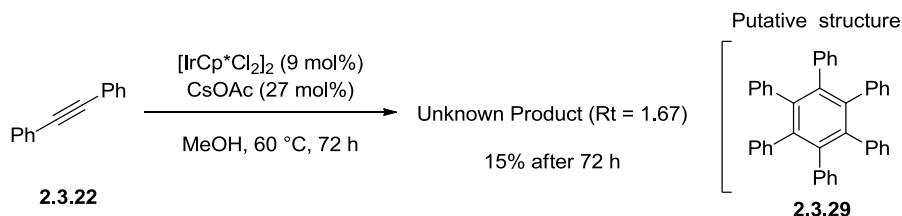
^a Unidentified by-product peak (*R*_t = 1.67) observed. ^b Values in parenthesis correspond to isolated yields. ^c Decomposition of the starting amide observed. ^d Percentage values were determined by LCMS analysis of the crude reaction mixtures.

Table 2.3.1 - Results of the initial C-H activation screening work.

The first series of experiments (**Table 2.3.1** – Entries 1-7) investigated the use of some of the most prevalent conditions in group 9 metal mediated C-H activation reactions, with cesium

acetate in methanol.^{299,301} Two sets of conditions were selected, to assess different reaction temperatures and cesium acetate loadings, with the different amide directing groups. The reactions were conducted under an air atmosphere, to facilitate any potential reoxidation of Rh(I) to Rh(III) (**Scheme 2.3.4**), which it was envisaged would be particularly important for the NHMe (**2.3.17**) substrate due to the absence of any potential internal oxidant. Unfortunately, only one reaction (**Table 2.3.1** - Entry 3) showed any discernible peaks with the anticipated masses for both the cyclised and uncyclised products. It was envisaged that both these species would possess significantly stronger UV chromophores than the starting materials, and therefore 1-2% peak area is likely to represent a significantly lower yield than this value. This low conversion and the relatively small reaction scale meant that the identities of the potential species could not be confirmed. In addition to this, under the reaction conditions the OPiv amide (**2.3.19**) was found to be unstable, potentially undergoing breakdown to liberate the corresponding primary amide. To the best of our knowledge the breakdown of OPiv amides under the typical C-H conditions has not been previously reported. This suggests that either conjugation to the aromatic ring confers some stability to the aromatic amides previously reported, or C-H activation in the literature examples occurs faster than any breakdown pathways.

In several instances, a new highly lipophilic, poorly ionising peak was formed (**Table 2.3.1** – Entries 1,2,4,9, and 12) ($R_t = 1.67$). Despite some of the reactions showing a significant peak area for this unidentified product, attempts to isolate this product were unsuccessful, with only small quantities of an unidentifiable product being recovered. The same peak was observed multiple times in various quantities, regardless of the identity of the directing group. It was postulated that the peak was not caused by a desirable C-H activation process, but instead a reaction between the alkyne (**2.3.22**) and the catalyst. To probe this, one of the reactions was replicated in the absence of the directing group (**Scheme 2.3.12**).



Scheme 2.3.12 – Exploring the proposed reaction between the alkyne (**2.3.22**) and $[\text{IrCp}^*\text{Cl}_2]_2$.

After 72 h, in the absence of any amide substrate, the unidentified peak was observed under the same reaction conditions. This supported the hypothesis that the observed peak was not a consequence of the desired C-H activation but an undesirable side reaction. The unidentified product was putatively assigned as the trimeric structure (**2.3.29**), due to the strong UV chromophore, lipophilic nature, and previous reports of the alkyne (**2.3.22**) to undergo cyclotrimerisation reactions.³⁰⁷ More work would be required to conclusively assign the identity of this product.

Due to the failure of the initial conditions to provide any significant C-H activation, alternative conditions were sought. The alcoholic solvent, *t*-AmOH, was identified for investigations into the influence of increasing the temperature on the reaction mixture (**Table 2.3.1** – Entries 8-9), due to its increased boiling point relative to methanol. One experiment was designed as a direct comparison to the methanol experiments (Entry 9). The second utilised conditions that had been reported by Rovis and Hyster using *t*-AmOH as the solvent for the oxidative cyclisation of alkyl amides with alkynes (Entry 8).³⁰⁰ Regrettably, under both sets of reaction conditions no product formation was observed, apart from the formation of the lipophilic by-product observed previously when using the CsOAc (Entry 9).

In addition to the polar protic solvents, polar aprotic solvents were also explored as part of the initial investigations. In 2013, Rovis *et al.* utilised a combination of cesium acetate and acetonitrile for the coupling of diazo species *via* C-H activation.³⁰⁸ As part of the optimisation work, a small set of protic and aprotic solvents were screened, with acetonitrile outperforming any of the protic solvents. The conditions were applied to the system of interest with both the alkyl amide (**2.3.17**) (**Table 2.3.1** – Entry 10) and OPiv amide (**2.3.19**) (**Table 2.3.1** – Entry 11) being evaluated under these conditions. In both instances no product formation was observed, although the OPiv amide (**2.3.19**) appeared stable in the reaction. Presumably the decomposition of (**2.3.19**) occurs *via* nucleophilic attack of the solvent in the alcohol solvents, liberating the free NH₂, a pathway that is not possible in the aprotic media.

Due to the modest success in the halogenation reaction (**Section 2.2.6**), demonstrating that the C-H activation could be achieved, conditions based on these results were investigated, replacing the NIS with the alkyne (**2.3.22**) (**Table 2.3.1** – Entries 12-17).²⁸⁷ Under these conditions, both with and without the external oxidant, no reaction was observed for the NHOPiv directing group (**Table 2.3.1** – Entries 13 and 16), apart from decomposition of the starting material. The combination of the NHOMe directing group and Cu(OAc)₂ additive also

showed no reaction. The addition of the pivalic acid additive gave rise to a small amount of potential product with the NHOMe directing group (**Table 2.3.1**, Entry 17), with the mass consistent with the uncyclised product (**2.3.27**). The low conversion and stronger chromophore of this product (**2.3.27**), relative to the starting materials, inhibited the isolation of the product and confirmation of the product identity. In addition to this, the protracted reaction times further limits the synthetic utility of this reaction. In contrast, with the NHMe directing group (**2.3.17**) both the use of the pivalic acid (**Table 2.3.1** – Entry 15) and Cu(OAc)₂ (**Table 2.3.1** – Entry 12) showed significant levels of product formation. In both, product could be observed by LCMS, and the uncyclised product (**2.3.27**) was confirmed by MDAP purification. In both cases, despite the high levels of conversion, no masses corresponding to the cyclised product (**2.3.23**) could be detected. The success of the NHMe directing group under these reaction conditions suggests that a more electron-rich amide is key for the reaction, with the electron-withdrawing NHOMe (**2.3.18**) and NHOPiv (**2.3.19**) inhibiting the desired transformation. The NHMe amide (**2.3.17**) confirmed that the desired C-H activation was occurring under the reaction conditions, demonstrating the feasibility of this novel directing group.

With the success of the conditions related to the previous iodination method leading to the synthesis of the non-cyclised product (**2.3.27**), conditions were extended in attempts to effect the cyclisation reaction. In 2012, Glorius *et al.* reported the use of directed rhodium (III) C-H activation with MIDA-alkynes to synthesise MIDA-substituted isoquinolines.³⁰⁹ The authors utilised a combination of Cu(OAc)₂ as an external oxidant, and CsOPiv as both a base and to facilitate the C-H activation step of the cycle. Unfortunately, no reaction was observed with these conditions (**Table 2.3.1** – Entry 18).

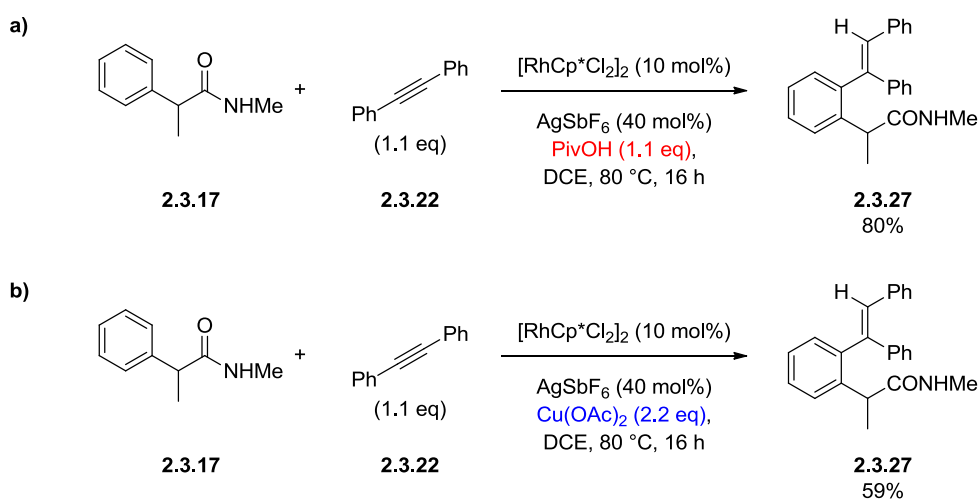
The final two entries (**Table 2.3.1** – Entries 19-20) are representative conditions for the use of iridium (III) catalysis in directed C-H activation reactions, based on conditions reported by Li *et al.* and Miura *et al.* respectively.^{285,310} It was postulated that the differences in electronics and reactivity of iridium may translate to improvements in the C-H activation reaction. In both instances, under the reaction conditions, no product formation or reaction was observed with the NHMe directing group.

Overall, two sets of conditions (**Table 2.3.1** – Entries 12 and 15) demonstrated the viability of the novel C-H activation process. To develop these results into a more generally effective methodology further research was concerned with the optimisation of the process and

developing a more detailed understanding of the importance of the specific reaction conditions.

2.3.5 Optimisation of the C-H Activation Reaction: Validation and Solvent Screening

Before any optimisation could be conducted, determination of an accurate yield for the successful reaction conditions was required (**Table 2.3.1** – Entries 12 and 15). Due to the small reaction scale, sampling techniques, and MDAP purification the yields initially obtained for both the copper (II) acetate (**Table 2.3.1** – Entry 12) and pivalic acid (**Table 2.3.1** – Entry 15) mediated reactions underestimate the efficiency and yields of both processes. The preliminary screening suggested that the copper (II) acetate promoted reaction proceeded significantly slower than the corresponding pivalic acid mediated process, and this also required verification. To explore the reaction rates and overall yields, both processes were scaled-up to a more practically convenient level scale enabling column chromatography (**Scheme 2.3.13**). To facilitate complete reaction conversion, due to the slow reaction progression in the copper-mediated reaction, both reactions were heated to 80 °C rather than 60 °C.

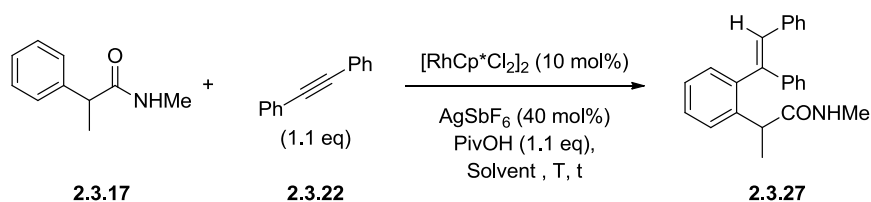


Scheme 2.3.13 – Scale-up of the successful C-H activation conditions; **a)** pivalic acid-mediated reaction; **b)** copper (II) acetate-mediated reaction.

Gratifyingly, in both instances the reaction was found to proceed in good yields (**Scheme 2.3.13**). In addition to this, the pivalic acid-mediated reaction also showed moderate levels of a di-C-H activation product. Unfortunately, the low purity of this product prevented the exact levels of this species to be discerned. The causes of the reduced yields for the copper (II) acetate case are attributed to two factors; the slower reaction rate, *vide supra*, and the levels of

the alkyne by-product formation through potential cyclotrimerization (**Scheme 2.3.12**). LCMS analysis showed that the copper (II) acetate reaction was associated with the formation of significantly increased levels of the by-product (see **Scheme 2.3.12**), relative to the pivalic acid-mediated reaction. It is proposed that this serves to reduce the levels of available alkyne for the C-H activation process and reduces the overall yields. The exact mechanism of this increased by-product formation are still unknown. It may be that under the copper-mediated conditions (**Scheme 2.3.13 b**) the desired C-H activation reaction proceeds more slowly, resulting in increased concentrations of the alkyne to partake in the side reaction. Alternatively, the copper may directly facilitate the side reaction. Without confirmation of the by-products structure, the exact role of the copper remains uncertain.

With the C-H activation affording a 80% yield of the product (**2.3.27**), attention was now turned to the optimisation of the reaction. In the initial screening (**Table 2.3.1**) a range of solvents were assessed, however, the combination of silver salts and pivalic acid or copper (II) acetate additives was only assessed in DCE. To assess if the success of the reaction is dependent on the use of DCE, the successful conditions (**Scheme 2.3.13**) were applied to a range of solvents with diverse properties (**Table 2.3.2**). Due to the increased yields and reaction rates of the pivalic acid-mediated reaction (**Scheme 2.3.13**) these conditions were chosen for the solvent screening.



Scheme 2.3.14 – General procedure for the C-H activation solvent screening.

Entry	Solvent	T (°C)	t (h)	LCMS (%)
1 ^a	DCE	60	16	34
2	Toluene	80	16	0
3	MeCN	60	40	0
4	MeOH	60	40	0
5 ^b	PhCl	80	16 (144)	15 (45)
6 ^b	^t AmOH	80	2 (16)	2 (2)
7 ^b	DCM	40	16 (40)	8 (13)
8	TBME	60	16	0
9 ^c	2-MeTHF	60 (80)	16 (56)	< 2 (18)

^a Reference reaction from **Table 2.3.1**. ^b Values in brackets indicate extended time periods. ^c Reaction was conducted at 60 °C for 16 h, before heating to 80 °C for a further 40 h.

Table 2.3.2 – Solvent screening for the C-H activation reaction.

The use of aromatic solvents, in particular toluene and chlorobenzene (**Table 2.3.2** – Entries 2 and 5), was reported in 2013 by Glorius *et al.* who identified both solvents for C-H activation reactions during a more extensive solvent screen.³¹¹ It was proposed that the weakly coordinating nature of the solvents would facilitate the coordination of the directing group to the catalyst and favour the metallocycle formation. The use of toluene as a solvent was unsuccessful, with no discernible reaction or side reactions occurring (**Table 2.3.2** – Entry 2). This may be a consequence of the poor solubility of the reagents in the reaction mixture, inhibiting both the reaction and the side reactions. The use of chlorobenzene was more successful (**Table 2.3.2** – Entry 5), with formation of the desired product (**2.3.27**) under the reaction conditions. It was postulated that the success of the reaction relative to that of toluene

was due to the increased polarity of the solvent, as chlorobenzene has a dielectric constant of 5.69,³¹² relative to a value of 2.38 for toluene.³¹² In addition to this, potential coordination between the chlorobenzene chlorine and the metal may also serve to solubilise the catalyst.³¹³ The reaction success is anticipated to be dependent on a subtle balance between the solubilisation of the reagents and the potential inhibition of the reaction by coordination of the catalyst. In the case of toluene it is thought that the polarity was too low to sufficiently solubilise the reagents and enable the reaction to occur. Unfortunately, in chlorobenzene the reaction still required elevated temperatures and protracted reaction times, relative to the DCE conditions (**Table 2.3.2** – Entry 1), and was subsequently not an appropriate alternative solvent.

The use of methanol or acetonitrile as solvents for rhodium(III) C-H activation reactions have already been discussed extensively, *vide supra*. It was envisaged that these solvents would provide a much safer and environmentally-friendly alternative to the chlorinated solvents that the reaction had been demonstrated in (**Table 2.3.2** – Entries 1 and 5). Unfortunately, no reaction was observed in either case with these solvents. It is thought that the relatively weak directing group, due to the weak-ligand ability and extended distance from the ring, is prevented from coordinating the catalyst by the stronger coordination from the solvent. As a consequence no reaction is observed in either instance.

It was postulated that the increased boiling point and steric bulk of *t*-AmOH would provide a solution to this problem. In contrast to methanol, the reaction could be heated to elevated temperatures to facilitate decooordination of the solvent. The clash between the other ligands and the bulky *tert*-butyl group was also anticipated to weaken the coordination. Gratifyingly, albeit in low conversions, some reaction was observed (**Table 2.3.2** – Entry 6) with this solvent at elevated temperatures, supporting the hypothesis of solvent deactivation. Unfortunately, despite the factors favouring the reaction, relative to that of the methanol example, only very low conversion was attained. This suggests that the solvent is still inhibiting the coordination of the directing group and preventing the reaction progression. Accordingly, the alcoholic solvents may not be appropriate for this transformation.

The similar properties of DCM and DCE meant that DCM was also explored as a replacement for DCE in the reaction (**Table 2.3.2** – Entry 7). The reaction was successful but was found to proceed significantly slower, with only a modest conversion after 40 hours, in addition to significant levels of unreacted starting materials. It is postulated that this is due to the

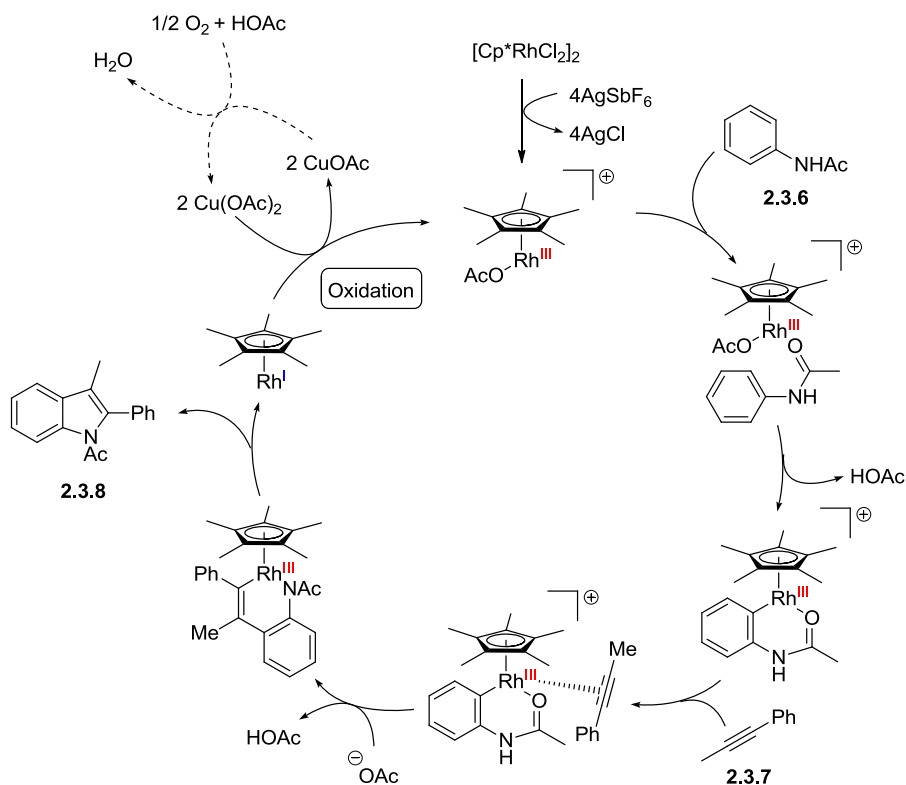
decreased reaction temperature, a limitation imparted on the reaction by the low boiling point of DCM. This issue could potentially be circumvented through the use of pressurised reaction vessels or microwave conditions, but this reduces the applicability of the process, particularly for larger scale synthesis.

The final class of solvent evaluated was the ethereal solvents, TBME and 2-MeTHF. Due to the issues of competitive binding of the catalyst by the solvent encountered in the case of acetonitrile (**Table 2.3.2** – Entry 3) and methanol (**Table 2.3.2** – Entry 4), two relatively bulky ether solvents were selected. It was postulated the steric bulk around the oxygen centre would weaken any potential coordination to the metal and favour coordination of the directing group. In the case of TBME (**Table 2.3.2** – Entry 8) no reaction was observed. There are several potential explanations for this: stronger coordination from the solvent, solvent coordination to the metal centre sterically shielding the approach of the directing group, or poor solubility of one or more reaction components. In contrast, 2-MeTHF was a viable solvent for the reaction (**Table 2.3.2** – Entry 9), requiring elevated temperatures and reaction times. Initial investigations only showed minimal reaction conversion after 16 hours at 60 °C. Increasing the reaction temperature was able to increase the reaction rate and conversion, but still significantly lower reaction conversions we attained relative to that of DCE (**Table 2.3.2** – Entry 1). The increased conversion after raising the reaction temperature supports the reversible association of the solvent with the catalyst, rather than complete deactivation *via* an unknown pathway. The enhanced coordination strength to the catalyst, relative to DCE, is thought to be the source of the reduced reaction rate.

Overall several different solvents have been demonstrated to enable the C-H reaction to various extents (**Table 2.3.2** – Entries 5, 6, 7, and 9). This demonstrates that the successful results in the initial screening (**Table 2.3.1**) are a consequence of the additives employed, although DCE also appears to be the optimal solvent for the reaction. The solvent screen suggested that the reaction conversion is dependent on a subtle balance between solubilising the reaction reagents and competitive binding between the solvent and the catalyst. It is thought that DCE is able to provide a weakly coordinating solvent that is readily displaced, while still providing the requisite solubility for the reaction progression.

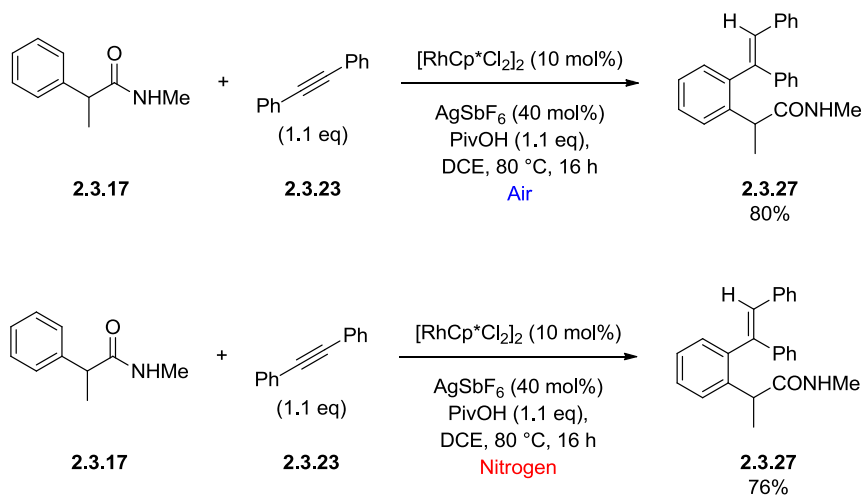
2.3.6 Optimisation of the C-H Activation Reaction: Exploring the Role of the Additives

The high yields for the uncyclised C-H product (**2.3.27**) (**Scheme 2.3.13**) in DCE, rather than any cyclised product (**2.3.23**), suggests a distinct mechanistic pathway to the typical cyclisation reactions (**Scheme 2.3.15**). These reactions typically utilise a Rh(III)/Rh(I) catalytic cycle, with the use of internal or additional oxidants to facilitate the reformation of the active Rh(III) catalyst.



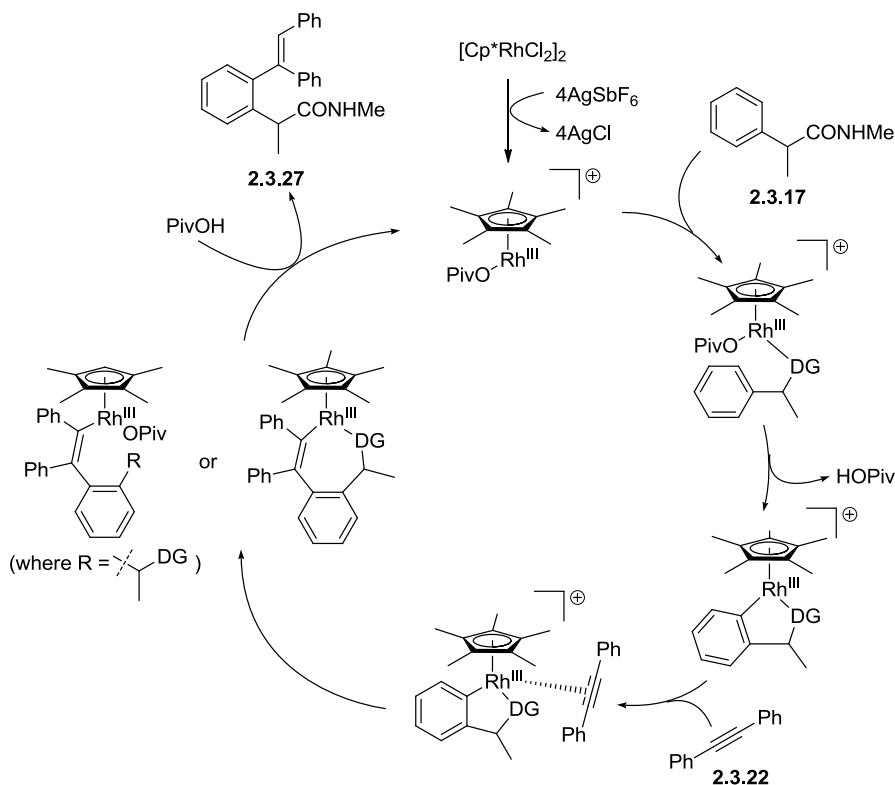
Scheme 2.3.15 – Mechanism for the synthesis of indoles using rhodium(III) C-H activation, highlighting the changes in the metal oxidation state and the oxidation step.²⁸⁸

The success of the NHMe directing group (**2.3.17**), in the absence of any external oxidants, and the relative oxidation state of the uncyclised product (**2.3.27**) implies that there is no oxidation event occurring. The initial screening (**Table 2.3.1**) and subsequent experiments were all conducted under an atmosphere of air. To support the hypothesis of an isohypsic mechanism, the reaction was conducted in parallel under both a nitrogen atmosphere and an air atmosphere (**Scheme 2.3.16**). It was postulated that as the proposed reaction mechanism does not require an oxidation step, that the two reactions would have comparable reaction rates and yields.



Scheme 2.3.16 – Investigating the role of the atmosphere on the C-H activation reaction. The reaction under the air atmosphere was reported previously, *vide supra*, (**Scheme 2.3.13**).

Under both an air or nitrogen atmosphere (**Scheme 2.3.16**) almost identical LCMS reaction profiles were observed, with comparable yields. Reaction monitoring by LCMS also suggested that similar reaction rates were observed, regardless of the atmosphere. These results support the hypothesis that there is no oxidation step occurring, and that an isohypsic mechanism is operative. The proposed mechanism is shown below (**Scheme 2.3.17**).



Scheme 2.3.17 – Proposed mechanism for the formation of the uncyclised product (2.3.27) with the use of the pivalic acid additive.

The first steps of the mechanism (**Scheme 2.3.17**) are proposed to be the same as the indole synthesis (**Scheme 2.3.15**). The silver salts serve to activate the pre-catalyst, sequestering the halogens to form the active cationic species. Coordination of the directing group (DG) and C-H activation forms the metallocyclic intermediate. Coordination of the alkyne to the vacant coordination site and migratory insertion forms the cyclic species. In the indole example (**Scheme 2.3.15**), exchange between coordination through the oxygen and the nitrogen enables a reductive elimination to form the indole and the rhodium(I) intermediate. In the new C-H activation process (**Scheme 2.3.17**), instead of a reductive elimination, it is proposed that a protonation occurs to yield the uncyclised product (2.3.27) and directly regenerates the catalyst without the requirement for re-oxidation. As a consequence no oxidants are required for the reaction (**Scheme 2.3.16**).

Based on this mechanism, it was proposed that rate of coordination to the nitrogen and reductive elimination must be slower than that of the protonation step (**Figure 2.3.3**). It is postulated that the primary cause of the absence of cyclisation is the difficulty in the formation of the metallocycle intermediate, after migratory insertion into the alkyne. The increased size

of the intermediate metallocycle, 8-membered in comparison to the 6-membered species in the mechanism proposed by Glorius *et al.*,²⁸⁸ inhibits the change of coordination between the carbonyl oxygen and the nitrogen of the amide. In addition to this, as depicted above (**Scheme 2.3.17**), the pivalic acid/pivalate group could displace the weak coordinating group, disrupting the formation of the large metallocycle. Consequentially, the inability to coordinate the metal *via* the nitrogen center prevents reductive elimination. Instead protonation of the intermediate, either by pivalic acid or the water associated with the copper acetate, leads to the formation of the uncyclised product (**2.3.27**) (**Figure 2.3.3**).

However, an alternative explanation for the formation of the non-cyclised product is that the reductive elimination step to form the 8-membered ring occurs significantly slower, even if coordination to the nitrogen center is occurring. If this pathway is operative, a double protonation of the amide directing group and the C-Rh bond then occurs to regenerate the catalyst and form the uncyclised product (**Figure 2.3.3**).

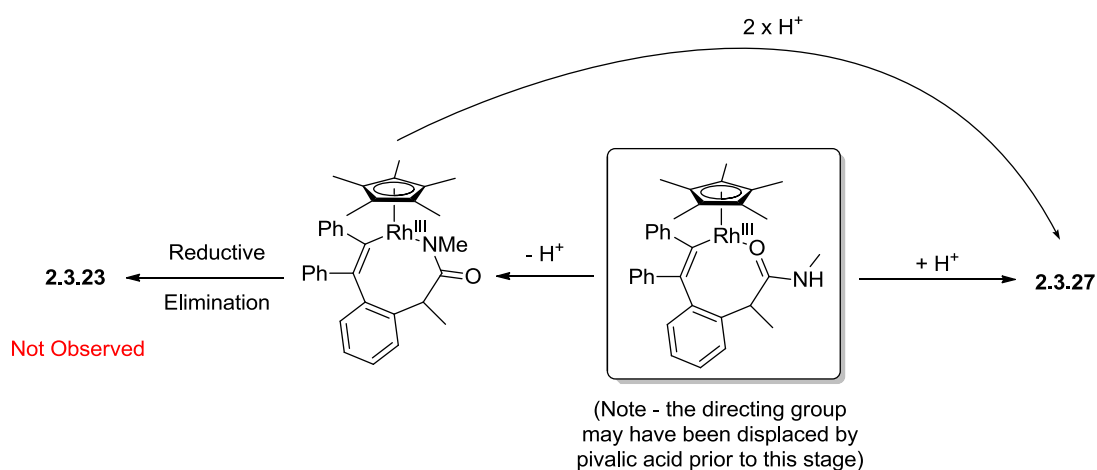
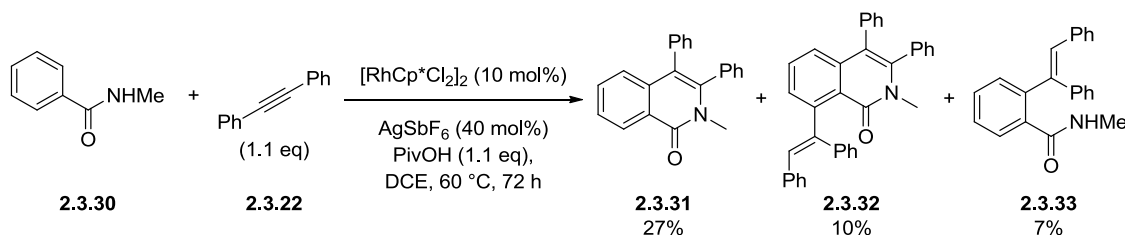


Figure 2.3.3 – Potential pathways to form either the cyclised or uncyclised products depending on the rates of protonation, change in coordination, and reductive elimination.

To ascertain if the absence of cyclisation is a consequence of the unprecedented system, the reaction was conducted with the directly linked amide directing group (**2.3.30**) (**Scheme 2.3.18**). It was hypothesised that the absence of cyclisation could be attributed to: the increased metallocycle size weakening coordination and inhibiting reductive elimination, the additional alkyl unit removing the directing amide from conjugation with the aromatic unit, or the reaction conditions favouring the protonation pathway/s. If the cyclisation occurs under these

conditions it would demonstrate that the reaction outcome is a consequence of the novel system, not the reaction conditions.



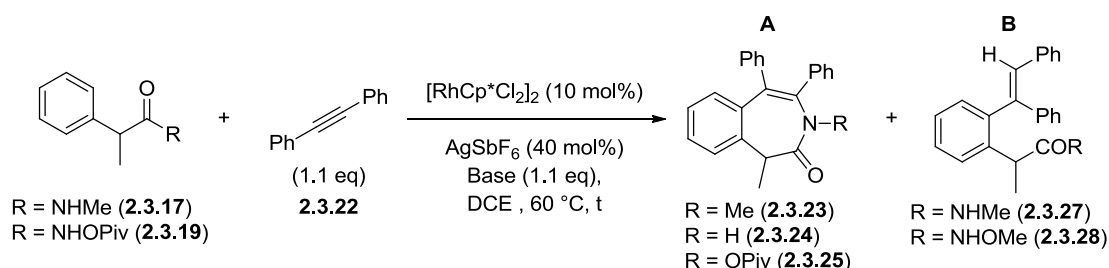
Scheme 2.3.18 – C-H activation with directly linked amide directing group (2.3.30). The product identities were proposed by based on the LCMS masses, with the yields representing the relative LCMS peak area.

Reaction of the directly-linked amide (2.3.30) under the typical conditions led to the formation of a mixture of products, with LCMS masses consistent with both cyclised and uncyclised products. Unfortunately, the mixture of products and other by-products inhibited the isolation and characterisation of the species. Two potential products from the cyclisation pathway were observed (2.3.31 and 2.3.32) as the major reaction products. The corresponding uncyclised product (2.3.33) was also observed as a minor reaction component. This demonstrates that although the reaction conditions do promote some formation of the uncyclised product (2.3.33), the major factor leading to the formation of the uncyclised product (2.3.27) is specific to the system, most likely due to the increased metallocycle size, *vide supra*. This weakens the coordination between the metal and the directing group and may even lead to the displacement of the directing group during the reaction.

With the exclusive formation of the uncyclised species (2.3.27) having been established for the novel amide directing group (2.3.17), the role of the additives on the reaction yield were explored. It was envisaged that alternative additives to copper (II) acetate (which is potentially an oxidant) or the pivalic acid may provide improved reaction yields, potentially removing the requirement for the activating silver salts. It was also proposed that the modification of the reactions condition could provide facile access to cyclic intermediates, further enhancing the scope of this novel methodology.

It was envisaged that formation of the cyclised product (2.3.23) could be promoted by enhancing the coordination strength between the directing group and the metal centre, and inhibiting the protonation of the metallocyclic intermediate (**Figure 2.3.2**). It was proposed

that the addition of a basic additive would fulfil both of these requirements. Coordination of the amide to the directing group is envisaged to enhance the acidity of the amide proton, facilitating the deprotonation and subsequent exchange from coordination of the oxygen to the nitrogen. Even if the reaction proceeds through the deprotonated cyclic system (**Figure 2.3.3**), it was envisaged that basic conditions would inhibit the proposed protonation of the metallocycle, allowing selective formation of the cyclic product (**2.3.23**). A range of different bases were assessed under the reaction conditions (**Scheme 2.3.19** and **Table 2.3.3**), with both the NHMe directing group (**2.3.17**), due to its established success in directing the desired C-H activation, and the NHOPiv directing group (**2.3.19**), due to its enhanced acidity.



Scheme 2.3.19 – General procedure for the base screening.

Entry	R	Base	t (h)	A (%) ^c	B (%) ^c
1	NHMe	CsOPiv	72	0	0
2	NHMe	CsOAc	72	0	39 ^a
3	NHMe	K ^t OBu	72	0	0
4	NHOPiv	CsOPiv	72	0	0
5	NHOPiv	CsOAc	72	0	0
6	NHOPiv	K ^t OBu	72	0	0

^aSignificant by-products observed and incomplete reaction profile. ^bBreakdown of the starting material observed. ^cPercentage product/s by LCMS.

Table 2.3.3 – Results of the screening into the C-H activation under basic conditions.

Three bases were selected for the screen with differing pK_a values to assess the influence of the base strength on the reaction.^{314,315} The use of the acetate bases is also commonly associated with concerted metallation-deprotonation reactions (**Figure 2.3.4**), and was anticipated to replace the pivalic acid or copper acetate promoters.³¹⁶

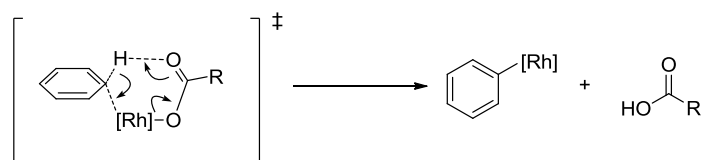


Figure 2.3.4 – Acetate-promoted C-H activation through a concerted metallation-deprotonation reaction.³¹⁶

In the case of the NHOPiv (**2.3.19**) directed reactions, despite it being anticipated that these amides would have lower pK_a values, complete degradation of the directing group was observed (**Table 2.3.3** – Entries 4-6). These results match those for the initial screening (**Table 2.3.1**), with hydrolysis of the directing group proposed to be occurring before any of the desired C-H activation processes. The use of the strong alkoxide base, potassium *tert*-butoxide, was unable to promote any C-H activation reactions (**Table 2.3.3** – Entry 3). Despite being the strongest base in the screen, the failure of the reaction may be due to coordination to the metal or the inability of the base to partake in the concerted metallation-deprotonation reaction postulated to be the mechanism for the C-H activation step.

The use of cesium pivalate (**Table 2.3.3** – Entry 1) was similarly ineffective at promoting the C-H activation reaction. It had been proposed that the use of the pivalate would be the optimal base for this reaction, due to the reported efficiencies of pivalate groups to affect concerted metallation-reactions.³¹⁶ No reaction, either cyclisation or formation of the uncyclised product, was observed suggesting that C-H activation does not occur under these conditions. This may be due to the pivalate group coordinating and sequestering the catalyst, or the steric bulk of the pivalate inhibiting the directing group coordination or other steps in the catalytic cycle.³¹⁶

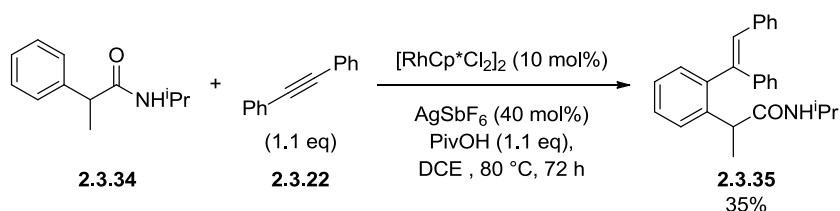
The only basic additive able to promote the reaction was cesium acetate (**Table 2.3.3** – Entry 2), in combination with the previously successful NHMe directing group. In contrast to the previously successful copper(II) acetate or pivalic acid conditions (**Scheme 2.3.13**), significant unidentified impurities were also observed in the reaction mixture, including the previously observed potential trimeric structure (**2.3.29**). These impurities inhibited the isolation of the product (**2.3.27**) and prevent cesium acetate being a viable alternative to the use of copper(II) acetate or pivalic acid.

In all instances (**Table 2.3.3**) no cyclisation products were detected under basic reaction conditions. It was determined that this new protocol is not currently suitable for the direct formation of cyclic products.

2.3.7 Investigations into Alternative Directing Groups

With the development of the novel directed C-H activation protocol for the formation of uncyclised products, attention was now turned to the directing group, to enhance the scope/applicability of the reaction. Three amide directing groups had been initially assessed for the reaction, *vide supra*, with the NHMe amide having optimal directing group capacity out of those explored. It was proposed that the electron-withdrawing oxygen groups in the NHOMe and NHOPiv amides weaken the coordination to the metal centre and prevent catalysis from occurring. In an effort to increase the scope and utility of the reaction a range of different directing groups were explored.

The first substrate investigated was the use of the NHⁱPr amide (**2.3.32**) directing group.³¹⁷ It was hypothesised that, due to the comparable electronics between the NHMe (**2.3.17**) amide and the NHⁱPr amide (**2.3.32**), the NHⁱPr amide (**2.3.32**) would be a competent directing group (**Scheme 2.3.20**).

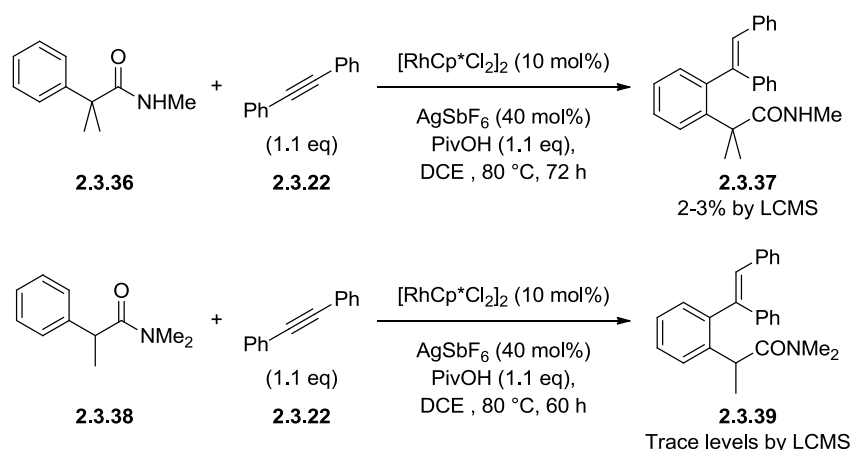


Scheme 2.3.20 – C-H activation with the alternative NHⁱPr amide (**2.3.32**).

Gratifyingly, under the optimised reaction conditions, the NHⁱPr amide (**2.3.34**) was observed to direct the C-H activation reaction, giving rise to the uncyclised product (**2.3.35**) in a 35% yield. The reaction was found to proceed significantly slower than for the NHMe amide (**2.3.17**), failing to attain full conversion after 72 h. The increased electron-donation of the ⁱPr group, relative to the Me group, was anticipated to enhance the coordination strength between the directing group and the catalyst, facilitating the C-H activation reaction and the rate of catalysis. The decrease in the rate suggests that the reaction is also highly susceptible to steric influences, in addition to the electronics of the directing group. It is proposed that the increased

steric bulk of the alkyl group in the amide (**2.3.34**) causes clashes with the catalyst and therefore slows the rate of the C-H activation process.

The reduced reactivity of the NHⁱPr amide (**2.3.34**) demonstrated that in addition to the electronic requirements of the directing group, there was also a significant steric factor which exerts a profound influence on the reactivity observed. To investigate the steric influences further, two alternative amide directing groups; the *gem*-dimethyl NHMe amide (**2.3.36**) and the NMe₂ amide (**2.3.38**), were investigated (**Scheme 2.3.21**). The *gem*-dimethyl substrate (**2.3.36**) was designed to investigate the influence of increased sterics in the linker. For the NMe₂ amide (**2.3.38**), the two electron donating alkyl groups in the amide could potentially enhance the coordination strength to the metal center. This directing group is also associated with an increased steric bulk, relative to the NHMe amide (**2.3.17**), which may debilitate the reaction. The relative reactivity enables the influence of both steric and electronic factors to be assessed.

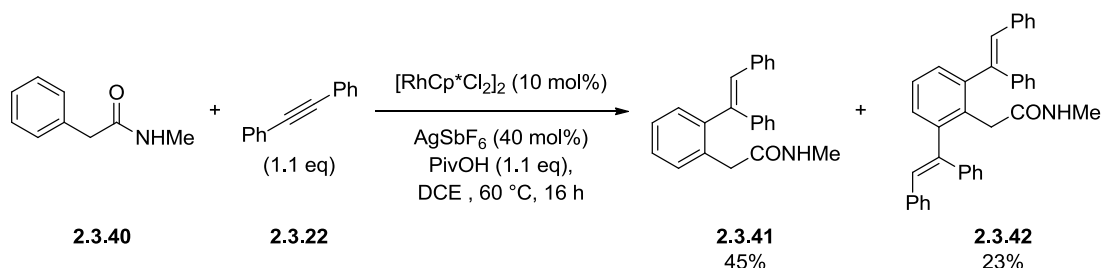


Scheme 2.3.21 – Attempted C-H activation reactions with the *gem*-dimethyl amide (**2.3.36**) and the NMe₂ amide (**2.3.38**).

In both instances only low levels of reactivity were observed, despite the comparatively forcing reaction conditions. The addition of a second methyl group into the linker (**2.3.36**) is hypothesised to increase the steric bulk at the *ortho* position of the ring. This steric clash may inhibit the C-H activation by the bulky catalyst, despite the Thorpe-Ingold effect favouring the cyclisation.³¹⁸ Low levels of potential product, consistent with the mass of the uncyclised product (**2.3.37**), could be observed by LCMS, but due to the predicted increased chromophore strength for the product, it is anticipated that under the reaction conditions negligible levels of C-H activation are occurring.

The replacement of the N-H (**2.3.17**) with an N-Me (**2.3.38**) also completely inhibits reactivity, with only trace levels of a potential product peak detected by LCMS. In a comparable fashion to the NHⁱPr amide (**2.3.34**) (**Scheme 2.3.20**), the increased steric bulk on the nitrogen decreases the reactivity, despite increasing the electron density on the carbonyl. In the case of the NMe₂ (**2.3.38**) this steric influence dominates, inhibiting product formation.

The three experiments with alternative alkyl amide directing groups (**Schemes 2.3.20** and **2.3.21**), clearly demonstrated that increasing the steric bulk has a detrimental influence on the reactivity. It was proposed that, conversely, a reduction in the steric bulk would have a beneficial influence on the reaction, potentially enabling higher yields and milder reaction conditions; such as a lowered temperatures and catalyst loadings. To probe this the reaction was conducted with the NHMe amide, with a less-hindered CH₂ linker (**2.3.40**) (**Scheme 2.3.22**).



Scheme 2.3.22 – C-H activation with the less sterically encumbered substrate (**2.3.40**).

Gratifyingly, under milder reaction conditions complete conversion of the alkyne was observed. In addition to the mono-C-H activation product (**2.3.41**) typically formed under the reaction conditions, the formation of significant quantities of the previously uncharacterised di-C-H activation product (**2.3.42**) was observed, with poor selectivity for the formation of the mono-C-H activation substrate. It is hypothesised that in the case of the methyl linker (**2.3.17**), after the first C-H activation, the steric clashes between the methyl group and the alkene inhibit the molecule from adopting the desired conformation to undergo a second C-H activation reaction (**Figure 2.3.5a**). Instead the molecule predominantly exists in the conformation with the hydrogen eclipsing the aromatic, with a large energy barrier to rotation inhibiting the molecule adopting the active conformation. Removal of this group alleviates the steric clash, reducing the energy between the lowest energy conformation and the reactive conformation,

enabling the molecule to adopt the required conformation for a second C-H activation reaction (Figure 2.3.5b).

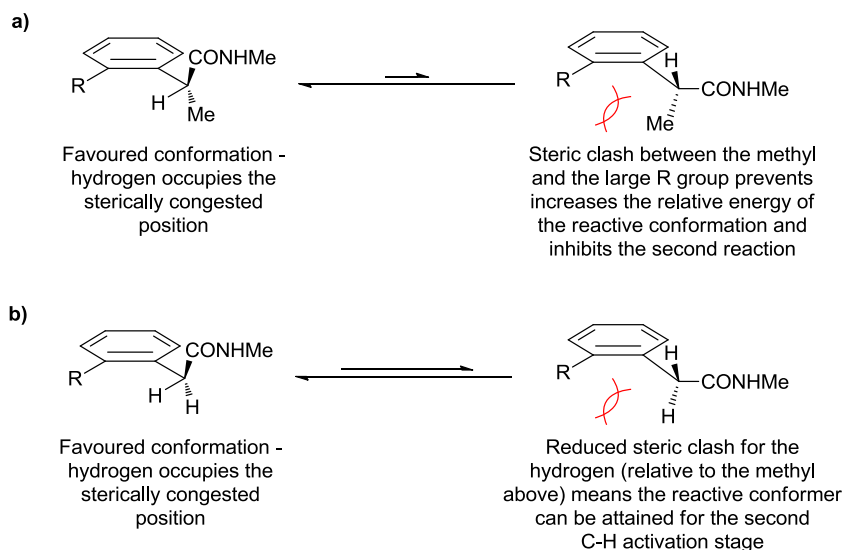
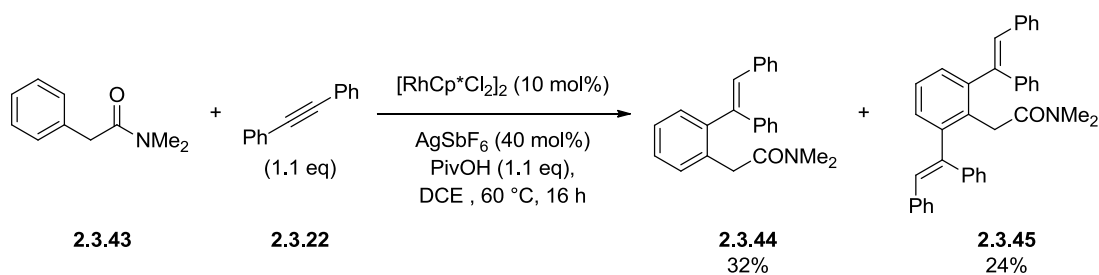


Figure 2.3.5 – a) Postulated steric clash between the methyl group and the alkene substrate, preventing further reactivity; b) Removal of the methyl enabling the second C-H activation reaction.

The experiments with different linkers, *vide infra*, demonstrated that the substrate sterics exert a profound influence on the reaction outcome. Increased steric bulk increases the selectivity for the mono-product, but debilitates the reaction. Conversely, reductions in the steric environment facilitate the reaction but at the expense of selectivity.

In order to further evaluate this subtle balance, the NMe₂ amide with a CH₂ linker (**2.3.43**) was subjected to the reaction conditions. Previously, the use of a NMe₂ amide (**2.3.38**) led to a complete loss of reactivity relative to the corresponding NHMe (**2.3.17**) amide (Scheme 2.3.23). It was envisaged that the additional methyl in this instance could modulate the reactivity, increasing the selectivity for the mono-C-H activation pathway. In addition to this, the presence of any di-C-H activation products would support the hypothesis for the mono:di selectivity based on conformational energies (Figure 2.3.5), as opposed to sterics inhibiting catalyst coordination and reaction.



Scheme 2.3.23 – C-H activation with the alternative NMe_2 amide (2.3.43).

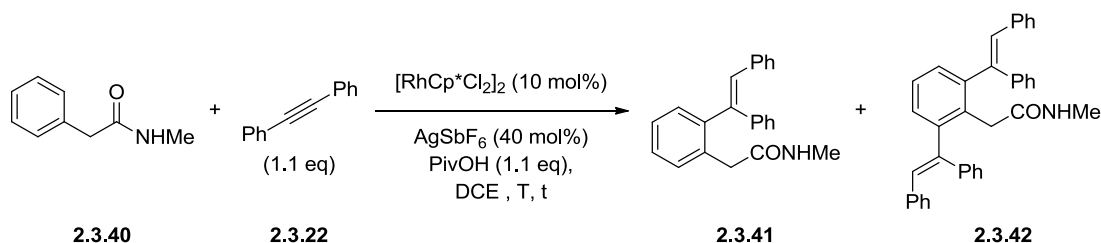
In contrast to the previous tertiary amide example (**Scheme 2.3.21**), the dimethyl amide (2.3.43) was found to be a competent directing group. As observed for the previous CH_2 -linked substrate, the reaction could be conducted under milder reaction conditions, with high conversions despite the lower temperature. Disappointingly, this reaction also suffered from the previously observed poor selectivity, adversely impacting the yields and purification of the compounds. The formation of the di-C-H activation product again illustrates the importance of the methyl group in the linker, supporting the hypothesis that this methyl exerts a profound influence on the relative energies of the potential conformations, and subsequently the reaction outcome.

In addition to developing the understanding of the role of the linker on the reaction outcome, the success of the NMe_2 amide (2.3.43) is informative from a more general mechanistic perspective. As this substrate cannot undergo protonation of the amide, it must undergo a single protonation event after undergoing the migratory insertion into the alkyne. While the double protonation pathway may be operative for the secondary amides, this demonstrates that in at least one example the proposed mono-protonation is the likely reaction pathway.

2.3.8 Exploring the Influence of Temperature on the Ratio of Mono-/Di-C-H Activation

Although the CH_2 -linked substrates (2.3.40 and 2.3.43) were competent directing groups, the poor selectivity between mono and di C-H activation limits the applicability of this substrate class. It was hypothesised that this decreased selectivity is a consequence of the reduced rotational energy barrier/s (**Figure 2.3.5**), enabling the reactive conformation for formation of the metallocycle to be attained for the second C-H activation. It was envisaged that the reaction temperature could be key for the control of the selectivity, with lower temperatures inhibiting the metallocycle formation for the more sterically encumbered mono-C-H activation product.

To evaluate if this potential energy difference could be utilised, while still maintaining a synthetically practical rate of reaction, the reaction with the NHMe amide (**2.3.40**) was replicated at a range of different temperatures (**Scheme 2.3.24**). Measuring the relative LCMS intensities then provides a measure of the ratio between the two products and subsequently the selectivity. A graph of the ratio between the mono/di products against time allows a measure of the influence of temperature on selectivity to be assessed (**Figure 2.3.6**).



Scheme 2.3.24 – General procedure for the investigation into the role of temperature on selectivity.

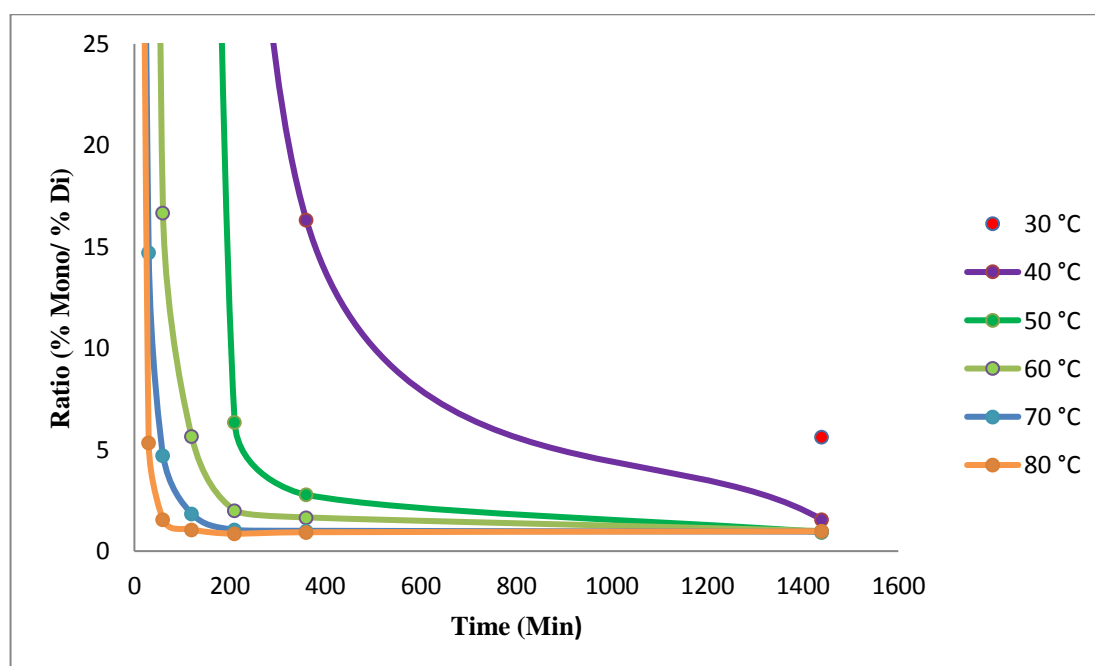


Figure 2.3.6 – Graph of the ratio of mono/di C-H activation at different temperatures. Ratio values were calculated from the integration of the LCMS peak areas (see experimental section). Low conversion for 30 °C resulted in insufficient data to accurately determine the selectivity pattern at this temperature.

Gratifyingly, in all instances appreciable levels of reaction were observed by LCMS within 24 h, including those conducted at lower temperatures. As the reactions progress, in all cases the ratio of mono:di decreases as anticipated. This is due to the rate of the di-C-H activation product (2.3.42) formation being dependent on the formation of the mono-C-H activation product (2.3.41). Subsequently, in all instances the reactions start with high ratios of selectivity, before tending to approximately equal levels of mono and di products by LCMS analysis in all instances.

Although the data (Figure 2.3.6) appears to implicate higher selectivities at lower temperatures, in particular at 30 °C and 40 °C, this may be a consequence of the reduced reaction conversion/s. To evaluate if there is any significant temperature dependence on the selectivity the ratio was plotted against the total integrated product area, which was used as a measure of the overall reaction progression (Figure 2.3.7).

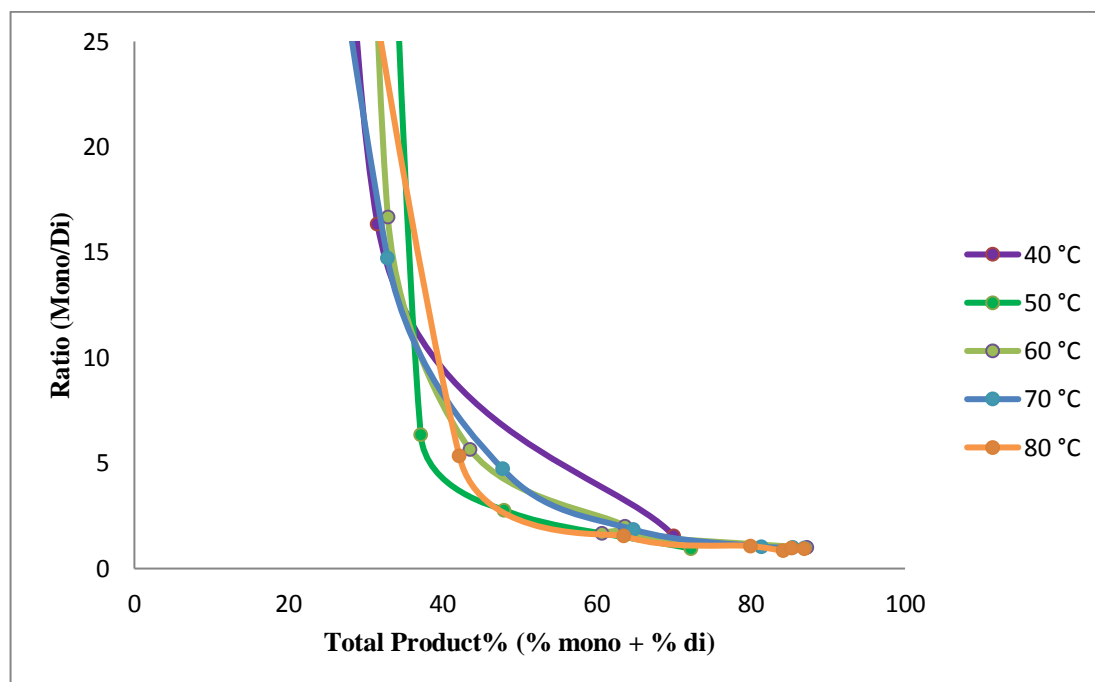


Figure 2.3.7 – Graph of the influence of the influence of total product formation against the ratios of different products. Total product% was calculated by the summation of the integrated peak areas for the mono (2.3.41) and di (2.3.42) C-H activation products. Again insufficient data was attained at 30 °C to accurately analyse this data.

In contrast to the ratio at different time points (Figure 2.3.7), comparable ratios of products were observed, independent of the temperature. This supports the hypothesis, *vide supra*, that

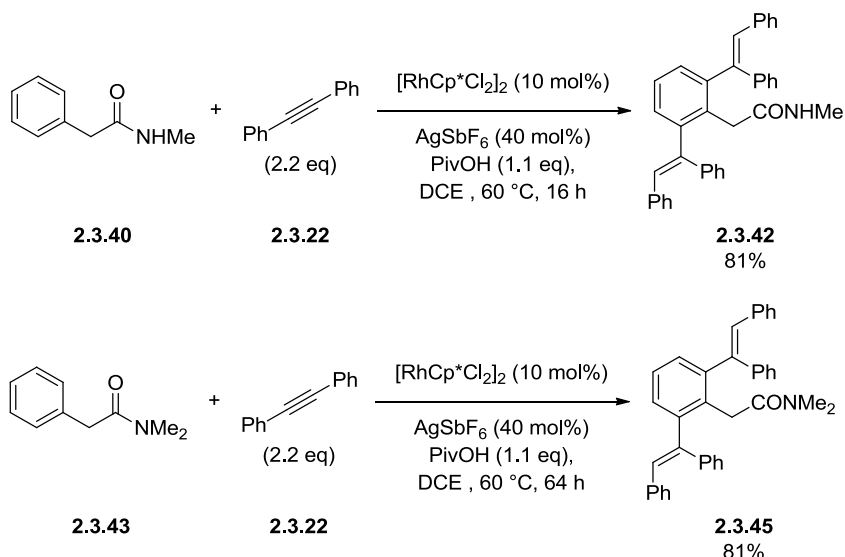
the higher product ratios observed at the lower reaction temperatures are a consequence of the lower conversions, thereby, minimising the concentration of the mono-C-H activation product (**2.3.41**). The significant decrease in the reaction rate at the lower reaction temperatures meant that further reductions in the temperature would not be appropriate due to the increased duration required. It was concluded that with the current directing groups (**2.3.40** and **2.3.42**), the absence of methyl group prevents any significant control over the mono:di-product ratios.

As the NMe₂ amide was demonstrated to be a competent directing group, it was demonstrated that the directing group did not require a potentially acidic proton to enhance coordination and direct the C-H activation. It was envisaged that by changing the strength of the coordination, the ratio of mono:di C-H activation could be controlled. It was hypothesised that weaker coordinating groups could favour the mono product, as the increased steric hindrance after the initial C-H activation could disrupt further catalyst coordination and debilitate the second reaction.

A range of different potentially coordinating groups were therefore assessed under the optimised reaction conditions. Disappointingly, in the case of alternative carbonyls, either an ester, acid, or ketone, no product formation could be observed (see experimental section). In the case of heterocyclic directing groups, only low levels of reaction were detected for tetrazole, pyridyl, and imidazole directing groups (see experimental section). In addition to this, these heterocyclic substrates also showed low levels of di-C-H activation occurring, and did not represent an alternative method to control the reaction outcome.

2.3.9 Evaluating of the Potential Double C-H Activation Process

With a variety of different directing groups being assessed for the reaction, methods to favour the mono-C-H activation product were restricted to the use of substitution in the linker region (**Section 2.3.7** and **Section 2.3.8**). Despite this outcome, it was envisaged that the use of the substituted amide directing groups (**2.3.41** and **2.3.43**) could be utilised to form the extremely hindered di-C-H activation products by increasing the alkyne stoichiometry (**Scheme 2.3.25**).



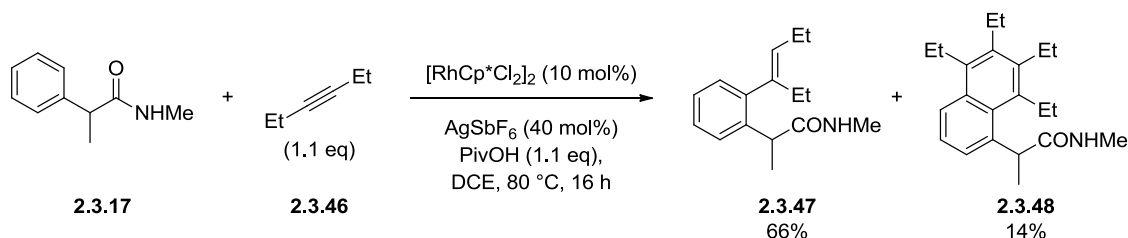
Scheme 2.3.25 – C-H activation reactions with increased alkyne levels.

Increasing the alkyne levels was able to increase the levels of conversion to the di-C-H activation products (**2.3.42** and **2.3.45**), enabling high yields of the sterically encumbered molecules. In the case of the dimethyl amide (**2.3.43**), slower reactivity was observed, relative to the NHMe amide (**2.3.40**). This could be a consequence of the increased steric bulk of the directing group, which when combined with the steric bulk of the alkene, decreases the reaction rate.

2.3.10 Exploring Alternative Alkynes

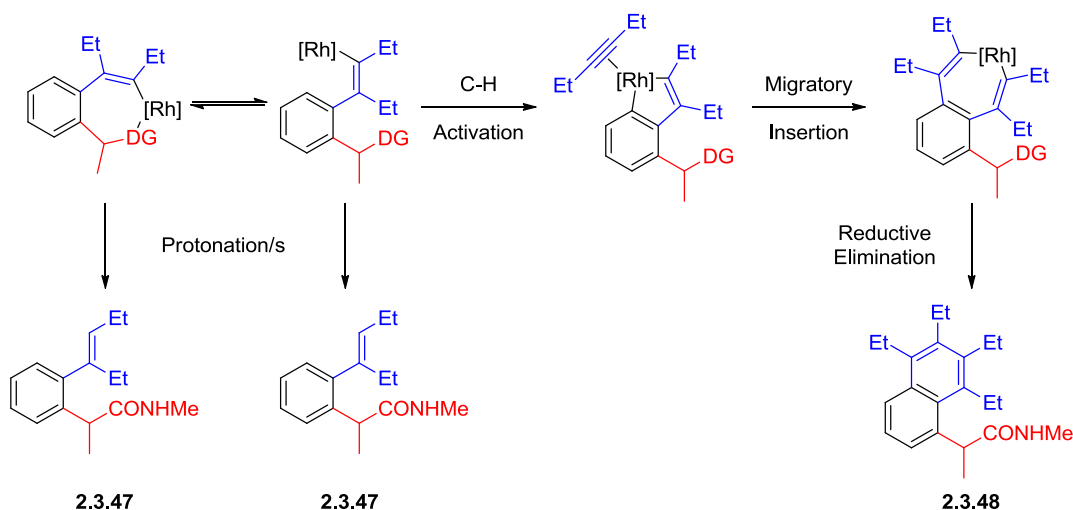
The studies into the directing group and linker have demonstrated that the reaction outcome is strongly influenced by both the sterics and electronics of the substrate. In order to increase the utility of the methodology and to further develop the understanding of the reaction, the alkyne component required evaluation.

To evaluate the potential alkyne scope, a small subset of alkynes were identified to investigate the influence of sterics and electronics on the reaction, as well as exploring the regioselectivity for non-symmetrical alkynes. In order to reduce the potential complexity of mixtures of mono and di C-H activation products, the investigations were restricted to the NHMe amide with the methyl substituted linker (**2.3.17**). The first substrate explored was the diethyl alkyne (**2.3.46**), investigating changing the aryl groups for less sterically encumbering alkyl substituents (**Scheme 2.3.26**).



Scheme 2.3.26 – Investigating the diethyl alkyne (**2.3.46**) as a potential substrate for the C-H activation reaction.

Gratifyingly, under the reaction conditions the reaction of the symmetric diethyl alkyne (**2.3.46**) was found to undergo the desired C-H activation reaction in a yield of 66%. In addition to this, a previously unobserved naphthalene product was formed in a 14% yield (**2.3.48**). It is proposed that this species is formed *via* a second C-H activation process of an intermediate rhodium species, rather than the protonation event/s typically observed (**Scheme 2.3.27**).



Scheme 2.3.27 – Proposed divergent mechanisms for the formation of both the uncyclised (**2.3.47**) and naphthalene (**2.3.48**).

The hypothesised mechanism for the formation of the naphthalene product (**2.3.48**) begins after the migratory insertion previously postulated (**Scheme 2.3.17**). The exact ligand sphere of the metal is unknown at this stage in the sequence, with a potential equilibrium being established between coordinated and non-coordinated by the directing group. Protonation of either these species generates the uncyclised species (**2.3.47**).

Alternatively, dissociation of the directing group enables a second C-H activation process, to form a 5-membered metallocycle. Formation of this species is dependent on dissociation of the directing group. This supports the hypothesis, *vide supra*, that the loss of the coordination of the directing group, potentially due to the increased ring-size, is responsible for the absence of any of the desired cyclisation. The coordination of the alkyne then enables a second migratory insertion reaction, forming a new 7-membered metallocycle. This then undergoes a reductive elimination to yield the product (**2.3.48**) and a rhodium(I) species, which is potentially re-oxidised by atmospheric oxygen. Preliminary studies have implicated this pathway, rather than a protonation followed by C-H activation of the alkene. The resubjection of the uncyclised product (**2.3.47**) to the reaction conditions is unable to form any of the desired naphthalene product (**2.3.48**), demonstrating that the naphthalene product (**2.3.48**) is not formed from the uncyclised product (**2.3.47**). Further studies are required to determine the influence of variation of the reaction conditions, such as the addition of external oxidants or conducting the reaction under an inert atmosphere.

The formation of the naphthalene product (**2.3.48**) for the reaction with diethyl alkyne (**2.3.46**) is thought to be due to the sterics of the reaction. It is proposed that the smaller ethyl substituent enables the rotation of intermediate rhodium species, allowing the correct orientation for the second C-H activation to occur (**Figure 2.3.8**). For the diphenyl alkyne (**2.3.22**) the bulkier phenyl group prevents the planar conformation being attained, preventing a second C-H activation reaction. The formation of naphthalene products in the reaction of other substrates, and the observed product distribution, may support this hypothesis or provide further information about the influence of other factors such as the disparate electronics of the alkynes.

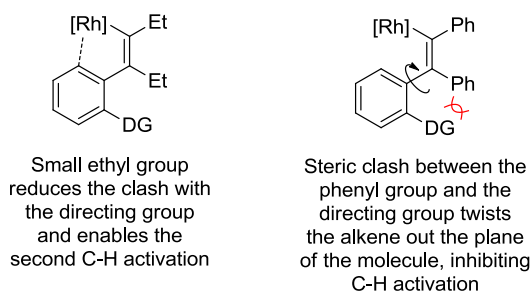
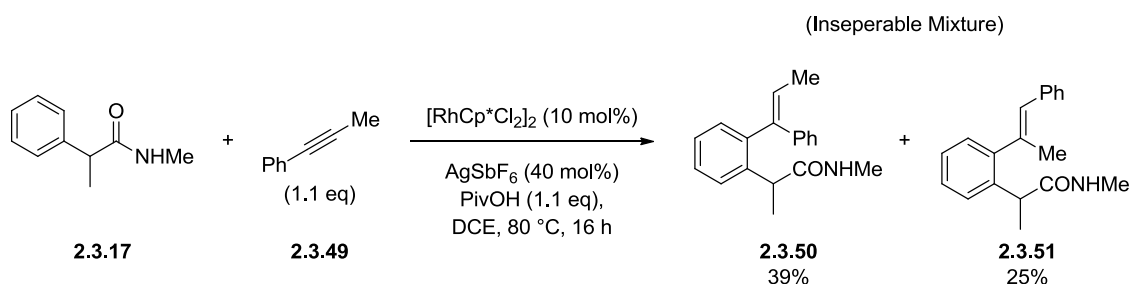


Figure 2.3.8 – Contrasting the postulated steric clashes for the diethyl and diphenyl substrates for the second C-H activation process.

With viability of the dialkyl alkyne (**2.3.46**) substrate having been established, the next alkyne selected was the unsymmetrical phenyl methyl alkyne (**2.3.49**). This was selected to evaluate the influence of the alkyne electronics; with an electronic environment between that of the previous two substrates (**2.3.22** and **2.3.46**). In addition to this, it also enabled the levels of regioselectivity to be investigated. In rhodium(III) catalysed C-H activation, this regioselectivity is typically attributed to a mixture of both steric and electronic factors, *vide supra*, although electronics is typically observed to dominate. The selectivity for the methyl substrate (**2.3.17**) will demonstrate if the same is true in the novel directing group series (**Scheme 2.3.28**).

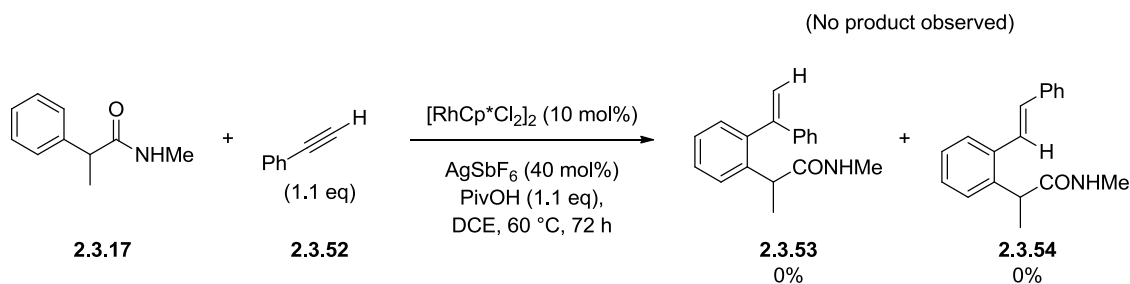


Scheme 2.3.28 – C-H activation with the unsymmetrical alkyne (**2.3.49**). Product identity was assigned using ROESY spectroscopy, specifically the correlations to the alkene hydrogen.

As anticipated, the reaction with the unsymmetrical alkyne (**2.3.49**) gave rise to a mixture of products. Due to the comparable polarities of the molecules, the individual isomers could not be separated and NMR analysis was used to assign and quantify the relative product levels. In contrast to the previously documented examples,^{285,288,301} an inversion and reduction of the regioselectivity was observed. Previous studies with unsymmetrical alkynes, both sterically and electronically, had demonstrated that with directly linked substrates the electronic factors dominate, *vide supra*. The result of the α -methyl suggests that the balance between selectivity and electronics is perturbed in this system. Potentially the absence of the conjugation between the directing group and the aromatic ring, in addition to the potential dissociation of the directing group prior to the migratory insertion, has a profound influence on both the sterics and electronics. As a result the steric factors outweigh the electronic factors, with the clash between the bulky phenyl group and the rhodium dictating the selectivity of the reaction.

In an effort to further explore the influence of sterics and electronics, and to increase the scope of the reaction further, the mono-substituted alkyne, phenylacetylene (**2.3.52**), was evaluated

as a potential substrate (**Scheme 2.3.29**). It was envisaged that if this substrate was tolerated it could further increase the utility of the reaction and the accessible substrates.



Scheme 2.3.29 – Attempted C-H activation with phenylacetylene (**2.3.52**).

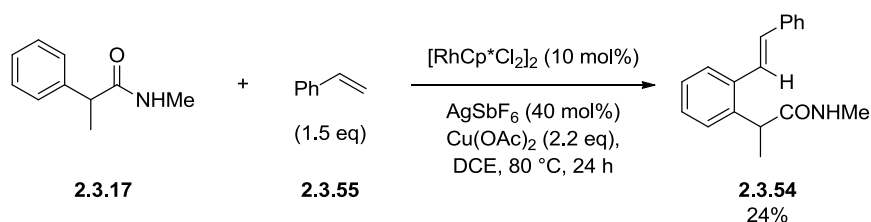
Under the reaction conditions (**Scheme 2.3.29**), the formation of a new peak consistent with the desired product mass (either **2.3.53** or **2.3.54**) was observed by LCMS. Unfortunately, this species degraded during the work-up, preventing product analysis and structural confirmation. Further experimentation demonstrated that this product was still formed in the absence of the rhodium catalyst and, therefore, it was concluded that the identity of this product was not one of the desired C-H activation products. Further studies are required to confirm the exact nature of this species, and the mechanism of its formation. However, this is beyond the scope of this thesis.

2.3.11 Alternative C-H Activation Reactions – Heck Reaction

Since the seminal reports by Miura *et al.*,²⁸⁵ group-nine mediated C-H activation reactions have been coupled to a range of different species, *vide supra*. With the C-H activation with a small subset of directing groups and alkynes being established, attention was now turned to the evaluation of alternative reactions. The Heck type reaction with an alkene was identified as a potential method to enable the synthesis of di-substituted alkene products, a class of substrate which at the time of writing cannot be accessed using the alkyne methodology. In addition to this, the differing reactivity of the alkene and alkyne may modify the reactivity enabling greater control of the mono/di selectivity.

The preliminary studies were conducted with styrene (**2.3.55**) and the α -methyl amide (**2.3.17**) (**Scheme 2.3.30**), due to the exclusive mono-selectivity previously observed with this substrate. This would enable the synthesis of one of the phenyl alkene substrates that were

previously inaccessible through use of the alkyne electrophile (**Scheme 2.3.29**). It was envisaged that if the reaction was successful then the result could be transferred to other directing groups and substrates.



Scheme 2.3.30 – Heck-type reaction of styrene (**2.3.55**) and the substituted amide (**2.3.17**). Alkene geometry for all Heck-reaction products was assigned based on the proton NMR coupling constants.

Both pivalic acid and copper acetate additives were assessed in the potential Heck reaction. Only low conversion was observed in the case of pivalic acid, presumably due to the slow rate of catalyst re-oxidation under the reaction conditions. Copper(II) acetate was found to give significantly higher levels of conversion. The copper is thought to fulfil the role of both an acetate source, to promote the C-H activation, and an oxidant to re-oxidise the catalyst (**Figure 2.3.9**). Unfortunately, the product (**2.3.54**) and styrene (**2.3.55**) were found to co-elute when analysed by LCMS, preventing accurate monitoring of the reaction conversions.

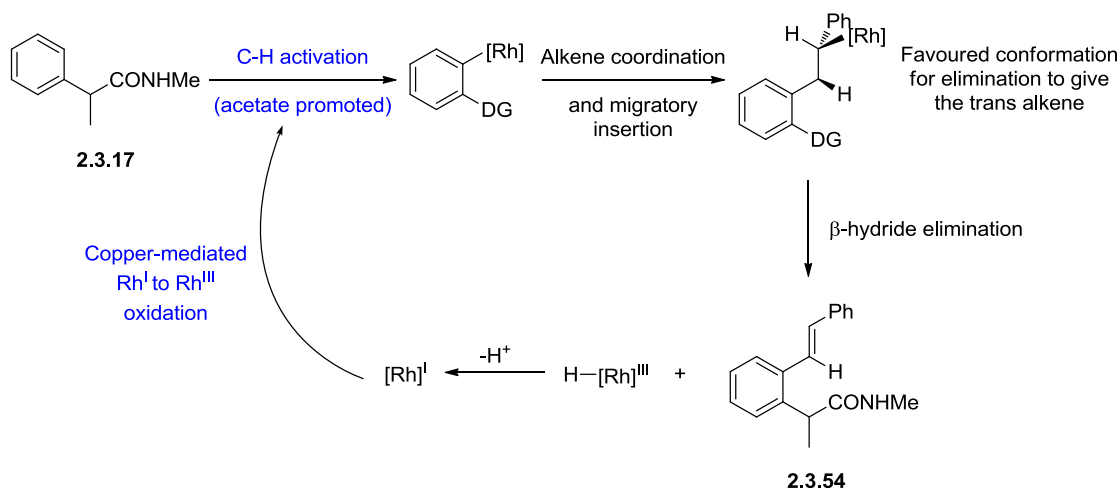
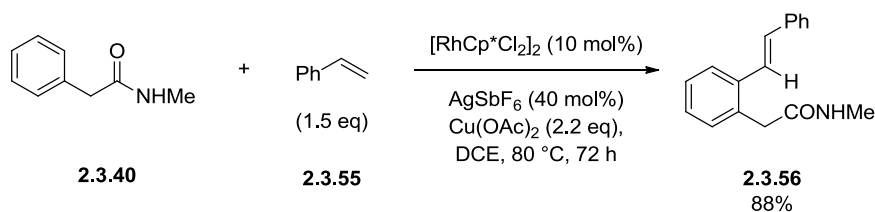


Figure 2.3.9 – Proposed roles of the copper(II) acetate in promoting the Heck-type reaction, highlighting the key stages in blue.

The proposed mechanism begins with an analogous C-H activation to that observed for the alkyne mechanism (**Figure 2.3.9**). The acetate from the copper acetate facilitates the concerted *ortho* metallation/deprotonation to generate the intermediate rhodium species, *vide supra*. Coordination of alkene and migratory insertion forms the C-C bond. Rotation around the single bond allows a *syn*-periplanar β -hydride elimination to form the *trans*-alkene (**2.3.54**). Deprotonation of the rhodium(III) hydride forms the rhodium(I) species. Re-oxidation of the catalyst by the copper regenerates the active rhodium(III) species, completing the catalytic cycle.

With the success of the Heck-type reaction having been established, albeit in modest yields, the reaction was replicated with the unsubstituted amide (**2.3.40**) (**Scheme 2.3.31**). It was envisaged that the reduced steric hindrance would increase the reaction rates, and the absence of the methyl group would reduce the lipophilicity enabling LCMS to be used to monitor the reaction conversion.



Scheme 2.3.31 – Heck-type reaction with the unsubstituted amide (**2.3.40**).

Gratifyingly, under the reaction conditions the mono C-H activation product (**2.3.56**) was attained in high yields, although protracted reaction times were required for complete reaction conversion. Again the use of copper(II) acetate as the additive was found to give significantly increased levels of reaction conversion, compared to the use of pivalic acid. In contrast to the alkyne case, *vide supra*, exclusively mono-C-H activation was observed. It is postulated that the absence of the second substituent reduces the level of twisting about the alkene bond (**Figure 2.3.9**). This in turn inhibits the amide from adopting the required conformation for the second C-H activation, and resulting in exclusive formation of the mono-product (**2.3.56**). The increased conjugation between the alkene and the aromatic may also have electronic influences on the rate of the second C-H activation.

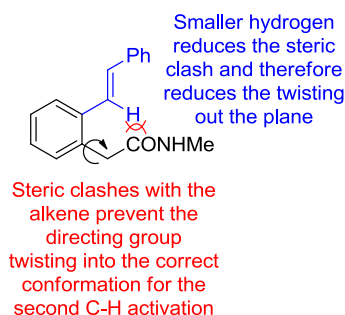
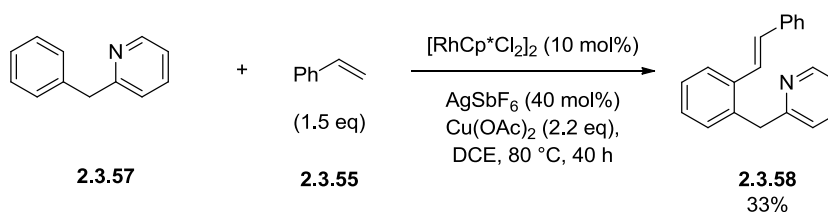


Figure 2.3.10 – Postulated steric clash preventing the second C-H activation.

As part of the work assessing alternative directing groups, *vide supra*, pyridyl directing groups were evaluated for the C-H activation reaction with the alkyne. Under these conditions only low levels of product were detected, despite elevated reaction times and temperatures. It was postulated that these low yields were a consequence of the pivalic acid additive, protonating the nitrogen, preventing the coordination to the catalyst *via* the Lewis-basic lone pair. As the previous Heck-type reactions were found to give higher conversions with copper(II) acetate, the pyridyl directing group was assessed for this reaction type (**Scheme 2.3.32**).

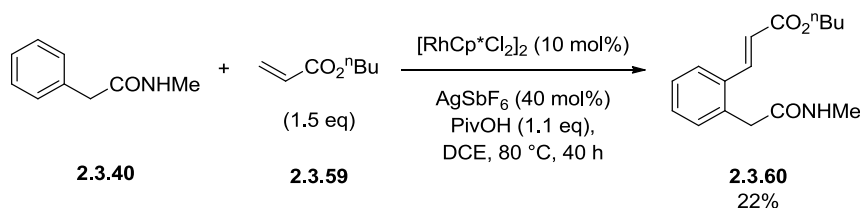


Scheme 2.3.32 – Heck-type reaction with the previously unsuccessful pyridyl directing group (**2.3.57**).

In contrast to the alkyne results, the desired alkene product (**2.3.58**) was formed in a 33% yield. The lower reactivity and reduced yield is thought to be attributed to the weaker directing group relative to the amide (**2.3.40**), slowing the rate of the C-H activation process. It is envisaged that optimisation of the reaction conditions could further enhance the yields and increase the reaction conversions.

With the success of the Heck-reaction with styrene (**2.3.55**), the application of the reaction to other alkenes was now evaluated. It was envisaged that improving the scope of the reaction would increase the viability and potential utility of the process, facilitating further studies. The enone (**2.3.59**) was selected as the resulting product (**2.3.60**) would possess a range of functionalities for further diversification. The butyl ester was used to avoid potential issues

with volatility at the elevated reaction temperatures (**Scheme 2.3.33**). The directed group selected was the unsubstituted amide (**2.3.40**), as this displayed the greatest levels of reactivity towards the C-H activation out of the directing groups studied thus far.

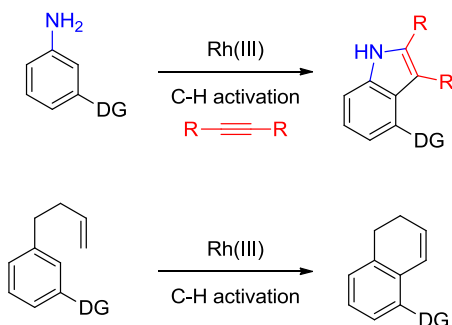


Scheme 2.3.33 – C-H activation of the amide (**2.3.40**) with the enone (**2.3.59**) electrophile.

In contrast to the previous Heck-reactions, the pivalic acid additive was found to give an improved reaction profile relative to the copper(II) acetate reaction. It is thought that the copper(II) acetate oxidant underwent side reactions with the enone (**2.3.59**), leading to increased levels of by-product formation, sequestering the enone (**2.3.59**). Despite the inability of the pivalic acid to promote the re-oxidation step (**Figure 2.3.8**), the absence of side-reactions led to the clean, albeit slower, conversion to the product (**2.3.60**). As observed for the pyridyl directing group (**2.3.57**), further optimisation of the reaction conditions can increase the yields and reaction rates. Despite this, the range of functionality installed under the reaction conditions, with the opportunity for further diversification, means this reaction could become a highly valuable synthetic process.

2.3.12 Conclusions and Future Work

Overall, significant progress towards the development of a novel directed C-H activation reaction has been achieved. Rational design and optimisation was able to develop conditions for the addition of alkynes in good yields with a model amide substrate (**2.3.17**). In addition to this, the impact of the solvent and additives was able to provide mechanistic insight into the reaction. Significant understanding of the reaction has been developed, with these studies laying the foundation for further research. At this stage, no C-H activation followed by subsequent cyclisation reaction has been demonstrated using this methodology, inhibiting the use of this chemistry to directly access BZP derivatives and other cyclic structures. However, it is envisaged that one potential solution to this is the use of internal tethers, exemplified below (**Scheme 2.3.34**). Future work will assess the viability of this strategy, which is outside the scope of this thesis.



Scheme 2.3.34 – Examples of the potential use of internal tethers to synthesise indole derivatives or other cyclic species using the novel C-H activation chemistry.

Several different novel groups have been demonstrated to direct the C-H activation reaction. Examples of both secondary and tertiary amides have shown these to be applicable directing groups, and preliminary results have demonstrated the viability of heterocyclic directing groups. Further research into optimisation of the conditions for heterocyclic directing groups, in particular Lewis-basic functionalities, and increased amide complexity could further enhance the utility of this methodology.

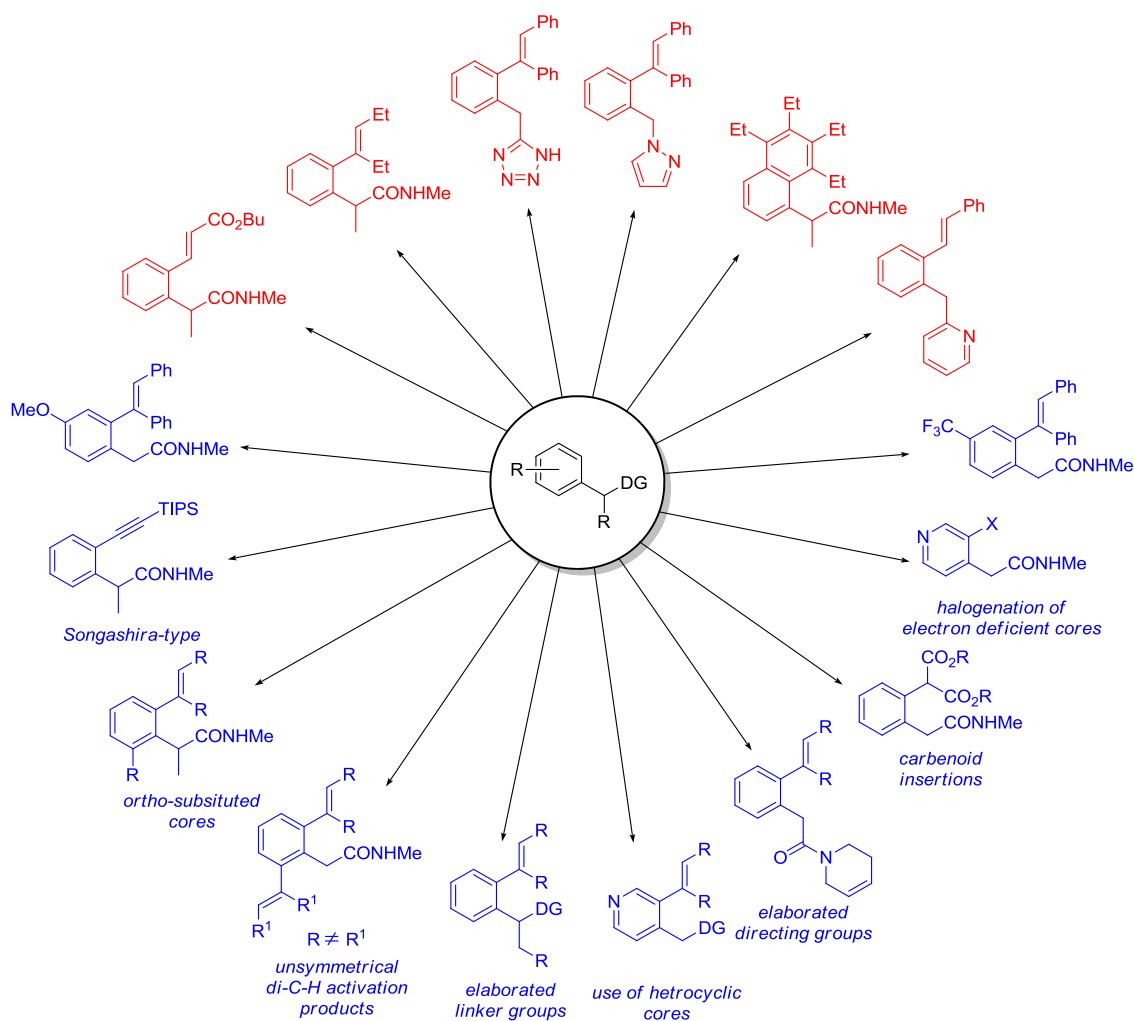
The role of the influence of the addition carbon-linker between the aromatic group and the amide has also been evaluated. A subtle interplay of steric and electronic effects has been found to control the propensity to undergo substitution. Unsubstituted amides (**2.3.40** and **2.3.43**) have been demonstrated to react multiple times (**Scheme 2.3.25**), providing access to highly hindered products that would be otherwise less accessible. The addition of a methyl group is able to modulate the reactivity, giving rise to exclusively mono-C-H activation. Further steric bulk, such as the *gem*-dimethyl linker (**2.3.36**), was found to completely debilitate the reaction. There is potential to develop new directing groups, which can be paired with an appropriate linker to control mono/di selectivity, or to enable differentiation between two directing functionalities within a molecule.

A subset of alkynes and alkenes have been investigated as electrophilic coupling partners. By judicious choice of the electrophile, a range of di- and tri-substituted alkenes can be synthesised utilising this novel methodology. Alkyl and aryl alkynes are tolerated under the reaction conditions, and unsymmetrical derivatives appear to exhibit the inverse selectivity to that reported previously.^{285,288,301} It is envisaged that further research into unsymmetrical

alkynes, in addition to exploring substitution on the aromatic ring, will provide a greater insight into the exact origins of the selectivity, enabling enhanced selectivities.

The expansion of the optimised conditions to the Heck-type reactions demonstrates that the methodology is not restricted to the coupling reaction with the alkynes. The mechanistic work and previous optimisation has developed an understanding of the role of different additives and conditions which can then be applied to alternative electrophiles. It is envisaged that future research will continue to expand the substrate scope, with some potential avenues of research highlighted below (**Figure 2.3.11**).

Current Examples of Reaction Scope



Potential Future Expansions of Reaction Scope

Figure 2.3.11 – Representative examples of current scope and potential avenues for future research.

Despite the research not enabling the synthesis of BZP derivatives at this current stage, the potential scope for this research is appreciable. The initial studies have developed a good amount of understanding of the reaction which will underpin future studies. It is envisaged that further development of this methodology will have ramifications for both total synthesis and medicinal chemistry, opening up the synthesis of a diverse range of previously synthetically less accessible molecules.

3. Experimental

General Methods

Unless otherwise stated, all reactions were carried out under an atmosphere of nitrogen in heat- or oven-dried glassware and using anhydrous solvent. Solvents and reagents were purchased from commercial suppliers and used as received unless otherwise indicated. Reactions were monitored by thin layer chromatography (TLC) or liquid chromatography-mass spectroscopy (LCMS).

Nuclear magnetic resonance (NMR)

NMR spectra were recorded at ambient temperature (unless otherwise stated) using standard pulse methods on a Bruker AV-400 (^1H = 400 MHz, ^{13}C = 100.6 MHz). Chemical shifts are reported in ppm and are referenced to tetramethylsilane (TMS) or the following solvent peaks: CDCl_3 (^1H = 7.27 ppm, ^{13}C = 77.00 ppm), $\text{DMSO-}d_6$ (^1H = 2.50 ppm, ^{13}C = 39.51 ppm) and $\text{MeOH-}d_4$ (^1H = 3.31 ppm, ^{13}C = 49.15 ppm). Coupling constants are quoted to the nearest 0.1 Hz and multiplicities are given by the following abbreviations and combinations thereof: s (singlet), d (doublet), t (triplet), q (quartet), quin (quintet), sxt (sextet), m (multiplet), and br (broad).

Infra-red spectroscopy (IR)

IR spectra were obtained on a Perkin Elmer Spectrum 1 machine.

Liquid chromatography mass spectroscopy (LCMS)

Liquid Chromatography Mass Spectroscopy (LCMS) was conducted on either a Acquity UPLC BEH C18 column (50 mm x 2.1 mm i.d. 1.7 μm packing diameter) at 40 °C eluting with either:

Method A/C - 0.1% v/v solution of formic acid in water (solvent A) and 0.1% v/v solution of formic acid in acetonitrile (solvent B); or

Method B/D - 10 mM ammonium bicarbonate in water adjusted to pH 10 with ammonia solution (solvent A) and acetonitrile (solvent B).

The UV detection is a summed signal from wavelength of 210 nm to 350 nm.

The mass spectra were recorded on a Waters ZQ spectrometer using electrospray positive and negative mode.

Confidential – Property of GSK – Do Not Copy

The following elution gradients were used:

Formic acid modifier (Method A)

Time (min)	Flow rate (mL / min)	% A	% B
0	1	97	3
1.5	1	0	100
1.9	1	0	100
2.0	1	97	3

High pH modifier (Method B)

Time (min)	Flow rate (mL / min)	% A	% B
0	1	99	1
1.5	1	3	97
1.9	1	3	97
2.0	1	99	1

Formic acid modifier (Method C)

Time (min)	Flow rate (mL / min)	% A	% B
0	1	97	3
1.5	1	5	95
1.9	1	5	95
2.0	1	97	3

High pH modifier (Method D)

Time (min)	Flow rate (mL / min)	% A	% B
0	1	97	3
0.05	1	97	3
1.50	1	5	95
1.90	1	5	95
2.00	1	97	3

Mass directed auto-preparative HPLC (MDAP)

Preparative mass directed HPLC (MDAP) was conducted on a Waters *MassLynx* system comprising of a Waters 515 pump with extended pump heads, Waters 2767 autosampler,

Confidential – Property of GSK – Do Not Copy

Waters 996 photodiode array detector, and Gilson 202 fraction collector on a XBridge or Sunfire C18 column (30 mm x 150 mm i.d. 5 µm packing diameter) at ambient temperature.

The mobile phase was:

Method A - 0.1% formic acid in water (solvent A) and 0.1% formic in acetonitrile (solvent B);
or

Method B - 10 mM ammonium bicarbonate in water adjusted to pH 10 with ammonia solution (solvent A) acetonitrile (solvent B).

The UV detection is a summed signal from wavelength of 210 nm to 350 nm. Mass spectra were recorded on Waters ZQ mass spectrometer using alternate-scan positive and negative electrospray ionization. The software used was *MassLynx* 3.5 with *FractionLynx* or using equivalent alternative systems.

The elution gradients used were at a flow rate of 40 mL/min over 10 or 20 min:

Gradient A	5-30% B
Gradient B	15-55% B
Gradient C	30-85% B
Gradient D	50-99% B
Gradient E	80-99% B

High resolution mass spectroscopy (HRMS)

ESI (+) high resolution mass spectra (HRMS) were obtained on a Micromass Q-ToF 2 hybrid quadrupole time-of-flight mass spectrometer, equipped with a Z-spray interface, over a mass range of 100 – 1100 Da, with a scan time of 0.9 s and an interscan delay of 0.1 s. Reserpine was used as the external mass calibrant ($[M+H]^+ = 609.2812$ Da). The Q-ToF 2 mass spectrometer was operated in W reflectron mode to give a resolution (FWHM) of 16000-20000. Ionisation was achieved with a spray voltage of 3.2 kV, a cone voltage of 50 V, with cone and desolvation gas flows of 10-20 and 600 L/h, respectively. The source block and desolvation temperatures were maintained at 120 °C and 250 °C, respectively. The elemental composition was calculated using *MassLynx* v4.1 for the $[M+H]^+$.

An Agilent 1100 Liquid Chromatograph equipped with a model G1367A autosampler, a model G1312A binary pump, and a HP1100 model G1315B diode array detector was used. The method used was generic for all experiments. All separations were achieved using a Phenomenex Luna C18 (2) reversed phase column (100 x 2.1 mm, 3 µm particle size).

Gradient elution was carried out with the mobile phases as (A) water containing 0.1% (v/v) formic acid and (B) acetonitrile containing 0.1% (v/v) formic acid. The conditions for the gradient elution were initially 5% B, increasing linearly to 100% B over 6 minutes, remaining at 100% B for 2.5 min then decreasing linearly to 5% B over 1 min, followed by an equilibration period of 2.5 min prior to the next injection. The flow rate was 0.5 mL/min, temperature controlled at 35 °C with an injection volume of between 2 to 5 µL. All samples were diluted with DMSO (99.9%) prior to LCMS analysis.

Purification by column chromatography

Column chromatography was conducted on a Combiflash® Rf, automated flash chromatography system, from Teledyne Isco using disposable, normal, or reverse phase, SPE Redisep or Grace cartridges (4 g to 330 g). The CombiFlash® Rf uses RFID (Radio Frequency Identification) technology to automate the setting of the parameters for purification runs and fraction collection. The system is equipped with a UV variable dual-wavelength and a Foxy® fraction collector enabling automated peak cutting, collection, and tracking.

Phase separators

Isolute® phase separator cartridges are fitted with a hydrophobic Teflon frit. These were used to separate chlorinated solvent from aqueous phase under gravity.

Isolute® 103

Isolute® 103 cartridges from Biotage are hydroxylated polystyrene-divinylbenzene copolymer resin. These were used to extract organic compounds from aqueous solution using a catch and release protocol.

Microwave

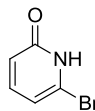
Microwave chemistry was typically performed in Biotage sealed vessels, irradiating with a Biotage Initiator™ Microwave Synthesiser.

Melting point

Melting points were measured on a Stuart automatic melting point apparatus, SMP40.

3.1 Lp-PLA₂ Experimental Section

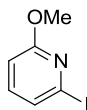
6-Bromopyridin-2(1H)-one – (1.2.5)¹²⁴



1.2.5

To a solution of potassium *tert*-butoxide (10.0 g, 89 mmol) in *tert*-butanol (50 mL) was added 2,6-dibromopyridine (2.0 g, 8.4 mmol). The resulting solution was refluxed at 130 °C under a nitrogen atmosphere for 16 h. The reaction was cooled to ambient temperature and to the reaction mixture was added cooled water. The mixture was acidified by the slow addition of 2M aqueous HCl. To the mixture was added ethyl acetate (50 mL) and the biphasic mixture separated. The aqueous phase was extracted with ethyl acetate (3 x 25 mL). The combined organic phases were washed with brine and passed through a hydrophobic frit. The mixture was concentrated under reduced pressure to give the crude product as an orange solid (1.8 g). The product was purified by automated flash column chromatography (cyclohexane: TBME 100:0 - 50:50, 120 g SiO₂) to give 6-bromopyridin-2(1H)-one (**1.2.5**) as a white crystalline solid (1.29 g, 88%). LCMS (Method A, UV, ESI) *R*_t = 0.48 min, [M-H]⁺ *m/z* = 173.9 and 175.9 (consistent with the two bromine isotopes), 100% purity. M.p. 122-124 °C (Lit. m.p. 119-120 °C).¹²⁴ ¹H NMR (400 MHz, *d*₆-DMSO): δ = 11.47 (1H, br, OH), 7.56 (1H, m, Ar-H), 7.05 (1H, d, *J* = 7.6 Hz, Ar-H), 6.64 (1H, d, *J* = 8.3 Hz, Ar-H). ¹³C NMR (100.6 MHz, *d*₆-DMSO): δ = 163.6, 141.9, 137.3, 118.5, 108.8. IR (*v*_{max}/cm⁻¹) = 1575, 1465, 780. HRMS (ESI-[+H]) *m/z*: Calcd for C₅H₄⁷⁹BrNO 173.9549; Found 173.9552.

2-Iodo-6-methoxypyridine (1.2.7)¹²³

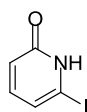


1.2.7

To an oven dried flask was added a solution of 2-bromo-6-methoxypyridine (4.0 mL, 32.5 mmol) and anhydrous THF (40 mL) and the solution cooled to -78 °C under a nitrogen atmosphere. To the mixture was added dropwise *n*-BuLi (1.6 M in hexanes, 22.4 mL, 35.8 mmol) whilst maintaining a temperature below -70 °C. The resulting solution was stirred at

-78 °C for 1 h. To the solution was added dropwise a solution of iodine (9.09 g, 35.8 mmol) in anhydrous THF (24 mL) and the resulting solution was warmed to ambient temperature. The reaction was quenched by the addition of 15% aqueous Na₂S₂O₃ (75 mL) and the biphasic mixture separated. The aqueous phase was extracted with Et₂O (3 x 50 mL). The combined organic extracts were washed with brine (50 mL) and passed through a hydrophobic frit. Removal of the solvent under reduced pressure gave the crude product as a brown solid (8.5 g). The crude product was purified by automated flash column chromatography (cyclohexane: TBME, 100:0 - 60:40, 120 g SiO₂). The appropriate fraction were combined and concentrated under reduced pressure to give 2-iodo-6-methoxypyridine (**1.2.7**) as a yellow solid (6.76 g, 88%). LCMS (Method A, UV, ESI) *R*_t = 1.07 min, [M-H]⁺ *m/z* = did not ionise, 92% purity. M.p. 42-43 °C (Lit. m.p. 43-45 °C). ¹²³H NMR (400 MHz, *d*₆-DMSO): δ = 7.43 (1H, d, *J* = 7.3 Hz, Ar-H), 7.40 (1H, m, Ar-H), 6.84 (1H, dd, *J* = 1.4, 7.6 Hz, Ar-H), 3.83 (3H, s). ¹³C NMR (100.6 MHz, *d*₆-DMSO): δ = 163.0, 140.8, 127.6, 114.1, 109.7, 53.7. IR (*ν*_{max}/cm⁻¹) = 2953, 1403, 1019. HRMS (ESI-[+H]) *m/z*: Calcd for C₆H₆INO 235.9567; Found 235.9561.

6-Iodopyridin-2(*1H*)-one (**1.2.8**)¹²³

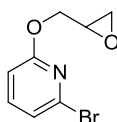


1.2.8

To a solution of 2-iodo-6-methoxypyridine (**1.2.7**) (4.80 g, 20.4 mmol) and NaI (9.18 g, 61.3 mmol) in anhydrous acetonitrile (30 mL) was added dropwise TMSCl (7.84 mL, 61.3 mmol). The resulting solution was heated to 80 °C and stirred under a nitrogen atmosphere for 5 h. The reaction mixture was cooled to ambient temperature. To the mixture was added 15% aqueous sodium thiosulfate (50 mL) and brine (40 mL) and ethyl acetate (40 mL). The biphasic mixture was separated and the aqueous phase extracted with ethyl acetate (3 x 40 mL). The combined organic extracts were passed through a hydrophobic frit and the solvent removed under reduced pressure to give the crude product as a yellow solid (6.0 g). The product was purified by automated flash column chromatography (cyclohexane: TBME, 100:0 - 30:70, 120 g SiO₂). Removal of the solvent under reduced pressure gave 6-iodopyridin-2(*1H*)-one (**1.2.8**) as a bright yellow solid (3.93 g, 87%). LCMS (Method A, UV, ESI) *R*_t = 0.48 min, [M-H]⁺ *m/z* = 221.9, 100% purity. M.p. 158-160 °C (Lit. m.p. 150-152 °C). ¹²³H NMR (400 MHz, *d*₆-DMSO): δ = 11.50 (1H, br, OH), 7.28 (1H, m, Ar-H), 7.15 (1H, d, *J* = 7.6 Hz, Ar-H), 6.57

(1H, d, $J = 8.0$ Hz, Ar-H). ^{13}C NMR (100.6 MHz, d_6 -DMSO): $\delta = 163.4, 141.1, 124.2, 111.2, 110.6$. IR ($\nu_{\text{max}}/\text{cm}^{-1}$) = 2845 (br), 1625, 1433, 785. HRMS (ESI-[+H]) m/z : Calcd for $\text{C}_5\text{H}_4\text{INO}$ 221.9410; Found 221.9403.

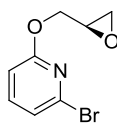
2-Bromo-6-(oxiran-2-ylmethoxy)pyridine (Table 1.2.1 – Entry 1)



To an oven dried flask was added 6-bromopyridin-2(1H)-one (**1.2.5**) (0.5 g, 2.87 mmol), cesium carbonate (2.34 g, 7.18 mmol) and anhydrous DMSO (2 mL) and the resulting mixture stirred for 15 min under a nitrogen atmosphere. To the solution was added oxiran-2-ylmethyl 4-methylbenzenesulfonate (0.79 g, 3.45 mmol). The resulting mixture was heated to 60 °C and stirred for 1.5 h. LCMS analysis at this stage revealed complete reaction conversion with an $N:O$ ratio of 19:81. The reaction was cooled to ambient temperature and to the mixture was added water (2 mL) and ethyl acetate (2 mL). The biphasic mixture was separated and the aqueous phase extracted with ethyl acetate (3 x 5 mL). The combined organic extracts were passed through a hydrophobic frit and the solvent removed under reduced pressure to give the crude product as a yellow solid (1.15 g). The crude mixture was purified by automated column chromatography (cyclohexane: ethyl acetate, 100:0 – 50:50, 80 g SiO_2). Removal of the solvent under reduced pressure gave 2-bromo-6-(oxiran-2-ylmethoxy)pyridine as a colourless oil (32 mg, 5%). LCMS (Method A, UV, ESI) $R_t = 0.94$ min, $[\text{M}-\text{H}]^+ m/z = 230.0$ and 232.0 (consistent with both bromine isotopes), 95% purity. ^1H NMR (400 MHz, d_6 -DMSO): $\delta = 7.69$ (1H, dd, $J = 7.6, 8.3$ Hz, Ar-H), 7.25 (1H, d, $J = 7.6$ Hz, Ar-H), 6.92 (1H, d, $J = 8.3$ Hz, Ar-H), 4.60 (1H, dd, $J = 2.8, 12.1$ Hz), 4.04 (1H, m), 3.33 (1H, m), 2.84 (1H, dd, $J = 4.3, 5.0$ Hz), 2.73 (1H, dd, $J = 2.8, 5.0$ Hz). ^{13}C NMR (100.6 MHz, d_6 -DMSO): $\delta = 178.6, 162.4, 142.0, 137.5, 120.8, 109.7, 72.0, 67.5$.

N-Alkylated product was not isolated due to product volatility or instability.

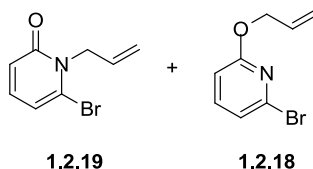
(R)-2-Bromo-6-(oxiran-2-ylmethoxy)pyridine (Table 1.2.1 – Entry 2)



To an oven dried flask was added 6-bromopyridin-2(1H)-one (**1.2.5**) (0.5 g, 2.87 mmol), cesium carbonate (1.12 g, 3.45 mmol) and anhydrous DMF (5 mL) under a nitrogen atmosphere. To the solution was added dropwise (*R*)-epichlorohydrin (0.27 mL, 3.45 mmol) and the resulting solution was heated to 85 °C under a nitrogen atmosphere for 3 h. LCMS analysis at this stage revealed complete reaction conversion with a *N*:*O* ratio of 24:76. The reaction mixture was cooled to ambient temperature and to the mixture was added ethyl acetate (30 mL) and water (30 mL). The biphasic mixture was separated and the aqueous phase extracted with ethyl acetate (3 x 15 mL). The combined organic extracts were washed with brine and passed through a hydrophobic frit. Removal of the solvent under reduced pressure gave the crude product as a red oil (1.1 g). The crude mixture was purified by automated column chromatography (TBME: cyclohexane, 0:100 - 100:0, 80 g SiO₂). Removal of the solvent under reduced pressure gave (*R*)-2-bromo-6-(oxiran-2-ylmethoxy)pyridine as a colourless oil (0.21 g, 31%). LCMS (Method A, UV, ESI) *R*_t = 0.94 min, [M-H]⁺ *m/z* = 230.0 and 232.0 (consistent with both bromine isotopes), 96% purity. ¹H NMR (400 MHz, CDCl₃): δ = 7.45 (1H, m), 7.10 (1H, d, *J* = 7.6 Hz), 6.76 (1H, d, *J* = 8.1 Hz), 4.67 (1H, dd, *J* = 3.3, 12.1 Hz), 4.20 (1H, dd, *J* = 6.2, 12.2 Hz), 3.38 (1H, m), 2.91 (1H, dd, *J* = 4.2, 4.9 Hz), 2.76 (1H, dd, *J* = 2.6, 4.9 Hz). ¹³C NMR (100.6 MHz, CDCl₃): δ = 179.2, 162.8, 140.6, 138.4, 120.7, 109.6, 76.3, 67.3.

N-Alkylated product was not isolated due to product volatility or instability.

1-Allyl-6-bromopyridin-2(1H)-one (1.2.19) and 2-(allyloxy)-6-bromopyridine (1.2.18) (Table 1.2.1 – Entry 3)



To a mixture of 6-bromopyridin-2(1H)-one (**1.2.5**) (0.5 g, 2.9 mmol) and cesium carbonate (1.12 g, 3.5 mmol) in anhydrous DMF (5 mL) was added 3-chloroprop-1-ene (0.26 g, 3.5

mmol) and the resulting solution heated at 85 °C for 3 h under a nitrogen atmosphere. LCMS analysis revealed the reaction had gone to completion at this stage, with an *N:O* ratio of 30:70. The reaction was cooled to ambient temperature and to the mixture was added DCM (30 mL) and water (30 mL). The biphasic mixture was separated and the aqueous phase extracted with DCM (3 x 30 mL). The combined organic phases were washed with brine (30 mL) and passed through a hydrophobic frit. Removal of the solvent under reduced pressure gave the crude product as a red liquid (2.0 g). The crude mixture was purified by automated column chromatography (cyclohexane: TBME, 100:0 - 0:100, 80 g SiO₂) to give 1-allyl-6-bromopyridin-2(*1H*)-one (**2.19**) as a yellow oil (171 mg, 28%) and the 2-(allyloxy)-6-bromopyridine (**2.18**) as a colourless oil (415 mg, 68%).

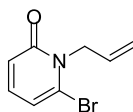
1-Allyl-6-bromopyridin-2(*1H*)-one (**2.19**):

LCMS (Method A, UV, ESI) $R_t = 0.71$ min, $[M-H]^+ m/z = 214.0$ and 216.0 (consistent with two bromine isotopes), 100% purity. ¹H NMR (400 MHz, CDCl₃): $\delta = 7.17$ (1H, m, Ar-H), 6.58 (1H, d, $J = 8.9$ Hz, Ar-H), 6.50 (1H, d, $J = 6.8$ Hz, Ar-H), 5.94 (1H, m), 5.27 (1H, d, $J = 10.4$ Hz), 5.19 (1H, d, $J = 17.2$ Hz), 4.97-4.92 (2H, m). ¹³C NMR (100.6 MHz, CDCl₃): $\delta = 162.7, 139.2, 131.0, 127.3, 119.0, 118.1, 111.4, 51.2$.

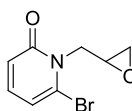
2-(Allyloxy)-6-bromopyridine (**2.18**):

LCMS (Method A, UV, ESI) $R_t = 1.16$ min, $[M-H]^+ m/z = 214.0$ and 216.0 (consistent with two bromine isotopes), 98% purity. ¹H NMR (400 MHz, CDCl₃): $\delta = 7.42$ (1H, m, Ar-H), 7.06 (1H, d, $J = 7.8$ Hz, Ar-H), 6.71 (1H, d, $J = 8.3$ Hz, Ar-H), 6.07 (1H, m), 5.41 (1H, d, $J = 17.9$ Hz), 5.27 (1H, d, $J = 10.9$ Hz), 4.88-4.83 (2H, m). ¹³C NMR (100.6 MHz, CDCl₃): $\delta = 163.0, 140.4, 138.5, 132.9, 120.3, 118.0, 109.6, 67.3$.

A full characterisation was not possible due to the volatility or instability of both products.

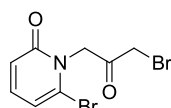
2-(Allyloxy)-6-bromopyridine (1.2.19)**1.2.19**

To a solution of palladium (II) chloride (0.017 g, 0.10 mmol) in anhydrous *p*-xylene (6 mL) was added a solution of 2-(allyloxy)-6-bromopyridine (**1.2.18**) (0.415 g, 1.94 mmol) in anhydrous *p*-xylene (1 mL) and the resulting solution heated at 80 °C under a nitrogen atmosphere for 3 h. The reaction was cooled to ambient temperature and the cooled mixture was filtered and the solvent removed under reduced pressure to give the crude product as a yellow oil (0.9 g). The crude product was purified by automated flash column chromatography (cyclohexane:TBME, 100:0 - 0:100, 80 g SiO₂). Removal of the solvent gave 2-(allyloxy)-6-bromopyridine (**1.2.19**) as a yellow oil (0.401 g, 97%). LCMS (Method A, UV, ESI) $R_t = 0.71$ min, $[M-H]^+ m/z = 214.0$ and 216.0 (consistent with two bromine isotopes), 100% purity. ¹H NMR (400 MHz, CDCl₃): $\delta = 7.17$ (1H, m, Ar-H), 6.58 (1H, d, $J = 8.9$ Hz, Ar-H), 6.50 (1H, d, $J = 6.8$ Hz, Ar-H), 5.94 (1H, m), 5.27 (1H, d, $J = 10.4$ Hz), 5.19 (1H, d, $J = 17.2$ Hz), 4.97-4.92 (2H, m). ¹³C NMR (100.6 MHz, CDCl₃): $\delta = 162.7, 139.2, 131.0, 127.3, 119.0, 118.1, 111.4, 51.2$.

6-Bromo-1-(oxiran-2-ylmethyl)pyridin-2(1H)-one (1.2.10)(*m*-CPBA epoxidation)**1.2.10**

To an oven dried flask was added 1-allyl-6-bromopyridin-2(1H)-one (**1.2.19**) (0.15 g, 0.70 mmol) and anhydrous DCM (6 mL) under a nitrogen atmosphere. The reaction was cooled to 0 °C and to the mixture was added *m*-CPBA (77% by weight) (1.57 g, 7.0 mmol). The resulting solution was warmed to ambient temperature and stirred for 72 h. LCMS at this stage showed no reaction had occurred and therefore the reaction was terminated at this stage.

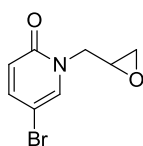
6-Bromo-1-(3-bromo-2-oxopropyl)pyridin-2(1H)-one (1.2.20) (IBX procedure)



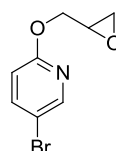
1.2.20

To an oven dried flask was added IBX (144 mg, 0.51 mmol), TEAB (108 mg, 0.51 mmol) and anhydrous DCM (4 mL) under a nitrogen atmosphere. The resulting solution was stirred for 5 minutes. To the reaction mixture was added 1-allyl-6-bromopyridin-2(1H)-one (**1.2.19**) (100 mg, 0.47 mmol) and the solution stirred until complete by LCMS. After 72 h LCMS analysis revealed complete reaction conversion, with a peak corresponding to the appropriate mass and isotopic pattern being detected. To the reaction mixture was added DCM (5 mL) and saturated aqueous NaHCO₃ (10 mL), followed by 10% aqueous sodium thiosulfate (10 mL). The biphasic mixture was separated and the organic phase washed with brine, passed through a hydrophobic frit, and concentrated under reduced pressure to give the crude product as brown oil (200 mg). Attempts to isolate the product using chromatographic methods were unsuccessful, and therefore the reaction was concluded.

5-Bromo-1-(oxiran-2-ylmethyl)pyridin-2(1H)-one (1.2.23) and 5-bromo-2-(oxiran-2-ylmethoxy)pyridine (1.2.24)



1.2.23



1.2.24

To an oven dried flask was added cesium carbonate (470 mg, 1.44 mmol) and anhydrous DMSO (0.6 mL) under a nitrogen atmosphere. To the solution was added 6-bromopyridin-2(1H)-one (100 mg, 0.58 mmol), followed by the addition of oxiran-2-ylmethyl 4-methylbenzenesulfonate (157 mg, 0.70 mmol) and the resulting solution stirred at ambient temperature for 2 h, under a nitrogen atmosphere. LCMS analysis at this stage revealed complete reaction conversion. To the reaction mixture was added water (1 mL) and ethyl acetate (2.5 mL). The biphasic mixture was separated and the aqueous phase extracted with ethyl acetate. The combined organic extracts were washed with brine and passed through a hydrophobic frit. Removal of the solvent under reduced pressure gave the crude product as a

yellow oil (250 mg). The crude mixture was purified by automated column chromatography (0:100 - 100:0, cyclohexane: ethyl acetate, 10 g SiO₂). Removal of the solvent under reduced pressure yielded 6-bromo-1-(oxiran-2-ylmethyl)pyridin-2(*IH*)-one (**1.2.23**) as a white solid (60 mg, 46%) and 2-bromo-6-(oxiran-2-ylmethoxy)pyridine (**1.2.24**) as a yellow solid (20 mg, 15%).

5-Bromo-1-(oxiran-2-ylmethyl)pyridin-2(*IH*)-one (**1.2.23**):

LCMS (Method A, UV, ESI) $R_t = 0.59$ min, $[M-H]^+ m/z = 230.0$ and 231.9 (consistent with two bromine isotopes), 100% purity. ¹H NMR (400 MHz, *d*₆-DMSO): $\delta = 7.90$ (1H, d, $J = 2.9$ Hz, Ar-H), 7.55 (1H, dd, $J = 2.8, 9.7$ Hz, Ar-H), 6.41 (1H, d, $J = 9.8$ Hz, Ar-H), 4.19 (1H, dd, $J = 3.7, 13.7$ Hz), 3.94 (1H, dd, $J = 5.6, 13.7$ Hz), 3.27 (1H, m), 2.78 (1H, m), 2.54 (1H, dd, $J = 2.6, 5.0$ Hz). ¹³C NMR (100.6 MHz, *d*₆-DMSO): $\delta = 160.2, 142.8, 139.3, 121.0, 96.2, 49.7, 49.1, 45.0$.

5-Bromo-2-(oxiran-2-ylmethoxy)pyridine (**1.2.24**):

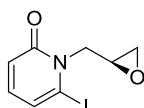
LCMS (Method A, UV, ESI) $R_t = 0.96$ min, $[M-H]^+ m/z = 230.0$ and 231.9 (consistent with two bromine isotopes), 100% purity. ¹H NMR (400 MHz, *d*₆-DMSO): $\delta = 8.28$ (1H, d, $J = 2.2$ Hz, Ar-H), 7.93 (1H, dd, $J = 8.8, 2.7$ Hz, Ar-H), 6.89 (1H, d, $J = 8.8$ Hz, Ar-H), 4.59 (1H, dd, $J = 2.7, 12.0$ Hz), 4.04 (1H, dd, $J = 6.6, 12.0$ Hz), 3.33 (1H, m), 2.83 (1H, dd, $J = 4.3, 5.0$ Hz), 2.70 (1H, dd, $J = 2.7, 5.0$ Hz). ¹³C NMR (100.6 MHz, *d*₆-DMSO): $\delta = 161.8, 147.1, 141.8, 112.9, 111.7, 67.1, 49.3, 43.9$.

General procedure for pyridone *N*-alkylation through the use of lithium additives (Curran procedure) (Table 1.2.2)¹⁵⁰

To an oven dried flask was added halo pyridone (1.0 eq) and anhydrous solvent/s under a nitrogen atmosphere. The solution was cooled to 0 °C and to the mixture was added NaH (60% dispersion in mineral oil) (1.05 eq) and the solution stirred under a nitrogen atmosphere for 10 minutes at 0 °C. To the cooled solution was added LiBr (2.0 eq) and the solution stirred at ambient temperature for 15 minutes. To the mixture was added the electrophile and the solution heated to 65 °C and stirred under a nitrogen atmosphere until complete as judged by LCMS. The reaction was cooled to ambient temperature, diluted with brine, and extracted with

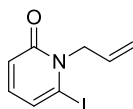
ethyl acetate. The combined organic extracts were passed through a hydrophobic frit and the solvent removed under reduced pressure to afford crude product. The crude product was purified by automated column chromatography.

(S)-6-Iodo-1-(oxiran-2-ylmethyl)pyridin-2(1H)-one (Table 1.2.2 – Entry 1)



To an oven dried flask was added 6-iodopyridin-2(1H)-one (**1.2.8**) (0.25 g, 1.13 mmol), anhydrous DME (2.0 mL) and DMF (0.5 mL). To the resulting solution was added sodium hydride (60% dispersion in mineral oil, 48 mg, 1.19 mmol) at 0 °C and stirred for 10 minutes under an inert atmosphere. To the cooled solution was added LiBr (0.196 g, 2.26 mmol) and the resulting mixture stirred at ambient temperature for 15 minutes. To the mixture was added (*R*)-2-(chloromethyl)oxirane (0.177 mL, 2.26 mmol) and the resulting mixture was heated to 65 °C and stirred under an inert atmosphere for 16 h. LCMS analysis at this stage revealed a complex mixture with no desired product formation. The reaction was therefore discontinued at this stage.

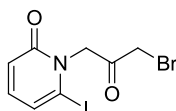
1-Allyl-6-iodopyridin-2(1H)-one (Table 1.2.2 – Entry 2)



To an oven dried flask was added 6-iodopyridin-2(1H)-one (**1.2.8**) (400 mg, 1.81 mmol), anhydrous DME (3.00 mL) and anhydrous DMF (0.50 mL). To the resulting solution was added sodium hydride (60% dispersion in mineral oil) (76 mg, 1.90 mmol) at 0 °C and the resulting mixture stirred for 10 minutes under a nitrogen atmosphere. To the cooled solution was added LiBr (314 mg, 3.62 mmol) and the resulting mixture stirred at ambient temperature for 15 minutes. To the mixture was added 3-chloroprop-1-ene (0.30 mL, 3.62 mmol). The reaction mixture was heated to 65 °C and stirred under a nitrogen atmosphere overnight. LCMS analysis at this stage showed no remaining starting material, with an *N*:*O* alkylation ratio of 77:23. The reaction was cooled to ambient temperature and to the cooled mixture was

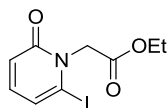
added brine (25 mL) and ethyl acetate (15 mL). The biphasic mixture was separated and the aqueous phase extracted with ethyl acetate (4 x 15 mL). The resulting organic extracts were combined, passed through a hydrophobic frit, and the solvent removed under reduced pressure to give the crude product as a yellow solid (700 mg). The crude product was purified by automated column chromatography (cyclohexane: TBME, 100:0, 50:50, 80 g SiO₂). Removal of the solvent under reduced pressure gave the desired product as a yellow solid (357 mg, 76%). LCMS (Method A, UV, ESI) $R_t = 0.72$ min, $[M-H]^+ m/z = 262.0$, 95% purity. M.p. 128-130 °C. ¹H NMR (400 MHz, *d*₆-DMSO): $\delta = 7.09$ (1H, dd, $J = 7.1, 9.1$ Hz, Ar-H), 6.87 (1H, dd, $J = 1.3, 7.1$ Hz, Ar-H), 6.37 (1H, dd, $J = 1.3, 9.1$ Hz, Ar-H), 5.89 (1H, m), 5.21 (1H, ddd, $J = 1.3, 1.8, 10.3$ Hz), 4.96 (1H, ddd, $J = 1.5, 1.8, 17.4$ Hz), 4.83–4.78 (2H, m). ¹³C NMR (100.6 MHz, *d*₆-DMSO): $\delta = 161.1, 140.4, 132.2, 118.8, 118.6, 116.7, 104.6, 54.7$. IR (ν_{\max} /cm⁻¹) = 3087, 1637, 1497, 782. HRMS (ESI-[+H]) m/z : Calcd for C₈H₈INO 261.9723; Found 261.9717.

6-Iodo-1-(3-bromo-2-oxopropyl)pyridin-2(1H)-one (Table 1.2.2 – Entry 3)

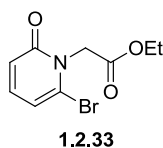


To an oven dried flask was added 6-iodopyridin-2(1H)-one (**1.2.8**) (0.1 g, 0.45 mmol), anhydrous DME (2.0 mL) and DMF (0.5 mL). To the resulting solution was added sodium hydride (60% dispersion in mineral oil, 19 mg, 0.48 mmol) at 0 °C and stirred for 10 minutes under a nitrogen atmosphere. To the cooled solution was added LiBr (0.08 g, 0.91 mmol) and the resulting mixture stirred at ambient temperature for 15 minutes. To the mixture was added 1,3-dibromopropan-2-one (76% by weight, 0.39 g, 1.36 mmol) and the reaction heated to 65 °C, and stirred under a nitrogen atmosphere. After 16 h LCMS analysis indicated the presence of a complicated reaction mixture with no desired product formation. The reaction was therefore concluded at this stage.

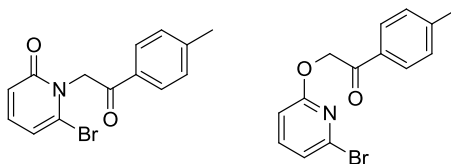
Ethyl 2-(6-iodo-2-oxopyridin-1(2H)-yl)acetate (Table 1.2.2 – Entry 4)



To an oven dried flask was added 6-iodopyridin-2(1H)-one (**1.2.8**) (200 mg, 0.91 mmol), anhydrous DMF (0.5 mL) and anhydrous DME (2 mL) and stirred under a nitrogen atmosphere. To the resulting solution was added sodium hydride (60% dispersion in mineral oil) (38 mg, 0.95 mmol) at 0 °C and stirred for 10 minutes under a nitrogen atmosphere. To the cooled solution was added lithium bromide (157 mg, 1.81 mmol) and the resulting mixture stirred at ambient temperature for 15 minutes. To the solution was added ethyl 2-bromoacetate (0.15 mL, 1.36 mmol) and the resulting solution heated to 65 °C and stirred overnight. After stirring overnight LCMS analysis showed the reaction had gone to completion, with an *N:O* alkylation ratio of 84:16. The solution was cooled to ambient temperature. To the mixture was added brine (5 mL) and ethyl acetate (5 mL). The biphasic mixture was separated and the aqueous phase extracted with ethyl acetate (4 x 5 mL). The combined organic extracts were passed through a hydrophobic frit and the solvent removed under reduced pressure to give the crude product as a pale yellow crystalline solid. The crude product was purified by automated column chromatography (cyclohexane: TBME, 100:0 - 0:100, 40 g SiO₂). The solvent was removed under reduced pressure to give ethyl 2-(6-iodo-2-oxopyridin-1(2H)-yl)acetate as a yellow solid (231 mg, 83%). LCMS (Method A, UV, ESI) $R_t = 0.71$ min, $[M-H]^+ m/z = 307.9$, 100% purity. M.p. 135-137 °C. ¹H NMR (400 MHz, *d*₆-DMSO): $\delta = 7.15$ (1H, dd, $J = 7.1, 9.1$ Hz, Ar-H), 6.92 (1H, dd, $J = 1.3, 7.1$ Hz, Ar-H), 6.40 (1H, dd, $J = 1.3, 9.3$ Hz, Ar-H), 4.98 (2H, s), 4.19 (2H, q, $J = 7.3$ Hz), 1.23 (3H, t, $J = 7.3$ Hz). ¹³C NMR (100.6 MHz, *d*₆-DMSO): $\delta = 167.4, 161.4, 141.0, 118.7, 118.4, 105.2, 61.3, 54.4, 14.0$. IR (ν_{max}/cm^{-1}) = 2983, 1731, 1644, 1496, 783. HRMS (ESI-[+H]) m/z : Calcd for C₉H₁₀INO₃ 307.9778; Found 307.9769.

Ethyl 2-(6-bromo-2-oxopyridin-1(2H)-yl)acetate (**1.2.33**) (Table 1.2.2 – Entry 5)

To an oven dried flask was added 6-bromopyridin-2(1H)-one (**1.2.5**) (3.00 g, 17.24 mmol), anhydrous DMF (7.5 mL) and anhydrous DME (30 mL). To the resulting solution was added sodium hydride (60% dispersion in mineral oil) (0.72 g, 18.19 mmol) at 0 °C and stirred for 10 minutes under a nitrogen atmosphere. To the cooled solution was added lithium bromide (2.99 g, 34.50 mmol) and the resulting mixture stirred at ambient temperature for 15 minutes. To the solution was added ethyl 2-bromoacetate (2.86 mL, 25.90 mmol) and the resulting solution heated to 65 °C and stirred for 16 h. LCMS analysis at this stage showed complete reaction conversion, with an *N:O* alkylation ratio of 93:7. The reaction was cooled to ambient temperature. To the mixture was added brine (50 mL) and ethyl acetate (50 mL). The biphasic mixture was separated and the aqueous phase extracted with ethyl acetate (4 x 50 mL). The combined organic extracts were passed through a hydrophobic frit and concentrated under reduced pressure to give the crude product as a purple oil. The crude product was purified by automated column chromatography (cyclohexane: TBME, 100:0 - 0:100, 120 g SiO₂). Removal of the solvent under reduced pressure gave ethyl 2-(6-bromo-2-oxopyridin-1(2H)-yl)acetate (**1.2.33**) as a white crystalline solid (3.66 g, 82% yield). LCMS (Method A, UV, ESI) $R_t = 0.71$ min, $[M-H]^+$ $m/z = 259.9$ and 261.9 (consistent with both bromine isotopes) 99% purity. M.p. 128-130 °C. ¹H NMR (400 MHz, *d*₆-DMSO): $\delta = 7.38$ (1H, dd, $J = 7.3, 9.3$ Hz, Ar-H), 6.68 (1H, dd, $J = 1.3, 7.3$ Hz, Ar-H), 6.47 (1H, dd, $J = 1.3, 9.3$ Hz, Ar-H), 4.98 (2H, s), 4.19 (2H, q, $J = 7.1$ Hz), 1.22 (3H, t, $J = 7.3$ Hz) (Sample also contained 16% ethyl acetate and 4% cyclohexane by mass, this is accounted for in the product yield). ¹³C NMR (100.6 MHz, *d*₆-DMSO): $\delta = 167.3, 161.9, 140.5, 127.4, 117.8, 110.7, 61.3, 49.5, 14.0$. IR ($\nu_{\max}/\text{cm}^{-1}$) = 2988, 1743, 1657, 1507, 782. HRMS (ESI-[+H]) m/z : Calcd for C₉H₁₀⁷⁹BrNO₃ 259.9917; Found 259.9909.

6-Bromo-1-(2-oxo-2-(*p*-tolyl)ethyl)pyridin-2(*1H*)-one (1.2.26) and 2-((6-bromopyridin-2-yl)oxy)-1-(*p*-tolyl)ethanone (Table 1.2.2 – Entry 6)**1.2.26**

To an oven dried flask was added 6-bromopyridin-2(*1H*)-one (**1.2.5**) (2.00 g, 11.49 mmol), anhydrous DMF (5 mL) and anhydrous DME (20 mL). To the resulting solution was added sodium hydride (60% dispersion in mineral oil) (0.48 g, 12.07 mmol) at 0 °C and the resulting solution stirred for 10 minutes under a nitrogen atmosphere. To the cooled solution was added LiBr (2.00 g, 22.99 mmol) and the resulting mixture stirred at ambient temperature for 15 minutes. To the solution was added 2-bromo-1-(*p*-tolyl)ethanone (3.67 g, 17.24 mmol) and the resulting solution heated to 65 °C and stirred for 16 h. LCMS analysis at this stage revealed the reaction had gone to completion at this stage, with an *N*:*O* alkylation ratio of 62:38. The reaction mixture was cooled to ambient temperature. To the mixture was added brine (50 mL) and ethyl acetate (50 mL). The biphasic mixture was separated and the aqueous phase extracted with ethyl acetate (4 x 50 mL). The combined organic extracts were passed through a hydrophobic frit and the solvent removed under reduced pressure to give the crude product as a brown oil. The product was purified by automated column chromatography (cyclohexane: ethyl acetate, 100:0 - 20:80, 120 g SiO₂) to give 6-bromo-1-(2-oxo-2-(*p*-tolyl)ethyl)pyridin-2(*1H*)-one (**1.2.26**) as a dark orange solid (1.70 g, 51%) and 2-((6-bromopyridin-2-yl)oxy)-1-(*p*-tolyl)ethanone (1.30 g, 37%) as a bright orange solid.

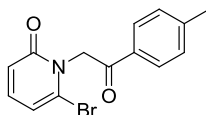
6-Bromo-1-(2-oxo-2-(*p*-tolyl)ethyl)pyridin-2(*1H*)-one (1.2.26):

LCMS (Method A, UV, ESI) $R_t = 0.92$ min, $[M-H]^+ m/z = 306.0$, 100% purity. M.p. 170-171 °C. ¹H NMR (400 MHz, *d*₆-DMSO): $\delta = 8.01$ (2H, d, $J = 8.3$ Hz, Ar-H), 7.46–7.37 (3H, m, Ar-H), 6.69 (1H, dd, $J = 1.0, 7.3$ Hz, Ar-H), 6.47 (1H, dd, $J = 1.0, 9.3$ Hz, Ar-H), 5.76 (2H, s), 2.42 (3H, s). ¹³C NMR (100.6 MHz, *d*₆-DMSO): $\delta = 187.7, 178.7, 162.0, 139.8, 136.4, 128.7, 125.7, 118.0, 110.7, 69.2, 55.7, 20.7$. IR (ν_{max}/cm^{-1}) = 2919, 1688, 1644, 803. HRMS (ESI-[+H]) m/z : Calcd for C₁₄H₁₂⁷⁹BrNO₂ 306.0124; Found 306.0126.

2-((6-Bromopyridin-2-yl)oxy)-1-(*p*-tolyl)ethanone:

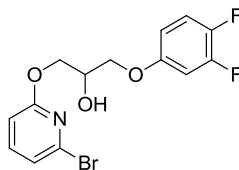
LCMS (Method A, UV, ESI) $R_t = 1.20$ min, $[M-H]^+ m/z = 306.0$, 95% purity. 1H NMR (400 MHz, d_6 -DMSO): $\delta = 7.92$ (2H, d, $J = 8.1$ Hz, Ar-H), 7.59 (1H, t, $J = 7.9$ Hz, Ar-H), 7.36 (2H, d, $J = 8.1$ Hz, Ar-H), 7.14 (1H, d, $J = 7.6$ Hz, Ar-H), 6.91 (1H, d, $J = 8.1$ Hz, Ar-H), 5.64 (2H, s), 2.44 (3H, s) (sample contained 3% cyclohexane by mass, this is accounted for in the product yield).

6-Bromo-1-(2-oxo-2-(*p*-tolyl)ethyl)pyridin-2(*1H*)-one (1.2.26) (Table 1.2.2 – Entry 7)



1.2.26

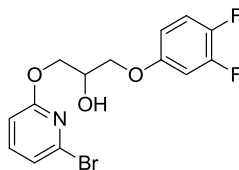
To an oven dried flask was added 6-bromopyridin-2(*1H*)-one (**1.2.5**) (1.00 g, 5.75 mmol) dissolved in anhydrous THF (20 mL). To the solution was added dropwise LHMDS (0.9 M in cyclohexane) (6.39 mL, 5.75 mmol) and the resulting solution stirred under a nitrogen atmosphere for 45 minutes. To the resulting solution was added 2-bromo-1-(*p*-tolyl)ethanone (1.84 g, 8.62 mmol) and the reaction heated to 65 °C and stirred under a nitrogen atmosphere for 16 h. LCMS analysis at this stage revealed an *N*:*O* ratio of 87:13, however, only minimal reaction progression was observed. Extended time increments, up to a total reaction time of 72 h, resulted in an unchanged reaction composition and the reaction was therefore concluded at this stage.

1-((6-Bromopyridin-2-yl)oxy)-3-(3,4-difluorophenoxy)propan-2-ol (Table 1.2.2 – Entry 8)

To a solution of cesium carbonate (468 mg, 1.44 mmol) in anhydrous DMSO (0.6 mL) was added 6-bromopyridin-2(*1H*)-one (**1.2.5**) (100 mg, 0.58 mmol) and the resulting mixture was stirred for 15 minutes under a nitrogen atmosphere. To the mixture was added dropwise oxiran-2-((3,4-difluorophenoxy)methyl)oxirane (118 mg, 0.63 mmol) and the resulting solution stirred under a nitrogen atmosphere for 72 h. After 72 h LCMS analysis still revealed significant quantities of starting materials. The reaction vessel was therefore heated to 60 °C for 5 h. LCMS analysis at this stage revealed the reaction had gone to completion; however, no *N*-alkylation product was detected. The reaction mixture was cooled to ambient temperature. To the cooled reaction mixture was added ethyl acetate (2 mL) and water (2 mL) and the biphasic mixture separated. The aqueous phase was extracted with ethyl acetate (3 x 2 mL). The combined organic phases were passed through a hydrophobic frit and the solvent removed under reduced pressure to give the crude product as a brown oil (0.3 g). The crude product was purified by mass directed auto purification to give exclusively the *O*-alkylated product (**3.36**) as a yellow oil (73 mg, 35%). LCMS (Method A, UV, ESI) $R_t = 1.15$ min, $[M-H]^+ m/z = 361.9$, 99% purity. 1H NMR (400 MHz, d_6 -DMSO): $\delta = 7.65$ (1H, m, Ar-H), 7.37–7.25 (1H, m, Ar-H), 7.21 (1H, dd, $J = 2.3, 7.6$ Hz, Ar-H), 7.11–7.01 (1H, m, Ar-H), 6.90–6.75 (2H, m, Ar-H), 4.35–4.23 (2H, m), 4.20–4.12 (1H, m), 4.09–3.98 (2H, m) – alcohol peak not observed due to exchange with the solvent.

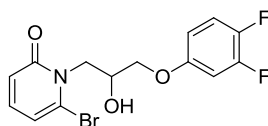
A complete characterisation was not carried out due to the undesired alkylation product being the sole product of the reaction.

1-((6-Bromopyridin-2-yl)oxy)-3-(3,4-difluorophenoxy)propan-2-ol (Table 1.2.2 – Entry 9)



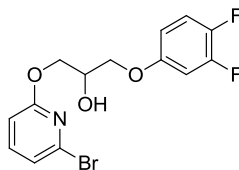
To an oven dried flask was added 6-bromopyridin-2(*1H*)-one (**1.2.5**) (100 mg, 0.58 mmol) dissolved in anhydrous DCM (10 mL). The resulting solution was cooled to 0 °C. To the mixture was added boron trifluoride diethyl etherate (0.152 mL, 1.21 mmol) and the reaction stirred for 5 minutes. To the cooled mixture was added dropwise 2-((3,4-difluorophenoxy)methyl)oxirane (118 mg, 0.63 mmol) in anhydrous DCM (7.5 mL) and the resulting mixture stirred for 30 minutes at 0 °C. After 30 minutes the solution was heated to 40 °C and stirred for 72 h. LCMS at this stage showed no reaction had occurred and therefore the reaction was concluded at this stage.

6-Bromo-1-(3-(3,4-difluorophenoxy)-2-hydroxypropyl)pyridin-2(*1H*)-one (Table 1.2.2 – Entry 10)



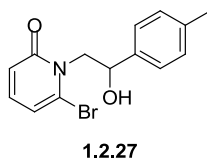
To an oven dried flask was added 6-bromopyridin-2(*1H*)-one (**1.2.5**) (100 mg, 0.58 mmol), anhydrous DME (0.8 mL) and DMF (0.2 mL). To the resulting solution was added sodium hydride (60% dispersion in mineral oil, 24 mg, 0.60 mmol) at 0 °C and stirred for 10 minutes under a nitrogen atmosphere. To the cooled solution was added LiBr (100 mg, 1.15 mmol) and the resulting mixture stirred at ambient temperature for 15 minutes. To the solution was added dropwise 2-((3,4-difluorophenoxy)methyl)oxirane (160 mg, 0.82 mmol). The reaction mixture was heated to 65 °C, and stirred for 16 h under a nitrogen atmosphere. LCMS analysis at this stage revealed a complicated reaction mixture with only trace amounts of potential *N*-alkylation product formation being detected.

1-((6-Bromopyridin-2-yl)oxy)-3-(3,4-difluorophenoxy)propan-2-ol (Table 1.2.2 – Entry 11)



To an oven dried flask was added 6-bromopyridin-2(*1H*)-one (**1.2.5**) (100 mg, 0.58 mmol), anhydrous DME (0.8 mL) and DMF (0.2 mL). To the resulting solution was added cesium carbonate (225 mg, 0.69 mmol) at 0 °C and the reaction was stirred for 10 minutes under a nitrogen atmosphere. To the cooled solution was added LiBr (100 mg, 1.15 mmol) and the resulting mixture stirred at ambient temperature for 15 minutes. To the solution was added dropwise 2-((3,4-difluorophenoxy)methyl)oxirane (160 mg, 0.86 mmol). The reaction mixture was heated to 65 °C, and stirred for 16 h under a nitrogen atmosphere. LCMS analysis at this stage revealed a complicated reaction mixture with an *N:O* alkylation ratio of 1:2.1. Significant by-product formation prevented isolation of the low levels of the alkylation products. The reaction was therefore concluded at this stage.

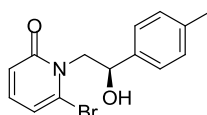
6-Bromo-1-(2-hydroxy-2-(*p*-tolyl)ethyl)pyridin-2(*1H*)-one (1.2.27)



To a solution of anhydrous DCM (20 mL) and anhydrous methanol (20 mL) was added 6-bromo-1-(2-oxo-2-(*p*-tolyl)ethyl)pyridin-2(*1H*)-one (**1.2.26**) (0.90 g, 2.94 mmol) and the resulting mixture cooled to 0 °C. To the cooled solution was added sodium borohydride (60% in mineral oil) (0.11 g, 2.94 mmol) and the resulting solution stirred at 0 °C under a nitrogen atmosphere for 2.5 h. The reaction mixture was warmed to ambient temperature and quenched by the dropwise addition of water (25 mL) and saturated aqueous NH₄Cl (25 mL). The resulting biphasic mixture was separated and the aqueous phase was extracted with ethyl acetate (3 x 50 mL). The combined organic extracts were washed with brine, passed through a hydrophobic frit, and the solvent removed under reduced pressure give the crude product

(1.1 g). The crude mixture was purified by automated column chromatography (cyclohexane: ethyl acetate, 100:0 - 0:100, 80 g SiO₂). Removal of the solvent gave 6-bromo-1-(2-hydroxy-2-(*p*-tolyl)ethyl)pyridin-2(1*H*)-one (**1.2.27**) as viscous colourless oil (0.84 g, 93%). LCMS (Method A, UV, ESI) $R_t = 0.89$ min, $[M-H]^+ m/z = 308.0$. ¹H NMR (400 MHz, *d*₆-DMSO): $\delta = 7.30$ (1H, dd, $J = 7.3, 9.1$ Hz, Ar-H), 7.26 (2H, d, $J = 8.1$ Hz, Ar-H), 7.15 (2H, d, $J = 8.1$ Hz, Ar-H), 6.57 (1H, dd, $J = 1.3, 7.3$ Hz, Ar-H), 6.42 (1H, dd, $J = 1.3, 9.1$ Hz, Ar-H), 5.50 (1H, d, $J = 4.5$ Hz), 4.95 (1H, m), 4.32 (1H, dd, $J = 8.8, 13.2$ Hz), 4.21 (1H, d, $J = 4.5, 13.2$ Hz), 2.29 (3H, s) (sample contained 12% ethyl acetate by mass, this is accounted for in the product yield). ¹³C NMR (100.6 MHz, *d*₆-DMSO): $\delta = 162.0, 139.8, 139.7, 136.4, 128.7, 128.4, 125.7, 110.7, 69.2, 55.7, 30.1, 20.7$. IR ($\nu_{\max}/\text{cm}^{-1}$) = 3356 (br), 1505, 782. HRMS (ESI-[+H]) m/z : Calcd for C₁₄H₁₄⁷⁹BrNO₂ 308.0281; Found 308.0277.

(*R*)-6-Bromo-1-(2-hydroxy-2-(*p*-tolyl)ethyl)pyridin-2(1*H*)-one (1.2.30)



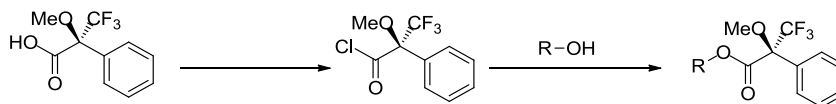
1.2.30

To an oven dried flask was added 6-bromo-1-(2-oxo-2-(*p*-tolyl)ethyl)pyridin-2(1*H*)-one (**1.2.26**) (400 mg, 1.31 mmol) dissolved in anhydrous THF (4 mL) and the resulting solution cooled to -78 °C and stirred under an inert atmosphere. To the cooled solution was slowly added (*R*)-1-methyl-3,3-diphenylhexahydropyrrolo[1,2-*c*][1,3,2]oxazaborole (1M in toluene) (0.26 mL, 0.26 mmol). To the resulting solution was added dropwise borane (1M in THF) (1.31 mL, 1.31 mmol) and the resulting solution stirred at -78 °C. The reaction was stirred for 16 h, after which the temperature had risen to -50 °C. LCMS analysis at this stage indicated no reaction had occurred. The reaction was therefore transferred to an ice bath and stirred at 0 °C. After 5 h, LCMS analysis revealed the slow reaction progression. The reaction was therefore stirred overnight by which time the temperature had risen to ambient temperature. To the solution was added a mixture of cooled water (10 mL) and methanol (10 mL). The resulting biphasic mixture was separated and the aqueous phase extracted with ethyl acetate (5 x 10 mL). The combined organic extracts were passed through a hydrophobic frit and the solvent removed under reduced pressure to give the crude product as a blue solid (600 mg). The crude product was purified by automated column chromatography (cyclohexane: TBME, 100:0 - 0:100, 80 g SiO₂) to give the desired product (**1.2.30**) as a viscous colourless oil (321

mg, 80%). LCMS (Method A, UV, ESI) $R_t = 0.89$ min, $[M-H]^+ m/z = 308.0$, 100% purity. 1H NMR (400 MHz, d_6 -DMSO): $\delta = 7.32$ – 7.22 (3H, m, Ar-H), 7.15 (2H, d, $J = 8.1$ Hz, Ar-H), 6.57 (1H, dd, $J = 1.3, 7.3$ Hz, Ar-H), 6.42 (1H, dd, $J = 1.3, 9.1$ Hz, Ar-H), 5.50 (1H, d, $J = 4.5$ Hz), 4.95 (1H, m), 4.32 (1H, dd, $J = 8.8, 13.3$ Hz), 4.21 (1H, d, $J = 4.5, 13.3$ Hz), 2.29 (3H, s). ^{13}C NMR (100.6 MHz, d_6 -DMSO): $\delta = 162.0, 139.9, 139.3, 136.4, 128.7, 128.4, 125.7, 110.7, 69.2, 55.7, 30.1, 20.7$. IR (ν_{max}/cm^{-1}) = 3356 (br), 1505, 782. HRMS (ESI-[+H]) m/z : Calcd for $C_{14}H_{14}^{79}BrNO_2$ 308.0281; Found 308.0277.

The ee of the reaction was determined in a subsequent experiment using the Mosher's acid chloride giving a % ee value of 60.

Mosher's acid method for determination of enantiomeric excess of secondary alcohols

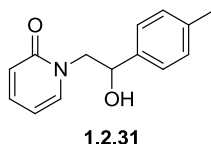


To a solution of (*S*)-3,3,3-trifluoro-2-methoxy-2-phenylpropanoic acid (100 mg, 0.48 mmol) in cyclohexane (20 mL) was added anhydrous DMF (0.033 mL, 0.43 mmol) followed by oxalyl chloride (0.17 mL, 2.0 mmol). The resulting solution was stirred under a nitrogen atmosphere for 1 h. The resulting mixture was filtered and the filtrate concentrated under reduced pressure to give the crude (*R*)-3,3,3-trifluoro-2-methoxy-2-phenylpropanoyl chloride which was used without further purification steps. To a solution of freshly prepared Mosher's acid chloride (45.1 mg, 0.18 mmol) and DMAP (23.8 mg, 0.20 mmol) in anhydrous DCM (2 mL) was added a solution of 6-bromo-1-(2-hydroxy-2-(*p*-tolyl)ethyl)pyridin-2(*1H*)-one (50 mg, 0.16 mmol) in anhydrous DCM (2 mL). To the solution was added DBU (0.027 mL, 0.18 mmol) and the resulting solution stirred under a nitrogen atmosphere until complete by LCMS (typically 16 h). To the mixture was added water (3 mL) and the biphasic mixture separated. The aqueous phase was extracted with DCM (3 x 10 mL) and the combined organic extracts passed through a hydrophobic frit. The solvent was removed under reduced pressure to give a yellow oil (190 mg). The crude mixture was assessed by NMR to determine the ee of the alcohol, through comparison with the racemic reference.

Determination of the ee for CBS reduction (**1.2.30**):

Enantiomeric excess determined by comparison of the $-OCH_3$ integrals for both diastereoisomers. 1H NMR (400 MHz, d_6 -DMSO) peaks at $\delta = 2.34$ and 2.33 , ratio of 3.91:1 \equiv 80:20. Therefore, the ee = $80 - 20 = 60\%$ for the asymmetric reduction.

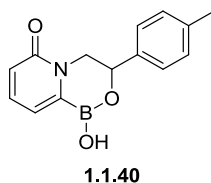
1-(2-Hydroxy-2-(*p*-tolyl)ethyl)pyridin-2(*1H*)-one (**1.2.31**) (Scheme 1.2.20)



To an oven dried flask was added 6-bromo-1-(2-hydroxy-2-(*p*-tolyl)ethyl)pyridin-2(*1H*)-one (**1.2.27**) (0.15 g, 0.49 mmol) in anhydrous THF (3 mL) and the resulting solution cooled to 0 °C and stirred under a nitrogen atmosphere. To the cooled solution was added dropwise *i*PrMgCl.LiCl (1M solution in THF) (1.17 mL, 1.17 mmol) and the resulting solution stirred at 0 °C for 30 minutes. LCMS at this stage (after quenching the sample with methanol) revealed complete dehalogenation consistent with the magnesium-halogen exchange. To the solution was added trimethyl borate (0.109 mL, 0.973 mmol) and the reaction stirred for 10 minutes. The reaction was quenched by the dropwise addition of 0.1 M aqueous HCl at 0 °C. The mixture was warmed to ambient temperature and diluted with ethyl acetate (5 mL). The resulting biphasic mixture was separated and the aqueous phase extracted with ethyl acetate (3 x 5 mL). The combined organic extracts were passed through a hydrophobic frit and the solvent removed *in vacuo* to give the undesired dehalogenation product (**1.2.31**) as a white solid (105 mg, 0.458 mmol, 94%). LCMS (Method A, UV, ESI) $R_t = 0.70$ min, $[M-H]^+$ $m/z = 230.1$, 99% purity. 1H NMR (400 MHz, d_6 -DMSO): $\delta = 7.51$ (1H, dd, $J = 1.8, 6.8$ Hz, Ar-H), 7.40 (1H, m, Ar-H), 7.27 (2H, d, $J = 8.1$ Hz, Ar-H), 7.17 (2H, d, $J = 8.1$ Hz, Ar-H), 6.40 (1H, d, $J = 9.1$ Hz, Ar-H), 6.15 (1H, m, Ar-H), 5.57 (1H, s, br), 4.83 (1H, m), 4.18 (1H, dd, $J = 3.9, 13.0$ Hz), 3.75 (1H, dd, $J = 8.8, 13.0$ Hz), 2.30 (3H). ^{13}C NMR (100.6 MHz, d_6 -DMSO): $\delta = 161.7, 140.3, 139.9, 139.8, 136.3, 128.7, 125.8, 119.2, 104.3, 69.8, 56.4, 20.6$.

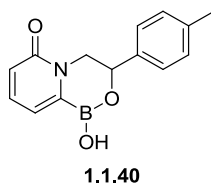
A complete characterisation was not carried out due to the undesired dehalogenation product being the sole product of this reaction

1-Hydroxy-3-(*p*-tolyl)-3,4-dihydropyrido[2,1-*c*][1,4,2]oxazaborinin-6(*1H*)-one
(1.1.40) (Scheme 1.2.21)



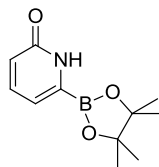
To a solution of 6-bromo-1-(2-hydroxy-2-(*p*-tolyl)ethyl)pyridin-2(*1H*)-one (**1.2.27**) (100 mg, 0.32 mmol) and potassium acetate (195 mg, 1.99 mmol) in anhydrous 1,4-dioxane (5 mL), in a pyrex sealed tube stirred at ambient temperature, was added 4,4,4',4',5,5,5',5'-octamethyl-2,2'-bi(1,3,2-dioxaborolane) (302 mg, 1.19 mmol). The reaction vessel was purged with nitrogen for 1 min after which PdCl₂(dppb) (19.3 mg, 0.032 mmol) was added. The reaction vessel was again purged with nitrogen for 1 min. The reaction mixture was heated to 100 °C and stirred for 16 h. LCMS analysis at this stage showed no remaining starting material, however, only the dehalogenation product rather was detected. Therefore, the reaction was discontinued at this stage.

1-Hydroxy-3-(*p*-tolyl)-3,4-dihydropyrido[2,1-*c*][1,4,2]oxazaborinin-6(*1H*)-one
(1.1.40) (Table 1.2.3 – Entry 1)



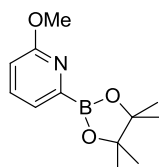
To a solution of 6-bromo-1-(2-hydroxy-2-(*p*-tolyl)ethyl)pyridin-2(*1H*)-one (**1.2.27**) (100 mg, 0.32 mmol) and triethylamine (0.27 mL, 1.95 mmol) in anhydrous 1,4-dioxane (1 mL) in a pyrex sealed tube stirred at ambient temperature and degassed for 10 minutes. To the mixture was added 4,4,5,5-tetramethyl-1,3,2-dioxaborolane (0.28 mL, 1.95 mmol). The reaction vessel was purged with nitrogen for 1 min after which tetrakis(triphenylphosphine)palladium(0) (38 mg, 0.032 mmol) was added. The reaction vessel was purged again with nitrogen for one 1 minute after which the reaction mixture was heated to 100 °C. After 16 h, LCMS analysis revealed no reaction had occurred. The reaction was therefore concluded at this stage.

6-(4,4,5,5-Tetramethyl-1,3,2-dioxaborolan-2-yl)pyridin-2(1H)-one (Table 1.2.3 – Entry 2)



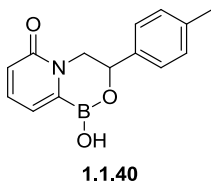
To a solution of 6-bromopyridin-2(1H)-one (**1.2.5**) (100 mg, 0.58 mmol) and triethylamine (0.50 mL, 3.45 mmol) in a pyrex sealed tube was added anhydrous 1,4-dioxane (1 mL) and the resulting solution degassed for 10 minutes. To the mixture was added 4,4,5,5-tetramethyl-1,3,2-dioxaborolane (0.50 mL, 3.45 mmol). The reaction vessel was purged with nitrogen for 1 min after which tetrakis(triphenylphosphine)palladium(0) (66 mg, 0.057 mmol) was added. The reaction vessel was again purged with nitrogen and heated to 100 °C. After 2 h, LCMS analysis revealed no product, despite complete consumption of the starting material. Therefore, the reaction was concluded at this stage.

2-Methoxy-6-(4,4,5,5-tetramethyl-1,3,2-dioxaborolan-2-yl)pyridine (Table 1.2.3 – Entry 3)



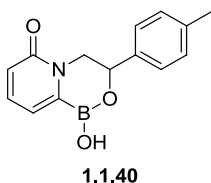
To a solution of 2-bromo-6-methoxypyridine (**1.2.6**) (0.165 mL, 1.33 mmol) and potassium acetate (0.80 g, 8.15 mmol) in anhydrous 1,4-dioxane (2.5 mL) in a pyrex sealed tube was added 4,4,4',4',5,5,5',5'-octamethyl-2,2'-bi(1,3,2-dioxaborolane) (1.239 g, 4.88 mmol). The reaction vessel was purged with nitrogen for 1 min after which PdCl₂(dppb) (80 mg, 0.133 mmol) was added. The reaction vessel was purged with nitrogen. The reaction mixture was heated under microwave irradiation at 100 °C for 15 min. LCMS analysis showed no reaction had occurred and the reaction was therefore concluded at this stage.

1-Hydroxy-3-(*p*-tolyl)-3,4-dihydropyrido[2,1-*c*][1,4,2]oxazaborinin-6(*1H*)-one
(1.1.40) (Table 1.2.3 – Entry 4)



To a solution of 6-bromo-1-(2-hydroxy-2-(*p*-tolyl)ethyl)pyridin-2(*1H*)-one (**1.2.27**) (80 mg, 0.26 mmol) and potassium acetate (156 mg, 1.59 mmol) in anhydrous 1,4-dioxane (5 mL) in a pyrex sealed tube was added 4,4,4',4',5,5,5',5'-octamethyl-2,2'-bi(1,3,2-dioxaborolane) (99 mg, 0.39 mmol). The reaction vessel was purged with nitrogen for 1 min after which PdCl₂(dppf) (9.5 mg, 0.013 mmol) was added. The reaction vessel was again purged with nitrogen. The resulting solution was heated to 130 °C under microwave irradiation for 15 min. At this stage LCMS analysis at this stage showed 21% dehalogenated by-product and 3.5% product formation (**1.1.40**) (approximate ratio of 6:1), with no remaining starting material. The low levels of desired product led to the reaction being concluded at this stage.

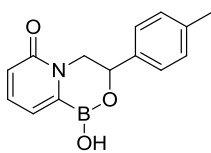
1-Hydroxy-3-(*p*-tolyl)-3,4-dihydropyrido[2,1-*c*][1,4,2]oxazaborinin-6(*1H*)-one
(1.1.40) (Entry 5, Table 1.2.3)



To a solution of 6-bromo-1-(2-hydroxy-2-(*p*-tolyl)ethyl)pyridin-2(*1H*)-one (**1.2.27**) (90 mg, 0.29 mmol) and potassium acetate (176 mg, 1.79 mmol) in anhydrous 1,4-dioxane (5 mL) in a pyrex sealed tube was added 4,4,4',4',5,5,5',5'-octamethyl-2,2'-bi(1,3,2-dioxaborolane) (111 mg, 0.44 mmol). The reaction vessel was purged with nitrogen for 1 min after which PdCl₂(dppf) (10.7 mg, 0.015 mmol) was added. The reaction vessel was again purged with nitrogen. The resulting solution was heated to 130 °C under microwave irradiation for 5 min. LCMS analysis at this stage showed 29% dehalogenated by-product and 7% product formation (approximate ratio of 4:1). The solvent was removed under reduced pressure and the resulting residue dissolved in DCM (15 mL). The organic phase was washed with water (2 x 10 mL), followed by brine (10 mL). The resulting organic phase was passed through a hydrophobic frit

and the solvent removed under reduced pressure to give the crude product as a brown solid. LCMS analysis at this stage revealed only low levels of the desired borolane (**1.1.40**) with predominately dehalogenated by-product (**1.2.31**) and the experiment was therefore concluded at this stage.

1-Hydroxy-3-(*p*-tolyl)-3,4-dihydropyrido[2,1-*c*][1,4,2]oxaborinin-6(*1H*)-one
(1.1.40) (Scheme 1.2.22)

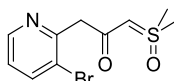


1.1.40

To a solution of 6-bromo-1-(2-hydroxy-2-(*p*-tolyl)ethyl)pyridin-2(*1H*)-one (**1.2.27**) (150 mg, 0.49 mmol) and potassium acetate (293 mg, 3.0 mmol) in anhydrous 1,4-dioxane (10 mL) in a pyrex sealed tube stirred at ambient temperature was added 4,4,4',4',5,5,5',5'-octamethyl-2,2'-bi(1,3,2-dioxaborolane) (185 mg, 0.73 mmol). The reaction vessel was purged with nitrogen for 1 min after which PdCl₂(dppf) (18 mg, 0.025 mmol) was added. The reaction vessel was again purged with nitrogen. The resulting solution was heated to 130 °C under microwave irradiation for 5 min. After this time the reaction was complete showing 49% dehalogenated product and only 12% desired product (ratio = 4:1). The solvent was removed under reduced pressure to give a brown solid that was purified by HPLC to give **1.1.40** as an off-white solid (10 mg, 8%). LCMS (Method A, UV, ESI) *R_t* = 0.81 min, [M-H]⁺ *m/z* = 256.3, 95% purity. ¹H NMR (400 MHz, *d*₆-DMSO): δ = 9.12 (1H, br), 7.42 (1H, dd, *J* = 6.6, 9.0 Hz, Ar-H), 7.32 (2H, d, *J* = 7.8 Hz, Ar-H), 7.21 (2H, d, *J* = 7.8 Hz, Ar-H), 6.72 (1H, d, *J* = 6.6 Hz, Ar-H), 6.51 (1H, d, *J* = 9.0 Hz, Ar-H), 5.36 (1H, dd, *J* = 2.7, 9.1 Hz), 4.47 (1H, dd, *J* = 2.7, 14.4 Hz), 3.81 (1H, dd, *J* = 9.1, 14.4 Hz), 2.31 (3H, s).

Insufficient material for full characterisation.

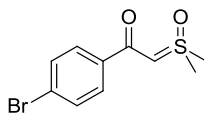
Ethyl 2-(3-bromopyridin-2-yl)acetate derived dimethylsulfoxonium (1.3.20)
(Scheme 1.3.10)



1.3.20

To an oven dried flask was added dried trimethylsulfoxonium iodide (2.70 g, 12.3 mmol), potassium *tert*-butoxide (1.38 g, 12.3 mmol), and anhydrous THF (20 mL). The resulting solution was heated to reflux for 2 h under a nitrogen atmosphere. The solution was cooled to ambient temperature and to the mixture was added dropwise ethyl 2-(3-bromopyridin-2-yl)acetate (**1.1.20**) (1.00 g, 4.10 mmol) over a period of 10 minutes. The resulting solution was stirred until complete by LCMS, monitoring the reaction at regular increments. After 16 h no product formation was observed and the reaction was therefore stirred for an additional 48 h. At this stage the reaction was complete, LCMS analysis indicating that complete hydrolysis of the ester (**1.1.20**) had occurred. In the absence of any desired product formation the reaction was concluded at this stage.

Dimethylsulfoxonium 2-oxo-3-(4-bromophenyl)propylide (1.3.24) (Scheme 1.3.11)



1.3.24

To an oven dried flask was added trimethylsulfoxonium chloride (1.68 g, 13.10 mmol) and potassium *tert*-butoxide (1.47 g, 13.10 mmol) in anhydrous THF (20 mL). The mixture was heated to reflux for 2 h under a nitrogen atmosphere before cooling to ambient temperature. To the cooled mixture was added ethyl 4-bromobenzoate (**1.3.23**) (0.71 mL, 4.37 mmol) and the resulting solution stirred under a nitrogen atmosphere for 16 h. LCMS analysis at this stage revealed 24% product (**1.3.24**) and 33% starting material, in addition to hydrolytic by-products. The evidence for successful ylide formation meant that the test reaction was concluded at this stage.

General procedure for the formation of Sulfur Ylides (Scheme 1.3.12) (Table 1.3.1)

General procedure: To an oven dried flask was added trimethylsulfoxonium chloride (1.58 g, 12.3 mmol, 3.0 eq), anhydrous THF (8 mL), and potassium *tert*-butoxide (1M in THF) (12.3 mL, 12.3 mmol, 3.0 eq) under a nitrogen atmosphere. The resulting solution was refluxed for 2 h and then cooled to the reaction temperature displayed in the table. To the solution was added ethyl 2-(3-bromopyridin-2-yl)acetate (**1.3.12**) (1.0 g, 4.10 mmol, 1.0 eq) and the resulting solution stirred under a nitrogen atmosphere. The reaction progression was monitored by LCMS analysis (Method A) at the indicated time increments.

Entry	Temperature (°C)	Amount of hydrolysis observed ^a	Reaction time	Product formation ^a	Remaining Starting material ^a
1	25	8% (10%) ^b	24 h (48 h) ^b	52% (54%) ^b	32% (29%) ^b
2	40	8% (9%) ^b	24 h (72 h)	75% (56%) ^b	14% (0%) ^b
3	50	14%	24 h	71%	7%
4	55	14% (19%) ^b	24 h (48 h)	67% (63%) ^b	10% (0%) ^b
5 ^c	70	9%	18 h	45%	18%

^a Determined by LCMS analysis. ^b Values in brackets correspond to experiments with extended time periods, denoted by the brackets in the time column. ^c Reaction at 70 °C was discontinued after 18 h due to significant by-product formation (representing approximately 30% of the total reaction composition).

Table 1.3.1 - Results of the formation of the sulfur ylide study.

Experiments into the influence of drying the sulfur salts on the levels of hydrolysis in the subsequent Ylide formation (Scheme 1.3.14) (Table 1.3.2)

General procedure: To a heat dried flask was added trimethylsulfoxonium chloride (a) and stirred under vacuum. The flask was heated to temperature (b) for time (c) before cooling to ambient temperature. The resulting salts were weighed and the mass difference recorded (d). The resulting salts were utilised for the formation of the sulfur ylides using the general procedure above (**Table 1.3.1** – General procedure) cooling to 50 °C. The resulting levels of hydrolysis (e) were obtained analysis of the LCMS data obtained from the crude reaction mixture.

Scheme 1.3.14, Table 1.3.2 – Entry 1:

a) 20.40 g, 159 mmol, b) 55 °C, c) 5 days, d) 0.96 g (4.7%), e) 0.95% hydrolysis by LCMS.

Scheme 1.3.14, Table 1.3.2 – Entry 2:

a) 10.74 g, 84 mmol, b) 55 °C, c) 3 days, d) 0.15 g (1.4%), e) no hydrolysis by LCMS.

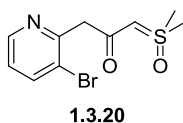
Scheme 1.3.14, Table 1.3.2 – Entry 3:

a) 28.05 g, 218 mmol, b) 60 °C, c) 4 days, d) 1.03 g (3.7%), e) no hydrolysis by LCMS.

Scheme 1.3.14, Table 1.3.2 – Entry 4:

a) 10.43 g, 81 mmol, b) 60 °C, c) 2 days, d) 0.35 g (3.4%), e) no hydrolysis by LCMS (alternative ester).

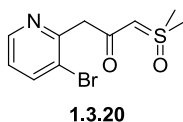
**Ethyl 2-(3-bromopyridin-2-yl)acetate derived dimethylsulfoxonium (1.3.20)
(Scheme 1.3.15)**



To an oven dried flask was added dried trimethylsulfoxonium chloride (19.4 g, 151 mmol) and anhydrous THF (150 mL). To the stirred solution was added potassium *tert*-butoxide (1M in THF) (150 mL, 150 mmol) and the resulting solution refluxed under a nitrogen atmosphere for 2 h. The resulting solution was cooled to 50 °C. To the suspension was added dropwise ethyl 2-(3-bromopyridin-2-yl)acetate (**1.1.20**) (12.2 mL, 50 mmol) over a period of 10 minutes and the reaction stirred at 50 °C for 40 h. LCMS analysis at this stage showed 5% remaining starting material. Stirring for an additional 8 h led to no changes in the reaction composition and the mixture was therefore progressed to work-up. The reaction mixture was cooled to ambient temperature. The reaction mixture was filtered and the solvent removed under reduced pressure. To the mixture was added ethyl acetate (150 mL) and water (100 mL). The biphasic mixture was separated and the aqueous layer extracted with ethyl acetate (10 x 150 mL) until no product remained in the aqueous layer. The combined organic extracts were passed through a hydrophobic frit and the solvent removed under reduced pressure to give a red oil which solidified into an orange solid upon agitation (16.62 g). The crude mixture was purified by

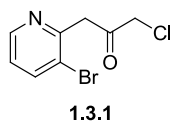
automated column chromatography (TBME:methanol, 100:0 - 70:30, 330 g SiO₂). Removal of the solvent under reduced pressure gave the product as a red oil which solidified upon the addition of ethyl acetate. The product (**1.3.20**) was isolated as an orange/brown solid (11.1 g, 76%). LCMS (Method A, UV, ESI) $R_t = 0.53$ min, $[M-H]^+ m/z = 289.9, 291.9$, 100% purity. M.p. 112-114 (dc) °C. ¹H NMR (400 MHz, *d*₆-DMSO): $\delta = 8.48$ (1H, dd, $J = 1.4, 4.7$ Hz, Ar-H), 8.01 (1H, dd, $J = 1.4, 8.1$ Hz, Ar-H), 7.21 (1H, dd, $J = 4.7, 8.1$ Hz, Ar-H), 4.56 (1H, s), 3.73 (2H, s), 3.42 (6H, s). ¹³C NMR (100.6 MHz, *d*₆-DMSO): $\delta = 183.4, 178.8, 156.0, 147.7, 140.0, 123.3, 121.7, 72.5, 49.3$. IR (ν_{max}/cm^{-1}) = 3005, 1734, 1581, 1371. HRMS (ESI-[+H]) m/z : Calcd for C₁₀H₁₃⁷⁹BrNO₂S 289.9850; Found 289.9863.

Ethyl 2-(3-bromopyridin-2-yl)acetate derived dimethylsulfoxonium with increased equivalents of base and sulfur salts (1.3.20) (Scheme 1.3.16)



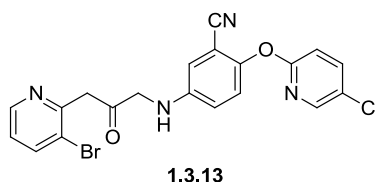
To an oven dried flask was added dried trimethylsulfoxonium chloride (27.0 g, 210 mmol) and anhydrous THF (60 mL). To the stirred solution was added potassium *tert*-butoxide (1M in THF) (210 mL, 210 mmol) and the resulting solution refluxed under a nitrogen atmosphere for 2 h. The resulting solution was cooled to 50 °C. To the suspension was added dropwise ethyl 2-(3-bromopyridin-2-yl)acetate (**1.1.20**) (8.95 mL, 53 mmol) over a period of 10 minutes and the reaction stirred at 50 °C for 24 h. LCMS analysis at this stage showed the reaction had gone to completion. The reaction mixture was cooled to ambient temperature. The reaction mixture was filtered and the solvent removed under reduced pressure to give a brown solid. The crude mixture was purified by automated column chromatography (Ethyl acetate:methanol, 100:0 – 75:25, 2 x 330 g SiO₂). Removal of the solvent under reduced pressure gave **1.3.20** as a red solid (12.66 g, 83%). LCMS (Method B, UV, ESI) $R_t = 0.42$ min, $[M-H]^+ m/z = 289.9, 291.9$, 94% purity. M.p. 112-114 (dc) °C. ¹H NMR (400 MHz, *d*₆-DMSO): $\delta = 8.48$ (1H, dd, $J = 1.4, 4.7$ Hz, Ar-H), 8.01 (1H, dd, $J = 1.4, 8.1$ Hz, Ar-H), 7.21 (1H, dd, $J = 4.7, 8.1$ Hz, Ar-H), 4.56 (1H, s), 3.73 (2H, s), 3.42 (6H, s). ¹³C NMR (100.6 MHz, *d*₆-DMSO): $\delta = 183.4, 178.8, 156.0, 147.7, 140.0, 123.3, 121.7, 72.5, 49.4$. IR (ν_{max}/cm^{-1}) = 3005, 1734, 1581, 1371. HRMS (ESI-[+H]) m/z : Calcd for C₁₀H₁₃⁷⁹BrNO₂S 289.9850; Found 289.9863.

1-(3-Bromopyridin-2-yl)-3-chloropropan-2-one (1.3.1) (Scheme 1.3.17)



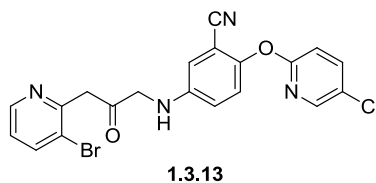
To an oven dried flask was added ethyl 2-(3-bromopyridin-2-yl)acetate derived dimethylsulfoxonium species (**1.3.20**) (1.00 g, 3.45 mmol) and anhydrous THF (20 mL) under a nitrogen atmosphere. The resulting solution was cooled to 0 °C. To the solution was added LiCl (0.18 g, 4.31 mmol) and methanesulfonic acid (0.54 mL, 8.27 mmol). The resulting solution was heated to 70 °C and stirred for 1 h. LCMS analysis indicated no remaining starting material at this stage. The reaction was cooled to ambient temperature and to the mixture was added diethyl ether (50 mL) to precipitate the desired product as the corresponding salt. The resulting black solid obtained showed no desired product when analysed by NMR and LCMS and therefore the reaction was concluded at this stage.

5-((3-(3-Bromopyridin-2-yl)-2-oxopropyl)amino)-2-((5-chloropyridin-2-yl)oxy)benzonitrile (1.3.13) (Scheme 1.3.18)



To an oven dried flask was added ethyl 2-(3-bromopyridin-2-yl)acetate derived dimethylsulfoxonium species (**1.3.20**) (1.00 g, 3.45 mmol) and anhydrous THF (15 mL) under a nitrogen atmosphere. The resulting solution was cooled to 0 °C. To the solution was added LiCl (0.18 g, 4.31 mmol) and methanesulfonic acid (0.54 mL, 8.27 mmol). The resulting solution was heated to 70 °C and stirred for 1 h under a nitrogen atmosphere. LCMS analysis indicated no remaining starting material at this stage. The reaction mixture was cooled to ambient temperature and 5-amino-2-((5-chloropyridin-2-yl)oxy)benzonitrile (**1.3.2**) (0.89 g, 3.62 mmol) was added, followed by the dropwise addition of DIPEA (2.11 mL, 12.06 mmol). The resulting solution was stirred at ambient temperature for 24 h. LCMS analysis at this stage showed no desired product formation and therefore the reaction was concluded.

5-((3-(3-Bromopyridin-2-yl)-2-oxopropyl)amino)-2-((5-chloropyridin-2-yl)oxy)benzonitrile (1.3.13) (Scheme 1.3.20)



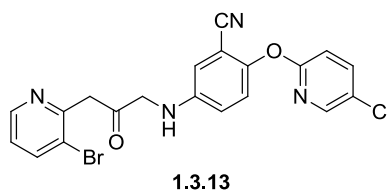
To an oven dried flask was added bis(1,5-cyclooctadiene)diiridium(I) dichloride (13 mg, 0.025 mmol), 5-amino-2-((5-chloropyridin-2-yl)oxy)benzonitrile (**1.3.2**) (1.22 g, 4.96 mmol) and anhydrous DCM (15 mL). To the resulting solution was added ethyl 2-(3-bromopyridin-2-yl)acetate derived dimethylsulfoxonium species (**1.3.20**) (0.72 g, 2.48 mmol). The resulting solution was stirred at ambient temperature under a nitrogen atmosphere. After stirring for 24 h LCMS analysis indicated 5% product formation. To the reaction was therefore added bis(1,5-cyclooctadiene)diiridium(I) dichloride (13 mg, 0.025 mmol). After a further 2 h, LCMS analysis showed 9% product formation. However, after an additional 22 h (total reaction time 48 h) this was unchanged. To the mixture was added bis(1,5-cyclooctadiene)diiridium(I) dichloride (13 mg, 0.025 mmol) (total catalyst loading of 3 mol%). After a further 1 h LCMS analysis showed 11% product formation. After a further 22 h, no significant changes were observed; therefore the reaction was stopped at this stage. The solvent was removed under reduced pressure and the crude mixture purified by mass directed auto purification. Removal of the solvent under reduced pressure gave the product (**1.3.13**) as a brown solid (76 mg, 7%). LCMS (Method A, UV, ESI) $R_t = 1.11$ min, $[M-H]^+ m/z = 457.3, 459.3, 461.3$ (consistent with both bromine and chlorine isotopes) 100% purity. M.p. 145-148 °C. 1H NMR (400 MHz, d_6 -DMSO): $\delta = 8.52$ (1H, dd, $J = 1.5, 4.8$ Hz, Ar-H), 8.19 (1H, d, $J = 2.5$ Hz, Ar-H), 8.08 (1H, dd, $J = 1.5, 8.1$ Hz, Ar-H), 7.98 (1H, dd, $J = 2.8, 8.8$ Hz, Ar-H), 7.28 (1H, dd, $J = 4.8, 8.3$ Hz, Ar-H), 7.18 (1H, d, $J = 8.8$ Hz, Ar-H), 7.12 Hz (1H, d, $J = 8.8$ Hz, Ar-H), 7.00 (1H, d, $J = 2.8$ Hz, Ar-H), 6.97 (1H, m, Ar-H), 6.50 (1H, t, $J = 5.8$ Hz, N-H), 4.28 (2H, d, $J = 5.8$ Hz, CH_2), 4.24 (2H, s, CH_2). ^{13}C NMR (100.6 MHz, d_6 -DMSO): $\delta = 203.8, 161.6, 154.1, 147.9, 146.0, 145.3, 144.7, 140.3, 140.1, 125.4, 124.0, 123.8, 121.6, 118.8, 116.2, 114.1, 112.5, 106.1, 52.6, 48.5$. IR (ν_{max}/cm^{-1}) = 3389, 1716, 1610, 1233. HRMS (ESI-[+H]) m/z : Calcd for $C_{20}H_{15}^{79}BrClN_4O_2$ 457.0067; Found 457.0068.

General procedure for aniline N-H insertion reactions (Scheme 1.3.21 and Table 1.3.3)

To an oven dried flask was added catalyst (a) and anhydrous solvent (b) and the resulting solution stirred under a nitrogen atmosphere. The solution was heated to the desired reaction temperature (c) and to the reaction was added aniline (d) followed by the ylide (e). The reaction was stirred at the indicated reaction temperature until complete as monitored by LCMS (f). The reaction was cooled to ambient temperature and the solvent removed under reduced pressure. The resulting mixture was purified by automated column chromatography (g).

Expanded experimental procedures for key experiments and the highest yielding processes (Table 1.3.3) are detailed below.

5-((3-(3-Bromopyridin-2-yl)-2-oxopropyl)amino)-2-((5-chloropyridin-2-yl)oxy)benzonitrile (1.3.13) (Scheme 1.3.21)



The reaction was conducted according to the general procedure above with bis(1,5-cyclooctadiene)diiridium(I) dichloride (0.116 g, 0.172 mmol), anhydrous toluene (1.5 mL), 5-amino-2-((5-chloropyridin-2-yl)oxy)benzonitrile (**1.3.2**) (0.51 g, 2.07 mmol) and ethyl 2-(3-bromopyridin-2-yl)acetate derived dimethylsulfoxonium species (**1.3.20**) (0.50 g, 1.72 mmol). The reaction was heated to 70 °C for 1 h, and LCMS analysis at this stage indicated the reaction was complete. The reaction was cooled to ambient temperature and concentrated under reduced pressure to give the crude product as a brown oil (1.2 g). The crude product was purified by automated column (cyclohexane:TBME, 100:0 – 0:100, then TBME:MeOH, 100:0 – 90:10, 80 g SiO₂). The appropriate fractions were combined and concentrated under reduced pressure to give 5-((3-(3-bromopyridin-2-yl)-2-oxopropyl)amino)-2-((5-chloropyridin-2-yl)oxy)benzonitrile (**1.3.13**) as a yellow/brown solid (0.623 g, 79%). LCMS (Method A, UV, ESI) $R_t = 1.11$ min, $[M-H]^+$ $m/z = 457.3, 459.3, 461.3$ (consistent with both bromine and chlorine isotopes) 100% purity. M.p. 145-148 °C. ¹H NMR (400 MHz, *d*₆-DMSO): $\delta = 8.52$

(1H, dd, $J = 1.5, 4.8$ Hz, Ar-H), 8.19 (1H, d, $J = 2.5$ Hz, Ar-H), 8.08 (1H, dd, $J = 1.5, 8.1$ Hz, Ar-H), 7.98 (1H, dd, $J = 2.8$ Hz, 8.8 Hz, Ar-H), 7.28 (1H, dd, $J = 4.8, 8.3$ Hz, Ar-H), 7.18 (1H, d, $J = 8.8$ Hz, Ar-H), 7.12 Hz (1H, d, $J = 8.8$ Hz, Ar-H), 7.00 (1H, d, $J = 2.8$ Hz, Ar-H), 6.97 (1H, m, Ar-H), 6.50 (1H, t, $J = 5.8$ Hz, N-H), 4.28 (2H, d, $J = 5.8$ Hz, CH₂), 4.24 (2H, s, CH₂). ¹³C NMR (100.6 MHz, *d*₆-DMSO): $\delta = 203.8, 161.6, 154.1, 147.9, 146.0, 145.3, 144.7, 140.3, 140.1, 125.4, 124.0, 123.8, 121.6, 118.8, 116.2, 114.1, 112.5, 106.1, 52.6, 48.5$. IR (ν_{\max} /cm⁻¹) = 3389, 1716, 1610, 1233. HRMS (ESI-[+H]) *m/z*: Calcd for C₂₀H₁₅⁷⁹BrClN₄O₂ 457.0067; Found 457.0068.

5-((3-(3-Bromopyridin-2-yl)-2-oxopropyl)amino)-2-((5-chloropyridin-2-yl)oxy)benzotrile (1.3.13) (Table 1.3.3 – Entry 1)

See **Scheme 1.3.20** and associated experimental.

5-((3-(3-Bromopyridin-2-yl)-2-oxopropyl)amino)-2-((5-chloropyridin-2-yl)oxy)benzotrile (1.3.13) (Table 1.3.3 – Entry 2)

Performed according to the general procedure:

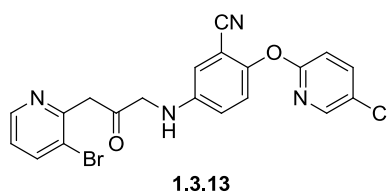
a) Bis(1,5-cyclooctadiene)diridium(I) dichloride (23 mg, 0.034 mmol); b) DCM (1.5 mL); c) 25 °C; d) 5-amino-2-((5-chloropyridin-2-yl)oxy)benzotrile (**1.3.2**) (127 mg, 0.527 mmol); e) ethyl 2-(3-bromopyridin-2-yl)acetate derived dimethylsulfoxonium species (**1.3.20**) (100 mg, 0.345 mmol); f) After 48 h LCMS analysis showed 16% product and no unreacted ylide, in-addition to significant quantities of aniline and unidentified by-products; g) Purified by automated column chromatography (cyclohexane:TBME, 100:0 – 0:100, 40 g SiO₂) however no product was isolated.

5-((3-(3-Bromopyridin-2-yl)-2-oxopropyl)amino)-2-((5-chloropyridin-2-yl)oxy)benzotrile (1.3.13) (Table 1.3.3 – Entry 3)

Performed according to the general procedure:

a) Bis(1,5-cyclooctadiene)diiridium(I) dichloride (2.3 mg, 3.4 μ mmol); b) Toluene (1.5 mL); c) 70 °C; d) 5-amino-2-((5-chloropyridin-2-yl)oxy)benzonitrile (**1.3.2**) (127 mg, 0.52 mmol); e) ethyl 2-(3-bromopyridin-2-yl)acetate derived dimethylsulfoxonium species (**1.3.20**) (100 mg, 0.35 mmol); f) After 48 h LCMS analysis showed 14% product with no ylide remaining; g) Purified by automated column chromatography (cyclohexane:TBME, 100:0 – 0:100, 40 g SiO₂) however no product was isolated.

5-((3-(3-Bromopyridin-2-yl)-2-oxopropyl)amino)-2-((5-chloropyridin-2-yl)oxy)benzonitrile (1.3.13) (Table 1.3.3 – Entry 4)



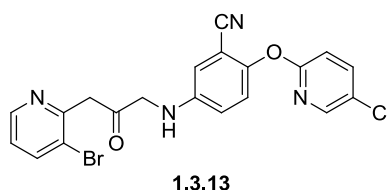
The reaction was conducted according to the general procedure above with bis(1,5-cyclooctadiene)diiridium(I) dichloride (23 mg, 0.034 mmol), anhydrous toluene (1.5 mL), 5-amino-2-((5-chloropyridin-2-yl)oxy)benzonitrile (**1.3.2**) (127 mg, 0.52 mmol) and ethyl 2-(3-bromopyridin-2-yl)acetate derived dimethylsulfoxonium species (**1.3.20**) (100 mg, 0.35 mmol). The reaction was heated at 45 °C for 2 h, and LCMS analysis at this stage indicated the reaction was complete. The mixture was purified by automated column *directly loading the reaction mixture onto the column* (cyclohexane:TBME, 100:0 – 0:100, 40 g SiO₂). Removal of the solvent under reduced pressure gave 5-((3-(3-bromopyridin-2-yl)-2-oxopropyl)amino)-2-((5-chloropyridin-2-yl)oxy)benzonitrile (**1.3.13**) as a brown solid (68 mg, 43%). LCMS (Method A, UV, ESI) $R_t = 1.11$ min, $[M-H]^+$ $m/z = 457.3, 459.3, 461.3$ (consistent with both bromine and chlorine isotopes) 100% purity. M.p. 145-148 °C. ¹H NMR (400 MHz, d_6 -DMSO): $\delta = 8.52$ (1H, dd, $J = 1.5, 4.8$ Hz, Ar-H), 8.19 (1H, d, $J = 2.5$ Hz, Ar-H), 8.08 (1H, dd, $J = 1.5, 8.1$ Hz, Ar-H), 7.98 (1H, dd, $J = 2.8$ Hz, 8.8 Hz, Ar-H), 7.28 (1H, dd, $J = 4.8, 8.3$ Hz, Ar-H), 7.18 (1H, d, $J = 8.8$ Hz, Ar-H), 7.12 Hz (1H, d, $J = 8.8$ Hz, Ar-H), 7.00 (1H, d, $J = 2.8$ Hz, Ar-H), 6.97 (1H, m, Ar-H), 6.50 (1H, t, $J = 5.8$ Hz, N-H), 4.28 (2H, d, $J = 5.8$ Hz, CH₂), 4.24 (2H, s, CH₂). ¹³C NMR (100.6 MHz, d_6 -DMSO): $\delta = 203.8, 161.6, 154.1, 147.9, 146.0, 145.3, 144.7, 140.3, 140.1, 125.4, 124.0, 123.8, 121.6, 118.8, 116.2, 114.1, 112.5, 106.1, 52.6, 48.5$. IR (ν_{max}/cm^{-1}) = 3389, 1716, 1610, 1233. HRMS (ESI-[+H]) m/z : Calcd for C₂₀H₁₅⁷⁹BrClN₄O₂ 457.0067; Found 457.0068.

5-((3-(3-Bromopyridin-2-yl)-2-oxopropyl)amino)-2-((5-chloropyridin-2-yl)oxy)benzonitrile (1.3.13) (Table 1.3.3 – Entry 5)

Performed according to the general procedure:

a) Bis(1,5-cyclooctadiene)diiridium(I) dichloride (231 mg, 0.35 mmol); b) Toluene (20 mL); c) 70 °C; d) 5-amino-2-((5-chloropyridin-2-yl)oxy)benzonitrile (**1.3.2**) (1.02 g, 4.14 mmol); e) ethyl 2-(3-bromopyridin-2-yl)acetate derived dimethylsulfoxonium species (**1.3.20**) (1.00 g, 3.45 mmol); f) After 30 min LCMS analysis showed no remaining ylide starting material; g) Purified by automated column chromatography (cyclohexane:TBME, 100:0 – 0:100, 120 g SiO₂) to give 5-((3-(3-bromopyridin-2-yl)-2-oxopropyl)amino)-2-((5-chloropyridin-2-yl)oxy)benzonitrile (**1.3.13**) as a brown solid (528 mg, 34%). Data consistent with that reported in other examples.

5-((3-(3-Bromopyridin-2-yl)-2-oxopropyl)amino)-2-((5-chloropyridin-2-yl)oxy)benzonitrile (1.3.13) (Table 1.3.3 – Entry 6)



The reaction was conducted according to the general procedure above with bis(1,5-cyclooctadiene)diiridium(I) dichloride (93 mg, 0.138 mmol), anhydrous toluene (2.5 mL), 5-amino-2-((5-chloropyridin-2-yl)oxy)benzonitrile (**1.3.2**) (677 mg, 2.76 mmol) and ethyl 2-(3-bromopyridin-2-yl)acetate derived dimethylsulfoxonium species (**1.3.20**) (400 mg, 1.38 mmol). The reaction was conducted at 70 °C for 30 minutes, and LCMS analysis at this stage indicated the reaction was complete. The mixture was purified by automated column (cyclohexane:ethyl acetate, 100:0 – 25:75, 40 g SiO₂). Removal of the solvent under reduced pressure gave 5-((3-(3-bromopyridin-2-yl)-2-oxopropyl)amino)-2-((5-chloropyridin-2-yl)oxy)benzonitrile (**1.3.13**) as a brown solid (378 mg, 60%). LCMS (Method A, UV, ESI) *R_t* = 1.11 min, [M-H]⁺ *m/z* = 457.3, 459.3, 461.3 (consistent with both bromine and chlorine isotopes) 100% purity. M.p. 145-148 °C. ¹H NMR (400 MHz, *d*₆-DMSO): δ = 8.52 (1H, dd, *J* = 1.5, 4.8 Hz, Ar-H), 8.19 (1H, d, *J* = 2.5 Hz, Ar-H), 8.08 (1H, dd, *J* = 1.5, 8.1 Hz, Ar-H),

7.98 (1H, dd, $J = 2.8$ Hz, 8.8 Hz, Ar-H), 7.28 (1H, dd, $J = 4.8$, 8.3 Hz, Ar-H), 7.18 (1H, d, $J = 8.8$ Hz, Ar-H), 7.12 Hz (1H, d, $J = 8.8$ Hz, Ar-H), 7.00 (1H, d, $J = 2.8$ Hz, Ar-H), 6.97 (1H, m, Ar-H), 6.50 (1H, t, $J = 5.8$ Hz, N-H), 4.28 (2H, d, $J = 5.8$ Hz, CH₂), 4.24 (2H, s, CH₂). ¹³C NMR (100.6 MHz, *d*₆-DMSO): $\delta = 203.8, 161.6, 154.1, 147.9, 146.0, 145.3, 144.7, 140.3, 140.1, 125.4, 124.0, 123.8, 121.6, 118.8, 116.2, 114.1, 112.5, 106.1, 52.6, 48.5$. IR ($\nu_{\max}/\text{cm}^{-1}$) = 3389, 1716, 1610, 1233. HRMS (ESI-[+H]) *m/z*: Calcd for C₂₀H₁₅⁷⁹BrCIN₄O₂ 457.0067; Found 457.0068.

5-(4-((3-(3-Bromopyridin-2-yl)-2-oxopropyl)amino)-2-cyanophenoxy)nicotinonitrile (Table 1.3.3 – Entry 7)

Performed according to the general procedure:

a) Bis(1,5-cyclooctadiene)diiridium(I) dichloride (46.2 mg, 0.090 mmol); b) Toluene (6 mL); c) 70 °C; d) 5-(4-amino-2-cyanophenoxy)nicotinonitrile (**1.3.28**) (233 mg, 0.986 mmol); e) ethyl 2-(3-bromopyridin-2-yl)acetate derived dimethylsulfoxonium species (**1.3.20**) (260 mg, 0.896 mmol); f) After 1 h LCMS analysis showed no remaining ylide starting material; g) Purified by automated column chromatography (cyclohexane:TBME, 100:0 – 0:100, 80 g SiO₂) to give 5-(4-((3-(3-bromopyridin-2-yl)-2-oxopropyl)amino)-2-cyanophenoxy)nicotinonitrile as a brown solid (79 mg, 20%). Data was found to be in agreement with other examples (e.g. **Table 1.3.3 – Entry 9**).

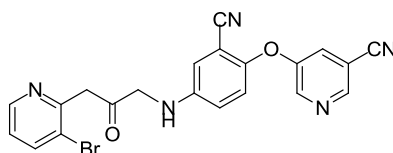
5-(4-((3-(3-Bromopyridin-2-yl)-2-oxopropyl)amino)-2-cyanophenoxy)nicotinonitrile (Table 1.3.3 – Entry 8)

Performed according to the general procedure:

a) Bis(1,5-cyclooctadiene)diiridium(I) dichloride (11.6 mg, 0.017 mmol); b) Toluene (1.5 mL); c) 70 °C; d) 5-(4-amino-2-cyanophenoxy)nicotinonitrile (**1.3.28**) (61 mg, 0.258 mmol); e) ethyl 2-(3-bromopyridin-2-yl)acetate derived dimethylsulfoxonium species (**1.3.20**) (50 mg, 0.172 mmol); f) After 20 min LCMS analysis showed no remaining ylide starting material; g) Purified by automated column chromatography (cyclohexane:TBME, 100:0 – 0:100, 12 g SiO₂) to give 5-(4-((3-(3-bromopyridin-2-yl)-2-oxopropyl)amino)-2-

cyanophenoxy)nicotinonitrile as a brown solid (16 mg, 21%). Data was found to be in agreement with other examples (e.g. Table 1.3.3 – Entry 9).

5-(4-((3-(3-Bromopyridin-2-yl)-2-oxopropyl)amino)-2-cyanophenoxy)nicotinonitrile (Table 1.3.3 – Entry 9)

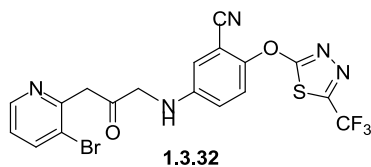


The reaction was conducted according to the general procedure above with bis(1,5-cyclooctadiene)diiridium(I) dichloride (11.6 mg, 0.0173 mmol), anhydrous toluene (2 mL), 5-(4-amino-2-cyanophenoxy)nicotinonitrile (81 mg, 0.345 mmol) and ethyl 2-(3-bromopyridin-2-yl)acetate derived dimethylsulfoxonium species (50 mg, 0.173 mmol). The reaction was conducted at 70 °C for 1 h, and LCMS analysis at this stage indicated the reaction was complete. The mixture was purified by automated column (TBME: cyclohexane, 0:100 - 100:0, 40 g SiO₂). Removal of the solvent under reduced pressure gave 5-(4-((3-(3-bromopyridin-2-yl)-2-oxopropyl)amino)-2-cyanophenoxy)nicotinonitrile as a brown solid (38 mg, 49%). LCMS (Method C, UV, ESI) $R_t = 1.03$ min, $[M-H]^+ m/z = 448.0, 450.0$ (consistent with both bromine isotopes) 100% purity. M.p. 98-100 °C. ¹H NMR (400 MHz, *d*₆-DMSO): $\delta = 8.80$ (1H, d, $J = 1.8$ Hz, Ar-H), 8.67 (1H, d, $J = 2.8$ Hz), 8.52 (1H, dd, $J = 1.5, 4.8$ Hz, Ar-H), 8.08 (1H, dd, $J = 1.5, 8.1$ Hz, Ar-H), 8.00 (1H, $J = 1.8, 2.8$ Hz, Ar-H), 7.29 (1H, dd, $J = 4.8, 8.1$ Hz, Ar-H), 7.14 (1H, d, $J = 8.8$ Hz, Ar-H), 7.05-6.99 (2H, m, Ar-H), 6.57 (1H, t, $J = 5.8$ Hz, N-H), 4.28 (2H, d, $J = 5.8$ Hz, CH₂), 4.24 (2H, s, CH₂). ¹³C NMR (100.6 MHz, *d*₆-DMSO): $\delta = 203.5, 154.1, 153.4, 147.9, 146.9, 146.1, 145.7, 143.6, 140.3, 127.1, 124.0, 121.7, 121.5, 119.2, 116.1, 115.8, 114.8, 109.7, 104.8, 52.6, 48.4$. IR (ν_{max}/cm^{-1}) = 3063, 1686, 1491. HRMS (ESI-[+H]) m/z : Calcd for C₂₁H₁₅⁷⁹BrN₅O₂ 448.0409; Found 448.0403.

5-((3-(3-Bromopyridin-2-yl)-2-oxopropyl)amino)-2-((5-(trifluoromethyl)-1,3,4-thiadiazol-2-yl)oxy)benzonitrile (Table 1.3.3 – Entry 10)

Performed according to the general procedure:

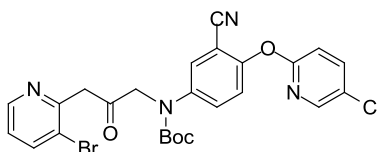
a) Bis(1,5-cyclooctadiene)diiridium(I) dichloride (11.6 mg, 0.017 mmol), b) Toluene (1.5 mL); c) 70 °C; d) 5-amino-2-((5-(trifluoromethyl)-1,3,4-thiadiazol-2-yl)oxy)benzonitrile (**1.3.29**) (74 mg, 0.258 mmol); e) ethyl 2-(3-bromopyridin-2-yl)acetate derived dimethylsulfoxonium species (**1.3.20**) (50 mg, 0.172 mmol); f) After 30 min LCMS analysis showed no remaining ylide starting material; g) Purified by automated column chromatography (cyclohexane:ethyl acetate, 100:0 – 30:70, 12 g SiO₂) to give 5-((3-(3-bromopyridin-2-yl)-2-oxopropyl)amino)-2-((5-(trifluoromethyl)-1,3,4-thiadiazol-2-yl)oxy)benzonitrile (**1.3.32**) (32 mg, 37%) as a brown solid. Data was found to be in agreement with other examples (e.g. **Table 1.3.3 – Entry 11**) (sample contained 25% ethyl acetate by mass, this is accounted for in the product yield).

5-((3-(3-Bromopyridin-2-yl)-2-oxopropyl)amino)-2-((5-(trifluoromethyl)-1,3,4-thiadiazol-2-yl)oxy)benzonitrile (Table 1.3.3 – Entry 11)

The reaction was conducted according to the general procedure above with bis(1,5-cyclooctadiene)diiridium(I) dichloride (44 mg, 0.066 mmol), anhydrous toluene (1.5 mL), 5-amino-2-((5-(trifluoromethyl)-1,3,4-thiadiazol-2-yl)oxy)benzonitrile (**1.3.29**) (375 mg, 1.31 mmol) and ethyl 2-(3-bromopyridin-2-yl)acetate derived dimethylsulfoxonium species (**1.3.20**) (190 mg, 0.66 mmol). The reaction was conducted at 70 °C for 1 h, and LCMS analysis at this stage indicated the reaction was complete. The mixture was purified by automated column (ethyl acetate: cyclohexane, 30:70 – 70:30, 80 g SiO₂). Removal of the solvent under reduced pressure gave 5-((3-(3-bromopyridin-2-yl)-2-oxopropyl)amino)-2-((5-(trifluoromethyl)-1,3,4-thiadiazol-2-yl)oxy)benzonitrile (**1.3.32**) (188 mg, 58%) as a brown solid. LCMS (Method A, UV, ESI) $R_t = 1.11$ min, $[M-H]^+ m/z = 497.9, 499.9$ (consistent with both bromine isotopes) 95% purity. M.p. 87- 90 °C. ¹H NMR (400 MHz, *d*₆-DMSO): $\delta = 8.52$ (1H, dd, $J = 1.4, 4.7$ Hz, Ar-H), 8.08 (1H, dd, $J = 1.5, 8.1$ Hz, Ar-H), 7.53 (1H, d, $J = 9.1$

Hz, Ar-H), 7.29 (1H, dd, $J = 4.8, 8.1$ Hz, Ar-H), 7.09-7.04 (2H, m, Ar-H), 6.80 (1H, t, $J = 5.8$ Hz, N-H), 4.32 (2H, d, $J = 5.8$ Hz), 4.24 (2H, s). ^{13}C NMR (100.6 MHz, d_6 -DMSO): $\delta = 203.3, 178.0, 154.1, 151.9, 151.5, 147.9, 147.6, 145.7, 140.3, 124.0, 121.5, 118.6, 118.5$ (q, $^1J_{\text{C-F}} = 256$ Hz), 114.9, 104.7, 91.2, 52.4, 48.3. IR ($\nu_{\text{max}}/\text{cm}^{-1}$) = 3064, 2235, 1700, 1606, 1460. HRMS (ESI-[+H]) m/z : Calcd for $\text{C}_{18}\text{H}_{12}^{81}\text{BrF}_3\text{N}_5\text{O}_2\text{S}$ 499.9769; Found 499.9828.

***tert*-Butyl (3-(3-bromopyridin-2-yl)-2-oxopropyl)(4-((5-chloropyridin-2-yl)oxy) - 3-cyanophenyl)carbamate (Table 1.3.3 – Entry 12)**



The reaction was conducted according to the general procedure above with bis(1,5-cyclooctadiene)diiridium(I) dichloride (0.116 g, 0.17 mmol), anhydrous toluene (1.5 mL), *tert*-butyl (4-((5-chloropyridin-2-yl)oxy)-3-cyanophenyl)carbamate (**1.1.16**) (1.19 g, 3.45 mmol) and ethyl 2-(3-bromopyridin-2-yl)acetate derived dimethylsulfoxonium species (**1.3.20**) (0.5 g, 1.72 mmol). The reaction was heated to 70 °C for 15 min. LCMS analysis at this stage showed the complete conversion of the ylide, but no discernible product formation. The reaction was therefore concluded at this stage.

5-(((3-(3-Bromopyridin-2-yl)-2-oxopropyl)amino)-2-((5-chloropyridin-2-yl)oxy)benzonitrile (1.3.13) (Table 1.3.3 – Entry 13)

Preformed according to the general procedure:

a) Ir(COD)(Imes)Cl (23 mg, 0.034 mmol); b) Dichloromethane (1.5 mL); c) ambient temperature; d) 5-amino-2-((5-chloropyridin-2-yl)oxy)benzonitrile (**1.3.2**) (127 mg, 0.517 mmol); e) ethyl 2-(3-bromopyridin-2-yl)acetate derived dimethylsulfoxonium species (**1.3.20**) (100 mg, 0.345 mmol); f) No reaction detected by LCMS analysis after 16 h; g) No purification possible.

5-((3-(3-Bromopyridin-2-yl)-2-oxopropyl)amino)-2-((5-chloropyridin-2-yl)oxy)benzonitrile (1.3.13) (Table 1.3.3 – Entry 14)

Performed according to the general procedure:

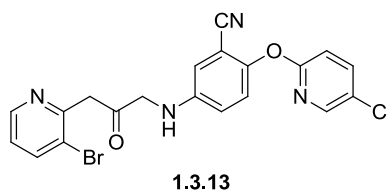
a) Ir(COD)(Imes)Cl (23 mg, 0.034 mmol); b) Toluene (1.5 mL); c) 70 °C; d) 5-amino-2-((5-chloropyridin-2-yl)oxy)benzonitrile (**1.3.2**) (169 mg, 0.689 mmol); e) ethyl 2-(3-bromopyridin-2-yl)acetate derived dimethylsulfoxonium species (**1.3.20**) (100 mg, 0.345 mmol); f) No reaction by LCMS analysis after 2 h; g) No purification possible.

5-((3-(3-Bromopyridin-2-yl)-2-oxopropyl)amino)-2-((5-chloropyridin-2-yl)oxy)benzonitrile (1.3.13) (Table 1.3.3 – Entry 15)

Performed according to the general procedure:

a) Chloro(dimethylsulfide)gold(I) (51 mg, 0.17 mmol); b) Toluene (10 mL); c) 70 °C; d) 5-amino-2-((5-chloropyridin-2-yl)oxy)benzonitrile (**1.3.2**) (635 mg, 2.58 mmol); e) ethyl 2-(3-bromopyridin-2-yl)acetate derived dimethylsulfoxonium species (**1.3.20**) (500 mg, 1.72 mmol); f) No reaction by LCMS analysis after 16 h; g) No purification possible.

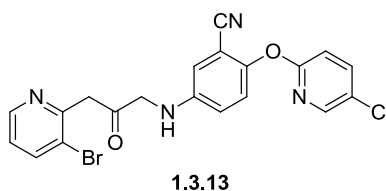
5-((3-(3-Bromopyridin-2-yl)-2-oxopropyl)amino)-2-((5-chloropyridin-2-yl)oxy)benzonitrile (1.3.13) (Scheme 1.3.23) – Inhibition Studies



To an oven dried flask was added bis(1,5-cyclooctadiene)diiridium(I) dichloride (137 mg, 0.204 mmol) and anhydrous toluene (3 mL) under a nitrogen atmosphere. The solution was heated to 70 °C and to the mixture was added 5-amino-2-((5-chloropyridin-2-yl)oxy)benzonitrile (**1.3.2**) (500 mg, 2.035 mmol). The resulting solution was stirred at 70 °C for 2 h. LCMS analysis at this stage showed no aniline degradation had occurred. To the solution was added ethyl 2-(3-bromopyridin-2-yl)acetate derived dimethylsulfoxonium species (**1.3.20**) (827 mg, 2.85 mmol) and the resulting solution was stirred at 70 °C under a

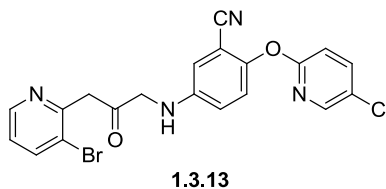
nitrogen atmosphere. After stirring for 15 minutes, LCMS analysis showed predominately unreacted starting materials with 49% aniline (**1.3.2**), with 4% of an unidentified by-product, mass and retention time were both inconsistent with the desired ketone (**1.3.13**). After stirring for 72 h, LCMS showed 51% aniline (**1.3.2**), 10% unidentified by-product, and 3% ylide (**1.3.20**). The reaction was therefore concluded at this stage.

5-((3-(3-Bromopyridin-2-yl)-2-oxopropyl)amino)-2-((5-chloropyridin-2-yl)oxy)benzotrile (1.3.13**) (Scheme 1.3.24) – Thermal Stability Assessment**



To an oven dried flask was anhydrous toluene (3 mL) under a nitrogen atmosphere and heated to 70 °C. 5-Amino-2-((5-chloropyridin-2-yl)oxy)benzotrile (**1.3.2**) (500 mg, 2.035 mmol) and ethyl 2-(3-bromopyridin-2-yl)acetate derived dimethylsulfoxonium species (**1.3.20**) (827 mg, 2.85 mmol) were added and the resulting solution was stirred at 70 °C under a nitrogen atmosphere. LCMS analysis after 72 h showed no desired product formation, with 10% unidentified by-product in addition to aniline (**1.3.2**) and reduced levels of unreacted ylide (**1.3.20**), relative to the start of the reaction. The reaction was therefore concluded at this stage.

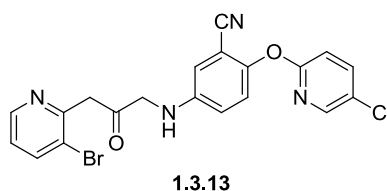
5-((3-(3-Bromopyridin-2-yl)-2-oxopropyl)amino)-2-((5-chloropyridin-2-yl)oxy)benzotrile (1.3.13**) (Scheme 1.3.25) – Catalyst Stability Assessment**



To an oven dried flask was added bis(1,5-cyclooctadiene)diiridium(I) dichloride (137 mg, 0.204 mmol) and anhydrous toluene (3 mL) under a nitrogen atmosphere. The solution was heated to 70 °C and stirred for 16 h. To the mixture was added 5-amino-2-((5-chloropyridin-2-yl)oxy)benzotrile (**1.3.2**) (500 mg, 2.035 mmol) and ethyl 2-(3-bromopyridin-2-yl)acetate

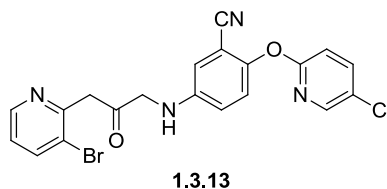
derived dimethylsulfoxonium species (**1.3.20**) (827 mg, 2.85 mmol) and the reaction stirred at 70 °C until complete by LCMS analysis. After 1 h, LCMS analysis showed 45% product (**1.3.13**) and 30% aniline (**1.3.2**) with no remaining ylide (**1.3.20**). The reaction was therefore concluded at this stage.

5-((3-(3-Bromopyridin-2-yl)-2-oxopropyl)amino)-2-((5-chloropyridin-2-yl)oxy)benzonitrile (1.3.13**) (Scheme 1.3.26) – Investigating the Influence of the Nitrile Group on Catalytic Activity**



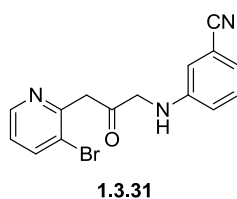
To an oven dried flask was added bis(1,5-cyclooctadiene)diiridium(I) dichloride (137 mg, 0.204 mmol) and anhydrous toluene (3 mL) under a nitrogen atmosphere. The reaction was heated to 70 °C and to the mixture was added benzonitrile (0.21 mL, 2.035 mmol). The resulting solution stirred at 70 °C for 2 h. To the mixture was added 5-amino-2-((5-chloropyridin-2-yl)oxy)benzonitrile (**1.3.2**) (500 mg, 2.035 mmol) and ethyl 2-(3-bromopyridin-2-yl)acetate derived dimethylsulfoxonium species (**1.3.20**) (827 mg, 2.85 mmol, 1.4 eq) and the reaction stirred at 70 °C until complete by LCMS. After 15 minutes, LCMS analysis showed no remaining ylide, with 55% product (**1.3.13**). The reaction was therefore concluded at this stage.

5-((3-(3-Bromopyridin-2-yl)-2-oxopropyl)amino)-2-((5-chloropyridin-2-yl)oxy)benzotrile (1.3.13) (Scheme 1.3.27) – Investigating the Influence of the Pyridyl Group on Catalytic Activity



To an oven dried flask was added bis(1,5-cyclooctadiene)diiridium(I) dichloride (137 mg, 0.204 mmol, 0.1 eq) and anhydrous toluene (3 mL) under a nitrogen atmosphere. The reaction was heated to 70 °C and to the mixture was added pyridine (0.164 mL, 2.035 mmol). The resulting solution stirred at 70 °C for 2 h. To the mixture was added 5-amino-2-((5-chloropyridin-2-yl)oxy)benzotrile (**1.3.2**) (500 mg, 2.035 mmol) and ethyl 2-(3-bromopyridin-2-yl)acetate derived dimethylsulfoxonium species (**1.3.20**) (827 mg, 2.85 mmol) and the reaction stirred at 70 °C until complete by LCMS. After 30 minutes LCMS analysis showed 5% product in addition to significant quantities of aniline and ylide. After 18 h no ylide was observed, with 48% product (**1.3.13**) in addition to aniline and potential decomposition by-products.

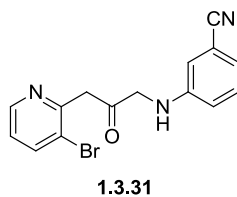
3-((3-(3-Bromopyridin-2-yl)-2-oxopropyl)amino)benzotrile (1.3.31) (Scheme 1.3.28)



To an oven dried flask was added bis(1,5-cyclooctadiene)diiridium(I) dichloride (136 mg, 0.203 mmol) and anhydrous toluene (3 mL) under a nitrogen atmosphere. The reaction was heated to 70 °C and to the mixture was added 3-aminobenzotrile (**1.3.30**) (240 mg, 2.032 mmol). The resulting solution was stirred for 2 h at 70 °C. To the mixture was added 5-ethyl 2-(3-bromopyridin-2-yl)acetate derived dimethylsulfoxonium species (**1.3.20**) (825 mg, 2.84 mmol) and the reaction stirred at 70 °C until complete by LCMS. After 15 minutes LCMS analysis showed 11% product, increasing to 30% after 1 h. After 16 h no ylide remained with

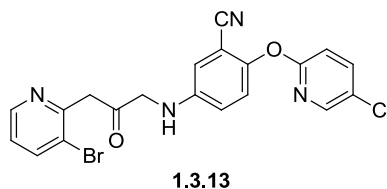
LCMS analysis showing 65% product formation. The reaction was cooled to ambient temperature and directly loaded onto a silica column. The reaction was purified by automated flash column chromatography (cyclohexane:ethyl acetate, 100:0 – 0:100, 80 g SiO₂). The appropriate fractions were combined and concentrated under reduced pressure to give 3-((3-(3-Bromopyridin-2-yl)-2-oxopropyl)amino)benzonitrile (**1.3.31**) as a brown gum (545 mg, 81%). LCMS (Method A, UV, ESI) $R_t = 0.95$ min, $[M-H]^+ m/z = 330.1, 332.1$ (consistent with both bromine isotopes) 97% purity. ¹H NMR (400 MHz, *d*₆-DMSO): $\delta = 8.52$ (1H, dd, $J = 1.3, 4.8$ Hz, Ar-H), 8.07 (1H, dd, $J = 1.5, 8.1$ Hz, Ar-H), $7.30 - 7.24$ (2H, m, Ar-H), $6.97 - 6.92$ (3H, m, Ar-H), 6.53 (1H, t, $J = 5.9$ Hz, NH), 4.26 (2H, d, $J = 5.9$ Hz), 4.23 (2H, s) (sample contained 12% ethyl acetate by mass, this is accounted for in the product yield). ¹³C NMR (100.6 MHz, *d*₆-DMSO): $\delta = 203.7, 170.7, 154.1, 148.7, 140.3, 130.0, 124.0, 121.6, 119.4, 117.2, 114.2, 111.6, 91.1, 52.3, 48.4$.

3-((3-(3-Bromopyridin-2-yl)-2-oxopropyl)amino)benzonitrile (1.3.31) (Scheme 1.3.29)



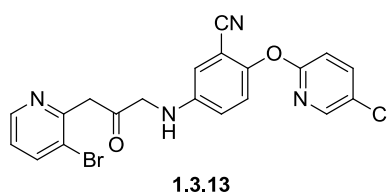
To an oven dried flask was added bis(1,5-cyclooctadiene)diiridium(I) dichloride (136 mg, 0.203 mmol) and anhydrous toluene (3 mL) under a nitrogen atmosphere. The reaction was heated to 70 °C and to the mixture was added 3-aminobenzonitrile (**1.3.30**) (240 mg, 2.032 mmol) and 5-ethyl 2-(3-bromopyridin-2-yl)acetate derived dimethylsulfoxonium species (**1.3.20**) (825 mg, 2.84 mmol) and the reaction stirred at 70 °C until complete by LCMS. After 15 minutes LCMS analysis showed 22% product, increasing to 55% after 1 h. After 16 h no ylide remained with LCMS analysis showing 64% product (**1.3.31**). The reaction was therefore concluded at this stage.

5-((3-(3-Bromopyridin-2-yl)-2-oxopropyl)amino)-2-((5-chloropyridin-2-yl)oxy)benzotrile (1.3.13) (Scheme 1.3.30) – Investigating the Influence of the Electron-Rich Pyridyl Group on Catalytic Activity



To an oven dried flask was added bis(1,5-cyclooctadiene)diiridium(I) dichloride (137 mg, 0.204 mmol) and anhydrous toluene (3 mL) under a nitrogen atmosphere. The reaction was heated to 70 °C and to the mixture was added 2-methoxypyridine (0.214 mL, 2.035 mmol). The resulting solution stirred at 70 °C for 1 h. To the mixture was added 5-amino-2-((5-chloropyridin-2-yl)oxy)benzotrile (**1.3.2**) (500 mg, 2.035 mmol) and ethyl 2-(3-bromopyridin-2-yl)acetate derived dimethylsulfoxonium species (**1.3.20**) (827 mg, 2.85 mmol) and the reaction stirred at 70 °C until complete by LCMS. After 30 minutes LCMS analysis showed 7% product (**1.3.13**) in addition to significant quantities of aniline and ylide. After 16 h no ylide was observed, with 33% product (**1.3.13**) in addition to aniline, pyridine, and potential decomposition by-products.

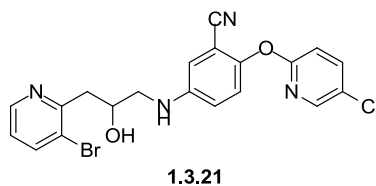
5-((3-(3-Bromopyridin-2-yl)-2-oxopropyl)amino)-2-((5-chloropyridin-2-yl)oxy)benzotrile (1.3.13) more concentrated example (Scheme 1.3.31)



The reaction was conducted according to the general procedure, above, with bis(1,5-cyclooctadiene)diiridium(I) dichloride (0.278 g, 0.414 mmol), anhydrous toluene (1.5 mL), 5-amino-2-((5-chloropyridin-2-yl)oxy)benzotrile (**1.3.2**) (1.22 g, 4.97 mmol) and ethyl 2-(3-bromopyridin-2-yl)acetate derived dimethylsulfoxonium species (**1.3.20**) (1.20 g, 4.14 mmol). The reaction was conducted at 70 °C for 1 h, and LCMS analysis at this stage indicated the reaction was complete. The mixture was purified by automated column (cyclohexane: TBME, 75:25 – 0:100, 120 g SiO₂). Removal of the solvent under reduced pressure gave 5-((3-(3-

bromopyridin-2-yl)-2-oxopropyl)amino)-2-((5-chloropyridin-2-yl)oxy)benzonitrile (**1.3.12**) as a yellow solid (1.43 g, 76%). LCMS (Method A, UV, ESI) $R_t = 1.11$ min, $[M-H]^+ m/z = 457.3, 459.3, 461.3$ (consistent with both bromine and chlorine isotopes) 100% purity. M.p. 145-148 °C. 1H NMR (400 MHz, d_6 -DMSO): $\delta = 8.52$ (1H, dd, $J = 1.5, 4.8$ Hz, Ar-H), 8.19 (1H, d, $J = 2.5$ Hz, Ar-H), 8.08 (1H, dd, $J = 1.5, 8.1$ Hz, Ar-H), 7.98 (1H, dd, $J = 2.8$ Hz, 8.8 Hz, Ar-H), 7.28 (1H, dd, $J = 4.8, 8.3$ Hz, Ar-H), 7.18 (1H, d, $J = 8.8$ Hz, Ar-H), 7.12 Hz (1H, d, $J = 8.8$ Hz, Ar-H), 7.00 (1H, d, $J = 2.8$ Hz, Ar-H), 6.97 Hz (1H, m, Ar-H), 6.50 (1H, t, $J = 5.8$ Hz, N-H), 4.28 (2H, d, $J = 5.8$ Hz, CH₂), 4.24 (2H, s, CH₂) (sample contained 8% ethyl acetate by mass, this is accounted for in the product yield). ^{13}C NMR (100.6 MHz, d_6 -DMSO): $\delta = 203.8, 161.6, 154.1, 147.9, 146.0, 145.3, 144.7, 140.3, 140.1, 125.4, 124.0, 123.8, 121.6, 118.8, 116.2, 114.1, 112.5, 106.1, 52.6, 48.5$. IR (ν_{max}/cm^{-1}) = 3389, 1716, 1610, 1233. HRMS (ESI-[+H]) m/z : Calcd for C₂₀H₁₅⁷⁹BrClN₄O₂ 457.0067; Found 457.0068.

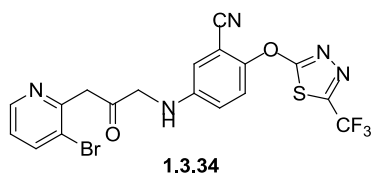
5-((3-(3-Bromopyridin-2-yl)-2-hydroxypropyl)amino)-2-((5-chloropyridin-2-yl)oxy)benzonitrile (1.3.21) (Scheme 1.3.32)



To a solution of anhydrous DCM (30 mL) and MeOH (30 mL) was added 5-((3-(3-bromopyridin-2-yl)-2-oxopropyl)amino)-2-((5-chloropyridin-2-yl)oxy) benzonitrile (**1.3.13**) (2.25 g, 4.92 mmol) and the resulting solution cooled to 0 °C. To the cooled solution was added sodium borohydride (0.19 g, 4.92 mmol) and the resulting solution was stirred at 0 °C under a nitrogen atmosphere for 20 minutes. The reaction was complete as monitored by LCMS at this stage. The reaction was quenched by the slow addition of water (25 mL) and saturated aqueous NH₄Cl (25 mL) and the resulting biphasic mixture separated. The aqueous phase was extracted with ethyl acetate (3 x 50 mL). The combined organic extracts were washed with brine (25 mL) and the organic phase passed through a hydrophobic frit. The solvent was removed under reduced pressure to give the crude product as a brown oil. The crude product was purified by automated flash column chromatography (ethyl acetate: cyclohexane, 0:100 - 100:0, 120 g SiO₂). Removal of the solvent under reduced pressure gave the product (**1.3.21**) as a pale white solid (2.13 g, 94%). LCMS (Method A, UV, ESI) $R_t = 1.07$ min, $[M-H]^+ m/z = 459.1, 461.1$ (consistent with both bromine isotopes) 100% purity.

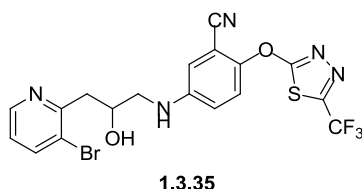
M.p. 77-80 °C. ¹H NMR (400 MHz, *d*₆-DMSO): δ = 8.53 (1H, dd, *J* = 1.4, 4.7 Hz, Ar-H), 8.19 (1H, d, *J* = 2.8 Hz, Ar-H), 8.04 (1H, dd, *J* = 1.5, 8.1 Hz, Ar-H), 7.98 (1H, dd, *J* = 2.8, 8.8 Hz, Ar-H), 7.22 (1H, dd, *J* = 4.8, 8.1 Hz, Ar-H), 7.17 (1H, d, *J* = 8.8 Hz, Ar-H), 7.09 (1H, d, *J* = 8.8 Hz, Ar-H), 6.97-6.93 (2H, m, Ar-H), 6.20 (1H, t, *J* = 5.9 Hz, N-H), 4.98 (1H, d, *J* = 5.29 Hz, O-H), 4.27 (1H, m), 3.19-3.16 (2H, m), 3.10-3.07 (2H, m). ¹³C NMR (100.6 MHz, *d*₆-DMSO): δ = 161.7, 157.2, 147.7, 146.8, 145.4, 144.2, 140.3, 140.1, 125.4, 123.9, 123.2, 121.5, 118.5, 116.3, 113.7, 112.4, 106.1, 67.7, 48.9, 42.1. IR (*ν*_{max}/cm⁻¹) = 3381 (br), 2925, 1611, 1456. HRMS (ESI-[+H]) *m/z*: Calcd for C₂₀H₁₇⁷⁹BrClN₄O₂ 459.0223; Found 459.0223.

5-((3-(3-Bromopyridin-2-yl)-2-oxopropyl)amino)-2-((5-(trifluoromethyl)-1,3,4-thiadiazol-2-yl)oxy)benzotrile (1.3.34) (Scheme 1.3.37)



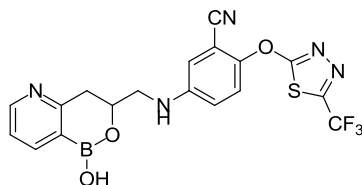
The reaction was conducted according to the general procedure above with bis(1,5-cyclooctadiene)diiridium(I) dichloride (0.235 g, 0.35 mmol), anhydrous toluene (1.5 mL), 5-amino-2-((5-(trifluoromethyl)-1,3,4-thiadiazol-2-yl)oxy)benzotrile (**1.3.29**) (1.48 g, 5.17 mmol) and ethyl 2-(3-bromopyridin-2-yl)acetate derived dimethylsulfoxonium (**1.3.20**) (1.0 g, 3.5 mmol). The reaction was conducted at 70 °C for 1 h, LCMS analysis at this stage indicated the reaction was complete. The reaction was cooled to ambient temperature and the mixture was purified by automated column (ethyl acetate: cyclohexane, 30:70 – 100:0, 120 g SiO₂). Removal of the solvent under reduced pressure gave 5-((3-(3-bromopyridin-2-yl)-2-oxopropyl)amino)-2-((5-(trifluoromethyl)-1,3,4-thiadiazol-2-yl)oxy)benzotrile (**1.3.34**) (1.04 g, 61%) as a dark brown solid. LCMS (Method A, UV, ESI) *R*_t = 1.11 min, [M-H]⁺ *m/z* = 497.9, 499.9 (consistent with both bromine isotopes) 100% purity. M.p. 87-90 °C. ¹H NMR (400 MHz, *d*₆-DMSO): δ = 8.52 (1H, dd, *J* = 1.4, 4.7 Hz, Ar-H), 8.08 (1H, dd, *J* = 1.5, 8.1 Hz, Ar-H), 7.53 (1H, d, *J* = 9.1 Hz, Ar-H), 7.29 (1H, dd, *J* = 4.8, 8.1 Hz, Ar-H), 7.09-7.04 (2H, m, Ar-H), 6.80 (1H, t, *J* = 5.8 Hz, N-H), 4.32 (2H, d, *J* = 5.8 Hz), 4.24 (2H, s). ¹³C NMR (100.6 MHz, *d*₆-DMSO): δ = 203.3, 178.0, 154.1, 151.9, 151.5, 147.9, 147.6, 145.7, 140.3, 124.0, 121.5, 118.6, 118.5 (q, ¹*J*_{C-F} = 256 Hz), 114.9, 104.7, 91.2, 52.4, 48.3. IR (*ν*_{max}/cm⁻¹) = 3064, 2235, 1700, 1606, 1460. HRMS (ESI-[+H]) *m/z*: Calcd for C₁₈H₁₂⁸¹BrF₃N₅O₂S 499.9769; Found 499.9828.

5-((3-(3-Bromopyridin-2-yl)-2-hydroxypropyl)amino)-2-((5-(trifluoromethyl)-1,3,4-thiadiazol-2-yl)oxy)benzonitrile (1.3.35)



To a solution of anhydrous DCM (10 mL) and anhydrous MeOH (10 mL) was added 5-((3-(3-bromopyridin-2-yl)-2-oxopropyl)amino)-2-((5-(trifluoromethyl)-1,3,4-thiadiazol-2-yl)oxy)benzonitrile (**1.3.34**) (720 mg, 1.45 mmol) and the resulting solution was cooled to 0 °C. To the cooled solution was added sodium borohydride (55 mg, 1.45 mmol) and the resulting solution was stirred at 0 °C under a nitrogen atmosphere for 1 h. LCMS analysis indicated the reaction was complete at this stage. The reaction was quenched by the slow addition of water (10 mL) and saturated aqueous NH₄Cl (10 mL) and the biphasic mixture separated. The aqueous phase was extracted with ethyl acetate (3 x 50 mL) and LCMS analysis indicated no remaining product in the aqueous phase at this stage. The combined organic extracts were passed through a hydrophobic frit and the solvent removed under reduced pressure to give the crude product as a brown oil (approximately 800 mg). The crude product was purified by automated column chromatography (cyclohexane: ethyl acetate, 80:20 - 0:100, 80 g SiO₂). The solvent was removed under reduced pressure to give 5-((3-(3-bromopyridin-2-yl)-2-hydroxypropyl)amino)-2-((5-(trifluoromethyl)-1,3,4-thiadiazol-2-yl)oxy)benzonitrile (**1.3.35**) (657 mg, 1.31 mmol, 91%) as a yellow gum. LCMS (Method A, UV, ESI) $R_t = 1.18$ min, $[M-H]^+$ $m/z = 500.0, 501.9$ (consistent with both bromine isotopes) 100% purity. ¹H NMR (400 MHz, *d*₆-DMSO): $\delta = 8.53$ (1H, dd, $J = 1.5, 4.5$, Ar-H), 8.04 (1H, dd, $J = 1.5, 8.1$ Hz, Ar-H), 7.50 (1H, d, $J = 9.1$ Hz, Ar-H), 7.22 (1H, dd, $J = 4.8, 8.1$ Hz, Ar-H), 7.05 (1H, d, $J = 3.0$ Hz, Ar-H), 7.02 (1H, dd, $J = 3.0, 9.1$ Hz, Ar-H), 6.54 (1H, t, $J = 5.8$ Hz, N-H), 5.00 (1H, d, $J = 5.3$ Hz, O-H), 4.28 (1H, m), 3.22 (1H, m), $3.16-3.06$ (3H, m) (sample contained 2% ethyl acetate by mass, this is accounted for in the product yield). ¹³C NMR (100.6 MHz, *d*₆-DMSO): $\delta = 178.3, 157.1, 152.1$ (q, $^2J_{C-F} = 38.2$ Hz), $148.4, 147.8, 145.2, 140.3, 123.8, 122.9, 122.0, 120.4$ (q, $^1J_{C-F} = 272.2$ Hz), $118.7, 115.6, 114.6, 105.3, 67.7, 48.7, 42.0$. ¹⁹F NMR (376.5 MHz, *d*₆-DMSO): $\delta = -59.43$ (CF₃). IR (ν_{max}/cm^{-1}) = 3381 (br), 1606, 1457, 1032. HRMS (ESI-[+H]) m/z : Calcd for C₁₈H₁₄⁷⁹BrF₃N₅O₂S 500.0004; Found 500.0014.

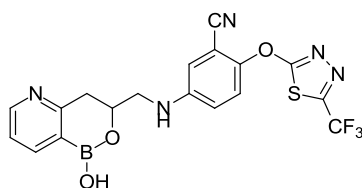
5-(((1-Hydroxy-3,4-dihydro-1*H*-[1,2]oxaborinino[4,3-*b*]pyridin-3-yl)methyl)amino)-2-((5-(trifluoromethyl)-1,3,4-thiadiazol-2-yl)oxy)benzonitrile (Scheme 1.3.39) (1.3.32)



1.3.32

To a solution of 5-((3-(3-bromopyridin-2-yl)-2-hydroxypropyl)amino)-2-((5-(trifluoromethyl)-1,3,4-thiadiazol-2-yl)oxy)benzonitrile (**1.3.35**) (50 mg, 0.10 mmol) and potassium acetate (60 mg, 0.61 mmol) in anhydrous 1,4-dioxane (2 mL) was added 4,4,4',4',5,5,5',5'-octamethyl-2,2'-bi(1,3,2-dioxaborolane) (93 mg, 0.37 mmol). The reaction vessel was purged with nitrogen after which 1,4-bis(diphenylphosphino)butane-palladium(II) chloride (7.3 mg, 0.01 mmol) was added to the mixture. The resulting reaction mixture was purged with nitrogen and heated to 100 °C for 16 h. LCMS analysis at this stage revealed potential fragmentation of the starting material and decomposition, with no desired product (**1.3.32**) formation. The reaction was therefore concluded at this stage.

5-(((1-Hydroxy-3,4-dihydro-1*H*-[1,2]oxaborinino[4,3-*b*]pyridin-3-yl)methyl)amino)-2-((5-(trifluoromethyl)-1,3,4-thiadiazol-2-yl)oxy)benzonitrile (Scheme 1.3.40) (1.3.32)

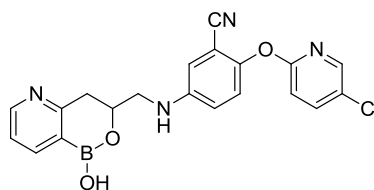


1.3.32

To a solution of 5-((3-(3-bromopyridin-2-yl)-2-hydroxypropyl)amino)-2-((5-(trifluoromethyl)-1,3,4-thiadiazol-2-yl)oxy)benzonitrile (**1.3.35**) (300 mg, 0.60 mmol) and potassium acetate (361 mg, 3.68 mmol) in anhydrous 1,4-dioxane (10 mL) in a pyrex sealed tube stirred at ambient temperature was added 4,4,4',4',5,5,5',5'-octamethyl-2,2'-bi(1,3,2-dioxaborolane) (228 mg, 0.90 mmol). The reaction vessel was purged with nitrogen for 1 min

after which PdCl₂(dppf) (22 mg, 0.03 mmol) was added. The reaction vessel was purged with nitrogen. The resulting solution was heated in Biotage Initiator (Microwave) for 30 minutes at 130 °C. The solvent was removed under reduced pressure and the resulting brown solid dissolved in DCM (100 mL). The organic phase was washed with water (50 mL) and brine (20 mL). LCMS of the aqueous phase showed no product. The organic phase was passed through a hydrophobic frit and the solvent removed under reduced pressure to give the crude mixture as a brown oil (100 mg). The crude product was dissolved in DMSO (1 mL) and purified by mass directed automatic purification. Removal of the solvent under reduced pressure gave 5-(((1-hydroxy-3,4-dihydro-1*H*-[1,2]oxaborinino[4,3-*b*]pyridin-3-yl)methyl)amino)-2-((5-(trifluoromethyl)-1,3,4-thiadiazol-2-yl)oxy)benzotrile (**1.3.32**) (101 mg, 38%). LCMS (Method A, UV, ESI) *R*_t = 0.77 min, [M-H]⁺ *m/z* = 466.2, 95% purity. ¹H NMR (400 MHz, *d*₆-DMSO): δ = 8.54 (1H, dd, *J* = 1.7, 4.9 Hz, Ar-H), 8.31 (1H, s, br), 8.03 (1H, dd, *J* = 1.5, 7.3, Ar-H), 7.52 (1H, d, *J* = 9.0 Hz, Ar-H), 7.28 (1H, dd, *J* = 5.0, 7.2 Hz, Ar-H), 7.04-7.14 (2H, m, Ar-H), 6.64 (1H, t, *J* = 5.6 Hz), 4.45 (1H, qd, *J* = 5.2, 9.7 Hz), 3.30-3.43 (2H, m), 3.00-3.08 (2H, m). ¹³C NMR (100.6 MHz, *d*₆-DMSO): δ = 178.3, 164.1, 151.6 (q, ²*J*_{C-F} = 38.9 Hz), 151.3, 148.2, 145.4, 140.5, 122.7, 122.5, 121.9, 118.5 (q, ¹*J*_{C-F} = 272.9 Hz), 118.2, 115.0, 114.2, 104.9, 71.4, 48.0, 37.4. IR (*v*_{max}/cm⁻¹) = 2901, 1606, 1585, 1458, 1326. HRMS (ESI-[+H]) *m/z*: Calcd for C₁₈H₁₄BF₃N₅O₃S 448.0863; Found 448.0872.

2-((5-Chloropyridin-2-yl)oxy)-5-(((1-hydroxy-3,4-dihydro-1*H*-[1,2]oxaborinino[4,3-*b*]pyridin-3-yl)methyl)amino)benzotrile (1.1.10**) (Scheme 1.4.2)**

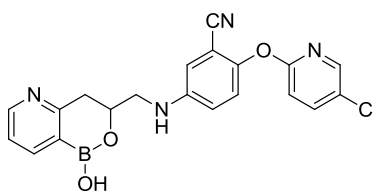


1.1.10

To a microwave vial was added 5-((3-(3-bromopyridin-2-yl)-2-hydroxypropyl)amino)-2-((5-chloropyridin-2-yl)oxy)benzotrile (**1.3.20**) (100 mg, 0.218 mmol, 1.0 eq), 4,4,4',4',5,5,5',5'-octamethyl-2,2'-bi(1,3,2-dioxaborolane) (203 mg, 0.798 mmol) and potassium acetate (132 mg, 1.342 mmol). The resulting solids were dissolved in anhydrous 1,4-dioxane (3 mL) and the solution degassed for 5 minutes. To the mixture was added PdCl₂(dppf) (8.0 mg, 0.011 mmol). The reaction mixture was degassed and heated to 100 °C. After 2 h LCMS analysis showed complete reaction conversion, with 55% product and 26% by-product. The reaction

was cooled to ambient temperature and the solvent removed under reduced pressure. The resulting mixture was purified by mass directed autopurification to give a brown gum (40 mg, 45%). LCMS analysis of this gum showed 89% product and 11% dehalogenated/deborylated by-product. The impure material was used in the following reaction without further purification.

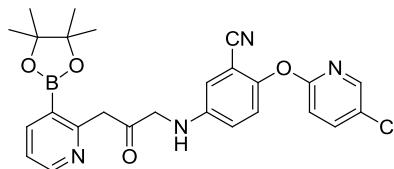
2-((5-Chloropyridin-2-yl)oxy)-5-(((1-hydroxy-3,4-dihydro-1*H*-[1,2]oxaborinino [4,3-*b*]pyridin-3-yl)methyl)amino)benzonitrile (1.1.10) (Scheme 1.4.3) – Stability assessment



1.1.10

To a microwave vial was added crude 2-((5-chloropyridin-2-yl)oxy)-5-(((1-hydroxy-3,4-dihydro-1*H*-[1,2]oxaborinino[4,3-*b*]pyridin-3-yl)methyl)amino)benzonitrile (**1.1.10**) (38 mg, 0.093 mmol), 4,4,4',4',5,5,5',5'-octamethyl-2,2'-bi(1,3,2-dioxaborolane) (87 mg, 0.343 mmol) and potassium acetate (57 mg, 0.577 mmol). The resulting solids were dissolved in anhydrous 1,4-dioxane (1.5 mL) and the solution degassed for 5 minutes. To the mixture was added PdCl₂(dppf) (3.4 mg, 4.7 μmol). LCMS analysis at stage showed 90% product in addition to by-product and low levels of catalyst. The reaction mixture was degassed and heated to 100 °C. LCMS analysis after 4 h and 16 h both showed an unchanged reaction composition, with 90% borylated product (**1.1.10**). The reaction was therefore concluded at this stage.

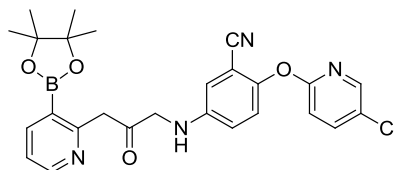
2-((5-Chloropyridin-2-yl)oxy)-5-((2-oxo-3-(3-(4,4,5,5-tetramethyl-1,3,2-dioxaborolan-2-yl)pyridin-2-yl)propyl)amino)benzonitrile (1.4.1) (Scheme 1.4.4 – a))



1.4.1

To a microwave vial was added 5-((3-(3-bromopyridin-2-yl)-2-oxopropyl)amino)-2-((5-chloropyridin-2-yl)oxy)benzonitrile (**1.3.13**) (18 mg, 0.039 mmol), 4,4,4',4',5,5,5',5'-octamethyl-2,2'-bi(1,3,2-dioxaborolane) (36.7 mg, 0.144 mmol) and potassium acetate (23 mg, 0.241 mmol). The resulting solids were dissolved in anhydrous 1,4-dioxane (1 mL) and the solution degassed for 5 minutes. To the mixture was added PdCl₂(dppf) (1.4 mg, 2.0 μmol, 0.05 eq). The reaction mixture was degassed and heated to 100 °C until complete by LCMS. After 16 h, LCMS analysis showed 20% aniline (**1.3.2**) in addition to a complicated mixture of unidentified products. The reaction was therefore concluded at this stage.

2-((5-Chloropyridin-2-yl)oxy)-5-((2-oxo-3-(3-(4,4,5,5-tetramethyl-1,3,2-dioxaborolan-2-yl)pyridin-2-yl)propyl)amino)benzonitrile (1.4.1) (Scheme 1.4.4 – b))

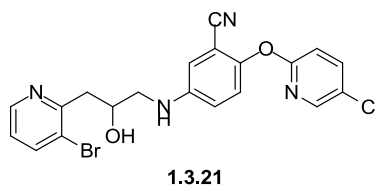


1.4.1

To a microwave vial was added tricyclohexylphosphine (4.4 mg, 0.016 mmol) and bis(dibenzylideneacetone)palladium(0) (3.8 mg, 6.60 μmol) under a nitrogen atmosphere. To the mixture was added 1,4-dioxane (4 mL) and the mixture stirred for 30 minutes. To the resulting mixture was added potassium acetate (32 mg, 0.328 mmol), 4,4,4',4',5,5,5',5'-octamethyl-2,2'-bi(1,3,2-dioxaborolane) (61 mg, 0.240 mmol) and 5-((3-(3-bromopyridin-2-yl)-2-oxopropyl)amino)-2-((5-chloropyridin-2-yl)oxy)benzonitrile (**1.3.13**) (100 mg, 0.218 mmol) successively and the resulting mixture placed under a nitrogen atmosphere and stirred

at 80 °C until complete by LCMS. After 16 h, LCMS analysis showed no significant reaction had occurred and the reaction was therefore concluded at this stage.

5-((3-(3-Bromopyridin-2-yl)-2-hydroxypropyl)amino)-2-((5-chloropyridin-2-yl)oxy)benzonitrile (1.3.21) (Attempted CBS Reduction)

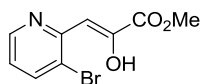


To an oven dried flask was added 5-((3-(3-bromopyridin-2-yl)-2-oxopropyl)amino)-2-((5-chloropyridin-2-yl)oxy)benzonitrile (**1.3.13**) (200 mg, 0.437 mmol) and anhydrous THF (3 mL) under a nitrogen atmosphere. The resulting solution was cooled to 0 °C and to the cooled solution was slowly added (*R*)-1-methyl-3,3-diphenylhexahydropyrrolo[1,2-*c*][1,3,2]oxazaborole (1M in toluene) (0.087 mL, 0.087 mmol). To the resulting solution was added dropwise borane (1M solution in THF) (0.437 mL, 0.437 mmol) and the resulting solution stirred at 0 °C until complete by LCMS. After 2 h no reaction was observed by LCMS. To the reaction was added borane (1M solution in THF) (1.31 mL, 1.31 mmol) was added dropwise and the reaction stirred at 0 °C for 3 h. The reaction was warmed to ambient temperature and stirred for 16 h. To the solution was added a mixture of cooled water (5 mL) and methanol (5 mL). The biphasic mixture was separated and the aqueous phase extracted with ethyl acetate (5 x 10 mL). The combined organic extracts were passed through a hydrophobic frit and the solvent removed under reduced pressure to give the crude product as a brown solid (250 mg). The crude product was purified by automated flash column chromatography (ethyl acetate: cyclohexane, 0:100 - 100:0, 12 g SiO₂). The solvent was removed under reduced pressure to give 5-((3-(3-bromopyridin-2-yl)-2-hydroxypropyl)amino)-2-((5-chloropyridin-2-yl)oxy)benzonitrile (**1.3.21**) (112 mg, 56%) as a pale white solid. LCMS (Method A, UV, ESI) $R_t = 1.07$ min, $[M-H]^+ m/z = 459.1, 461.1$ (consistent with both bromine isotopes) 100% purity. M.p. 77-80 °C. ¹H NMR (400 MHz, *d*₆-DMSO): $\delta = 8.53$ (1H, dd, $J = 1.4, 4.7$ Hz, Ar-H), 8.19 (1H, d, $J = 2.8$ Hz, Ar-H), 8.04 (1H, dd, $J = 1.5, 8.1$ Hz, Ar-H), 7.98 (1H, dd, $J = 2.8, 8.8$, Ar-H), 7.22 (1H, dd, $J = 4.8, 8.1$ Hz, Ar-H), 7.17 (1H, d, $J = 8.8$ Hz, Ar-H), 7.09 (1H, d, $J = 8.8$ Hz, Ar-H), 6.97-6.93 (2H, m, Ar-H), 6.20 (1H, t, $J = 5.9$ Hz, N-H), 4.98 (1H, d, $J = 5.29$ Hz, O-H), 4.27 (1H, m), 3.19-3.16 (2H, m), 3.10-3.07 (2H, m). ¹³C NMR (100.6 MHz, *d*₆-DMSO): $\delta = 161.7, 157.2, 147.7, 146.8,$

145.4, 144.2, 140.3, 140.1, 125.4, 123.9, 123.2, 121.5, 118.5, 116.3, 113.7, 112.4, 106.1, 67.7, 48.9, 42.1. IR ($\nu_{\max}/\text{cm}^{-1}$) = 3381 (br), 2925, 1611, 1456. HRMS (ESI-[+H]) m/z : Calcd for $\text{C}_{20}\text{H}_{17}^{79}\text{BrClN}_4\text{O}_2$ 459.0223; Found 459.0223.

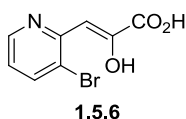
*Chiral HPLC and Mosher's acid method both showed no enantioselectivity for the reaction.*³¹⁹

(Z)-Methyl 3-(3-bromopyridin-2-yl)-2-hydroxyacrylate (**1.5.7**)

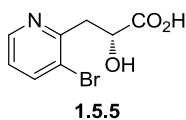


1.5.7

A mixture of methyl 2,2,2-trimethoxyacetate (3.59 mL, 24.71 mmol) and anhydrous tetrahydrofuran (20 mL) was cooled to 0 °C under a nitrogen atmosphere. To the mixture was added dropwise 3-bromo-2-methylpyridine (1.67 mL, 14.53 mmol) and the resulting mixture stirred for 10 min. To the cooled solution was added dropwise lithium bis(trimethylsilyl)amide (1M in THF) (31.20 mL, 31.20 mmol) and the resulting solution warmed to ambient temperature and stirred for 16 h. To the mixture was added 2M aqueous HCl (40 mL) and the resulting mixture stirred for 1 h. The reaction was neutralised by the addition of saturated aqueous NaHCO_3 and to the mixture was added ethyl acetate (50 mL). The resulting biphasic mixture was separated and the aqueous phase extracted with ethyl acetate (3 x 50 mL). The combined organic extracts were washed with brine, passed through a hydrophobic frit, and concentrated under reduced pressure to give the crude product as a yellow solid (3.2 g). The crude product was purified by automated flash column chromatography (cyclohexane:TBME, 100:0 - 40:60, 120 g SiO_2). The appropriate fractions were combined and concentrated under reduced pressure to give methyl (Z)-3-(3-bromopyridin-2-yl)-2-hydroxyacrylate (**1.5.7**) (2.90 g, 77%) as a yellow solid. LCMS (Method C, UV, ESI) R_t = 0.94, $[\text{M}-\text{H}]^+$ m/z = 258.0, 260.0 (consistent with both bromine isotopes), 100% purity. M.p. 118-120 °C. ^1H NMR (400 MHz, d_6 -DMSO): δ = 14.62 (1H, s), 8.55 (1H, dd, J = 1.3, 5.0 Hz), 8.24 (1H, dd, J = 1.3, 8.2 Hz), 7.29 (1H, dd, J = 5.1, 8.1 Hz), 6.79 (1H, s), 3.82 (3H, s). ^{13}C NMR (100.6 MHz, d_6 -DMSO): δ = 163.3, 154.0, 153.6, 144.6, 142.2, 122.8, 117.9, 99.8, 52.5. IR ($\nu_{\max}/\text{cm}^{-1}$) = 3080, 2948, 1726, 1612, 1569. HRMS (ESI-[+H]) m/z : Calcd for $\text{C}_9\text{H}_9^{79}\text{BrNO}_3$ 257.9760; Found 257.9755.

(Z)-3-(3-Bromopyridin-2-yl)-2-hydroxyacrylic acid (1.5.6)

To a solution of methyl (Z)-3-(3-bromopyridin-2-yl)-2-hydroxyacrylate (**1.5.7**) (1.13 g, 4.38 mmol) in anhydrous 1,4-dioxane (20 mL) was added lithium hydroxide (1M aqueous solution) (8.76 mL, 8.76 mmol) and the resulting solution heated to 60 °C for 1 h. The reaction was cooled to ambient temperature and acidified by the slow addition of 2M aqueous HCl. To the mixture was added DCM (25 mL) and the resulting biphasic mixture separated. The aqueous phase was extracted with DCM (3 x 20 mL). The combined organic extracts were washed with brine, passed through a hydrophobic frit, and concentrated under reduced pressure to afford (Z)-3-(3-bromopyridin-2-yl)-2-hydroxyacrylic acid (**1.5.6**) (0.975 g, 91%) as a yellow solid. LCMS (Method C, UV, ESI) $R_t = 0.76$, $[M-H]^+$ $m/z = 244.0, 246.0$ (consistent with both bromine isotopes), 100% purity. M.p. 185-186 °C. 1H NMR (400 MHz, d_6 -DMSO): $\delta = 14.42$ (1H, s), 13.30 (1H, s), 8.56 (1H, dd, $J = 1.3, 5.0$ Hz), 8.24 (1H, dd, $J = 1.3, 8.2$ Hz), 7.29 (1H, dd, $J = 4.9, 8.1$ Hz), 6.81 (1H, s). ^{13}C NMR (100.6 MHz, d_6 -DMSO): $\delta = 164.2, 154.7, 153.9, 144.8, 142.2, 122.7, 117.9, 99.6$. IR (ν_{max}/cm^{-1}) = 3458, 3099, 1731, 1609, 1564, 1235. HRMS (ESI-[+H]) m/z : Calcd for $C_8H_7^{79}BrNO_3$ 243.9604; Found 243.9598.

(R)-3-(3-Bromopyridin-2-yl)-2-hydroxypropanoic acid (1.5.5)

To a mixture of (Z)-3-(3-bromopyridin-2-yl)-2-hydroxyacrylic acid (**1.5.6**) (870 mg, 3.56 mmol), (*R,R*)-teth-TsDPEN RuCl (11.05 mg, 0.018 mmol), and anhydrous methanol (20 mL) was added triethylamine (1.491 mL, 10.69 mmol), followed by formic acid (0.547 mL, 14.26 mmol) and the resulting mixture stirred under a nitrogen atmosphere for 16 h. To the mixture was added 2-MeTHF (20 mL) and 1M aqueous NaOH (15 mL). The biphasic mixture was separated and the organic phase extracted with 1M aqueous NaOH (3 x 5 mL). The combined aqueous extracts were acidified to pH 2-3 by the addition of 2M aqueous HCl. To the mixture was added 2-MeTHF (20 mL) and the biphasic was separated. The aqueous phase was extracted with 2-MeTHF (3 x 20 mL). The combined organic extracts were concentrated under

reduced pressure to give (*R*)-3-(3-bromopyridin-2-yl)-2-hydroxypropanoic acid (**1.5.5**) (850 mg, 97%) a yellow gum. LCMS (Method C, UV, ESI) $R_t = 0.49$, $[M-H]^+ m/z = 246.0, 248.0$ (consistent with both bromine isotopes), 94% purity. 1H NMR (400 MHz, d_6 -DMSO): $\delta = 8.49$ (1H, dd, $J = 1.2, 4.6$ Hz), 8.02 (1H, dd, $J = 1.5, 8.1$ Hz), 7.21 (1H, dd, $J = 4.6, 8.1$ Hz), 4.55 (1H, dd, $J = 5.7, 7.7$ Hz), $3.28-3.15$ (2H, m), 2 exchangeable protons not observed. ^{13}C NMR (100.6 MHz, d_6 -DMSO): $\delta = 174.9, 156.1, 147.7, 140.2, 123.3, 121.4, 68.9, 41.0$. IR (ν_{max}/cm^{-1}) = 3397, 2912, 1713, 1037. HRMS (ESI-[+H]) m/z : Calcd for $C_8H_9^{79}BrNO_3$ 245.9766; Found 245.9769.

Chiral analytical chromatography was carried out by Eric Hortense, Analytical Chemistry, GSK, Stevenage.²³² The HPLC was conducted on a Chiralpak ICTM column (250 mm x 4.6 mm i.d. 5 μ m packing diameter).

The solvents employed were:

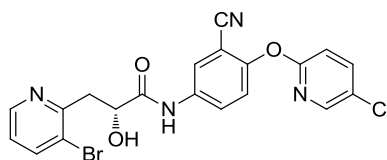
A = 0.1% v/v TFA in heptane.

B = EtOH.

The elution gradient used was 0.7:0.3 A:B with a flow rate of 1 mL/min over 20 min.

$R_t = 6.65$ min (*R*)-enantiomer and 6.80 min (*S*)-enantiomer. Integration of the relative peaks areas gave a ee value 99% for the (*R*)-enantiomer (**1.5.5**).

(*R*)-3-(3-Bromopyridin-2-yl)-*N*-(4-((5-chloropyridin-2-yl)oxy)-3-cyanophenyl)-2-hydroxypropanamide (1.5.4)

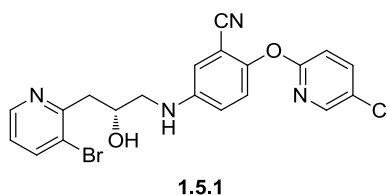


1.5.4

A mixture of anhydrous *N,N*-dimethylacetamide (5 mL), 5-amino-2-((5-chloropyridin-2-yl)oxy)benzotrile (**1.3.2**) (879 mg, 3.58 mmol), and (*R*)-3-(3-bromopyridin-2-yl)-2-hydroxypropanoic acid (**1.5.5**) (800 mg, 3.25 mmol) was cooled to 0 °C and to the mixture was added EDC.HCl (935 mg, 4.88 mmol). The reaction was stirred at 0 °C for 1 h. To the mixture was added water (15 mL) and the resulting mixture stirred at ambient temperature overnight. The resulting mixture was filtered, washing with water, and the resulting solid dried under reduced pressure to give the crude product as a yellow solid (2 g). The crude product

was purified by automated column chromatography (cyclohexane:ethyl acetate, 100:0 - 0:100, 120 g SiO₂). The appropriate fractions were combined and concentrated under reduced pressure to give a mixture of aniline and product. Addition of methanol and filtration gave (*R*)-3-(3-bromopyridin-2-yl)-*N*-(4-((5-chloropyridin-2-yl)oxy)-3-cyanophenyl)-2-hydroxypropanamide (**1.5.4**) (950 mg, 62%) as a white solid. LCMS (Method C, UV, ESI) $R_t = 1.12$, $[M-H]^+ m/z = 473, 475$ (consistent with both bromine isotopes), 99% purity. M.p. 207-208 °C. ¹H NMR (400 MHz, *d*₆-DMSO): $\delta = 10.23$ (1H, s), 8.51 (1H, dd, $J = 1.5, 4.6$ Hz), 8.25-8.20 (2H, m), 8.07-8.01 (3H, m), 7.37 (1H, d, $J = 9.0$ Hz), 7.28 (1H, d, $J = 8.6$ Hz), 7.22 (1H, dd, $J = 4.6, 8.1$ Hz), 6.03 (1H, s), 4.71 (1H, m), 3.20-3.18 (2H, m). ¹³C NMR (100.6 MHz, *d*₆-DMSO): $\delta = 172.8, 161.0, 156.1, 150.3, 147.7, 145.5, 140.4, 140.2, 136.3, 126.4, 126.1, 123.7, 123.4, 121.5, 115.5, 113.0, 105.7, 70.8, 48.6$ (one carbon not observed). IR ($\nu_{\max}/\text{cm}^{-1}$) = 3287, 1666, 1549, 1457. HRMS (ESI-[+H]) m/z : Calcd for C₂₀H₁₅⁷⁹BrClN₄O₃ 473.0016; Found 472.9996.

(*R*)-5-((3-(3-Bromopyridin-2-yl)-2-hydroxypropyl)amino)-2-((5-chloropyridin-2-yl)oxy)benzonitrile (1.5.1)



To a heat dried flask was added (*R*)-3-(3-bromopyridin-2-yl)-*N*-(4-((5-chloropyridin-2-yl)oxy)-3-cyanophenyl)-2-hydroxypropanamide (**1.5.4**) (0.250 g, 0.528 mmol) and anhydrous tetrahydrofuran (7.5 mL) under a nitrogen atmosphere. To the reaction was added boron trifluoride diethyl etherate (0.130 mL, 1.055 mmol), followed by the dropwise addition of borane tetrahydrofuran complex (1M in THF) (1.583 mL, 0.633 mmol). The resulting mixture was heated to 65 °C and stirred for 48 h. The reaction was cooled to 0 °C and to the mixture was added methanol (2 mL). The reaction was stirred for 5 min and to the mixture was added 2M aqueous NaOH (2 mL). The resulting mixture was stirred for 1 h. To the mixture was added water (10 mL) and DCM (10 mL) and the biphasic mixture separated. The aqueous phase was extracted with DCM (3 x 10 mL). The combined organic extracts were passed through a hydrophobic frit and concentrated under reduced pressure to give the crude product as a yellow oil (600 mg). The crude product was purified by automated flash column

Confidential – Property of GSK – Do Not Copy

chromatography (cyclohexane:TBME, 100:0 – 0:100, 80 g SiO₂). The appropriate fractions were combined and concentrated under reduced pressure to give (*R*)-5-((3-(3-bromopyridin-2-yl)-2-hydroxypropyl)amino)-2-((5-chloropyridin-2-yl)oxy)benzo nitrile (**1.5.1**) (214 mg, 88%) as a white solid. LCMS (Method C, UV, ESI) $R_t = 1.14$, $[M-H]^+ m/z = 459, 461$ (consistent with both bromine isotopes), 100% purity. ¹H NMR (400 MHz, *d*₆-DMSO): $\delta = 8.52$ (1H, dd, $J = 1.5, 4.9$ Hz), 8.18 (1H, d, $J = 2.2$ Hz), 8.03 (1H, dd, $J = 1.5, 8.1$ Hz), 7.97 (1H, dd, $J = 2.8, 8.7$ Hz), 7.22 (1H, dd, $J = 4.6, 8.1$ Hz), 7.16 (1H, d, $J = 8.8$ Hz), 7.08 (1H, d, $J = 8.8$ Hz), 6.97 - 6.91 (2H, m), 6.19 (1H, m), 4.97 (1H, d, $J = 5.4$ Hz), 4.27 (1H, m), 3.23 - 3.04 (4H, m) (sample contained 3% TBME by mass, this is accounted for in the product yield). HRMS (ESI-[+H]) m/z : Calcd for C₂₀H₁₇⁸¹BrClN₄O₂ 459.0223; Found 459.0223.

Data in agreement with that reported previously.

Chiral analytical chromatography was carried out by Eric Hortense, Analytical Chemistry, GSK, Stevenage.²³² The HPLC was conducted on a Chiralpak ICTM column (250 mm x 4.6 mm i.d. 5 μ m packing diameter).

The solvents employed were:

A = 0.1% v/v *iso*-propylamine in heptane.

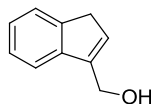
B = EtOH.

The elution gradient used was 0.5:0.5 A:B with a flow rate of 1 mL/min over 20 min.

$R_t = 11.59$ min (*R*)-enantiomer and 14.72 min (*S*)-enantiomer. Integration of the relative peaks areas gave a ee value 99.5% for the (*R*)-enantiomer (**1.5.1**).

3.2 BET Experimental Section

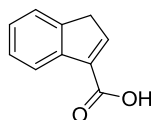
(1*H*-Inden-3-yl)methanol (2.2.13)²⁶⁹



2.2.13

To a heat dried flask was added 1*H*-indene (1.00 mL, 8.61 mmol) and anhydrous tetrahydrofuran (20 mL) under a nitrogen atmosphere. The solution was cooled to - 78 °C and to the mixture was added dropwise *n*-BuLi (2.5 M in hexanes, 3.62 mL, 9.04 mmol). The resulting solution was warmed to 0 °C and stirred for 30 min. The reaction mixture was cooled to - 78 °C and to the cooled solution was added paraformaldehyde (0.284 g, 9.47 mmol). The reaction was warmed to ambient temperature and stirred for 16 h. LCMS at this stage showed no significant reaction and therefore the reaction was terminated at this stage.

1*H*-Indene-3-carboxylic acid (2.2.14)³²⁰

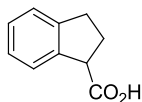


2.2.14

To a heat dried flask was added 1*H*-indene (3.01 mL, 25.8 mmol) and anhydrous tetrahydrofuran (THF) (50 mL) under a nitrogen atmosphere. The solution was cooled to - 78 °C and to the mixture was added dropwise *n*-BuLi (2.5 M in hexanes, 10.85 mL, 27.1 mmol). The resulting solution was stirred for 30 minutes at 0 °C. The solution was cooled to - 78 °C and to the cooled solution was added dry ice and the reaction was stirred overnight at ambient temperature. The reaction was acidified by the addition of aqueous 2M HCl and to the mixture was added ethyl acetate (75 mL). The resulting biphasic mixture was separated and the aqueous phase extracted with ethyl acetate (3 x 75 mL). The combined organic extracts were washed with brine (25 mL), passed through a hydrophobic frit, and concentrated under reduced pressure to afford the crude product as a yellow solid (4.0 g). The crude product was purified by automated column chromatography (cyclohexane:ethyl acetate + 1% vol. AcOH, 0:100 - 50:50, 120 g SiO₂). The appropriate fractions were combined and concentrated under reduced pressure to afford 1*H*-indene-3-carboxylic acid (2.2.14) as a yellow solid (3.61 g, 87%). LCMS

(Method C, UV, ESI) $R_t = 0.86$ min, $[M-H]^+ m/z$ = did not ionise, 100% purity. 1H NMR (400 MHz, $CDCl_3$): $\delta = 8.13$ (1H, d, $J = 7.6$ Hz), 7.68 (1H, t, $J = 2.0$ Hz), 7.53 (1H, d, $J = 7.3$ Hz), 7.41 (1H, m), 7.32 (1H, m), 3.62 (2H, d, $J = 1.7$ Hz), acid OH not observed due to exchange. Data was in agreement with that previously reported.³²⁰

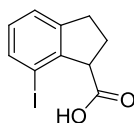
2,3-Dihydro-1*H*-indene-1-carboxylic acid (**2.2.16**)³²⁰



2.2.16

Palladium on carbon (5%) (2.66 g, 1.249 mmol), acetic acid (30 mL), and 1*H*-indene-3-carboxylic acid (**2.2.14**) (2.00 g, 12.49 mmol) were added to one chamber of the COware apparatus under a flow of nitrogen. The first reaction chamber was sealed and to the second was added aqueous HCl (4M, 35 mL, 140 mmol), followed by zinc (3.06 g, 46.8 mmol), while retaining a flow of nitrogen. The second tube was sealed and the reaction stirred over the weekend. To the mixture was added celite, and the solution stirred for 15 minutes. The resulting mixture was filtered through celite and concentrated under reduced pressure to give the crude product as a yellow oil (1.95 g). The crude product was purified by automated flash column chromatography (cyclohexane:TBME (+ 5% AcOH), 100:0 - 40:60, 120 g SiO_2). The appropriate fractions were combined and concentrated under reduced pressure to give 2,3-dihydro-1*H*-indene-1-carboxylic acid (**2.2.16**) as a white solid (1.82 g, 90%). LCMS (Method C, UV, ESI) $R_t = 0.84$ min, $[M-H]^+ m/z$ = did not ionise, 97% purity. 1H NMR (400 MHz, d_6 -DMSO): $\delta = 12.38$ (1H, s), 7.34 (1H, m), 7.25 (1H, m), 7.22-7.14 (2H, m), 3.97 (1H, m), 2.98 (1H, m), 2.85 (1H, m), 2.30-2.22 (2H, m). Data was in agreement with that previously reported.³²⁰

7-Iodo-2,3-dihydro-1H-indene-1-carboxylic acid (2.2.25)

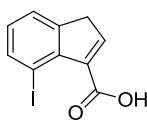


2.2.25

To a microwave vial was added 2,3-dihydro-1H-indene-1-carboxylic acid (**2.2.16**) (100 mg, 0.617 mmol), diacetoxypalladium (6.92 mg, 0.031 mmol), iodine (117 mg, 0.462 mmol), (diacetoxyiodo)benzene (149 mg, 0.462 mmol), and anhydrous *N,N*-dimethylformamide (3 mL) under air. The vial was sealed, covered with aluminium foil, heated thermally to 60 °C, and stirred for 24 h. The reaction was cooled to ambient temperature and concentrated under reduced pressure to give the crude reaction mixture as a brown oil. The crude product was purified by automated flash column chromatography (cyclohexane:ethyl acetate (+ 1% AcOH), 100:0 - 50:50, 40 g SiO₂). The appropriate fractions were combined and concentrated under reduced pressure to give a orange gum (51 mg). The mixture was dissolved in DMSO:MeOH (1:1) and purified by MDAP. The appropriate fractions were combined and concentrated to give 7-iodo-2,3-dihydro-1H-indene-1-carboxylic acid (**2.2.25**) as a white solid (20 mg, 11%). LCMS (Method D, UV, ESI) *R*_t = 0.55 min, [M-H]⁺ *m/z* = did not ionise, 100% purity. ¹H NMR (400 MHz, *d*₆-DMSO): δ = 7.55 (1H, d, *J* = 7.6 Hz), 7.25 (1H, d, *J* = 7.3 Hz), 6.94 (1H, m), 3.78 (1H, dd, *J* = 2.4, 9.4 Hz), 3.10 (1H, m), 2.98 (1H, m), 2.36 (1H, m), 2.18 (1H, m). ¹³C NMR (100.6 MHz, CDCl₃): δ = 174.4, 146.7, 145.7, 135.5, 128.9, 124.2, 94.8, 55.3, 32.8, 29.4. ROESY spectroscopy was used to confirm the product was the desired regioisomer.

Full characterisation not conducted due to insufficient material.

4-Iodo-1H-indene-3-carboxylic acid (2.2.26)

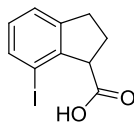


2.2.26

A microwave vial containing a mixture of 1H-indene-3-carboxylic acid (**2.2.16**) (100 mg, 0.624 mmol), diacetoxypalladium (7 mg, 0.031 mmol), iodine (119 mg, 0.468 mmol), (diacetoxyiodo)benzene (151 mg, 0.468 mmol), and *N,N*-dimethylformamide (3 mL) was

sealed, covered with aluminium foil, and heated to 60 °C. After 24 h, LCMS showed no significant reaction and therefore the reaction was terminated at this stage.

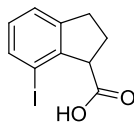
7-Iodo-2,3-dihydro-1H-indene-1-carboxylic acid (2.2.25) (Scheme 2.2.10)



2.2.25

A mixture of 2,3-dihydro-1H-indene-1-carboxylic acid (**2.2.16**) (250 mg, 1.541 mmol), diacetoxypalladium (17 mg, 0.077 mmol), iodine (782 mg, 3.080 mmol), (diacetoxyiodo)benzene (993 mg, 3.080 mmol), and *N,N*-dimethylformamide (8 mL) was sealed, covered with aluminium foil, and heated to 60 °C. After 5 h, no product or starting material could be observed by LCMS and significant pressure build up was observed. The reaction was therefore terminated at this stage.

7-Iodo-2,3-dihydro-1H-indene-1-carboxylic acid (2.2.25) (Scheme 2.2.10 – Reaction A)

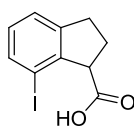


2.2.25

A mixture of 2,3-dihydro-1H-indene-1-carboxylic acid (**2.2.16**) (250 mg, 1.541 mmol), diacetoxypalladium (17 mg, 0.077 mmol), iodine (293 mg, 1.156 mmol), (diacetoxyiodo)benzene (372 mg, 1.156 mmol), and *N,N*-dimethylformamide (8 mL) was sealed, covered with aluminium foil and heated to 60 °C. After 16 h, LCMS showed unreacted starting material with 71% reaction conversion. To the reaction was added iodine (195 mg, 0.771 mmol) and (diacetoxyiodo)benzene (248 mg, 0.771 mmol) and the reaction was stirred at 60 °C for a further 6 h. LCMS at this stage showed 80% reaction conversion. The reaction was cooled to ambient temperature and to the mixture was added 5% aqueous sodium metabisulfite (25 mL) and ethyl acetate (25 mL). The biphasic mixture was separated and the aqueous phase extracted with ethyl acetate (3 x 25 mL). The combined organic extracts were

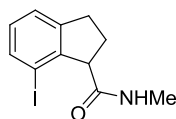
washed with brine, passed through a hydrophobic frit, and concentrated under reduced pressure to give the crude product as a dark brown oil (1 g). The crude product was purified by automated flash column chromatography (cyclohexane:TBME (+ 5% AcOH), 100:0 - 50:50, 80 g SiO₂). The appropriate fractions were combined and concentrated under reduced pressure to give a yellow/orange oil (270 mg). LCMS and NMR showed significant remaining impurities and therefore the reaction was terminated at this stage.

7-Iodo-2,3-dihydro-1H-indene-1-carboxylic acid (2.2.25) (Scheme 2.2.10 – Reaction B)



2.2.25

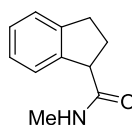
A mixture of 2,3-dihydro-1H-indene-1-carboxylic acid (**2.2.16**) (250 mg, 1.541 mmol), diacetoxy palladium (35 mg, 0.154 mmol), iodine (391 mg, 1.541 mmol), (diacetoxyiodo)benzene (496 mg, 1.541 mmol), and *N,N*-dimethylformamide (8 mL) was sealed, covered with aluminium foil, and heated to 60 °C for 16 h. LCMS at this stage showed 88% reaction conversion. The reaction was cooled to ambient temperature and to the mixture was added 5% aqueous sodium metabisulfite (25 mL) and ethyl acetate (25 mL). The resulting biphasic mixture was separated and the aqueous phase extracted with ethyl acetate (3 x 25 mL). The combined organic extracts were washed with brine, passed through a hydrophobic frit, and concentrated under reduced pressure to give the crude product as a dark brown oil (1 g). The crude product was purified by automated flash column chromatography (cyclohexane:TBME (+ 5% AcOH), 100:0 - 50:50, 80 g SiO₂). The appropriate fractions were combined and concentrated under reduced pressure to give 220 mg of impure material - in addition to this a methanol wash liberated another 120 mg of material which showed significant levels of product. The reaction was terminated at this stage.

7-Iodo-*N*-methyl-2,3-dihydro-1*H*-indene-1-carboxamide (2.2.28)**2.2.28**

A mixture of 2,3-dihydro-1*H*-indene-1-carboxylic acid (**2.2.16**) (1.00 g, 6.17 mmol), diacetoxypalladium (0.069 g, 0.308 mmol), iodine (1.57 g, 6.17 mmol), (diacetoxyiodo)benzene (1.99 g, 6.17 mmol), and *N,N*-dimethylformamide (25 mL) was sealed, covered with aluminium foil, and heated to 60 °C. After 6.5 h, the reaction was cooled to ambient temperature and to the mixture was added iodine (0.78 g, 3.09 mmol) and (diacetoxyiodo)benzene (0.99 g, 3.09 mmol). The reaction was heated to 60 °C and stirred for 16 h. The reaction was cooled to ambient temperature and to the mixture was added 5% aqueous sodium metabisulfide (25 mL) and ethyl acetate (25 mL). The resulting biphasic mixture was separated and the aqueous phase was extracted with ethyl acetate (3 x 25 mL). The combined organic extracts were washed with 2M aqueous NaOH (3 x 20 mL). The combined aqueous extracts were acidified by the addition of 2M aqueous HCl and to the mixture was added ethyl acetate (50 mL). The biphasic mixture was separated and the aqueous phase extracted with ethyl acetate (3 x 50 mL). The combined organic extracts were washed with brine, passed through a hydrophobic frit, and concentrated under reduced pressure to give crude as 7-iodo-2,3-dihydro-1*H*-indene-1-carboxylic acid (**2.2.25**) as a brown gum (950 mg) of sufficient purity to be used in the next stage of the reaction without further purification. To a mixture of crude 7-iodo-2,3-dihydro-1*H*-indene-1-carboxylic acid (**2.2.25**) (910 mg) and anhydrous tetrahydrofuran (10 mL) was added methanamine (2M in THF, 1.90 mL, 3.79 mmol) and DIPEA (1.10 mL, 6.32 mmol) under a nitrogen atmosphere. To the solution was added 2,4,6-tripropyl-1,3,5,2,4,6-trioxatriphosphinane 2,4,6-trioxide (50% in ethyl acetate, 4.70 mL, 7.90 mmol) and the reaction stirred at 70 °C for 5 h. The reaction was cooled to ambient temperature and to the mixture was added water (50 mL) and ethyl acetate (50 mL). The biphasic mixture was separated and the aqueous phase extracted with ethyl acetate (3 x 50 mL). The combined organic extracts were washed with brine, passed through a hydrophobic frit, and concentrated under reduced pressure to give the crude product as an off-yellow solid (1.4 g). The crude product was purified by automated column chromatography (cyclohexane:TBME, 100:0 - 0:100, 80 g SiO₂). The appropriate fractions were combined and concentrated under reduced pressure to give 7-iodo-*N*-methyl-2,3-dihydro-1*H*-indene-1-carboxamide (940 mg, 53% over 2 steps) as a white solid. LCMS (Method C, UV, ESI) $R_t =$

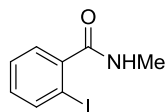
0.82, [M-H]⁺ *m/z* = 301.9, 100% purity. M.p. 214-215 °C. ¹H NMR (400 MHz, *d*₆-DMSO): δ = 8.10 (1H, m), 7.89 (1H, d, *J* = 4.2 Hz), 7.54 (1H, d, *J* = 7.8 Hz), 7.26 (1H, d, *J* = 7.1 Hz), 6.94 (1H, m), 3.79 (1H, dd, *J* = 3.3, 9.2 Hz), 3.11 (1H, m), 2.94 (1H, ddd, *J* = 3.7, 8.9, 15.8 Hz), 2.60 (3H, d, *J* = 4.6 Hz), 2.31 (1H, m), 2.03 (1H, m). ¹³C NMR (100.6 MHz, *d*₆-DMSO): δ = 172.7, 146.5, 146.3, 135.7, 129.0, 124.2, 94.3, 55.2, 32.8, 29.8, 25.7. IR (*v*_{max}/cm⁻¹) = 3278, 2933, 1636, 1558. HRMS (ESI-[+H]) *m/z*: Calcd for C₁₁H₁₃INO 302.0036; Found 302.0036.

***N*-Methyl-2,3-dihydro-1*H*-indene-1-carboxamide (2.2.29)**

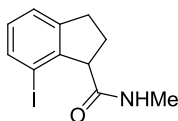


2.2.29

To a mixture of 2,3-dihydro-1*H*-indene-1-carboxylic acid (**2.2.16**) (3.13 g, 19.30 mmol) and anhydrous tetrahydrofuran (50 mL) was added methanamine (2M in THF) (11.58 mL, 23.16 mmol) and DIPEA (6.74 mL, 38.60 mmol) under a nitrogen atmosphere. To the solution was added 2,4,6-tripropyl-1,3,5,2,4,6-trioxatriphosphinane 2,4,6-trioxide (50% in ethyl acetate) (28.7 mL, 48.20 mmol). The resulting mixture was heated to 70 °C and stirred under a nitrogen atmosphere for 3 h. The reaction was cooled to ambient temperature and to the mixture was added water (100 mL) and ethyl acetate (100 mL). The resulting biphasic mixture was separated and the aqueous phase extracted with ethyl acetate (3 x 100 mL). The combined organic extracts were washed with brine, passed through a hydrophobic frit, and concentrated under reduced pressure to give the crude product as a orange oil (6.21 g). The crude product was purified by automated column chromatography (cyclohexane:ethyl acetate, 100:0 - 0:100, 80 g SiO₂). The appropriate fractions were combined and concentrated under reduced pressure to give *N*-methyl-2,3-dihydro-1*H*-indene-1-carboxamide (**2.2.29**) as a white solid (3.31 g, 98%). LCMS (Method C, UV, ESI) *R*_t = 0.69 min, [M-H]⁺ *m/z* = 176.1, 100% purity. M.p. 114-115 °C. ¹H NMR (400 MHz, *d*₄-MeOD): δ = 7.24-7.11 (4H, m), 3.91 (1H, t, *J* = 7.6 Hz), 3.08 (1H, m), 2.90 (1H, m), 2.77 (3H, s), 2.33-2.26 (2H, m). ¹³C NMR (100.6 MHz, *d*₄-MeOD): δ = 177.6, 145.7, 143.4, 128.4, 127.5, 125.6, 125.1, 53.0, 32.9, 30.7, 26.5. IR (*v*_{max}/cm⁻¹) = 3276, 1646, 1548, 700. HRMS (ESI-[+H]) *m/z*: Calcd for C₁₁H₁₄NO 176.1075; Found 176.1078.

2-Iodo-*N*-methylbenzamide (2.2.31)**2.2.31**

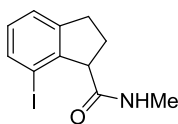
To a heat dried microwave vial was added $[\text{RhCp}^*\text{Cl}_2]_2$ (15 mg, 0.025 mmol), AgSbF_6 (34 mg, 0.100 mmol), pivalic acid (112 mg, 1.100 mmol), and anhydrous 1,2-dichloroethane (5 mL) under a nitrogen atmosphere. To the vial was added *N*-methylbenzamide (135 mg, 1.00 mmol) and *N*-iodosuccinimide (247 mg, 1.100 mmol) and the resulting mixture heated to 60 °C and stirred for 16 h. LCMS at this stage showed 6% starting material, 77% mono-iodinated product, and 17% di-iodinated. The reaction was terminated at this stage.

7-Iodo-*N*-methyl-2,3-dihydro-1*H*-indene-1-carboxamide (2.2.28)**2.2.28**

To a heat dried microwave vial was added $[\text{RhCp}^*\text{Cl}_2]_2$ (9 mg, 0.014 mmol), AgSbF_6 (20 mg, 0.057 mmol), pivalic acid (64 mg, 0.628 mmol), and anhydrous 1,2-dichloroethane (3 mL) under a nitrogen atmosphere. To the vial was added *N*-methyl-2,3-dihydro-1*H*-indene-1-carboxamide (**2.2.29**) (100 mg, 0.571 mmol) and *N*-iodosuccinimide (141 mg, 0.628 mmol) and the resulting mixture heated to 60 °C and stirred for 16 h. LCMS analysis at this stage 18% starting material, 25% product, and 19% of an undetermined isomer/s. The reaction was cooled to ambient temperature and to the mixture was added ethyl acetate (10 mL). The resulting mixture was filtered through a silica plug, eluting with ethyl acetate (50 mL) and concentrated under reduced pressure to give the crude product as a red gum (250 mg). The crude product was purified by mass directed automated purification (formic modifier). The appropriate fractions were combined and concentrated under reduced pressure to give 7-iodo-*N*-methyl-2,3-dihydro-1*H*-indene-1-carboxamide (**2.2.28**) as a white solid (28 mg, 16%) and an undetermined mixture of other isomers as a yellow gum (12 mg, 7%). LCMS (Method C, UV, ESI) $R_t = 0.82$, $[\text{M-H}]^+ m/z = 301.9$, 100% purity. $^1\text{H NMR}$ (400 MHz, d_6 -DMSO): $\delta =$

7.89 (1H, d, $J = 4.2$ Hz), 7.54 (1H, d, $J = 7.8$ Hz), 7.26 (1H, d, $J = 7.1$ Hz), 6.94 (1H, m), 3.79 (1H, dd, $J = 3.3, 9.2$ Hz), 3.11 (1H, m), 2.94 (1H, ddd, $J = 3.7, 8.9, 15.8$ Hz), 2.60 (3H, d, $J = 4.6$ Hz), 2.31 (1H, m), 2.03 (1H, m). *Data in agreement with that above.*

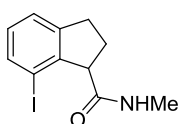
7-Iodo-*N*-methyl-2,3-dihydro-1*H*-indene-1-carboxamide (2.2.28) (Control no rhodium)



2.2.28

To a heat dried microwave vial was added AgSbF_6 (20 mg, 0.057 mmol), pivalic acid (64 mg, 0.628 mmol), and anhydrous 1,2-dichloroethane (3 mL) under a nitrogen atmosphere. To the vial was added *N*-methyl-2,3-dihydro-1*H*-indene-1-carboxamide (**2.2.29**) (100 mg, 0.571 mmol) and *N*-iodosuccinimide (141 mg, 0.628 mmol). The resulting mixture was heated to 60 °C and stirred for 16 h. LCMS analysis at this stage showed 10% product (**2.2.28**), 13% starting material (**2.2.29**), and 35% of the alternative regioisomer/s. The reaction was terminated at this stage.

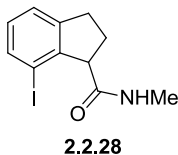
7-Iodo-*N*-methyl-2,3-dihydro-1*H*-indene-1-carboxamide (2.2.28) (Control no silver salts)



2.2.28

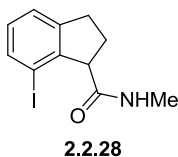
To a heat dried microwave vial was added $[\text{RhCp}^*\text{Cl}_2]_2$ (9 mg, 0.014 mmol), pivalic acid (64 mg, 0.628 mmol), and anhydrous 1,2-dichloroethane (3 mL) under a nitrogen atmosphere. To the vial was added *N*-methyl-2,3-dihydro-1*H*-indene-1-carboxamide (**2.2.29**) (100 mg, 0.571 mmol) and *N*-iodosuccinimide (141 mg, 0.628 mmol) and the resulting mixture heated to 60 °C for 40 h. LCMS at this stage showed no reaction, therefore the reaction was terminated at this stage.

7-Iodo-*N*-methyl-2,3-dihydro-1*H*-indene-1-carboxamide (2.2.28) (Alternative Rh(III) catalyst)



To a heat dried microwave vial was added tris(acetonitrile) pentamethylcyclopentadienylrhodium(III) hexafluoroantimonate (12 mg, 0.014 mmol), pivalic acid (64 mg, 0.628 mmol), and anhydrous 1,2-dichloroethane (3 mL) under a nitrogen atmosphere. To the vial was added *N*-methyl-2,3-dihydro-1*H*-indene-1-carboxamide (**2.2.29**) (100 mg, 0.571 mmol) and *N*-iodosuccinimide (141 mg, 0.628 mmol) and the resulting mixture heated to 60 °C and stirred for 16 h. LCMS at this stage showed only low levels of reaction were observed and, therefore, the reaction was terminated at this stage.

7-Iodo-*N*-methyl-2,3-dihydro-1*H*-indene-1-carboxamide (2.2.28) (Alternative Rh(III) catalyst with additional silver additives)



To a heat dried microwave vial was added tris(acetonitrile) pentamethylcyclopentadienylrhodium(III) hexafluoroantimonate (12 mg, 0.014 mmol), pivalic acid (64 mg, 0.628 mmol), AgSbF₆ (20 mg, 0.057 mmol), and anhydrous 1,2-dichloroethane (3 mL) under a nitrogen atmosphere. To the vial was added *N*-methyl-2,3-dihydro-1*H*-indene-1-carboxamide (**2.2.29**) (100 mg, 0.571 mmol) and *N*-iodosuccinimide (141 mg, 0.628 mmol) and the resulting mixture heated to 60 °C and stirred for 16 h. LCMS analysis at this stage showed 12% desired product (**2.2.28**) and 14% of a mixture of the other isomers.

Rh(III) Catalysed C-H Activation/Iodination Screening (Table 2.2.1)

To a heat dried microwave vial was added [RhCp*Cl₂]₂ (a), AgSbF₆ (b), pivalic acid (64 mg, 0.628 mmol) and anhydrous 1,2-dichloroethane (3 mL) under a nitrogen atmosphere. To the mixture was added substrate (c) and NXS (d) and the resulting mixture heated to T (e) for time (f). LCMS analysis at this stage showed (g).

Table 2.2.1 – Entry 1

a) 9 mg, 0.014 mmol; b) 20 mg, 0.057 mmol; c) *N*-methyl-2,3-dihydro-1*H*-indene-1-carboxamide (**2.2.29**) (100 mg, 0.571 mmol); d) NBS (112 mg, 0.628 mmol); e) 60 °C; f) 16 h; g) Complex mixture with no discernible product or by-product.

Table 2.2.1 – Entry 2

a) 9 mg, 0.014 mmol; b) 20 mg, 0.057 mmol; c) 2,3-dihydro-1*H*-indene-1-carboxylic acid (**2.2.16**) (92 mg, 0.571 mmol); d) NIS (141 mg, 0.628 mmol); e) 60 °C; f) 16 h; g) No starting material or products detected, however a gaseous evolution was observed.

Table 2.2.1 – Entry 3

a) 3.5 mg, 0.0057 mmol; b) 7.8 mg, 0.023 mmol; c) *N*-methyl-2,3-dihydro-1*H*-indene-1-carboxamide (**2.2.29**) (100 mg, 0.571 mmol); d) NIS (141 mg, 0.628 mmol); e) 60 °C; f) 16 h; g) 8% desired product (P), 10% undesired regioisomer/s (BP), and 23% unreacted starting material (SM).

Table 2.2.1 – Entry 4

a) 70.5 mg, 0.114 mmol; b) 157 mg, 0.457 mmol; c) *N*-methyl-2,3-dihydro-1*H*-indene-1-carboxamide (**2.2.29**) (100 mg, 0.571 mmol); d) NIS (141 mg, 0.628 mmol); e) 60 °C; f) 24 h; g) 18% desired product (P), 42% undesired regioisomer/s (BP), and 22% unreacted starting material (SM).

Table 2.2.1 – Entry 5

a) 9 mg, 0.014 mmol; b) 4.9 mg, 0.014 mmol; c) *N*-methyl-2,3-dihydro-1*H*-indene-1-carboxamide (**2.2.29**) (100 mg, 0.571 mmol); d) NIS (141 mg, 0.628 mmol); e) 60 °C; f) 16 h; g) Trace levels of reaction.

Table 2.2.1 – Entry 6

a) 9 mg, 0.014 mmol; b) 20 mg, 0.057 mmol; c) *N*-methyl-2,3-dihydro-1*H*-indene-1-carboxamide (**2.2.29**) (100 mg, 0.571 mmol); d) NIS (385 mg, 1.712 mmol); e) 25 °C; f) 16 h; g) 16% desired product (P), 4% undesired regioisomer/s (BP), and 67% unreacted starting material (SM), no changes after 40 h.

Table 2.2.1 – Entry 7

a) 9 mg, 0.014 mmol; b) 20 mg, 0.057 mmol; c) *N*-methyl-2,3-dihydro-1*H*-indene-1-carboxamide (**2.2.29**) (100 mg, 0.571 mmol); d) NIS (141 mg, 0.628 mmol); e) 30 °C; f) 16 h; g) 6% desired product (P), 2% undesired regioisomer/s (BP), and 22% unreacted starting material (SM).

Table 2.2.1 – Entry 8

a) 9 mg, 0.014 mmol; b) 20 mg, 0.057 mmol; c) *N*-methyl-2,3-dihydro-1*H*-indene-1-carboxamide (**2.2.29**) (100 mg, 0.571 mmol); d) NIS (141 mg, 0.628 mmol); e) 40 °C; f) 16 h; g) 13% desired product (P), 5% undesired regioisomer/s (BP), and 24% unreacted starting material (SM).

Table 2.2.1 – Entry 9

a) 9 mg, 0.014 mmol; b) 20 mg, 0.057 mmol; c) *N*-methyl-2,3-dihydro-1*H*-indene-1-carboxamide (**2.2.29**) (100 mg, 0.571 mmol); d) NIS (141 mg, 0.628 mmol); e) 50 °C; f) 16 h; g) 16% desired product (P), 5% undesired regioisomer/s (BP), and 17% unreacted starting material (SM).

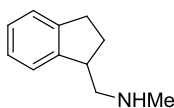
Table 2.2.1 – Entry 10

a) 9 mg, 0.014 mmol; b) 20 mg, 0.057 mmol; c) *N*-methyl-2,3-dihydro-1*H*-indene-1-carboxamide (**2.2.29**) (100 mg, 0.571 mmol); d) NIS (141 mg, 0.628 mmol); e) 60 °C; f) 16 h; g) 9% desired product (P), 9% undesired regioisomer/s (BP), and 18% unreacted starting material (SM).

Table 2.2.1 – Entry 11

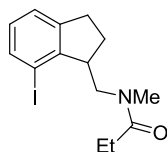
a) 9 mg, 0.014 mmol; b) 20 mg, 0.057 mmol; c) *N*-methyl-2,3-dihydro-1*H*-indene-1-carboxamide (**2.2.29**) (100 mg, 0.571 mmol); d) NIS (141 mg, 0.628 mmol); e) 70 °C; f) 16 h; g) 7% desired product (P), 8% undesired regioisomer/s (BP), and 23% unreacted starting material (SM).

1-(2,3-Dihydro-1*H*-inden-1-yl)-*N*-methylmethanamine (**2.2.39**)



2.2.39

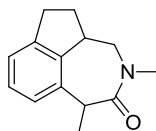
To a heat dried flask was added *N*-methyl-2,3-dihydro-1*H*-indene-1-carboxamide (**2.2.29**) (250 mg, 1.427 mmol) and anhydrous tetrahydrofuran (6 mL) under a nitrogen atmosphere. To the solution was added dropwise lithium aluminum hydride (2.3 M in 2-MeTHF, 1.24 mL, 2.85 mmol) and the resulting solution stirred at ambient temperature for 5 h. LCMS at this stage showed no reaction. The reaction was heated to 50 °C and stirred for 16 h. The resulting mixture was cooled to ambient temperature. To the mixture was added ether (10 mL), followed by the slow addition of water (2 mL). To the mixture was added 2M NaOH (2 mL), followed by water (6 mL) and resulting solution stirred for 15 minutes. To the mixture was added anhydrous magnesium sulfate, and the reaction stirred for an additional 15 minutes. The mixture was filtered and the biphasic mixture separated. The organic phase was passed through a hydrophobic frit, and concentrated under reduced pressure to give the crude product as a black gum (210 mg). LCMS at this stage only showed trace levels of product (**2.2.29**) and, therefore, the reaction was terminated at this stage.

***N*-((7-Iodo-2,3-dihydro-1*H*-inden-1-yl)methyl)-*N*-methylpropionamide (2.2.41)****2.2.41**

To a heat dried microwave vial was added $[\text{Ir}(\text{COE})_2\text{Cl}]_2$ (47.6 mg, 0.053 mmol), diethylsilane (0.826 mL, 6.38 mmol) and anhydrous toluene (2 mL) under a nitrogen atmosphere. To the resulting solution was added 7-iodo-*N*-methyl-2,3-dihydro-1*H*-indene-1-carboxamide (**2.2.28**) (320 mg, 1.063 mmol) in anhydrous dichloromethane (2 mL) and the resulting mixture stirred at ambient temperature for 14 h. To the mixture was added DCM (20 mL) and 2M aqueous HCl (10 mL). The resulting biphasic mixture was separated and the organic phase washed with 2 M aqueous HCl (3 x 10 mL). The combined aqueous extracts were basified with NaOH (2M aqueous) and extracted with DCM (3 x 40 mL). The combined organic extracts were washed with brine, passed through a hydrophobic frit, and concentrated under reduced pressure to afford the crude 1-(7-iodo-2,3-dihydro-1*H*-inden-1-yl)-*N*-methylmethanamine (**2.2.40**) as a dark brown oil (250 mg) of sufficient purity to be used in the next stage of the reaction without further purification. To a mixture of crude 1-(7-iodo-2,3-dihydro-1*H*-inden-1-yl)-*N*-methylmethanamine (**2.2.40**) (305 mg) and anhydrous tetrahydrofuran (10 mL) was added dropwise propionyl chloride (0.209 mL, 2.392 mmol) under a nitrogen atmosphere and the resulting mixture stirred for 20 h. To the mixture was added DCM (25 mL) and saturated aqueous sodium carbonate (25 mL). The biphasic mixture was separated and the aqueous phase washed with DCM (3 x 20 mL). The combined organic extracts were washed with brine, passed through a hydrophobic frit, and concentrated under reduced pressure to give the crude product as a dark brown oil (350 mg). The crude product was purified by automated flash column chromatography (cyclohexane:TBME, 100:0 - 0:100, 12 g SiO_2). The appropriate fractions were combined and concentrated under reduced pressure to give *N*-((7-iodo-2,3-dihydro-1*H*-inden-1-yl)methyl)-*N*-methylpropionamide (**2.2.41**) as a yellow oil (199 mg, 55% over two steps). LCMS (Method C, UV, ESI) $R_t = 1.19$, $[\text{M}-\text{H}]^+ m/z = 344.0$, 100% purity. ^1H NMR (400 MHz, d_6 -DMSO, 120 °C): $\delta = 7.55$ (1H, d, $J = 7.8$ Hz), 7.25 (1H, d, $J = 7.3$ Hz), 6.93 (1H, m), 3.60 (1H, m), 3.42 (1H, m), 3.11 (1H, m), 2.96 (3H, s), 2.95-2.84 (2H, m), 2.32 (2H, q, $J = 7.3$ Hz), 2.06 (1H, m), 1.96 (1H, m), 1.04 (3H, t, $J = 7.3$ Hz). ^{13}C NMR (100.6 MHz, d_6 -DMSO, 120 °C): $\delta = 173.2$, 148.2, 145.5, 135.9, 129.1, 124.6, 93.0, 48.4, 47.5, 31.7, 27.2, 25.8, 9.1 (one aromatic proton not observed). IR ($\nu_{\text{max}}/\text{cm}^{-1}$) =

2935, 1639, 1444, 765. HRMS (ESI-[+H]) m/z : Calcd for $C_{14}H_{19}NOI$ 344.0511; Found 344.0511.

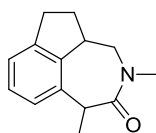
1,3-Dimethyl-4,4a,5,6-tetrahydro-1H-indeno[1,7-*cd*]azepin-2(3H)-one (2.2.10)



2.2.10

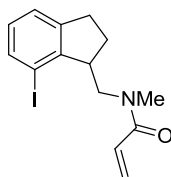
To a heat dried microwave vial was added BINAP (2.7 mg, 4.37 μ mol), $Pd_2(dba)_3$ (2.7 mg, 2.91 μ mol), and sodium *tert*-butoxide (8.4 mg, 0.087 mmol). To the mixture was added *N*-((7-iodo-2,3-dihydro-1*H*-inden-1-yl)methyl)-*N*-methylpropionamide (**2.2.41**) (20 mg, 0.058 mmol) and anhydrous 1,4-dioxane (1 mL) and the resulting mixture heated to 100 °C and stirred for 112 h. LCMS at this stage showed no product formation and therefore the reaction was terminated at this stage.

1,3-Dimethyl-4,4a,5,6-tetrahydro-1H-indeno[1,7-*cd*]azepin-2(3H)-one (2.2.10)



2.2.10

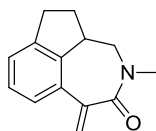
To a heat dried microwave vial was added BINAP (2.7 mg, 4.37 μ mol), $Pd_2(dba)_3$ (2.67 mg, 2.91 μ mol), and potassium hexamethyldisilazide (23.25 mg, 0.117 mmol) under a nitrogen atmosphere. To the mixture was added *N*-((7-iodo-2,3-dihydro-1*H*-inden-1-yl)methyl)-*N*-methylpropionamide (**2.2.41**) (20 mg, 0.058 mmol) in anhydrous 1,4-dioxane (1 mL) and the resulting mixture heated to 100 °C and stirred for 24 h. LCMS at this stage showed a mixture of starting material and dehalogenated by-product with no product formation. Therefore, the reaction was terminated at this stage.

***N*-((7-Iodo-2,3-dihydro-1*H*-inden-1-yl)methyl)-*N*-methylacrylamide (2.2.42)****2.2.42**

To a microwave vial was added [Ir(COE)₂Cl]₂ (119 mg, 0.133 mmol) and diethylsilane (2.07 mL, 15.94 mmol) and the resulting mixture was stirred for 5 min. To the mixture was added a mixture of 7-iodo-*N*-methyl-2,3-dihydro-1*H*-indene-1-carboxamide (**2.2.28**) (800 mg, 2.66 mmol) and anhydrous toluene (2 mL). The reaction vessel was sealed and the resulting mixture was stirred at ambient temperature for 40 h. To the mixture was added dropwise 2M aqueous HCl (10 mL), followed by ethyl acetate (15 mL). The resulting biphasic mixture was separated and the organic phase extracted with 2M aqueous HCl (2 x 5 mL). The combined aqueous extracts were basified by the addition of 2M aqueous NaOH and to the mixture was added ethyl acetate (20 mL). The resulting biphasic mixture was separated and the aqueous phase extracted with ethyl acetate (3 x 20 mL). The combined organic extracts were passed through a hydrophobic frit and concentrated under reduced pressure to give crude 1-(7-iodo-2,3-dihydro-1*H*-inden-1-yl)-*N*-methylmethanamine (**2.2.40**) as a brown gum (550 mg) of sufficient purity to be used in the next stage without further purification. To a mixture of crude 1-(7-iodo-2,3-dihydro-1*H*-inden-1-yl)-*N*-methylmethanamine (**2.2.40**) (649 mg) in anhydrous tetrahydrofuran (15 mL) was added dropwise acryloyl chloride (0.413 mL, 5.09 mmol) and the resulting mixture stirred for 1.5 h under a nitrogen atmosphere. To the reaction was added DCM (25 mL) and saturated aqueous sodium carbonate (25 mL). The resulting biphasic mixture was separated and the aqueous phase extracted with DCM (3 x 25 mL). The combined organic extracts were washed with brine (50 mL), passed through a hydrophobic frit, and concentrated under reduced pressure to give the crude product as a yellow gum (900 mg). The crude product was purified by automated flash column chromatography (cyclohexane:TBME, 100:0 - 50:50, 80 g SiO₂). The appropriate fractions were combined and concentrated under reduced pressure to give *N*-((7-iodo-2,3-dihydro-1*H*-inden-1-yl)methyl)-*N*-methylacrylamide (**2.2.42**) as a yellow gum (551 mg, 72%). LCMS (Method C, UV, ESI) *R*_t = 1.16, [M-H]⁺ *m/z* = 342.0, 100% purity. ¹H NMR (400 MHz, *d*₆-DMSO, 120 °C): δ = 7.56 (1H, d, *J* = 7.7 Hz), 7.26 (1H, d, *J* = 7.3 Hz), 6.95 (1H, m), 6.71 (1H, dd, *J* = 10.6, 16.8 Hz), 6.09 (1H, dd, *J* = 2.4, 16.9 Hz), 5.63 (1H, dd, *J* = 2.4, 10.5 Hz), 3.65 (1H, m), 3.50-3.40 (2H, m), 3.12 (1H, m), 3.02 (3H, s), 2.93 (1H, m), 2.08 (1H, m), 1.97 (1H, dd, *J* = 7.8, 13.0 Hz). ¹³C NMR (100.6 MHz, *d*₆

–DMSO, 120 °C): $\delta = 166.2, 147.9, 145.5, 136.0, 129.2, 129.1, 126.0, 124.7, 93.0, 49.4, 47.6, 34.7, 31.6, 27.2$. IR ($\nu_{\max}/\text{cm}^{-1}$) = 2933, 1644, 1607, 765. HRMS (ESI-[+H]) m/z : Calcd for $\text{C}_{14}\text{H}_{17}\text{INO}$ 342.0349; Found 342.0344.

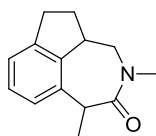
3-Methyl-1-methylene-4,4a,5,6-tetrahydro-1H-indeno[1,7-*cd*]azepin-2(3H)-one (2.2.43)



2.2.43

To a microwave vial was added (**2.2.42**) *N*-((7-iodo-2,3-dihydro-1*H*-inden-1-yl)methyl)-*N*-methylacrylamide (300 mg, 0.879 mmol), $\text{PdCl}_2(\text{dppf})$ (32 mg, 0.044 mmol), and anhydrous acetonitrile (10 mL). The vial was sealed and degassed for 5 minutes. To the mixture was added triethylamine (0.306 mL, 2.198 mmol) and the reaction heated to 110 °C under microwave irradiation for 15 minutes. The resulting mixture was filtered through celite, washing with ethyl acetate (50 mL), and concentrated under reduced pressure to give the crude product as a brown solid (600 mg). The crude product was purified by automated flash column chromatography (cyclohexane/TBME, 100:0 - 0:100, 80 g SiO_2). The appropriate fractions were combined and concentrated to give 3-methyl-1-methylene-4,4a,5,6-tetrahydro-1*H*-indeno[1,7-*cd*]azepin-2(3*H*)-one (**2.2.43**) as a light brown solid (179 mg, 95%). LCMS (Method C, UV, ESI) $R_t = 0.92$, $[\text{M}-\text{H}]^+ m/z = 214.2$, 100% purity. ^1H NMR (400 MHz, d_6 –DMSO): $\delta = 7.27$ (1H, d, $J = 7.3$ Hz), 7.24–7.16 (2H, m), 5.69 (1H, d, $J = 1.2$ Hz), 5.57 (1H, d, $J = 1.2$ Hz), 3.52 (1H, dd, $J = 10.5, 14.4$ Hz), 3.40 (1H, dd, $J = 2.4, 14.2$ Hz), 3.21 (1H, m), 3.03 (3H, s), 2.87 (1H, m), 2.75 (1H, dd, $J = 7.8, 15.2$ Hz), 2.20 (1H, m), 1.55 (1H, m). ^{13}C NMR (100.6 MHz, d_6 –DMSO): $\delta = 170.1, 145.3, 144.1, 143.3, 130.2, 127.2, 124.4, 123.9, 121.3, 51.9, 44.5, 34.4, 31.5, 31.0$. IR ($\nu_{\max}/\text{cm}^{-1}$) = 2946, 1630, 1602, 750. HRMS (ESI-[+H]) m/z : Calcd for $\text{C}_{14}\text{H}_{16}\text{NO}$ 214.1226; Found 214.1222.

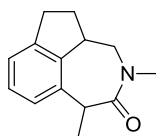
1,3-Dimethyl-4,4a,5,6-tetrahydro-1H-indeno[1,7-*cd*]azepin-2(3H)-one (2.2.10)



2.2.10

Palladium on carbon (5%) (28 mg, 0.013 mmol), anhydrous ethanol (0.5 mL), anhydrous tetrahydrofuran (0.5 mL), and 3-methyl-1-methylene-4,4a,5,6-tetrahydro-1H-indeno[1,7-*cd*]azepin-2(3H)-one (**2.2.43**) (28 mg, 0.132 mmol) were added to one chamber of the COware apparatus under a flow of nitrogen. The first chamber was sealed and to the second was added HCl (4M) (0.132 mL, 0.528 mmol), followed by zinc (0.030 g, 0.462 mmol), under a flow of nitrogen. The second chamber was sealed and the reaction stirred overnight. No reaction was observed after 72 h, therefore, the reaction was terminated at this stage.

1,3-Dimethyl-4,4a,5,6-tetrahydro-1H-indeno[1,7-*cd*]azepin-2(3H)-one (2.2.10)



2.2.10

To a microwave vial was added 3-methyl-1-methylene-4,4a,5,6-tetrahydro-1H-indeno[1,7-*cd*]azepin-2(3H)-one (**2.2.43**) (150 mg, 0.703 mmol) and anhydrous methanol (10 mL). To the mixture was added magnesium (68 mg, 2.81 mmol) and the reaction stirred at ambient temperature under nitrogen for 1 h. To the mixture was added ethyl acetate (20 mL) and saturated aqueous ammonium chloride (20 mL). The resulting biphasic mixture was separated and the aqueous phase extracted with ethyl acetate (20 mL). The combined organic extracts were washed with brine (20 mL), passed through a hydrophobic frit, and concentrated under reduced pressure to give the crude product as a cloudy gum (200 mg). The crude product was purified by automated flash column chromatography (cyclohexane/TBME, 100:0 - 50:50, 12 g SiO₂). The appropriate fractions were combined and concentrated to give 1,3-dimethyl-1,3,4,4a,5,6-hexahydro-2H-indeno[1,7-*cd*]azepin-2-one (**2.2.10**) as a white solid (142 mg, 94%) as a 5:1 mixture of diastereoisomers. LCMS (Method C, UV, ESI) $R_t = 0.94$ and 0.98 , $[M-H]^+ m/z = 216.2$, 19% and 80% purity respectively for each diastereoisomer. ¹H NMR (400 MHz, *d*₆ -DMSO): $\delta = 7.16$ - 7.11 (2H, m, *major diastereoisomer*), 7.11 - 7.08 (2H, m,

minor diastereoisomer), 7.04 (1H, m, *major diastereoisomer*), 6.94 (1H, m, *minor diastereoisomer*), 4.29 (1H, m, *both diastereoisomers*), 4.22 (1H, dd, $J = 6.4, 15.4$ Hz, *minor diastereoisomer*), 4.12 (1H, dd, $J = 11.4, 14.5$ Hz, *major diastereoisomer*), 3.40 (1H, dd, $J = 2.9, 15.4$ Hz, *minor diastereoisomer*), 3.34 (1H, dd, $J = 2.7, 14.7$ Hz, *major diastereoisomer*), 3.11 (1H, m, *both diastereoisomers*), 2.96 (3H, s, *major diastereoisomer*), 2.88 (3H, s, *minor diastereoisomer*), 2.86-2.70 (2H, m, *both diastereoisomers*), 2.27 (1H, m, *minor diastereoisomer*), 2.17 (1H, m, *major diastereoisomer*), 1.68 (1H, m, *minor diastereoisomer*), 1.58 (1H, m, *major diastereoisomer*), 1.40 (3H, d, $J = 6.8$ Hz, *major diastereoisomer*), 1.36 (3H, d, $J = 7.1$ Hz, *minor diastereoisomer*).

*Full characterisation was not conducted due to insufficient material, the sample was separated by chiral HPLC.*²⁹⁴

Chiral purification chromatography was carried out by Steve Jackson, Analytical Chemistry, GSK, Stevenage.²⁹⁴ The purification was conducted on a Chiralpak ICTM column (250 mm x 30 mm i.d. 5 μ m packing diameter).

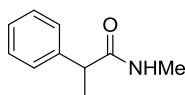
The solvents employed were:

A = Heptane.

B = EtOH.

The elution gradient used was 0.7:0.3 A:B.

***N*-Methyl-2-phenylpropanamide (2.3.17)**

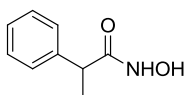


2.3.17

To a mixture of 2-phenylpropanoic acid (**2.3.20**) (0.91 mL, 6.66 mmol) and anhydrous tetrahydrofuran (10 mL) was added methanamine (2M in THF, 4.00 mL, 7.99 mmol) and DIPEA (2.33 mL, 13.32 mmol) under nitrogen atmosphere. To the resulting solution was added 2,4,6-tripropyl-1,3,5,2,4,6-trioxatriphosphinane 2,4,6-trioxide (50% in ethyl acetate, 9.91 mL, 16.65 mmol) and the resulting mixture heated to 70 °C and stirred for 1 h. The reaction was cooled to ambient temperature and to the mixture was added water (20 mL) and ethyl acetate (25 mL). The resulting biphasic mixture was separated and the aqueous phase extracted with ethyl acetate (3 x 20 mL). The combined organic extracts were washed with

brine, passed through a hydrophobic frit, and concentrated under reduced pressure give the crude product as a yellow gum (1.5 g). The crude product was purified by automated column chromatography (cyclohexane: TBME, 100:0 - 0:100, 80 g SiO₂). The appropriate fractions were combined and concentrated under reduced pressure to give *N*-methyl-2-phenylpropanamide (**2.3.17**) as a white solid (0.987 g, 91%). LCMS (Method C, UV, ESI) $R_t = 0.66$, $[M-H]^+ m/z = 164.1$. ¹H NMR (400 MHz, *d*₆-DMSO): $\delta = 7.84$ (1H, s), 7.33-7.25 (4H, m), 7.21 (1H, m), 3.55 (1H, q, $J = 7.1$ Hz), 2.56-2.54 (3H, m), 1.32 (3H, d, $J = 7.1$ Hz). Data was in agreement with that reported previously.³²¹

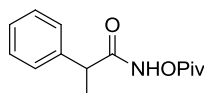
N-Hydroxy-2-phenylpropanamide (**2.3.21**)



2.3.21

To a solution of CDI (1.19 g, 7.32 mmol) in anhydrous tetrahydrofuran (10 mL) was added dropwise 2-phenylpropanoic acid (**2.3.20**) (0.91 mL, 6.66 mmol) in anhydrous tetrahydrofuran (2.5 mL). The resulting solution was stirred at ambient temperature for 1 h. The reaction mixture was cooled to 0 °C and to the mixture was added dropwise hydroxylamine (50% aqueous) (1.63 mL, 26.60 mmol). The reaction was warmed to ambient temperature and stirred for 15 min. To the reaction was added water (10 mL) and ethyl acetate (25 mL), and the biphasic mixture was separated. The organic phase was washed with brine and concentrated under reduced pressure to give the crude product as a colourless oil (1.5 g). The crude product was purified by automated flash column chromatography (cyclohexane:TBME, 70:30 - 0:100, 80 g SiO₂). The appropriate fractions were collected and combined under reduced pressure to give *N*-hydroxy-2-phenylpropanamide (**2.3.21**) as a white solid (651 mg, 59%). LCMS (Method C, UV, ESI) $R_t = 0.55$, $[M-H]^+ m/z = 166.1$. ¹H NMR (400 MHz, *d*₆-DMSO): $\delta = 10.60$ (1H, s), 8.78 (1H, s), 7.35-7.27 (4H, m), 7.22 (1H, m), 3.43 (1H, q, $J = 7.1$ Hz), 1.34 (3H, d, $J = 7.1$ Hz). ¹³C NMR (100.6 MHz, CDCl₃): $\delta = 170.2$, 141.8, 128.1, 127.2, 126.5, 42.1, 18.2.

Data in agreement with that previously reported.³²²

2-Phenyl-*N*-(pivaloyloxy)propanamide (2.3.19)**2.3.19**

To a solution of *N*-hydroxy-2-phenylpropanamide (**2.3.21**) (636 mg, 3.85 mmol), triethylamine (0.563 mL, 4.04 mmol), and anhydrous tetrahydrofuran (20 mL) was added pivaloyl chloride (0.497 mL, 4.04 mmol) and the resulting solution stirred at ambient temperature for 16 h under a nitrogen atmosphere. The reaction was diluted with ethyl acetate (20 mL) and washed with 1M aqueous HCl (20 mL), water (20 mL), and brine. The organic layer was passed through a hydrophobic frit and concentrated under reduced pressure to give the crude product as an off-white solid (1.1 g). The crude product was purified by automated flash column chromatography (cyclohexane:TBME, 100:0 - 0:100. 80 g SiO₂). The appropriate fractions were combined and concentrated under reduced pressure to give 2-phenyl-*N*-(pivaloyloxy)propanamide (**2.3.19**) as a white solid (720 mg, 75%). LCMS (Method D, UV, ESI) $R_t = 0.67$, $[M-H]^+ m/z = 250.2$. M.p. 98-100 °C. ¹H NMR (400 MHz, *d*₆-DMSO): $\delta = 11.82$ (1H, s), 7.38-7.20 (5H, m), 3.63 (1H, q, $J = 7.1$ Hz), 1.38 (3H, d, $J = 7.1$ Hz), 1.22 (9H, s). ¹³C NMR (100.6 MHz, CDCl₃): $\delta = 175.5, 170.7, 140.8, 128.3, 127.3, 126.8, 42.0, 37.6, 26.7, 18.3$. IR ($\nu_{\max}/\text{cm}^{-1}$) = 3132, 2974, 1780, 1664.

Rh(III) Catalysed C-H Activation Screening (Table 2.3.1)

To a heat dried microwave vial was added substrate (a) (0.125 mmol), 1,2-diphenylethyne (**2.3.22**) (25 mg, 0.138 mmol), catalyst (b) (0.013 mmol, 10 mol%), additive/s (c), and solvent (d) (0.625 mL). The vial was sealed and heated to T (e) for time (f). LCMS at this stage showed (g).

Table 2.3.1 – Entry 1

a) *N*-methyl-2-phenylpropanamide (**2.3.17**) (20 mg); b) [RhCp*Cl₂]₂ (7.7 mg); c) cesium acetate (7.2 mg, 0.038 mmol); d) methanol; e) 60 °C; f) 90 h; g) by-product formation ($R_t = 1.67$, method C) with no product formation.

Table 2.3.1 – Entry 2

a) *N*-methyl-2-phenylpropanamide (**2.3.17**) (20 mg); b) [IrCp*Cl₂]₂ (10.0 mg); c) cesium acetate (7.2 mg, 0.038 mmol); d) methanol; e) 60 °C; f) 90 h; g) by-product formation (*R_t* = 1.67, method C) with no product formation.

Table 2.3.1 – Entry 3

a) *N*-methoxy-2-phenylpropanamide (**2.3.18**) (22 mg); b) [RhCp*Cl₂]₂ (7.7 mg); c) cesium acetate (7.2 mg, 0.038 mmol); d) methanol; e) 60 °C; f) 40 h; g) 1% cyclised potential product with loss of OMe and 2% potential uncyclised product.

Table 2.3.1 – Entry 4

a) 2-phenyl-*N*-(pivaloyloxy)propanamide (**2.3.19**) (31 mg); b) [RhCp*Cl₂]₂ (7.7 mg); c) cesium acetate (7.2 mg, 0.038 mmol); d) methanol; e) 60 °C; f) 16 h; g) potential by-product and loss of the OPiv group but no product formation.

Table 2.3.1 – Entry 5

a) 2-phenyl-*N*-(pivaloyloxy)propanamide (**2.3.19**) (31 mg); b) [IrCp*Cl₂]₂ (10.0 mg); c) cesium acetate (7.2 mg, 0.038 mmol); d) methanol; e) 60 °C; f) 16 h; g) loss of the OPiv group but no product formation.

Table 2.3.1 – Entry 6

a) *N*-methyl-2-phenylpropanamide (**2.3.17**) (20 mg); b) [RhCp*Cl₂]₂ (7.7 mg); c) cesium acetate (48 mg, 0.250 mmol); d) methanol; e) ambient; f) 90 h; g) no reaction.

Table 2.3.1 – Entry 7

a) 2-phenyl-*N*-(pivaloyloxy)propanamide (**2.3.19**) (31 mg); b) [RhCp*Cl₂]₂ (7.7 mg); c) cesium acetate (48 mg, 0.250 mmol); d) methanol; e) ambient; f) 72 h; g) some breakdown of the starting material but no product formation.

Table 2.3.1 – Entry 8

a) *N*-methyl-2-phenylpropanamide (**2.3.17**) (20 mg); b) [RhCp*Cl₂]₂ (7.7 mg); c) copper (II) acetate (48 mg, 0.263 mmol); d) ^tAmOH; e) 110 °C; f) 16 h; g) no reaction.

Table 2.3.1 – Entry 9

a) *N*-methyl-2-phenylpropanamide (**2.3.17**) (20 mg); b) [RhCp*Cl₂]₂ (7.7 mg); c) cesium acetate (48 mg, 0.250 mmol); d) ^tAmOH; e) 110 °C; f) 72 h; g) by-product formation (*R_t* = 1.67, method C) with no product formation.

Table 2.3.1 – Entry 10

a) *N*-methyl-2-phenylpropanamide (**2.3.17**) (20 mg); b) [RhCp*Cl₂]₂ (7.7 mg); c) cesium acetate (7.2 mg, 0.038 mmol); d) acetonitrile; e) 60 °C; f) 90 h; g) trace amounts of the by-product formation (*R_t* = 1.67, method C) with no product formation.

Table 2.3.1 – Entry 11

a) 2-phenyl-*N*-(pivaloyloxy)propanamide (**2.3.19**) (31 mg); b) [RhCp*Cl₂]₂ (7.7 mg); c) cesium acetate (7.2 mg, 0.038 mmol); d) acetonitrile; e) 60 °C; f) 72 h; g) no product formation with trace levels of decomposition.

Table 2.3.1 – Entry 12

a) *N*-methyl-2-phenylpropanamide (**2.3.17**) (20 mg); b) [RhCp*Cl₂]₂ (7.7 mg); c) copper (II) acetate (50 mg, 0.275 mmol) and AgSbF₆ (17 mg, 0.050 mmol); d) DCE; e) 60 °C; f) 144 h; g) LCMS showed 39% product. The reaction was cooled to ambient temperature and concentrated under reduced pressure to give the crude product as a green solid (110 mg). The crude product was dissolved in DMSO:MeOH (1:1) purified by MDAP (formic modifier). The appropriate fractions were combined and concentrated under reduced pressure to give (*E*)-2-(2-(1,2-diphenylvinyl)phenyl)-*N*-methylpropanamide (**2.3.27**) (3 mg, 7%) as a yellow gum.

Data in agreement with that reported below.

Table 2.3.1 – Entry 13

a) 2-phenyl-*N*-(pivaloyloxy)propanamide (**2.3.19**) (31 mg); b) [RhCp*Cl₂]₂ (7.7 mg); c) copper (II) acetate (50 mg, 0.275 mmol) and AgSbF₆ (17 mg, 0.050 mmol); d) DCE; e) 60 °C; f) 72 h; g) Complex mixture of peaks with no product detected.

Table 2.3.1 – Entry 14

a) *N*-methoxy-2-phenylpropanamide (**2.3.18**) (22 mg); b) [RhCp*Cl₂]₂ (7.7 mg); c) copper (II) acetate (50 mg, 0.275 mmol) and AgSbF₆ (17 mg, 0.050 mmol); d) DCE; e) 60 °C; f) 40 h; g) No reaction.

Table 2.3.1 – Entry 15

a) *N*-methyl-2-phenylpropanamide (**2.3.17**) (20 mg); b) [RhCp*Cl₂]₂ (7.7 mg); c) PivOH (14 mg, 0.138 mmol) and AgSbF₆ (17 mg, 0.050 mmol); d) DCE; e) 60 °C; f) 16 h; g) LCMS showed 34% product. The reaction was cooled to ambient temperature and concentrated under reduced pressure to give the crude product as a yellow solid (103 mg). The crude product was dissolved in DMSO:MeOH (1:1) purified by MDAP (formic modifier). The appropriate fractions were combined and concentrated under reduced pressure to give (*E*)-2-(2-(1,2-diphenylvinyl)phenyl)-*N*-methylpropanamide (**2.3.27**) (8 mg, 19%) as a yellow gum.

Data in agreement with that reported below.

Table 2.3.1 – Entry 16

a) 2-phenyl-*N*-(pivaloyloxy)propanamide (**2.3.19**) (31 mg); b) [RhCp*Cl₂]₂ (7.7 mg); c) PivOH (14 mg, 0.138 mmol) and AgSbF₆ (17 mg, 0.050 mmol); d) DCE; e) 60 °C; f) 16 h; g) Some breakdown of the starting material with no product formation.

Table 2.3.1 – Entry 17

a) *N*-methoxy-2-phenylpropanamide (**2.3.18**) (22 mg); b) [RhCp*Cl₂]₂ (7.7 mg); c) PivOH (14 mg, 0.138 mmol) and AgSbF₆ (17 mg, 0.050 mmol); d) DCE; e) 60 °C; f) 144 h; g) 10% potential uncyclised product formation.

Table 2.3.1 – Entry 18

a) *N*-methyl-2-phenylpropanamide (**2.3.17**) (20 mg); b) [RhCp*Cl₂]₂ (7.7 mg); c) cesium pivalate (59 mg, 0.250 mmol) and copper (II) acetate (9.1 mg, 0.050 mmol); d) acetonitrile; e) 60 °C; f) 60 h; g) no reaction.

Table 2.3.1 – Entry 19

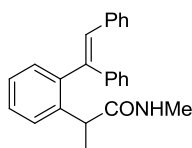
a) *N*-methyl-2-phenylpropanamide (**2.3.17**) (20 mg); b) [IrCp*Cl₂]₂ (10.0 mg); c) (1,1,1-trifluoro-*N*-((trifluoromethyl)sulfonyl)methylsulfonamido)silver (19 mg, 0.050 mmol); d) DCE; e) 60 °C; f) 72 h; g) no significant reaction.

Table 2.3.1 – Entry 20

a) *N*-methyl-2-phenylpropanamide (**2.3.17**) (20 mg); b) [IrCp*Cl₂]₂ (10.0 mg); c) silver carbonate (69 mg, 0.250 mmol); d) *o*-xylene; e) 160 °C; f) 24 h; g) no reaction.

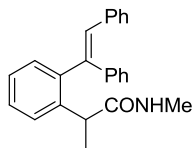
Control Reaction Without the Amide (Scheme 2.3.12)

To a microwave vial was added [IrCp*Cl₂]₂ (10.0 mg, 0.013 mmol), 1,2-diphenylethyne (25 mg, 0.140 mmol), and cesium acetate (7.34 mg, 0.038 mmol). The vial was sealed and to the mixture was added anhydrous methanol (0.625 mL). The reaction was heated to 60 °C and stirred for 72 h. LCMS analysis at this stage showed 15% formation of a new peak (*R*_t = 1.67, method C) consistent with that of the previously observed by-product. The reaction was terminated at this stage.

(E)-2-(2-(1,2-diphenylvinyl)phenyl)-N-methylpropanamide (2.3.27) (Scheme 2.3.13)**2.3.27**

To a heat dried microwave vial was added $[\text{RhCp}^*\text{Cl}_2]_2$ (31 mg, 0.05 mmol), AgSbF_6 (69 mg, 0.20 mmol), pivalic acid (56 mg, 0.55 mmol), *N*-methyl-2-phenylpropanamide (**2.3.17**) (82 mg, 0.50 mmol), and 1,2-diphenylethyne (98 mg, 0.55 mmol). The vial was sealed and to the mixture was added anhydrous DCE (2.5 mL). The resulting mixture was heated to 80 °C and stirred for 16 h. The reaction was cooled to ambient temperature and concentrated under reduced pressure to give the crude product as a dark brown solid (250 mg). The crude product was purified by automated flash column chromatography (cyclohexane:ethyl acetate, 100:0 – 50:50, 12 g SiO_2). The appropriate fractions were combined and concentrated under reduced pressure to give (*E*)-2-(2-(1,2-diphenylvinyl)phenyl)-*N*-methylpropanamide (**2.3.27**) as a yellow gum (136 mg, 80%). LCMS (Method C, UV, ESI) $R_t = 1.33$ min, $[\text{M-H}]^+ m/z = 342.1$, 97% purity. ^1H NMR (400 MHz, d_6 -DMSO, 120 °C): $\delta = 7.59$ (1H, s), 7.44-7.23 (8H, m), 7.17-7.09 (4H, m), 7.08-6.98 (2H, m), 6.02 (1H, s), 3.57 (1H, m), 2.37-2.22 (3H, m), 1.07 (3H, d, $J = 7.1$ Hz). ^{13}C NMR (100.6 MHz, d_6 -DMSO, 120 °C): $\delta = 173.7, 142.6, 140.9, 139.2, 137.3, 130.4, 129.6, 128.8, 128.7, 128.4, 128.3, 127.8, 127.4, 127.4, 127.0, 42.6, 26.0, 19.4$ (two aromatic peaks not observed due converging peaks, rotamers, and isomers). IR ($\nu_{\text{max}}/\text{cm}^{-1}$) = 2911, 1712, 1210. HRMS (ESI-[+H]) m/z : Calcd for $\text{C}_{24}\text{H}_{24}\text{NO}$ 342.1852; Found 342.1848.

(*E*)-2-(2-(1,2-diphenylvinyl)phenyl)-*N*-methylpropanamide (2.3.27) (Scheme 2.3.13)



2.3.27

To a heat dried microwave vial was added [RhCp*Cl₂]₂ (31 mg, 0.05 mmol), AgSbF₆ (69 mg, 0.20 mmol), copper (II) acetate (200 mg, 1.10 mmol), *N*-methyl-2-phenylpropanamide (**2.3.17**) (82 mg, 0.50 mmol), and 1,2-diphenylethyne (98 mg, 0.55 mmol). The vial was sealed and to the mixture was added anhydrous DCE (2.5 mL). The resulting mixture was heated to 80 °C and stirred for 16 h. The reaction was cooled to ambient temperature and concentrated under reduced pressure. The crude product was purified by automated flash column chromatography (cyclohexane:ethyl acetate, 100:0 – 50:50, 12 g SiO₂). The appropriate fractions were combined and concentrated under reduced pressure to give (*E*)-2-(2-(1,2-diphenylvinyl)phenyl)-*N*-methylpropanamide (**2.3.27**) as a yellow gum (100 mg, 59%). LCMS (Method C, UV, ESI) *R*_t = 1.33 min, [M-H]⁺ *m/z* = 342.1, 97% purity. ¹H NMR (400 MHz, *d*₆-DMSO, 120 °C): δ = 7.59 (1H, s), 7.44-7.23 (8H, m), 7.17-7.09 (4H, m), 7.08-6.98 (2H, m), 6.02 (1H, s), 3.57 (1H, m), 2.37-2.22 (3H, m), 1.07 (3H, d, *J* = 7.1 Hz). ¹³C NMR (100.6 MHz, *d*₆-DMSO, 120 °C): δ = 173.7, 142.6, 140.9, 139.2, 137.3, 130.4, 129.6, 128.8, 128.7, 128.4, 128.3, 127.8, 127.4, 127.4, 127.0, 42.6, 26.0, 19.4 (one aromatic peak not observed due converging peaks, rotamers, and isomers). IR (*v*_{max}/cm⁻¹) = 2911, 1712, 1210. HRMS (ESI-[+H]) *m/z*: Calcd for C₂₄H₂₄NO 342.1852; Found 342.1848.

Rh(III) Catalysed C-H Activation Solvent Screening (Table 2.3.2)

To a heat dried microwave vial was added *N*-methyl-2-phenylpropanamide (**2.3.17**) (82 mg, 0.50 mmol), 1,2-diphenylethyne (**2.3.22**) (98 mg, 0.55 mmol), [RhCp*Cl₂]₂ (31 mg, 0.05 mmol, 10 mol%), AgSbF₆ (69 mg, 0.20 mmol), pivalic acid (56 mg, 0.55 mmol), and solvent (a) (2.5 mL). The vial was sealed and heated to T (b) for time (c). LCMS at this stage showed (d).

Table 2.3.2 – Entry 2

a) toluene; b) 80 °C; c) 16 h; d) no reaction.

Table 2.3.2 – Entry 3

a) acetonitrile; b) 60 °C; c) 40 h; d) no reaction.

Table 2.3.2 – Entry 4

a) methanol; b) 60 °C; c) 40 h; d) no reaction.

Table 2.3.2 – Entry 5

a) PhCl; b) 60 °C; c) 16 h; d) 15% product in addition to starting materials and the solvent. After 144 h the reaction was complete showing 45% product in addition to low levels of the alkyne (2.3.22) starting material.

Table 2.3.2 – Entry 6

a) ^tAmOH; b) 80 °C; c) 2 h; d) 2% product after 2 h. This was unchanged after 16 h and, therefore, the reaction was concluded at this stage.

Table 2.3.2 – Entry 7

a) DCM; b) 40 °C; c) 16 h; d) 8% product after 16 h. After 40 h this had increased to 13%.

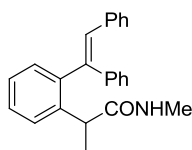
Table 2.3.2 – Entry 8

a) TBME; b) 60 °C; c) 16 h; d) No reaction.

Table 2.3.2 – Entry 9

a) 2-MeTHF; b) 60 °C; c) 16 h; d) < 2% product after 16 h. The reaction was heated to 80 °C and stirred for an additional 40 h (56 h in total). LCMS at this stage showed 18% product in addition to significant levels of remaining starting materials.

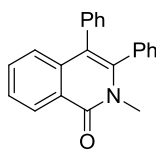
(*E*)-2-(2-(1,2-diphenylvinyl)phenyl)-*N*-methylpropanamide (2.3.27) (Scheme 2.3.16)



2.3.27

To a heat dried microwave vial was added [RhCp*Cl₂]₂ (31 mg, 0.05 mmol), AgSbF₆ (69 mg, 0.20 mmol), pivalic acid (56 mg, 0.55 mmol), *N*-methyl-2-phenylpropanamide (**2.3.17**) (82 mg, 0.50 mmol), and 1,2-diphenylethyne (98 mg, 0.55 mmol). The vial was sealed and placed under a nitrogen atmosphere. To the mixture was added anhydrous DCE (2.5 mL) and the resulting mixture heated to 80 °C and stirred for 16 h. The reaction was cooled to ambient temperature and concentrated under reduced pressure. The crude product was purified by automated flash column chromatography (cyclohexane/ethyl acetate, 100:0 – 50:50, 12 g SiO₂). The appropriate fractions were combined and concentrated under reduced pressure to give (*E*)-2-(2-(1,2-diphenylvinyl)phenyl)-*N*-methylpropanamide (**2.3.27**) as a yellow gum (130 mg, 76%). LCMS (Method C, UV, ESI) *R*_t = 1.33 min, [M-H]⁺ *m/z* = 342.1, 97% purity. ¹H NMR (400 MHz, *d*₆-DMSO, 120 °C): δ = 7.59 (1H, s), 7.44-7.23 (8H, m), 7.17-7.09 (4H, m), 7.08-6.98 (2H, m), 6.02 (1H, s), 3.57 (1H, m), 2.37-2.22 (3H, m), 1.07 (3H, d, *J* = 7.1 Hz). ¹³C NMR (100.6 MHz, *d*₆-DMSO, 120 °C): δ = 173.7, 142.6, 140.9, 139.2, 137.3, 130.4, 129.6, 128.8, 128.7, 128.4, 128.3, 127.8, 127.4, 127.4, 127.0, 42.6, 26.0, 19.4 (one aromatic peak not observed due converging peaks, rotamers, and isomers). IR (*ν*_{max}/cm⁻¹) = 2911, 1712, 1210. HRMS (ESI-[+H]) *m/z*: Calcd for C₂₄H₂₄NO 342.1852; Found 342.1848.

2-Methyl-3,4-diphenylisoquinolin-1(2H)-one (2.3.31)



2.3.31

To a microwave vial was added [RhCp*Cl₂]₂ (31 mg, 0.05 mmol), AgSbF₆ (69 mg, 0.20 mmol), pivalic acid (56 mg, 0.55 mmol), *N*-methylbenzamide (**2.3.30**) (68 mg, 0.50 mmol), and 1,2-diphenylethyne (**2.3.22**) (98 mg, 0.55 mmol). The vial was sealed and to the mixture was added anhydrous 1,2-dichloroethane (2.5 mL). The resulting mixture was heated to 60 °C and stirred for 72 h. LCMS at this stage showed masses corresponding to 27% cyclised product (**2.3.31**), 10% cyclised with a second C-H activation (**2.3.32**), and 7% non-cyclised (**2.3.33**). The reaction was cooled to ambient temperature and concentrated under reduced pressure to give the crude product as a dark brown solid (190 mg). The crude product was dissolved in DMSO:MeOH (1:1) and purified by formic MDAP. No product was isolated due to MDAP error and the reaction was terminated at this stage.

Rh(III) Catalysed C-H Activation Base Screening (Table 2.3.3)

To a heat dried microwave vial was added substrate (a), 1,2-diphenylethyne (**2.3.22**) (25 mg, 0.138 mmol mg), [RhCp*Cl₂]₂ (7.7 mg, 0.013 mmol, 10 mol%), AgSbF₆ (17 mg, 0.05 mmol), base (b), and anhydrous DCE (0.625 mL). The vial was sealed and heated to 60 °C for 72 h. LCMS at this stage showed (c).

Table 2.3.3 – Entry 1

a) *N*-methyl-2-phenylpropanamide (**2.3.17**) (20 mg, 0.125 mmol); b) CsOPiv (32 mg, 0.138 mmol); c) no reaction.

Table 2.3.3 – Entry 2

a) *N*-methyl-2-phenylpropanamide (**2.3.17**) (20 mg, 0.125 mmol); b) CsOAc (26 mg, 0.138 mmol); c) 3% starting material (**2.3.17**), 39% product (**2.3.27**), 10% unreacted alkyne (**2.3.22**), and 35% alkyne by-product.

Table 2.3.3 – Entry 3

a) *N*-methyl-2-phenylpropanamide (**2.3.17**) (20 mg, 0.125 mmol); b) KO^tBu (15 mg, 0.138 mmol); c) no reaction.

Table 2.3.3 – Entry 4

a) 2-phenyl-*N*-(pivaloyloxy)propanamide (**2.3.19**) (31 mg, 0.125 mmol); b) CsOPiv (32 mg, 0.138 mmol); c) no reaction.

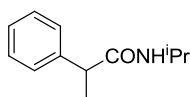
Table 2.3.3 – Entry 5

a) 2-phenyl-*N*-(pivaloyloxy)propanamide (**2.3.19**) (31 mg, 0.125 mmol); b) CsOAc (26 mg, 0.138 mmol); c) no reaction.

Table 2.3.3 – Entry 6

a) 2-phenyl-*N*-(pivaloyloxy)propanamide (**2.3.19**) (31 mg, 0.125 mmol); b) KO^tBu (15 mg, 0.138 mmol); c) no reaction.

***N*-Isopropyl-2-phenylpropanamide (**2.3.34**)³¹⁷**

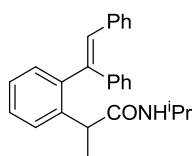


2.3.34

Prepared within our laboratories according to the following procedure.³¹⁷ A mixture of 2-phenylpropanoic acid (**2.3.20**) (0.45 mL, 3.33 mmol) and ethyl acetate (5 mL) was cooled to 0 °C. To the mixture was added CDI (702 mg, 4.33 mmol) and the resulting mixture stirred for 15 min. To the reaction was added propan-2-amine (0.37 mL, 4.33 mmol) and the resulting mixture stirred overnight at ambient temperature. To the mixture was added propan-2-amine (0.26 mL, 3.03 mmol) and the reaction stirred for an additional 1 h. The reaction was concentrated under reduced pressure to give the crude product. The crude product was purified

by automated flash column chromatography (cyclohexane:ethyl acetate, 90:10 – 50:50, 40 g SiO₂). The appropriate fractions were combined and concentrated under reduced pressure to give *N*-isopropyl-2-phenylpropanamide (**2.3.34**) as an off-white solid (368 mg, 49%). LCMS (Method D, UV, ESI) $R_t = 0.88$ min, $[M-H]^+ m/z = 192.1$, 99% purity. ¹H NMR (400 MHz, *d*₃-MeOD): $\delta = 7.37$ -7.27 (4H, m), 7.23 (1H, m), 3.95 (1H, td, $J = 6.6, 13.1$ Hz), 3.60 (1H, m), 1.43 (1H, d, $J = 7.1$ Hz), 1.18-1.04 (6H, m) (NH proton not observed) (low-levels of unknown impurities by NMR).

(*E*)-2-(2-(1,2-Diphenylvinyl)phenyl)-*N*-isopropylpropanamide (2.3.35)

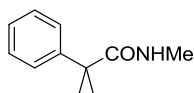


2.3.35

To a heat dried microwave vial was added [RhCp*Cl₂] (8 mg, 0.013 mmol), AgSbF₆ (17 mg, 0.050 mmol), pivalic acid (14 mg, 0.138 mmol), *N*-isopropyl-2-phenylpropanamide (**2.3.34**) (24 mg, 0.125 mmol), and 1,2-diphenylethyne (25 mg, 0.138 mmol). The vial was sealed and to the mixture was added anhydrous DCE (0.625 mL). The resulting mixture was heated to 80 °C and stirred for 72 h. LCMS analysis at this stage showed 50% product, 3% starting amide (**2.3.34**), and 22% alkyne. The reaction was cooled to ambient temperature and concentrated under reduced pressure. The crude product was purified by formic MDAP. The appropriate fractions were combined and concentrated under reduced pressure to give (*E*)-2-(2-(1,2-diphenylvinyl)phenyl)-*N*-isopropylpropanamide (**2.3.35**) as an orange oil (16 mg, 35%). LCMS (Method C, UV, ESI) $R_t = 1.44$ min, $[M-H]^+ m/z = 370.2$, 92% purity. ¹H NMR (400 MHz, *d*₆-DMSO, 120 °C): $\delta = 7.59$ (1H, m), 7.44-7.09 (12H, m), 7.06-6.99 (2H, m), 5.84 (m, *NH rotameric proton*, combined integration of 1H) and 5.60 (m, *NH rotameric proton*, combined integration of 1H), 3.54 (1H, m), 1.02 (3H, d, $J = 7.1$ Hz), 0.85 (6H, d, $J = 6.6$ Hz, *iPr rotameric protons*), 0.74 (6H, d, $J = 6.4$ Hz), (¹Pr hydrogen could not be distinguished due to the complex coupling and rotameric structures).

Insufficient material for full characterisation.

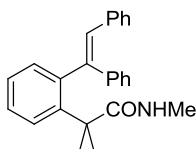
***N*,2-Dimethyl-2-phenylpropanamide (2.3.36)**



2.3.36

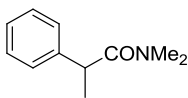
To a mixture of 2-methyl-2-phenylpropanoic acid (650 mg, 3.96 mmol) and 2-methyltetrahydrofuran (10 mL) was added methanamine (2M in THF, 2.38 mL, 4.75 mmol) and DIPEA (1.38 mL, 7.92 mmol) under a nitrogen atmosphere. To the mixture was added T3P (50% in ethyl acetate, 3.53 mL, 5.94 mmol). The resulting mixture was stirred for 16 h at ambient temperature. To the mixture was added ethyl acetate (15 mL) and water (15 mL). The resulting biphasic mixture was separated and the aqueous phase extracted with ethyl acetate (3 x 20 mL). The combined organic extracts were washed with brine (50 mL), passed through a hydrophobic frit, and concentrated under reduced pressure to give the crude product as a yellow oil (800 mg). The crude product was purified by automated flash column chromatography (cyclohexane:TBME, 100:0 – 0:100, 80 g SiO₂). The appropriate fractions were combined and concentrated under reduced pressure to give *N*,2-dimethyl-2-phenylpropanamide (**2.3.36**) as a yellow oil (380 mg, 54%). LCMS (Method C, UV, ESI) *R*_t = 0.75, [M-H]⁺ *m/z* = 178.1, 100% purity. ¹H NMR (400 MHz, *d*₆-DMSO): δ = 7.32-7.28 (5H, m), 7.21 (1H, m), 2.56 (3H, d, *J* = 4.6 Hz), 1.44 (6H, s).

***(E)*-2-(2-(1,2-Diphenylvinyl)phenyl)-*N*,2-dimethylpropanamide (2.3.37)**

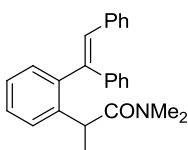


2.3.37

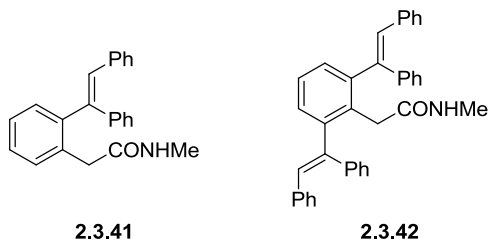
To a heat dried microwave vial was added [RhCp*Cl₂] (8 mg, 0.013 mmol), AgSbF₆ (17 mg, 0.050 mmol), pivalic acid (14 mg, 0.138 mmol), *N*,2-dimethyl-2-phenylpropanamide (**2.3.36**) (22 mg, 0.125 mmol), and 1,2-diphenylethyne (25 mg, 0.138 mmol). The vial was sealed and to the mixture was added anhydrous DCE (0.625 mL). The resulting mixture was heated to 80 °C and stirred for 72 h. LCMS analysis at this stage showed 2-3% potential product in addition to unreacted starting materials. The reaction was therefore terminated at this stage.

***N,N*-Dimethyl-2-phenylpropanamide (2.3.38)****2.3.38**

To a mixture of 2-phenylpropanoic acid (**2.3.20**) (0.91 mL, 6.66 mmol) and anhydrous THF (10 mL) was added dimethylamine (4.00 mL, 7.99 mmol) and DIPEA (2.33 mL, 13.32 mmol) under a nitrogen atmosphere. To the solution was added T3P (50% in ethyl acetate, 5.95 mL, 9.99 mmol). The reaction was heated to 70 °C and stirred for 1 h. The reaction was cooled to ambient temperature and to the mixture was added water (20 mL) and ethyl acetate (20 mL). The resulting biphasic mixture was separated and the aqueous phase extracted with ethyl acetate (3 x 15 mL). The combined organic extracts were washed with brine, passed through a hydrophobic frit, and concentrated under reduced pressure to give the crude product as a yellow oil (1.6 g). The crude product was purified by automated flash column chromatography (cyclohexane:TBME, 100:0 – 0:100, 120 g SiO₂). The appropriate fractions were combined and concentrated under reduced pressure to give *N,N*-dimethyl-2-phenylpropanamide (**2.3.38**) as a yellow oil (1.11 g, 91%). LCMS (Method C, UV, ESI) $R_t = 0.80$, $[M-H]^+ m/z = 178.2$, 100% purity. ¹H NMR (400 MHz, *d*₆-DMSO): $\delta = 7.34$ -7.19 (5H, m), 4.05 (1H, q, $J = 6.7$ Hz), 2.87 (3H, s), 2.82 (3H, s), 1.27 (3H, d, $J = 6.8$ Hz).

***(E)*-2-(2-(1,2-Diphenylvinyl)phenyl)-*N,N*-dimethylpropanamide (2.3.39)****2.3.39**

To a heat dried microwave vial was added [RhCp*Cl₂] (31 mg, 0.05 mmol), AgSbF₆ (69 mg, 0.20 mmol), pivalic acid (56 mg, 0.55 mmol), *N,N*-dimethyl-2-phenylpropanamide (**2.3.38**) (0.085 mL, 0.50 mmol), and 1,2-diphenylethyne (98 mg, 0.55 mmol). The vial was sealed and to the mixture was added anhydrous DCE (2.5 mL). The resulting mixture was heated to 80 °C and stirred for 60 h. LCMS at this stage showed only trace levels of potential product and therefore the reaction was concluded at this stage.

(E)-2-(2-(1,2-Diphenylvinyl)phenyl)-N-methylacetamide (2.3.41) and 2-(2,6-Bis((E)-1,2-diphenylvinyl)phenyl)-N-methylacetamide (2.3.42)

To a heat dried microwave vial was added [RhCp*Cl₂] (31 mg, 0.05 mmol), AgSbF₆ (69 mg, 0.20 mmol), pivalic acid (56 mg, 0.55 mmol), *N*-methyl-2-phenylacetamide (**2.3.40**) (75 mg, 0.50 mmol), and 1,2-diphenylethyne (98 mg, 0.55 mmol). The vial was sealed and to the mixture was added anhydrous DCE (2.5 mL). The resulting mixture was heated to 60 °C and stirred for 16 h. LCMS analysis at this stage showed only low levels of unreacted starting materials at this stage. The reaction was cooled to ambient temperature and concentrated under reduced pressure. The crude product was purified by automated column chromatography (cyclohexane/TBME, 100:0 - 60:40, 24 g SiO₂). The appropriate fractions were combined and concentrated to give 2-(2,6-bis((*E*)-1,2-diphenylvinyl)phenyl)-*N*-methylacetamide (**2.3.41**) as a white solid (58 mg, 23%) and (*E*)-2-(2-(1,2-diphenylvinyl)phenyl)-*N*-methylacetamide (**2.3.42**) as a white solid (74 mg, 45%).

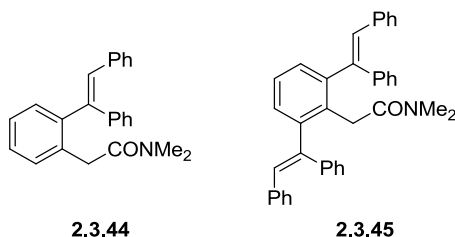
(E)-2-(2-(1,2-Diphenylvinyl)phenyl)-N-methylacetamide (2.3.41):

LCMS (Method C, UV, ESI) $R_t = 1.24$ min, $[M-H]^+ m/z = 328.1$, 100% purity. M.p. 137-142 °C. ¹H NMR (400 MHz, *d*₆-DMSO): $\delta = 7.50$ (1H, d, 4.2 Hz), 7.40-7.24 (8H, m), 7.16 (5H, m), 7.09-6.97 (3H, m), 3.22 (d, $J = 15.2$ Hz, CH₂ rotameric protons, combined integration of 2H) and 3.11 (d, $J = 15.2$ Hz, CH₂ rotameric protons, combined integration of 2H), 2.37 (3H, d, $J = 4.4$ Hz). ¹³C NMR (100.6 MHz, *d*₆-DMSO, 120 °C): $\delta = 170.3, 142.5, 141.1, 140.0, 137.4, 135.3, 131.1, 130.5, 129.5, 129.0, 128.6, 128.3, 128.0, 127.8, 127.4, 127.3, 127.1, 40.1, 25.9$. IR (ν_{max}/cm^{-1}) = 3343, 1643, 1554, 757. HRMS (ESI-[+H]) m/z : Calcd for C₂₃H₂₂NO 328.1696; Found 328.1699.

2-(2,6-Bis((*E*)-1,2-diphenylvinyl)phenyl)-*N*-methylacetamide (**2.3.42**):

LCMS (Method C, UV, ESI) $R_t = 1.64$ min, $[M-H]^+ m/z = 506.2$, 98% purity. M.p. 190-192 °C. 1H NMR (400 MHz, d_6 -DMSO): $\delta = 7.44$ -7.38 (4H, m), 7.36-7.30 (6H, m), 7.29-7.13 (13H, m), 7.10 (2H, d, $J = 7.6$ Hz), 6.83 (q, $J = 4.6$ Hz, *NH rotameric proton*, combined integration of 1H) and 6.68 (q, $J = 4.4$ Hz, *NH rotameric proton*, combined integration of 1H), 3.15 (d, $J = 15.7$ Hz, *CH₂ rotameric protons*, combined integration of 2H) and 2.93 (s, *CH₂ rotameric protons*, combined integration of 2H) and 2.76 (d, $J = 15.9$ Hz, *CH₂ rotameric protons*, combined integration of 2H), 2.06-2.01 (3H, m). ^{13}C NMR (100.6 MHz, d_6 -DMSO, 120 °C): $\delta = 168.7$, 141.8, 140.8, 136.9, 133.6, 130.6, 129.4, 128.6, 128.1, 127.7, 127.7, 127.2, 126.9, 126.5, 37.7, 25.0 (one aromatic carbon not observed). IR (ν_{max}/cm^{-1}) = 3444, 3053, 1664, 1445, 695. HRMS (ESI-[+H]) m/z : Calcd for $C_{37}H_{32}NO$ 506.2478; Found 506.2487.

(*E*)-2-(2-(1,2-Diphenylvinyl)phenyl)-*N*-methylacetamide (2.3.44) and 2-(2,6-bis((*E*)-1,2-diphenylvinyl)phenyl)-*N,N*-dimethylacetamide (2.3.45)



To a heat dried microwave vial was added $[RhCp^*Cl_2]$ (31 mg, 0.05 mmol), $AgSbF_6$ (69 mg, 0.20 mmol), pivalic acid (56 mg, 0.55 mmol), *N,N*-dimethyl-2-phenylacetamide (**2.3.43**) (82 mg, 0.50 mmol), and 1,2-diphenylethyne (98 mg, 0.55 mmol). The vial was sealed and to the mixture was added anhydrous DCE (2.5 mL). The resulting mixture was heated to 60 °C and stirred for 16 h. The reaction was cooled to ambient temperature and concentrated under reduced pressure. The crude product was purified by automated column chromatography (cyclohexane/TBME, 100:0 - 60:40, 24 g SiO_2). The crude product was purified by automated column chromatography (cyclohexane/TBME, 100:0 - 60:40, 24 g SiO_2). The appropriate fractions were combined and concentrated to give 2-(2,6-bis((*E*)-1,2-diphenylvinyl)phenyl)-*N,N*-dimethylacetamide (**2.3.45**) as a white solid (63 mg, 24%) and (*E*)-2-(2-(1,2-diphenylvinyl)phenyl)-*N,N*-dimethylacetamide (**2.3.44**) as a colourless gum (55 mg, 32%).

(*E*)-2-(2-(1,2-diphenylvinyl)phenyl)-*N,N*-dimethylacetamide (**2.3.44**):

LCMS (Method C, UV, ESI) $R_t = 1.33$ min, $[M-H]^+ m/z = 342.1$, 99% purity. 1H NMR (400 MHz, d_6 -DMSO, 120 °C): $\delta = 7.39-7.11$ (13H, m), 7.06-7.02 (2H, m), 3.36 (2H, s), 2.65 (6H, s). ^{13}C NMR (100.6 MHz, d_6 -DMSO, 120 °C): $\delta = 169.5, 141.6, 140.5, 139.2, 136.8, 134.4, 130.2, 128.9, 128.5, 128.2, 128.1, 127.8, 127.6, 127.4, 126.9, 126.9, 126.5, 36.9, 35.9$. IR (ν_{max}/cm^{-1}) = 3021, 1642, 1491, 693. HRMS (ESI-[+H]) m/z : Calcd for $C_{24}H_{24}NO$ 342.1852; Found 342.1844.

2-(2,6-bis((*E*)-1,2-diphenylvinyl)phenyl)-*N,N*-dimethylacetamide (**2.3.45**):

LCMS (Method C, UV, ESI) $R_t = 1.67$ min, $[M-H]^+ m/z = 520.3$, 83% purity. M.p. 98-102 °C. 1H NMR (400 MHz, d_6 -DMSO, 120 °C): $\delta = 7.49-7.02$ (24H, m), 6.69 (1H, s), 3.66-3.25 (2H, m), 2.72 (1H, s, *NMe*₂ rotameric protons), 2.58-2.54 (5H, m, *NMe*₂ rotameric protons). ^{13}C NMR (100.6 MHz, d_6 -DMSO, 120 °C): $\delta = 168.6, 142.0, 141.5, 141.1, 136.9, 134.8, 130.6, 130.5, 129.6, 129.5, 129.4, 129.2, 129.0, 128.8, 128.2, 128.0, 127.9, 127.8, 127.6, 127.3, 127.2, 127.1, 126.9, 126.8, 126.7, 126.6, 35.6, 24.2$ (NMR complicated by the presence of overlapping peaks and rotameric structures). IR (ν_{max}/cm^{-1}) = 3021, 1642, 1491, 693. HRMS (ESI-[+H]) m/z : Calcd for $C_{38}H_{34}NO$ 520.2635; Found 520.2630.

Study into the Influence of Temperature into the Mono-/Di-C-H Activation Reactions (Scheme 2.3.24)

To a microwave vial was added a mixture of $[RhCp^*Cl_2]$ (31 mg, 0.05 mmol), $AgSbF_6$ (69 mg, 0.20 mmol), pivalic acid (56 mg, 0.55 mmol), *N*-methyl-2-phenylacetamide (**2.3.40**) (75 mg, 0.50 mmol), and 1,2-diphenylethyne (**2.3.22**) (98 mg, 0.55 mmol). The vial was sealed and to the mixture was added anhydrous DCE (2.5 mL). The reaction was heated to the stated temperature and monitored periodically by LCMS (see below).

Confidential – Property of GSK – Do Not Copy

After 30 min:

Temperature	% starting material (2.3.40)	% mono-product (2.3.41)	% di-product (2.3.42)	Ratio of mono/di
30 °C	4.91	2.95	0	-
40 °C	4.30	5.80	0	-
50 °C	3.79	9.80	0	-
60 °C	3.23	23.17	0	-
70 °C	2.31	30.76	2.09	14.72
80 °C	1.69	35.51	6.65	5.34

After 60 min:

Temperature	% starting material (2.3.40)	% mono-product (2.3.41)	% di-product (2.3.42)	Ratio of mono/di
30 °C	4.98	3.03	0	-
40 °C	4.13	8.89	0	-
50 °C	3.22	18.22	0	-
60 °C	2.41	31.03	1.86	16.68
70 °C	1.78	39.44	8.35	4.72
80 °C	1.19	38.58	24.89	1.55

After 120 min:

Temperature	% starting material (2.3.40)	% mono-product (2.3.41)	% di-product (2.3.42)	Ratio of mono/di
30 °C	4.62	9.31	0	-
40 °C	3.56	14.20	0	-
50 °C	2.62	25.87	Trace	-
60 °C	1.82	37.00	6.55	5.65
70 °C	1.26	42.03	22.75	1.85
80 °C	1.10	41.30	38.66	1.07

After 210 min:

Temperature	% starting material (2.3.40)	% mono-product (2.3.41)	% di-product (2.3.42)	Ratio of mono/di
30 °C	4.56	15.00	0	-
40 °C	3.01	23.49	Trace	-
50 °C	1.84	32.10	5.05	6.36
60 °C	1.28	42.51	21.13	2.01
70 °C	1.07	41.61	39.80	1.05
80 °C	1.02	38.84	45.36	0.86

After 360 min:

Temperature	% starting material (2.3.40)	% mono-product (2.3.41)	% di-product (2.3.42)	Ratio of mono/di
30 °C	3.29	14.15	0	-
40 °C	2.31	29.73	1.82	16.34
50 °C	1.28	35.28	12.71	2.78
60 °C	0.97	37.87	22.78	1.66
70 °C	0.99	42.79	42.66	1.00
80 °C	1.07	41.93	44.97	0.93

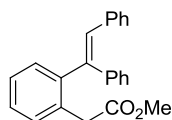
After 24 h:

Temperature	% starting material (2.3.40)	% mono-product (2.3.41)	% di-product (2.3.42)	Ratio of mono/di
30 °C	2.06	38.32	6.80	5.64
40 °C	1.10	42.53	27.48	1.55
50 °C	0.60	34.98	37.29	0.94
60 °C	0.69	43.49	43.76	0.99
70 °C	0.88	42.63	44.31	0.96
80 °C	0.82	42.12	43.19	0.98

Rh(III) Catalysed C-H Activation Directing Group Screening

To a heat dried microwave vial was added substrate (a), 1,2-diphenylethyne (b), [RhCp*Cl₂]₂ (10 mol%) (c), AgSbF₆ (40 mol%) (d), pivalic acid (1.1 eq) (e), and anhydrous DCE (f). The vial was sealed and heated to T (g) for time (h).

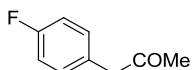
(E)-Methyl 2-(2-(1,2-diphenylvinyl)phenyl)acetate



a) methyl 2-phenylacetate (0.07 mL, 0.50 mmol); b) 98 mg, 0.55 mmol; c) 31 mg, 0.05 mmol; d) 69 mg, 0.20 mmol; e) 56 mg, 0.55 mmol; f) 2.5 mL, g) 120 °C; h) 96 h. LCMS at this stage

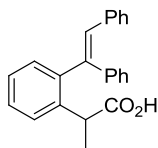
24% of an unidentified peak. Due to low conversion and the forcing reaction conditions the reaction was concluded at this stage.

1-(4-Fluorophenyl)propan-2-one



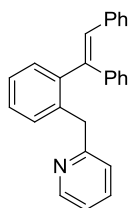
a) 1-(4-fluorophenyl)propan-2-one (0.017 mL, 0.125 mmol); b) 25 mg, 0.138 mmol; c) 8 mg, 0.013 mmol; d) 17 mg, 0.050 mmol; e) 14 mg, 0.138 mmol; f) 0.625 mL, g) 80 °C; h) 16 h. LCMS at this stage 30% unknown product. The reaction was cooled ambient temperature and concentrated under reduced pressure. The crude product was purified by formic MDAP. Unfortunately none of the unknown peak was isolated and the reaction was concluded at this stage.

(E)-2-(2-(1,2-Diphenylvinyl)phenyl)propanoic acid



a) 2-phenylpropanoic acid (0.017 mL, 0.125 mmol); b) 25 mg, 0.138 mmol; c) 8 mg, 0.013 mmol; d) 17 mg, 0.050 mmol; e) 14 mg, 0.138 mmol; f) 0.625 mL, g) 80 °C; h) 16 h. LCMS at this stage showed 25% of an unknown product. Due to the low conversion levels and the identical retention time of this product in both acidic and basic modifiers the reaction was terminated at this stage.

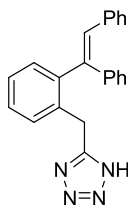
(E)-2-(2-(1,2-Diphenylvinyl)benzyl)pyridine



a) 2-benzylpyridine (0.02 mL, 0.125 mmol); b) 25 mg, 0.138 mmol; c) 8 mg, 0.013 mmol; d) 17 mg, 0.050 mmol; e) 14 mg, 0.138 mmol; f) 0.625 mL, g) 80 °C; h) 72 h. The reaction was cooled to ambient temperature and concentrated under reduced pressure to give the crude product as a brown gum (70 mg). The crude product was dissolved in DMSO:MeOH (1:1) and purified by formic MDAP. The appropriate fractions were combined and concentrated under reduced pressure to give (*E*)-2-(2-(1,2-diphenylvinyl)benzyl)pyridine as a light brown gum (4 mg, 9%). LCMS (Method C, UV, ESI) $R_t = 1.14$ min, $[M-H]^+$ $m/z = 348.2$, 90% purity. NMR (400 MHz, d_6 -DMSO, 120 °C): $\delta = 8.45$ (1H, d, $J = 4.2$ Hz), 7.60 (1H, dt, $J = 1.8, 7.6$ Hz), 7.27-7.08 (13H, m), 7.06-7.02 (2H, m), 6.97 (1H, d, $J = 7.8$ Hz), 6.57 (1H, s), 4.14 (2H, s).

Insufficient material for complete characterisation.

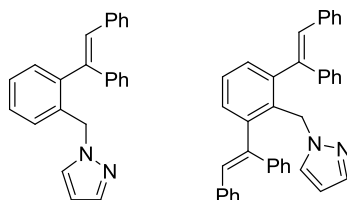
(E)-5-(2-(1,2-Diphenylvinyl)benzyl)-1H-tetrazole



a) 5-benzyl-1H-tetrazole (20 mg, 0.125 mmol); b) 25 mg, 0.138 mmol; c) 8 mg, 0.013 mmol; d) 17 mg, 0.050 mmol; e) 14 mg, 0.138 mmol; f) 0.625 mL, g) 80 °C; h) 64 h. The reaction was cooled to ambient temperature and concentrated under reduced pressure to give the crude product as a yellow solid (70 mg). The crude product was dissolved in DMSO:MeOH (1:1) and purified by formic MDAP. The appropriate fractions were combined and concentrated under reduced pressure to give (*E*)-5-(2-(1,2-diphenylvinyl)benzyl)-1H-tetrazole as an off-white solid (7 mg, 17%). LCMS (Method C, UV, ESI) $R_t = 1.31$ min, $[M-H]^+$ $m/z = 339.1$, 99% purity. NMR (400 MHz, d_6 -DMSO): $\delta = 7.42$ -7.24 (7H, m), 7.20 (1H, s), 7.17-7.11 (4H, m), 6.95-6.90 (2H, m), 4.32 (2H, s).

Insufficient material for complete characterisation.

(*E*)-1-(2-(1,2-Diphenylvinyl)benzyl)-1*H*-pyrazole **and** **1-(2,6-bis((*E*)-1,2-diphenylvinyl)benzyl)-1*H*-pyrazole**



a) 1-benzyl-1*H*-pyrazole (0.07 mL, 0.50 mmol); b) 98 mg, 0.55 mmol; c) 31 mg, 0.05 mmol; d) 69 mg, 0.20 mmol; e) 56 mg, 0.55 mmol; f) 2.5 mL, g) 60 °C; h) 112 h. The reaction was cooled to ambient temperature and concentrated under reduced pressure. The crude product was purified by automated column chromatography (cyclohexane/TBME, 100:0 – 80:20, 24 g SiO₂). The appropriate fractions were combined and concentrated under reduced pressure to give (*E*)-1-(2-(1,2-diphenylvinyl)benzyl)-1*H*-pyrazole as a colourless oil (27 mg, 16%) and 1-(2,6-bis((*E*)-1,2-diphenylvinyl)benzyl)-1*H*-pyrazole as a colourless gum (15 mg, 6%).

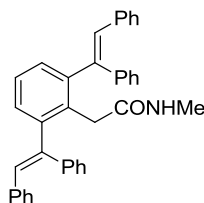
(*E*)-1-(2-(1,2-diphenylvinyl)benzyl)-1*H*-pyrazole (**2.3.48**):

LCMS (Method C, UV, ESI) $R_t = 1.46$ min, $[M-H]^+ m/z = 337.1$, 90% purity. ¹H NMR (400 MHz, *d*₆-DMSO, 120 °C): $\delta = 7.46$ (2H, dd, $J = 2.0, 5.6$ Hz), 7.34-7.25 (6H, m), 7.23-7.11 (7H, m), 7.06 (1H, m), 6.67 (1H, s), 6.24 (1H, t, $J = 2.0$ Hz), 5.34 (2H, s). ¹³C NMR (100.6 MHz, *d*₆-DMSO, 120 °C): $\delta = 143.1, 140.7, 140.0, 138.7, 136.8, 134.8, 131.1, 130.0, 129.8, 128.7, 128.3, 127.9, 127.5, 126.9, 126.5, 105.2, 52.7$. HRMS (ESI-[+H]) m/z : Calcd for C₂₄H₂₁N₂ 337.1699; Found 337.1684.

1-(2,6-bis((*E*)-1,2-diphenylvinyl)benzyl)-1*H*-pyrazole:

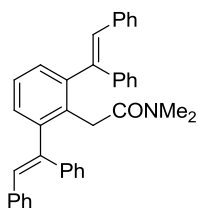
LCMS (Method C, UV, ESI) $R_t = 1.75$ min, $[M-H]^+ m/z = 515.2$, 94% purity. ¹H NMR (400 MHz, *d*₆-DMSO, 120 °C): $\delta = 7.45$ -7.38 (2H, m), 7.31-7.27 (2H, m), 7.24-7.12 (13 H, m), 7.09-7.04 (4H, m), 7.02-6.97 (4H, m), 6.59 (2H, s), 6.14 (1H, t, $J = 2.1$ Hz), 5.39 (2H, s). ¹³C NMR (100.6 MHz, *d*₆-DMSO, 120 °C): $\delta = 145.8, 140.8, 139.8, 138.1, 136.8, 131.0, 130.9, 129.7, 129.3, 129.3, 128.9, 128.1, 127.9, 127.8, 127.3, 126.8, 104.6, 50.0$. HRMS (ESI-[+H]) m/z : Calcd for C₃₈H₃₁N₂ 515.2482; Found 515.2461.

2-(2,6-Bis((*E*)-1,2-diphenylvinyl)phenyl)-*N*-methylacetamide (2.3.42) (2.2 equivalents of alkyne)



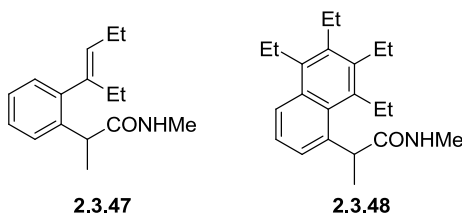
2.3.42

To a heat dried microwave vial was added [RhCp*Cl₂] (31 mg, 0.05 mmol), AgSbF₆ (69 mg, 0.20 mmol), pivalic acid (56 mg, 0.55 mmol), *N*-methyl-2-phenylacetamide (**2.3.40**) (75 mg, 0.50 mmol), and 1,2-diphenylethyne (196 mg, 1.10 mmol). The vial was sealed and to the mixture was added anhydrous DCE (2.5 mL). The resulting mixture was heated to 60 °C and stirred for 16 h. The reaction was cooled to ambient temperature and concentrated under reduced pressure. The crude product was purified by automated column chromatography (cyclohexane/TBME, 100:0 - 50:50, 24 g SiO₂). The appropriate fractions were combined and concentrated to give 2-(2,6-bis((*E*)-1,2-diphenylvinyl)phenyl)-*N*-methylacetamide (**2.3.42**) as a white solid (206 mg, 81%). LCMS (Method C, UV, ESI) *R*_t = 1.64 min, [M-H]⁺ *m/z* = 506.2, 98% purity. M.p. 190-192 °C. ¹H NMR (400 MHz, *d*₆-DMSO): δ = 7.44-7.38 (4H, m), 7.36-7.30 (6H, m), 7.29-7.13 (13H, m), 7.10 (2H, d, *J* = 7.6 Hz), 6.83 (q, *J* = 4.6 Hz, *NH rotameric proton*, combined integration of 1H) and 6.68 (q, *J* = 4.4 Hz, *NH rotameric proton*, combined integration of 1H), 3.15 (d, *J* = 15.7 Hz, *CH₂ rotameric protons*, combined integration of 2H) and 2.93 (s, *CH₂ rotameric protons*, combined integration of 2H) and 2.76 (d, *J* = 15.9 Hz, *CH₂ rotameric protons*, combined integration of 2H), 2.06-2.01 (3H, m). ¹³C NMR (100.6 MHz, *d*₆-DMSO, 120 °C): δ = 168.7, 141.8, 140.8, 136.9, 133.6, 130.6, 129.4, 128.6, 128.1, 127.7, 127.7, 127.2, 126.9, 126.5, 37.7, 25.0 (one aromatic carbon not observed). IR (*ν*_{max}/cm⁻¹) = 3444, 3053, 1664, 1445, 695. HRMS (ESI-[+H]) *m/z*: Calcd for C₃₇H₃₂NO 506.2478; Found 506.2487.

2-(2,6-Bis((E)-1,2-diphenylvinyl)phenyl)-N,N-dimethylacetamide (2.3.45)**2.3.45**

To a heat dried microwave vial was added [RhCp*Cl₂] (31 mg, 0.05 mmol), AgSbF₆ (69 mg, 0.20 mmol), pivalic acid (56 mg, 0.55 mmol), *N,N*-dimethyl-2-phenylacetamide (**2.3.43**) (82 mg, 0.50 mmol), and 1,2-diphenylethyne (196 mg, 1.10 mmol). The vial was sealed and to the mixture was added anhydrous DCE (2.5 mL). The resulting mixture was heated to 60 °C and stirred for 64 h. The reaction was cooled to ambient temperature and concentrated under reduced pressure. The crude product was purified by automated flash column chromatography (cyclohexane/TBME, 100:0 – 60:40, 24 g SiO₂). The appropriate fractions were combined and concentrated under reduced pressure to give 2-(2,6-bis((*E*)-1,2-diphenylvinyl)phenyl)-*N,N*-dimethylacetamide (**2.3.45**) as a white solid (211 mg, 81%). LCMS (Method C, UV, ESI) *R*_t = 1.67 min, [M-H]⁺ *m/z* = 520.3, 83% purity. M.p. 98-102 °C. ¹H NMR (400 MHz, *d*₆-DMSO, 120 °C): δ = 7.49-7.02 (24H, m), 6.69 (1H, s), 3.66-3.25 (2H, m), 2.72 (1H, s, *NMe*₂ rotameric protons), 2.58-2.54 (5H, m, *NMe*₂ rotameric protons). ¹³C NMR (100.6 MHz, *d*₆-DMSO, 120 °C): δ = 168.6, 142.0, 141.5, 141.1, 136.9, 134.8, 130.6, 130.5, 129.6, 129.5, 129.4, 129.2, 129.0, 128.8, 128.2, 128.0, 127.9, 127.8, 127.6, 127.3, 127.2, 127.1, 126.9, 126.8, 126.7, 126.6, 35.6, 24.2 (NMR complicated by the presence of overlapping peaks and rotameric structures). IR (*ν*_{max} /cm⁻¹) = 3021, 1642, 1491, 693. HRMS (ESI-[+H]) *m/z*: Calcd for C₃₈H₃₄NO 520.2635; Found 520.2630.

(E)-2-(2-(Hex-3-en-3-yl)phenyl)-N-methylpropanamide (2.3.47) and N-methyl-2-(5,6,7,8-tetraethylnaphthalen-1-yl)propanamide (2.3.48)



To a heat dried microwave vial was added [RhCp*Cl₂] (31 mg, 0.05 mmol), AgSbF₆ (69 mg, 0.20 mmol), pivalic acid (56 mg, 0.55 mmol), *N*-methyl-2-phenylpropanamide (**2.3.17**) (82 mg, 0.50 mmol), and hex-3-yne (**2.3.46**) (0.062 mL, 0.55 mmol). The vial was sealed and to the mixture was added anhydrous DCE (2.5 mL). The resulting mixture was heated to 80 °C and stirred for 16 h. The reaction was cooled to ambient temperature and concentrated under reduced pressure. The crude product was purified by automated flash column chromatography (cyclohexane/TBME, 100:0 – 50:50, 24 g SiO₂). The appropriate fractions were combined and concentrated under reduced pressure to give (*E*)-2-(2-(hex-3-en-3-yl)phenyl)-*N*-methylpropanamide (**2.3.47**) as a colourless solid (81 mg, 66%) and *N*-methyl-2-(5,6,7,8-tetraethylnaphthalen-1-yl)propanamide (**2.3.48**) (22 mg, 14%) as a white solid.

(E)-2-(2-(hex-3-en-3-yl)phenyl)-N-methylpropanamide (2.3.47):

LCMS (Method C, UV, ESI) $R_t = 1.20$ min, [M-H]⁺ $m/z = 246.2$, 100% purity. M.p. 47-48 °C. ¹H NMR (400 MHz, *d*₆-DMSO, 120 °C): $\delta = 7.42$ (1H, dd, $J = 7.8, 1.2$ Hz), 7.21 (1H, m), 7.15 (1H, m), 7.01 (1H, dd, $J = 7.3, 1.5$ Hz), 6.78 (1H, m), 5.20 (1H, t, $J = 7.2$ Hz), 3.75 (1H, q, $J = 7.2$ Hz), 2.6 (3H, d, $J = 4.6$ Hz), 2.38 (2H, q, $J = 7.6$ Hz), 2.26-2.16 (2H, m), 1.35 (3H, d, $J = 7.1$ Hz), 1.05 (3H, t, $J = 7.5$ Hz), 0.90 (3H, t, $J = 7.6$ Hz). ¹³C NMR (100.6 MHz, *d*₆-DMSO, 120 °C): $\delta = 174.0, 143.4, 140.5, 139.6, 131.2, 128.7, 127.2, 126.4, 125.6, 42.0, 25.7, 24.8, 20.6, 19.7, 13.9, 12.4$. IR ($\nu_{\max}/\text{cm}^{-1}$) = 3316, 2965, 1649, 1529. HRMS (ESI-[+H]) m/z : Calcd for C₁₆H₂₃NO 246.1852; Found 246.1846.

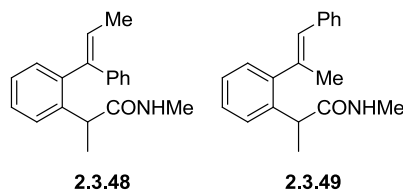
N-methyl-2-(5,6,7,8-tetraethylnaphthalen-1-yl)propanamide (2.3.48):

LCMS (Method C, UV, ESI) $R_t = 1.43$, [M-H]⁺ $m/z = 326.2$, 100% purity. ¹H NMR (400 MHz, *d*₆-DMSO, 120 °C): $\delta = 7.92$ (1H, dd, $J = 1.1, 8.4$ Hz), 7.47 (1H, dd, $J = 1.2, 7.1$ Hz), 7.35

(1H, m), 6.88 (1H, m), 4.48 (1H, q, $J = 6.8$ Hz), 3.22-3.06 (4H, m), 2.96-2.83 (4H, m), 2.60 (3H, d, $J = 4.6$ Hz), 1.51 (3H, d, $J = 7.1$ Hz), 1.34-1.20 (12H, m).

Insufficient material for complete characterisation.

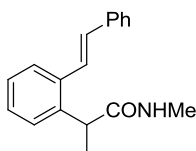
(*E*)-*N*-Methyl-2-(2-(1-phenylprop-1-en-1-yl)phenyl)propanamide (2.3.50) and (*E*)-*N*-methyl-2-(2-(1-phenylprop-1-en-2-yl)phenyl)propanamide (2.3.51)



To a heat dried microwave vial was added [RhCp*Cl₂] (31 mg, 0.05 mmol), AgSbF₆ (69 mg, 0.20 mmol), pivalic acid (56 mg, 0.55 mmol), *N*-methyl-2-phenylpropanamide (**2.3.17**) (82 mg, 0.50 mmol), and prop-1-en-1-ylbenzene (**2.3.49**) (0.069 mL, 0.55 mmol). The vial was sealed and to the mixture was added anhydrous DCE (2.5 mL). The resulting mixture was heated to 80 °C and stirred for 16 h. The reaction was cooled to ambient temperature and concentrated under reduced pressure. The crude product was purified by automated flash column chromatography (cyclohexane/TBME, 100:0 - 50:50, 24 g SiO₂). The appropriate fractions were combined and concentrated under reduced pressure to give a mixture of (*E*)-*N*-methyl-2-(2-(1-phenylprop-1-en-1-yl)phenyl)propanamide (**2.3.50**) and (*E*)-*N*-methyl-2-(2-(1-phenylprop-1-en-2-yl)phenyl)propanamide (**2.3.51**) as a pale yellow solid (90 mg, 64%, 61:39 ratio of products). LCMS (Method C, UV, ESI) $R_t = 1.18$ min, $[M-H]^+ m/z = 280.2$, 73% purity. ¹H NMR (400 MHz, *d*₆-DMSO): $\delta = 7.60$ (1H, d, $J = 3.9$ Hz, *NH* proton for the major isomer), 7.55-7.01 (7H, m, *aromatic protons for both isomers*), 6.87-6.77 (2H, m, *aromatic protons for both isomers*), 6.60 (1H, s, *alkene proton for the minor isomer*), 6.57 (1H, s, *alkene proton for the major isomer*), 6.23 (1H, d, $J = 3.4$ Hz, *NH* proton for the minor isomer), 3.59 (1H, q, $J = 7.0$ Hz, *both isomers*), 2.55 (3H, d, $J = 4.7$ Hz, *major isomer*), 2.18-2.14 (3H, m, *major isomer*), 2.14-2.10 (6H, m, *minor isomer*), 1.31 (3H, d, $J = 7.1$ Hz, *minor isomer*), 0.94 (3H, d, $J = 7.1$ Hz, *major isomer*). ¹³C NMR (100.6 MHz, *d*₆-DMSO, 120 °C): $\delta = 173.5$, 141.3, 138.6, 137.9, 137.0, 129.3, 128.7, 128.1, 127.9, 127.7, 127.7, 127.3, 127.2, 126.8, 126.4, 126.2, 41.9, 27.7, 25.6, 20.4, 19.7, 19.0 (several peaks not observed due converging

peaks, rotamers, and isomers). HRMS (ESI-[+H]) m/z : Calcd for C₁₉H₂₂NO 280.1696; Found 280.1684.

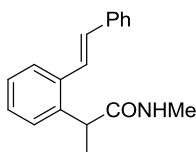
(E)-N-Methyl-2-(2-styrylphenyl)propanamide (2.3.53)



2.3.53

To a heat dried microwave vial was added [RhCp*Cl₂] (8 mg, 0.013 mmol), AgSbF₆ (17 mg, 0.050 mmol), pivalic acid (14 mg, 0.138 mmol), *N*-methyl-2-phenylpropanamide (**2.3.17**) (20 mg, 0.125 mmol), and ethynylbenzene (**2.3.52**) (0.015 mL, 0.138 mmol). The vial was sealed and to the mixture was added anhydrous DCE (0.625 mL). The resulting mixture was heated to 60 °C and stirred for 72 h. LCMS at this stage showed 40% of new peaks (14% and 26%) consistent with the mass of the product. The reaction was cooled to ambient temperature and concentrated under reduced pressure to give the crude product as a black gum (101 mg). The crude product was purified by formic MDAP. Unfortunately neither of the peaks could be isolated, appearing to degrade during the isolation stage. *Repeating the reaction in the absence of the rhodium catalyst showed the formation of the same peak, implying that this not a product of C-H activation but a side reaction.*

(E)-N-Methyl-2-(2-styrylphenyl)propanamide (2.3.53)



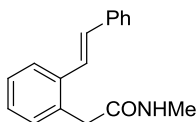
2.3.53

To a heat dried microwave vial was added [RhCp*Cl₂] (8 mg, 0.013 mmol), AgSbF₆ (17 mg, 0.050 mmol), copper(II) acetate (50 mg, 0.275 mmol), *N*-methyl-2-phenylpropanamide (**2.3.17**) (20 mg, 0.125 mmol), and styrene (**2.3.55**) (0.022 mL, 0.188 mmol). The vial was sealed and to the mixture was added anhydrous DCE (0.625 mL). The resulting mixture was heated to 80 °C and stirred for 24 h. The reaction was cooled to ambient temperature and to

concentrated under reduced pressure to give the crude product as a brown solid (80 mg). The crude product was dissolved in DMSO:MeOH (1:1) and purified by formic MDAP. The appropriate fractions were combined and concentrated under reduced pressure to give (*E*)-*N*-methyl-2-(2-styrylphenyl)propanamide (**2.3.53**) (8 mg, 24%). LCMS (Method C, UV, ESI) R_t = 1.11 min, $[M-H]^+$ m/z = 266.2, 100% purity. 1H NMR (400 MHz, d_6 -DMSO): δ = 7.84 (1H, d, J = 4.4 Hz), 7.68-7.63 (3H, m), 7.60 (1H, d, J = 16.1 Hz), 7.44-7.38 (3H, m), 7.32-7.23 (3H, m), 7.08 (1H, d, J = 16.1 Hz), 4.03 (1H, q, J = 7.0 Hz), 2.57 (3H, d, J = 4.4 Hz), 1.33 (3H, d, J = 6.8 Hz).

Insufficient material for complete characterisation. Replacement of the copper(II) acetate with pivalic acid led to only trace levels of reaction after 24 h by LCMS.

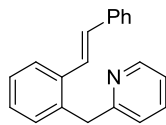
(*E*)-*N*-Methyl-2-(2-styrylphenyl)acetamide (**2.3.56**)



2.3.56

To a heat dried microwave vial was added $[RhCp^*Cl_2]$ (62 mg, 0.10 mmol), $AgSbF_6$ (137 mg, 0.40 mmol), copper(II) acetate (400 mg, 2.20 mmol), *N*-methyl-2-phenylacetamide (**2.3.40**) (149 mg, 1.00 mmol), and styrene (**2.3.55**) (0.17 mL, 1.50 mmol). The vial was sealed and to the mixture was added anhydrous DCE (5.00 mL). The resulting mixture was heated to 80 °C and stirred for 72 h. The reaction was cooled to ambient temperature and concentrated under reduced pressure. The crude product was purified by automated column chromatography (cyclohexane/TBME, 100:0 – 0:100, 80 g SiO_2). The appropriate fractions were combined and concentrated under reduced pressure to give (*E*)-*N*-methyl-2-(2-styrylphenyl)acetamide (**2.3.56**) as a white solid (222 mg, 88%). LCMS (Method C, UV, ESI) R_t = 1.03 min, $[M-H]^+$ m/z = 252.2, 100% purity. M.p. 154-155 °C. 1H NMR (400 MHz, d_6 -DMSO): δ = 7.96 (1H, d, J = 3.7 Hz), 7.70 (1H, m), 7.60 (2H, d, J = 7.1 Hz), 7.51 (1H, d, J = 16.4 Hz), 7.39 (2H, t, J = 7.6 Hz), 7.31-7.19 (4H, m), 7.11 (1H, d, J = 16.1 Hz), 3.60 (2H, s), 2.58 (3H, d, J = 4.4 Hz). ^{13}C NMR (100.6 MHz, $CDCl_3$): δ = 170.4, 137.3, 136.2, 134.4, 130.9, 129.7, 128.6, 127.6, 127.4, 126.9, 126.5, 126.0, 125.2, 25.6 (One carbon not observed due to converging and overlapping aromatic peaks). IR (ν_{max}/cm^{-1}) = 3306, 2924, 1712, 1634, 699. HRMS (ESI-[+H]) m/z : Calcd for $C_{17}H_{18}NO$ 252.1388; Found 252.1389.

(E)-2-(2-Styrylbenzyl)pyridine (2.3.58)

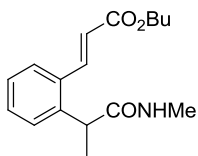


2.3.58

To a heat dried microwave vial was added [RhCp*Cl₂] (8 mg, 0.013 mmol), AgSbF₆ (17 mg, 0.050 mmol), copper(II) acetate (50 mg, 0.275 mmol), 2-benzylpyridine (**2.3.57**) (20 mg, 0.125 mmol), and styrene (**2.3.55**) (0.022 mL, 0.188 mmol). The vial was sealed and to the mixture was added anhydrous DCE (0.625 mL). The resulting mixture was heated to 80 °C and stirred for 40 h. The reaction was cooled to ambient temperature and concentrated under reduced pressure to give the crude product as a green solid (105 mg). The crude product was dissolved in DMSO:MeOH (1:1) and purified by formic MDAP. The appropriate fractions were combined and concentrated under reduced pressure to give (E)-2-(2-styrylbenzyl)pyridine (**2.3.58**) as a yellow solid (11 mg, 33%). LCMS (Method C, UV, ESI) *R*_t = 0.99 min, [M-H]⁺ *m/z* = 272.2, 100% purity. ¹H NMR (400 MHz, *d*₆-DMSO): δ = 8.49 (1H, m), 7.72 (1H, m), 7.67 (1H, dt, *J* = 1.8, 7.6 Hz), 7.58 (1H, d, *J* = 16.6 Hz), 7.57-7.52 (2H, m), 7.40-7.34 (2H, m), 7.33-7.23 (4H, m), 7.21-7.15 (2H, m), 7.09 (1H, d, *J* = 16.1 Hz), 4.28 (2H, s). ¹³C NMR (100.6 MHz, *d*₆-DMSO): δ = 160.5, 149.0, 137.5, 137.2, 136.6, 135.9, 130.9, 129.6, 128.7, 128.2, 127.7, 126.9, 126.5, 126.0, 125.4, 122.9, 121.3, 41.5.

Insufficient material for complete characterisation.

(E)-Butyl 3-(2-(1-(methylamino)-1-oxopropan-2-yl)phenyl)acrylate (2.3.60)



2.3.60

To a heat dried microwave vial was added [RhCp*Cl₂] (8 mg, 0.013 mmol), AgSbF₆ (17 mg, 0.050 mmol), pivalic acid (13 mg, 0.125 mmol), *N*-methyl-2-phenylpropanamide (**2.3.17**) (20 mg, 0.125 mmol), and butyl acrylate (**2.3.59**) (0.022 mL, 0.188 mmol). The vial was sealed and to the mixture was added anhydrous DCE (0.625 mL). The resulting mixture was heated to 80 °C and stirred for 40 h. The reaction was cooled to ambient temperature and concentrated

under reduced pressure to give the crude product as an orange oil (60 mg). The crude product was dissolved in DMSO:MeOH (1:1) and purified by formic MDAP. The appropriate fractions were combined and concentrated under reduced pressure to give (*E*)-butyl 3-(2-(1-(methylamino)-1-oxopropan-2-yl)phenyl)acrylate (**2.3.60**) (8 mg, 22%). LCMS (Method C, UV, ESI) $R_t = 1.10$, $[M-H]^+ m/z = 290.2$, 100% purity. 1H NMR (400 MHz, d_6 -DMSO): $\delta = 8.05$ (1H, d, $J = 15.7$ Hz), 7.89 (1H, d, $J = 4.4$ Hz), 7.68 (1H, d, $J = 7.8$ Hz), 7.43-7.34 (2H, m), 7.26 (1H, dt, $J = 1.3, 7.4$ Hz), 6.47 (1H, d, $J = 15.7$ Hz), 4.16 (2H, t, $J = 6.6$ Hz), 3.93 (1H, q, $J = 7.1$ Hz), 2.56 (3H, d, $J = 4.4$ Hz), 1.68 (2H, m), 1.39 (2H, qd, $J = 7.4, 14.8$ Hz), 1.28 (3H, d, $J = 7.1$ Hz), 0.92 (3H, t, $J = 7.3$ Hz). ^{13}C NMR (100.6 MHz, $CDCl_3$): $\delta = 173.1, 166.1, 141.8, 132.4, 130.2, 127.3, 127.0, 126.9, 120.0, 63.7, 41.2, 30.3, 25.7, 19.3, 18.6, 13.5$.

Reaction with copper(II) acetate showed a complex mixture of products, with the major peak not corresponding to the desired product.

4. Appendix

4.1 Lp-PLA₂ and PLA₂-VIIB Biological Assay Information

1-*O*-Hexadecyl-2-deoxy-2-thio-*S*-acetyl-*sn*-glyceryl-3-phosphorylcholine (2-thio-PAF) is a substrate for PAF-hydrolases (PAF-AH) commercially available from Cayman Chemical. Upon cleavage with PAF-AH, the free thiol is released at the *sn*-2 position and can then react with 7-diethylamino-3-(4'-maleimidylphenyl)-4-methylcoumarin (CPM) a thiol-reactive coumarin. This reaction (Michael addition) results in an increase in fluorescence. Inhibitors of PLA₂ therefore prevent this cleavage and no fluorescent increase is observed.

i) Recombinant human Lp-PLA₂ assay

The thio-PAF assay was run as an unquenched 20 µL assay. The source plate containing the compounds to be tested was prepared by making 1:3 (by volume) serial dilution of the compounds within DMSO on a 384-well microplate. Then, 5 µL of the compounds on the compound source plate were transferred into 384 well Greiner 784076 (black) plates using a STAR+ (Hamilton) liquid dispenser. 10µL of recombinant human Lp-PLA₂ enzyme (20 pM rhLp-PLA₂ in an assay buffer of 50 mM HEPES, pH 7.4, 150 mM NaCl, 1 mM CHAPS) was added to each well of the plate. 5 µL of substrate comprising 40 µM 2-thio-PAF [from ethanol stock], 40 µM CPM [from a DMSO stock] and 400 µM NEM (*N*-ethylmaleimide) [made fresh daily in DMSO] in an assay buffer (50 mM HEPES, pH 7.4, 150 mM NaCl, 1 mM CHAPS) was added to the 384 well Greiner 784076 black plates. The plates were vortexed for 10 sec. The plate was covered to protect it from light and incubated for 20 min at 25 °C. The plates were read for fluorescence intensity at ex: 380 nm / em: 485 nm using an Envision plate reader (Perkin Elmer). Raw data are transferred to Excel software and pIC₅₀ data, curve, and QC analysis was conducted by using the XL fit module in Excel.

IC₅₀ values quoted correspond to the IC₅₀ values after 20 minutes unless otherwise indicated.

ii) Recombinant human PLA₂-VIIB assay

The thio-PAF assay was run as an unquenched 20 µL assay. The source plate containing the compounds to be tested was prepared by making 1:3 (by volume) serial dilution of the

compounds within DMSO on a 384-well microplate. Then, 5 μL of the compounds on the compound source plate were transferred into 384 well Greiner 784076 (black) plates using a STAR+ (Hamilton) liquid dispenser. 10 μL of recombinant human PLA₂ –VIIB enzyme (200 pM rhPLA₂ –VIIB in an assay buffer of 50 mM HEPES, pH 7.4, 150 mM NaCl, 1 mM CHAPS) was added to each well of the plate. 5 μL of substrate comprising 40 μM 2-thio-PAF [from ethanol stock], 40 μM CPM [from a DMSO stock] and 400 μM NEM (*N*-ethylmaleimide) [made fresh daily in DMSO] in an assay buffer (50 mM HEPES, pH 7.4, 150 mM NaCl, 1 mM CHAPS) was added to 384 well Greiner 784076 black plates. The plates were vortexed for 10 sec. The plate was covered to protect it from light and incubated for 20 min at 25 °C. The plates were read for fluorescence intensity at ex: 380 nm / em: 485 nm using an Envision plate reader (Perkin Elmer). Raw data were transferred to Excel software and pIC₅₀ data, curve, and QC analysis was conducted by using the XL fit module in Excel.

IC₅₀ values quoted correspond to the IC₅₀ values after 20 minutes unless otherwise indicated.

iii) Lipoprotein-associated phospholipase A₂ (Lp-PLA₂) Human Plasma

The human plasma assay utilizes the same thioester analog of PAF as described in the HR thioPAF assay. This assay may detect the activity of Lp-PLA₂ in human plasma, as determined by specific inhibition by Lp-PLA₂ inhibitors.

The thio-PAF assay was run as a quenched 20 μL assay. The compounds source plate was prepared by making 1:3 (by volume) serial dilution of the compounds into pure DMSO on a 96-well microplate. 5 μL of compounds on the compound source plate were transferred to 96-well Corning 3686 (black) low-volume plates by a STAR+ (Hamilton) liquid dispenser. 10 μL pooled human plasma, which was previously aliquoted and frozen, was added. Plates were centrifuged for 30 sec at 1000 rpm. After 15 minutes preincubation at room temperature, 5 μL of the substrate solution comprising 2 mM 2-thio-PAF [from ethanol stock], 52 μM CPM [from a DMSO stock] and 2.5 mM NEM (*N*-ethylmaleimide) [made fresh daily in DMSO] in assay buffer (50mM HEPES, pH 7.4, 150 mM NaCl, 1 mM CHAPS) was added to 96-well Corning 3686 (black) low-volume plates. After 3 mins, the reaction was quenched with 10 μL of 5% aqueous trifluoroacetic acid (TFA). The plates were centrifuged 30 sec at 1000 rpm, covered to protect from light and incubated for 10 min at room temperature. Plates were read at ex: 380 nm / em: 485 nm using an Envision plate reader (Perkin Elmer). Raw data were

transferred to Excel software and pIC₅₀ data, curve, and QC analysis was conducted by using the XL fit module in Excel.

IC₅₀ values quoted correspond to the IC₅₀ value after 20 minutes unless otherwise indicated.

iv) Selectivities

The selectivity was determined by measuring the pIC₅₀ values for Lp-PLA₂ and PLA₂-VIIB at the limits of the assay stability, after 180 minutes and 60 minutes, respectively.

4.2 Determination of *N*-/*O*-Alkylation

Assignment of *N*:*O* alkylation was conducted using a combination of NMR and LCMS techniques. ¹³C NMR was found to provide the most conclusive method for the differentiation of the *N*-alkylated and *O*-alkylated products as exemplified below (Figure 4.2.1).

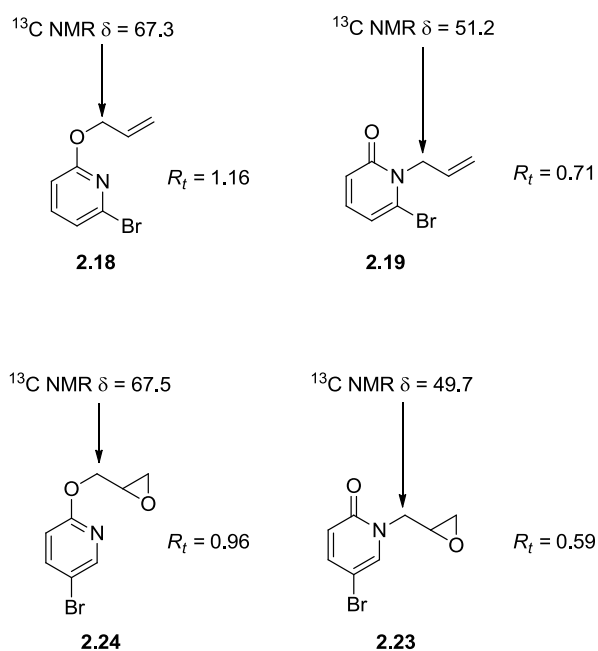


Figure 4.2.1 – Examples of key NMR (DMSO solvent) discrepancies utilised in *N*:*O* alkylation assignment and the differences in the LCMS retention times. LCMS values obtained using: Method A, UV, ESI.

In instances where both the isomers were isolated, the products could be distinguished by comparison of the marked carbon shifts (**Figure 4.2.1**), as a consequence of the disparate electronegativities of the adjacent heteroatoms.

In all instances there was a significant difference in the polarity of the two molecules, which was evident in the LCMS spectrum of each isomer. The greater hydrophilicity of the *N*-alkylated molecule, relative to the *O*-alkylated isomer, resulted in reduced retention times. In cases when one (or both) isomer was not isolated, the LCMS analysis was used to assign the regiochemistry of the reaction outcome, with the *N*-alkylated molecule possessing the lower relative retention time of the two. Ratios recorded were obtained by LCMS analysis of the crude reaction mixture, unless otherwise stated.

4.3 BET Biological Assay Information

BET proteins were produced using protocols given in the literature.²⁴⁹ Compounds were screened against either 6H-Thr BRD4 (1-477) (Y390A) (BRD4 BD2 mutation to monitor compound binding to BD1) or 6H-Thr BRD4 (1-477) (Y97A) (BRD4 BD1 mutation to monitor compound binding to BD2) in a dose-response format in a TR-FRET assay measuring competition between test compound and an Alexa Fluor 647 derivative of I-BET762.1 Compounds were titrated from 10 mM in 100% DMSO and 50 nL transferred to a low volume black 384 well micro titre plate using a Labcyte Echo 555. A Thermo Scientific Multidrop Combi was used to dispense 5 μ L of 20 nM protein in an assay buffer of 50 mM HEPES, 150 mM NaCl, 5% glycerol, 1 mM DTT and 1 mM CHAPS, pH 7.4, and in the presence of 100 nM fluorescent ligand ($\sim K_d$ concentration for the interaction between BRD4 BD1 and ligand). After equilibrating for 30 min in the dark at rt, the bromodomain protein:fluorescent ligand interaction was detected using TR-FRET following a 5 μ L addition of 3 nM europium chelate labelled anti-6His antibody (Perkin Elmer, W1024, AD0111) in assay buffer. Time resolved fluorescence (TRF) was then detected on a TRF laser equipped Perkin Elmer Envision multimode plate reader (excitation = 337 nm; emission 1 = 615 nm; emission 2 = 665 nm; 317 dual wavelength bias dichroic = 400 nm, 630 nm). TR-FRET ratio was calculated using the following equation: Ratio = ((Acceptor fluorescence at 665 nm) / (Donor fluorescence at 615 nm)) * 1000. TR-FRET ratio data was normalised to high (DMSO) and low (compound control derivative of I-BET762) controls and IC₅₀ values determined for each of the compounds tested by fitting the fluorescence ratio data to a four parameter model: $y = a + ((b - a) / (1 + (10 \wedge$

Confidential – Property of GSK – Do Not Copy

$x / 10^{(c-d)}$ where 'a' is the minimum, 'b' is the Hill slope, 'c' is the IC₅₀ and 'd' is the maximum.

5. Bibliography

- (1) Zalewski, A.; Macphee, C. *Arterioscler. Thromb. Vasc. Biol.* **2005**, *25*, 923–931.
- (2) Mallat, Z.; Lambeau, G.; Tedgui, A. *Circulation.* **2010**, *122*, 2183–2200.
- (3) Prescott, S. M.; Zimmerman, G. A.; Stafforini, D. M.; McIntyre, T. M. *Annu. Rev. Biochem.* **2000**, *69*, 419–445.
- (4) Nelson, D. L.; Cox, M. M. *Lehninger Principles of Biochemistry*, 4th Edition.; W. H. Freeman: New York, 2004.
- (5) Khalil, M. B.; Hou, W.; Zhou, H.; Elisma, F.; Swayne, L. A.; Blanchard, A. P.; Yao, Z.; Bennett, S. A. L.; Figeys, D. *Mass Spectrosc. Rev.* **2012**, *29*, 877–929.
- (6) Chester, M. A. *Eur. J. Biochem.* **1998**, *257*, 293–298.
- (7) Wolfrom, M. L. *J. Org. Chem.* **1963**, *28*, 281–291.
- (8) Cahn, R. S.; Ingold, C.; Prelog, V. *Angew. Chemie Int. Ed.* **1966**, *5*, 385–415.
- (9) Tjoelker, L. W.; Wilder, C.; Eberhardt, C.; Stafforini, D. M.; Dietsch, G.; Schimpf, B.; Hooper, S.; Trong, H. L.; Cousens, L. S.; Zimmerman, G. A.; Yamadat, Y.; McIntyre, T. M.; Prescott, S. M.; Gray, P. W. *Nature* **1994**, *374*, 549–553.
- (10) Rosenson, R. S.; Stafforini, D. M. *J. Lipid Res.* **2012**, *53*, 1767–1782.
- (11) Aloulou, A.; Ali, Y. B.; Bezzine, S.; Gargouri, Y.; Gelb, M. H. *Lipases and Phospholipases: Methods and Protocols*; Sandoval, G., Ed.; Springer Science + Business Media: New York, 2012.
- (12) Six, D. A.; Dennis, E. A. *Biochim. Biophys. Acta.* **2000**, *1488*, 1–19.
- (13) Münzel, T.; Gori, T. *Eur. Heart J.* **2009**, *30*, 2829–2831.
- (14) Rosenson, R. S. *Curr. Opin. Lipidol.* **2010**, *21*, 473–480.
- (15) Packard, C. J.; Shepherd, J.; Cobbe, S. M.; Ford, I.; Isles, C. G.; McKillop, J. H.; MacFarlane, P. W.; Lorimer, A. R.; Norrie, J. *Circulation* **1998**, *97*, 1440–1445.
- (16) Packard, C. J.; O'Reilly, D. S. J.; Caslake, M. J.; McMahan, A. D.; Ford, I.; Cooney, J.; Macphee, C. H.; Suckling, K. E.; Krishna, M.; Wilkinson, F. E.; Rumley, A.; Docherty, G.; Burczak, J. D.; Lowe, G. D. O. *N. Engl. J. Med.* **2000**, *343*, 1148–1155.

- (17) <http://clinicaltrials.gov/show/NCT01428453>. First accessed on 4th July 2014.
- (18) Maxwell, A. **2014**, GlaxoSmithKline, Unpublished Work.
- (19) White, H. D.; Held, C.; Stewart, R.; Tarka, E.; Brown, R.; Davies, R. Y.; Budaj, A.; Harrington, R. A.; Steg, P. G.; Ardissino, D.; Armstrong, P. W.; Avezum, A.; Aylward, P. E.; Bryce, A.; Chen, H.; Chen, M.-F.; Corbalan, R.; Dalby, A. J.; Danchin, N.; De Winter, R. J.; Denchev, S.; Diaz, R.; Elisaf, M.; Flather, M. D.; Goudev, A. R.; Granger, C. B.; Grinfeld, L.; Hochman, J. S.; Husted, S.; Kim, H.-S.; Koenig, W.; Linhart, A.; Lonn, E.; López-Sendón, J.; Manolis, A. J.; Mohler III, E. R.; Nicolau, J. C.; Pais, P.; Parkhomenko, A.; Pedersen, T. R.; Pella, D.; Ramos-Corrales, M. A.; Ruda, M.; Sereg, M.; Siddique, S.; Sinnaeve, P.; Smith, P.; Sritara, P.; Swart, H. P.; Sy, R. G.; Teramoto, T.; Tse, H.-F.; Watson, D.; Weaver, W. D.; Weiss, R.; Viigimaa, M.; Vinereanu, D.; Zhu, J.; Cannon, C. P.; Wallentin, L. *N. Engl. J. Med.* **2014**, *370*, 1702–1711.
- (20) <http://www.gsk.com/media/press-releases/2014/gsk-announces-phase-iii-study-with-darapladib-did-not-meet-prima.html>. First Accessed 7th July 2014.
- (21) McLaughlin, M. In *A Phase IIa Study of Darapladib, an Oral Lipoprotein-Associated Phospholipase A2 Inhibitor, in Diabetic Macular Edema. Presented at the 6th Ocular Diseases & Drug Discovery, San Diego, CA, 20th March 2014*.
- (22) Blackie, J. A.; Bloomer, J. C.; Brown, M. J. B.; Cheng, H.-Y.; Elliott, R. L.; Hammond, B.; Hickey, D. M. B.; Ife, R. J.; Leach, C. A.; Lewis, V. A.; Macphee, C. H.; Milliner, K. J.; Moores, K. E.; Pinto, I. L.; Smith, S. A.; Stansfield, I. G.; Stanway, S. J.; Taylor, M. A.; Theobald, C. J.; Whittaker, C. M. *Bioorg. Med. Chem. Lett.* **2002**, *12*, 2603–2606.
- (23) Blackie, J. A.; Bloomer, J. C.; Brown, M. J. B.; Cheng, H.-Y.; Hammond, B.; Hickey, D. M. B.; Ife, R. J.; Leach, C. A.; Lewis, V. A.; Macphee, C. H.; Milliner, K. J.; Moores, K. E.; Pinto, I. L.; Smith, S. A.; Stansfield, I. G.; Stanway, S. J.; Taylor, M. A.; Theobald, C. J. *Bioorg. Med. Chem. Lett.* **2003**, *13*, 1067–1070.
- (24) Segen, J. C. *The Dictionary of Modern Medicine*; CRC Press: Boca Raton, 2012.
- (25) Tjoelker, L. W.; Eberhardt, C.; Unger, J.; Trong, H. L.; Zimmerman, G. A.;

- McIntyre, T. M.; Stafforini, D. M.; Prescott, S. M.; Gray, P. W. *J. Biol. Chemistry* **1995**, *270*, 25481–25487.
- (26) Samanta, U.; Bahnson, B. J. *J Biol Chem* **2008**, *283*, 31617–31624.
- (27) Freer, S. T.; Kraut, J.; Robertus, J. D.; Wright, H. T. *Biochemistry* **1970**, *9*, 1997–2009.
- (28) Hedstrom, L. *Chem. Rev.* **2002**, *102*, 4501–4523.
- (29) Fersht, A. *Enzyme Structure and Mechanism*, 2nd Editio.; W. H. Freeman and Company: New York, 1984.
- (30) Kamerlin, S. C. L.; Chu, Z. T.; Warshel, A. *J. Org. Chem.* **2010**, *75*, 6391–6401.
- (31) Zhang, Y.; Kua, J.; McCammon, J. A. *J. Am. Chem. Soc.* **2002**, *124*, 10572–10577.
- (32) Gao, J.; Ma, S.; Major, D. T.; Nam, K.; Pu, J.; Truhlar, D. G. *Chem. Rev.* **2006**, *106*, 3188–3209.
- (33) Manas, E. **2013**, GlaxoSmithKline, Unpublished Work.
- (34) Krantz, A. *Bioorg. Med. Chem. Lett.* **1992**, *2*, 1327–1334.
- (35) Powers, J. C.; Asgian, J. L.; Ekici, O. D.; James, K. E. *Chem. Rev.* **2002**, *102*, 4639–4750.
- (36) Prorok, M.; Albeck, A.; Foxman, B. M.; Abeles, R. H. *Biochemistry* **1994**, *33*, 9784–9790.
- (37) Serafimova, I. M.; Pufall, M. A.; Krishnan, S.; Duda, K.; Cohen, M. S.; Maglathlin, R. L.; McFarland, J. M.; Miller, R. M.; Frödin, M.; Taunton, J. *Nat. Chem. Biol.* **2012**, *8*, 471–476.
- (38) Johnson, D. S.; Weerapana, E.; Cravatt, B. F. *Futur. Med. Chem.* **2010**, *2*, 949–964.
- (39) Singh, J.; Petter, R. C.; Baillie, T. A.; Whitty, A. *Nat. Rev. Drug Discov.* **2011**, *10*, 307–317.
- (40) Szedlacsek, S. E.; Duggleby, R. G. *Methods Enzymol.* **1995**, *249*, 144–180.
- (41) Morrison, J. F. *Biochim. Biophys. Acta - Enzymol.* **1969**, *185*, 269–286.
- (42) Hall, D. G. *Structure, Properties, and Preparation of Boronic Acid Derivatives. Overview of Their Reactions and Applications*; Hall, D. G., Ed.; Wiley-VCH Verlag GmbH & Co. KGaA: Weinheim, 2005.
- (43) Summers, D. **2014**, GlaxoSmithKline, Unpublished Work.

- (44) Groll, M.; Berkers, C. R.; Ploegh, H. L.; Ovaa, H. *Structure* **2006**, *14*, 451–456.
- (45) ProductsandTobacco/CDER/ucm094929.htm, H. fda.gov/AboutFDA/CentersOffices/OfficeofMedica. First Accessed 6th August 2014.
- (46) Baker, S. J.; Tomsho, J. W.; Benkovic, S. J. *Chem. Soc. Rev.* **2011**, *40*, 4279–4285.
- (47) Boyd, H. F.; Flynn, S. T.; Hickey, D. M. B.; Ife, R. J.; Jones, M.; Leach, C. A.; Macphee, C. H.; Milliner, K. J.; Rawlings, D. A.; Slingsby, B. P.; Smith, S. A.; Stansfield, I. G.; Tew, D. G.; Theobald, C. J. *Bioorg. Med. Chem. Lett.* **2000**, *10*, 395–398.
- (48) Mishra, K. P.; Ganju, L.; Sairam, M.; Banerjee, P. K.; Sawhney, R. C. *Biomed. Pharmacother.* **2008**, *62*, 94–98.
- (49) Macarron, R.; Banks, M. N.; Bojanic, D.; Burns, D. J.; Cirovic, D. A.; Garyantes, T.; Green, D. V. S.; Hertzberg, R. P.; Janzen, W. P.; Paslay, J. W.; Schopfer, U.; Sittampalam, G. S. *Nat. Rev. Drug Discov.* **2011**, *10*, 188–195.
- (50) Congreve, M.; Murray, C. W.; Blundell, T. L. *Drug Discov. Today* **2005**, *10*, 895–907.
- (51) Rees, D. C.; Congreve, M.; Murray, C. W.; Carr, R. *Nat. Rev. Drug Discov.* **2004**, *3*, 660–672.
- (52) Arnott, J. A.; Planey, S. L. *Expert Opin. Drug Discov.* **2012**, *7*, 863–875.
- (53) Leeson, P. D.; Springthorpe, B. *Nat. Rev. Drug Discov.* **2007**, *6*, 881–890.
- (54) Murray, C. W.; Verdonk, M. L.; Rees, D. C. *Trends Pharmacol. Sci.* **2012**, *33*, 224–232.
- (55) Hopkins, A. L.; Groom, C. R.; Alex, A. *Drug Discov. Today* **2004**, *9*, 430–431.
- (56) Schultes, S.; de Graaf, C.; Haaksma, E. E. J.; de Esch, I. J. P.; Leurs, R.; Krämer, O. *Drug Discov. Today. Technol.* **2010**, *7*, e147-202.
- (57) Lipinski, C. A.; Lombadro, F.; Dominy, B. W.; Feeney, P. J. *Adv. Drug Deliv. Rev.* **2001**, *46*, 3–26.
- (58) Congreve, M.; Carr, R.; Murray, C.; Jhoti, H. *Drug Discov. Today* **2003**, *8*, 876–877.
- (59) <http://www.daylight.com/dayhtml/doc/clogp/#PCMsc1.1.2>. First Accessed 14th March 2014.

- (60) Goodwin, J. T.; Conradi, R. A.; Ho, N. F. H.; Burton, P. S. *J. Med. Chem.* **2001**, *44*, 3721–3729.
- (61) Veber, D. F.; Johnson, S. R.; Cheng, H.-Y.; Smith, B. R.; Ward, K. W.; Kopple, K. D. *J. Med. Chem.* **2002**, *45*, 2615–2623.
- (62) Patel, V. **2011**, GlaxoSmithKline, Unpublished Work.
- (63) Day, P. **2011**, Astex Pharmaceuticals, Unpublished Work.
- (64) Nadin, A. **2011**, GlaxoSmithKline, Unpublished Work.
- (65) Faitg, T. **2009**, GlaxoSmithKline, Unpublished Work.
- (66) Rust, T. **2010**, GlaxoSmithKline, Unpublished Work.
- (67) Ethiraj, K.; Pradhan, T. **2012**, GVKBio, Unpublished Work.
- (68) Curtis, N.; Faucher, N.; Donche, F.; Sautet, S.; Martin, F.; Lamoureux, L.; Moquette, A.; Daugan, A.; Livia, S. **2012**, GlaxoSmithKline, Unpublished Work.
- (69) Woolford, A.; Day, P. **2012**, Astex Pharmaceuticals, Unpublished Work.
- (70) Patel, V. **2014**, GlaxoSmithKline, Unpublished Work.
- (71) Summers, D. **2012**, GlaxoSmithKline, Unpublished Work.
- (72) Hattori, K.; Adachi, H.; Matsuzawa, A.; Yamamoto, K.; Tsujimoto, M.; Aoki, J.; Hattori, M.; Arai, H.; Inoue, K. *J. Biol. Chem.* **1996**, *271*, 33032–33038.
- (73) O’Donoghue, M. L.; Braunwald, E.; White, H. D.; Steen, D. L.; Lukas, M. A.; Tarka, E.; Steg, P. G.; Hochman, J. S.; Bode, C.; Maggioni, A. P.; Im, K.; Shannon, J. B.; Davies, R. Y.; Murphy, S. A.; Crugnale, S. E.; Wiviott, S. D.; Bonaca, M. P.; Watson, D. F.; Weaver, W. D.; Serruys, P. W.; Cannon, C. P. *J. Am. Med. Assoc.* **2014**, *312*, 1006–1015.
- (74) Patel, V. **2015**, GlaxoSmithKline, Unpublished Work.
- (75) Potvain, F. **2011**, GlaxoSmithKline, Unpublished Work.
- (76) Valkó, K.; Bevan, C.; Reynolds, D. *Anal. Chemistry* **1997**, *69*, 2022–2029.
- (77) Gogisetti, G. **2011**, GlaxoSmithKline, Unpublished Work.
- (78) Patel, V. **2011**, GlaxoSmithKline, Unpublished Work.
- (79) Hutchinson, S. **2011**, GlaxoSmithKline, Unpublished Work.
- (80) Summers, D. **2012**, GlaxoSmithKline, Unpublished Work.
- (81) Summers, D. **2013**, GlaxoSmithKline, Unpublished Work.
- (82) Mortelmans, K.; Zeiger, E. *Mutat. Res. Mol. Mech. Mutagen.* **2000**, *455*, 29–

- 60.
- (83) Baxter, A. **2013**, GlaxoSmithKline, Unpublished Work.
- (84) Potvain, F. **2011**, GlaxoSmithKline, Unpublished Work.
- (85) Donche, F. **2013**, GlaxoSmithKline, Unpublished Work.
- (86) Lewis, D. F. V.; Jacobs, M. N.; Dickins, M. *Drug Discov. Today* **2004**, *9*, 530–537.
- (87) Potvain, F. **2012**, GlaxoSmithKline, Unpublished Work.
- (88) Davies, S. **2013**, GlaxoSmithKline, Unpublished Work.
- (89) Nguyen, V. L. **2013**, GlaxoSmithKline, Unpublished Work.
- (90) Summers, D. **2013**, GlaxoSmithKline, Unpublished Work.
- (91) Liang, X. **2013**, GlaxoSmithKline, Unpublished Work.
- (92) Potvain, F. **2014**, GlaxoSmithKline, Unpublished Work.
- (93) Summers, D. **2014**, GlaxoSmithKline, Unpublished Work.
- (94) Krapcho, A. P.; Weimaster, J. F.; Eldridge, J. M.; Jahngen Jr., E. G. E.; Lovey, A. J.; Stephens, W. P. *J. Org. Chem.* **1978**, *43*, 138–147.
- (95) Fouchet, M. A. **2013**, GlaxoSmithKline, Unpublished Work.
- (96) Malik, H. A.; Taylor, B. L. H.; Kerrigan, J. R.; Grob, J. E.; Houk, K. N.; Bois, J. D.; Hamann, L. G.; Patterson, A. W. *Chem. Sci.* **2014**, *5*, 2352–2361.
- (97) Tidwell, T. T. *e-EROS Encycl. Reagents Org. Synth.* **2001**.
- (98) Propst III, R. M.; Trzupsek, L. S. *J. Am. Chem. Soc.* **1981**, *103*, 3233–3235.
- (99) Barchéath, S. D.; Tawatao, R. I.; Corr, M.; Carson, D. A.; Cottam, H. B. *Bioorg. Med. Chem. Lett.* **2005**, *15*, 1785–1788.
- (100) Bordwell, F. G. *Acc. Chem. Res.* **1988**, *21*, 456–463.
- (101) Joule, J. A.; Mills, K. *Heterocyclic Chemistry*, 5th ed.; Blackwell Publishing Ltd: Chichester, 2010.
- (102) Bordwell, F. G.; Algrim, D.; Vanier, N. R. *J. Org. Chem.* **1977**, *42*, 1817–1819.
- (103) White, G. **2013**, GlaxoSmithKline, Unpublished Work.
- (104) Abedi, S. A. **2014**, GlaxoSmithKline, Unpublished Work.
- (105) Matondo, H.; Souirti, S.; Baboulène, M. *Synth. Commun.* **2006**, *33*, 795–800.
- (106) Craven, A. **2014**, GlaxoSmithKline, Unpublished Work.
- (107) Rach, S. F.; Kühn, F. E. *Chem. Rev.* **2009**, *109*, 2061–2080.
- (108) Chen, K.; Peterson, R.; Math, S. K.; LaMunyon, J. B.; Testa, C. A.; Cefalo, D.

- R. *Tetrahedron Lett.* **2012**, *53*, 4873–4876.
- (109) Curtis, N. **2013**, GlaxoSmithKline, Unpublished Work.
- (110) Gray, M. **2013**, GlaxoSmithKline, Unpublished Work.
- (111) Boudier, A.; Bromm, L. O.; Lotz, M.; Knochel, P. *Angew. Chemie Int. Ed.* **2000**, *39*, 4414–4435.
- (112) Lipshutz, B. H.; Sengupta, S. *Org. React.* **2004**, *41*, 135–631.
- (113) Knochel, P.; Singer, R. D. *Chem. Rev.* **1993**, *93*, 2117–2188.
- (114) Bunnett, J. F.; Davis, G. T. *J. Am. Chem. Soc.* **1958**, *80*, 4337–4339.
- (115) Clayden, J.; Greeves, N.; Warren, S.; Wothers, P. *Organic Chemistry*; Oxford University Press: Oxford, 2001.
- (116) Reddy, S. *Example of poor aniline nucleophilicity*; Unpublished Work; GlaxoSmithKline.
- (117) Corey, E. J.; Helal, C. J. *Angew. Chemie Int. Ed.* **1998**, *37*, 1986–2012.
- (118) Craven, A. **2014**, GlaxoSmithKline, Unpublished Work.
- (119) Potvain, F. **2013**, GlaxoSmithKline, Unpublished Work.
- (120) Li, D. **2012**, GlaxoSmithKline, Unpublished Work.
- (121) Zhan, H. **2012**, GlaxoSmithKline, Unpublished Work.
- (122) Potvain, F. **2012**, GlaxoSmithKline, Unpublished Work.
- (123) Knapp, D. M.; Gillis, E. P.; Burke, M. D. *J. Am. Chem. Soc.* **2009**, *131*, 6961–6963.
- (124) Curran, D. P.; Liu, H.; Josien, H.; Ko, S.-B. *Tetrahedron* **1996**, *52*, 11385–11404.
- (125) Newkome, G. R.; Broussard, J.; Staires, S. K.; Sauer, J. D. *Synthesis (Stuttg.)* **1974**, 707.
- (126) Shiao, M. J.; Lai, L. L.; Ku, W. S.; Lin, P. Y.; Hwu, J. R. *J. Org. Chem.* **1993**, *58*, 4742–4744.
- (127) Hammett, L. P. *J. Am. Chem. Soc.* **1937**, *59*, 96–103.
- (128) Taft Jr., R. W. *J. Am. Chem. Soc.* **1952**, *74*, 2729–2732.
- (129) Blanksby, S. J.; Ellison, G. B. *Acc. Chem. Res.* **2003**, *36*, 255–263.
- (130) Sarveswara, R. **2014**, GVKBio, Unpublished Work.
- (131) Jessen, H. J.; Gademann, K. *Nat. Prod. Rep.* **2010**, *27*, 1168–1185.
- (132) Li, Q.; Mitscher, L. A.; Shen, L. L. *Med. Res. Rev.* **2000**, *20*, 231–293.

- (133) Liang, G.-B.; Qiana, X.; Biftua, T.; Singha, S.; Gaoa, Y.-D.; Scapinb, G.; Patel, S.; Leiting, B.; Patel, R.; Wu, J.; Zhang, X.; Thornberry, N. A.; Webera, A. E. *Bioorg. Med. Chem. Lett.* **2008**, *18*, 3706–3710.
- (134) Stenkamp, D.; Budzinski, R. M.; Heckel, A.; Kley, J.; Lehmann-Lintz, T.; Mueller, S. G.; Oost, T.; Roth, G. J. WO 2009/103478 A1.
- (135) De, S. R.; Ghorai, S. K.; Mal, D. *J. Org. Chem.* **2009**, *74*, 1598–1604.
- (136) Shimizu, S.; Ogata, M. *J. Org. Chem.* **1988**, *53*, 5160–5163.
- (137) Girdardin, M.; Ouellet, S. G.; Gauvreau, D.; Moore, J. C.; Hughes, G.; Devine, P. N.; O’Shea, P. D.; Campeau, L. C. *Org. Process Res. Dev.* **2013**, *17*, 61.
- (138) Itami, K.; Yamazaki, D.; Yoshida, J.-I. *Org. Lett.* **2003**, *5*, 2161–2164.
- (139) Dinan, F. J.; Tieckelmann, H. *J. Org. Chem.* **1964**, *29*, 892–895.
- (140) Moffett, R. B. *J. Org. Chem.* **1963**, *28*, 2885–2886.
- (141) Overman, L. E. *Angew. Chem. Int. Ed.* **1984**, *23*, 579–586.
- (142) Espeel, P. H.; Peuter, G. D.; Tielen, M. C.; Jacobs, P. A. *J. Phys. Chemistry* **1994**, *98*, 11588–11596.
- (143) Deshmukh, S. S.; Chaudhari, K. H.; Akamanchi, K. G. *Synlett* **2011**, 81–83.
- (144) Katsuki, T.; Sharpless, K. B. *J. Am. Chem. Soc.* **1980**, *102*, 5974–5976.
- (145) Hulce, M. *2-Pyridone. e-EROS Encycl. Reagents Org. Synth.* **2001**.
- (146) Frank, J.; Katritzky, A. R. *J. Chem. Soc., Perkin Trans. 2* **1976**, 1428–1431.
- (147) Kocak, A.; Kurbanli, S.; Malkondu, S. *Synth. Commun.* **2007**, *37*, 3697–3708.
- (148) Saroj, R. D.; Sujit, K. G.; Dipakranjan, M. *J. Org. Chem.* **2009**, *74*, 1598–1604.
- (149) Vavilina, G.; Zicmanis, A.; Mekss, P.; Klavins, M. *Chem. Heterocycl. Compd.* **2008**, *44*, 549–558.
- (150) Hopkins, G.; Jonak, J.; Minnemeyer, H.; Tieckelmann, H. *J. Org. Chem.* **1967**, *32*, 4040–4044.
- (151) Liu, H.; Ko, S.-B.; Josien, H.; Curran, D. P. *Tetrahedron Lett.* **1995**, *36*, 8917–8920.
- (152) Breugst, M.; Mayr, H. *J. Am. Chem. Soc.* **2010**, *132*, 15380–15389.
- (153) Ikariya, T.; Murata, K.; Noyori, R. *Org. Biomol. Chem.* **2006**, *4*, 393–406.
- (154) Ikariya, T.; Blacker, A. J. *Acc. Chem. Res.* **2007**, *40*, 1300–1308.
- (155) Leitner, W.; Brown, J. M.; Brunner, H. *J. Am. Chem. Soc.* **1993**, *115*, 152–159.
- (156) Jensen, F. R.; Bushweller, C. H.; Beck, B. H. *J. Am. Chem. Soc.* **1968**, *91*, 344–

351.

- (157) Miyaura, N.; Suzuki, A. *Chem. Rev.* **1995**, *95*, 2457–2483.
- (158) Corbet, J.-P.; Mignani, G. *Chem. Rev.* **2006**, *106*, 2651–2710.
- (159) Sumrell, G. *J. Org. Chem.* **1954**, *19*, 817–819.
- (160) Leermann, T.; Leroux, F. R.; Colobert, F. *Org. Lett.* **2011**, *13*, 4479–4481.
- (161) Blasberg, F.; Bolte, M.; Wagner, M.; Lerner, H.-W. *Organometallics* **2012**, *31*, 1001–1005.
- (162) Curtis, N.; Faucher, N.; Donche, F.; Sautet, S.; Martin, F.; Lamoureux, L.; Moquette, A.; Daugan, A.; Livia, S. **2009**, GlaxoSmithKline, Unpublished Work.
- (163) Liang, X. **2013**, GlaxoSmithKline, Unpublished Work.
- (164) Campbell, M. **2013**, GlaxoSmithKline, Unpublished Work.
- (165) Donche, F. **2013**, GlaxoSmithKline, Unpublished Work.
- (166) Potvain, F. **2014**, GlaxoSmithKline, Unpublished Work.
- (167) Albeck, A.; Persky, R. *Tetrahedron* **1994**, *50*, 6333–6346.
- (168) Podlech, J. *J. für Prakt. Chemie/Chemiker-Zeitung* **1998**, *340*, 679–682.
- (169) Wang, D.; Schwinden, M. D.; Radesca, L.; Patel, B.; Kronenthal, D.; Huang, M.-H.; Nugent, W. A. *J. Org. Chem.* **2004**, *69*, 1629–1633.
- (170) Ohno, F.; Kawashima, T.; Okazaki, R. *J. Am. Chem. Soc.* **1996**, *118*, 697–698.
- (171) Baldwin, J. E.; Adlington, R. M.; Godfrey, C. R. A.; Gollins, D. W.; Vaughan, J. G. *Chem. Commun.* **1993**, 1434–1435.
- (172) Mangion, I. K.; Nwamba, I. K.; Shevlin, M.; Huffman, M. A. *Org. Lett.* **2009**, *11*, 3566–3569.
- (173) Molinaro, C.; Bulger, P. G.; Lee, E. E.; Kosjek, B.; Lau, S.; Gauvreau, D.; Howard, M. E.; Wallace, D. J.; O’Shea, P. D. *J. Org. Chem.* **2012**, *77*, 2299–2309.
- (174) Mangion, I. K.; Weisel, M. *Tetrahedron Lett.* **2010**, *51*, 5490–5492.
- (175) Luong, H.; Luss-Lusis, E.; Tanoury, G. J.; Nugent, W. A. *Eur. J. Org. Chem.* **2013**, No. 20, 4238–4241.
- (176) Mangion, I. K.; Ruck, R. T.; Rivera, N.; Huffman, M. A.; Shelvin, M. *Org. Lett.* **2011**, *13*, 5480–5483.
- (177) Leggio, A.; De Marco, R.; Perri, F.; Spinella, M.; Liguori, A. *Eur. J. Org. Chem.*

2012, No. 1, 114–118.

- (178) Fischer, K. *Angew. Chemie* **1935**, 48, 394–396.
- (179) Craven, A. **2014**, GlaxoSmithKline, Unpublished Work.
- (180) Crabtree, R. *Acc. Chem. Res.* **1979**, 12, 331–337.
- (181) Craven, A. **2014**, GlaxoSmithKline, Unpublished Work.
- (182) Baskaran, S. **2013**, GlaxoSmithKline, Unpublished Work.
- (183) Cochrane, A. R.; Irvine, S.; Kerr, W. J.; Reid, M.; Andersson, S.; Nilsson, G. *N. J. Label. Compd. Radiopharm.* **2013**, 56, 451–454.
- (184) Balakrishna, P. **2014**, GVKBio, Unpublished Work.
- (185) Raghuramarao, I. **2014**, GlaxoSmithKline, Unpublished Work.
- (186) Lamoureux, P. **2013**, GlaxoSmithKline, Unpublished Work.
- (187) McFadyen, R. **2013**, GlaxoSmithKline, Unpublished Work.
- (188) Mamidi, R. **2014**, GVKBio, Unpublished Work.
- (189) Potvain, F. **2014**, GlaxoSmithKline, Unpublished Work.
- (190) Moquette, A. **2014**, GlaxoSmithKline, Unpublished Work.
- (191) Donche, F. **2014**, GlaxoSmithKline, Unpublished Work.
- (192) Lamoureux, P. **2014**, GlaxoSmithKline, Unpublished Work.
- (193) Clohessy, T. **2013**, GlaxoSmithKline, Unpublished Work.
- (194) Ishiyama, T.; Ishida, K.; Miyaura, M. *Tetrahedron* **2001**, 57, 9813–9816.
- (195) Mitchell, M. **2014**, GlaxoSmithKline, Unpublished Work.
- (196) Irigineni, R. **2014**, GVKBio, Unpublished Work.
- (197) Carrow, B. P.; Hartwig, J. F. *J. Am. Chem. Soc.* **2011**, 133, 2116–2119.
- (198) McNaught, A. D.; Wilkinson, A. *IUPAC. Compendium of Chemical Terminology, 2nd ed. (the “Gold Book”)*; Blackwell Scientific Publications: Oxford, 1997.
- (199) Walsh, P. J.; Kozlowski, M. C. *Fundamentals of Asymmetric Catalysis*, 1st Editio.; University Science Books: Sausalito, 2009.
- (200) Sih, C. J.; Chen, C. S. *Angew. Chem. Int. Ed.* **1984**, 23, 570–578.
- (201) Hashiguchi, S.; Fujii, A.; Takehara, J.; Ikariya, T.; Noyori, R. *J. Am. Chem. Soc.* **1995**, 117, 7562–7563.
- (202) Moore, J. C.; Pollard, D. J.; Kosjek, B.; Devine, P. N. *Acc. Chem. Res.* **2007**, 40, 1412–1419.

- (203) Kamal, A.; Laxminarayana, B.; Gayatri, N. L. *Tetrahedron Lett.* **1997**, *38*, 6871–6874.
- (204) Gröger, H.; Hummel, W.; Buchholz, S.; Drauz, K.; Nguyen, T. Van; Rollmann, C.; Hüsken, H.; Abokitse, K. *Org. Lett.* **2003**, *5*, 173–176.
- (205) Hummel, W.; Schütte, H.; Schmidt, E.; Wandrey, C.; Kula, M.-R. *Appl. Microbiol. Biotechnol.* **1987**, *26*, 409–416.
- (206) Zhou, B. N.; Gopalan, A. S.; VanMiddlesworth, F.; Shieh, W. R.; Sih, C. J. *J. Am. Chem. Soc.* **1983**, *105*, 5925–5926.
- (207) Curtis, N. **2014**, GlaxoSmithKline, Unpublished Work.
- (208) Craven, A. **2014**, GlaxoSmithKline, Unpublished Work.
- (209) Roiban, D. **2014**, GlaxoSmithKline, Unpublished Work.
- (210) Murata, K.; Fukuda, Y.; Simosaka, M.; Watanabe, K.; Saikusa, T.; Kimura, A. *Eur. J. Biochem.* **1985**, *151*, 631–636.
- (211) Harris, E. **2014**, GlaxoSmithKline, Unpublished Work.
- (212) Fox, R. J.; Huisman, G. W. *Trends Biotechnol.* **2008**, *26*, 132–138.
- (213) Dalby, P. A. *Curr. Opin. Struct. Biol.* **2003**, *13*, 500–505.
- (214) Currin, A.; Swainston, N.; Day, P. J.; Kell, D. B. *Chem. Soc. Rev.* **2015**, *44*, 1172–1239.
- (215) Zanotti-Gerosa, A.; Hems, W.; Groarke, M.; Hancock, F. *Platin. Met. Rev.* **2005**, *49*, 158–165.
- (216) Noyori, R.; Ohkuma, T.; Kitamura, M.; Takaya, H.; Sayo, N.; Kumobayashi, H.; Akutagawa, S. *J. Am. Chem. Soc.* **1987**, *109*, 5856–5858.
- (217) Ohkuma, T.; Ooka, H.; Hashiguchi, S.; Ikariya, T.; Noyori, R. *J. Am. Chem. Soc.* **1995**, *117*, 2675–2676.
- (218) Matsumura, K.; Aria, N.; Kiyoto, H.; Saito, T.; Sayo, N.; Ohkuma, T. *J. Am. Chem. Soc.* **2011**, *133*, 10696–10966.
- (219) Ye, C.; Liu, J.; Ren, F.; Okafo, N. *J. Pharm. Biomed. Anal.* **2000**, *23*, 581–589.
- (220) Gooding, O. W. *Curr. Opin. Chem. Biol.* **2004**, *8*, 297–304.
- (221) Denmark, S. E.; Butler, C. R. *J. Am. Chem. Soc.* **2008**, *130*, 3690–3704.
- (222) Zhu, L.; Vimolratana, M.; Brown, S. P.; Medina, J. C. *Tetrahedron Lett.* **2008**, *49*, 1768–1770.
- (223) Meerwein, H.; Schmidt, R. *Justus Liebig's Ann. der Chemie* **1925**, *444*, 221–

- 238.
- (224) Hashiguchi, S.; Fujii, A.; Takehara, J.; Ikariya, T.; Noyori, R. *J. Am. Chem. Soc.* **1995**, *117*, 7562–7563.
- (225) Fujii, A.; Hashiguchi, S.; Uematsu, N.; Ikariya, T.; Noyori, R. *J. Am. Chem. Soc.* **1996**, *118*, 2521–2522.
- (226) Zhou, X.; Wu, X.; Yang, B.; Xiao, J. *J. Mol. Catal. A Chem.* **2012**, *357*, 133–140.
- (227) Kazuhiko Matsumura; Shohei Hashiguchi; Takao Ikariya, and; Ryoji Noyori*, †. **1997**.
- (228) Václavík, J.; Kačer, P.; Kuzma, M.; Červený, L. *Molecules* **2011**, *16*, 5460–5495.
- (229) Cross, D. J.; Houson, I.; Kawamoto, A. M.; Wills, M. *Tetrahedron Lett.* **2004**, *45*, 843–846.
- (230) Hannedouche, J.; Clarkson, G. J.; Wills, M. *J. Am. Chem. Soc.* **2004**, *126*, 986–987.
- (231) Hayes, A. M.; Morris, D. J.; Clarkson, G. J.; Wills, M. *J. Am. Chem. Soc.* **2005**, *127*, 7318–7319.
- (232) Hortense, E. **2016**, GlaxoSmithKline, Unpublished Work.
- (233) Yamakawa, M.; Yamada, I.; Noyori, R. *Angew. Chemie Int. Ed.* **2001**, *40*, 2818–2821.
- (234) Václavík, J.; Kuzma, M.; Přeč, J.; Kačer, P. *Organometallics* **2011**, *30*, 4822–4829.
- (235) Das, S.; Addis, D.; Zhou, S.; Junge, K.; Beller, M. *J. Am. Chem. Soc.* **2010**, *132*, 1770–1771.
- (236) Kovalenko, O. O.; Volkov, A.; Adolfsson, H. *Org. Lett.* **2015**, *17*, 446–449.
- (237) Doležel, J.; Bartoš, J.; Voglmayr, H.; Greilhuber, J. *Cytometry* **2003**, *51A*, 127–128.
- (238) Annunziato, A. T. *Nat. Educ.* **2008**, *1*, 26.
- (239) Larkin, J.; Goh, X. Y.; Vetter, M.; Pickering, L.; Swanton, C. *Nat. Rev. Urol.* **2012**, *9*, 147–155.
- (240) Bhasin, M.; Reinherz, E. L.; Reche, P. A. *J. Comput. Biol.* **2006**, *13*, 102–112.
- (241) Strahl, B. D.; Allis, C. D. *Nature* **2000**, *403*, 41–45.

- (242) Smith, S. G.; Zhou, M.-M. *ACS Chem. Biol.* **2016**, *11*, 598–608.
- (243) Chiang, C.-M. *F1000 Biol. Rep.* **2009**, *1*, 98.
- (244) Duffy, B. C.; Liu, S.; Martin, G. S.; Wang, R.; Hsia, M. M.; Zhao, H.; Guo, C.; Ellis, M.; Quinn, J. F.; Kharenko, O. A.; Norek, K.; Gesner, E. M.; Young, P. R.; McLure, K. G.; Wagner, G. S.; Lakshminarasimhan, D.; White, A.; Suto, R. K.; Hansen, H. C.; Kitchen, D. B. *Bioorg. Med. Chem. Lett.* **2015**, *25*, 2818–2823.
- (245) Chung, C. *Prog. Med. Chem.* **2012**, *51*, 1–55.
- (246) Raux, B.; Voitovich, Y.; Derviaux, C.; Lugari, A.; Rebuffet, E.; Milhas, S.; Priet, S.; Roux, T.; Trinquet, E.; Guillemot, J.-C.; Knapp, S.; Brunel, J.-M.; Fedorov, A. Y.; Collette, Y.; Roche, P.; Betzi, S.; Combes, S.; Morelli, X. *J. Med. Chem.* **2016**, *59*, 1634–1641.
- (247) White, G. **2016**, GlaxoSmithKline, Internal Presentation.
- (248) Dhalluin, C.; Carlson, J. E.; Zeng, L.; He, C.; Aggarwal, A. K.; Zhou, M.-M.; Zhou, M.-M. *Nature* **1999**, *399*, 491–496.
- (249) Chung, C.; Coste, H.; White, J. H.; Mirguet, O.; Wilde, J.; Gosmini, R. L.; Delves, C.; Magny, S. M.; Woodward, R.; Hughes, S. A.; Boursier, E. V.; Flynn, H.; Bouillot, A. M.; Bamborough, P.; Brusq, J.-M. G.; Gellibert, F. J.; Jones, E. J.; Riou, A. M.; Homes, P.; Martin, S. L.; Uings, I. J.; Toum, J.; Clément, C. A.; Boullay, A.-B.; Grimley, R. L.; Blandel, F. M.; Prinjha, R. K.; Lee, K.; Kirilovsky, J.; Nicodeme, E. *J. Med. Chem.* **2011**, *54*, 3827–3838.
- (250) Bamborough, P. **2016**, GlaxoSmithKline, Unpublished Work.
- (251) Zeng, L.; Li, J.; Muller, M.; Yan, S.; Mujtaba, S.; Pan, C.; Wang, Z.; Zhou, M.-M. *J. Am. Chem. Soc.* **2005**, *127*, 2376–2377.
- (252) White, G.; Wall, I.; Bamborough, P. **2014**, GlaxoSmithKline, Unpublished Work.
- (253) Hortense, E.; Jackson, S. **2014**, GlaxoSmithKline, Unpublished Work.
- (254) White, G.; Baxter, A.; Dalton, T.; Gray, M.; Hirst, D.; Anderson, N.; Barker, M.; Cooper, T.; Wellaway, N.; Poole, D.; Wall, I.; Barnett, H.; McGonagle, G. **2015**, GlaxoSmithKline, Unpublished Work.
- (255) Fournier, J.; Hart, S. **2015**, GlaxoSmithKline, Unpublished Work.
- (256) Fournier, J.; Hart, S. **2016**, GlaxoSmithKline, Unpublished Work.

- (257) Wall, I. **2015**, GlaxoSmithKline, Unpublished Work.
- (258) Weinstock, J.; Oh, H.-J.; DeBrosse, C. W.; Eggleston, D. S.; Wise, M.; Flaim, K. E.; Gessner, G. W.; Sawyer, J. L.; Kaiser, C. *J. Med. Chem.* **1987**, *30*, 1303–1308.
- (259) Shaughnessy, K. H.; Hamann, B. C.; Hartwig, J. F. *J. Org. Chem.* **1998**, *63*, 6546–6553.
- (260) Donets, P. A.; Goeman, J. L.; Van der Eycken, J.; Robeyns, K.; Van Meervelt, L.; Van der Eycken, E. V. *Eur. J. Org. Chem.* **2009**, *2009*, 793–796.
- (261) Cornella, J.; Righi, M.; Larrosa, I. *Angew. Chemie Int. Ed.* **2011**, *50*, 9429–9432.
- (262) Arroniz, C.; Ironmonger, A.; Rassias, G.; Larrosa, I. *Org. Lett.* **2013**, *15*, 910–913.
- (263) Luo, J.; Preciado, S.; Larrosa, I. *J. Am. Chem. Soc.* **2014**, *136*, 4109–4112.
- (264) Luo, J.; Preciado, S.; Larrosa, I. *Chem. Commun.* **2015**, *51*, 3127–3130.
- (265) Mei, T.-S.; Wang, D.-H.; Yu, J.-Q. *Org. Lett.* **2010**, *12*, 3140–3143.
- (266) Giri, R.; Mangel, N.; Li, J.-J.; Wang, D.-H.; Breazzano, S. P.; Saunders, L. B.; Yu, J.-Q. *J. Am. Chem. Soc.* **2007**, *129*, 3510–3511.
- (267) Giri, R.; Yu, J.-Q. *J. Am. Chem. Soc.* **2008**, *130*, 14082–14083.
- (268) Thuy-Boun, P. S.; Villa, G.; Dang, D.; Richardson, P.; Su, S.; Yu, J.-Q. *J. Am. Chem. Soc.* **2013**, *135*, 17508–17513.
- (269) Kosaka, Y.; Kawauchi, S.; Goseki, R.; Ishizone, T. *Macromolecules* **2015**, *48*, 4421–4430.
- (270) Watson, A. J. A.; Maxwell, A. C.; Williams, J. M. J. *J. Org. Chem.* **2011**, *76*, 2328–2331.
- (271) Leonard, J.; Blacker, A. J.; Marsden, S. P.; Jones, M. F.; Mulholland, K. R.; Newton, R. *Org. Process Res. Dev.* **2015**, *19*, 1400–1410.
- (272) Pietruszka, J.; Simon, R. C.; Kruska, F.; Braun, M. *Eur. J. Org. Chem.* **2009**, *2009*, 6217–6224.
- (273) Khumsubdee, S.; Burgess, K. *ACS Catal.* **2013**, *3*, 237–249.
- (274) Stowers, K. J.; Sanford, M. S. *Org. Lett.* **2009**, *11*, 4584–4587.
- (275) Lyons, T. W.; Sanford, M. S. *Chem. Rev.* **2010**, *110*, 1147–1169.
- (276) Giri, R.; Yu, J.-Q.; Giri, R.; Yu, J. *Encycl. Reagents Org. Synth.* **2008**, Iodine

Monoacetate.

- (277) McGonagle, F. I.; Sneddon, H. F.; Jamieson, C.; Watson, A. J. B. *ACS Sustain. Chem. Eng.* **2014**, *2*, 523–532.
- (278) Daugulis, O.; Roane, J.; Tran, L. D. *Acc. Chem. Res.* **2015**, *48*, 1053–1064.
- (279) Kuppusamy, R.; Muralirajan, K.; Cheng, C.-H. *ACS Catal.* **2016**, *6*, 3909–3913.
- (280) Zhang, Z.-Z.; Liu, B.; Wang, C.-Y.; Shi, B.-F. *Org. Lett.* **2015**, *17*, 4094–4097.
- (281) Kim, J. H.; Greßies, S.; Glorius, F. *Angew. Chemie Int. Ed.* **2016**, *55*, 5577–5581.
- (282) Liu, W.; Ackermann, L. *ACS Catal.* **2016**, *6*, 3743–3752.
- (283) Su, M.; Li, C.; Ma, J. *J. Chinese Chem. Soc.* **2016**, *63*, 828–840.
- (284) Guimond, N.; Fagnou, K. *J. Am. Chem. Soc.* **2009**, *131*, 12050–12051.
- (285) Ueura, K.; Satoh, T.; Miura, M. *J. Org. Chem.* **2007**, *72*, 5362–5367.
- (286) Feng, C.; Loh, T. P. *Angew. Chemie Int. Ed.* **2014**, *53*, 2722–2726.
- (287) Schröder, N.; Wencel-Delord, J.; Glorius, F. *J. Am. Chem. Soc.* **2012**, *134*, 8298–8301.
- (288) Stuart, D. R.; Alsabeh, P.; Kuhn, M.; Fagnou, K. *J. Am. Chem. Soc.* **2010**, *132*, 18326–18339.
- (289) Racys, D. T.; Sharif, S. A. I.; Pimlott, S. L.; Sutherland, A. *J. Org. Chem.* **2016**, *81*, 772–780.
- (290) Cheng, C.; Brookhart, M. *J. Am. Chem. Soc.* **2012**, *134*, 11304–11307.
- (291) Beletskaya, I. P.; Cheprakov, A. V. *Chem. Rev.* **2000**, *100*, 3009–3066.
- (292) Dounay, A. B.; Overman, L. E. *Chem. Rev.* **2003**, *103*, 2945–2964.
- (293) Das, B.; Kashinatham, A.; Venkataiah, B. *Synth. Commun.* **1999**, *29*, 3799–3804.
- (294) Hortense, E.; Jackson, S. **2016**, GlaxoSmithKline, Unpublished Work.
- (295) Wang, F.; Wang, H.; Wang, Q.; Yu, S.; Li, X. *Org. Lett.* **2016**, *18*, 1306–1309.
- (296) Ueura, K.; Satoh, T.; Miura, M. *Org. Lett.* **2007**, *9*, 1407–1409.
- (297) Stuart, D. R.; Bertrand-Laperle, M.; Burgess, K. M. N.; Fagnou, K. *J. Am. Chem. Soc.* **2008**, *130*, 16474–16475.
- (298) Rakshit, S.; Patureau, F. W.; Glorius, F. *J. Am. Chem. Soc.* **2010**, *132*, 9585–9587.
- (299) Guimond, N.; Gouliaras, C.; Fagnou, K. *J. Am. Chem. Soc.* **2010**, *132*, 6908–

- 6909.
- (300) Hyster, T. K.; Rovis, T. *J. Am. Chem. Soc.* **2010**, *132*, 10565–10569.
- (301) Guimond, N.; Gorelsky, S. I.; Fagnou, K. *J. Am. Chem. Soc.* **2011**, *133*, 6449–6457.
- (302) Yang, Y.-F.; Houk, K. N.; Wu, Y.-D. *J. Am. Chem. Soc.* **2016**, *138*, 6861–6868.
- (303) Chan, W.-W.; Lo, S.-F.; Zhou, Z.; Yu, W.-Y. *J. Am. Chem. Soc.* **2012**, *134*, 13565–13568.
- (304) Shi, Z.; Koester, D. C.; Boultadakis-Arapinis, M.; Glorius, F. *J. Am. Chem. Soc.* **2013**, *135*, 12204–12207.
- (305) Hart, S.; Fournier, J. **2015**, GlaxoSmithKline, Unpublished Work.
- (306) Dalton, T. **2016**, GlaxoSmithKline, Unpublished Work.
- (307) Angermund, K. P.; Betz, P.; Butenschön, H. *Chem. Ber.* **1993**, *126*, 713–724.
- (308) Hyster, T. K.; Ruhl, K. E.; Rovis, T. *J. Am. Chem. Soc.* **2013**, *135*, 5364–5367.
- (309) Wang, H.; Grohmann, C.; Nimphius, C.; Glorius, F. *J. Am. Chem. Soc.* **2012**, *134*, 19592–19595.
- (310) Xie, F.; Qi, Z.; Yu, S.; Li, X. *J. Am. Chem. Soc.* **2014**, *136*, 4780–4787.
- (311) Wang, H.; Schröder, N.; Glorius, F. *Angew. Chemie Int. Ed.* **2013**, *52*, 5386–5389.
- (312) Wohlfarth, C. *Static Dielectric Constants of Pure Liquids and Binary Liquid Mixtures*, 1st Editio.; Springer-Verlag: Heidelberg, 2008.
- (313) Klahn, A. H.; Morales, V.; Oelckers, B.; Buono-Core, G. E.; Gomez, J.; Godoy, F. *J. Chil. Chem. Soc.* **2011**, *56*, 819–822.
- (314) Olmstead, W. N.; Margolin, Z.; Bordwell, F. G. *J. Org. Chem.* **1980**, *45*, 3295–3299.
- (315) Bordwell, F. G.; Algrim, D. *J. Org. Chem.* **1976**, *41*, 2507–2508.
- (316) Lapointe, D.; Fagnou, K. *Chem. Lett.* **2010**, *39*, 1118–1126.
- (317) Dalton, T. **2016**, GlaxoSmithKline, Unpublished Work.
- (318) Beesley, R. M.; Ingold, C. K.; Thorpe, J. F. *J. Chem. Soc., Trans.* **1915**, *107*, 1080–1106.
- (319) Hortense, E. **2014**, GlaxoSmithKline, Unpublished Work.
- (320) Pietruszka, J.; Simon, R. C.; Kruska, F.; Braun, M. *Eur. J. Org. Chem.* **2009**, *2009*, 6217–6224.

- (321) Hanada, S.; Ishida, T.; Motoyama, Y.; Nagashima, H. *J. Org. Chem.* **2007**, *72*, 7551–7559.
- (322) Dettori, G.; Gaspa, S.; Porcheddu, A.; De Luca, L. *Adv. Synth. Catal.* **2014**, *356*, 2709–2713.